

NASA Contractor Report 3100

NASA-CR-3100

19800010753

Rotary Balance Data for a Typical
Single-Engine General Aviation
Design for an Angle-of-Attack
Range of 8° to 90°

I - Low-Wing Model A

FOR REFERENCE
NOT TO BE TAKEN FROM THIS ROOM

Randy S. Hultberg and William Mulcay

CONTRACT NAS1-14849
FEBRUARY 1980

NASA

NASA Contractor Report 3100

Rotary Balance Data for a Typical
Single-Engine General Aviation
Design for an Angle-of-Attack
Range of 8° to 90°

I - Low-Wing Model A

Randy S. Hultberg and William Mulcay
Bihrlé Applied Research, Inc.
Jericho, New York

Prepared for
Langley Research Center
under Contract NAS1-14849



National Aeronautics
and Space Administration

**Scientific and Technical
Information Office**

1980

SUMMARY

Aerodynamic characteristics obtained in a rotational flow environment utilizing a rotary balance located in the Langley spin tunnel are presented in plotted form for a 1/5-scale, single-engine, low-wing, general aviation airplane model. The configurations tested included the basic airplane, various control deflections, tail designs, fuselage shapes and wing leading edges. Data are presented without analysis for an angle-of-attack range of 8° to 90° and clockwise and counter-clockwise rotations covering an $\frac{\Omega b}{2V}$ range from 0 to 0.85.

INTRODUCTION

The NASA Langley Research Center has initiated a broad general aviation stall/spin research program which includes spin-tunnel and free-flight radio control model tests, as well as full-scale flight tests for a number of configurations typical of light, general aviation airplanes. To support this effort, rotary balance wind tunnel force tests covering these same configurations will be conducted to establish a data base for analysis of model and full-scale flight results, and to develop design charts for desirable stall/spin characteristics.

A 1/5-scale, single-engine, general aviation airplane model, referred to as model A, having a low-wing location was tested in a rotational flow environment utilizing a rotary balance located in the Langley spin tunnel. This report presents the data obtained for the basic airplane, various control deflections, tail designs, fuselage shapes and wing leading edges. These data supplement the rotary balance data presented in references 1 and 2.

Reference 1 data is mainly concerned with the fuselage modifications and airplane components previously tested statically (reference 3) at a low and high Reynolds number in the Ames Research Center 12-foot Pressure Tunnel. Data solely relative to leading-edge wing modifications are presented in reference 2. Data for model A having a high-wing location are presented in reference 4.

SYMBOLS

The units for physical quantities used herein are presented in the International System of Units (SI) and U.S. Customary Units. The measurements were made in the U.S. Customary Units; equivalent dimensions were determined by using the conversion factors given in reference 5.

b	wing span, m (ft)
\bar{c}	mean aerodynamic chord, cm (in.)
C_L	lift-force coefficient, $\frac{\text{Lift force}}{qS}$
C_N	normal-force coefficient, $\frac{\text{Normal force}}{qS}$
C_A	axial-force coefficient, $\frac{\text{Axial force}}{qS}$
C_Y	side-force coefficient, $\frac{\text{Side force}}{qS}$
C_λ	rolling moment coefficient, $\frac{\text{Rolling moment}}{qSb}$
C_m	pitching-moment coefficient, $\frac{\text{Pitching moment}}{qS\bar{c}}$
C_n	yawing moment coefficient, $\frac{\text{Yawing moment}}{qSb}$
q	free-stream dynamic pressure, N/m ² (lb/ft ²)
S	wing area, m ² (ft ²)
V	free-stream velocity, m/sec (ft/sec)
α	angle of attack, deg

β angle of sideslip, deg
 Ω angular velocity about spin axis, rad/sec
 $\frac{\Omega b}{2V}$ spin coefficient, positive for clockwise spin
 δ_a aileron deflection, positive when right aileron is down
 $(\delta_{a_{\text{right}}} - \delta_{a_{\text{left}}})/2$, deg
 δ_e elevator deflection, positive when trailing edge is down, deg
 δ_r rudder deflection, positive when trailing edge is to left,
deg

Abbreviations:

cg center of gravity
SR spin radius
TE trailing edge

TEST EQUIPMENT

A rotary balance measures the forces and moments acting on an airplane while subjected to rotational flow conditions; the background for this apparatus is discussed in reference 1. A photograph and sketch of the rotary balance apparatus installed in the Langley spin tunnel are shown in figures 1 and 2, respectively. The rotating portion of the balance system, mounted on a horizontal supporting boom which is hinged at the wall, is moved from the wall to the center of the tunnel by cables. The rotary arm of the balance system, which rotates about a vertical axis, is attached to the outer end of the horizontal supporting boom and is driven by a drive shaft through couplings and gears.

A test model is mounted on a strain gauge balance which is affixed to the bottom of the rotary balance apparatus. Controls located outside the tunnel are used to activate motors on the rig which position the model to the desired attitude. The angle-of-attack range of the rig is 8 to 90 degrees and the sideslip angle range is ± 15 degrees. The spin radius and the lateral displacement motors allow the operator to position the moment center of the balance on the spin axis or at a specific distance from the spin axis. This is done for each combination of angle of attack and sideslip angle. The general practice is to mount the moment center of the balance at the cg location about which the aerodynamic moments are desired. Electrical current from the balance, and to the motors on the rig, is conducted through slip-rings located at the rig head. Examples of how the rig is positioned for different angle of attack and sideslip angles are shown in figures 2a and 2b, respectively.

The model can be rotated up to 90 rpm in either direction. By using different rotational speeds and a specific airflow in the tunnel, the motions of a steady spinning airplane can be simulated. The aerodynamic forces and moments can then be measured for values of $\frac{\Omega b}{2V}$, including the case of $\frac{\Omega b}{2V} = 0$, where static aerodynamic forces and moments can be obtained.

A NASA six-component strain gauge balance is mounted inside the model and measures the normal, lateral and longitudinal forces and the yawing, rolling and pitching moments acting about the model body axis. The interactions that exist between the six compo-

nents are available from balance calibration tests and are accounted for after the balance voltages are converted to forces and moments.

The data acquisition, reduction and presentation system for the rotary balance set-up is composed of a 12-channel scanner/voltmeter, a mini-computer and a plotter. With this equipment, on-line digital print-out and/or graphical plots of data are possible.

TEST PROCEDURES

Rotary aerodynamic data are obtained in two steps. The first step is to record the inertial forces and moments (tares) acting on the model at different attitudes and rotational speeds. To accomplish this, a covered bird-cage like structure is mounted to the upper rig which encloses the model without touching it. In this manner, the air immediately surrounding the model is rotated with it. As the rig is rotated at the desired attitude and rate, the inertial forces and moments generated by the model are measured and stored on magnetic tape for later use.

The second step in the data-gathering process is to measure aerodynamic and inertial forces at different attitudes and rotational speeds for a selected tunnel velocity with, of course, the cage structure removed. The tares are subtracted from these values, and the remaining aerodynamic forces and moments are then converted to coefficient form and stored on magnetic tape.

MODEL

A 1/5-scale fiberglass/foam/plywood model of a configuration considered to be a typical low-wing, single-engine, light general

aviation airplane was tested in the present study. A three-view drawing of this model is shown in figure 3, dimensional characteristics of the model are presented in Table I, and a photograph of the model installed on the rotary balance located in the Langley spin tunnel is presented in figure 1.

The model was fabricated such that various wing, tail and fuselage configurations could be tested. The two tail configurations tested involved different locations of the horizontal tail as shown in figure 4. The fuselage shape and wing leading edge modifications tested are shown in figure 5 and 6 respectively.

The model control surfaces could be set at any position prior to the test. The maximum deflections for the control surfaces were:

Elevator, deg	25 up, 15 down
Rudder, deg	25 right, 25 left
Aileron, deg	25 up, 20 down

TEST CONDITIONS

The tests were conducted in the spin tunnel at a tunnel velocity of 7.62 m/sec (25 ft/sec) which corresponds to a Reynolds number of 128,000 based on the model mean aerodynamic chord. Unless noted otherwise in Table II, all the configurations were tested through an angle-of-attack range of 8 to 90° at a zero sideslip angle with the spin axis passing through the full-scale airplane cg location of .255 \bar{c} for angles of attack above 30°. For angles of attack below 35°, the spin axis was set 76.2 cm (30 in.) forward of the cg. Consequently, data was obtained for both a 0

and 76.2 cm (30 in.) spin radius at angles of attack of 30 and 35°. At each spin attitude, measurements were obtained for nominal $\frac{\Omega b}{2V}$ values of .1, .2, .3, .4, .45, .55, .65, .75 and .85 in both clockwise and counter-clockwise directions, as well as for $\frac{\Omega b}{2V} = 0$ (static value).

DATA PRESENTATION

Table II identifies the configurations tested and the corresponding appendix figure numbers which present the aerodynamic data. The aerodynamic coefficients vs. $\frac{\Omega b}{2V}$ are presented for each configuration in six sequentially numbered figures in the following order: C_n , C_ℓ , C_m , C_N , C_Y and C_A . Each figure, in turn, consists of four pages which present the subject aerodynamic coefficient vs. $\frac{\Omega b}{2V}$ for the following angles of attack and spin radii, unless noted otherwise in Table II.

- a) $\alpha = 8, 10, 12, 14, 16$ deg SR= 76.2 cm (30 in.)
- b) $\alpha = 18, 20, 25, 30, 35$ deg SR= 76.2 cm (30 in.)
- c) $\alpha = 30, 35, 40, 45, 50$ deg SR= 0
- d) $\alpha = 55, 60, 70, 80, 90$ deg SR= 0

All the moment data are presented for a cg position of $0.255\bar{c}$.

Lift coefficient as a function of angle of attack for zero rotation rate is presented at the end of the Appendix for the configurations cited in Table II.

REFERENCES

1. Bihrlle, William, Jr.; Hultberg, Randy S.; Mulcay, William:
Rotary Balance Data for a Typical Single-Engine Low-Wing
General Aviation Design for an Angle-of-Attack Range of
 30° to 90° . NASA CR-2972, 1978.
2. Bihrlle, William, Jr.; Mulcay, William: Rotary Balance Data
for a Typical Single-Engine General Aviation Design for an
Angle-Of-Attack Range of 8° to 35° . III- Effect of Wing
Leading-Edge Modifications Model A. NASA CR-3102, 1979.
3. Bihrlle, William, Jr.; Barnhart, Billy; Pantason, Paul:
Static Aerodynamic Characteristics of a Typical Single-Engine
Low-Wing General Aviation Design for an Angle-of-Attack
Range of -8° to 90° . NASA CR 2971, 1978
4. Mulcay, William ; Rose, Robert: Rotary Balance Data for
a Typical Single-Engine General Aviation Design for an
Angle-of-Attack Range of 8° to 90° . II- High Wing Model A.
NASA CR-3101, 1979.
5. Mechtly, E.A.: The International System of Units - Physical
Constants and Conversion Factors. NASA SP-7012, 1973.

TABLE I.- DIMENSIONAL CHARACTERISTICS OF THE BASIC MODEL

Overall length with tail #4, m (ft) 1.23 (4.05)

Wing:

Span, m (ft) 1.46 (4.80)

Area, m² (ft²) 0.36 (3.87)

Root chord, cm (in.) 24.54 (9.66)

Tip chord, cm (in.) 24.54 (9.66)

Mean aerodynamic chord, cm (in.) 24.54 (9.66)

Leading edge of \bar{c} , distance rearward of leading

edge of root chord, cm (in.) 0

Aspect ratio 5.9

Dihedral, deg 5.0

Incidence:

Root, deg 3.5

Tip, deg 3.5

Airfoil section NACA 64₂-415 modified

Horizontal tail:

Span, m (ft) 0.47 (1.53)

Incidence, deg -3.0

Airfoil section NACA 65₁-012

Vertical tail:

Airfoil section NACA 65₁-012

TABLE II.- CONFIGURATIONS TESTED AND FIGURE INDEX
(Unless noted otherwise, all configurations tested through $\alpha = 8$ to 90° at $\beta = 0^\circ$.)

FIGURE NO.	CONFIGURATION	δ_e deg	δ_a deg	δ_r deg	REMARKS
^a A1-A6	Basic (#4 Horizontal tail)	0	0	0	
A7-A12				-25	
A13-A18		+15			
A19-A24		-15			
A25-A30		-25			
A31-A36			+22.5		
A37-A42			-22.5		
A43-A48			+22.5	0	
A49-A54		0	0		$\beta = +10^\circ$
A55-A60					$\beta = -10^\circ$
A61-A66	with rounded fuselage bottom aft of wing TE				only $\alpha = 30$ to 90° , SR=0
A67-A72	with rounded fuselage bottom aft of engine cowling				only $\alpha = 30$ to 90° , SR=0
A73-A78	with rounded fuselage bottom aft of engine cowling and wing fairings removed				only $\alpha = 55$ to 90° , SR=0
^a A79-A84	Y with full-span leading-edge wing droop				
A85-A90	#3 Horizontal tail				
A91-A96	with rounded fuselage bottom aft of wing TE				only $\alpha = 30$ to 90° , SR=0
A97-A102	with rounded fuselage bottom aft of engine cowling				only $\alpha = 30$ to 90° , SR=0
A103-A108	with rounded fuselage bottom aft of engine cowling and wing fairings removed				only $\alpha = 30$ to 90° , SR=0
A109-A114	Y with full-span leading-edge wing droop				

^a C_L vs α presented in figure A115.

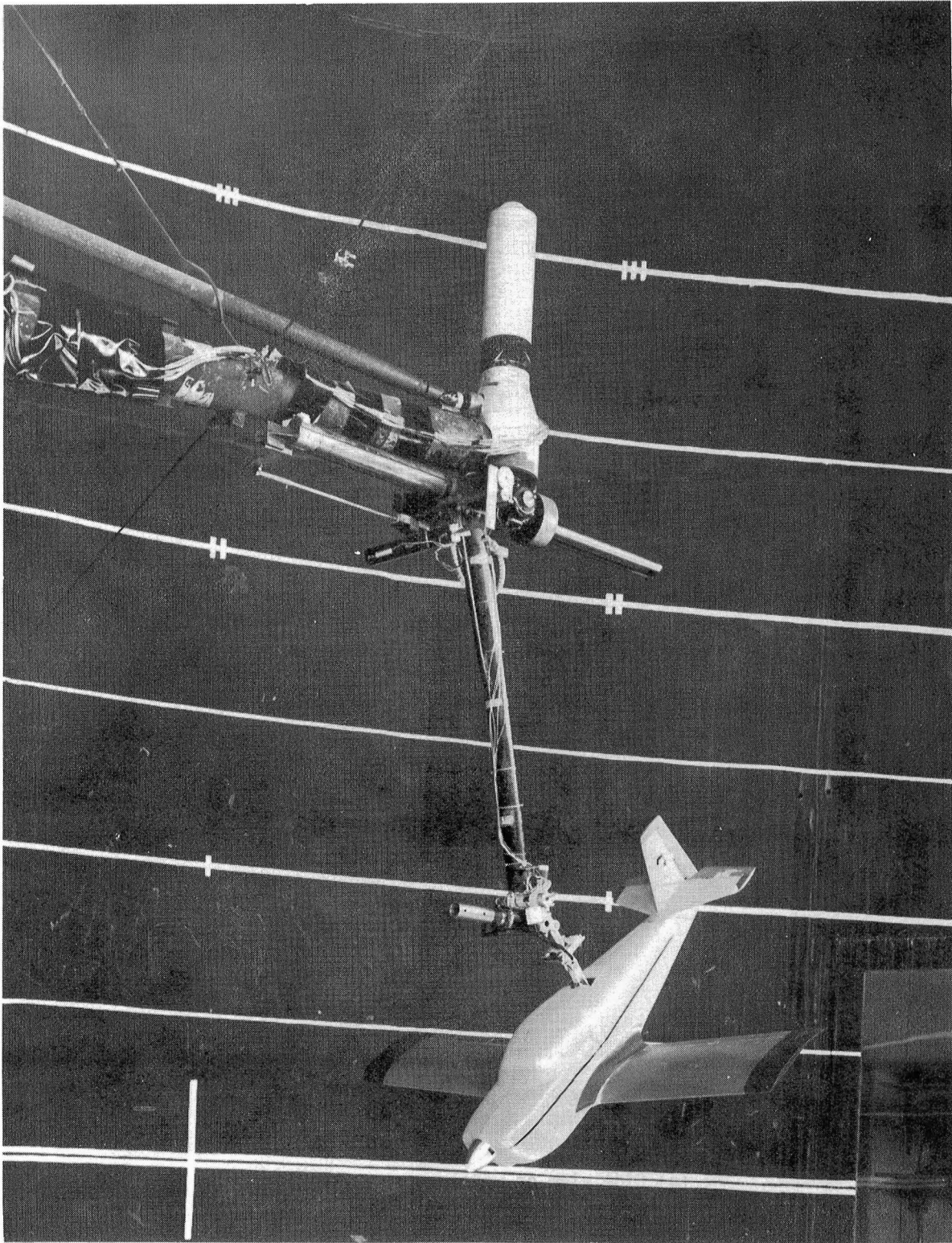
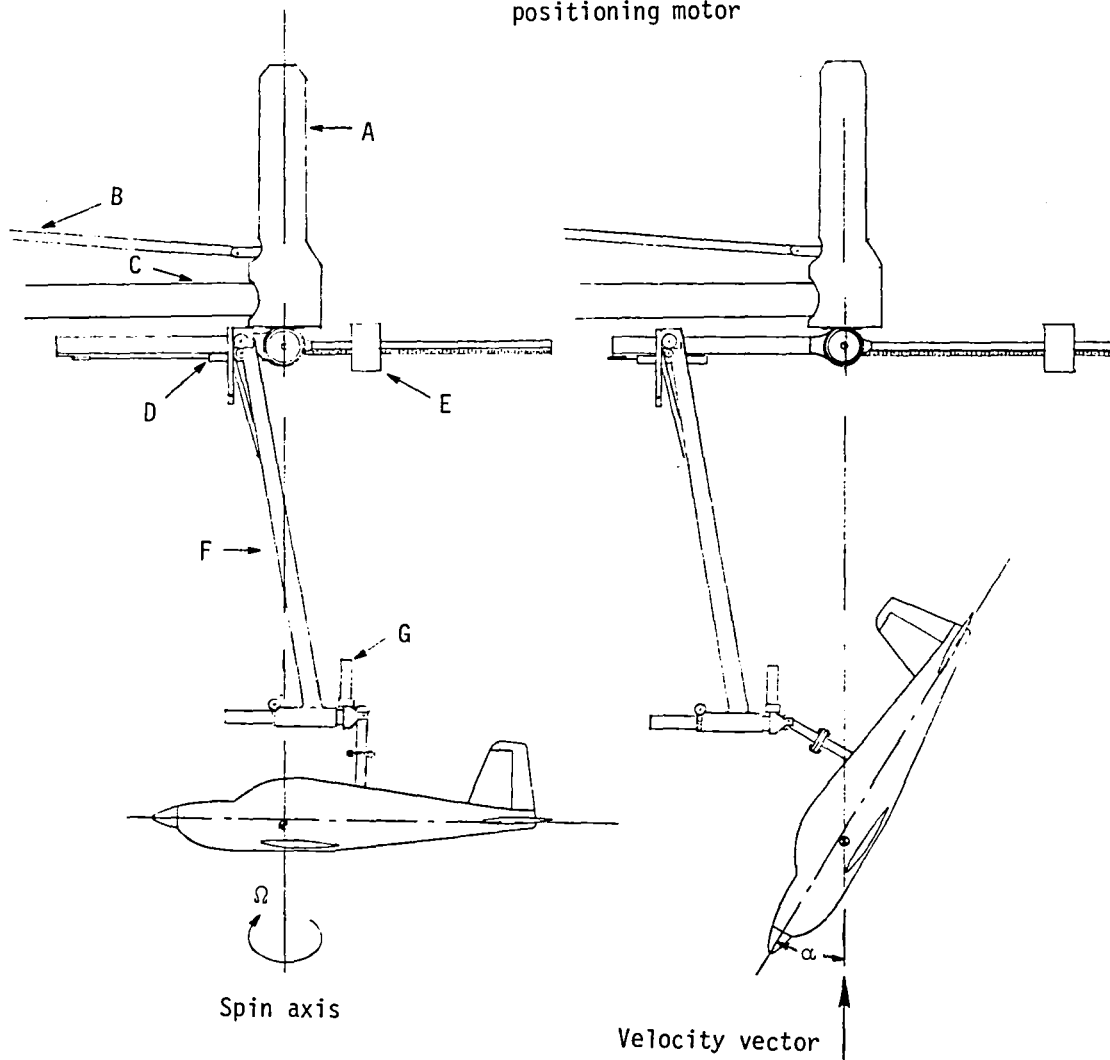


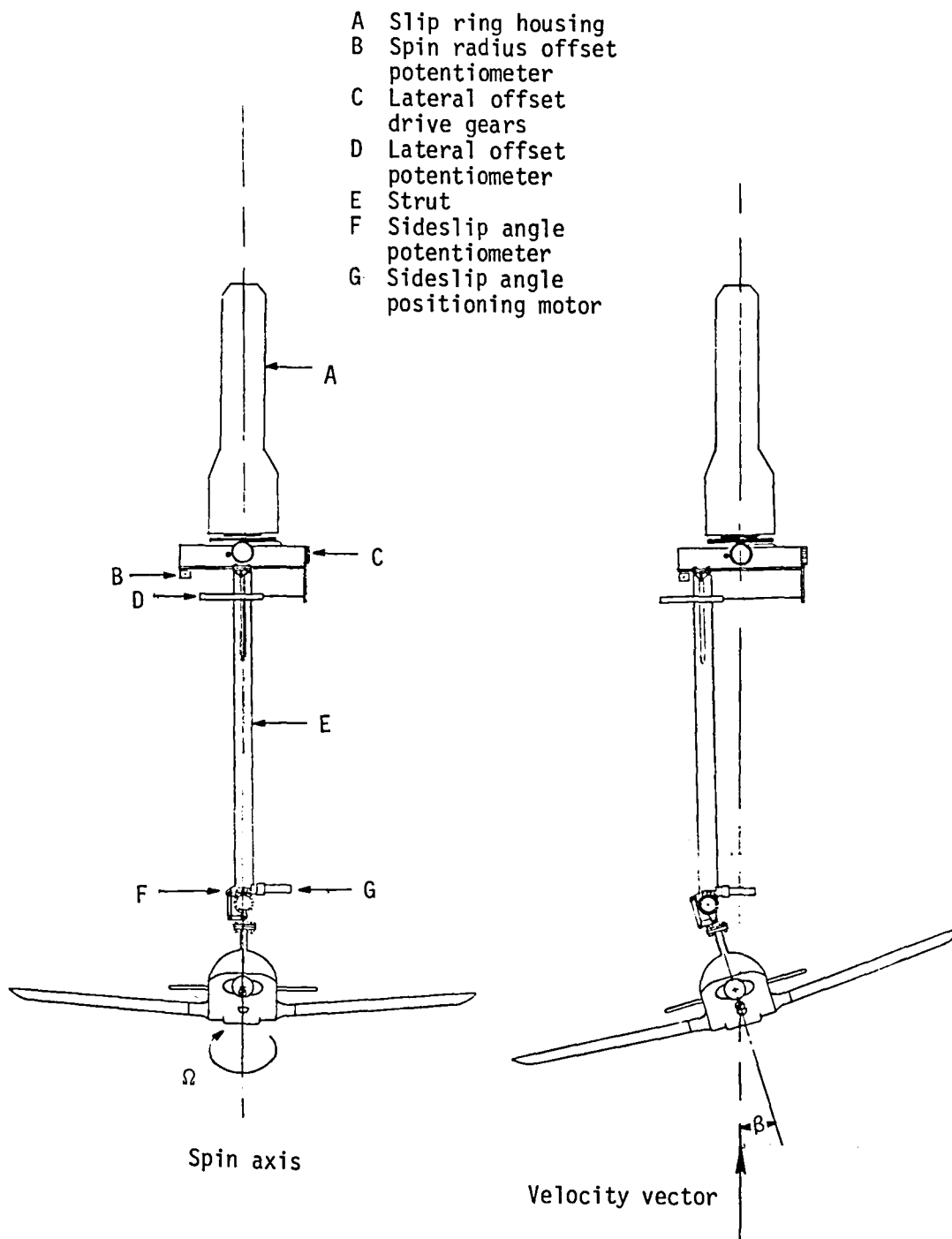
Figure 1.- Photograph of 1/5-scale model installed on rotary balance apparatus.

- A Slip ring housing
- B Drive shaft
- C Support boom
- D Spin radius offset potentiometer
- E Counterweight
- F Strut
- G Angle of attack positioning motor



(a) Side view of model.

Figure 2.- Sketch of rotary balance apparatus.



(b) Front view of model.

Figure 2.- Concluded.

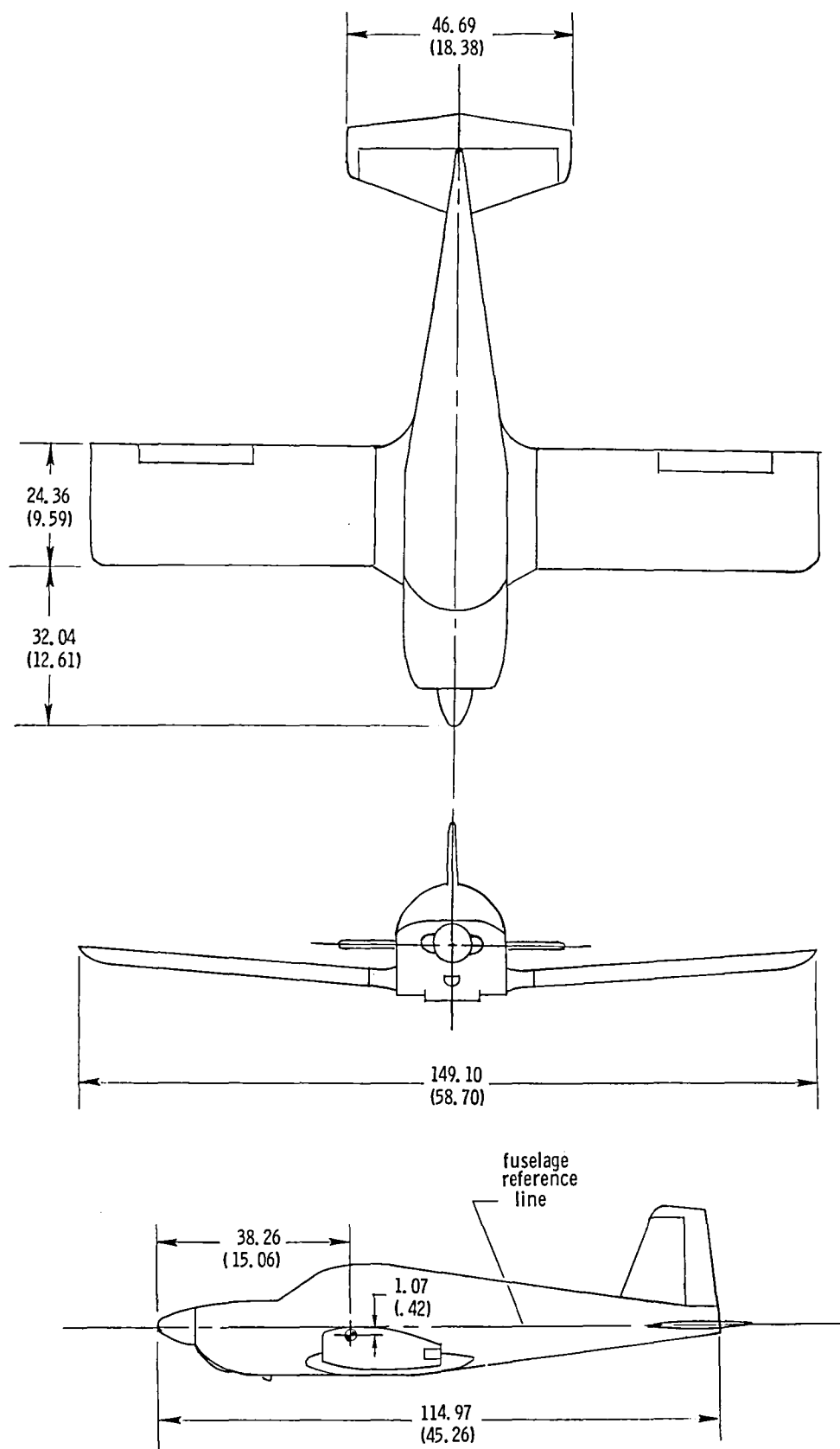
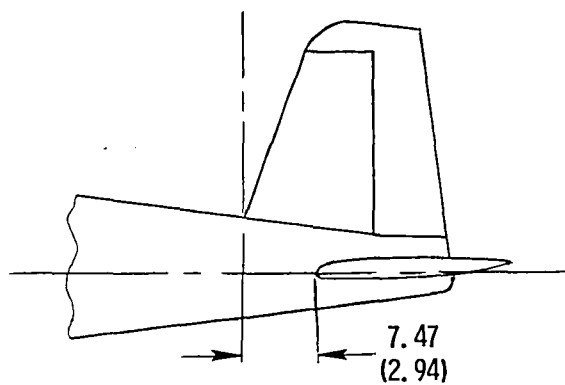
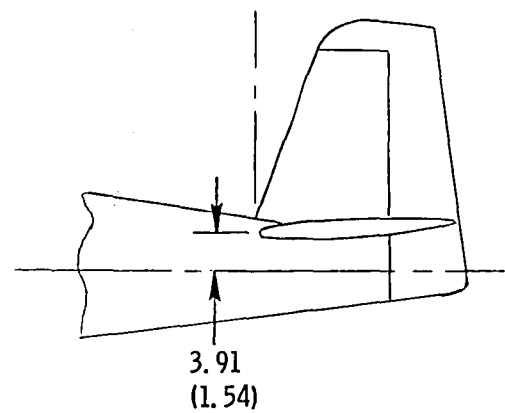
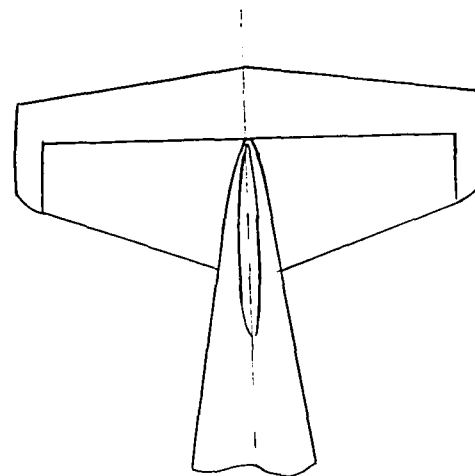


Figure 3. - Three-view drawing of 1/5-scale low-wing general aviation model A. Center-of-gravity positioned at 0.255C. Dimensions are given in centimeters(inches), model scale.



b) Tail 4



a) Tail 3

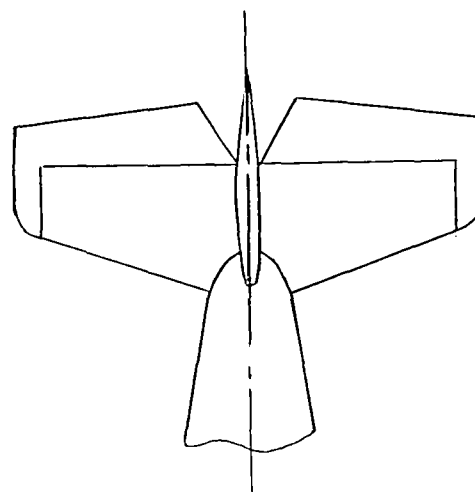


Figure 4. -Tail configurations tested on model. Dimensions are given in centimeters (inches), model scale.

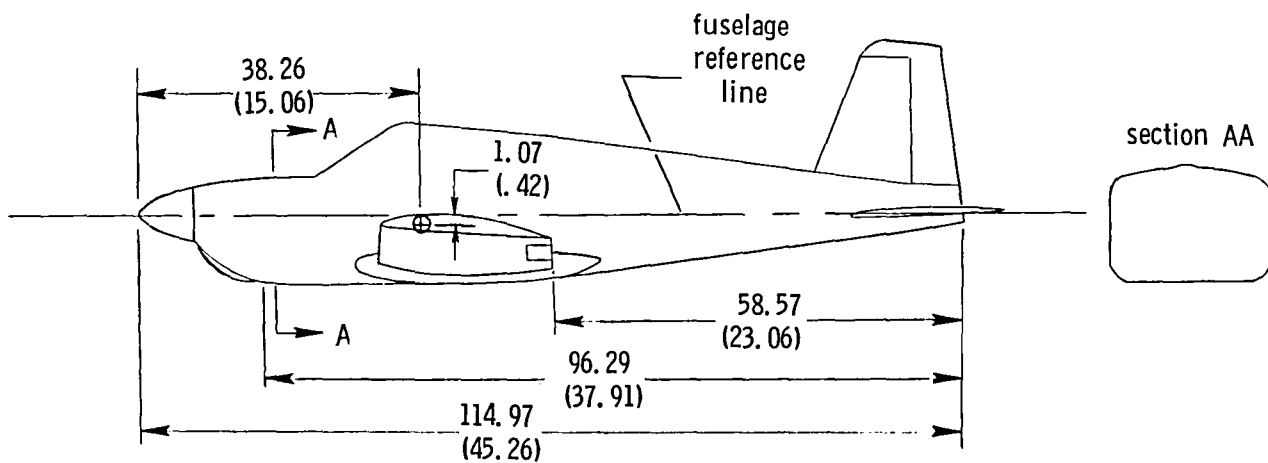
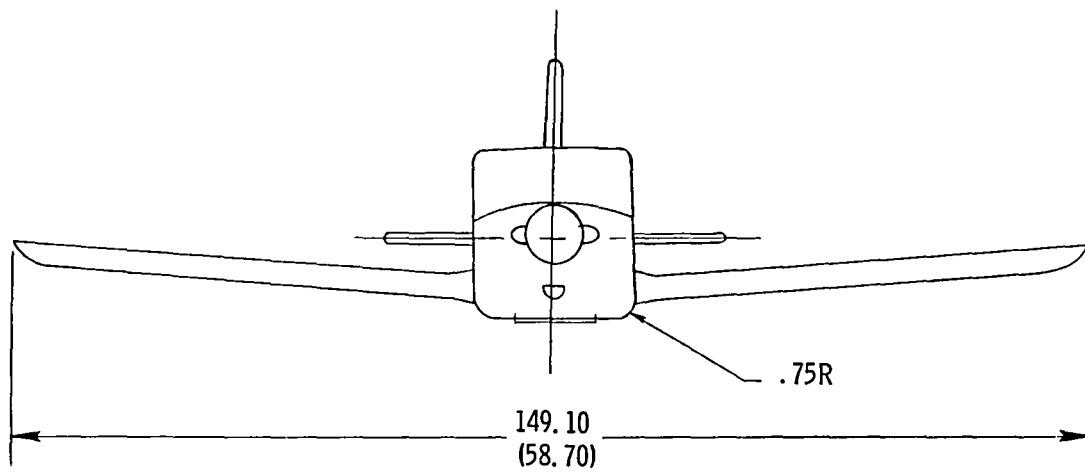


Figure 5. - Fuselage modifications for model. Dimensions are given in centimeters (inches).

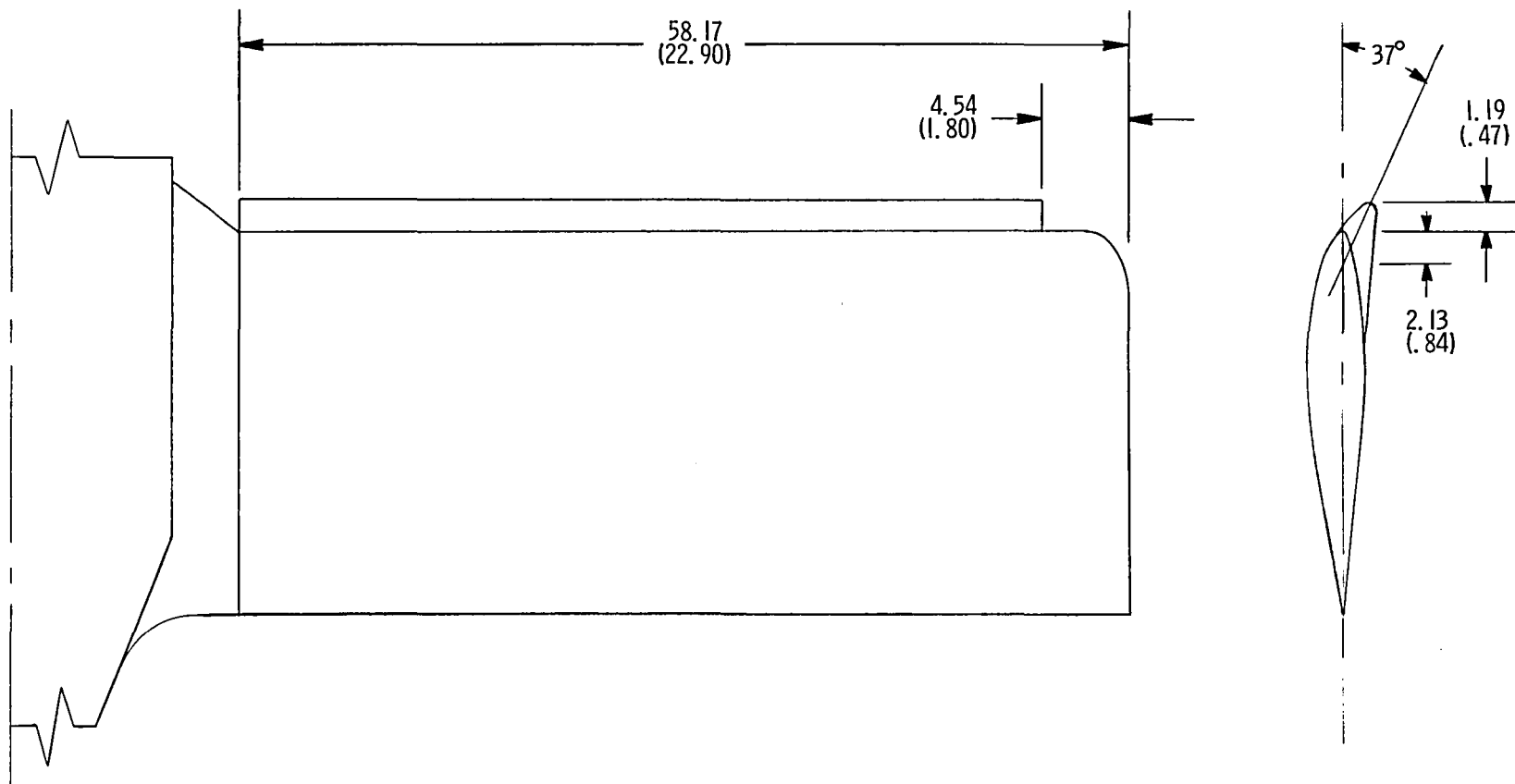
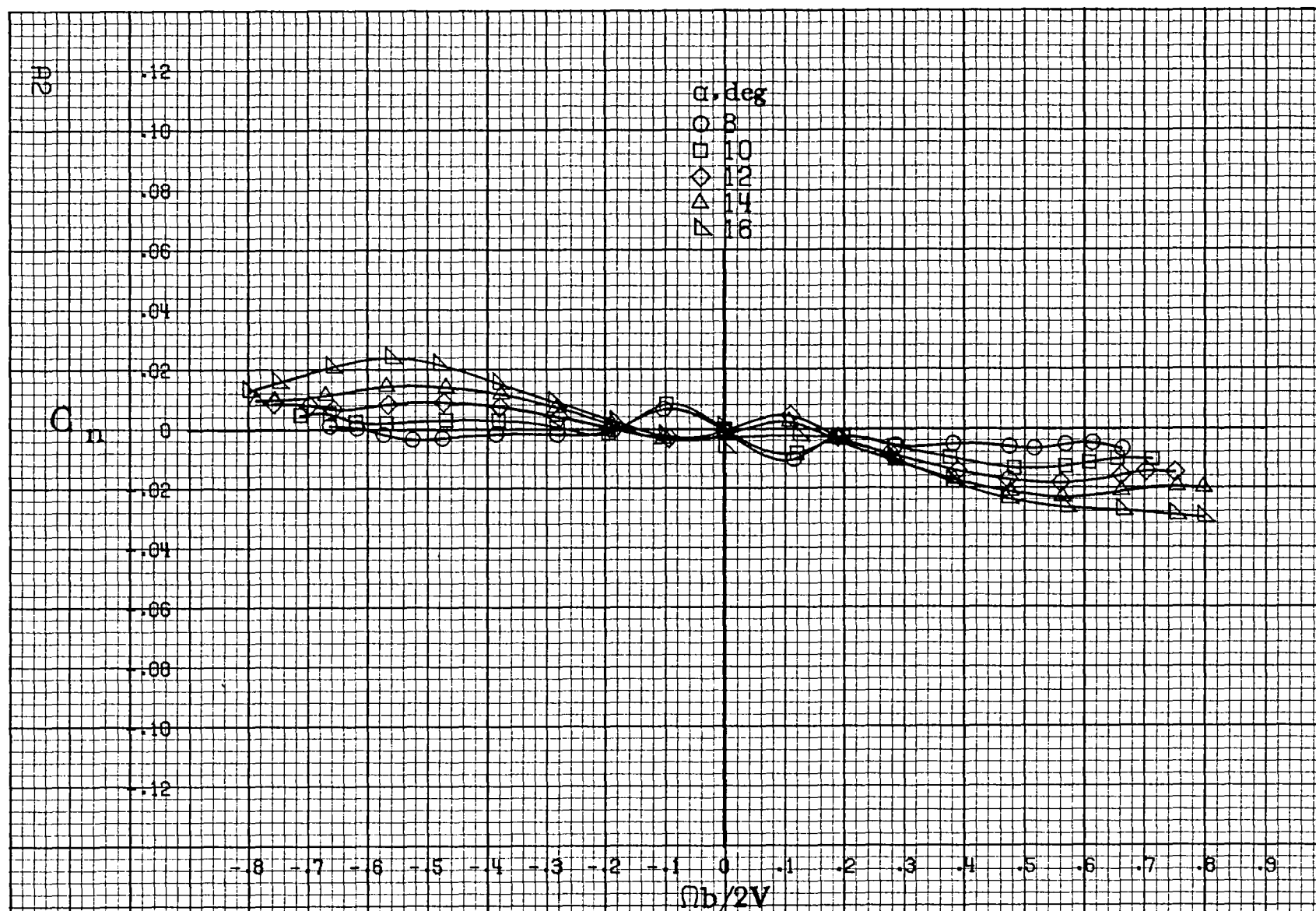


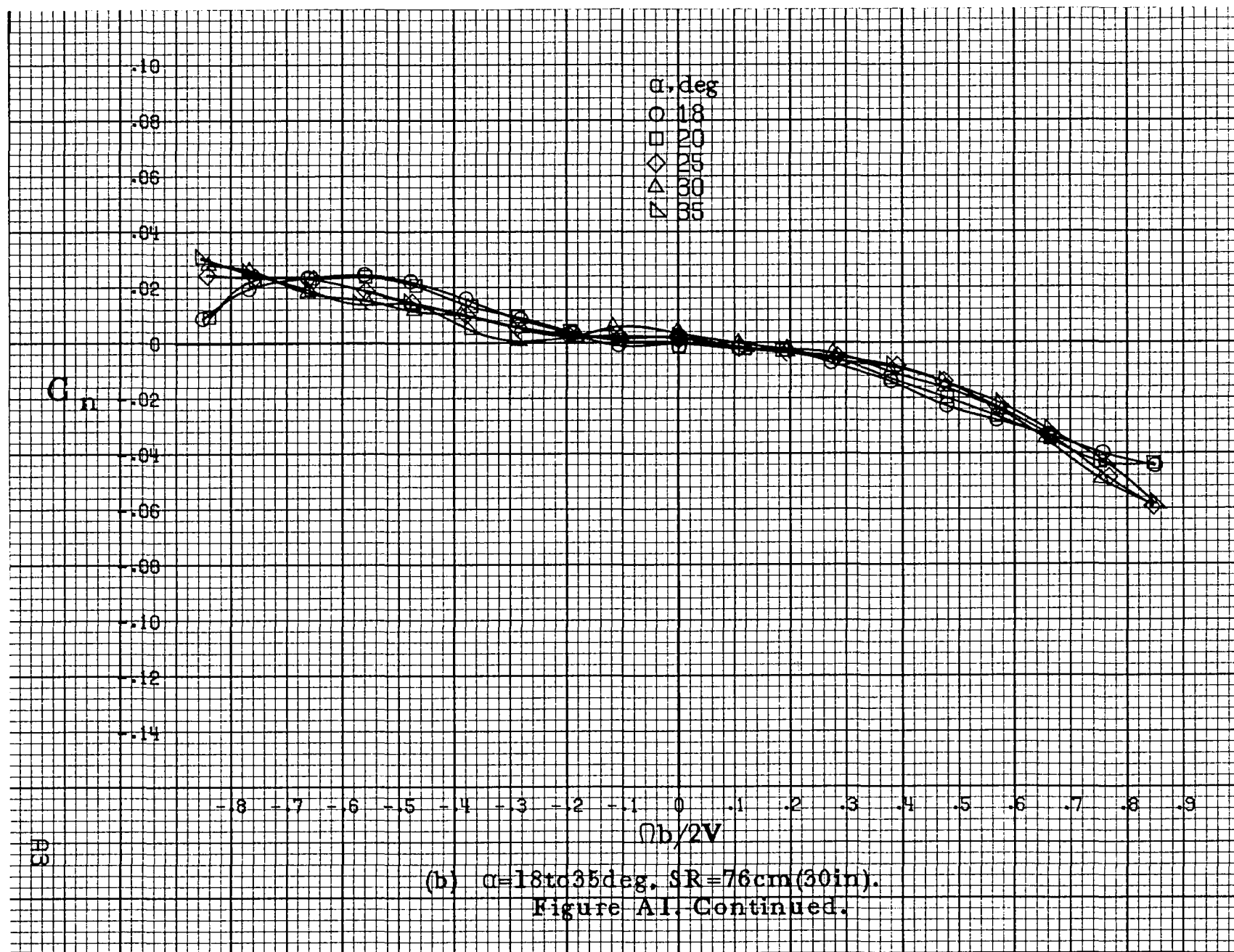
Figure 6. - Basic airfoil with leading edge droop tested on model. Dimensions are given in centimeters (inches), model scale.

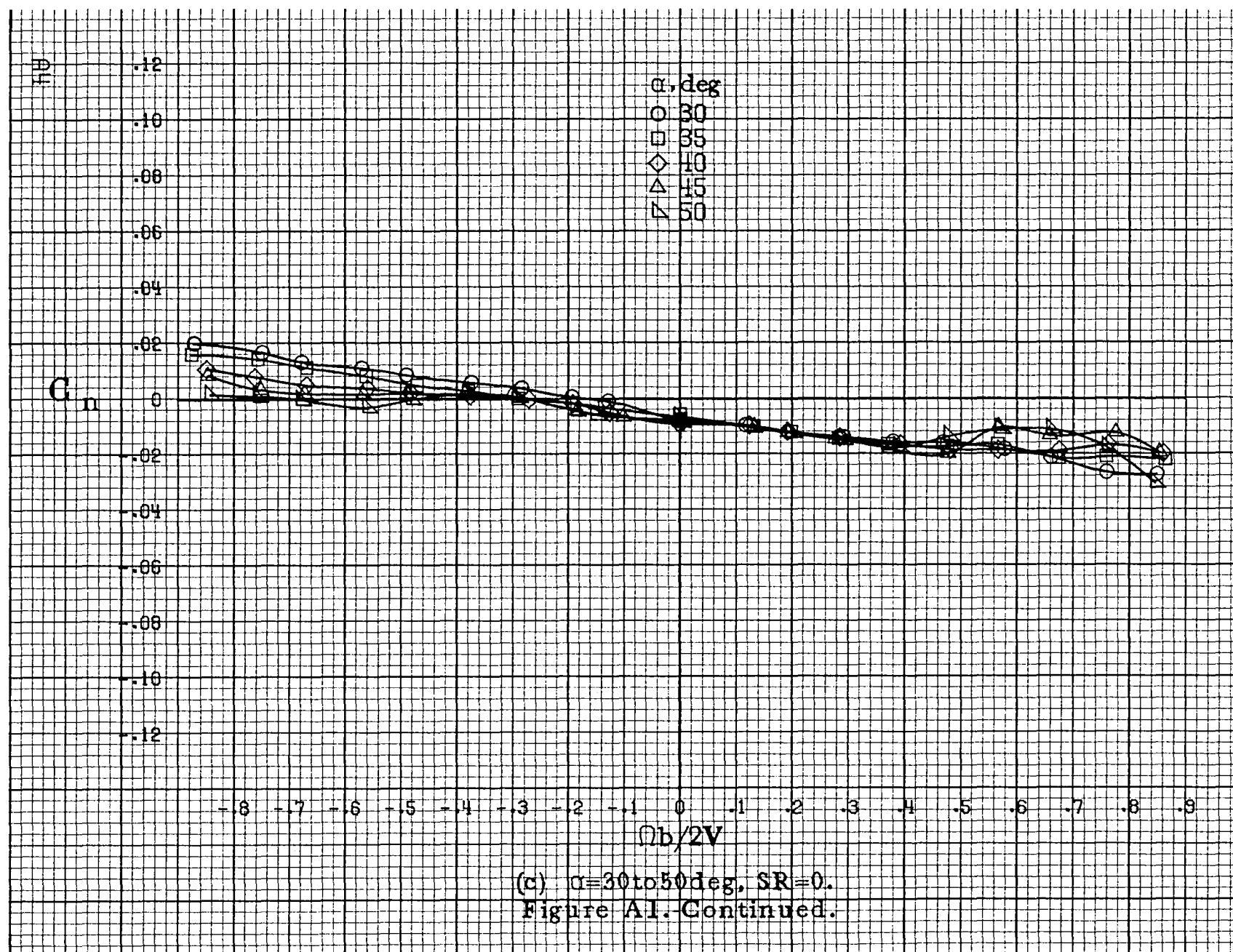
APPENDIX

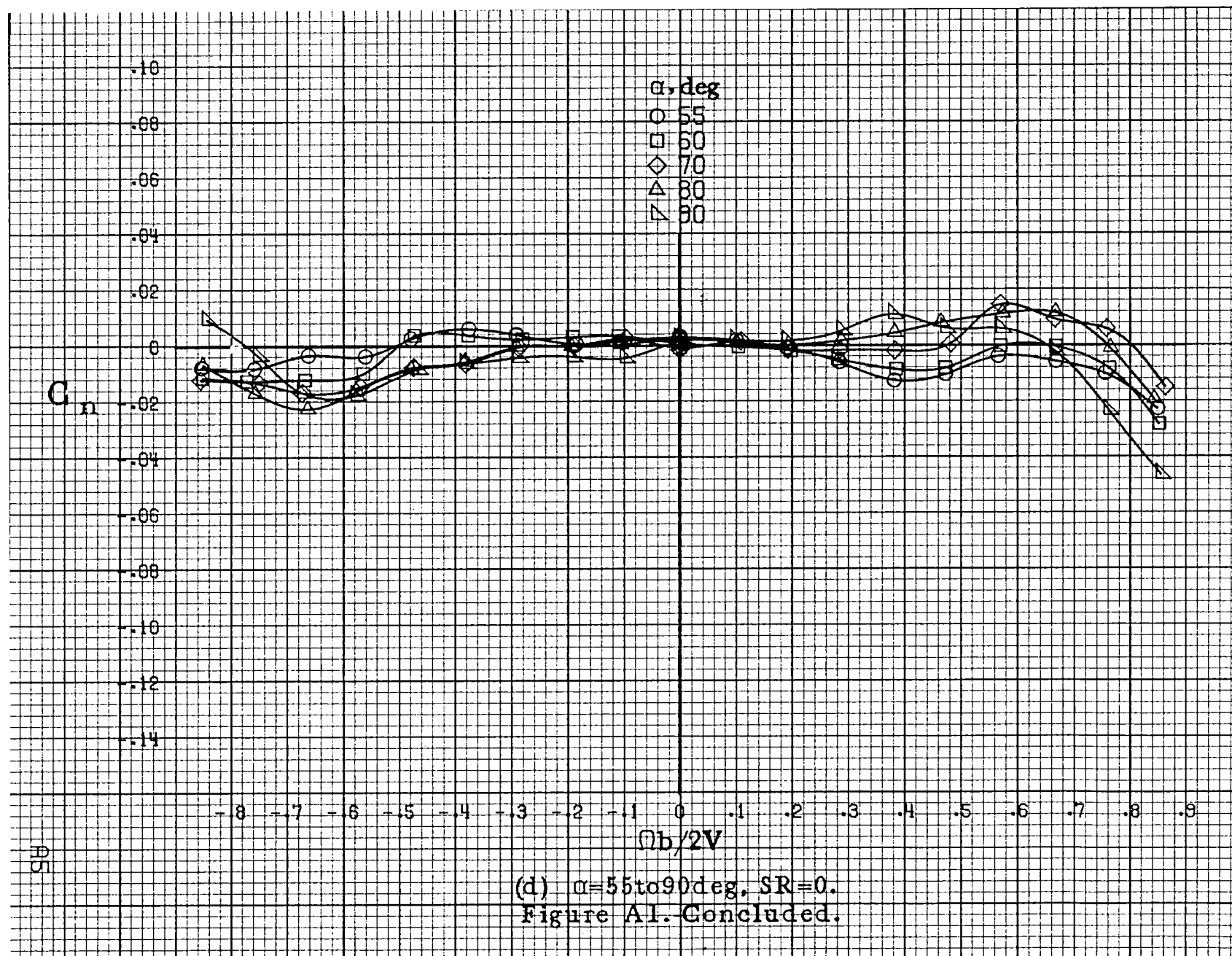


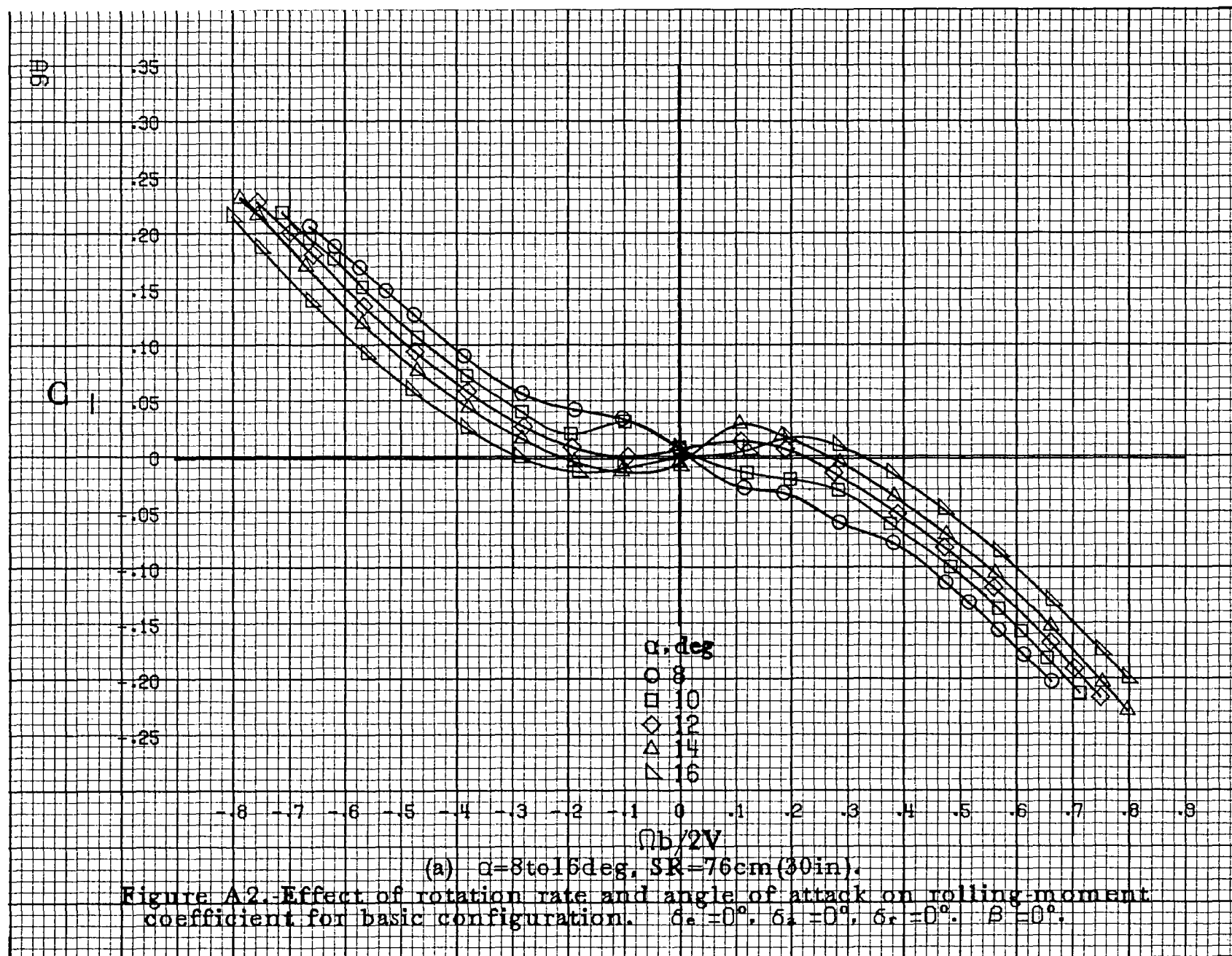
(a) $\alpha=8$ to 16 deg. $SR=76$ cm (30 in).

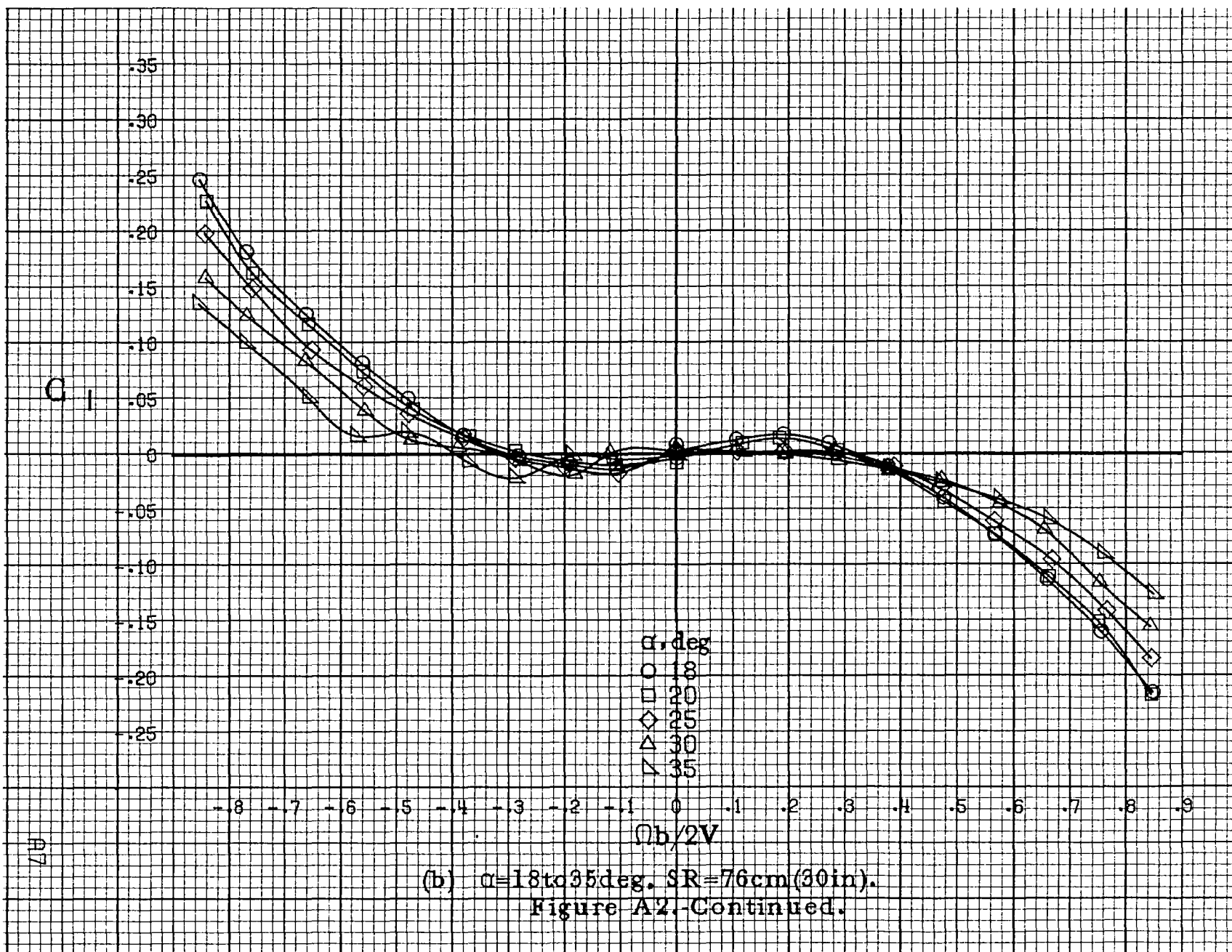
Figure A1. Effect of rotation rate and angle of attack on yawing-moment coefficient for basic configuration. $\delta_e = 0^\circ$, $\delta_a = 0^\circ$, $\delta_r = 0^\circ$. $\beta = 0^\circ$.

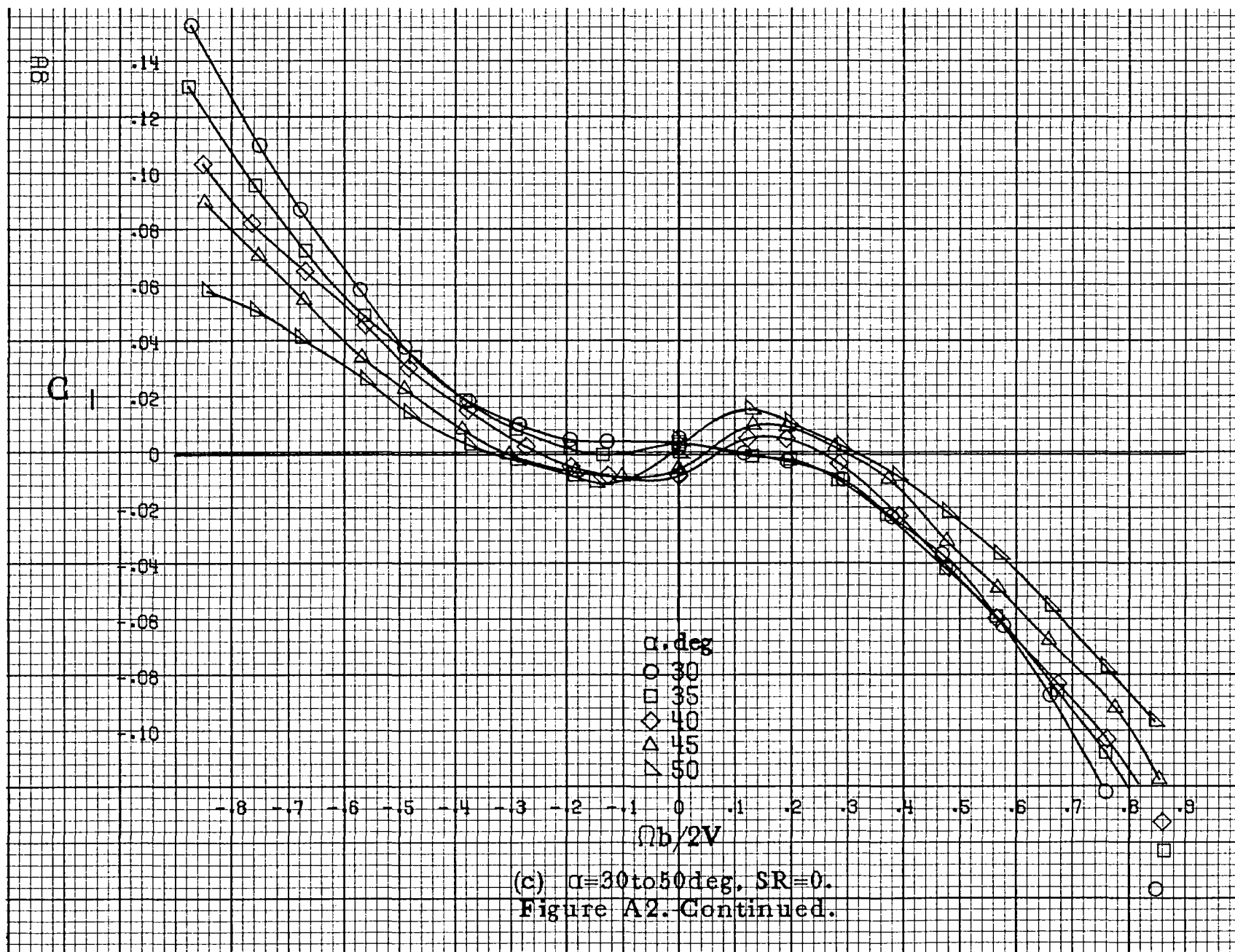


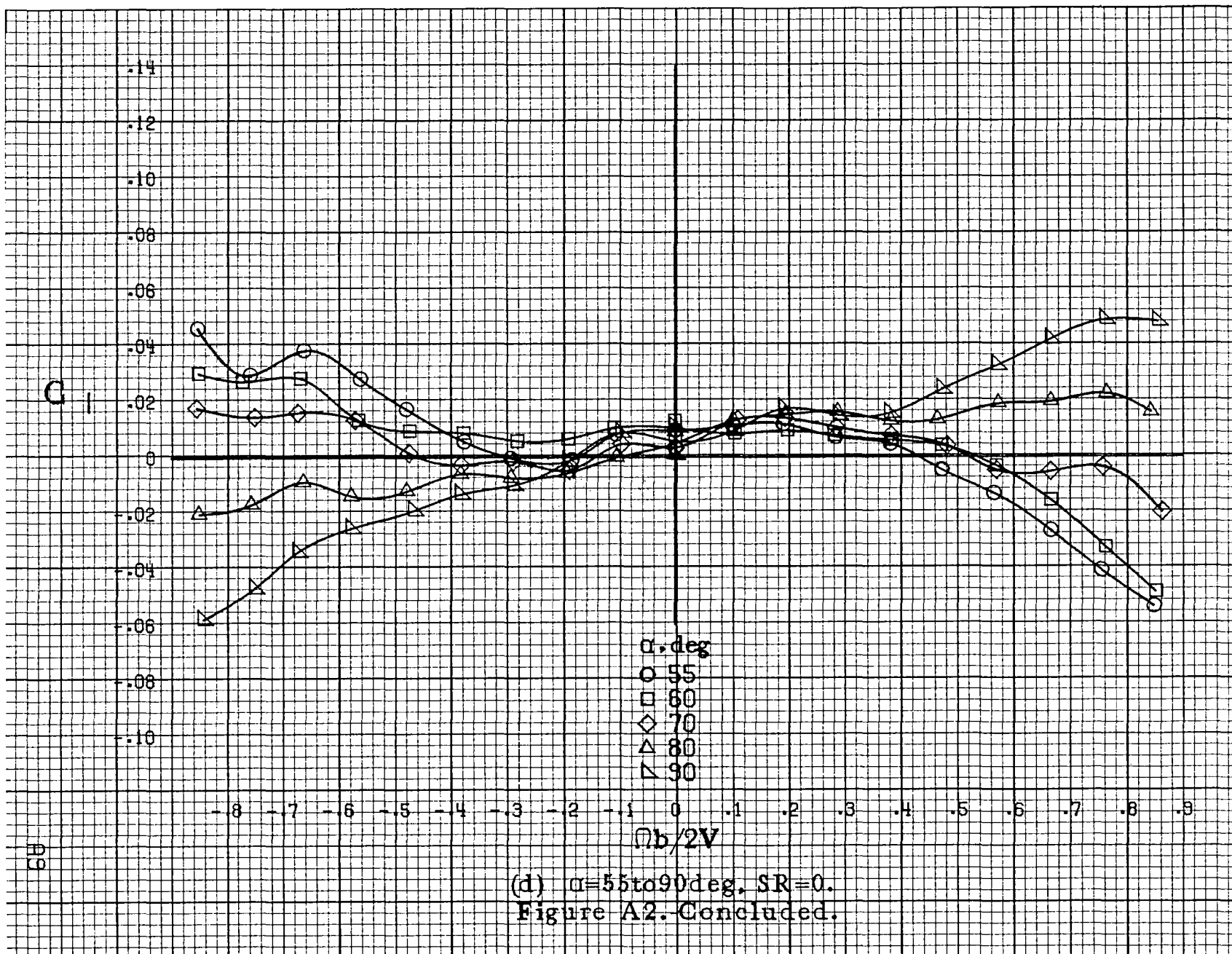


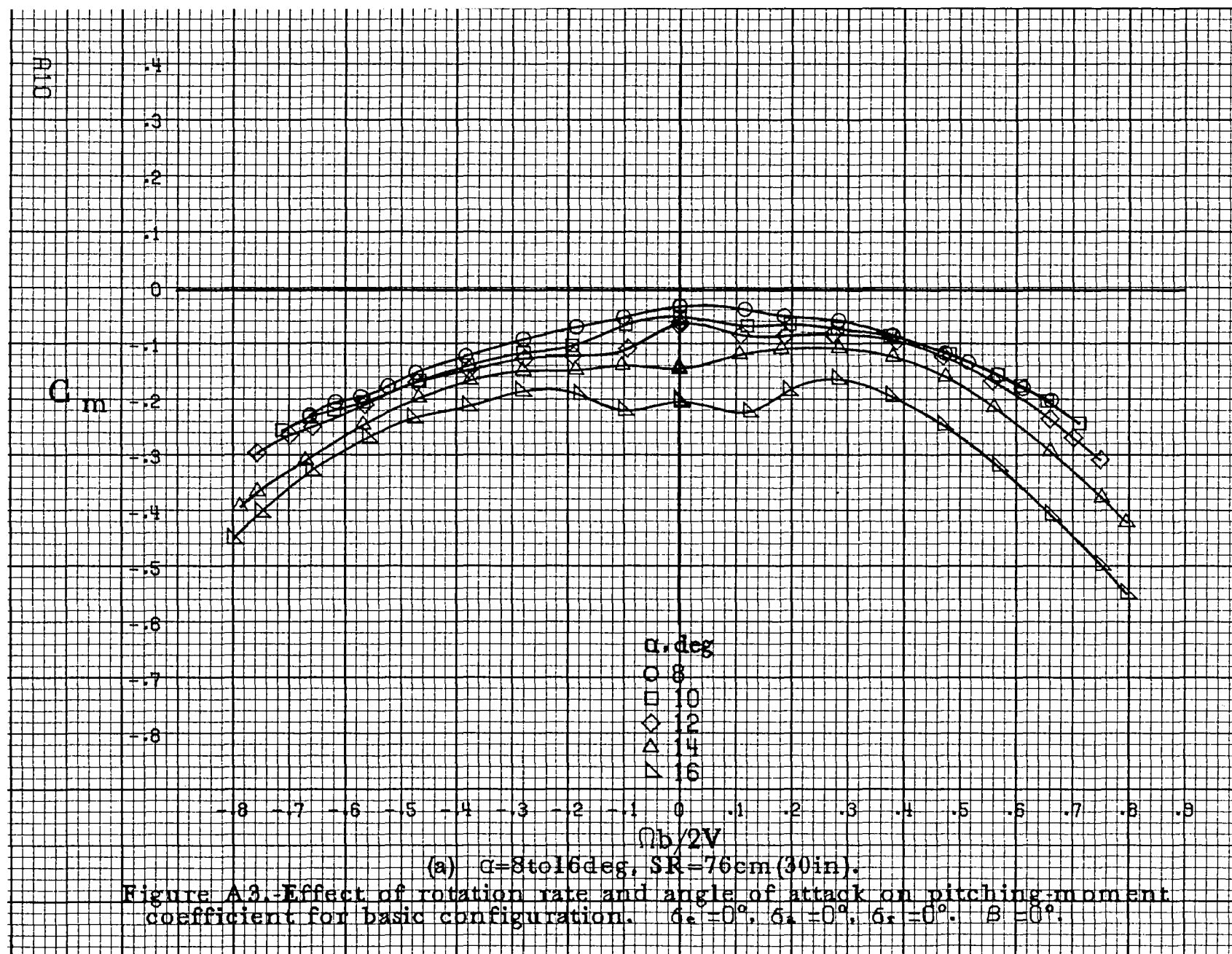


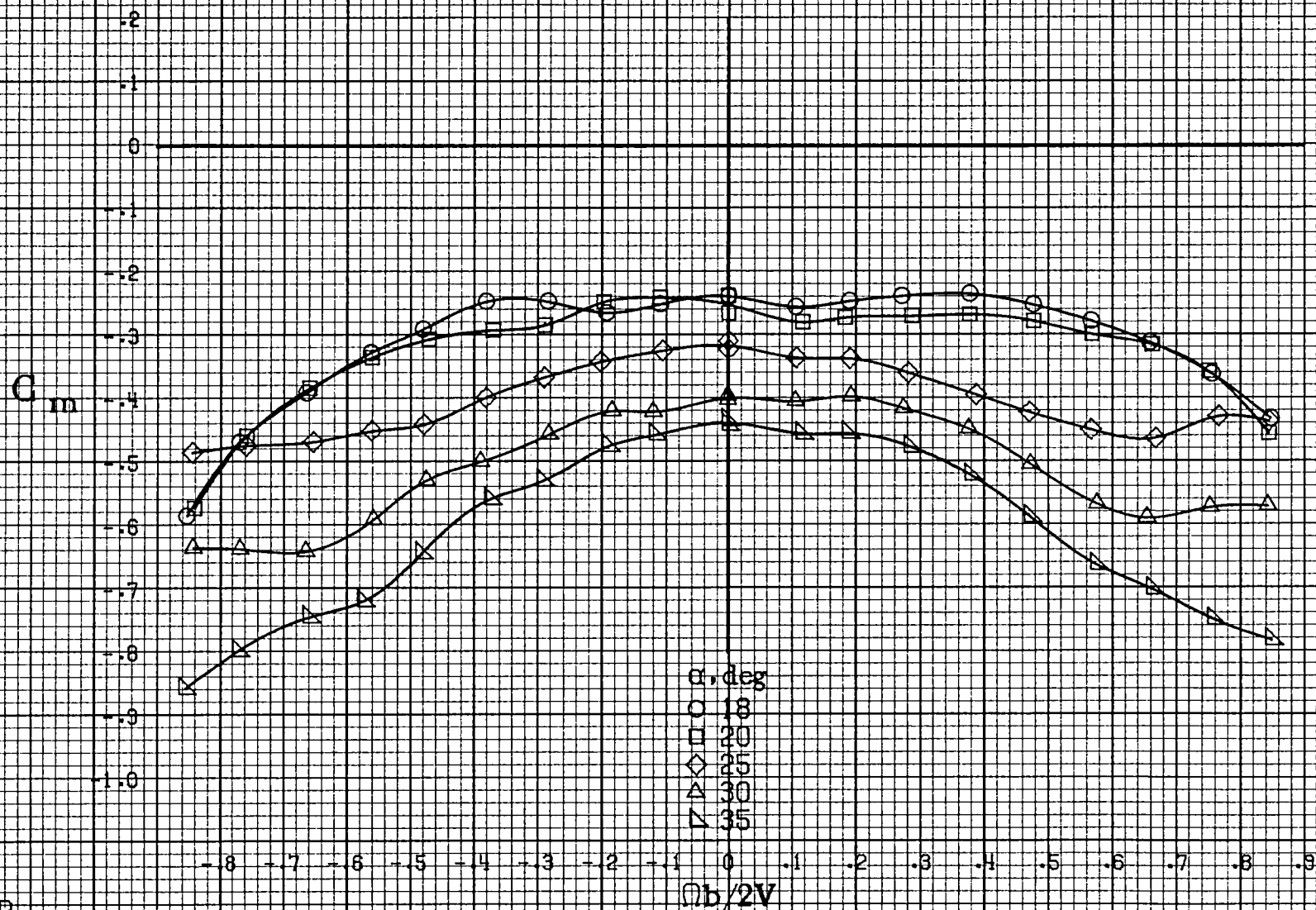




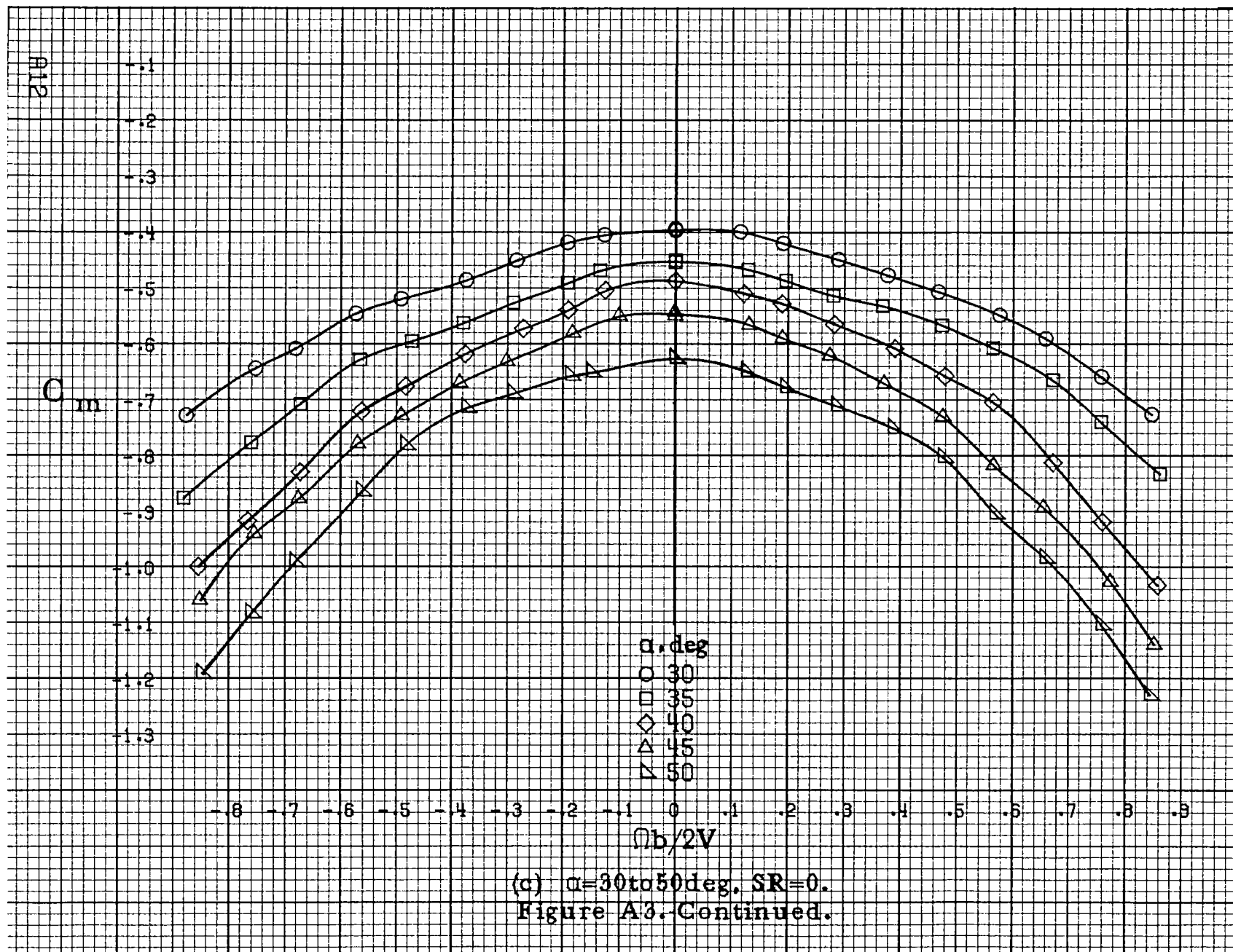


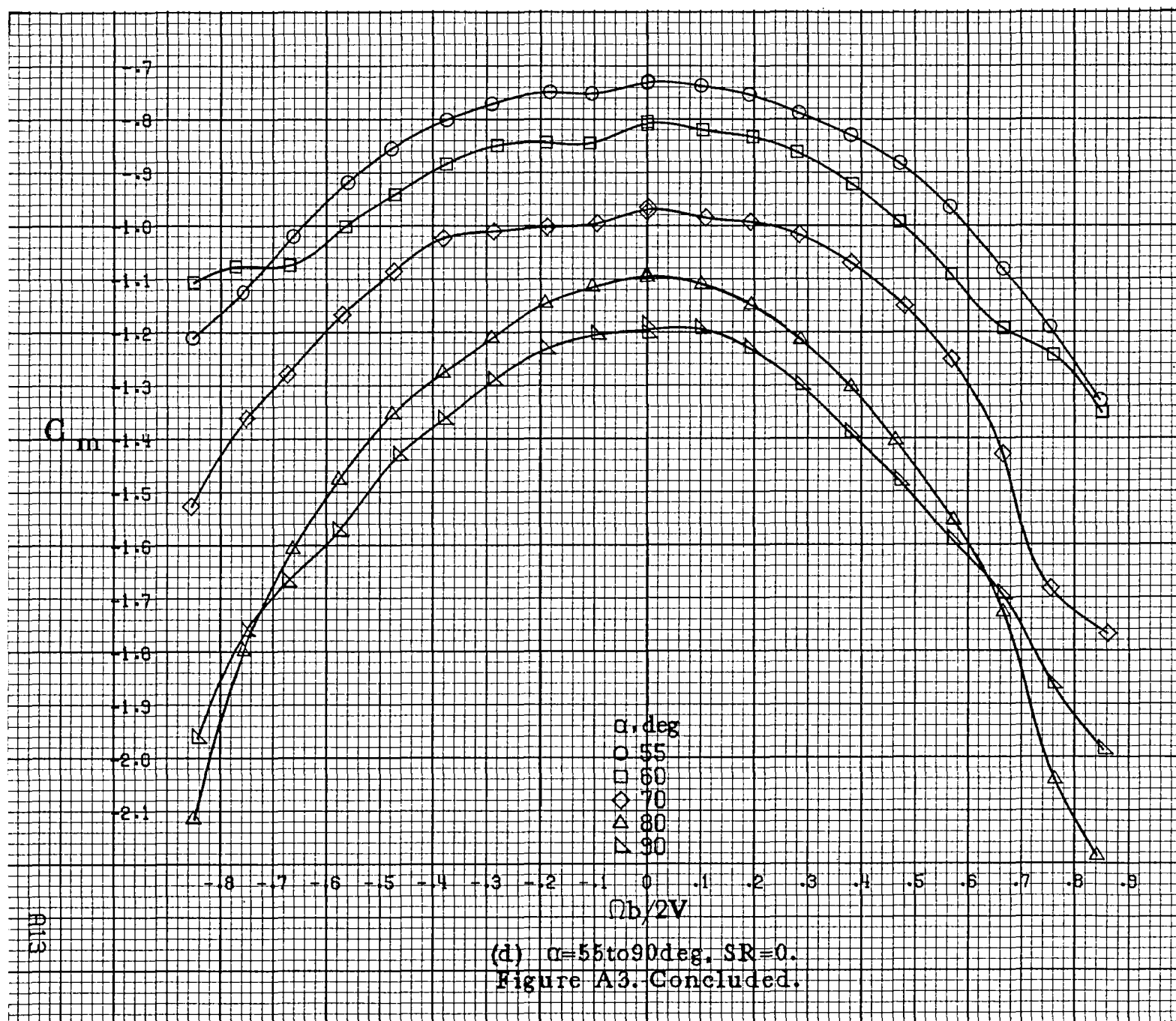


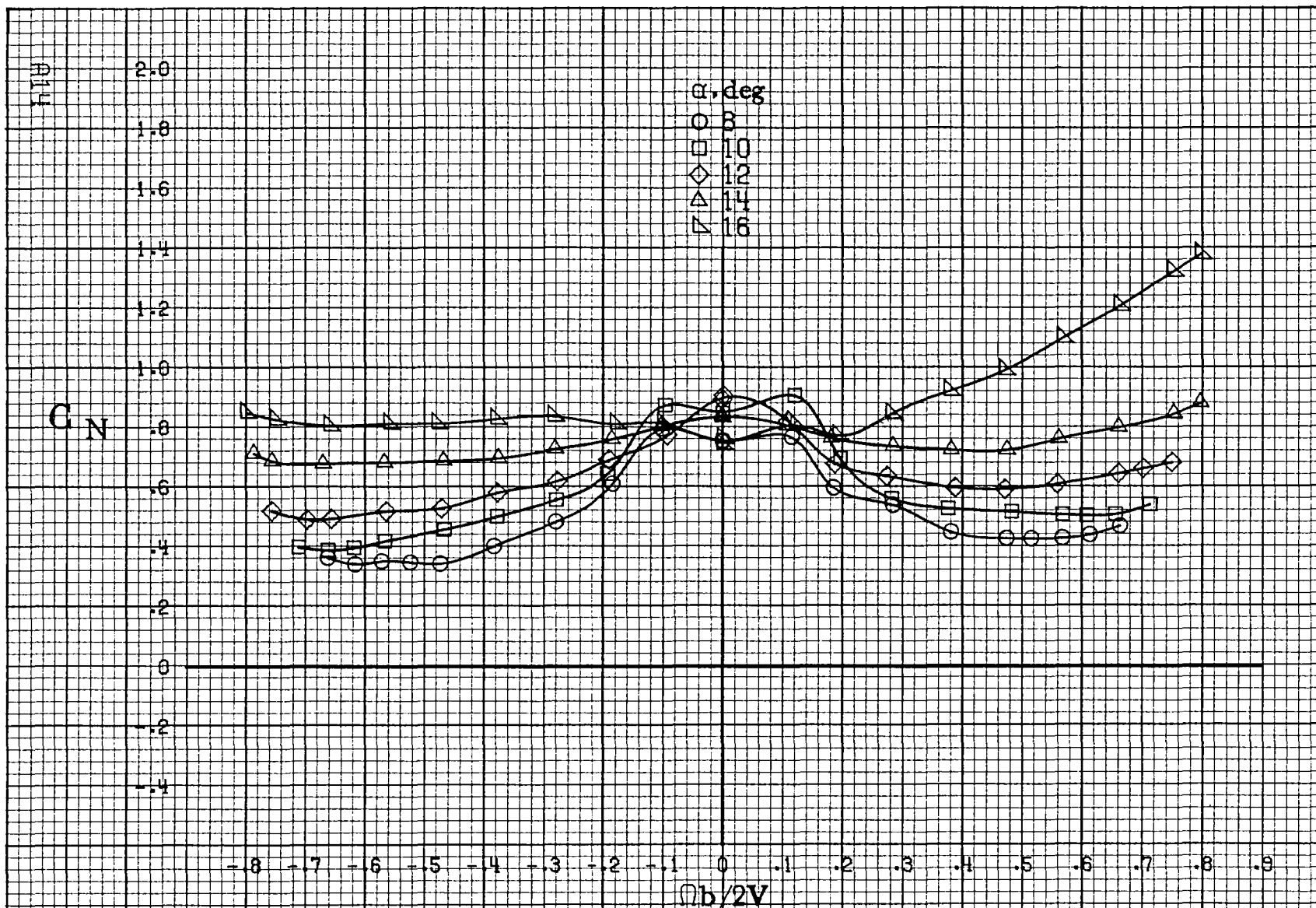




(b) $\alpha = 18$ to 35° , $SR = 76\text{ cm (30 in.)}$.
Figure A3. Continued.

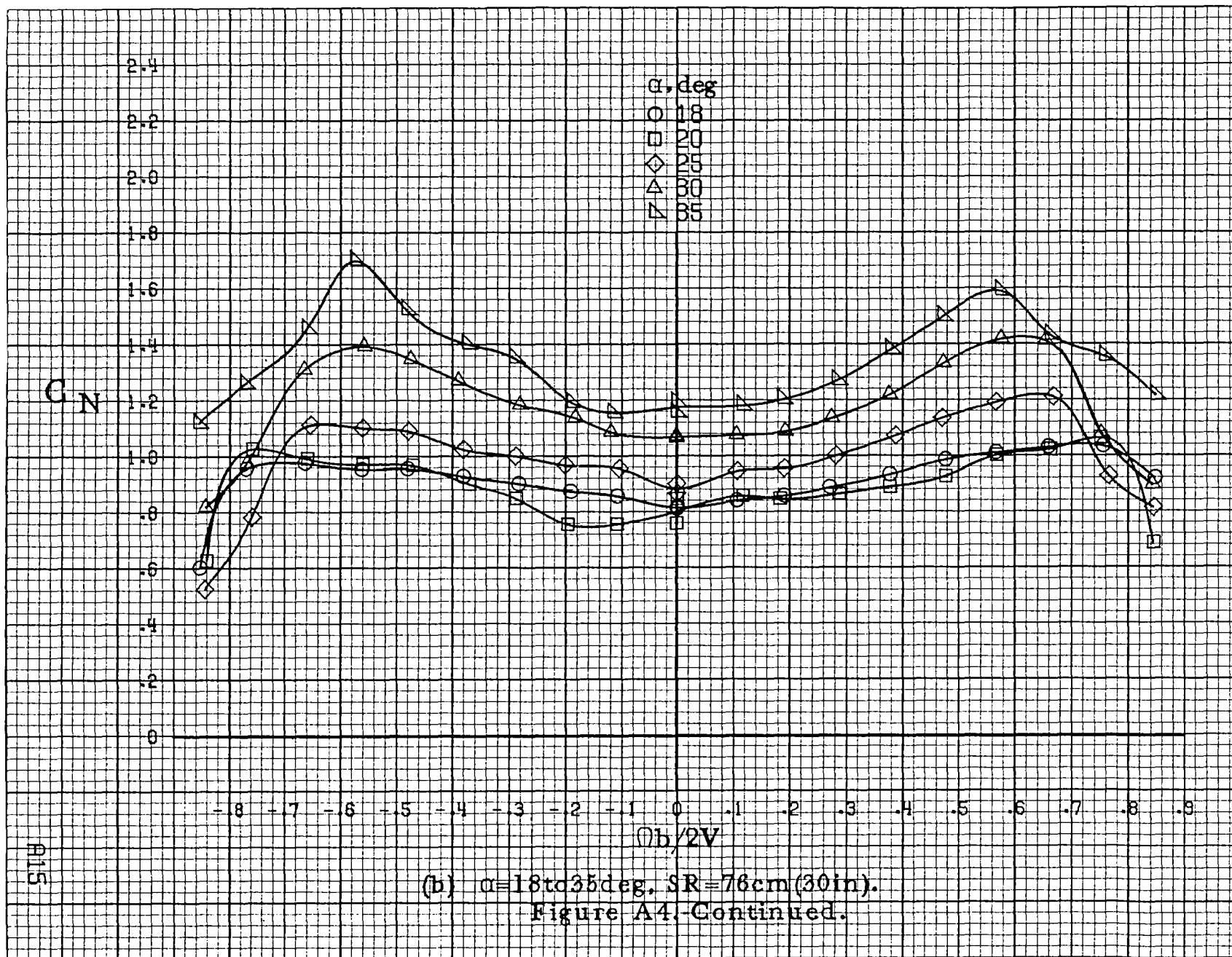


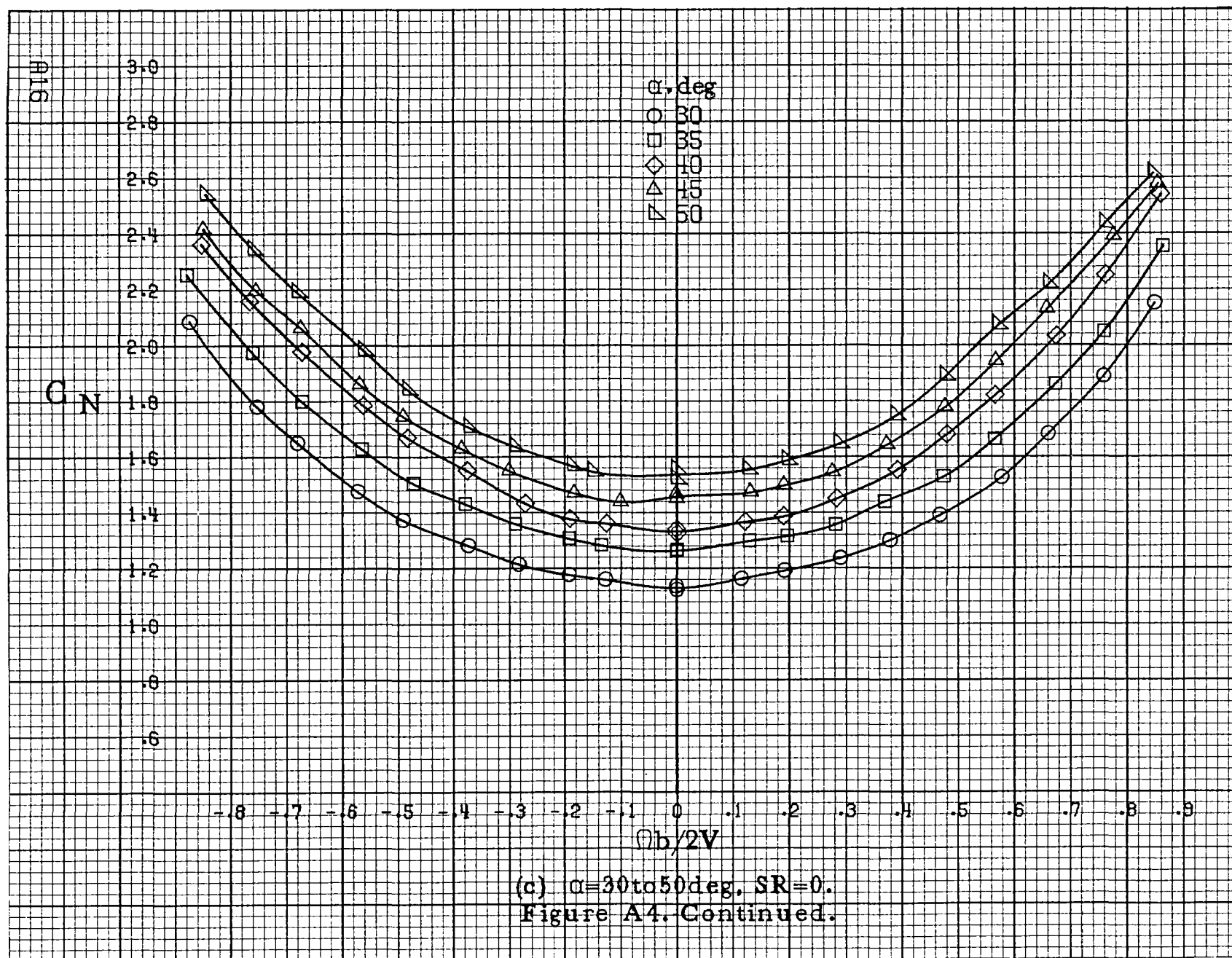


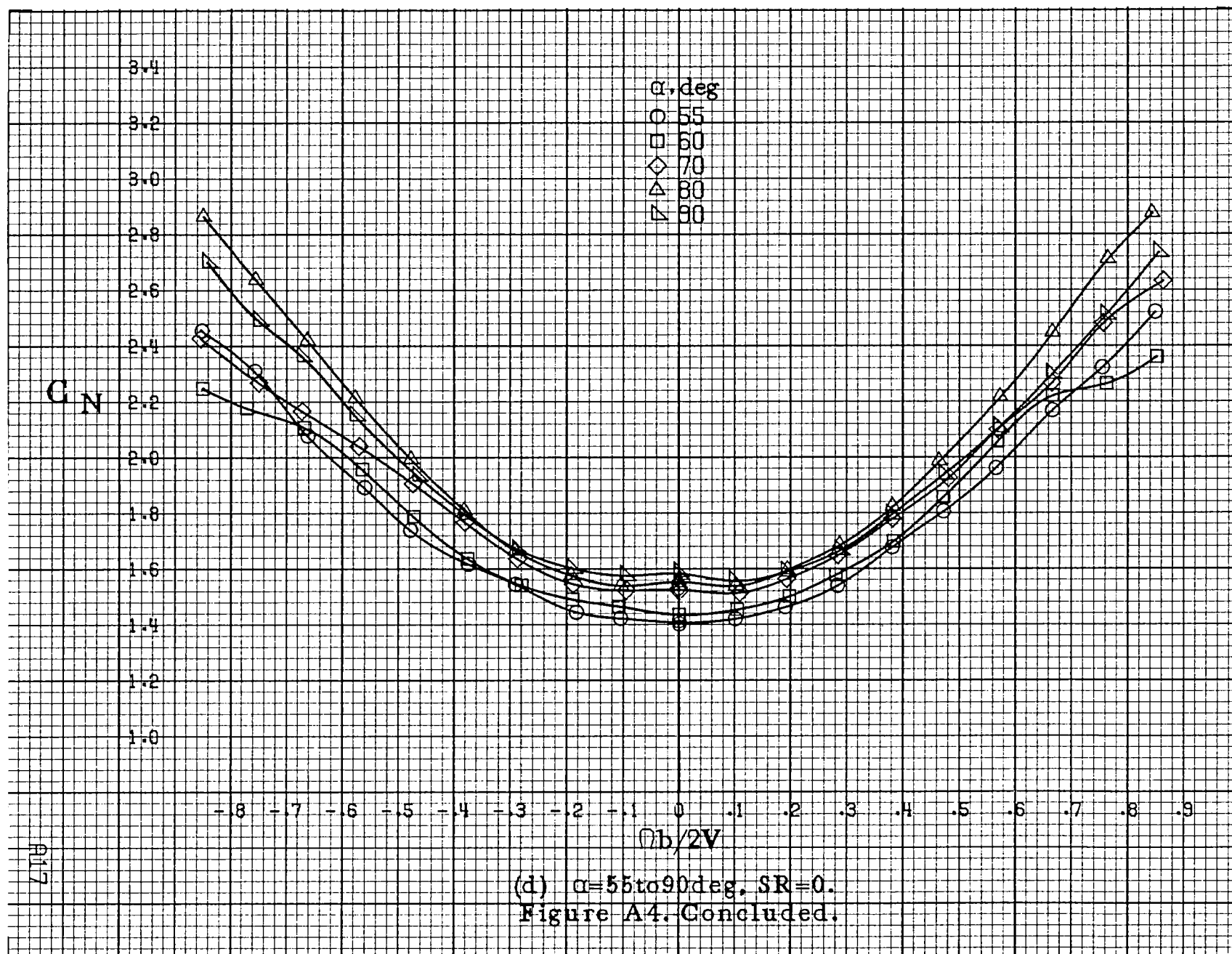


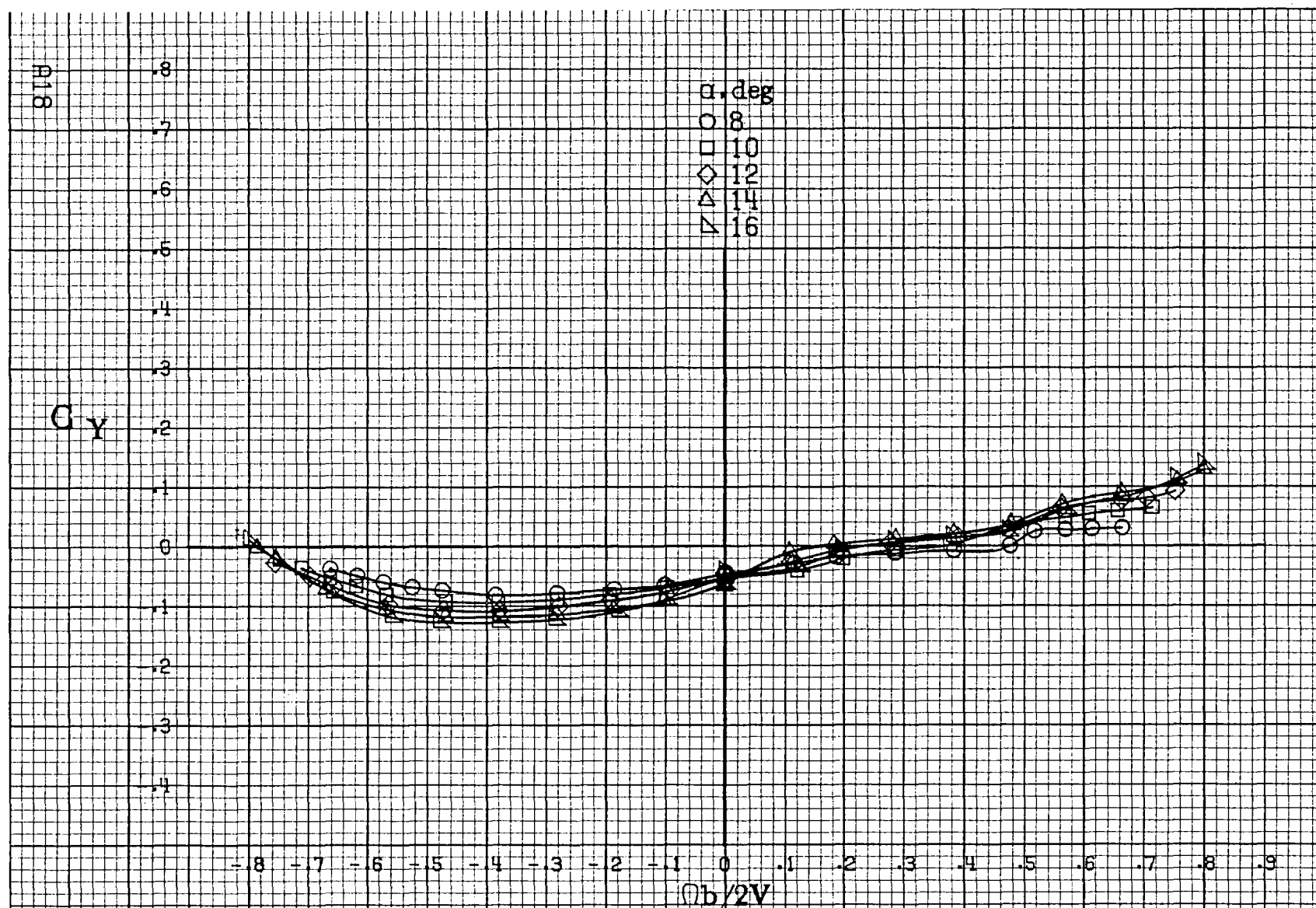
(a) $\alpha=8$ to 16° , $SR=76\text{cm}(30\text{in})$.

Figure A4. Effect of rotation rate and angle of attack on normal-force coefficient for basic configuration. $\delta_e=0^\circ$, $\delta_a=0^\circ$, $\delta_r=0^\circ$. $\beta=0^\circ$.



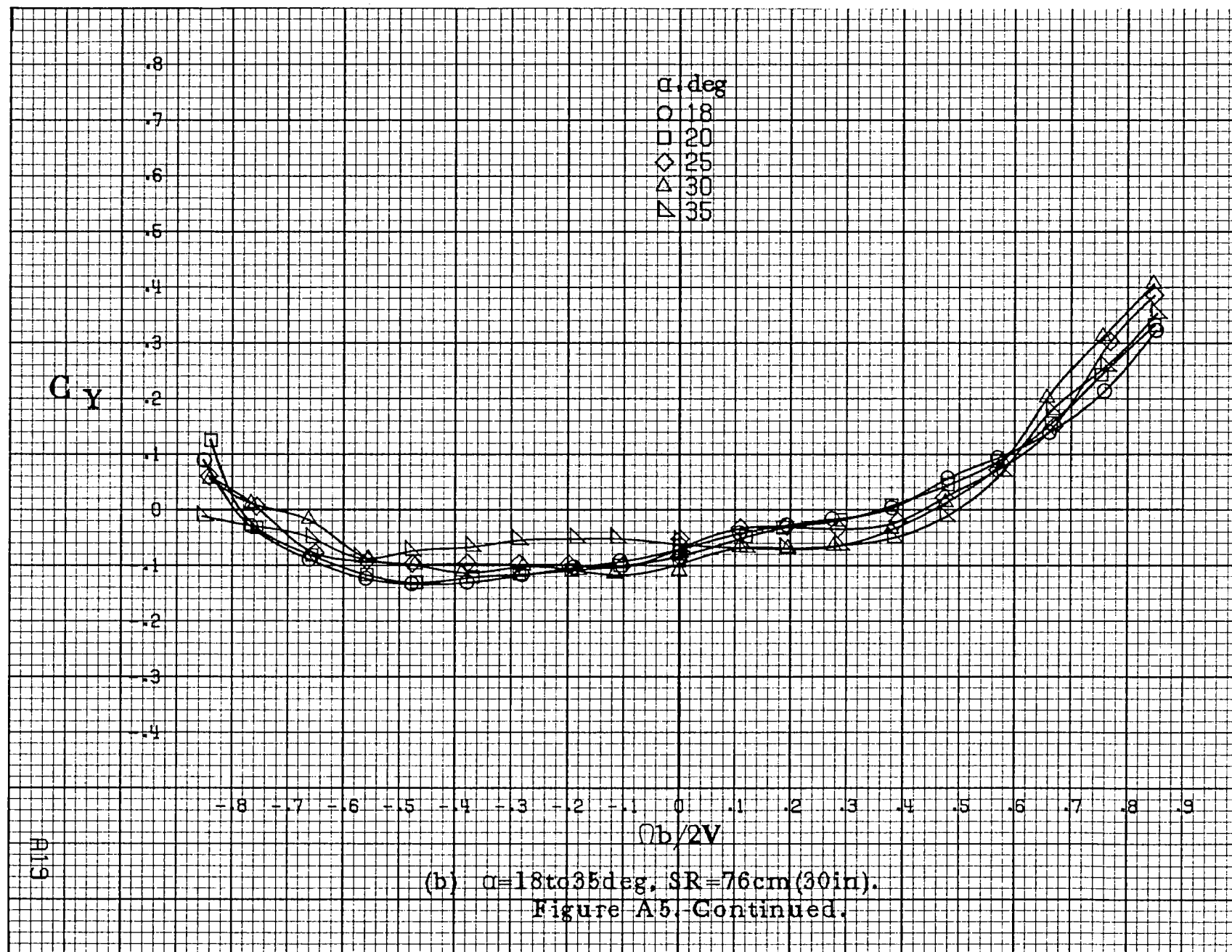


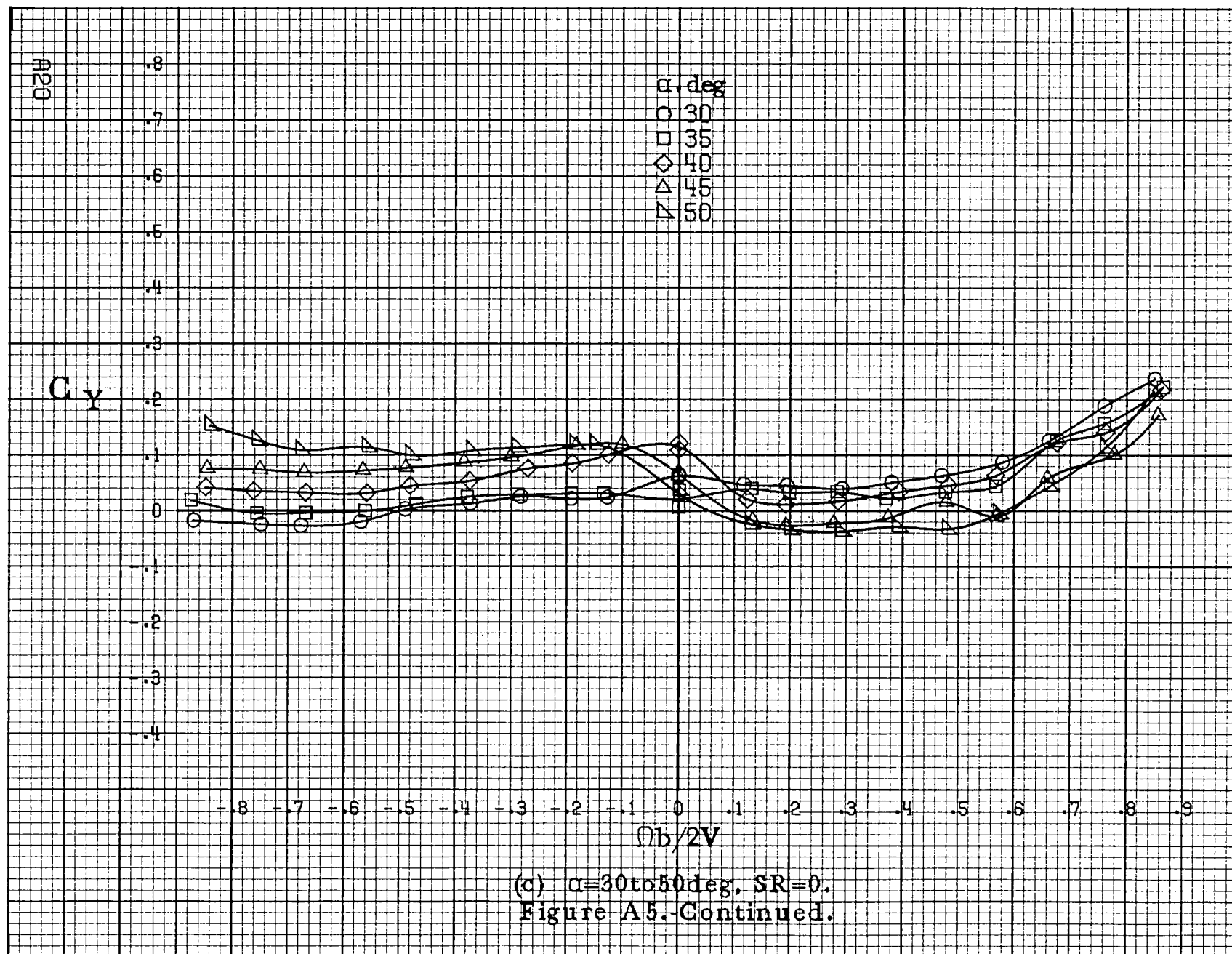


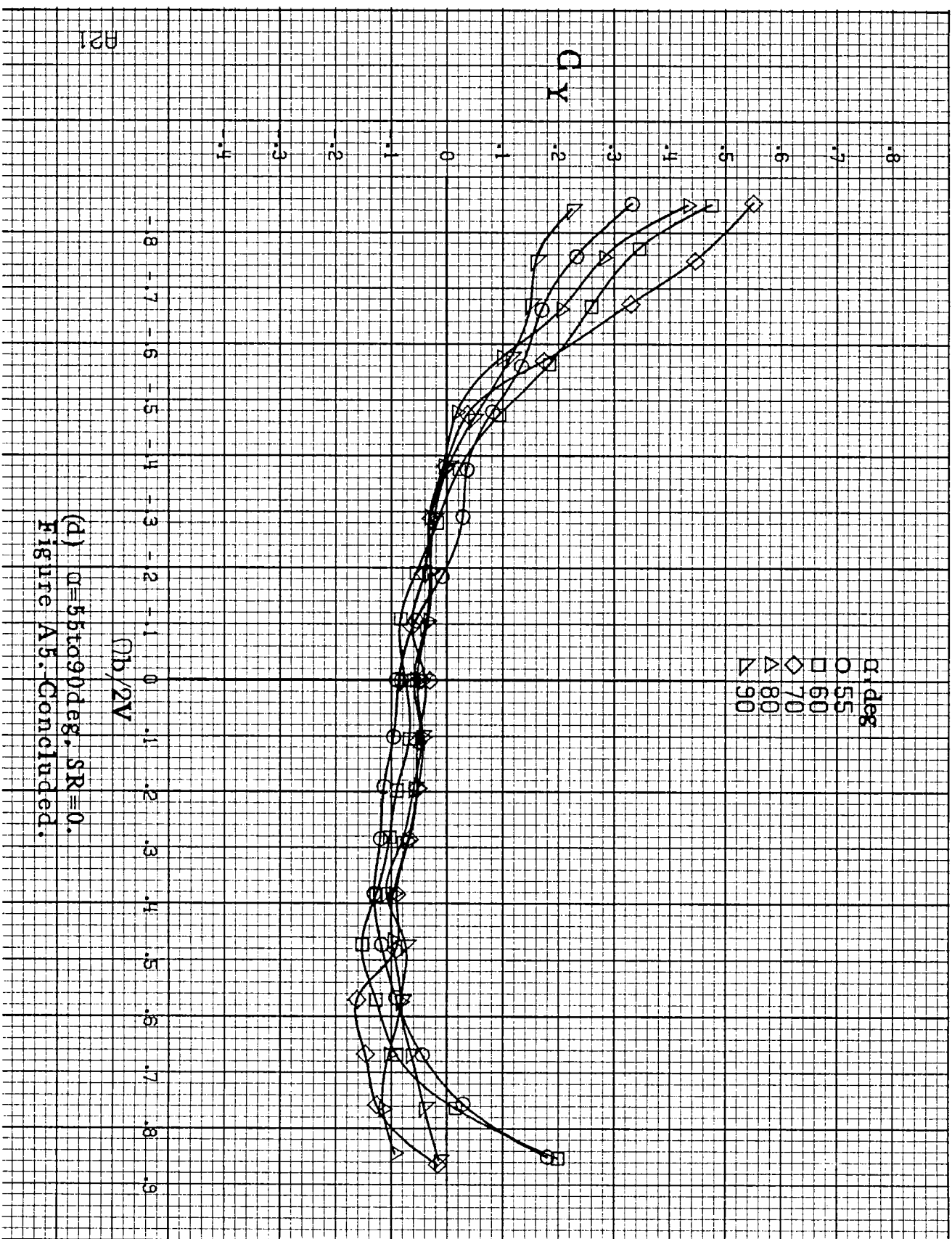


(a) $\alpha = 8$ to 16° , $SR = 76\text{cm}(30\text{in})$.

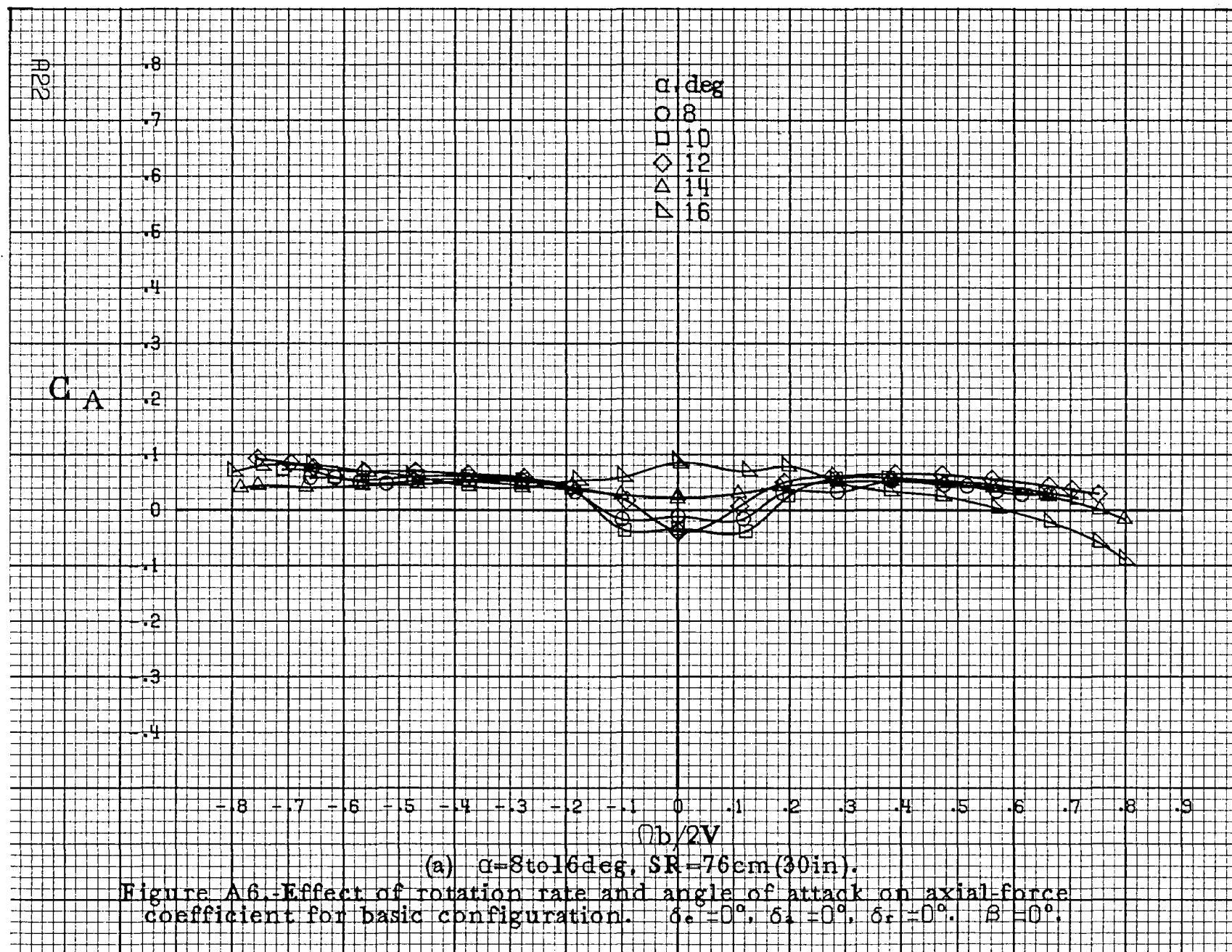
Figure A5.-Effect of rotation rate and angle of attack on side-force coefficient for basic configuration. $\delta_e = 0^\circ$, $\delta_a = 0^\circ$, $\delta_r = 0^\circ$, $\beta = 0^\circ$.

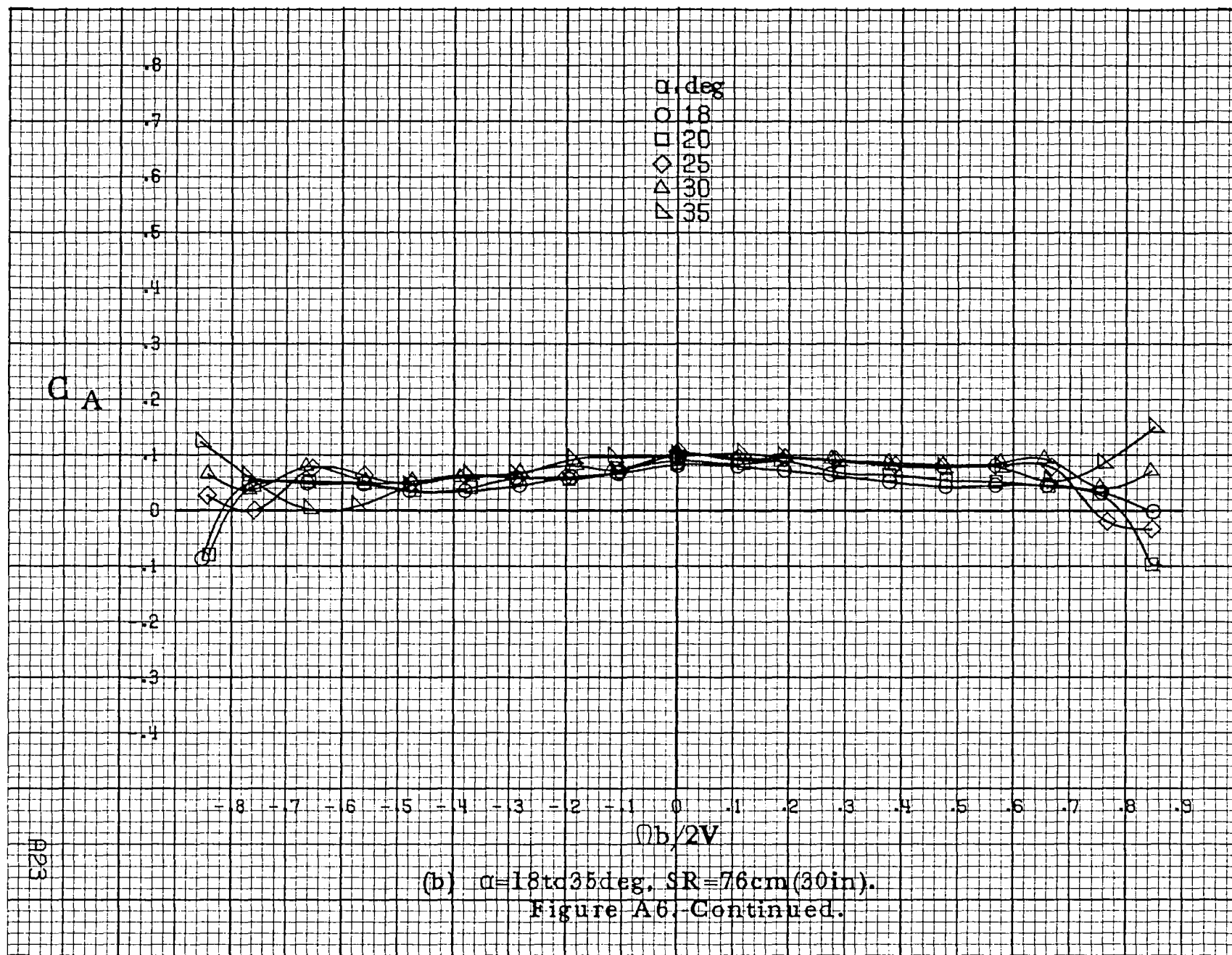


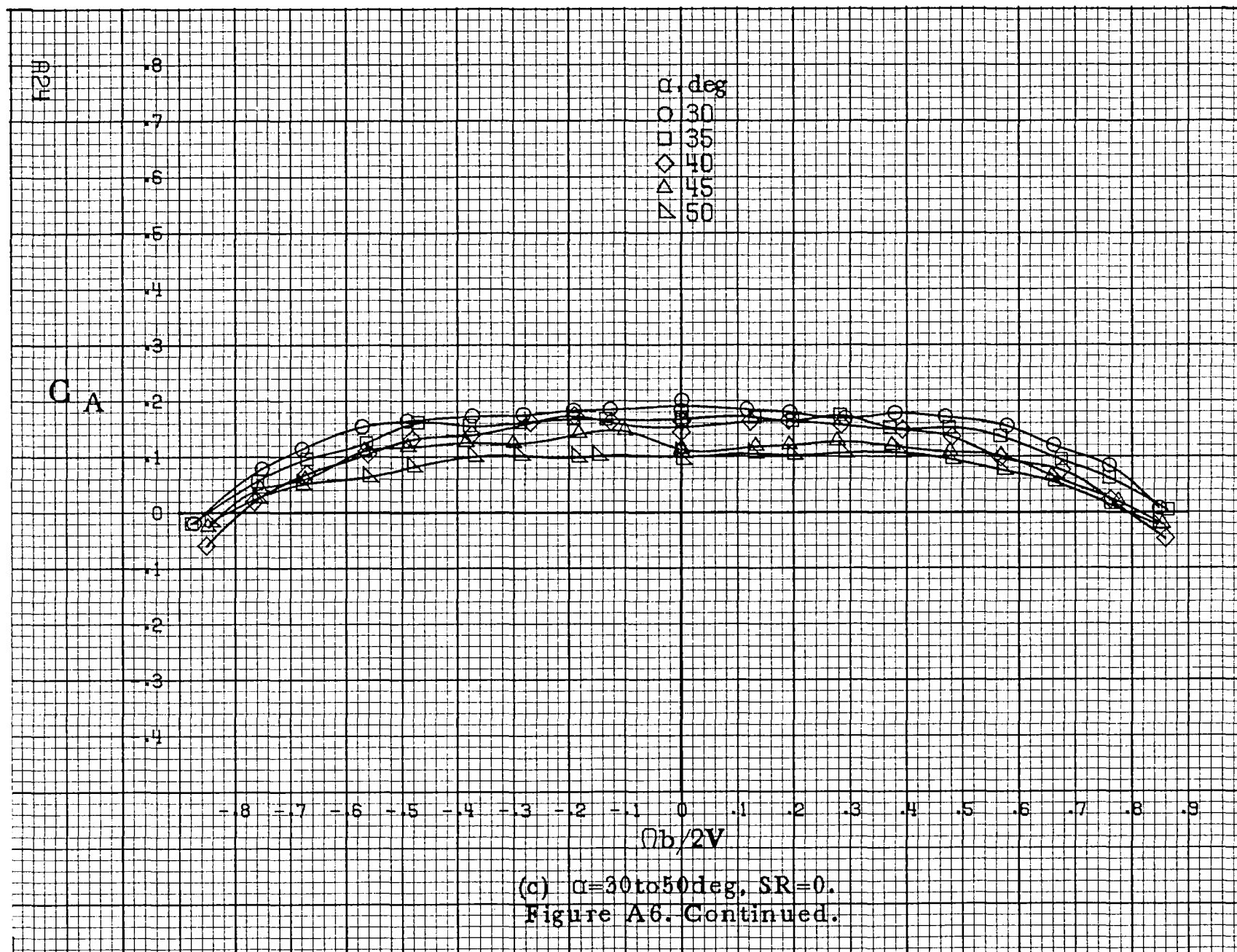


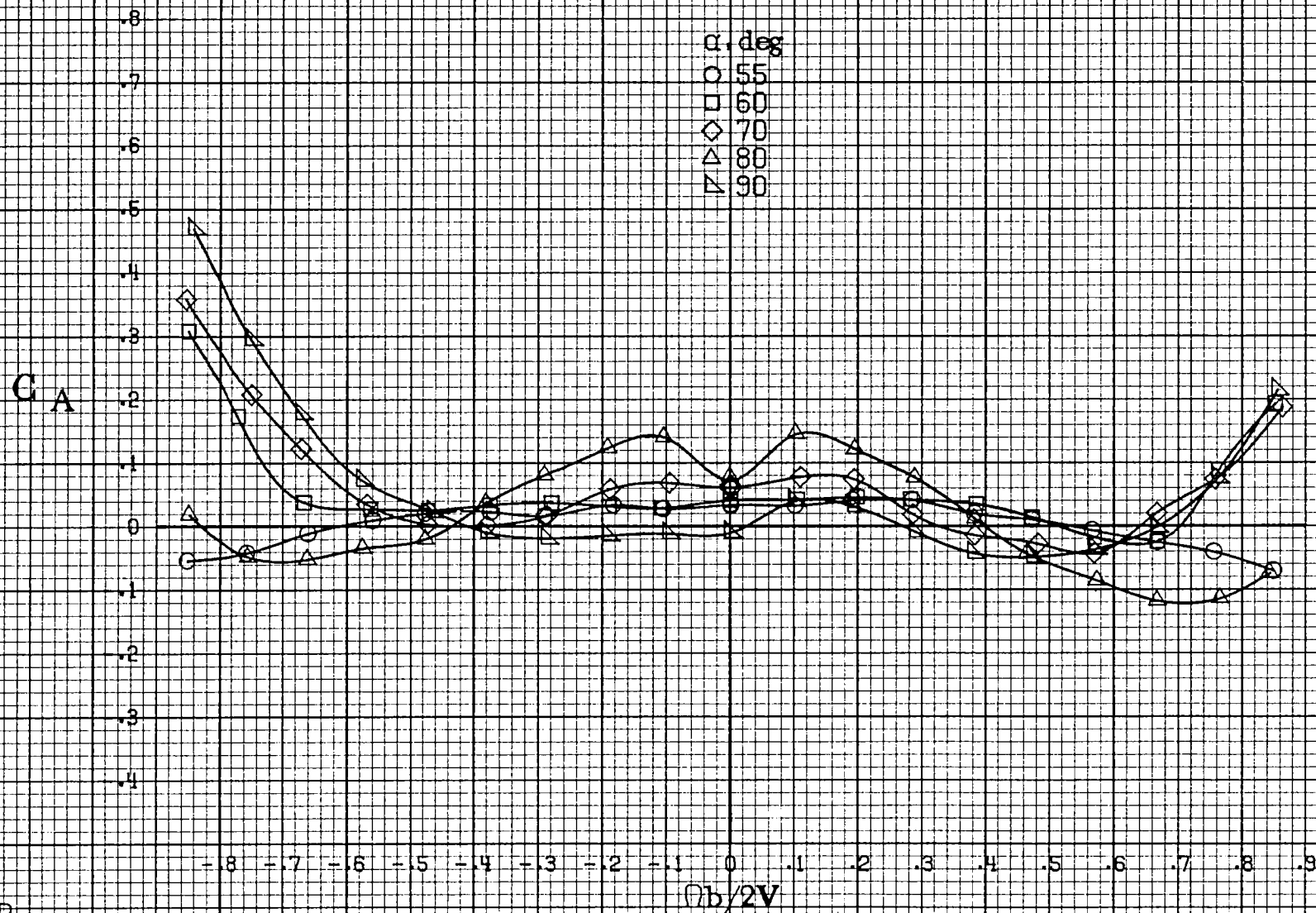


(d) $\omega = 55$ to 90° deg, $SR = 0$.
Figure A5. Concluded.

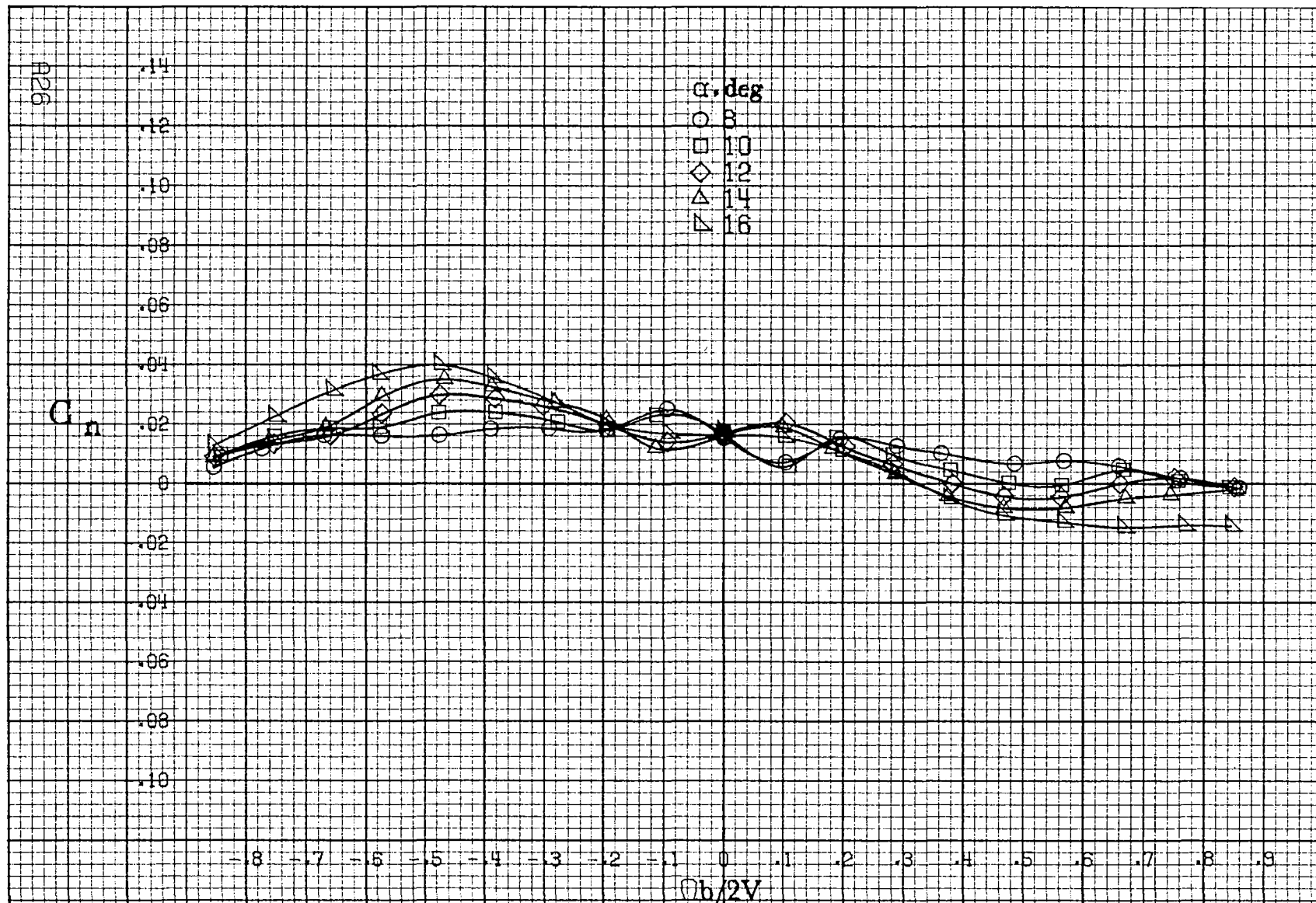






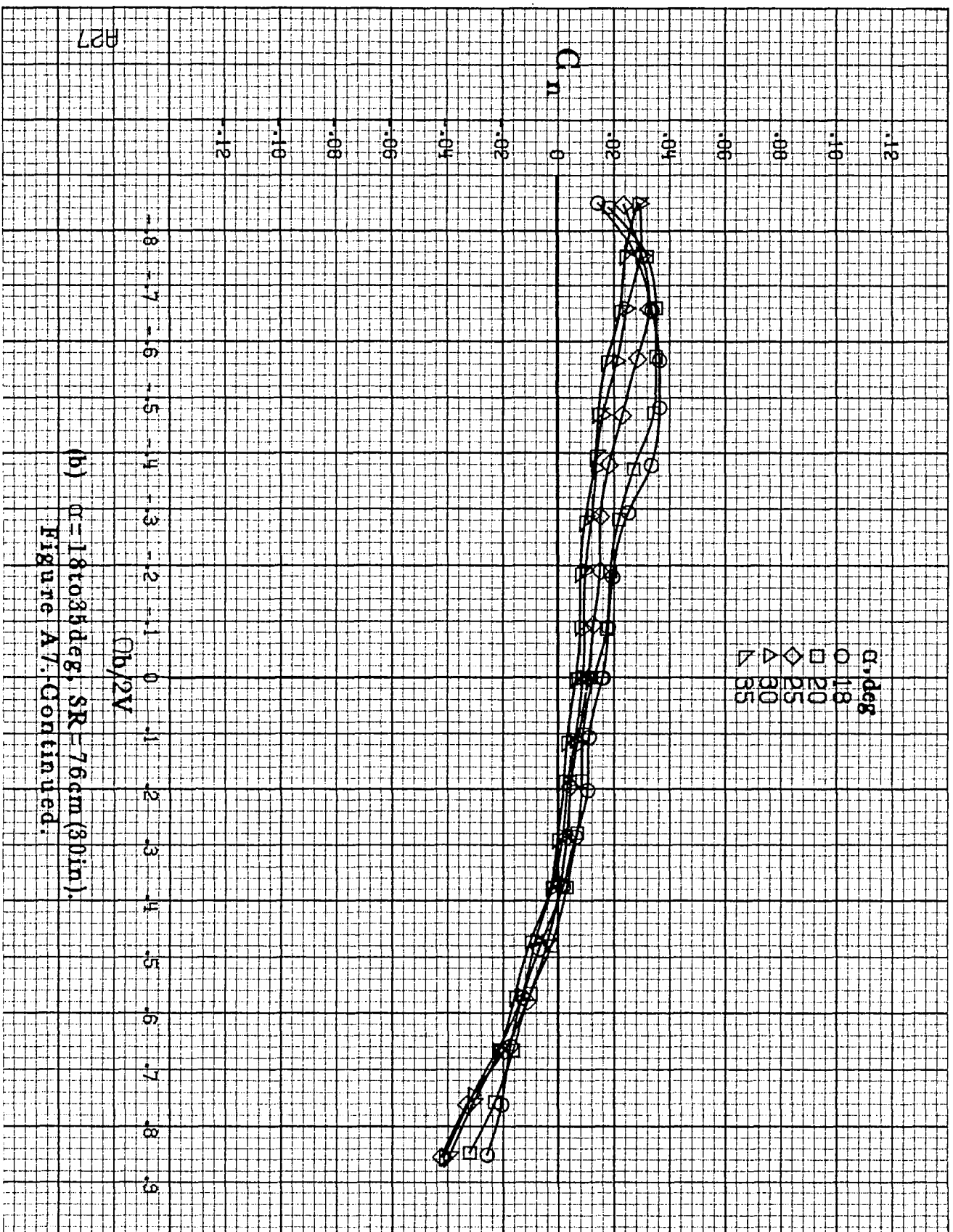


(d) $\alpha=55$ to 90° , $SR=0$.
Figure A6. Concluded.

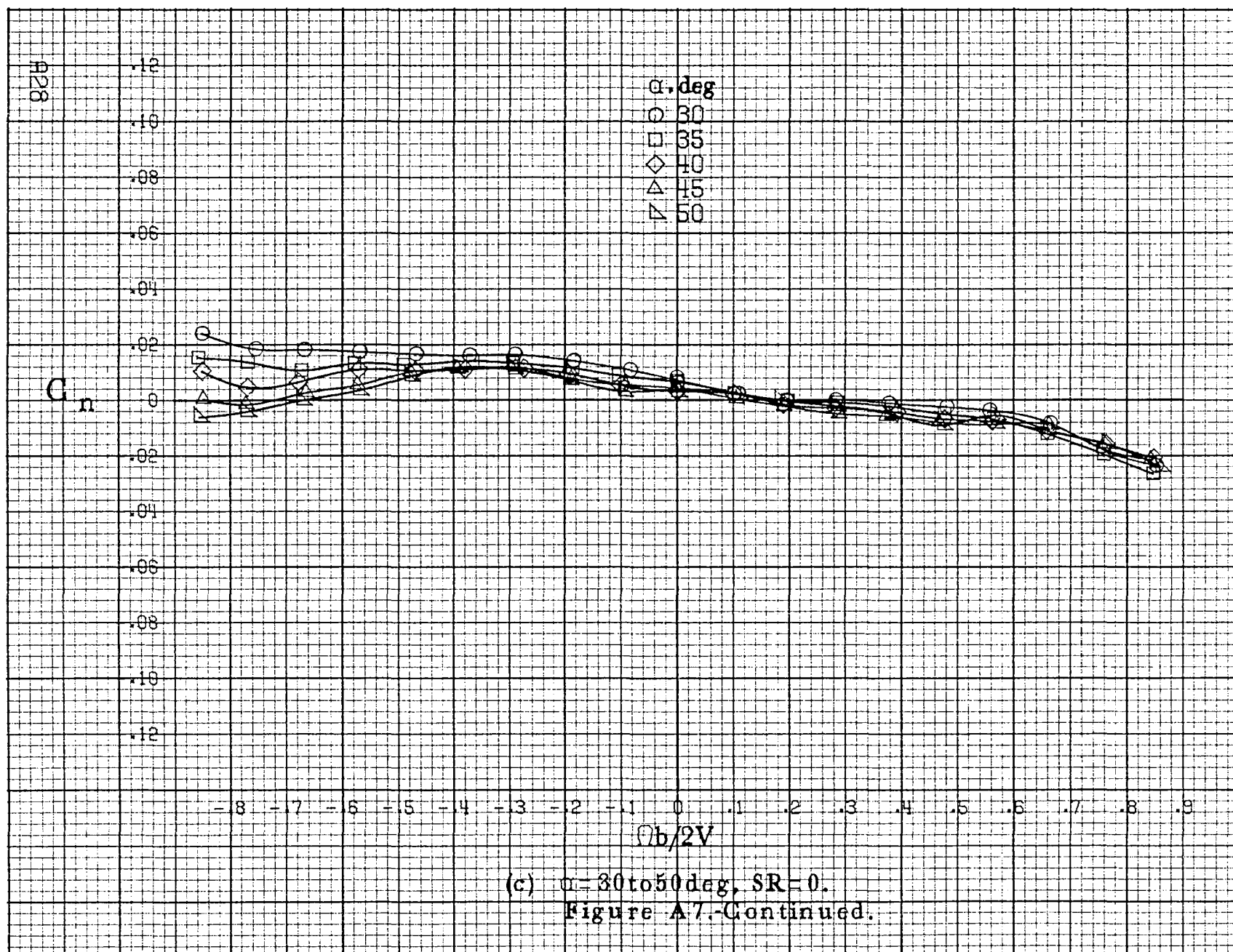


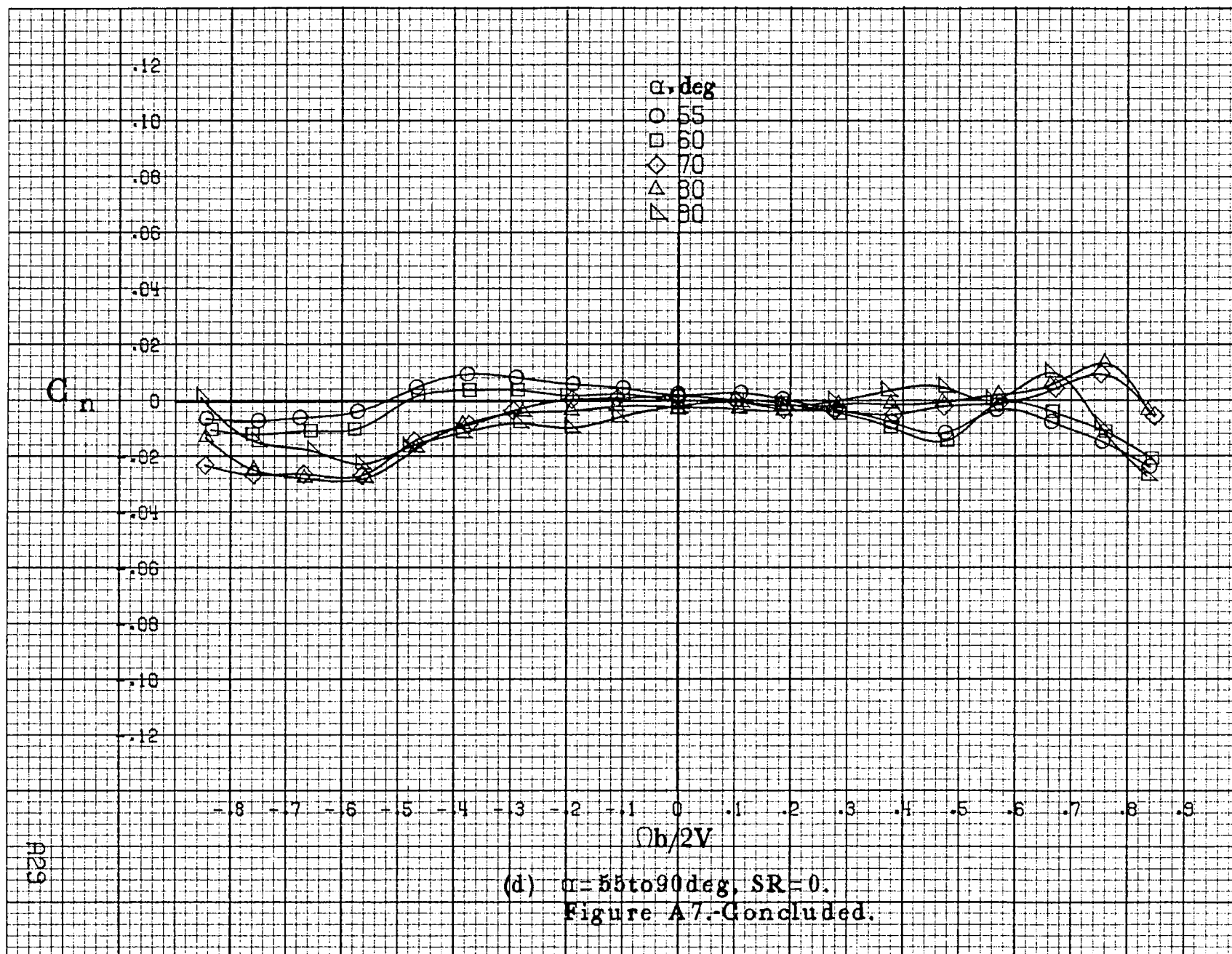
(a) $\alpha = 8 \text{ to } 16 \text{ deg}$, $SR = 76 \text{ cm (30 in)}$.

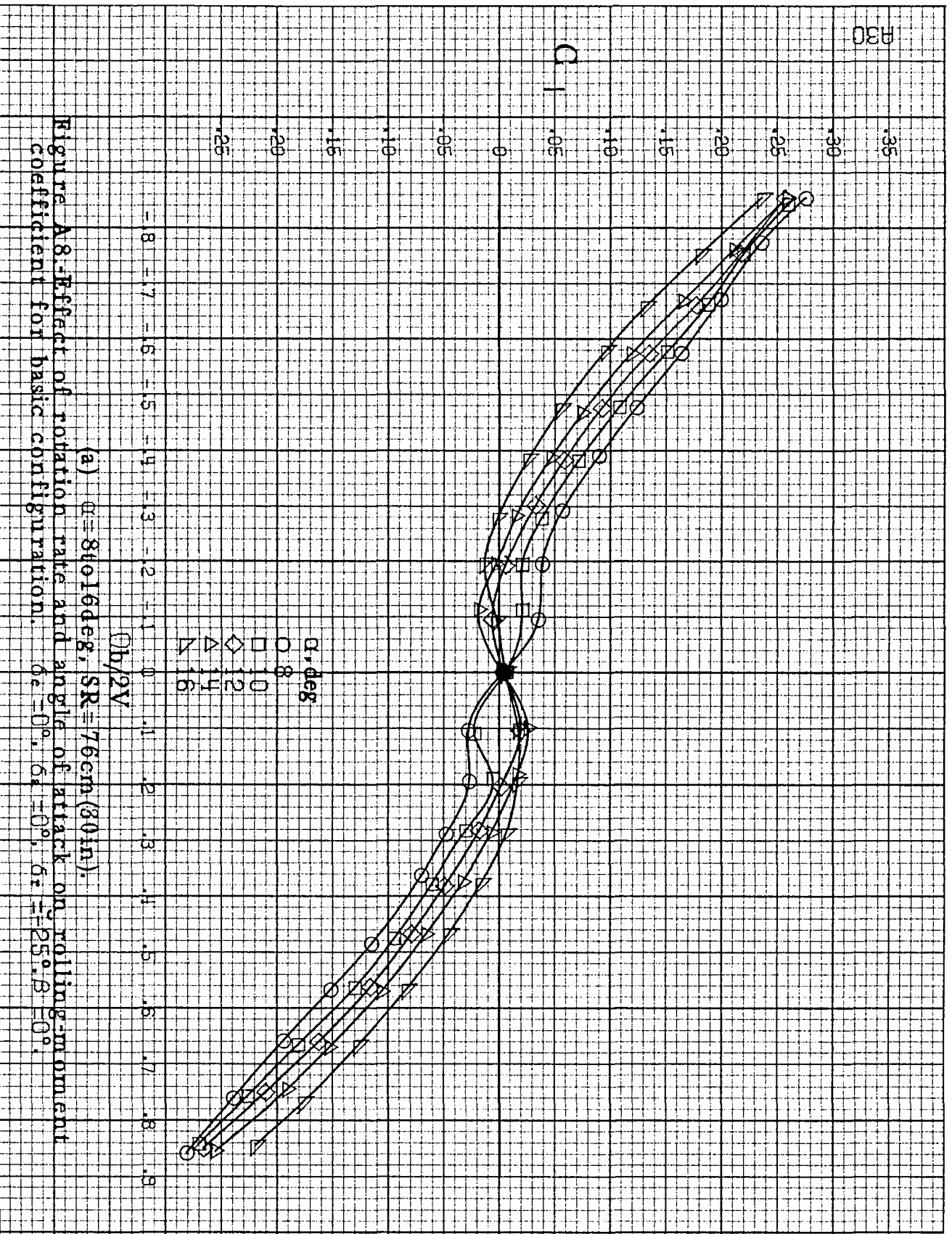
Figure A7-Effect of rotation rate and angle of attack on yawing-moment coefficient for basic configuration. $\delta_e = 0^\circ$, $\delta_a = 0^\circ$, $\delta_r = 25^\circ$, $\beta = 0^\circ$.

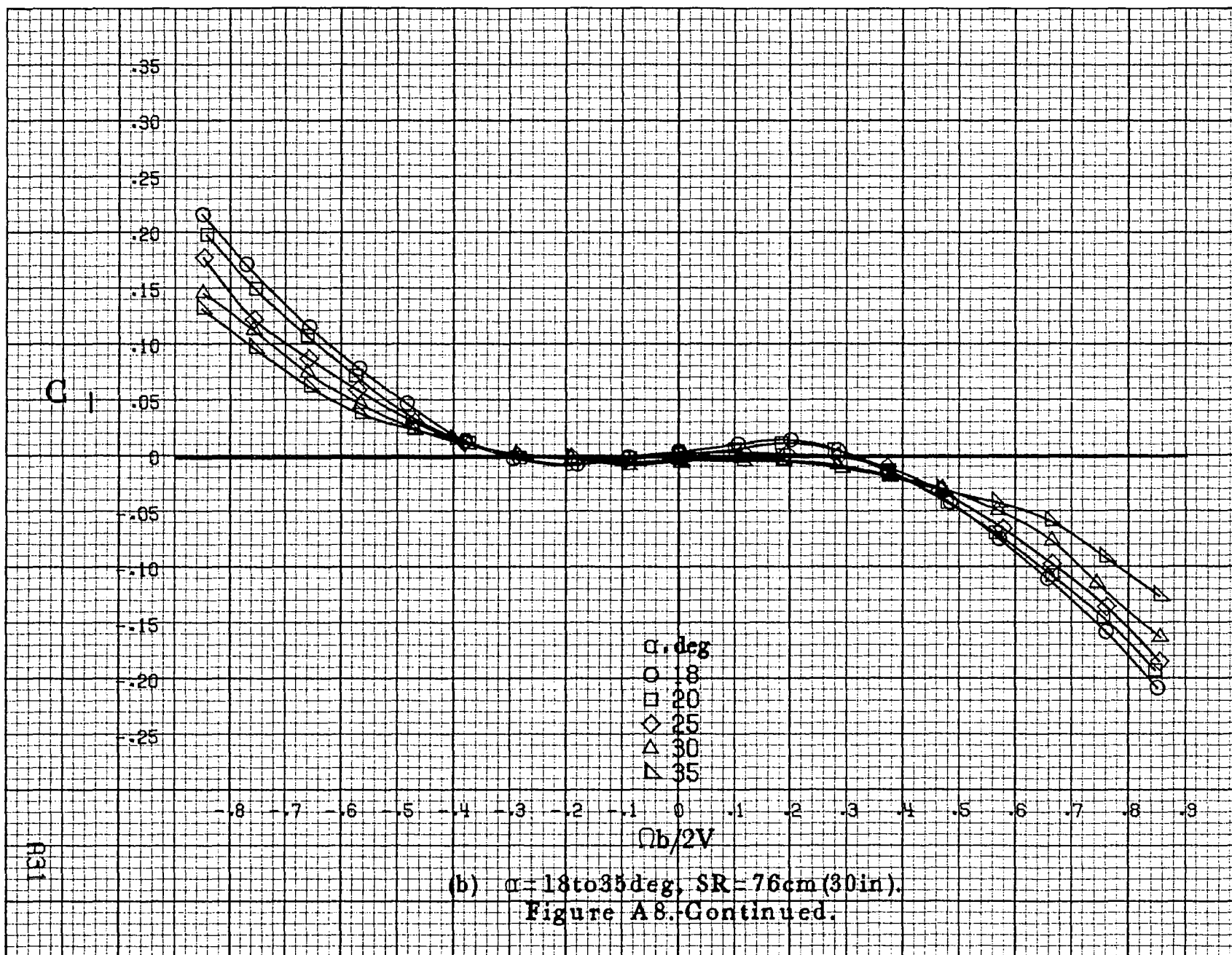


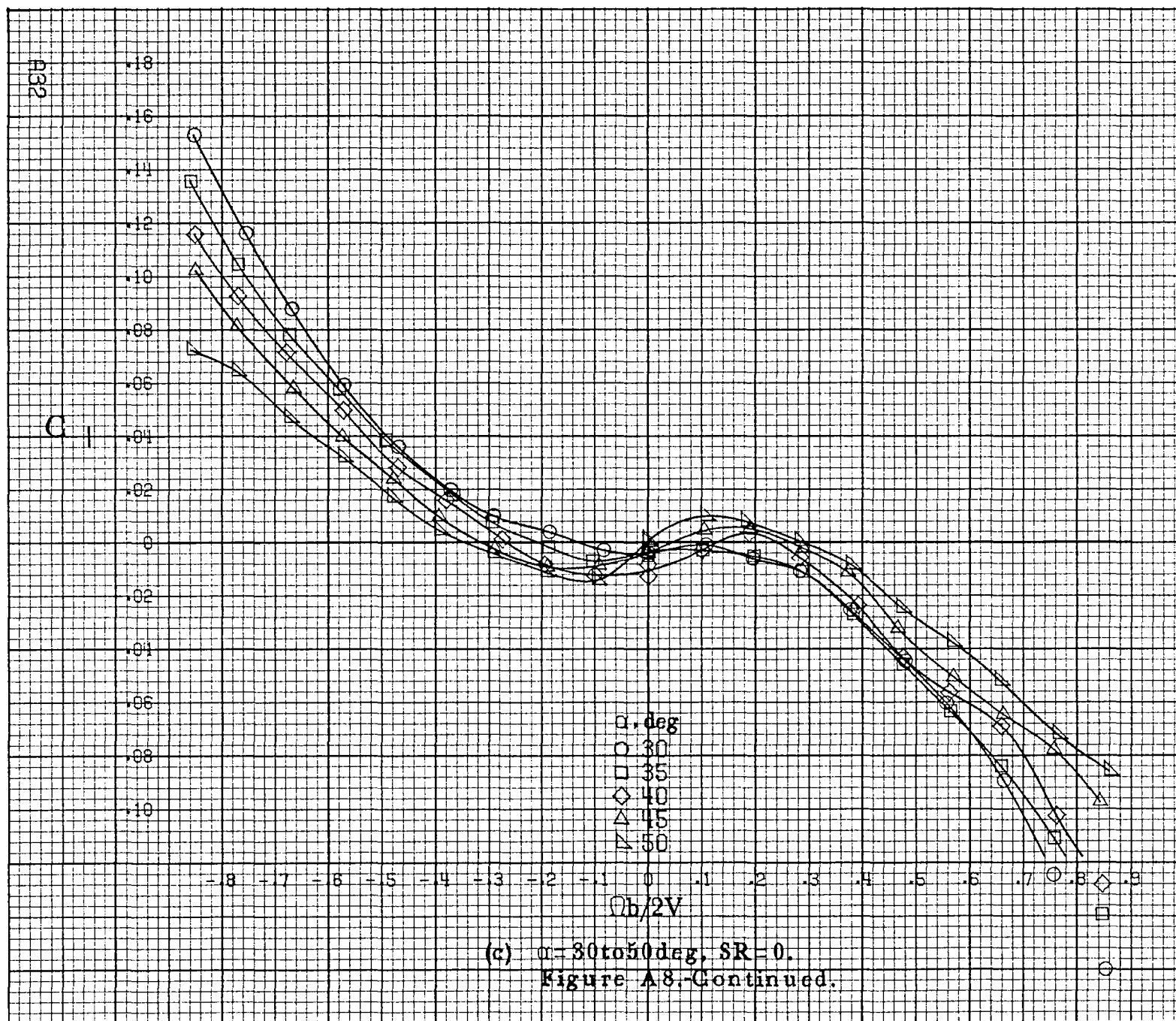
(b) $\alpha = 18$ to 35 deg, $SR = 76$ cm (30 in).
Figure A7. Continued.

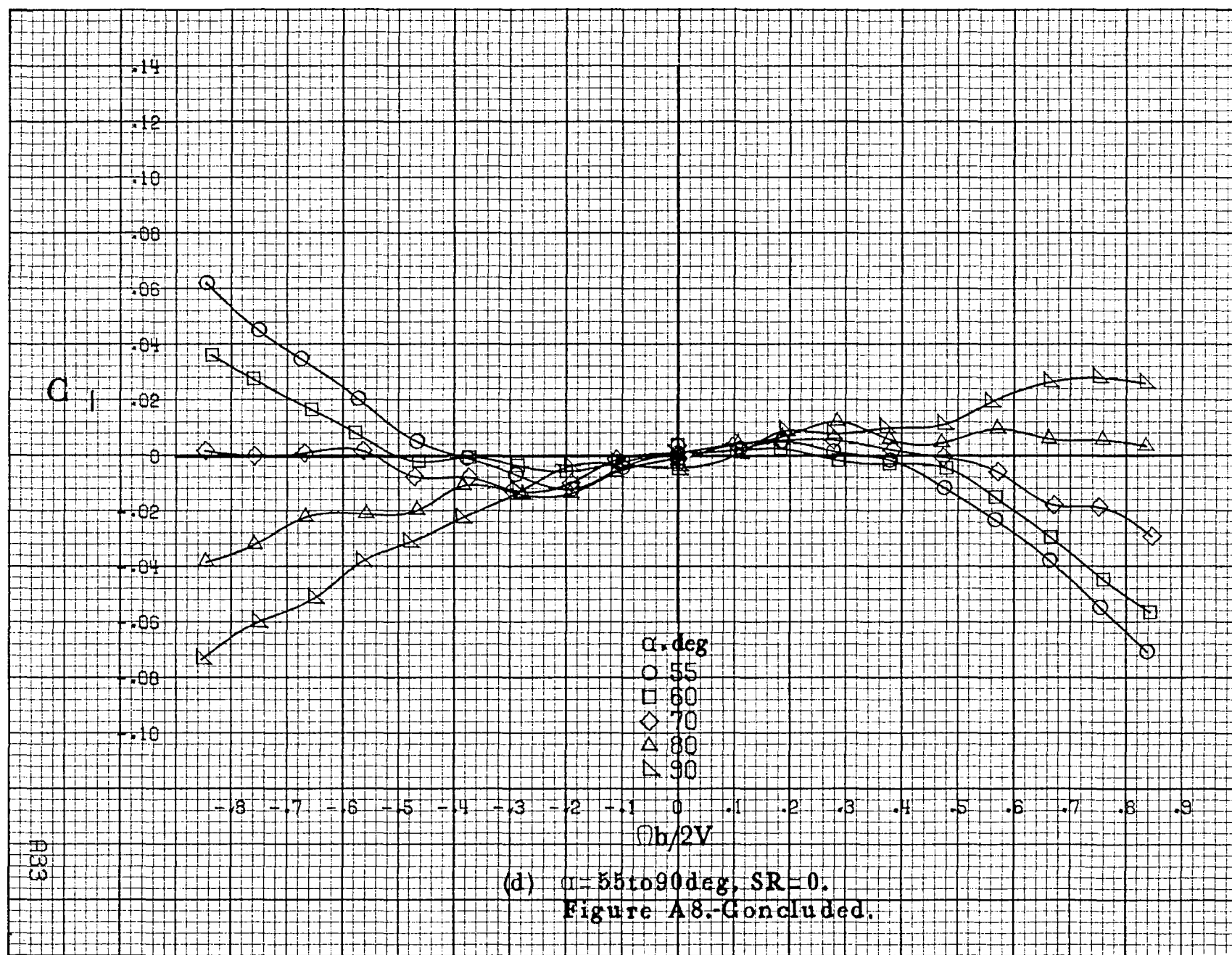


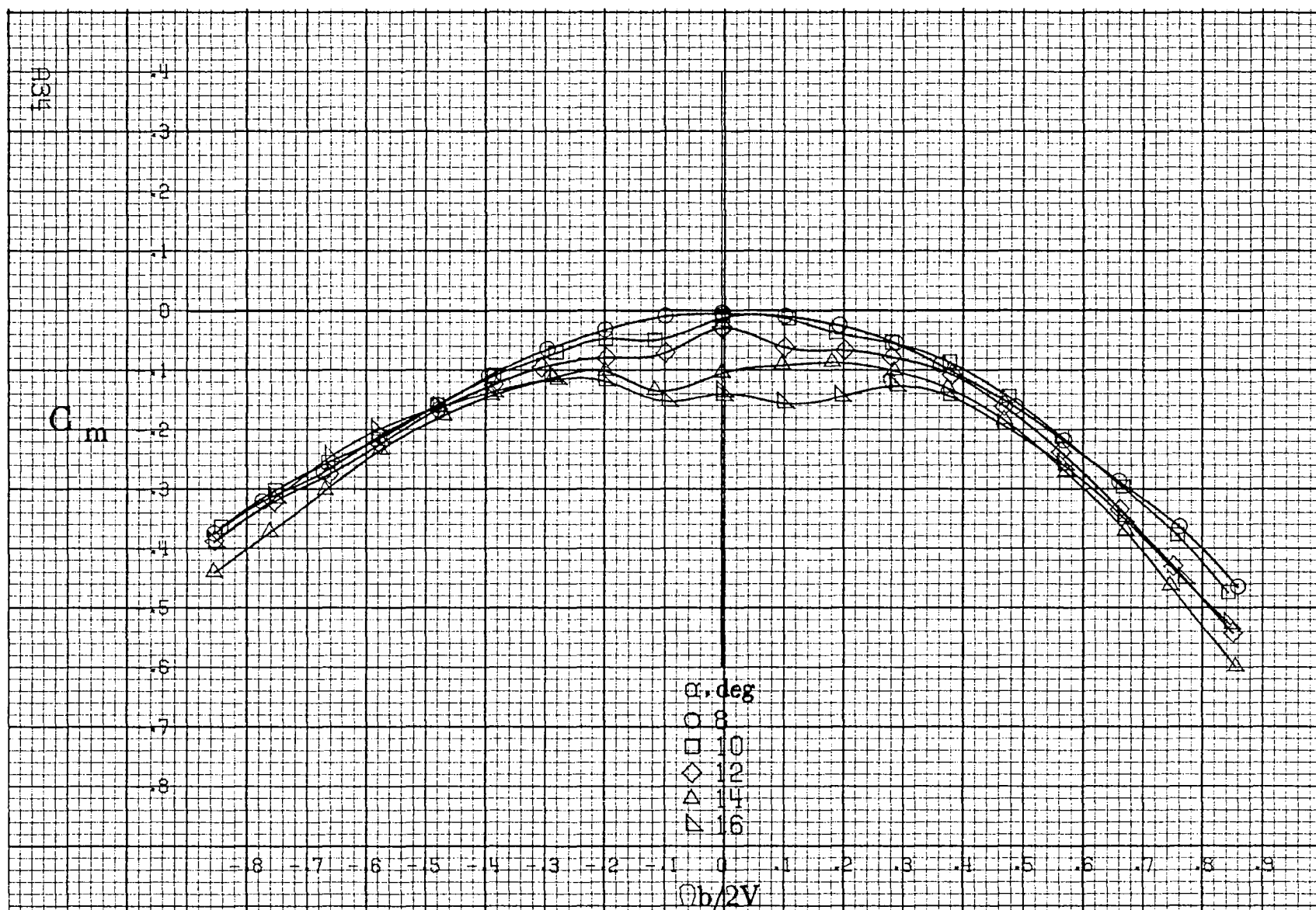






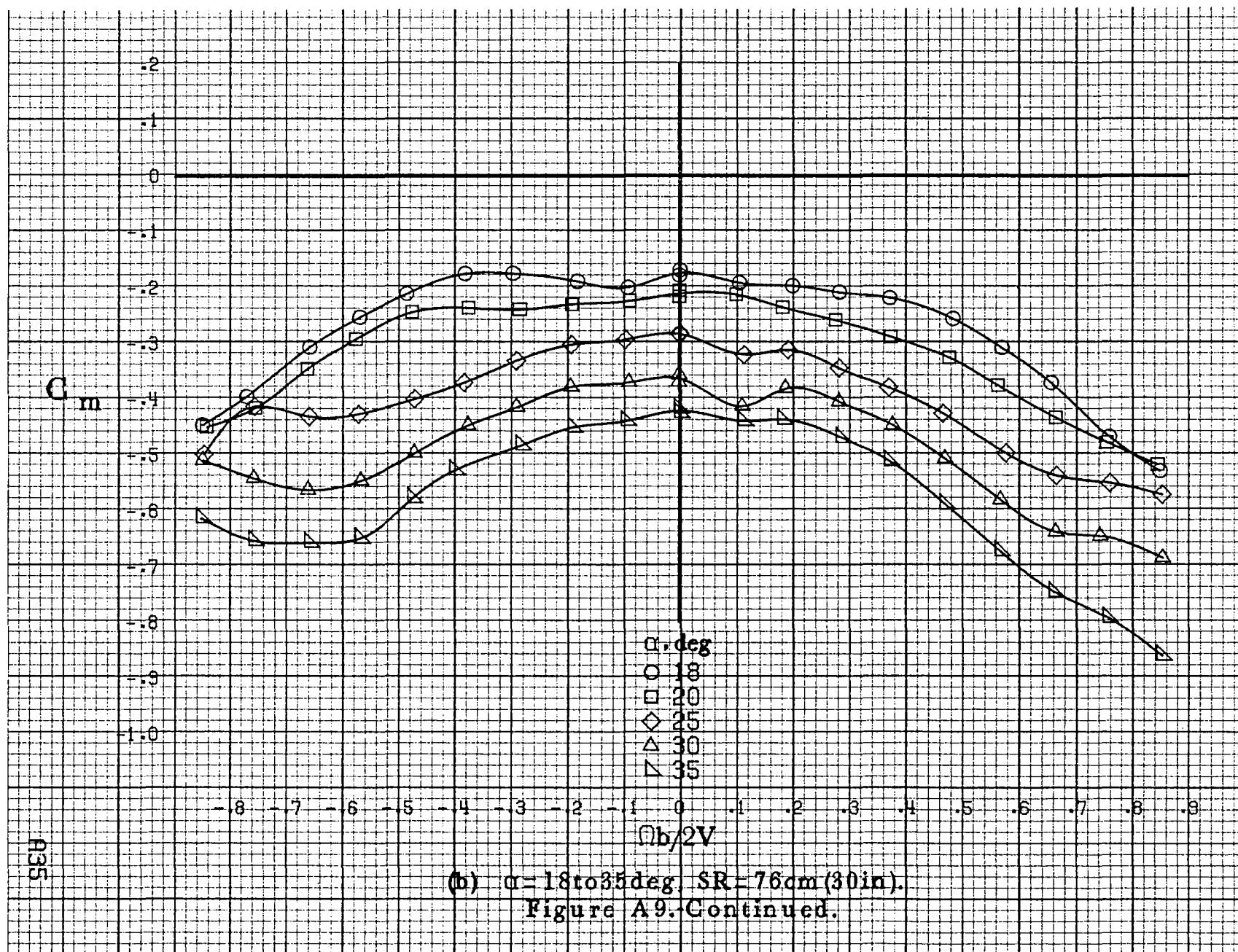


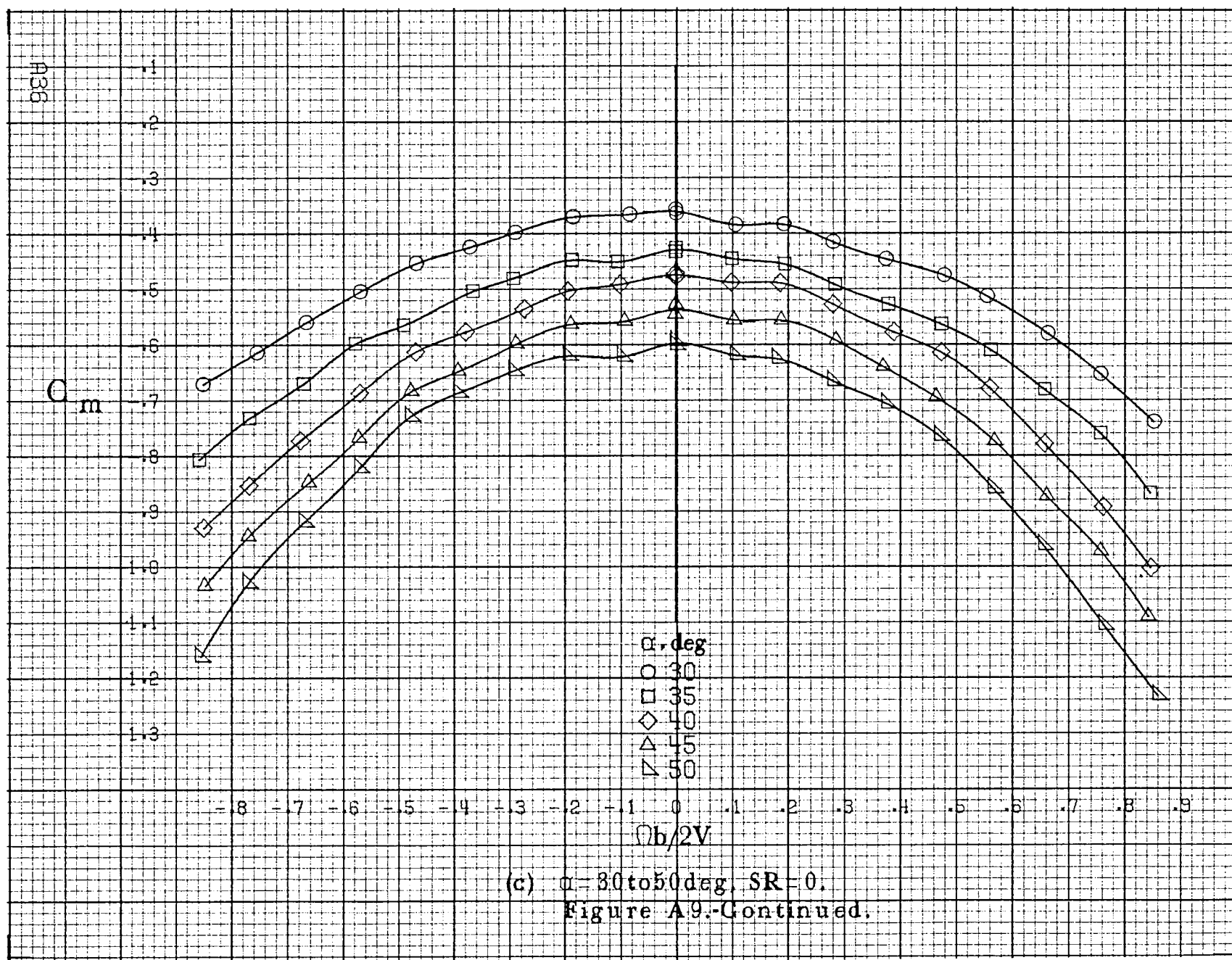


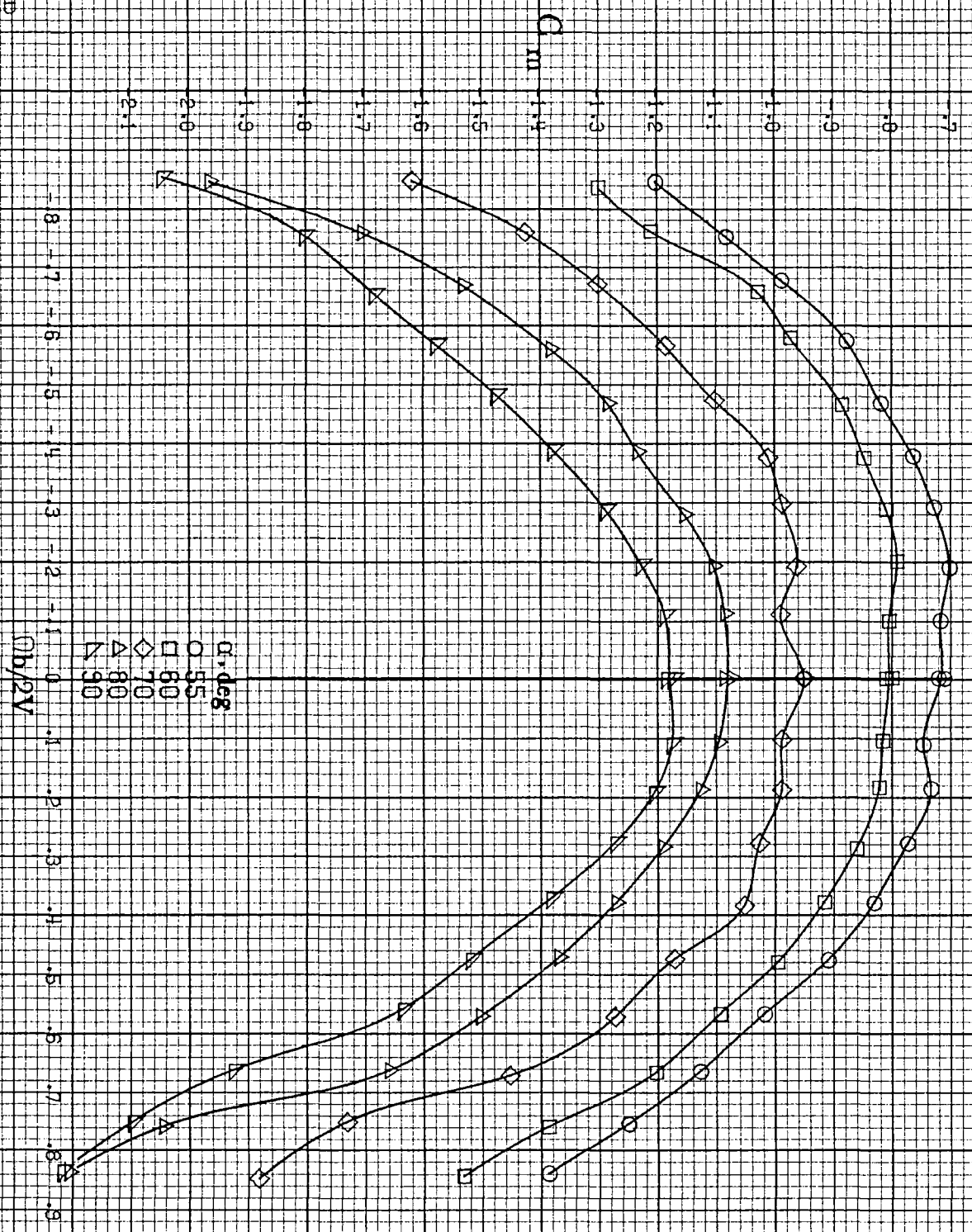


(a) $\alpha=8$ to 16° , $SR=76\text{cm}(30\text{in})$.

Figure A9-Effect of rotation rate and angle of attack on pitching-moment coefficient for basic configuration. $\delta_a=0^\circ$, $\delta_r=0^\circ$, $\delta_s=-25^\circ$, $\beta=0^\circ$.







(a) $\alpha=55$ to 90° , $SR=0$,
Figure A.9-Continued.

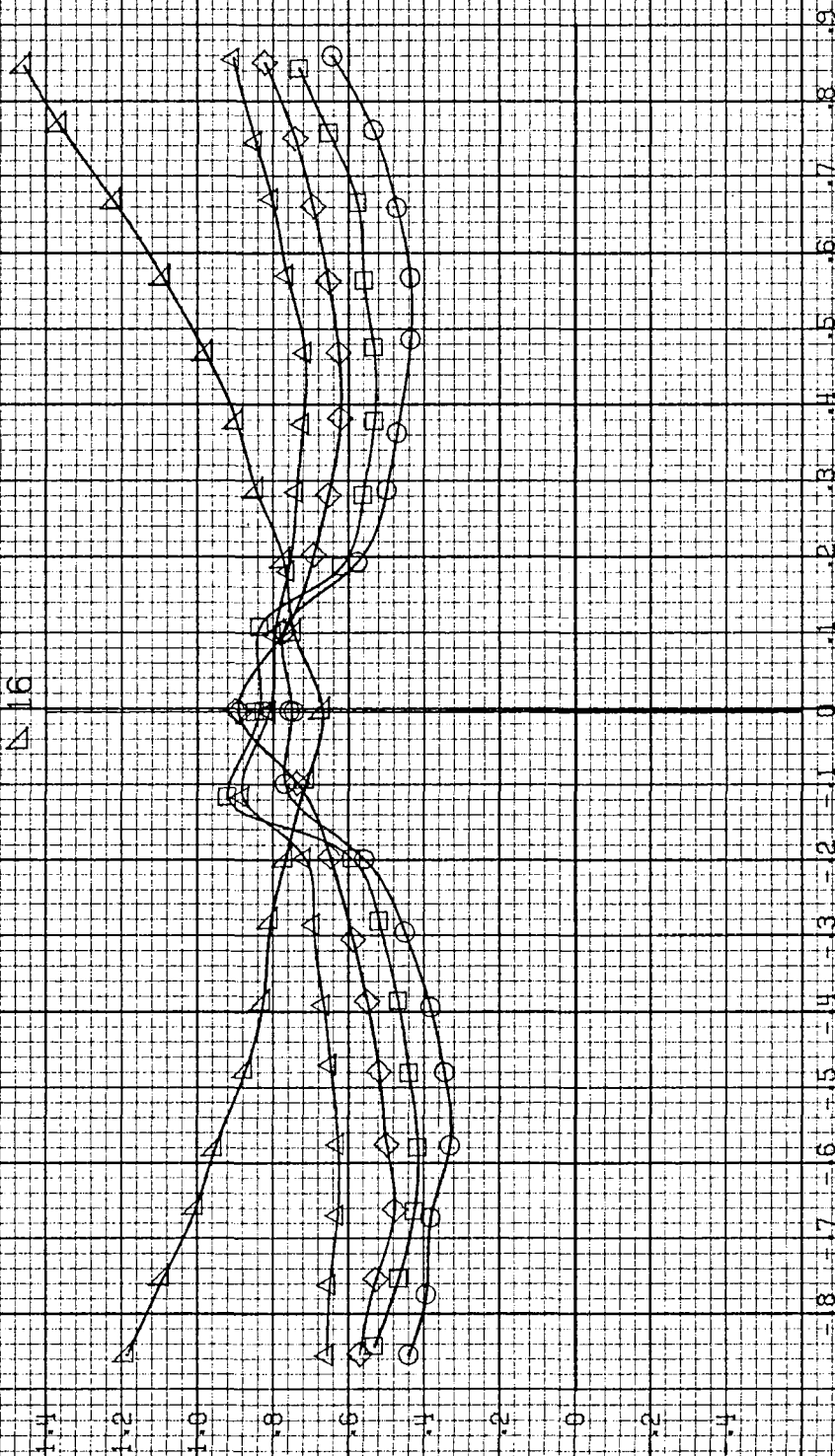
α , deg

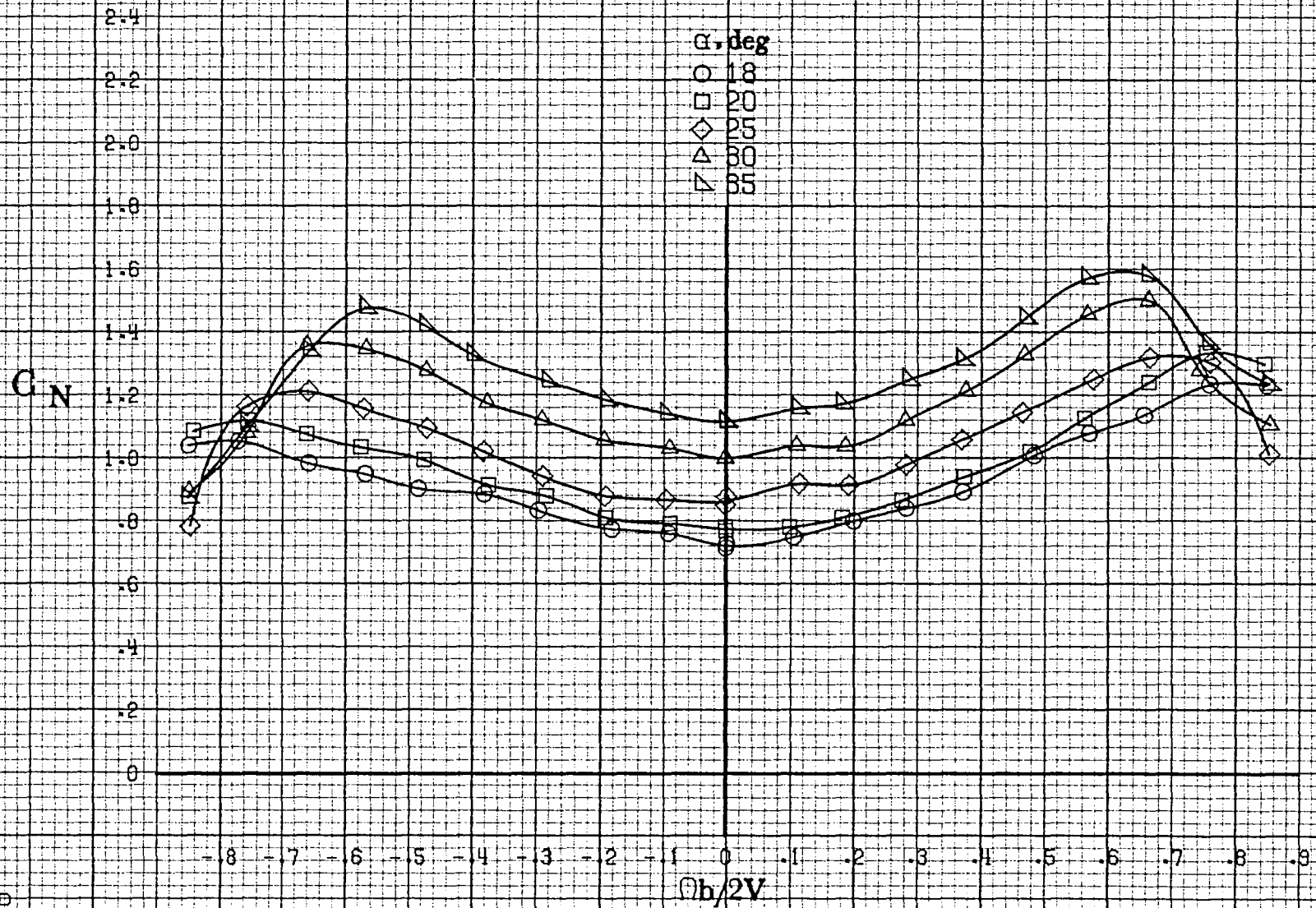
\circ 8
 \square 10
 \diamond 12
 \triangle 14
 ∇ 16

C/N

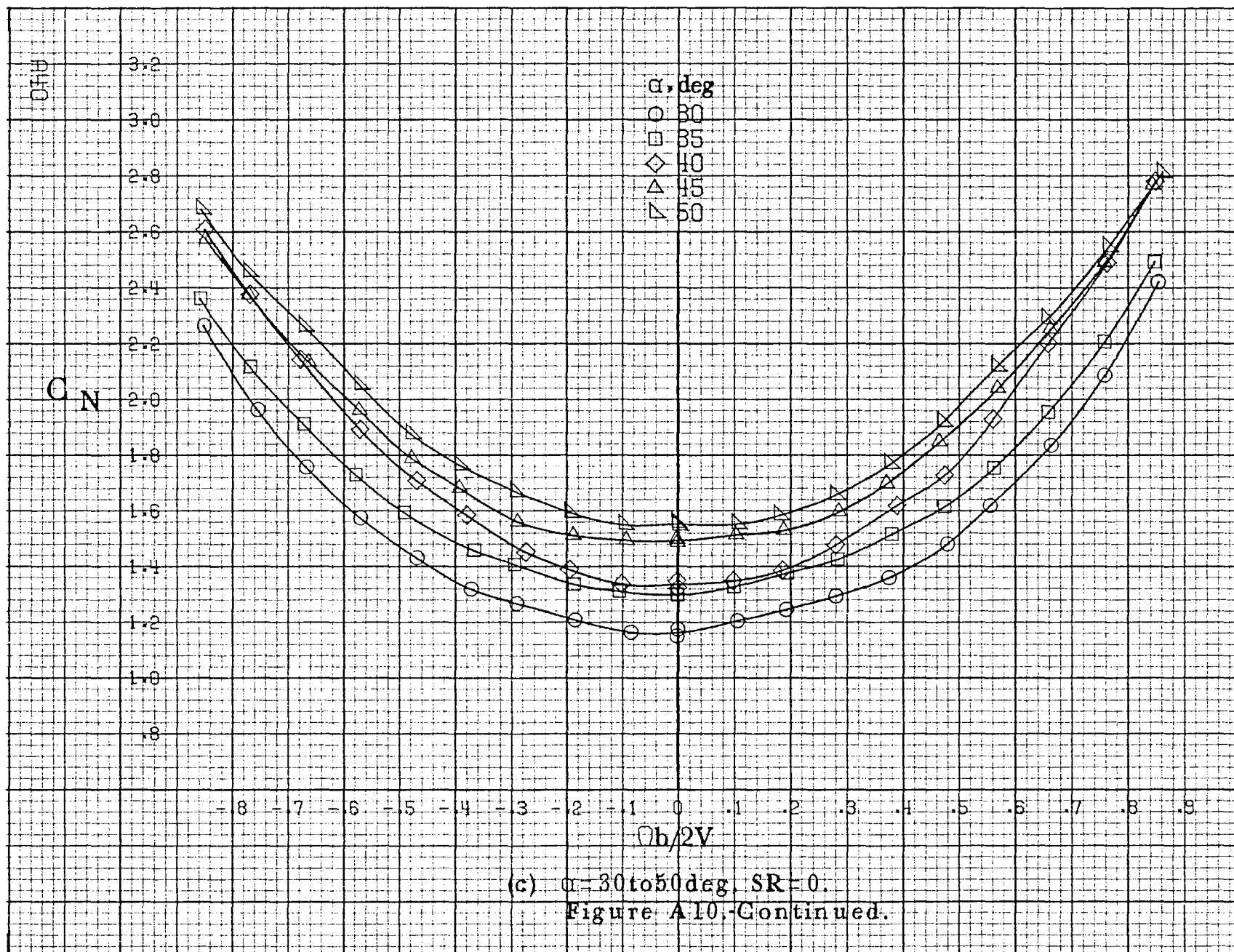
 $\phi b/2V$ (a) $\alpha = 8$ to 16 deg, $SR = 76$ cm (30 in).

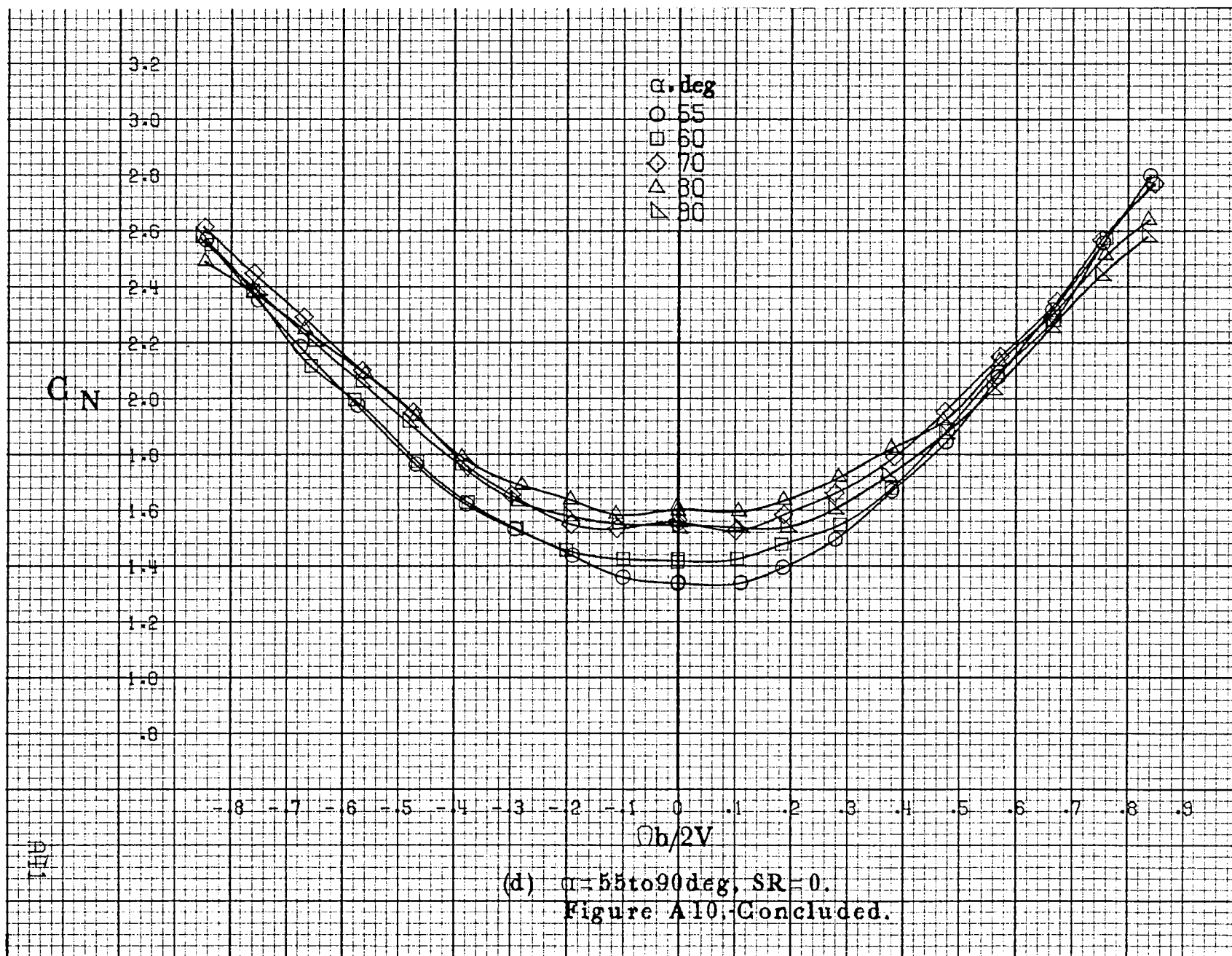
Figure A10. Effect of rotation rate and angle of attack on normal-force coefficient for basic configuration. $\delta_a = 0^\circ$, $\delta_n = 0^\circ$, $\delta_r = -25^\circ$, $\beta = 0^\circ$.

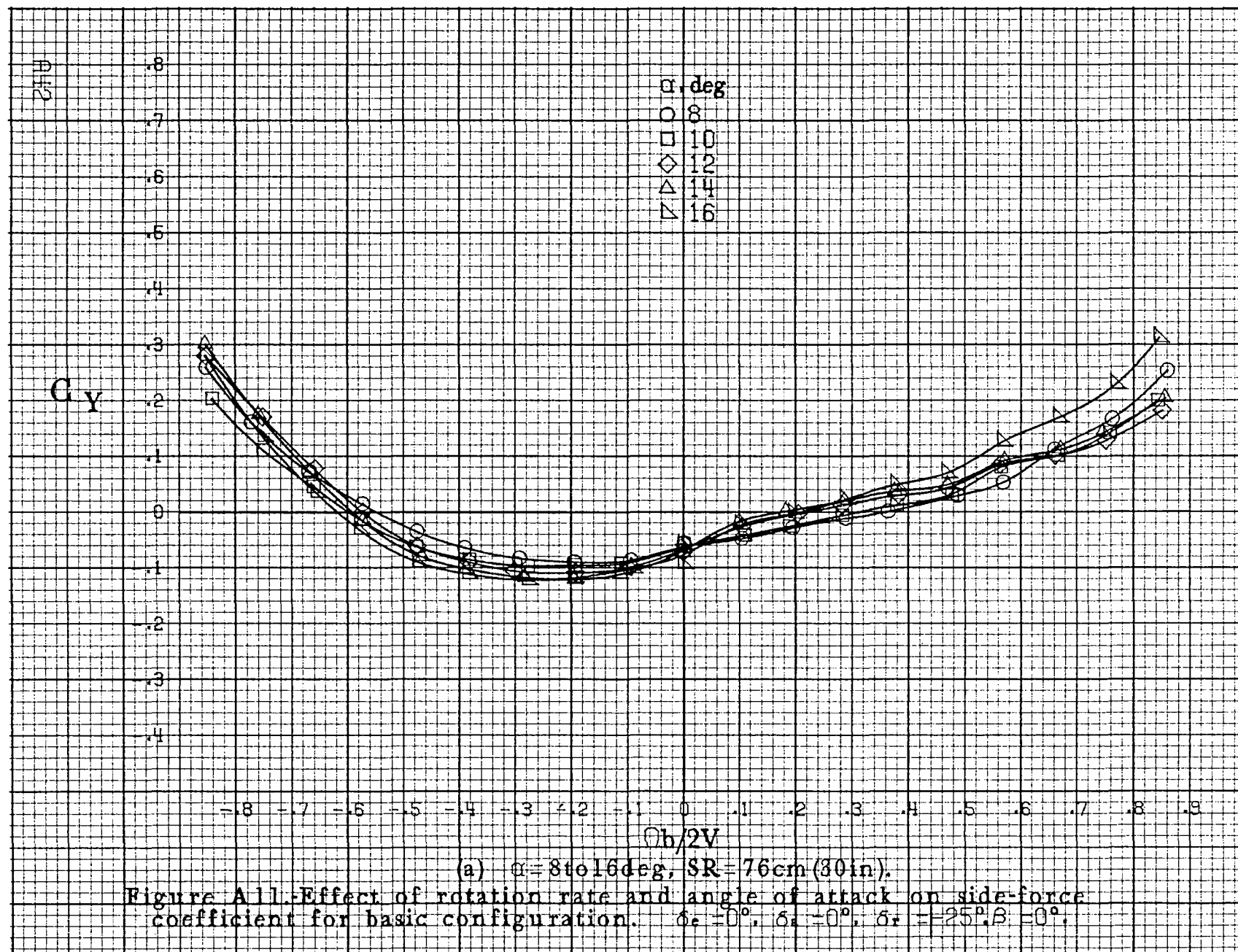


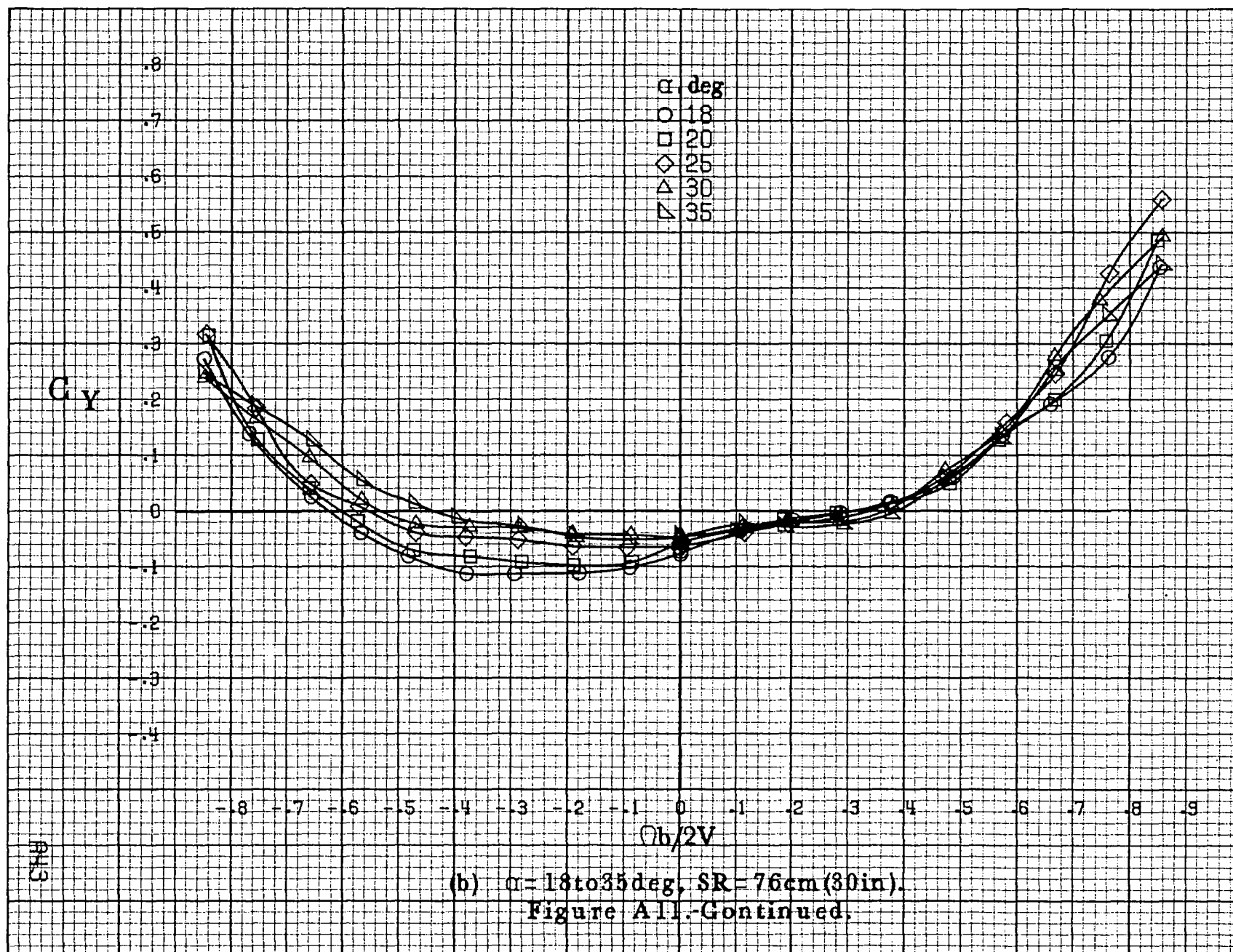


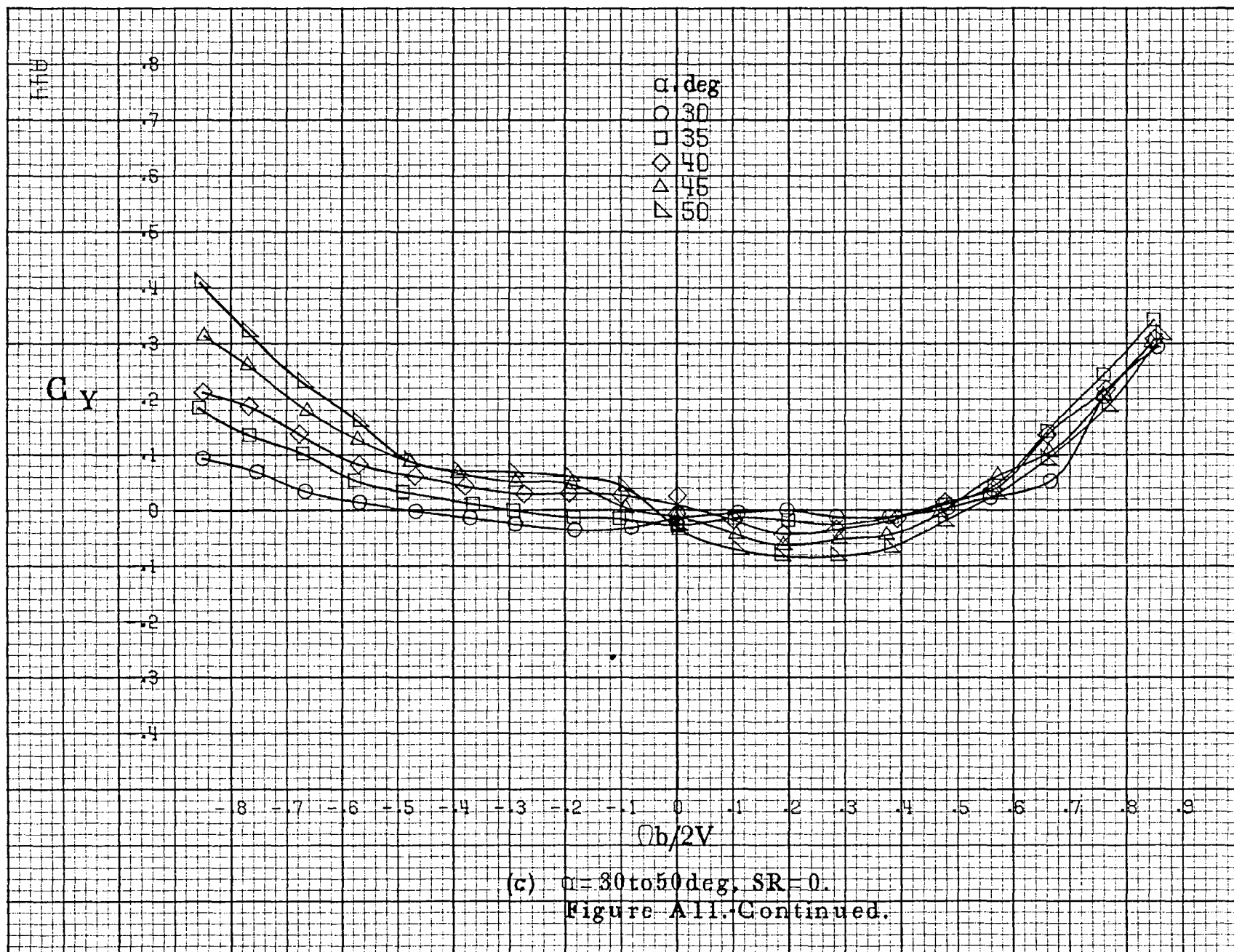
(b) $\alpha = 18$ to 35 deg. SR = 76 cm (30 in).
Figure A10.-Continued.

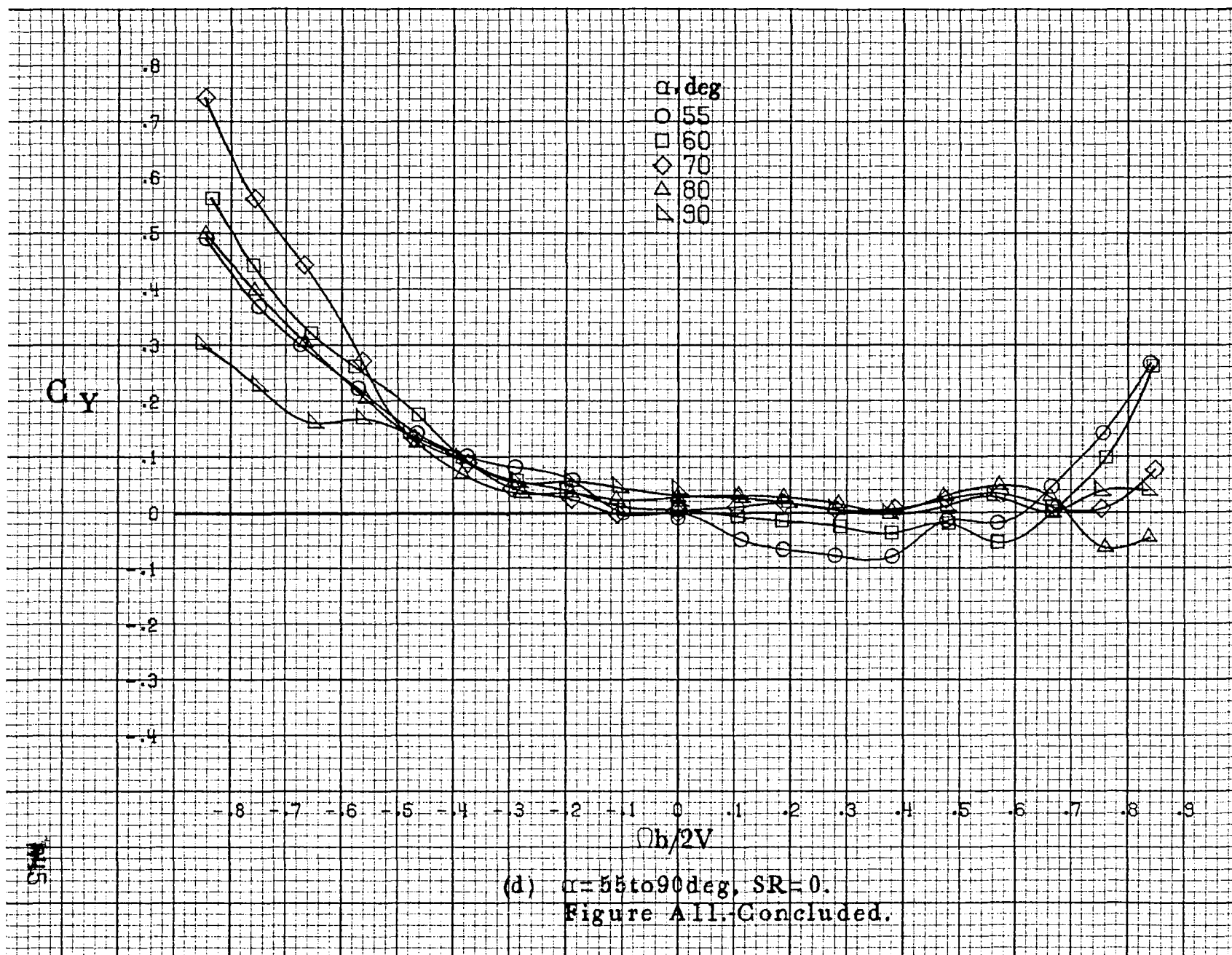


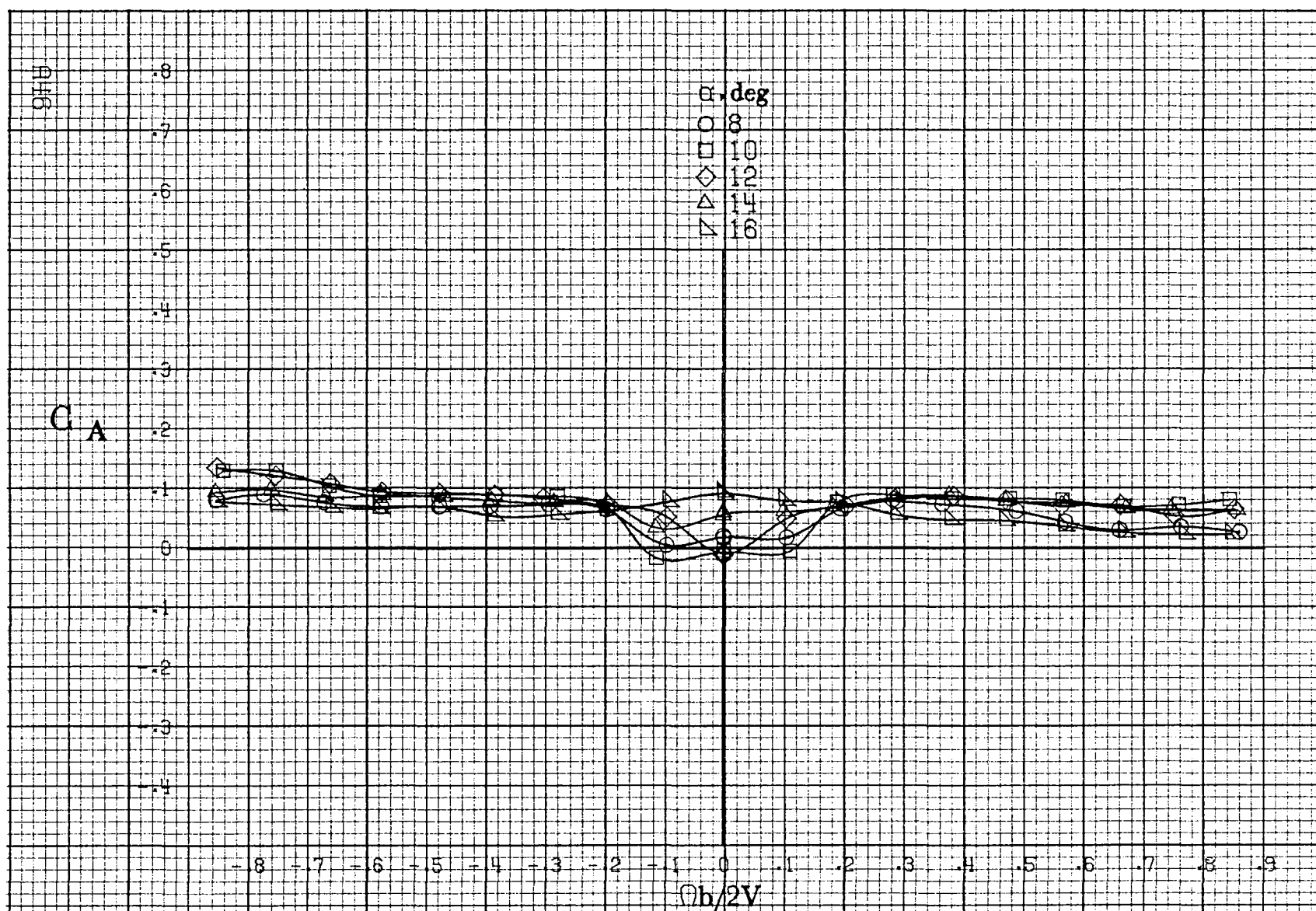






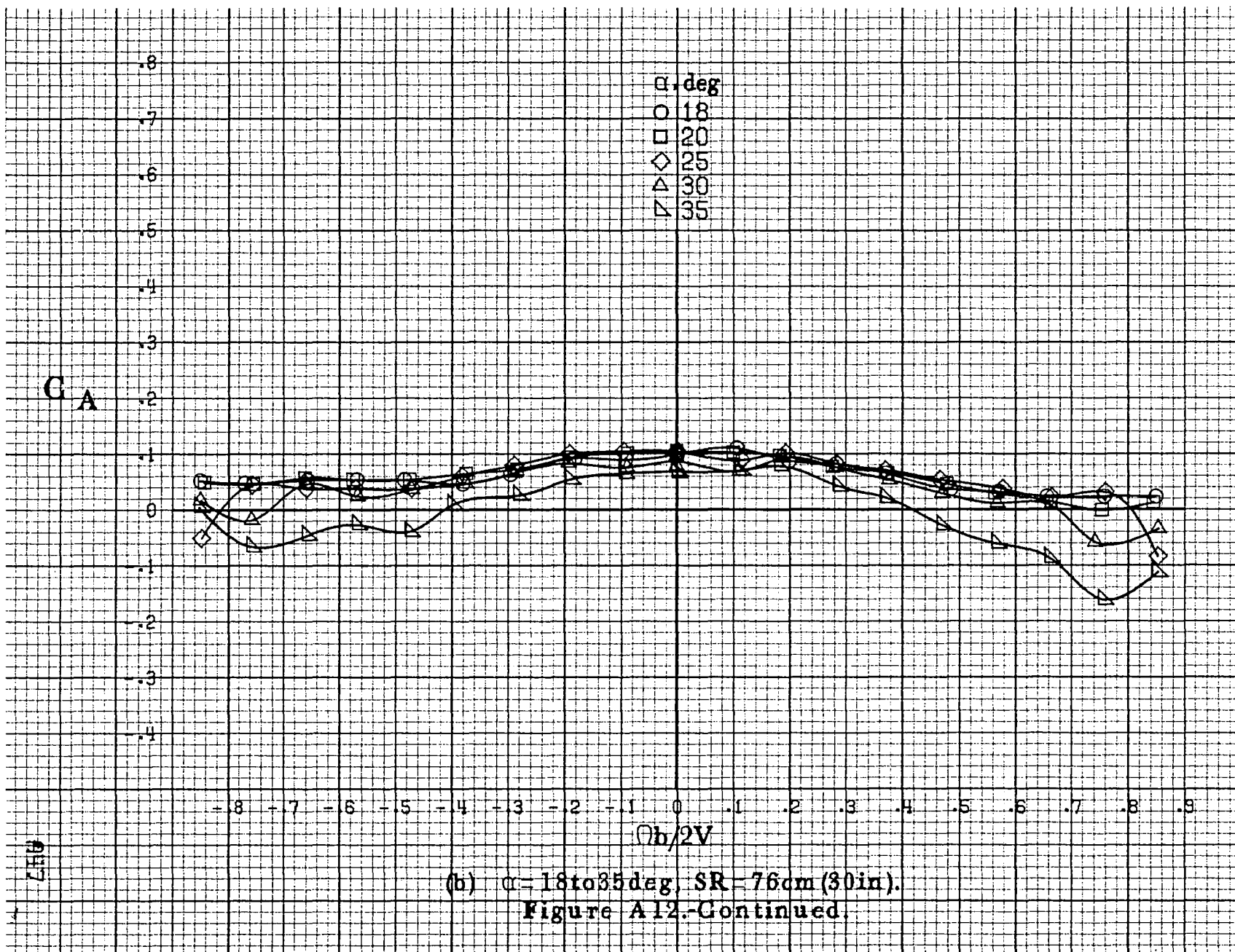




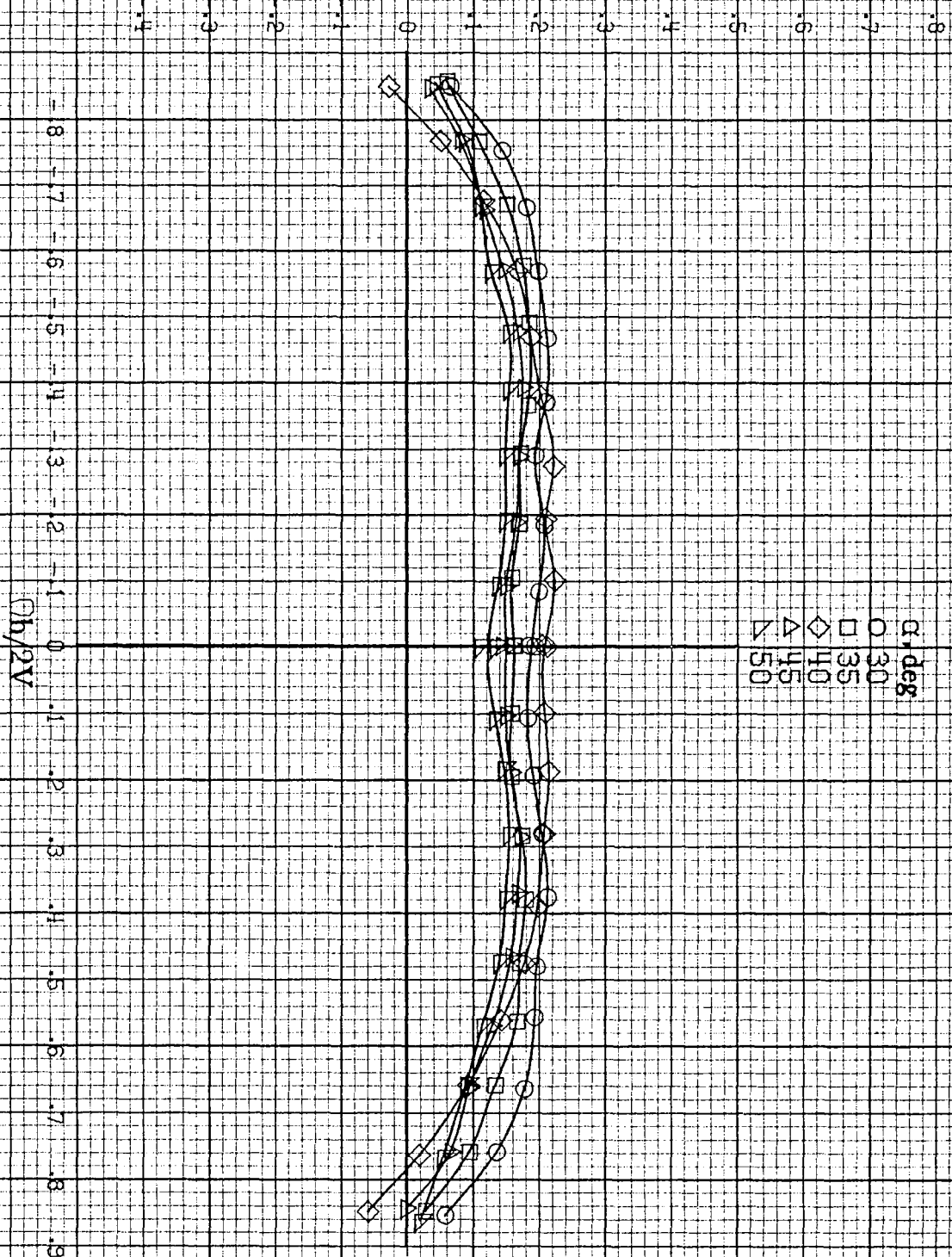


(a) $\alpha = 8$ to 16° , $SR = 76 \text{ cm (30 in.)}$.

Figure A12. Effect of rotation rate and angle of attack on axial force coefficient for basic configuration. $\delta_a = 0^\circ$, $\delta_r = 0^\circ$, $\delta_z = -25^\circ$, $\delta = 0^\circ$.

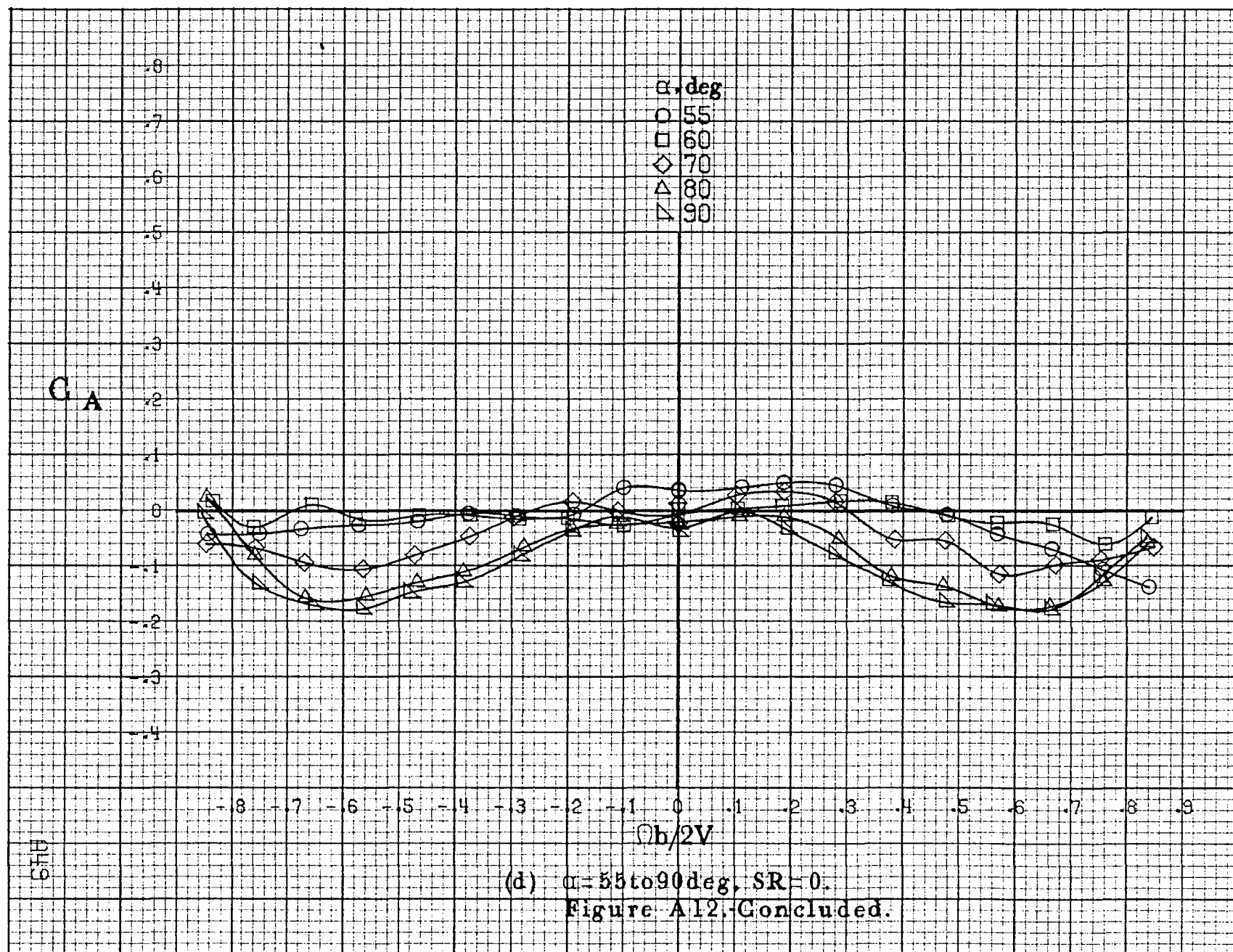


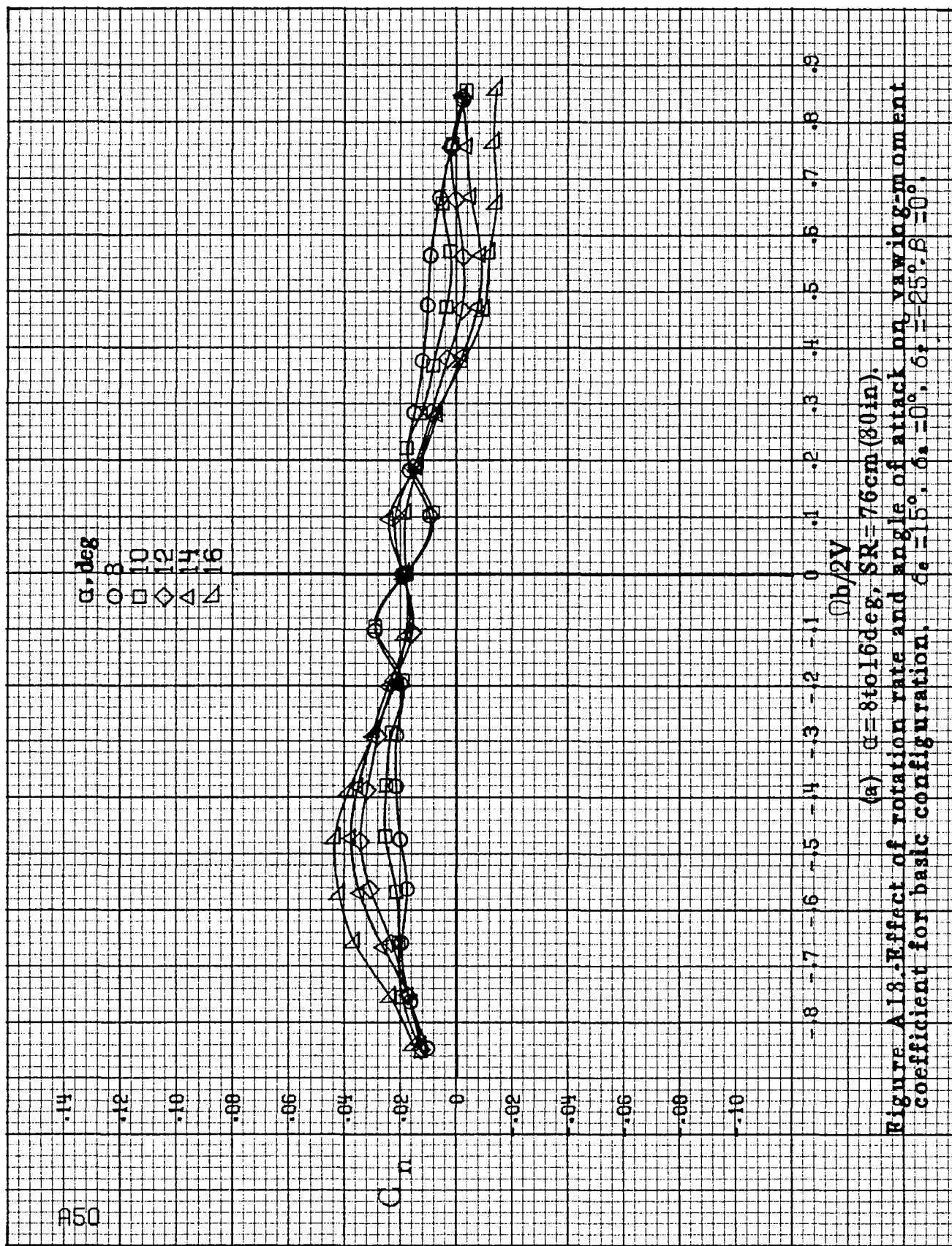
C A

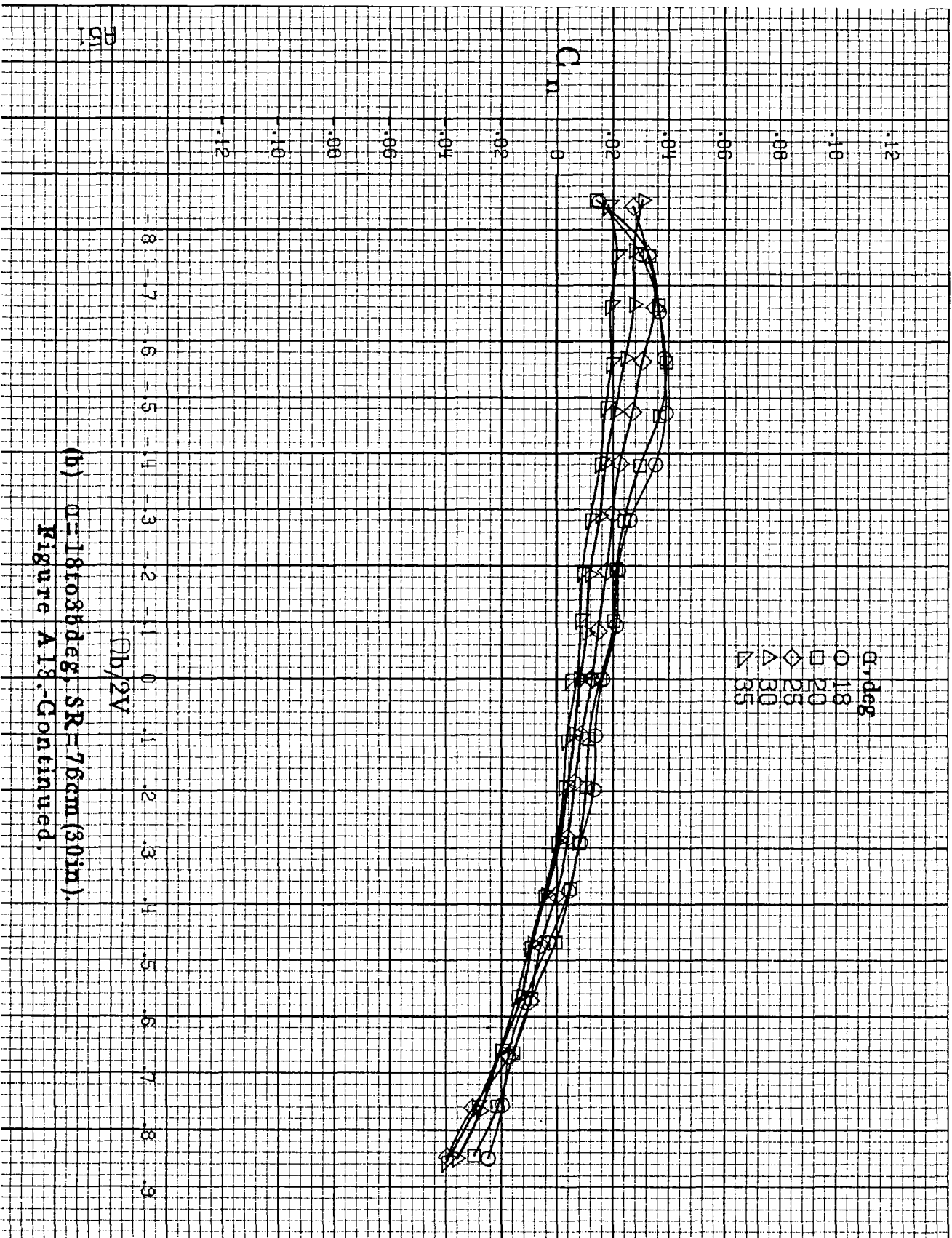


(c) $\omega = 30$ to 50 deg, $SR = 0$.

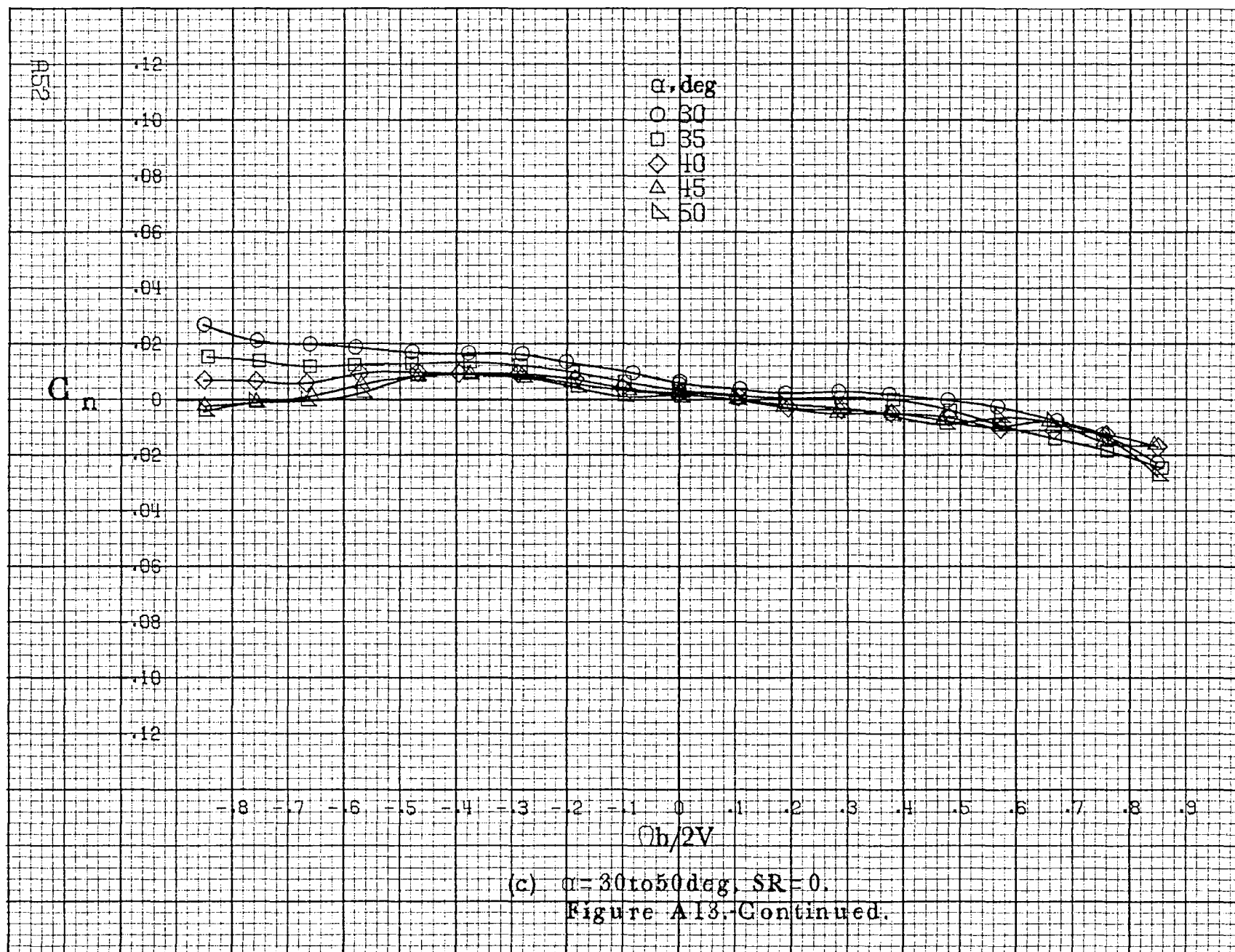
Figure A12. Continued.

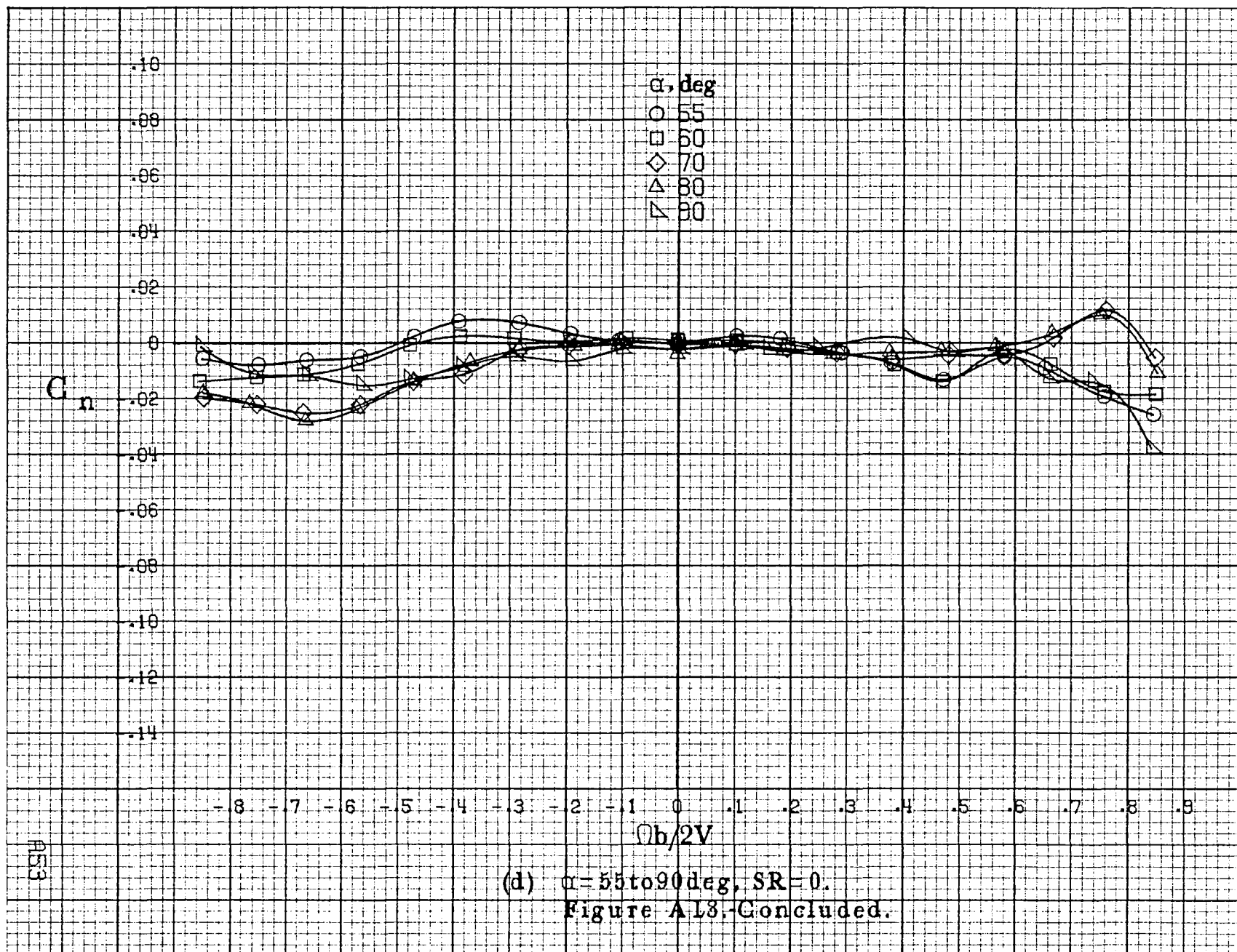


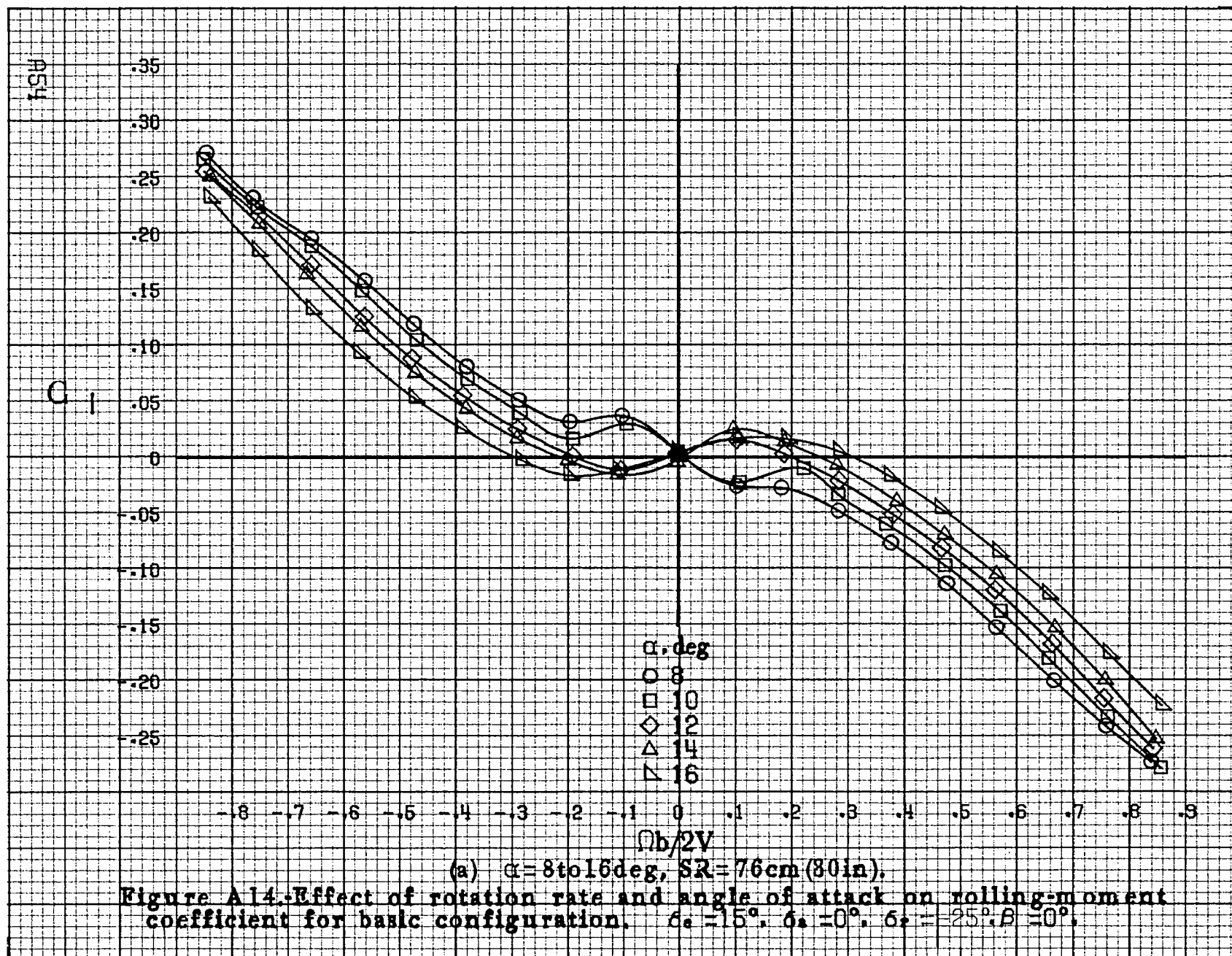


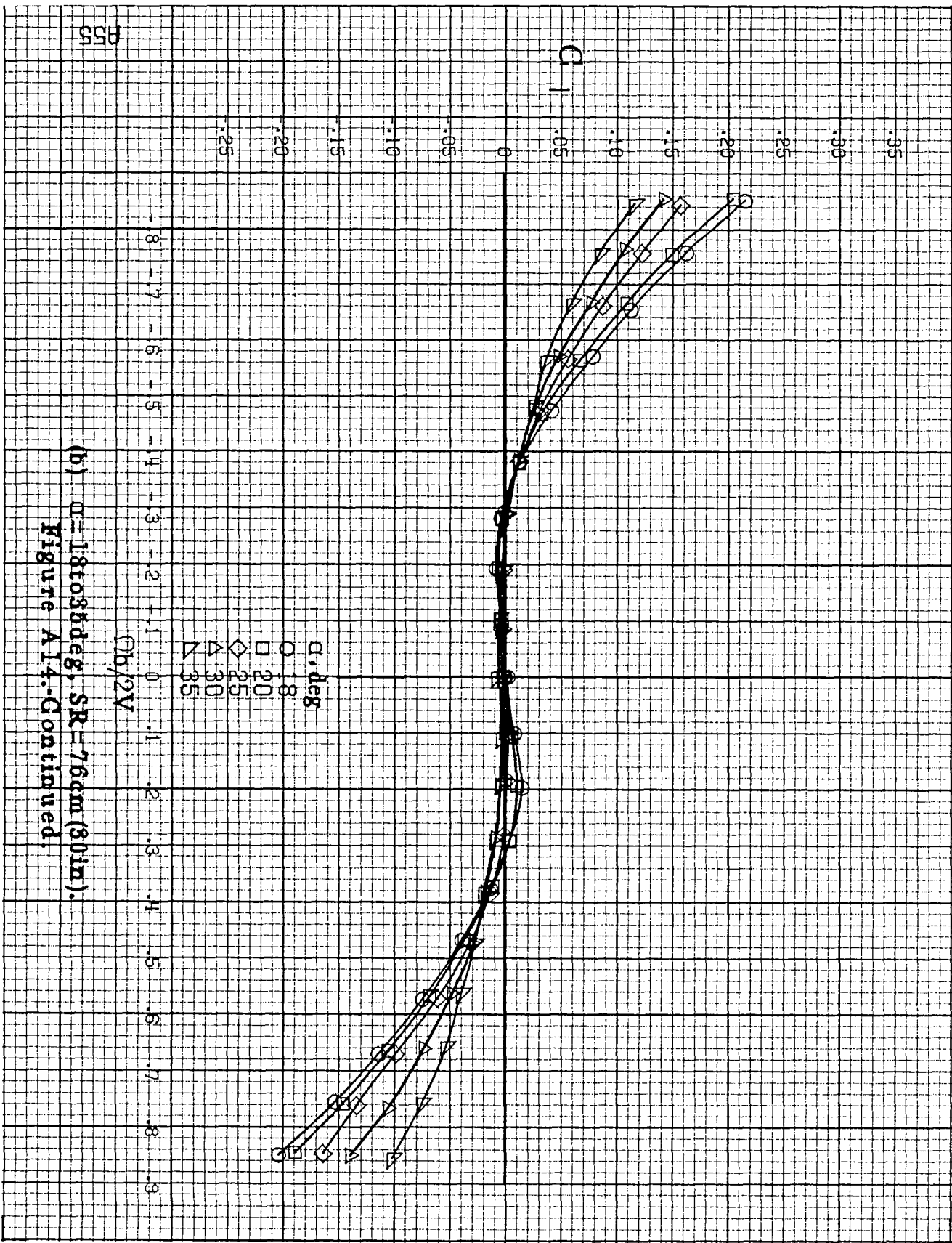


(b) $\alpha = 18.18 \text{ deg}$, $SR = 7.6 \text{ cm (30 in)}$.
 Figure A13.-Continued.

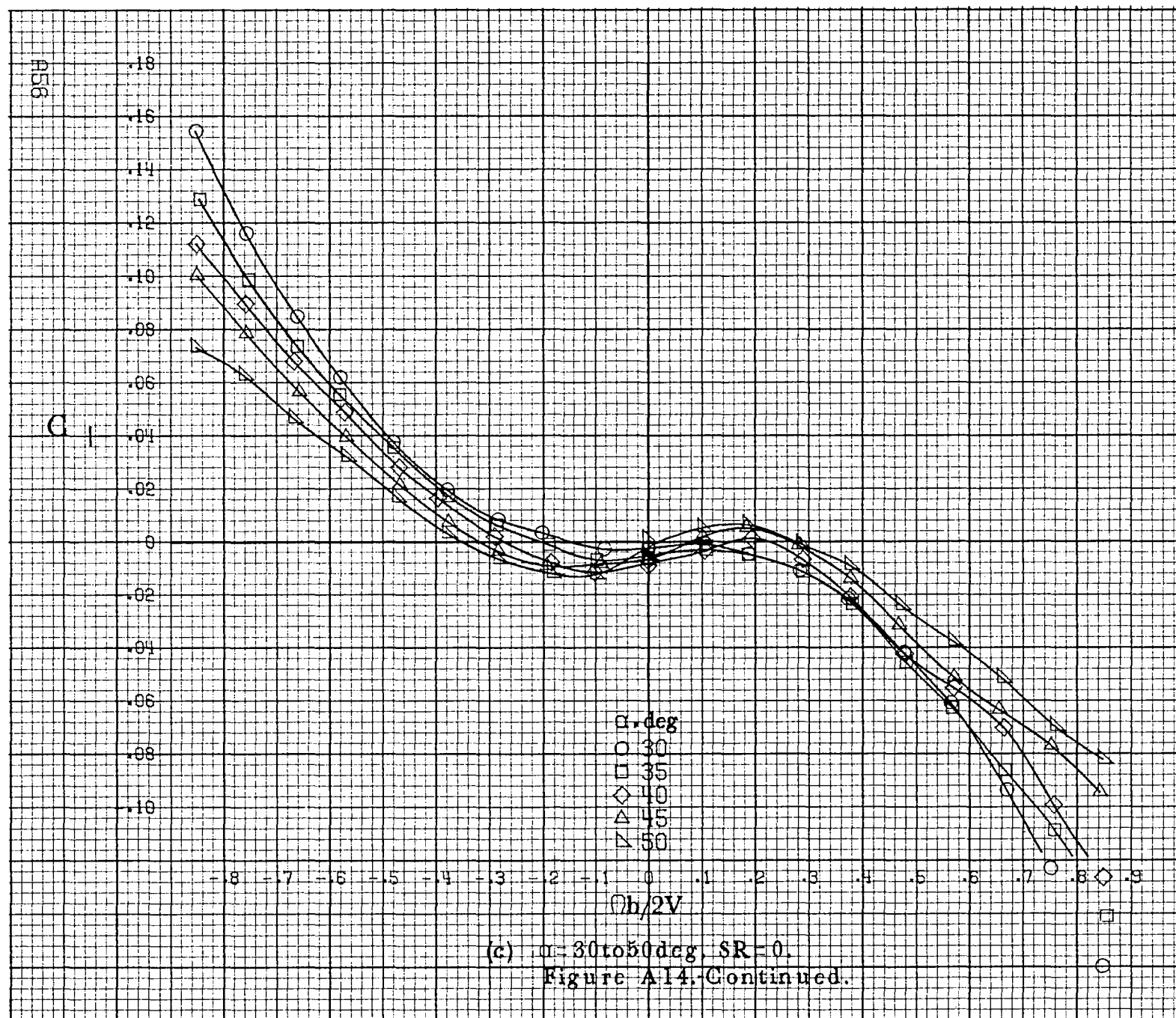


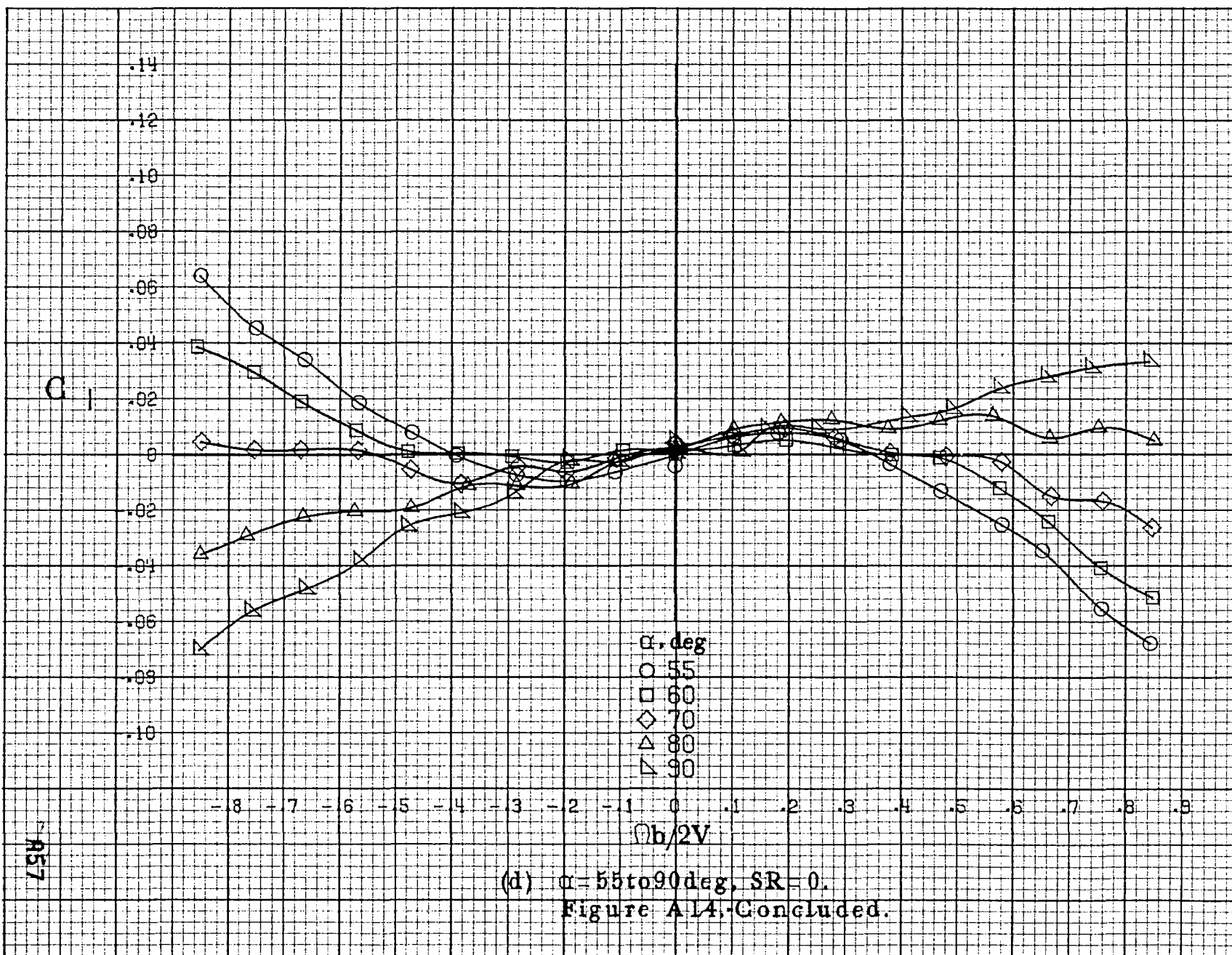


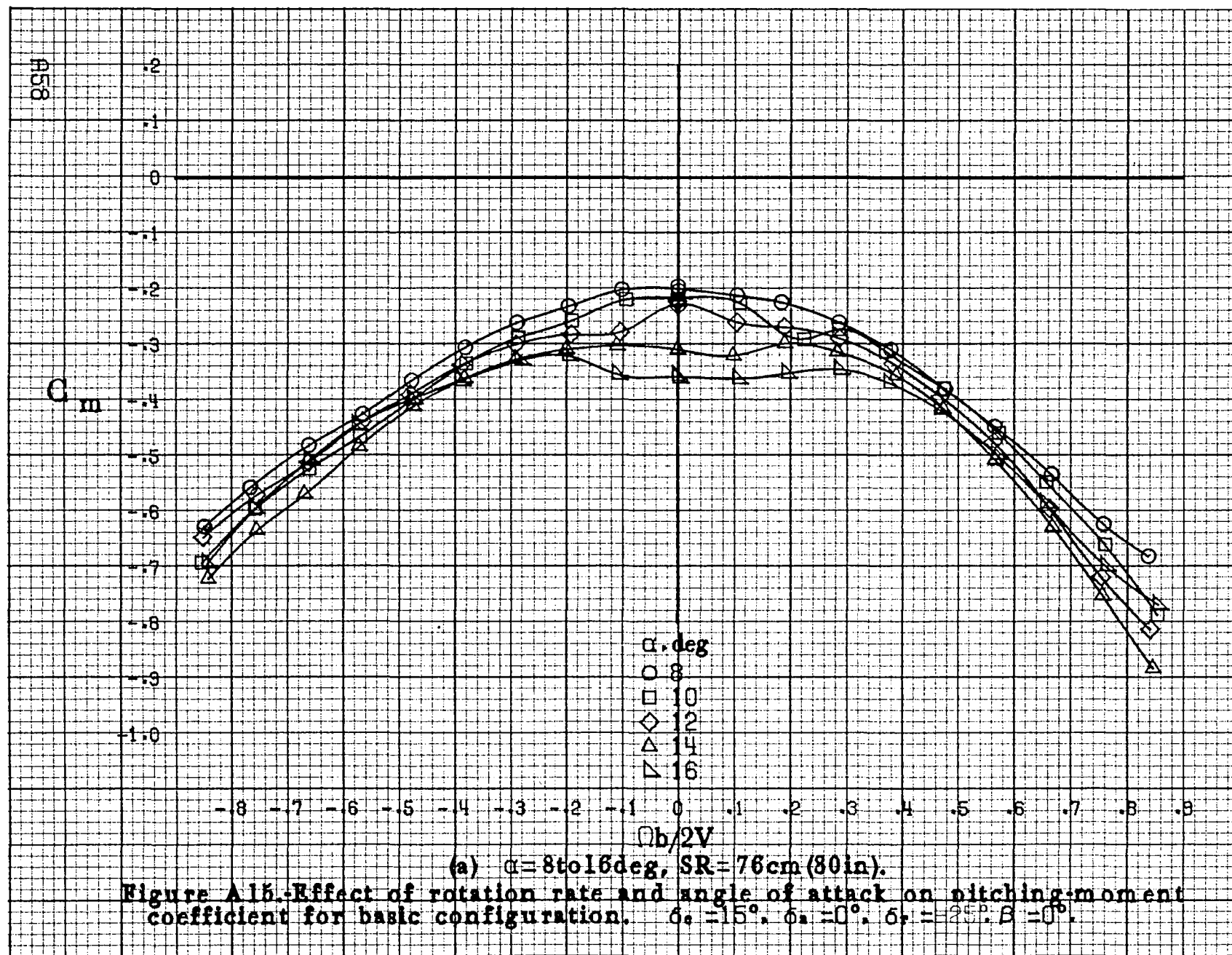


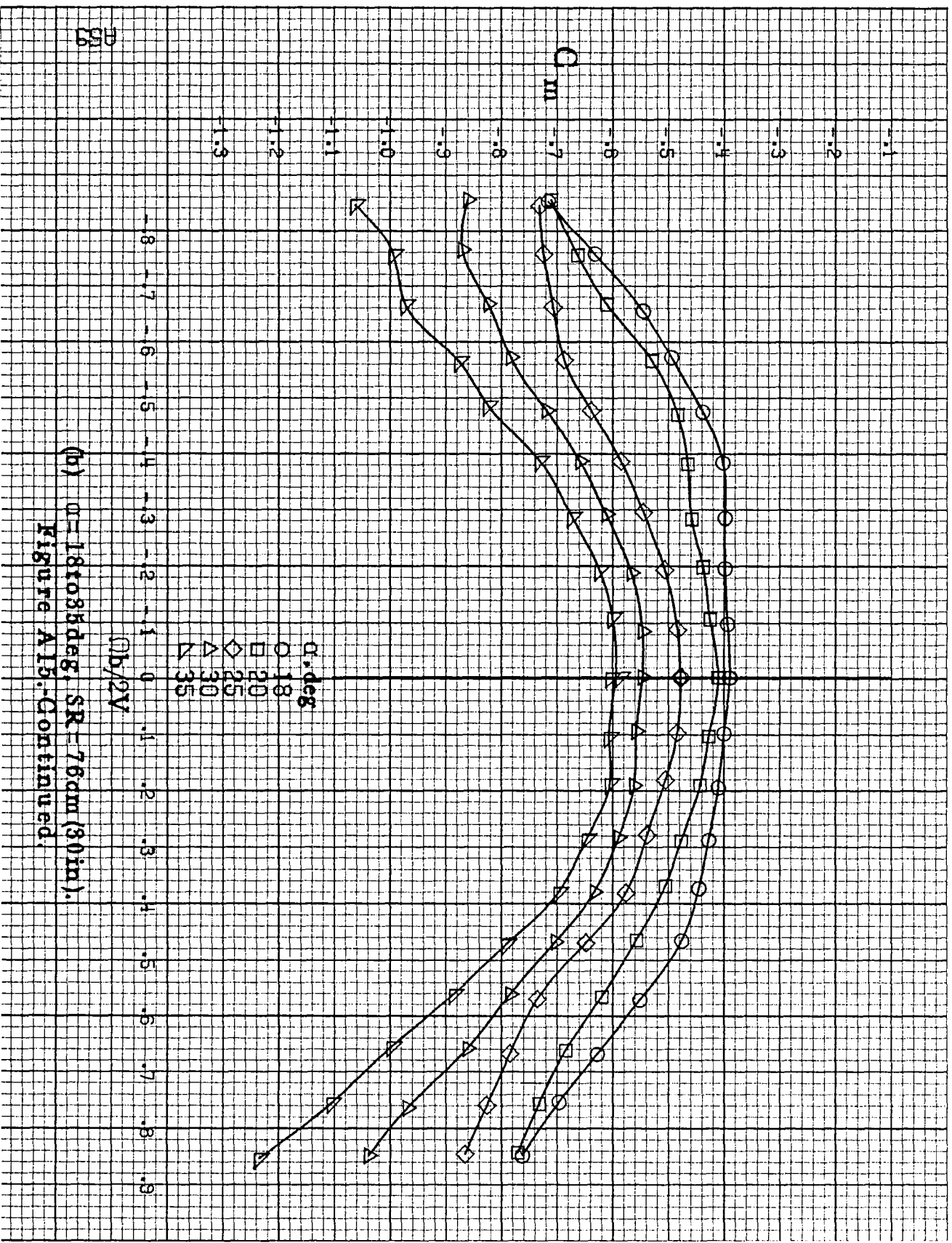


(b) $\alpha = 18$ to 35 deg, $SR = 76$ cm (30 in).
Figure A14-Continued.

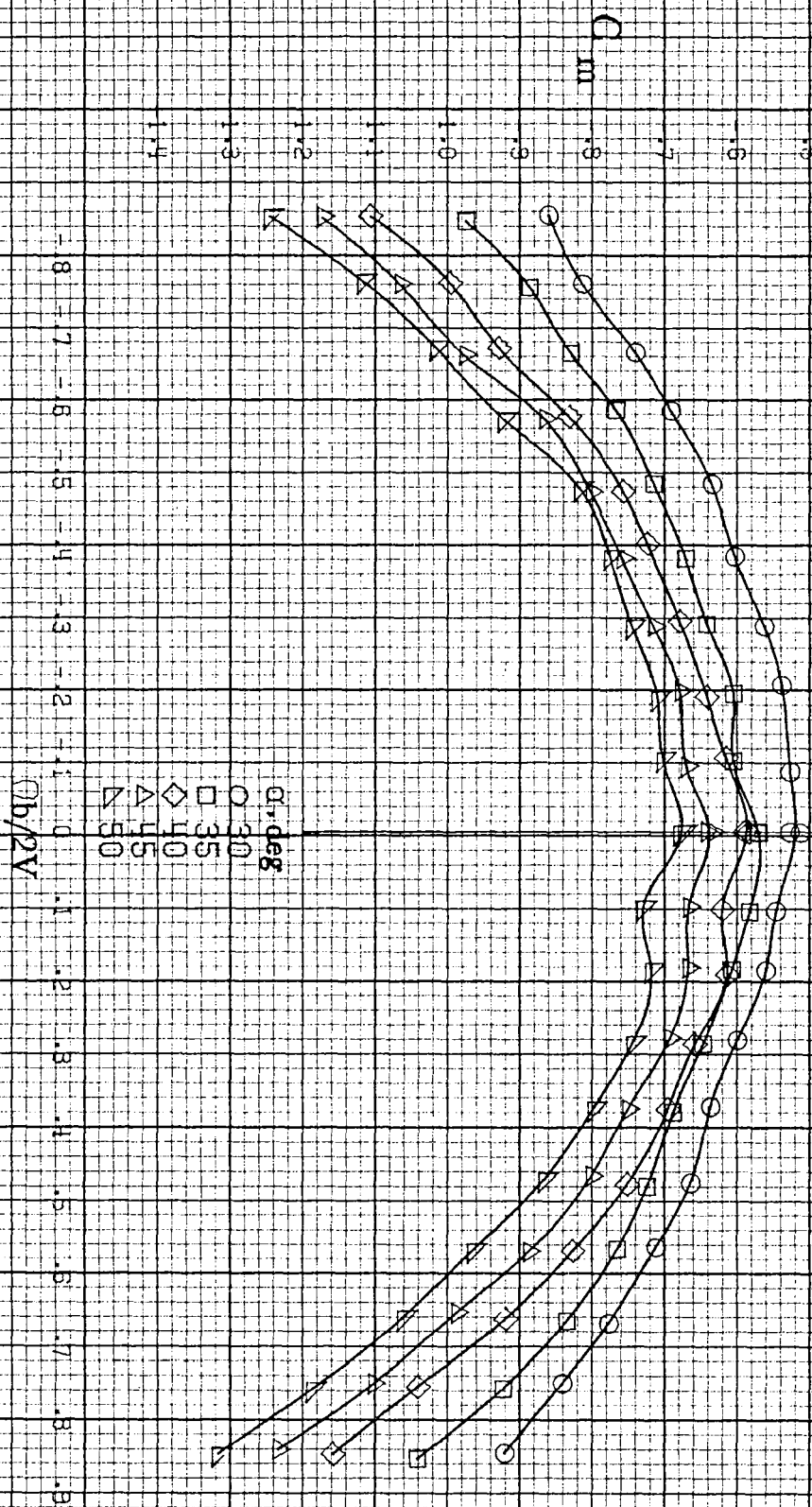




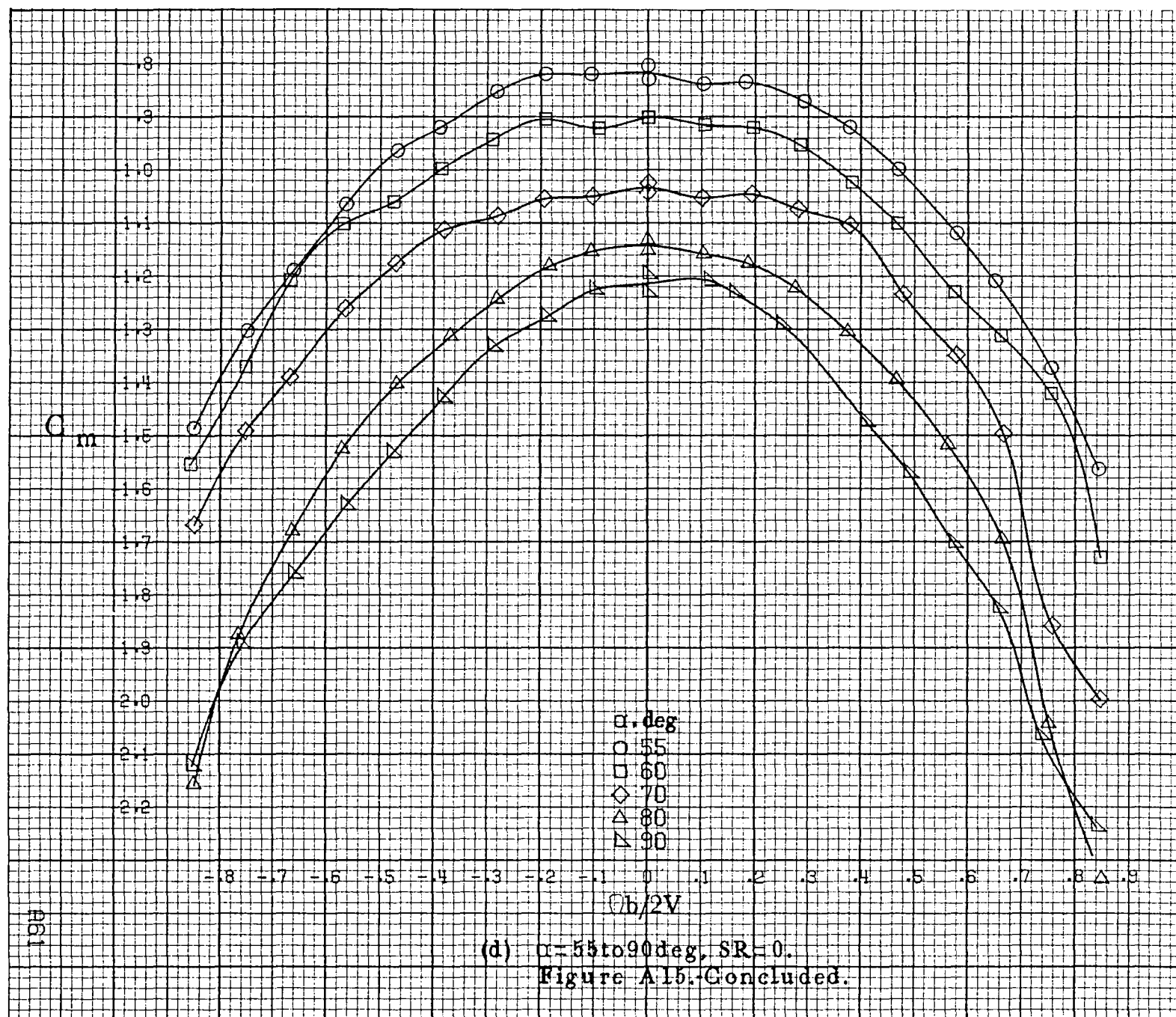


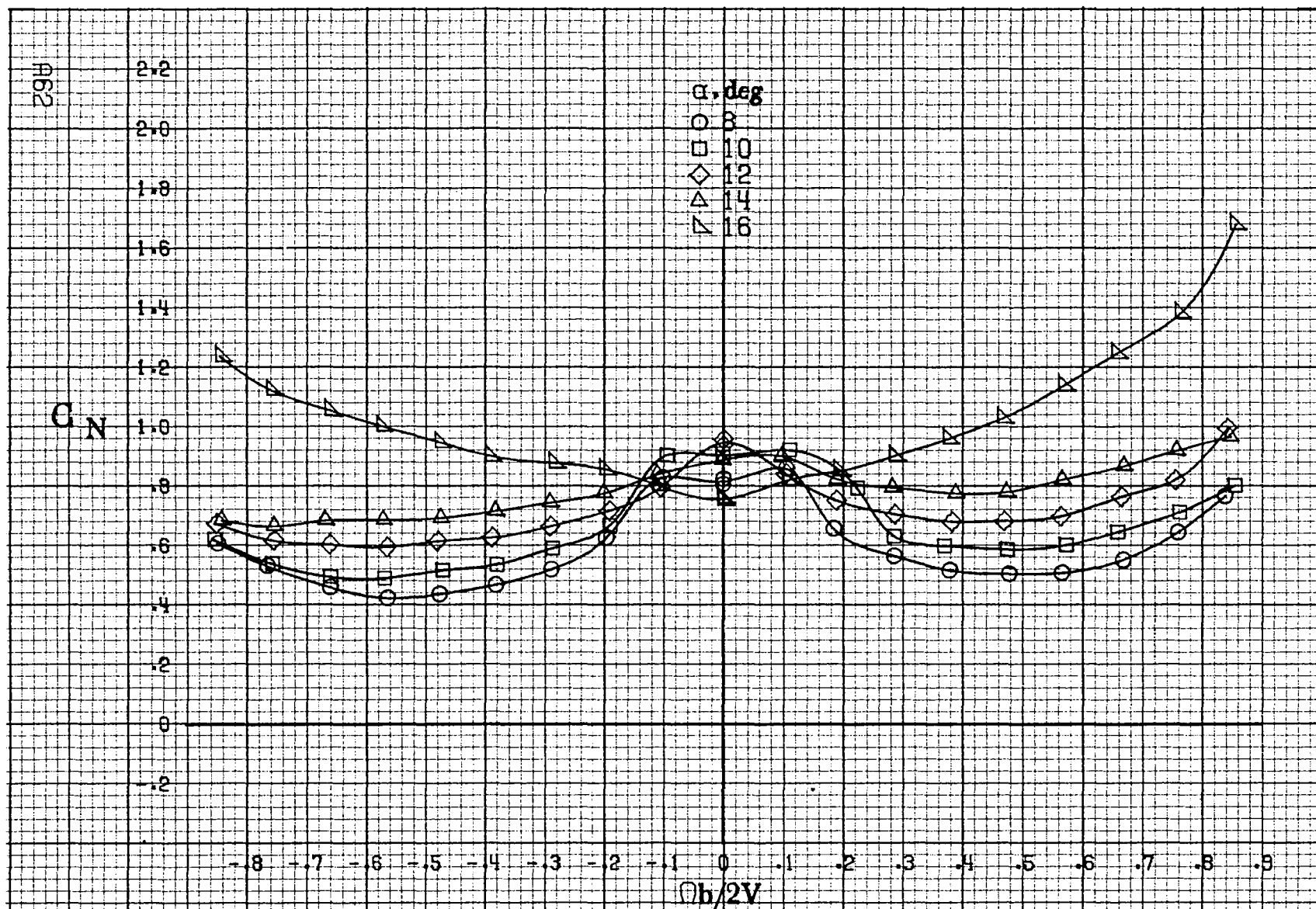


(b) $\alpha = 18$ to 35 deg, $SR = 76$ cm (30 in.).
Figure A15.-Continued.



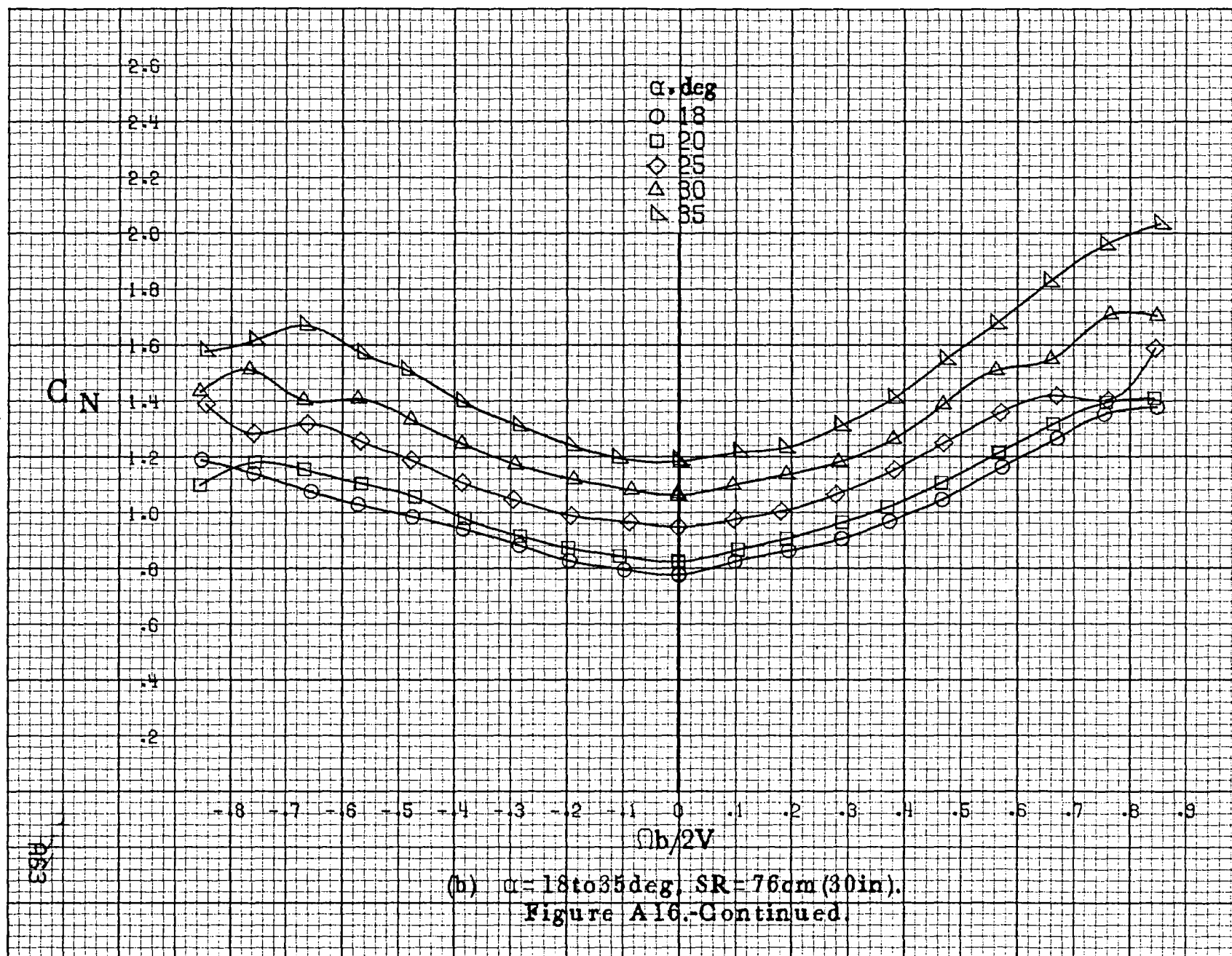
(c) $\alpha = 30$ to 50 deg, $SR = 0$.
Figure A15-Continued.

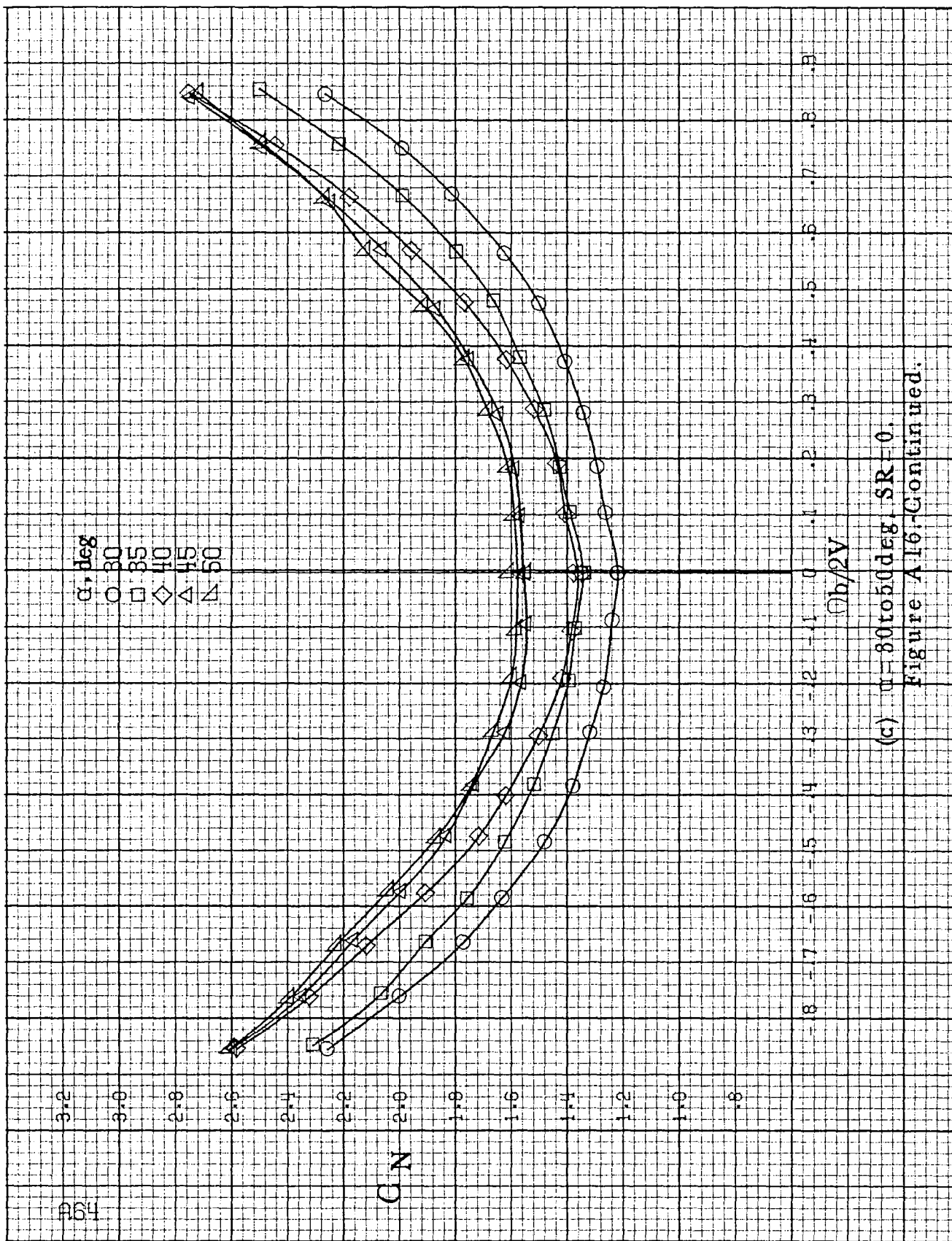




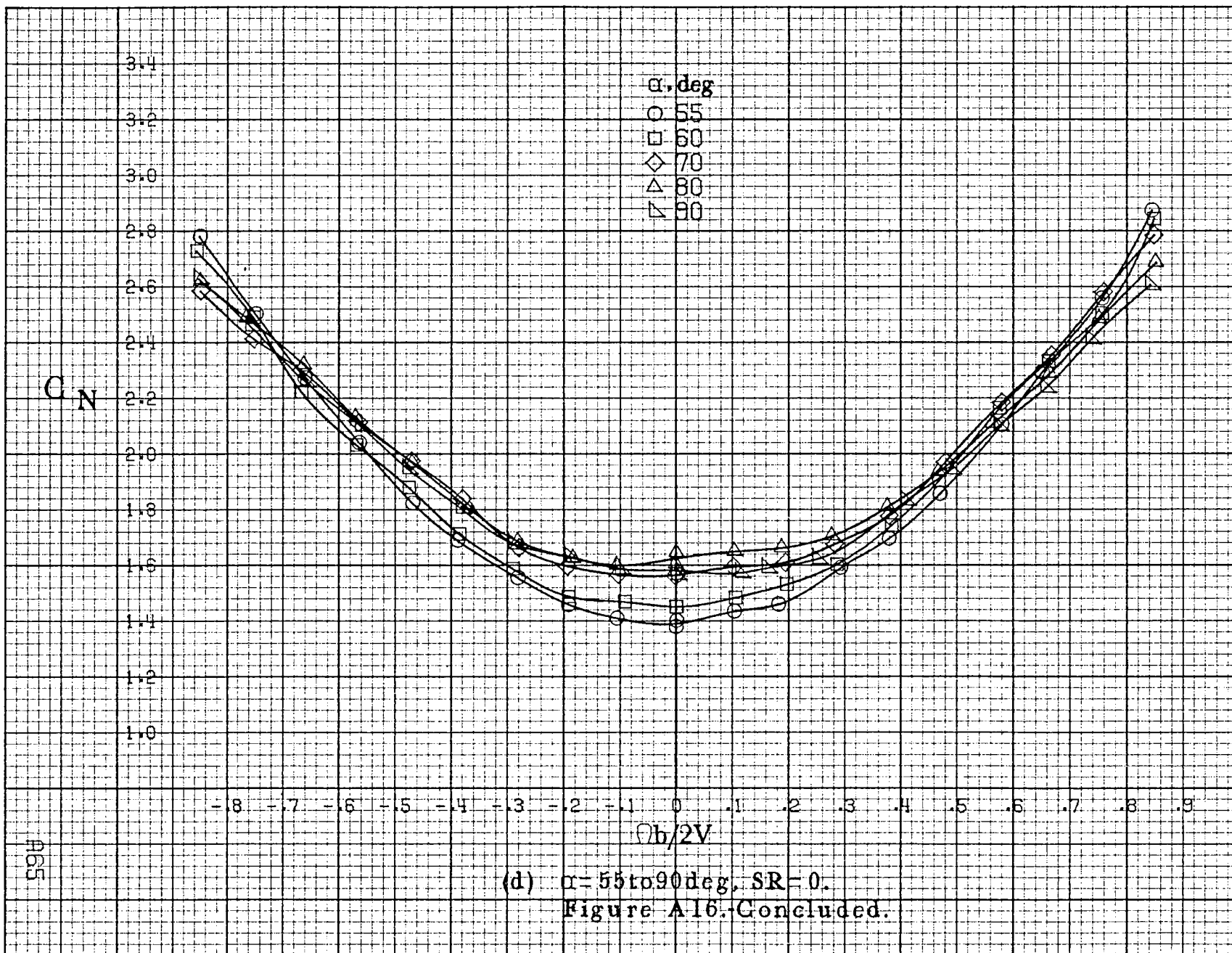
(a) $\alpha = 8$ to 16° , $SR = 76\text{cm} (80\text{in})$.

Figure A16. Effect of rotation rate and angle of attack on normal force coefficient for basic configuration. $\delta_a = 15^\circ$, $\delta_s = 0^\circ$, $\delta_r = 25^\circ$, $\beta = 0^\circ$.

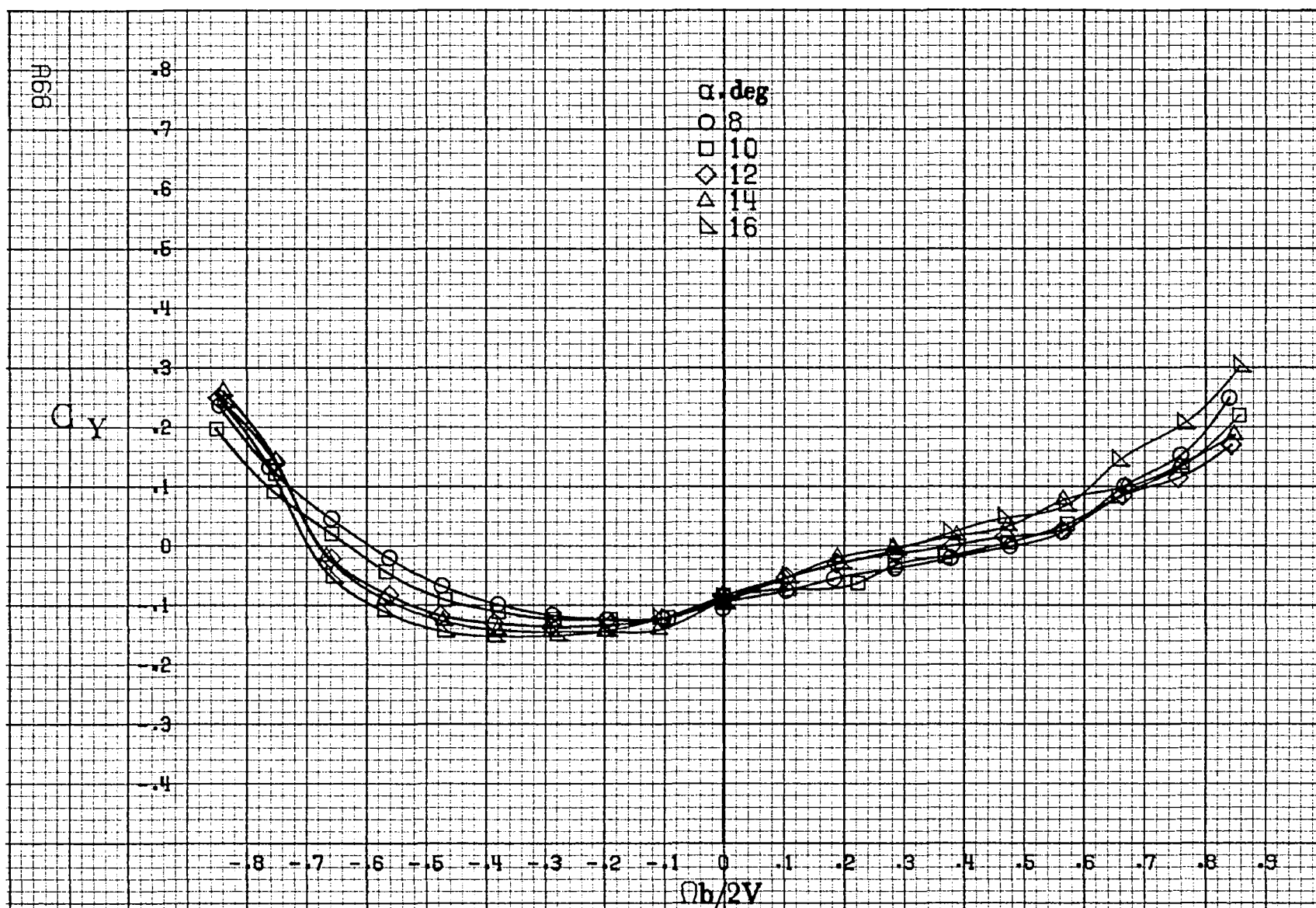




(c) $\alpha=30$ to 50 deg, $SR=0$.
Figure A16-Continued.

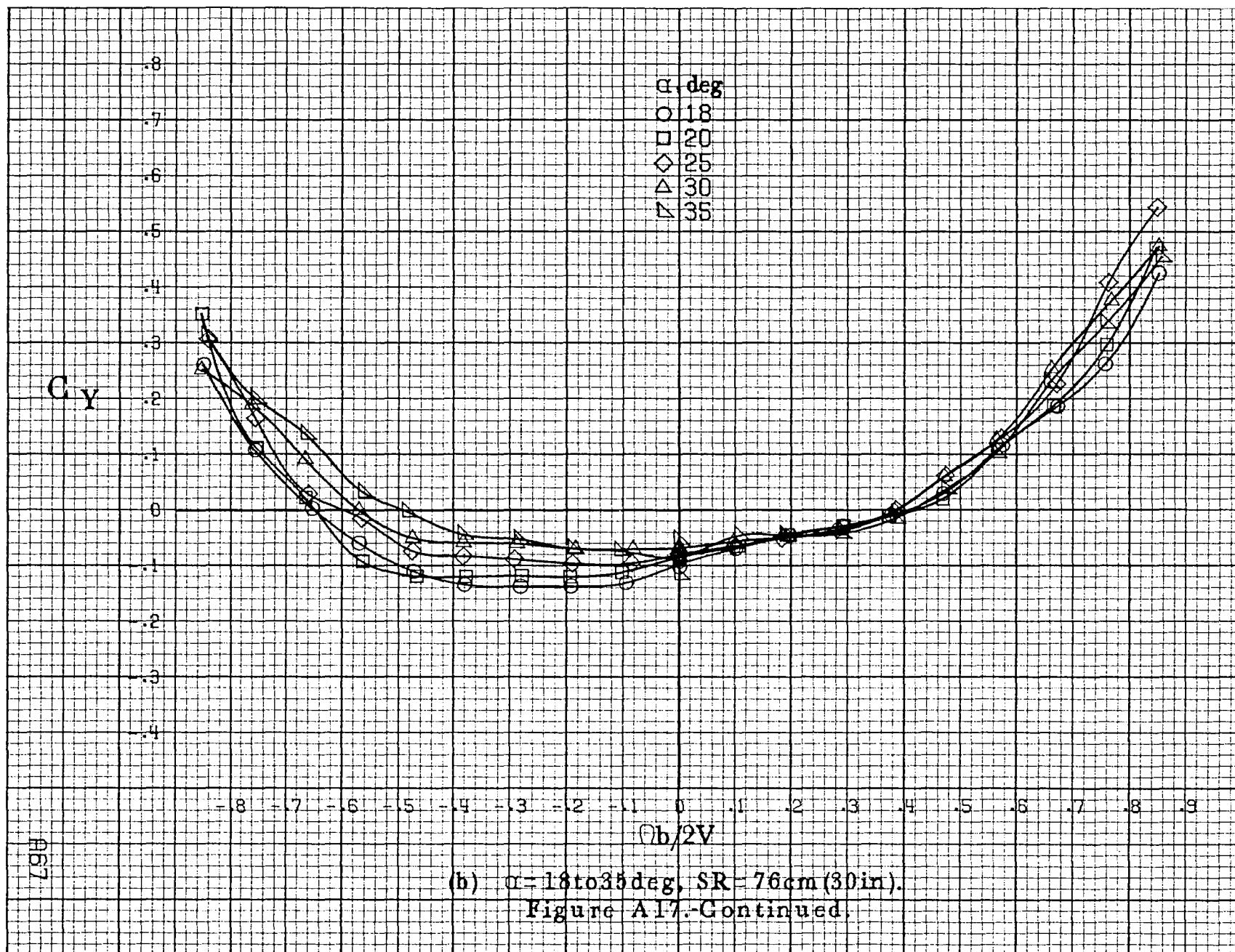


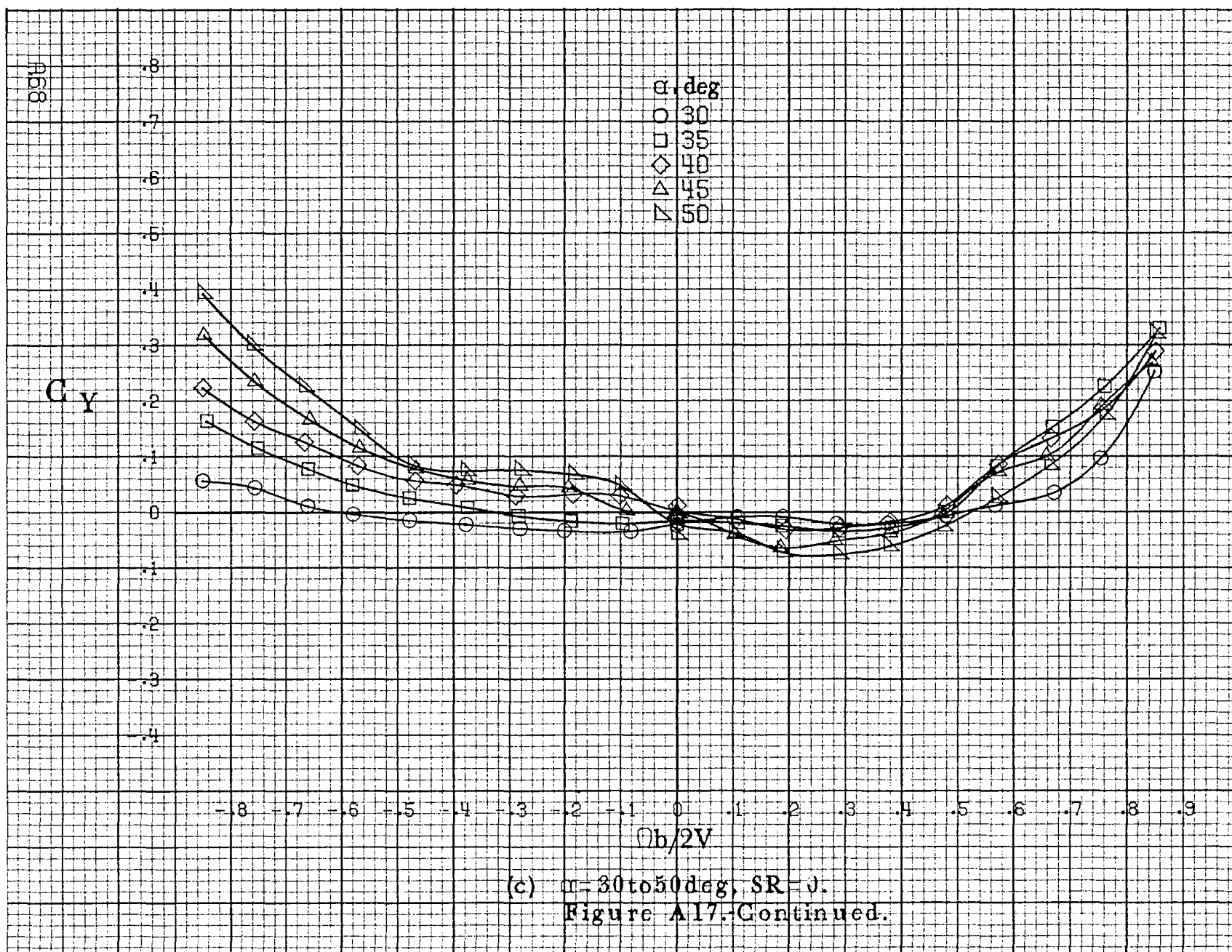
(d) $\alpha = 55$ to 90 deg, $SR = 0$.
Figure A16.-Concluded.

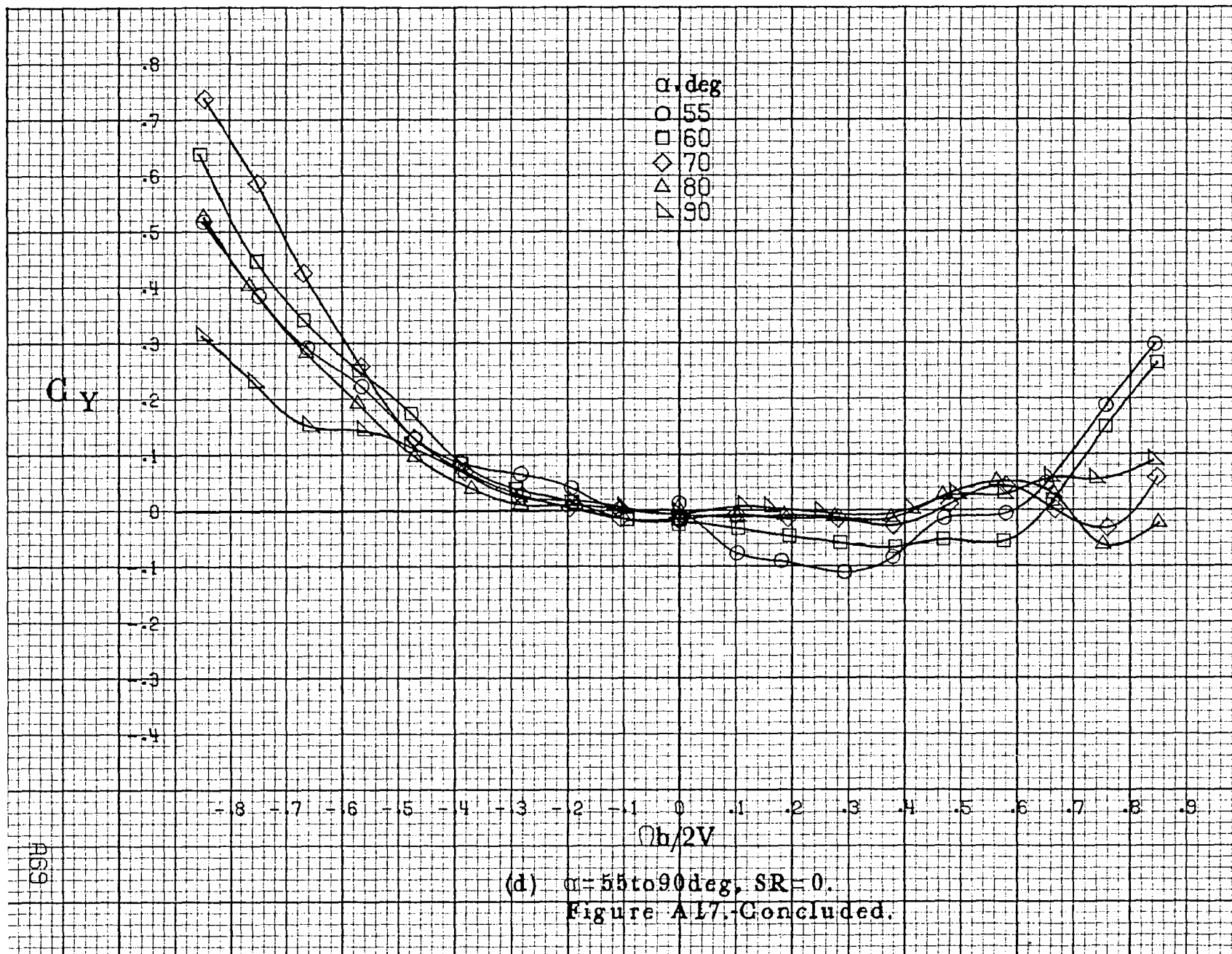


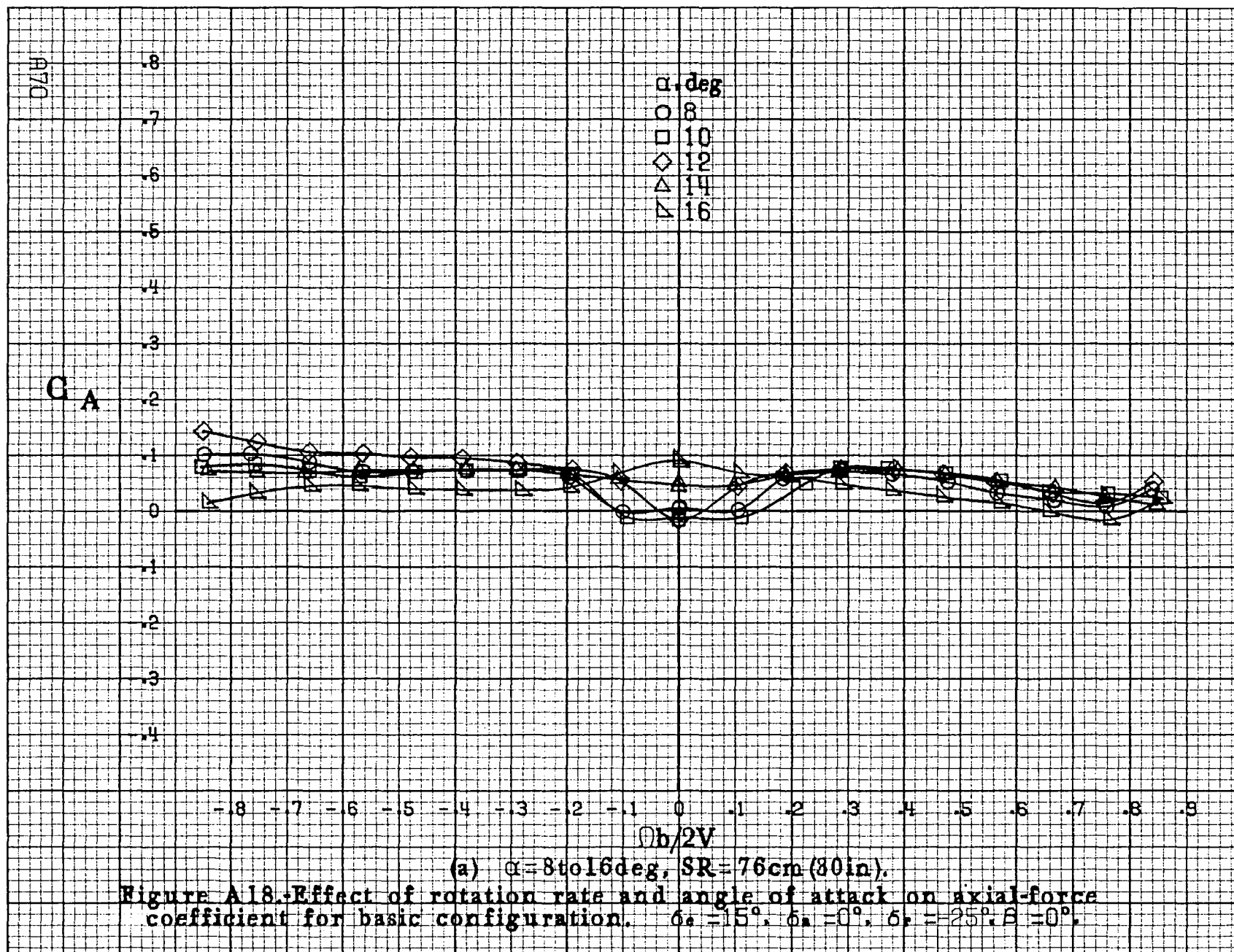
(a) $\alpha = 8$ to 16° , $SR = 76 \text{ cm (30 in.)}$.

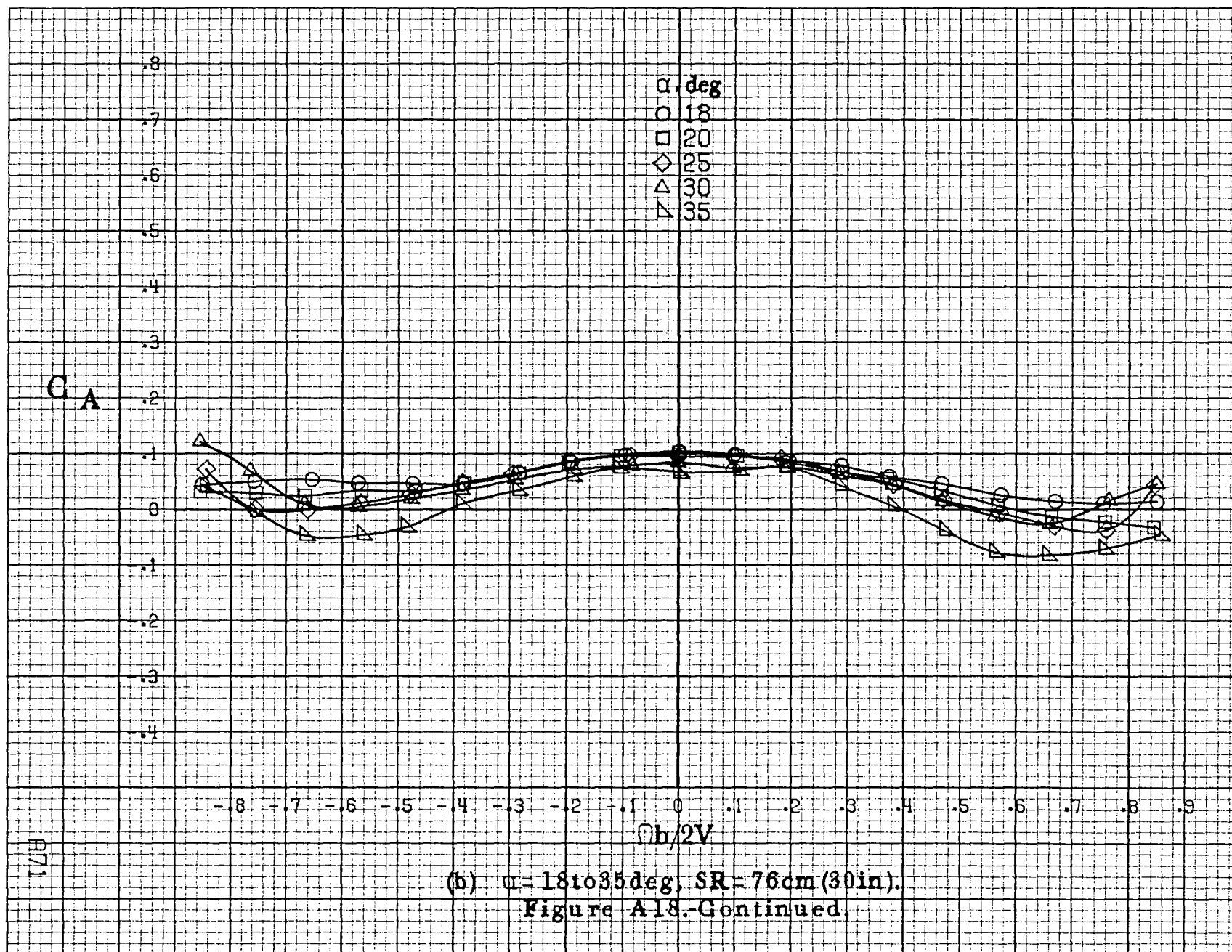
Figure A17. Effect of rotation rate and angle of attack on side-force coefficient for basic configuration. $\delta_e = 15^\circ$, $\delta_a = 0^\circ$, $\delta_r = -25^\circ$, $\beta = 0^\circ$.

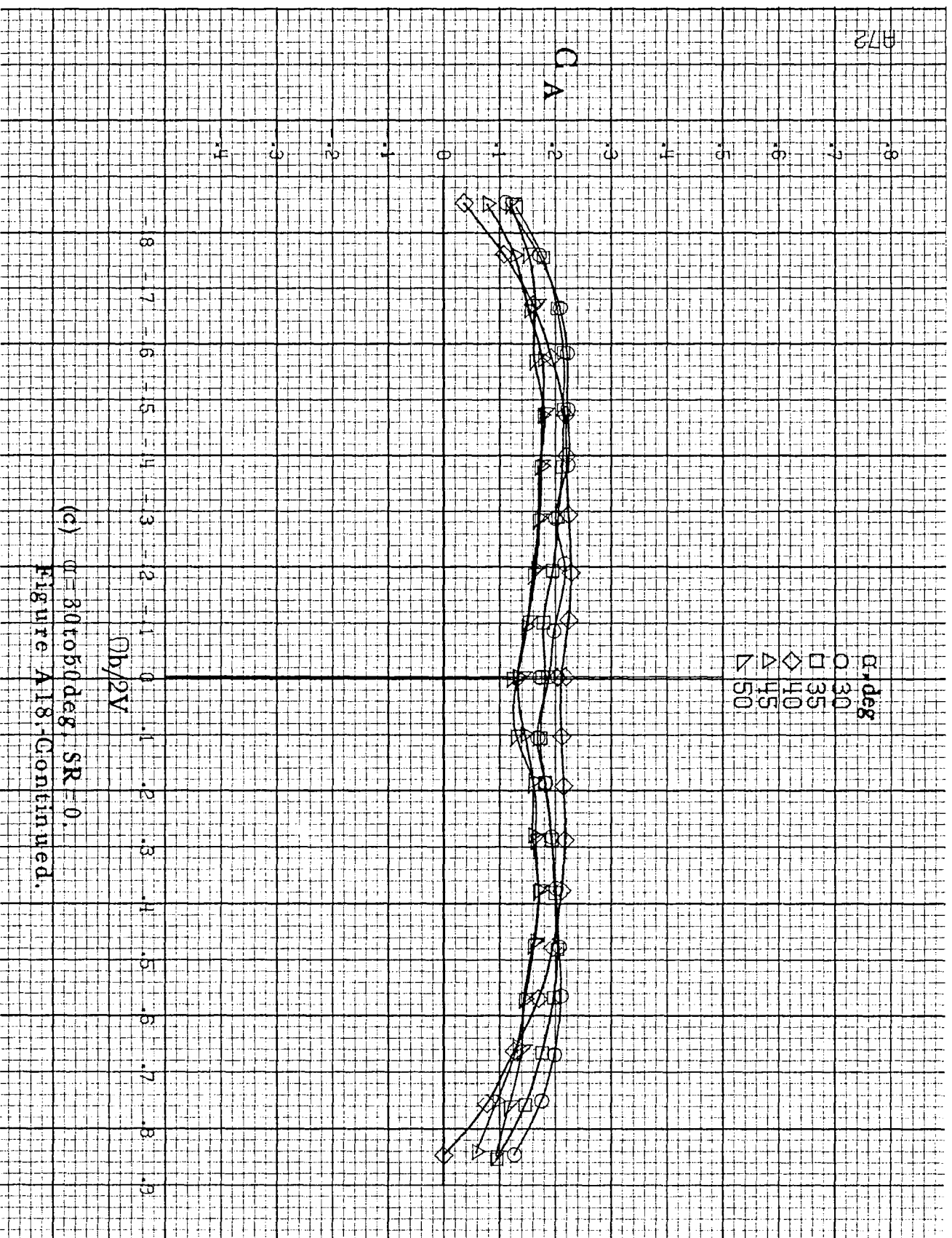


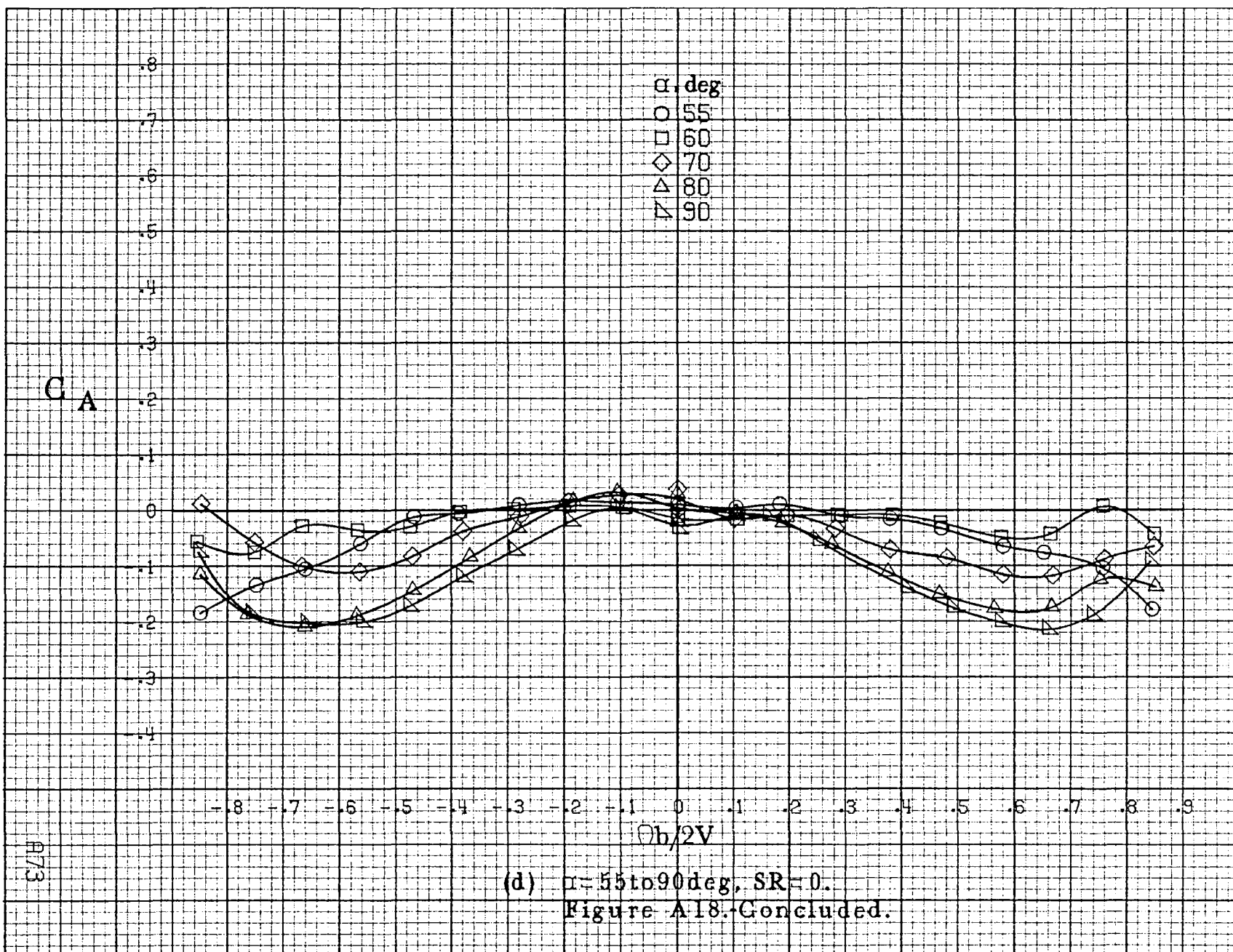


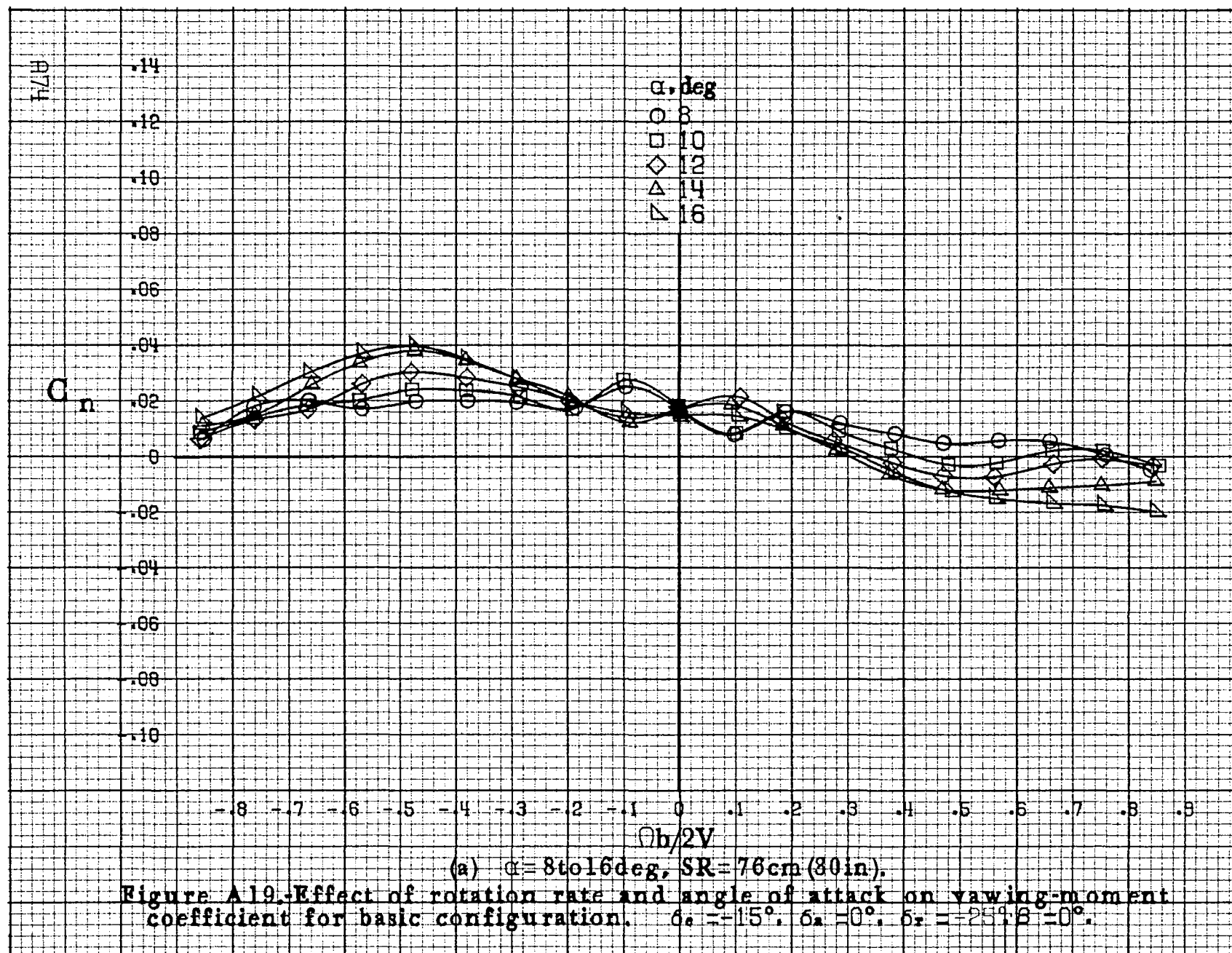


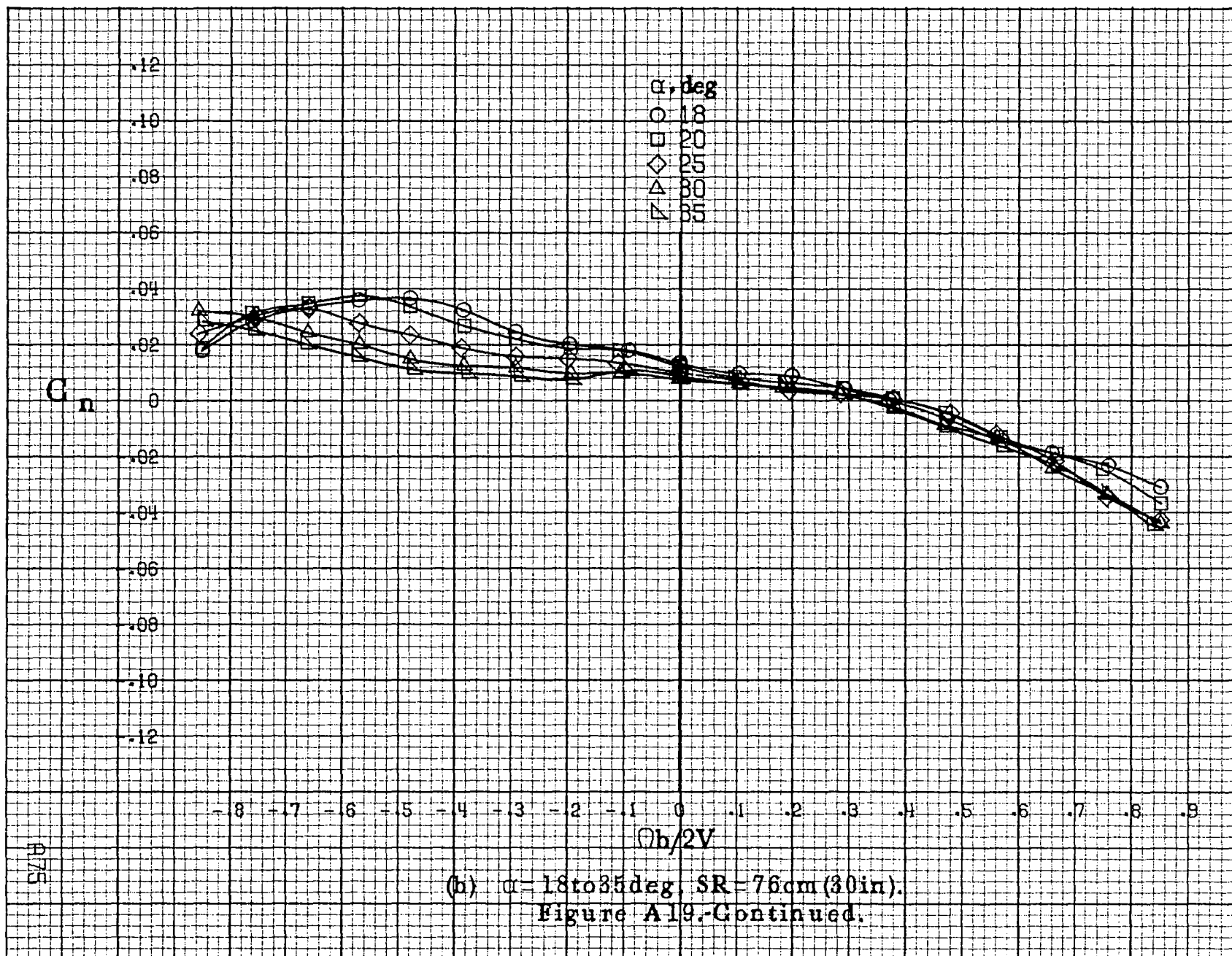


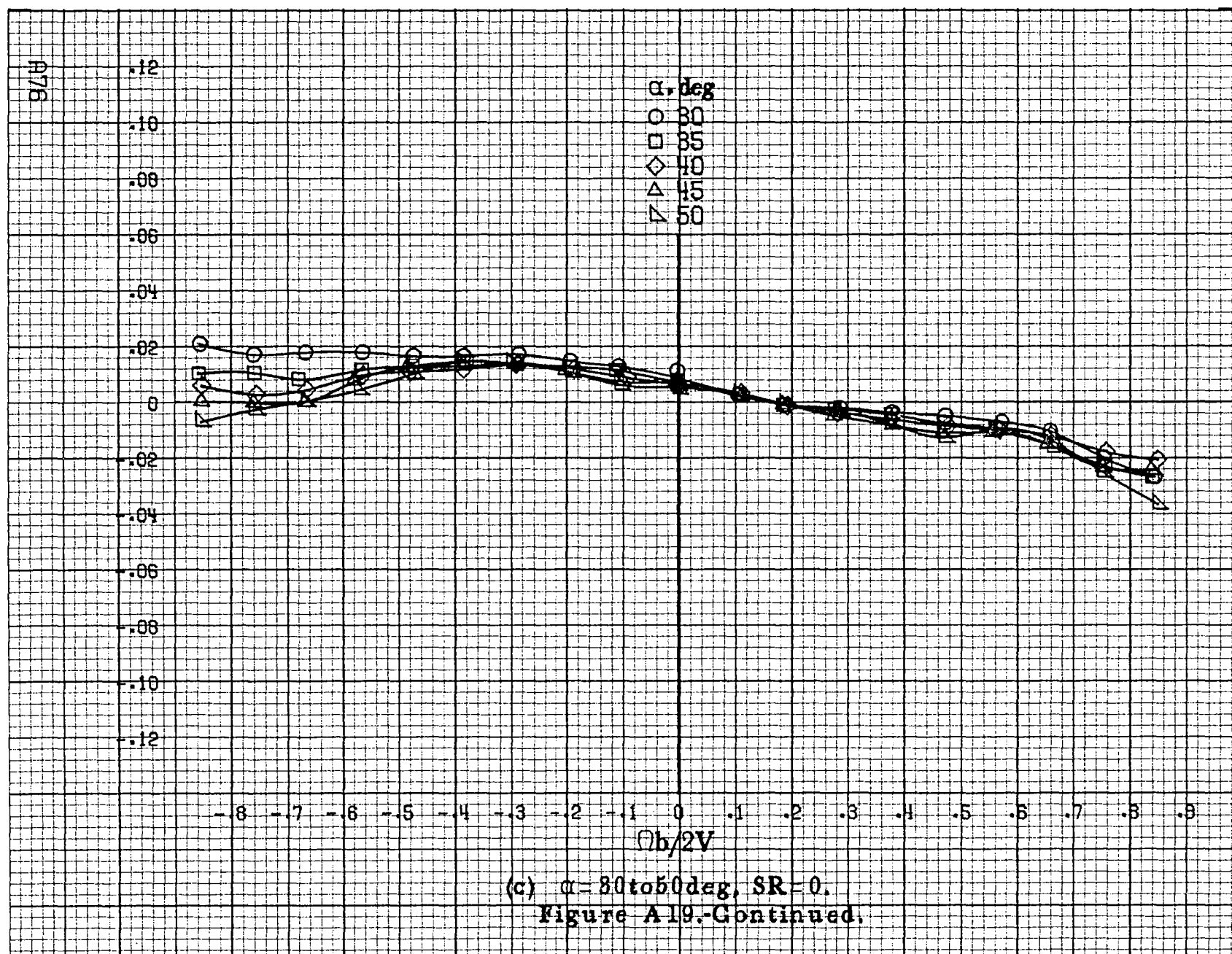


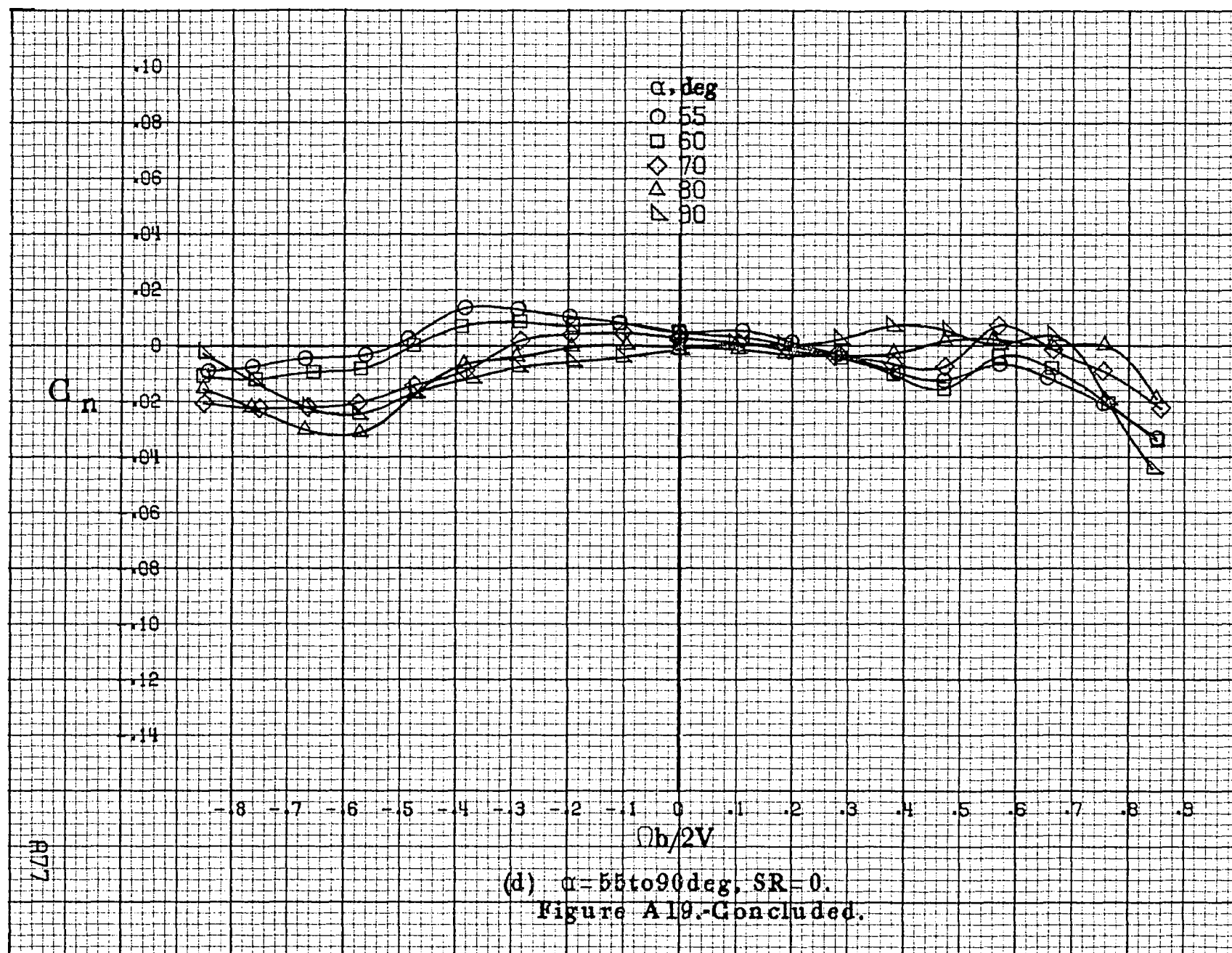


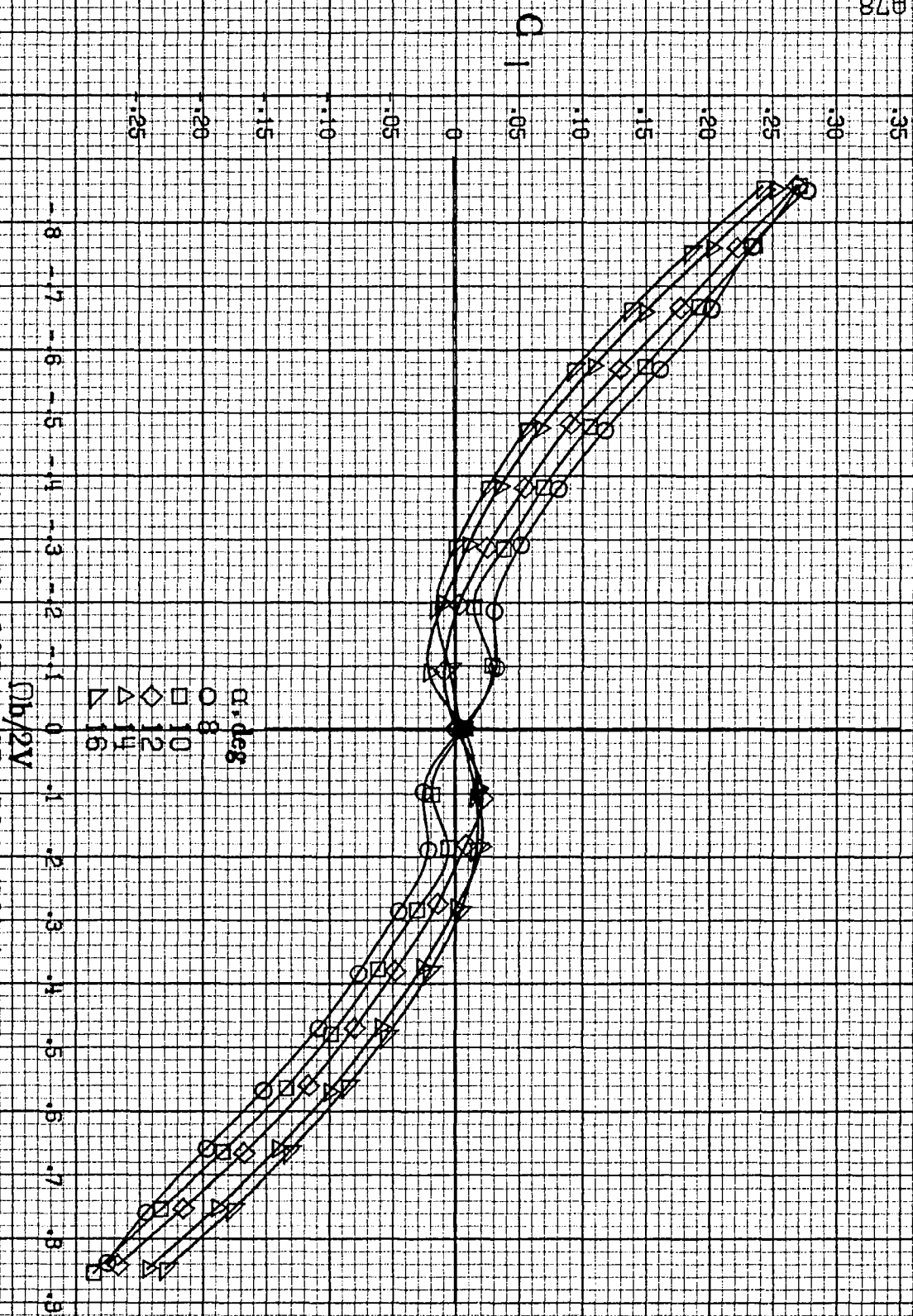




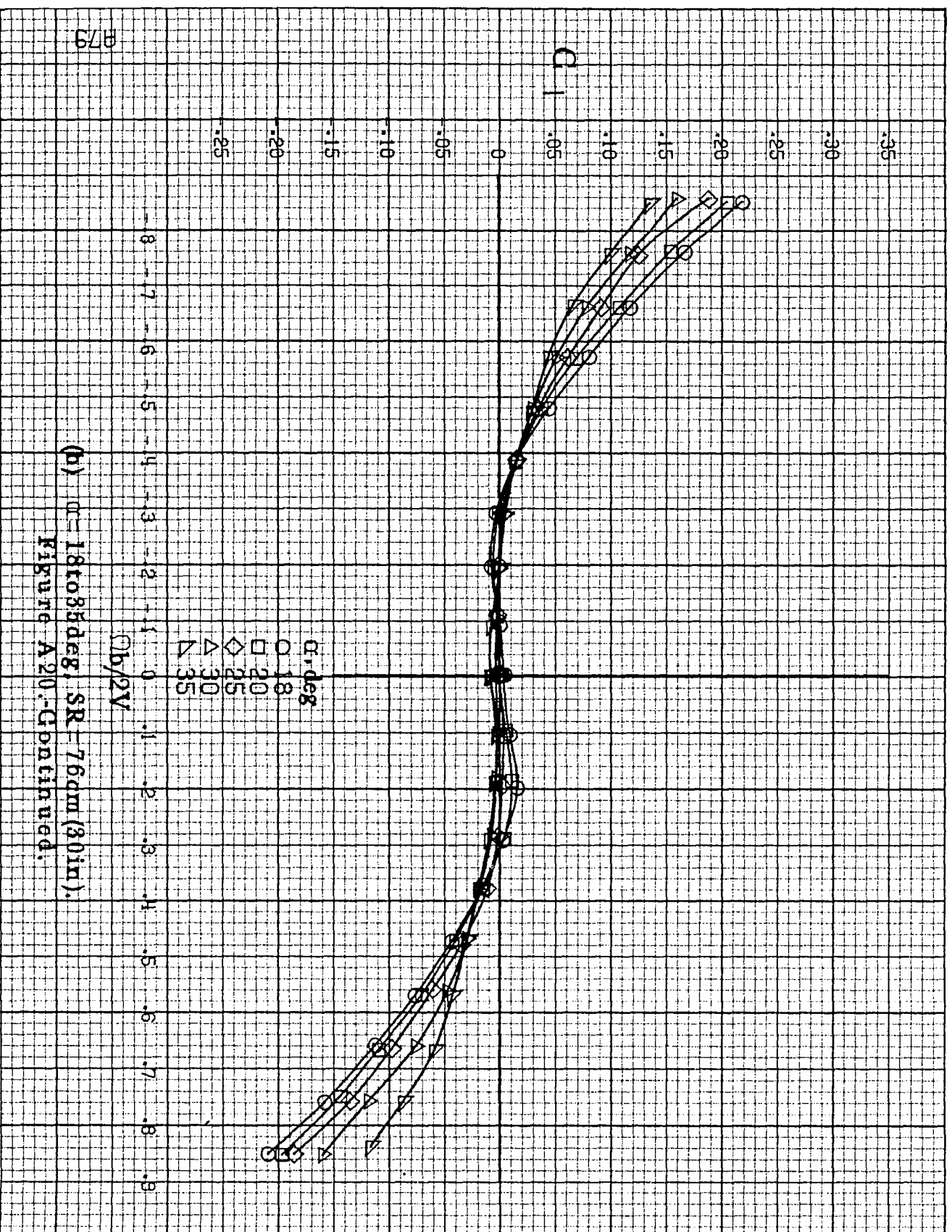




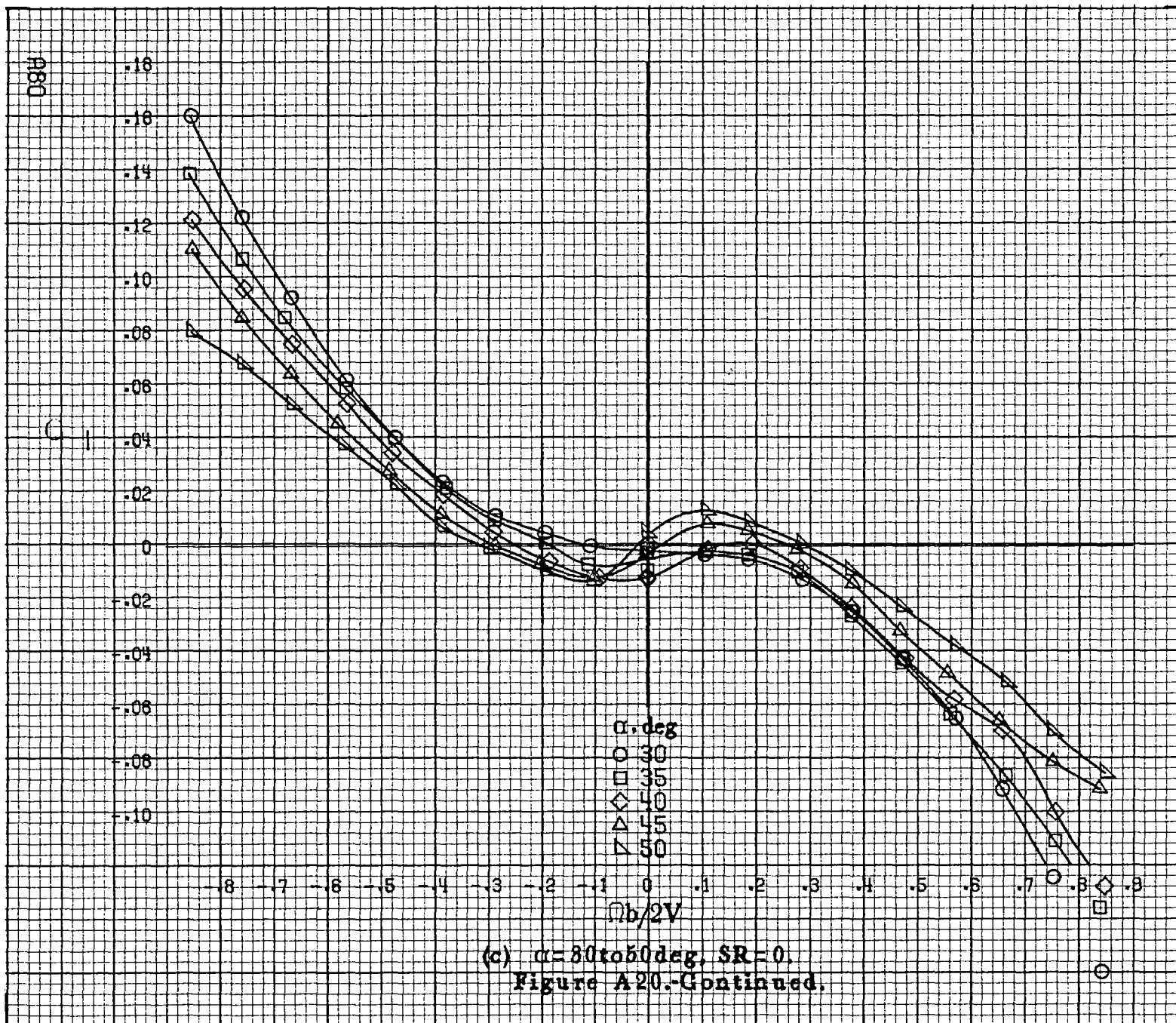


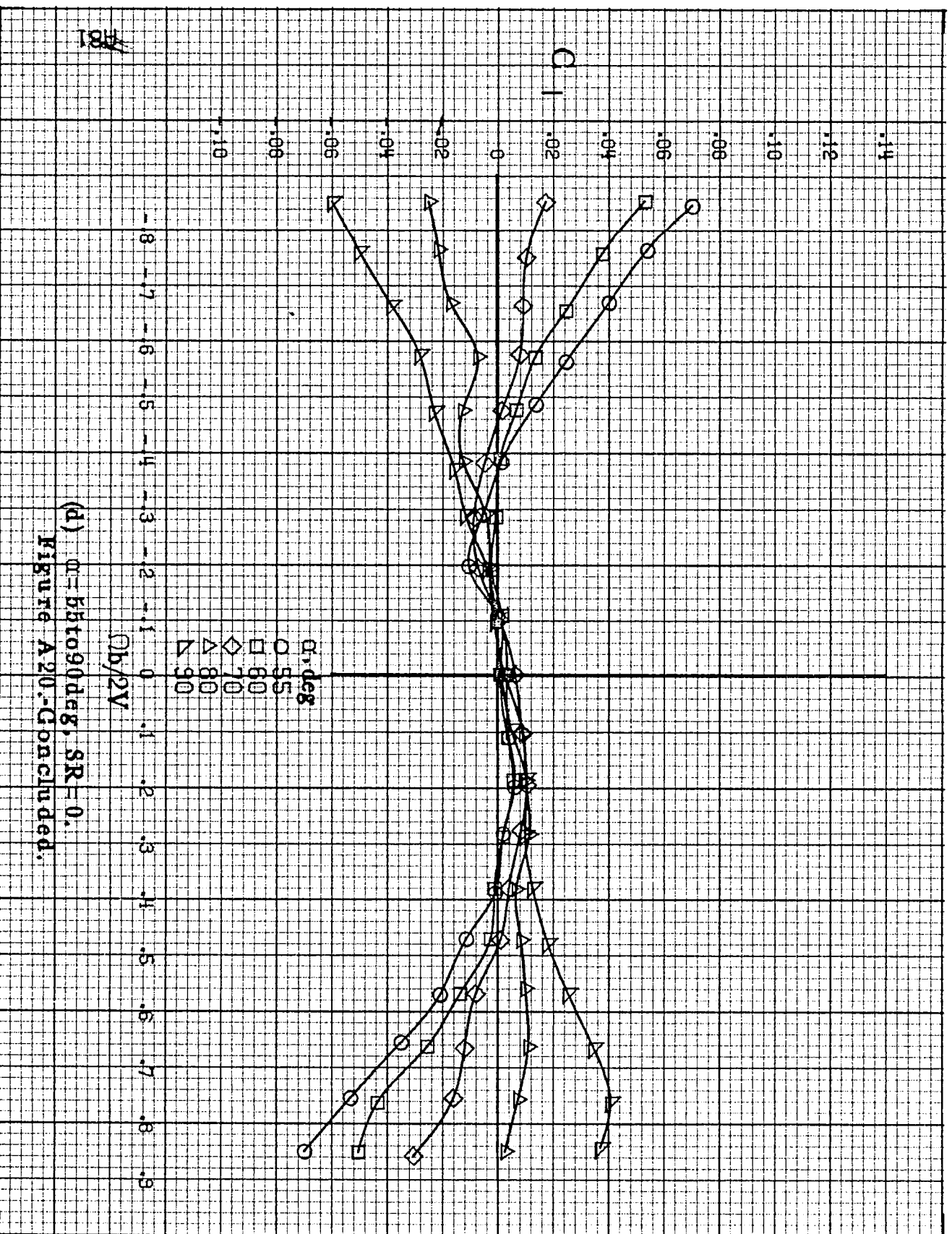


(a) $\alpha = 8$ to 16° , $SR = 76$ cm (30 in).
 Figure A20. Effect of rotation rate and angle of attack on rolling-moment coefficient for basic configuration. $\delta_e = -15^\circ$, $\delta_a = 0^\circ$, $\delta_r = -25^\circ$, $\delta = 0^\circ$.



(b) $\alpha = 18$ to 35 deg, SR = 76 gm (30 in).
Figure A20.-Continued.





(d) $\alpha = 55$ to 90 deg, $SR = 0$.
Figure A20.-Concluded.

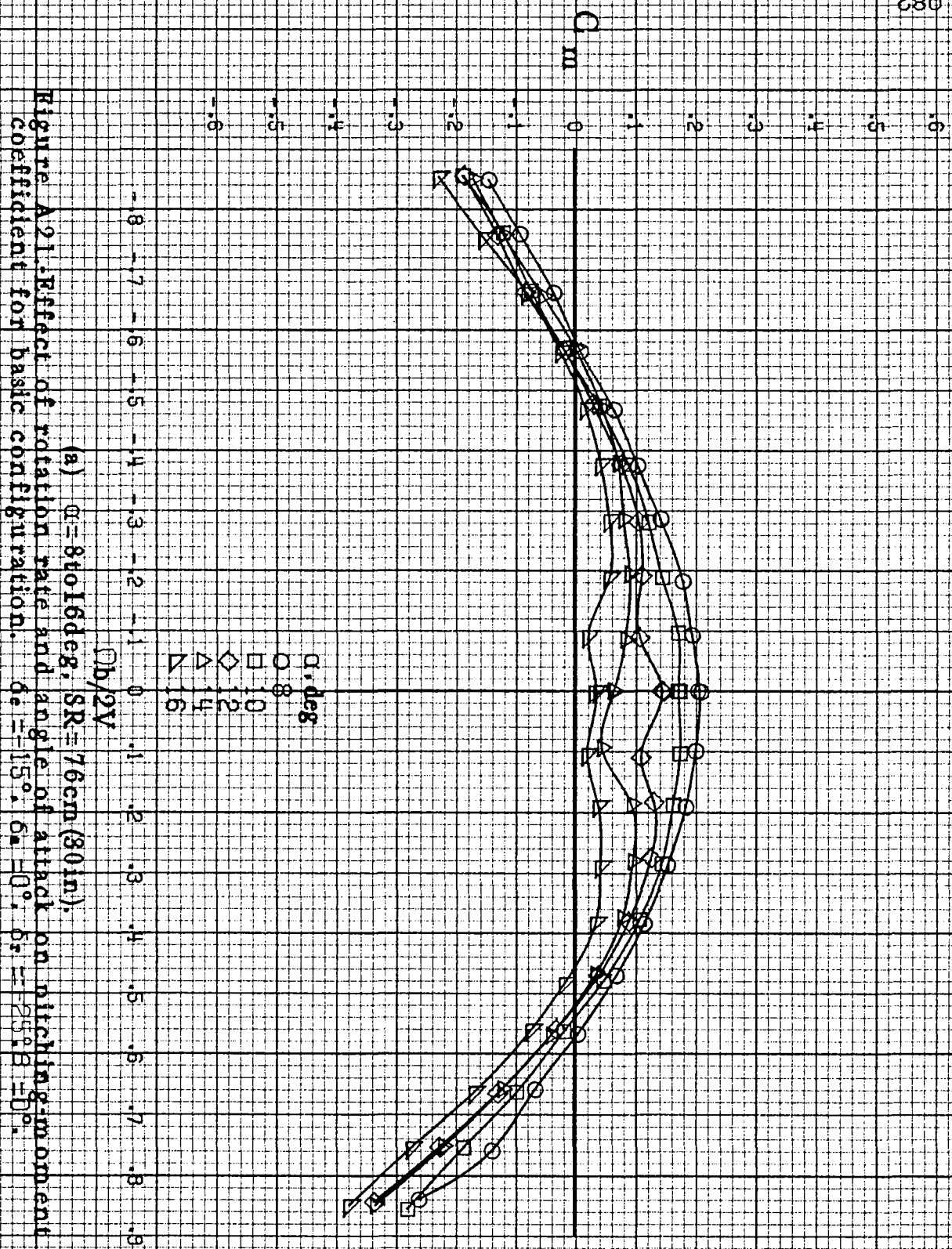
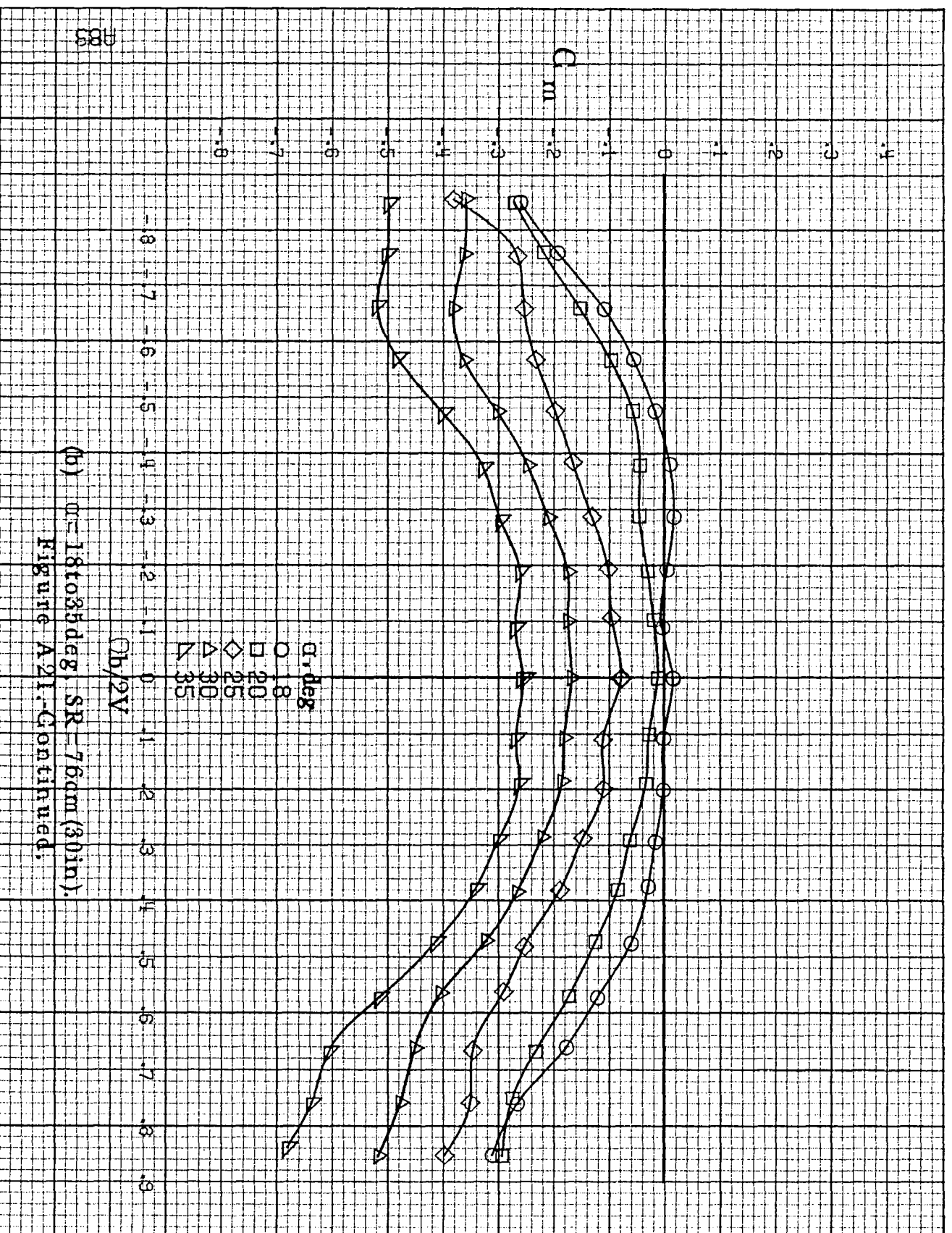
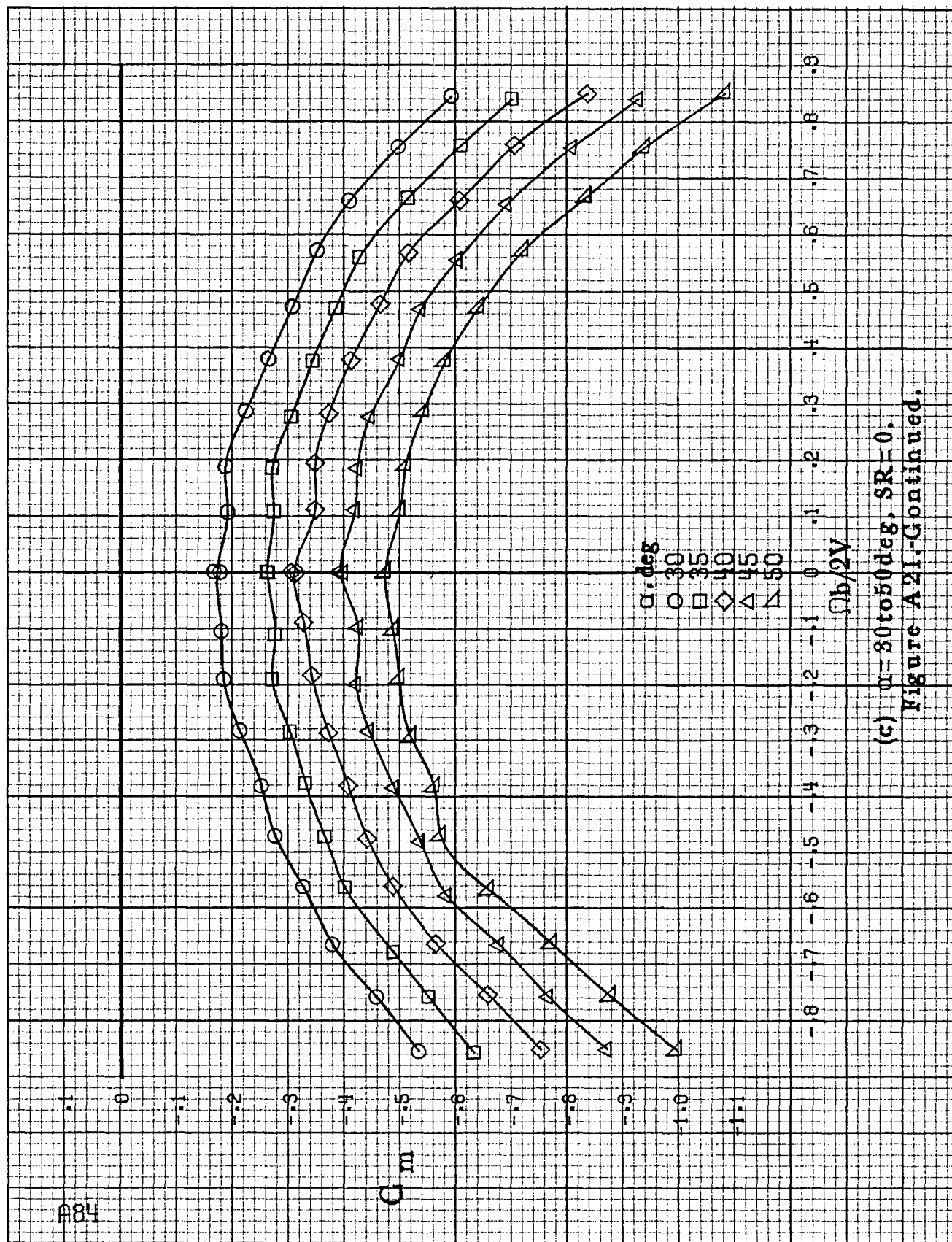


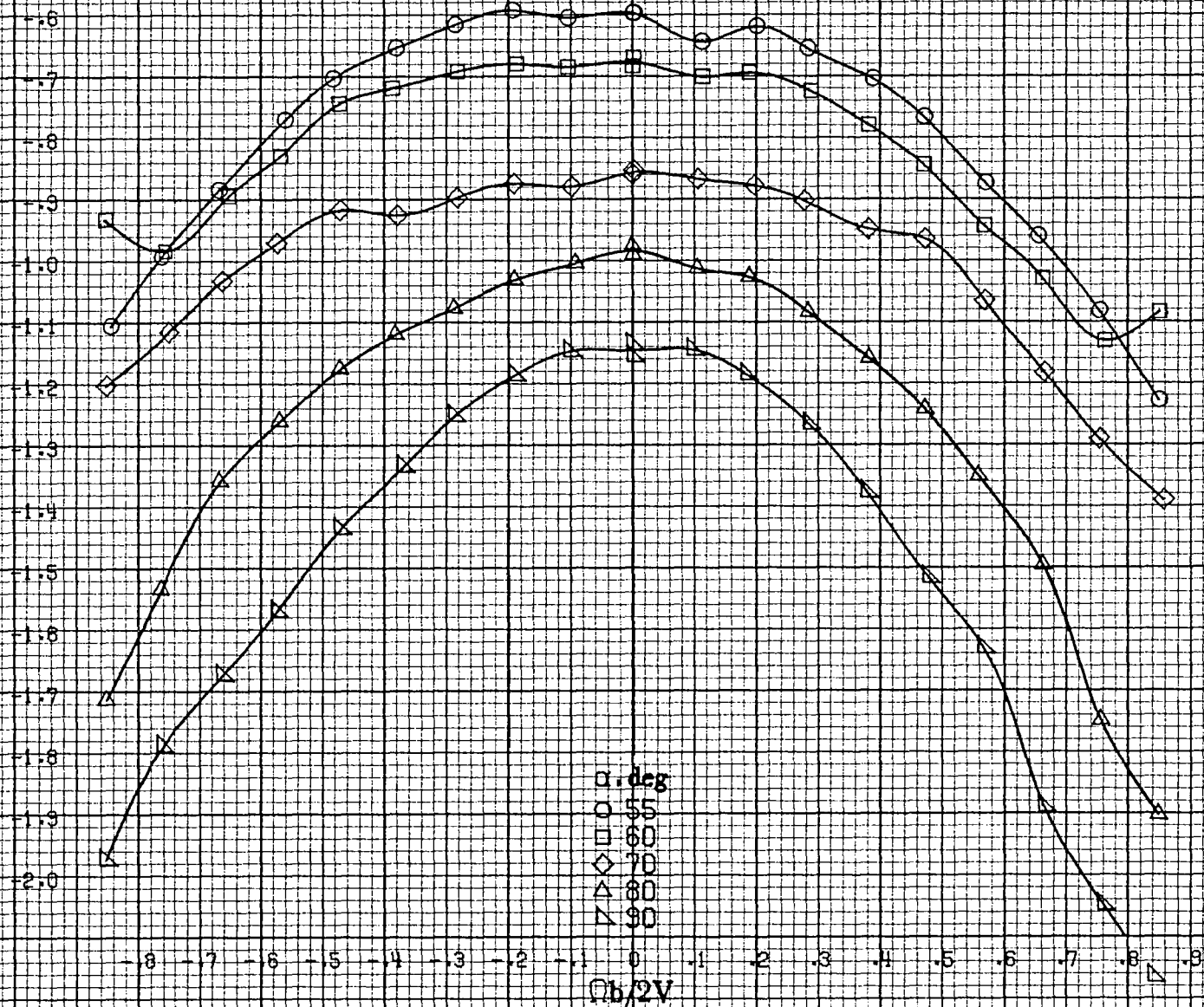
Figure A21. Effect of rotation rate and angle of attack on pitching moment coefficient for basic configuration. $\alpha = -15^\circ$, $\Omega_b = 0^\circ$, $\delta = -25.25^\circ$.



(b) $\omega = 181035 \text{ deg}$, $SR = 76 \text{ cm (30 in.)}$.
Figure A21. Continued.



C_m



(d) $\alpha=55$ to 90 deg. $SR=0$.
Figure A21-Concluded.

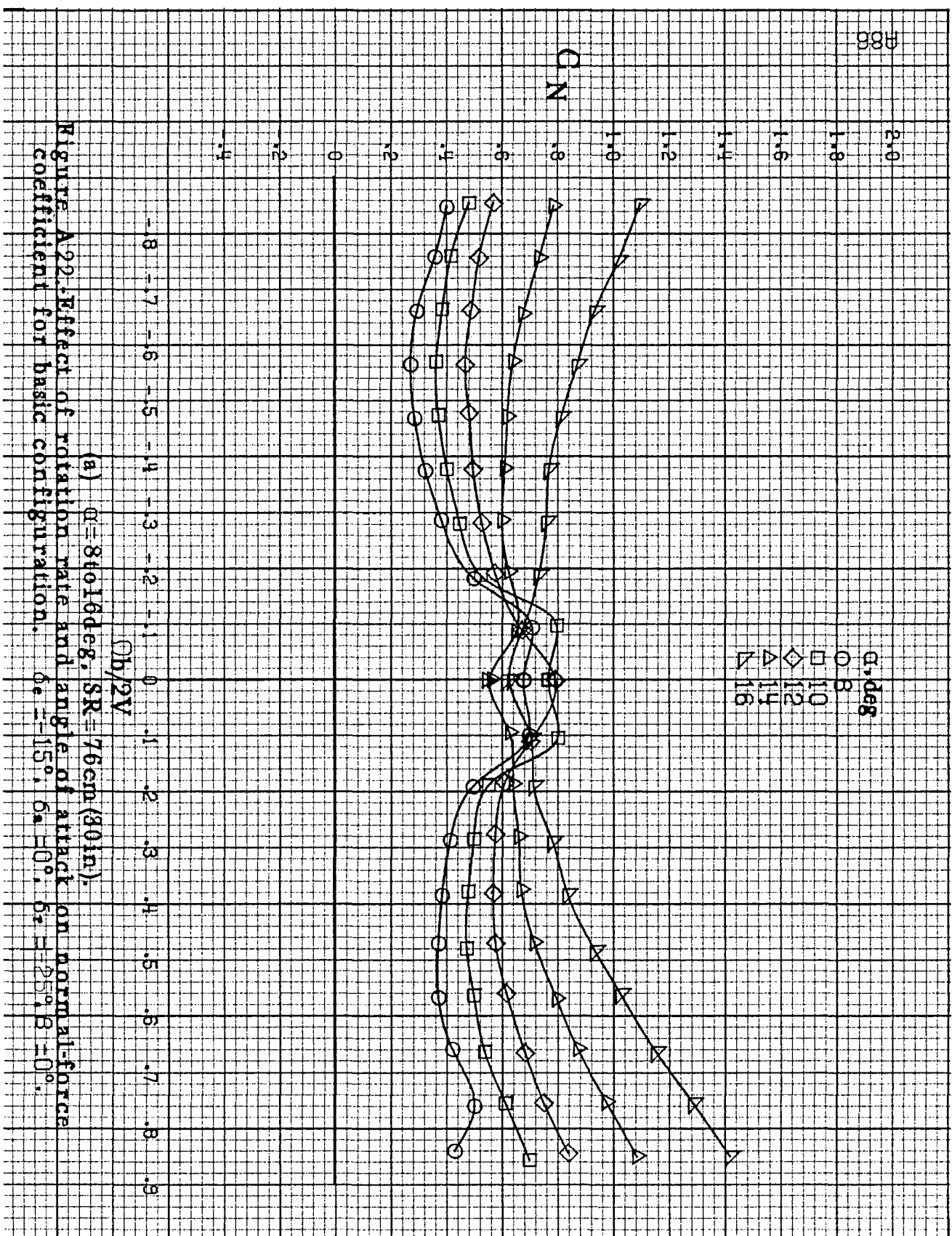
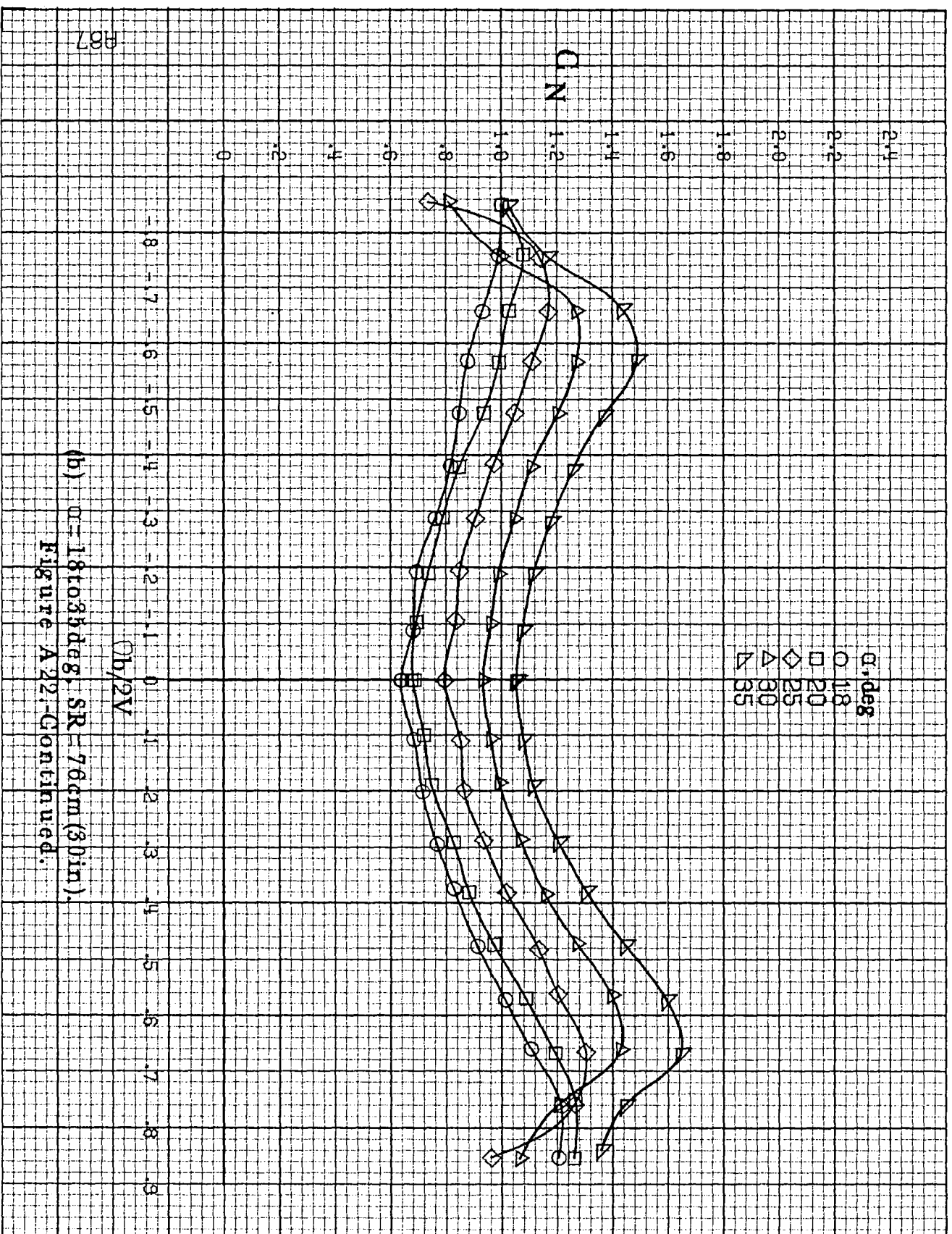
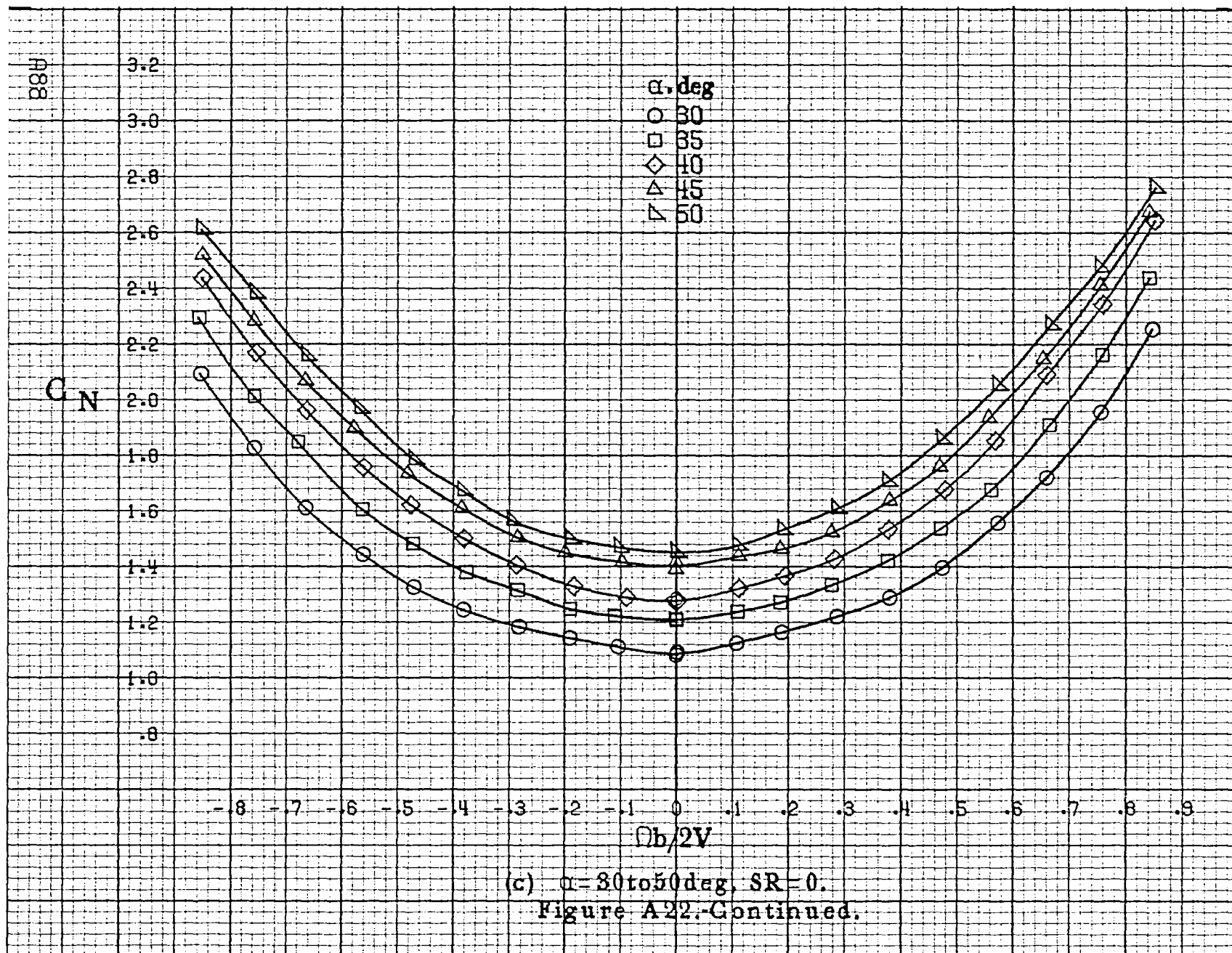
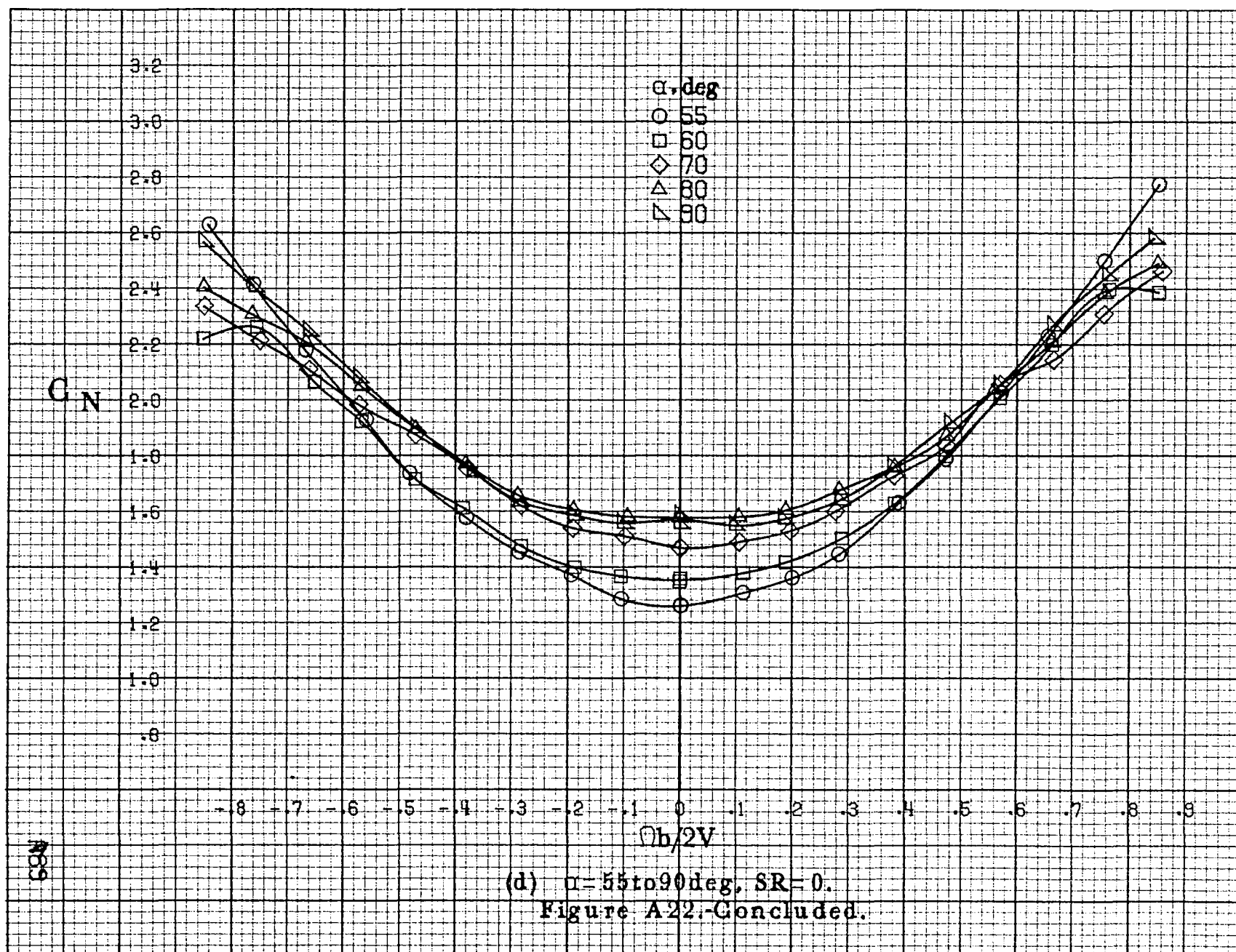
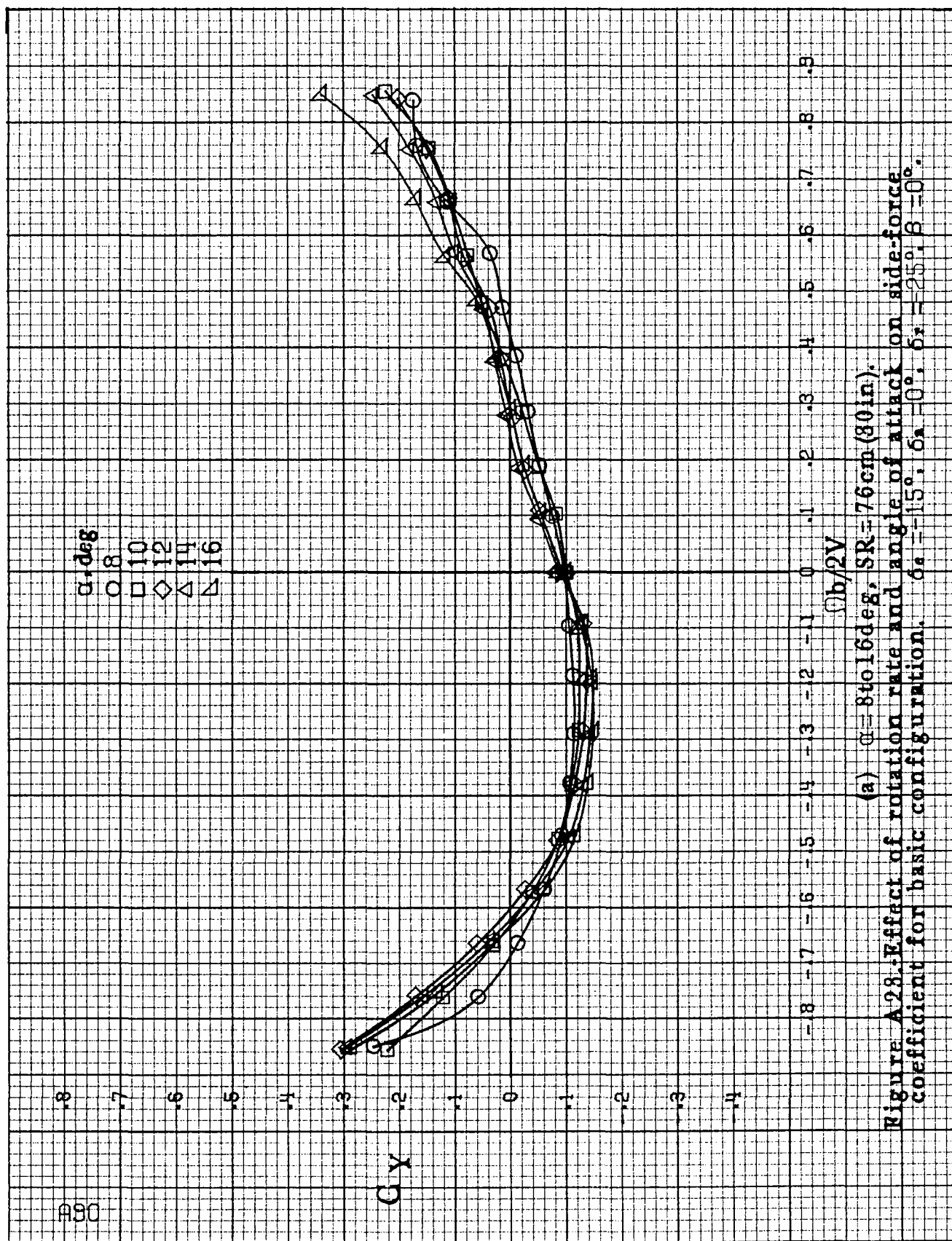


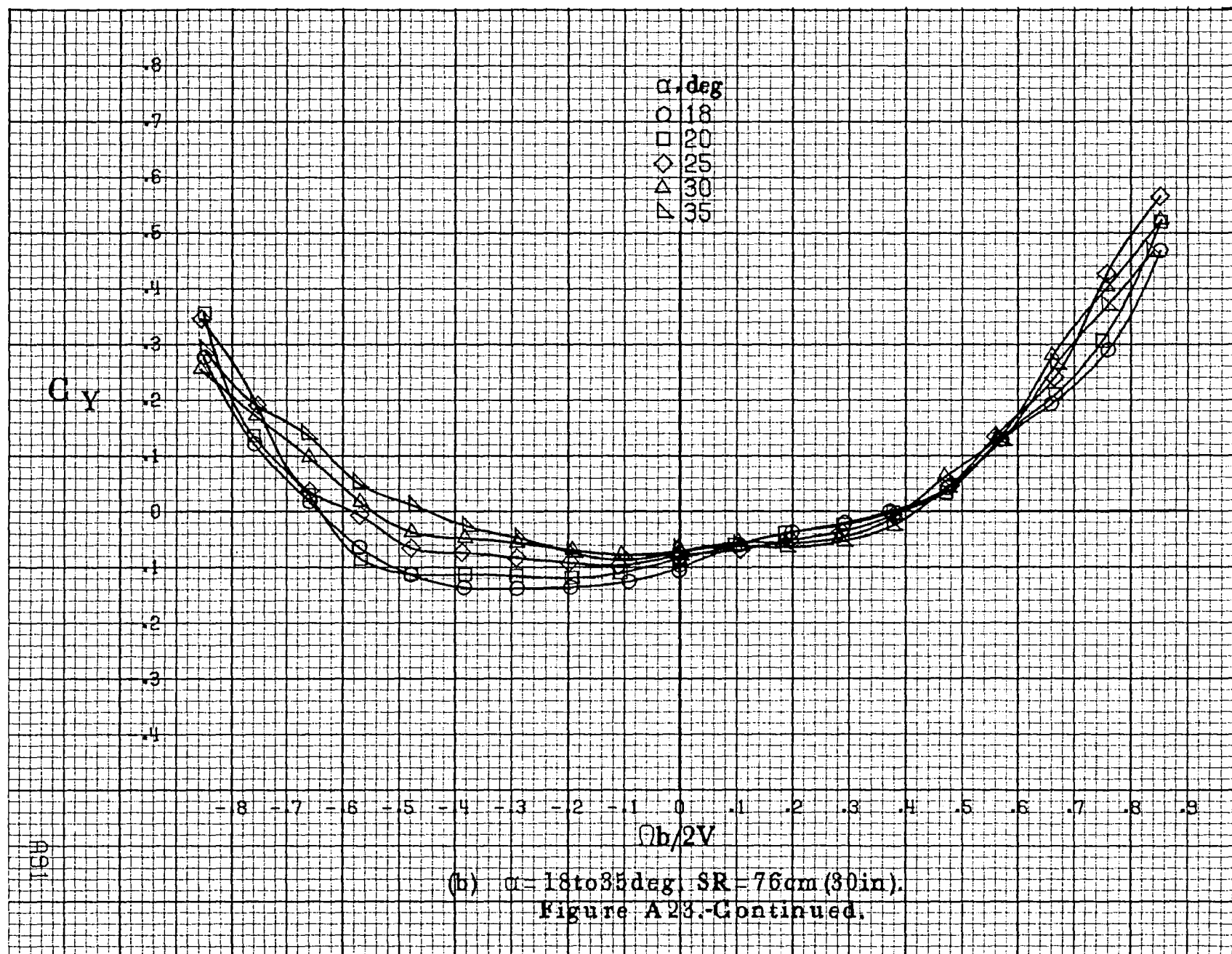
Figure A22. Effect of rotation rate and angle of attack on normal-force coefficient for basic configuration. $\alpha = 8^\circ, 10^\circ, 12^\circ, 14^\circ, 16^\circ$.

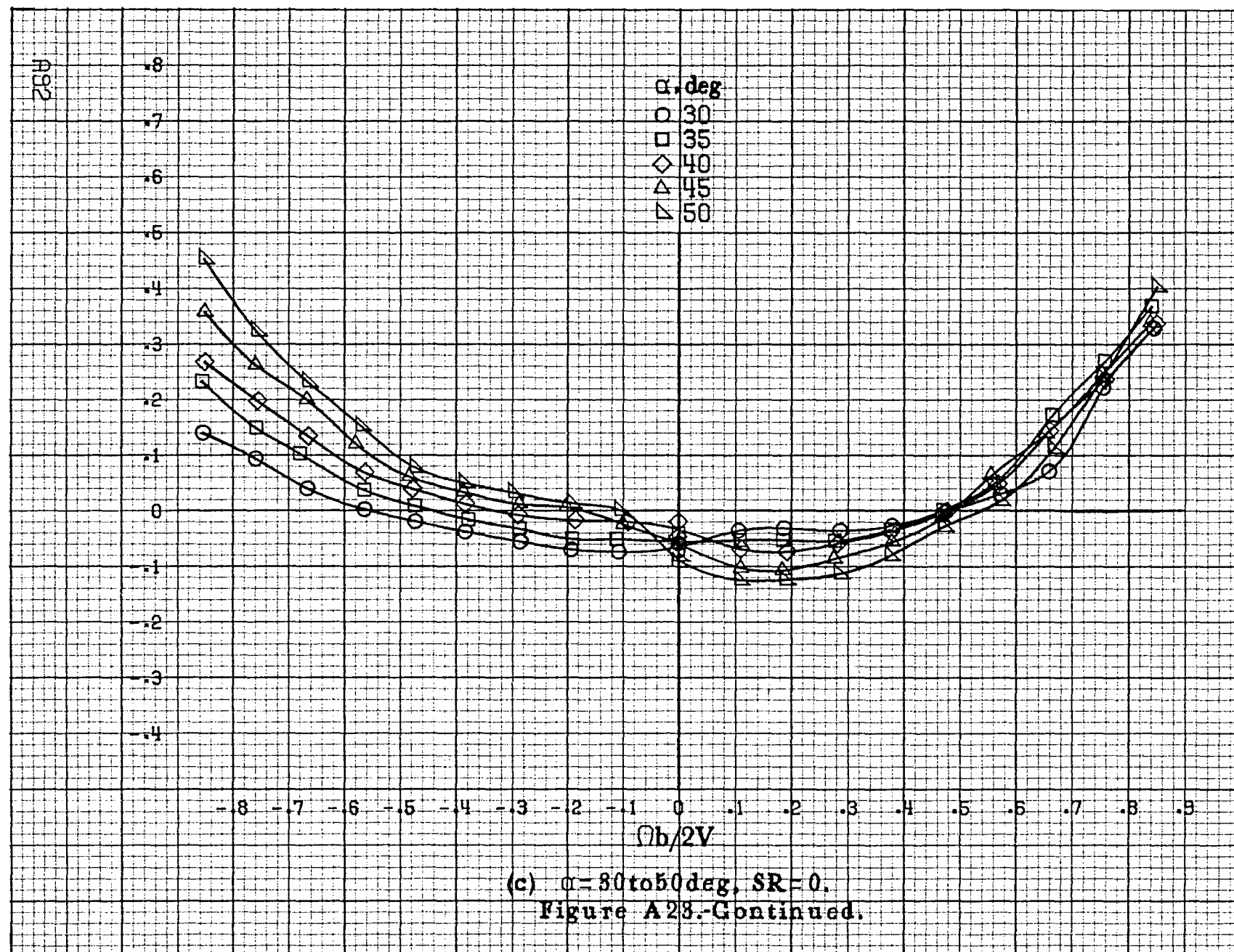


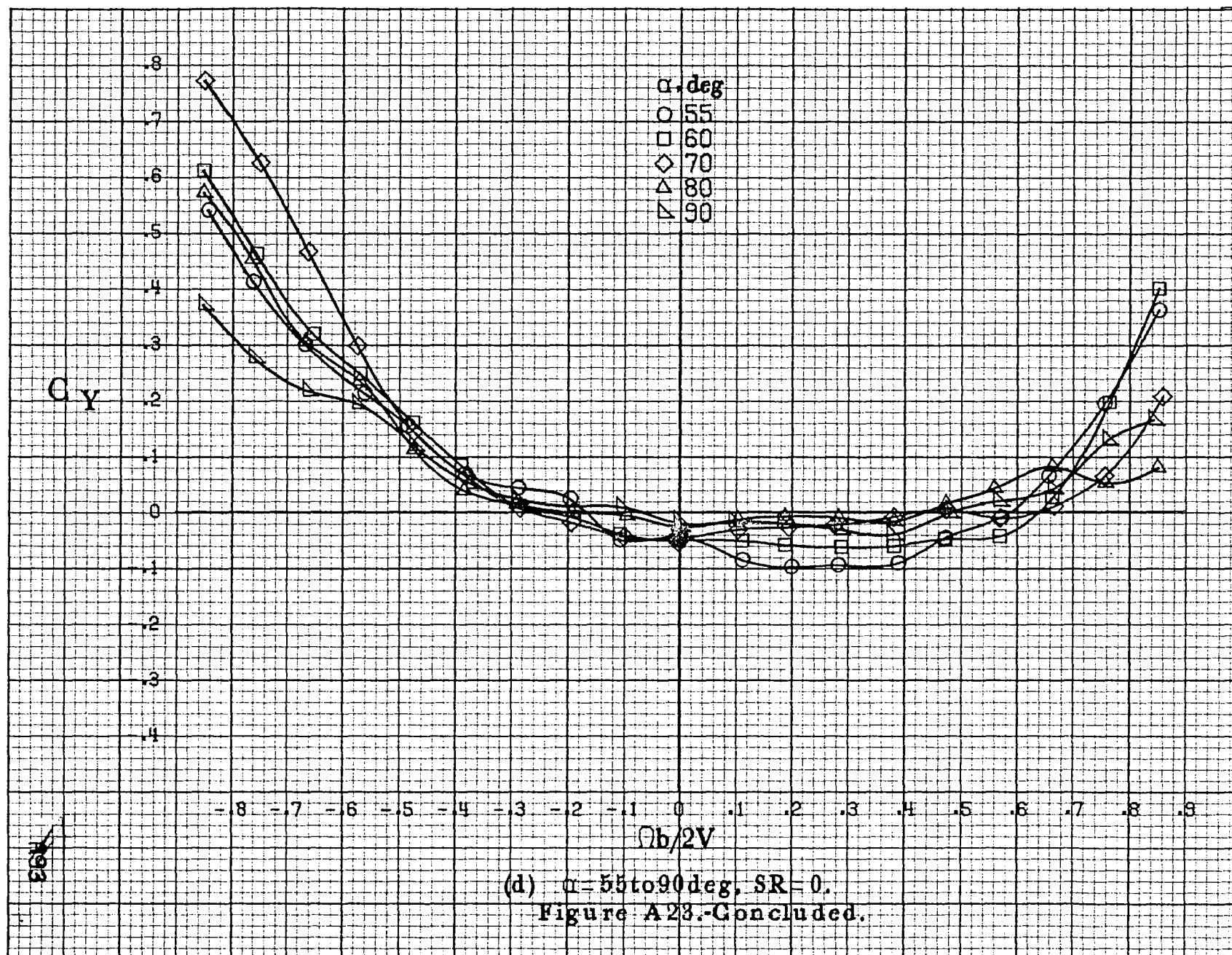


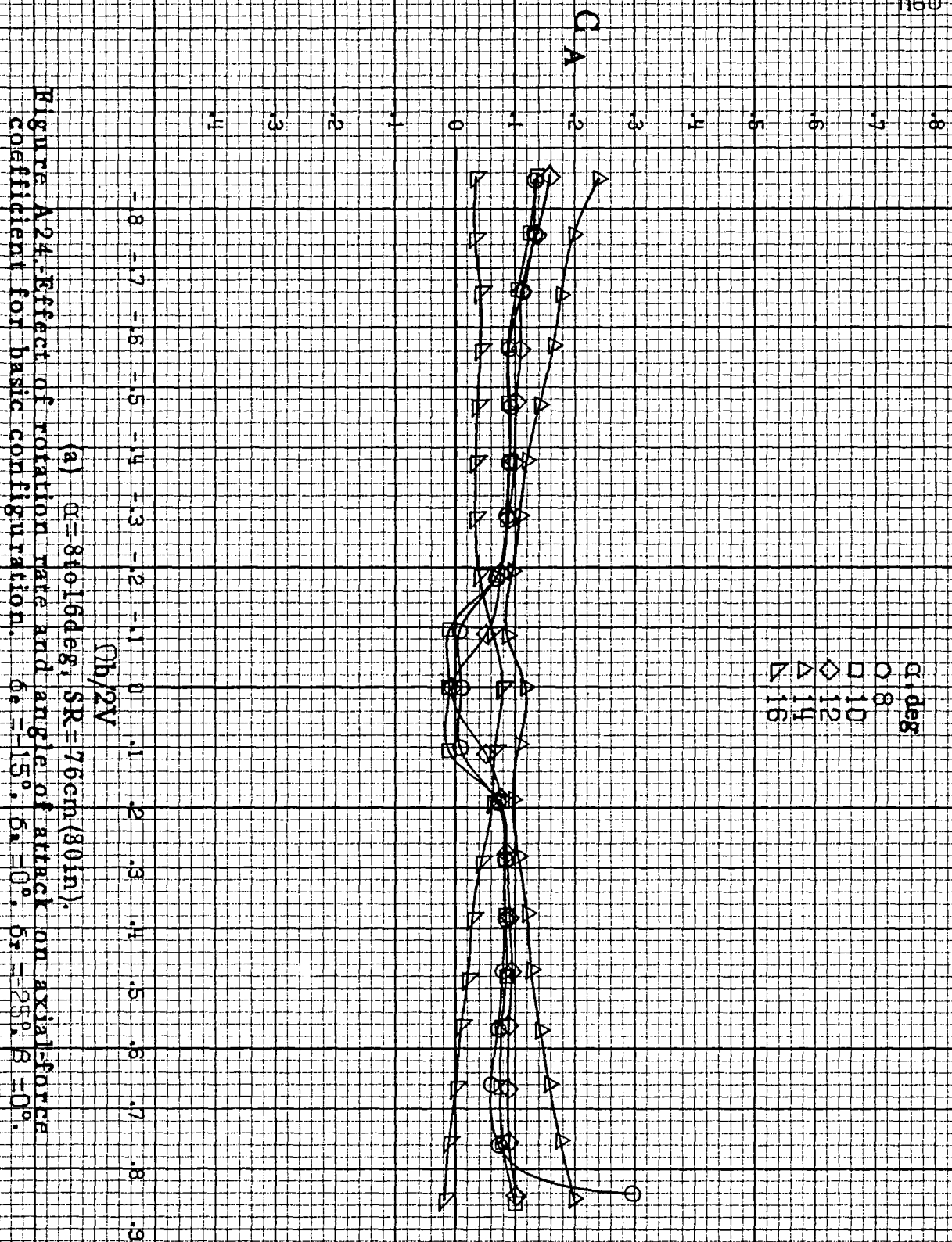


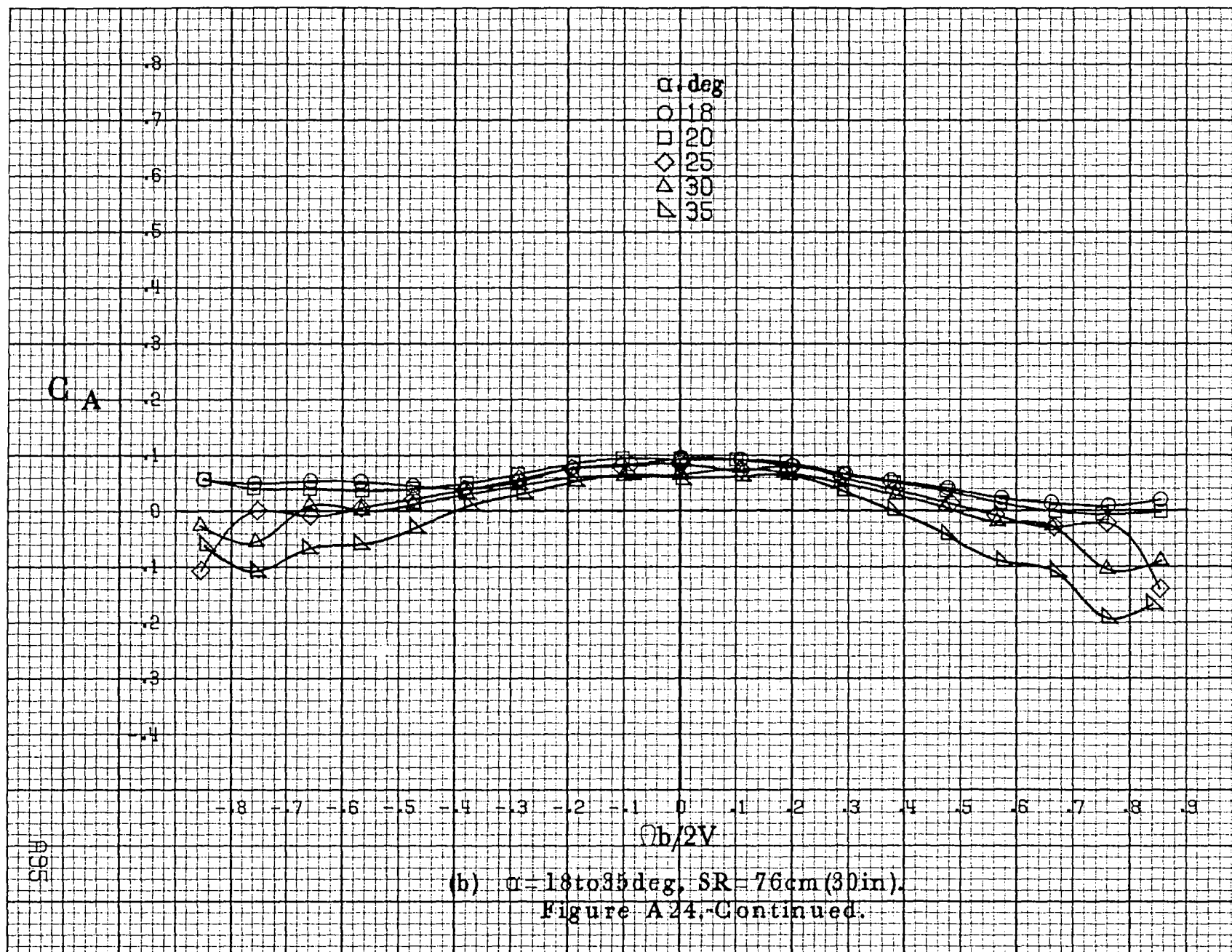


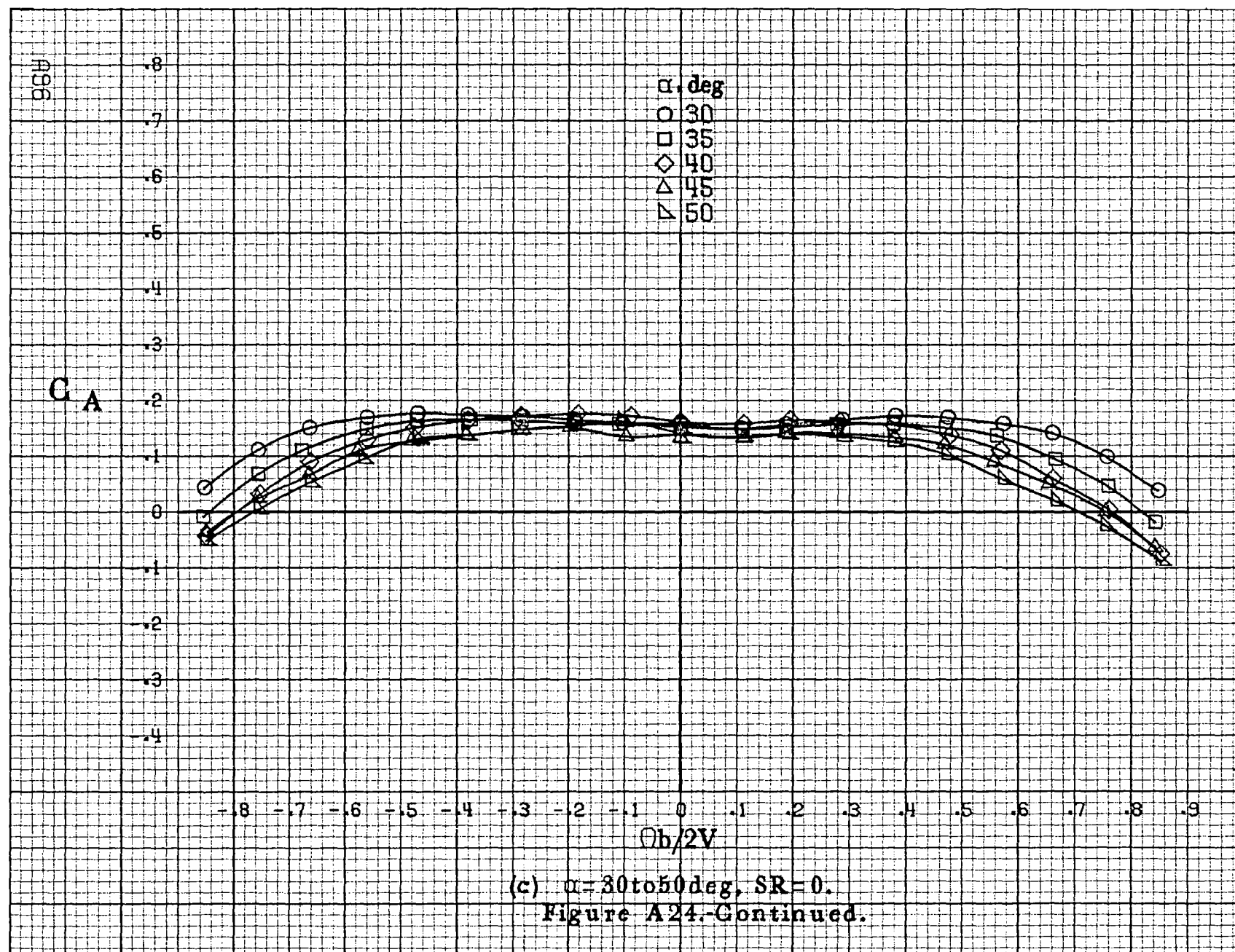


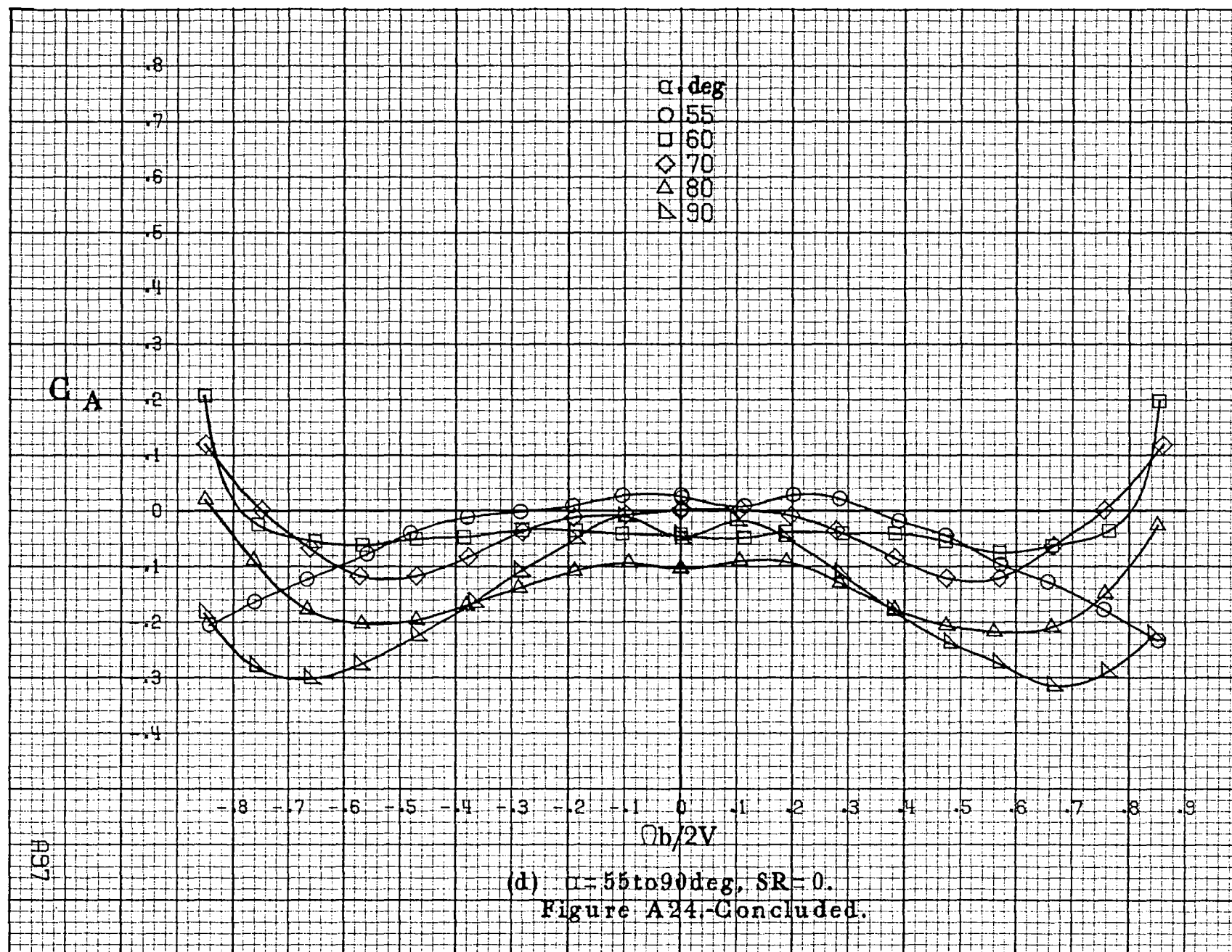


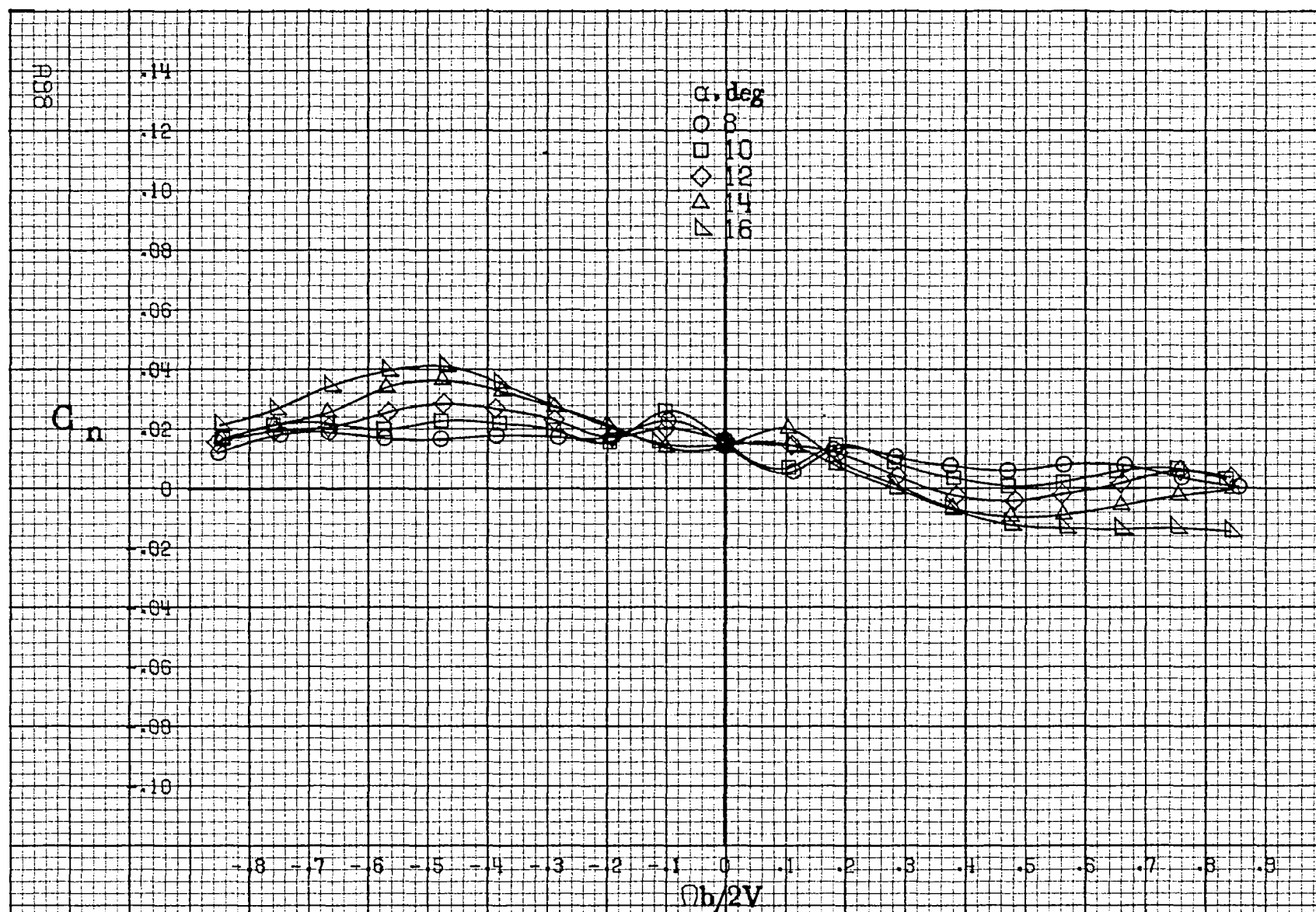






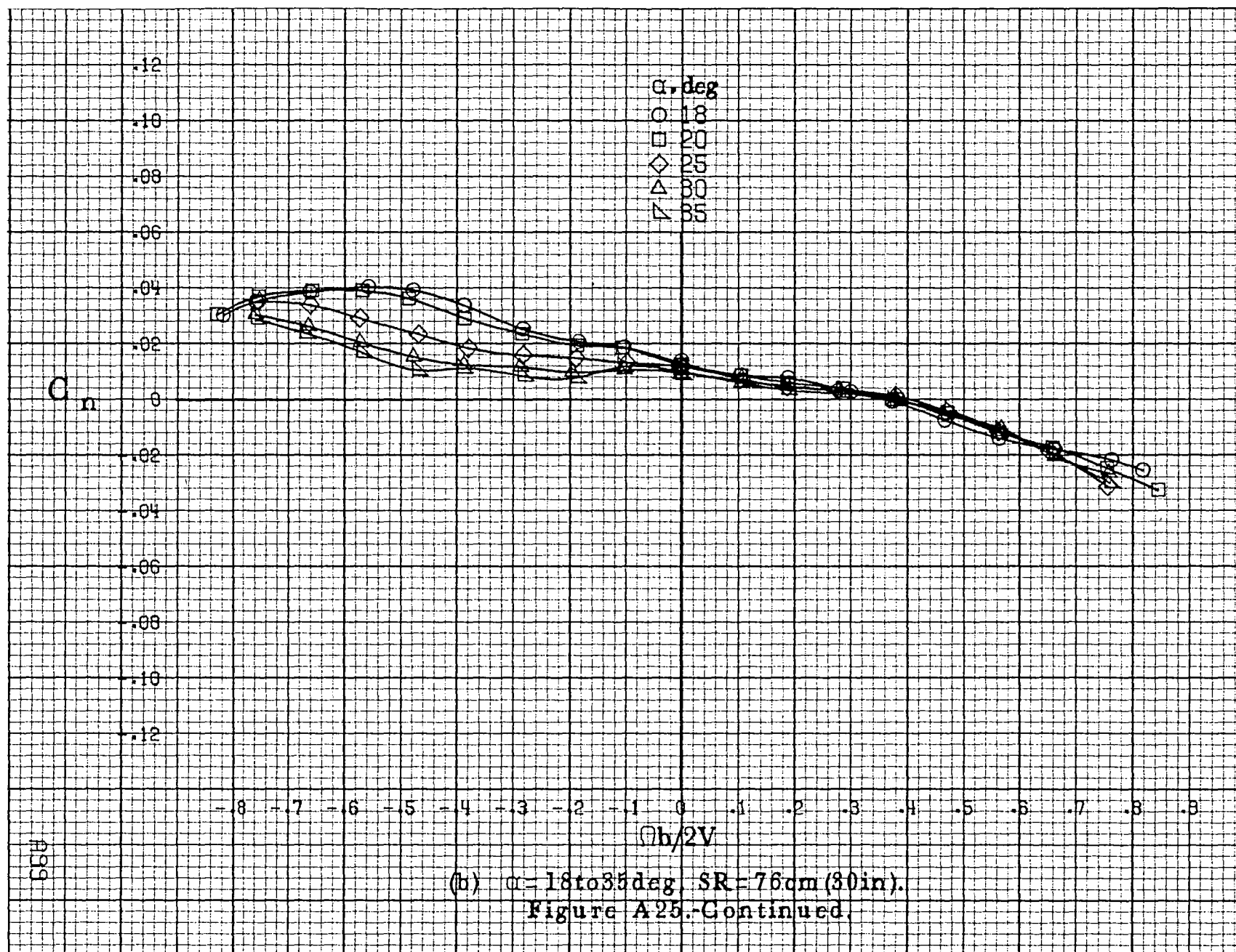


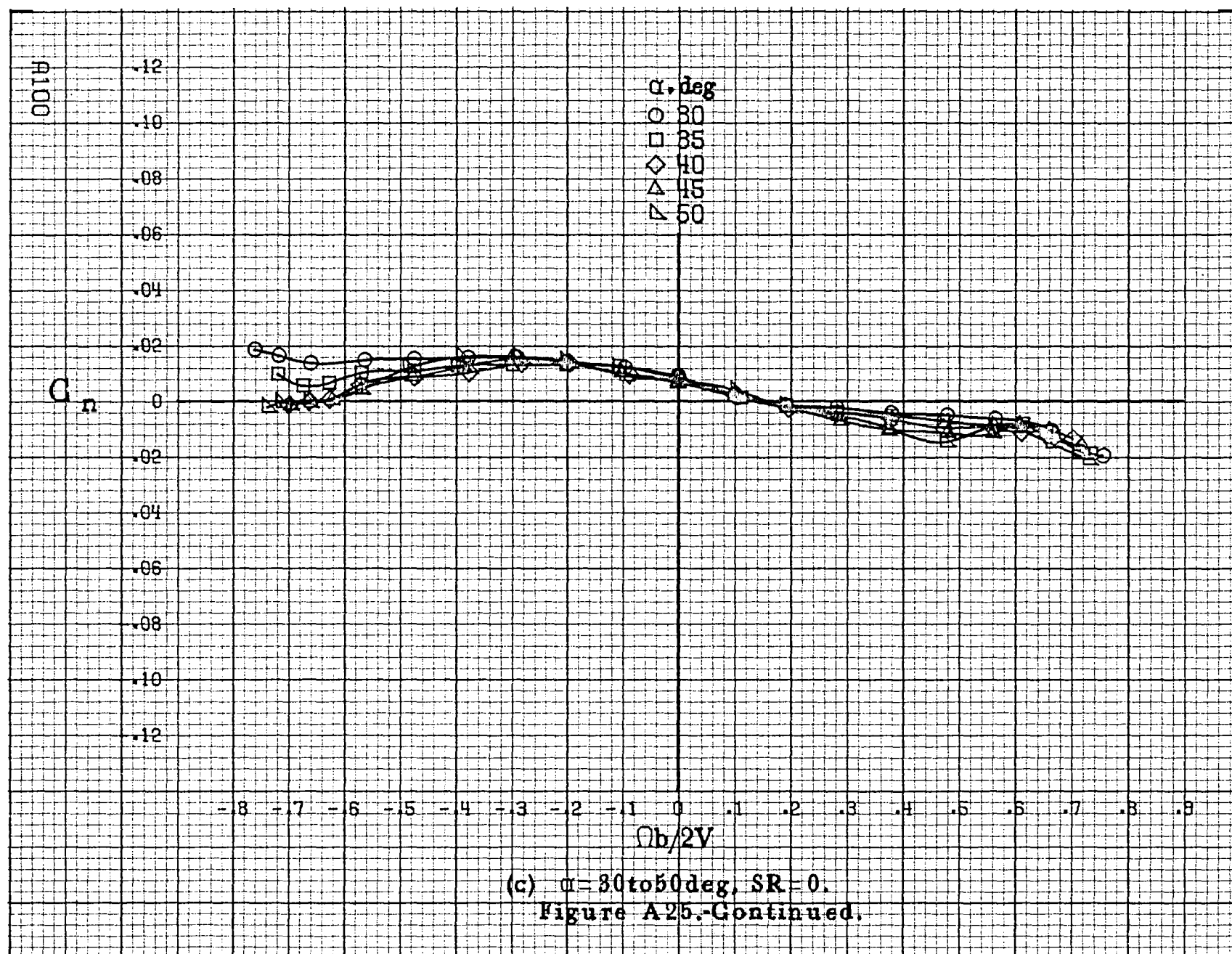


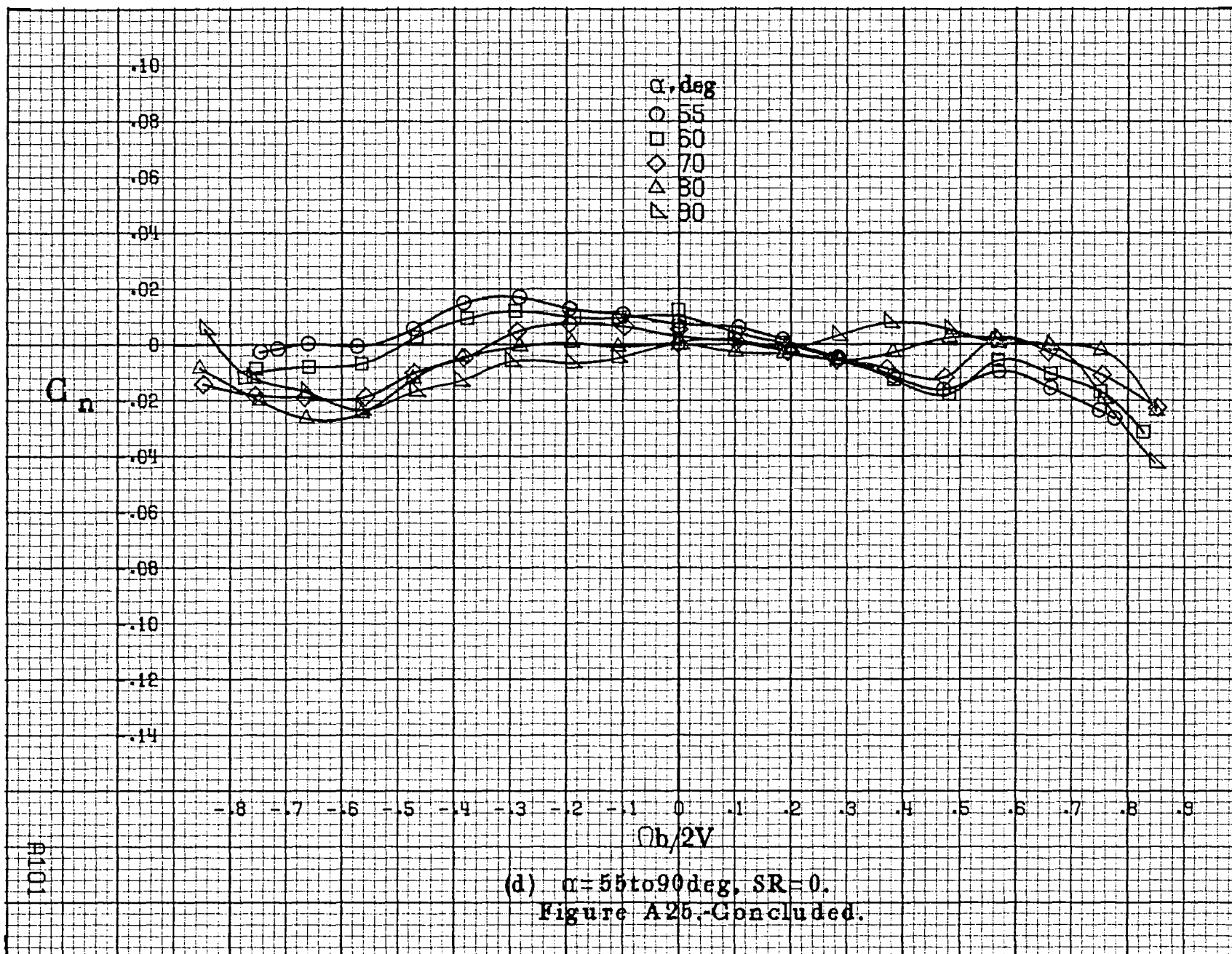


(a) $\alpha = 8$ to 16° , $SR = 76\text{ cm (30 in.)}$.

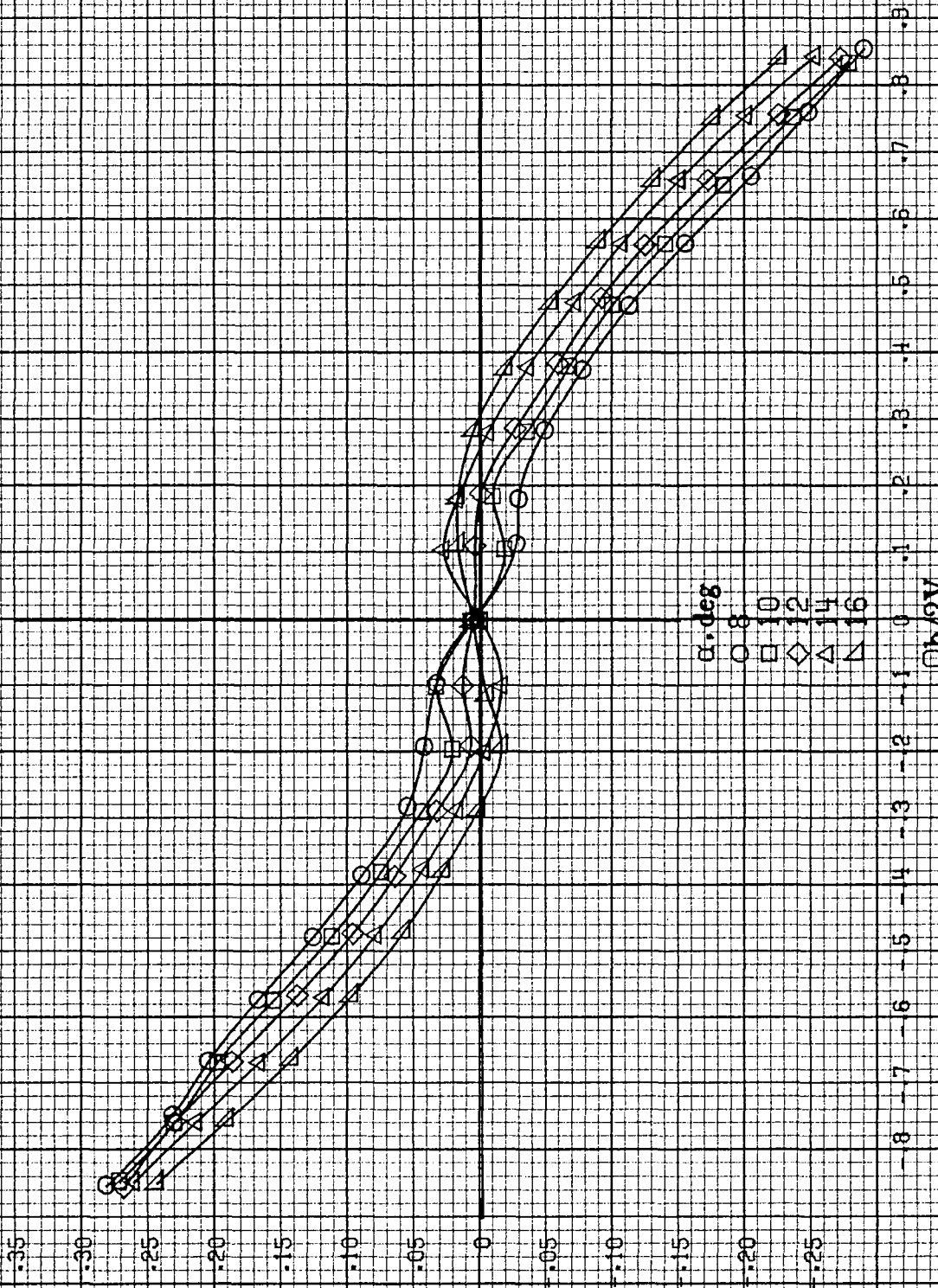
Figure A25. Effect of rotation rate and angle of attack on yawing-moment coefficient for basic configuration. $\delta_a = \pm 25^\circ$, $\delta_s = 0^\circ$, $\delta_r = \pm 25^\circ$, $\delta = 0^\circ$.





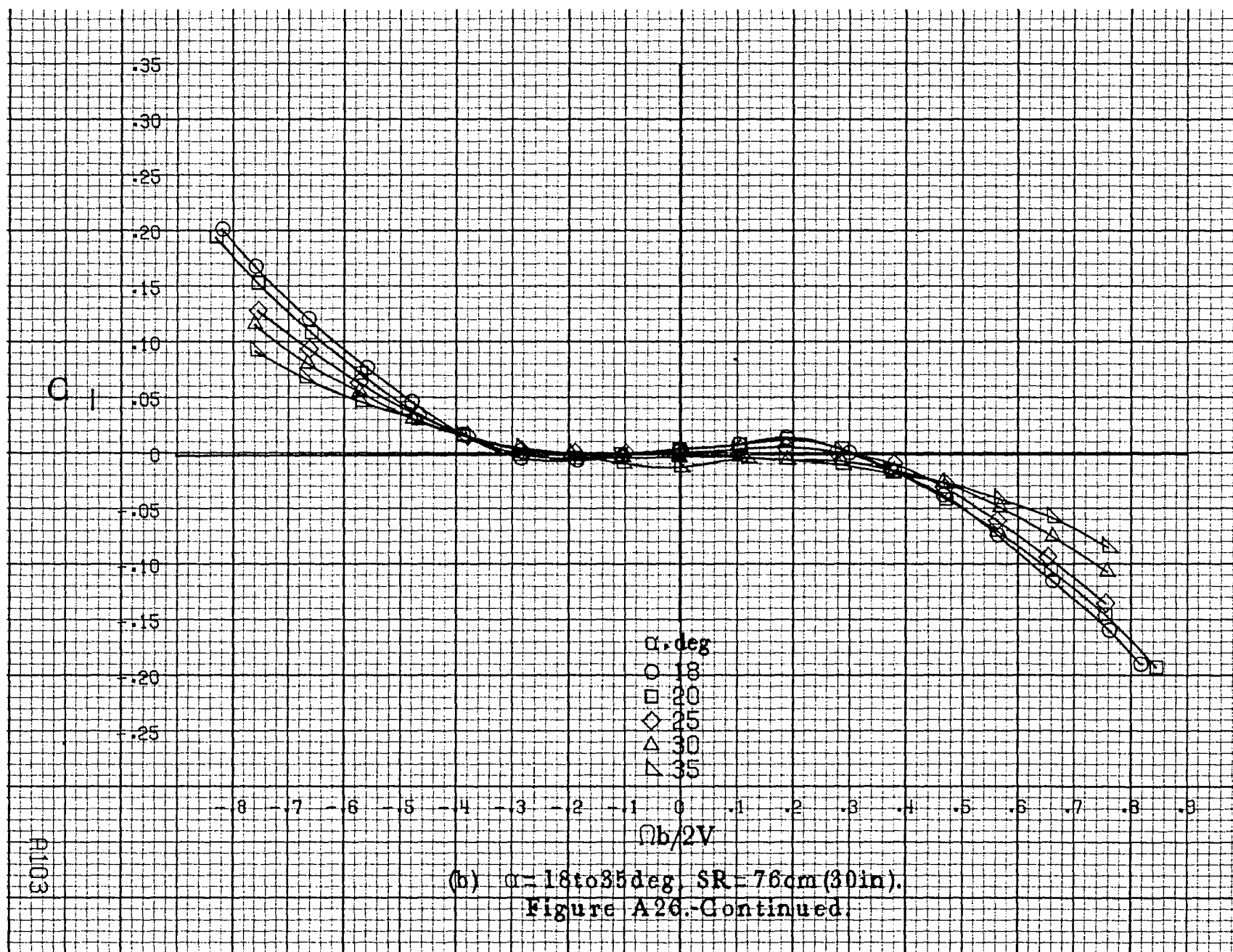


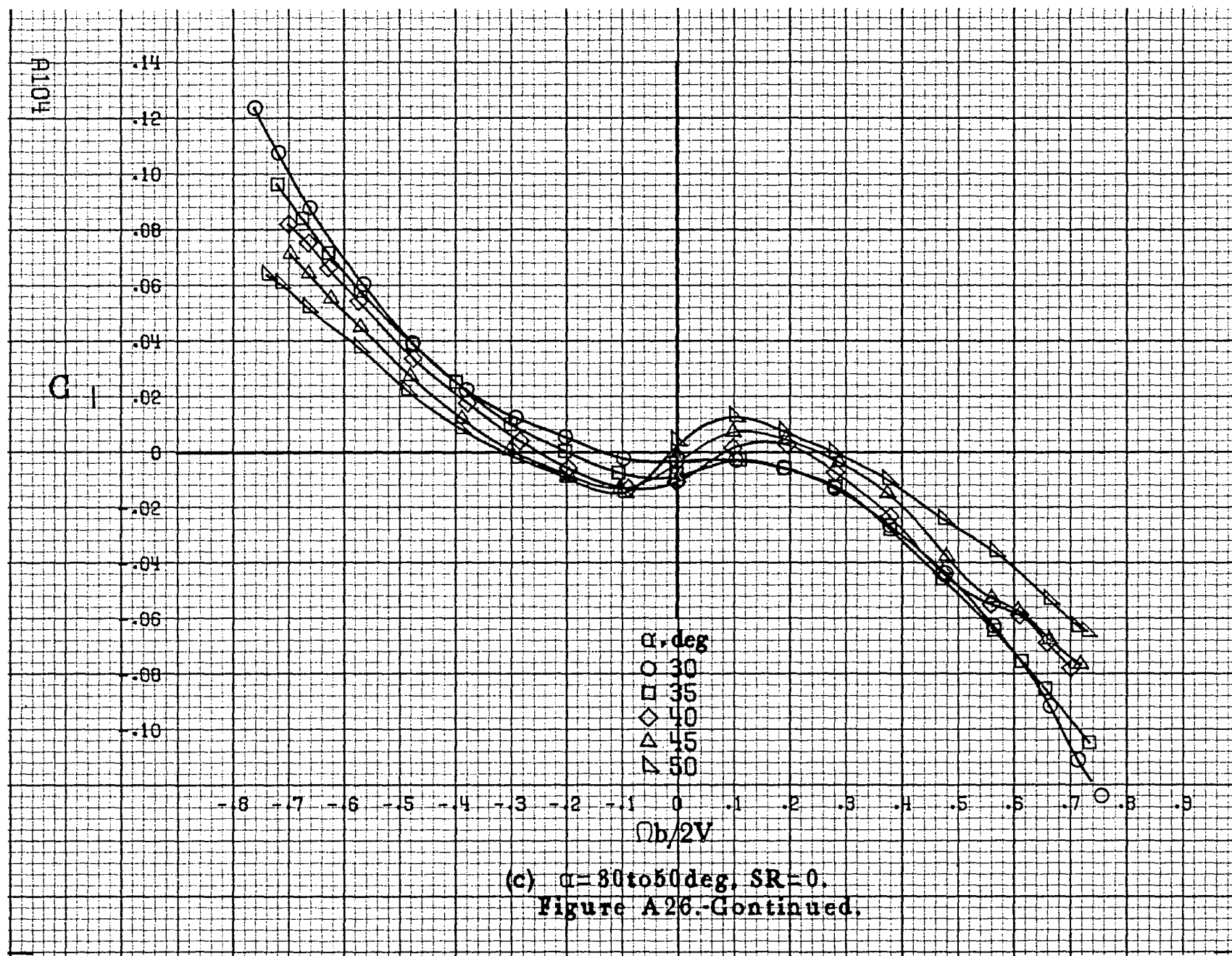
A102

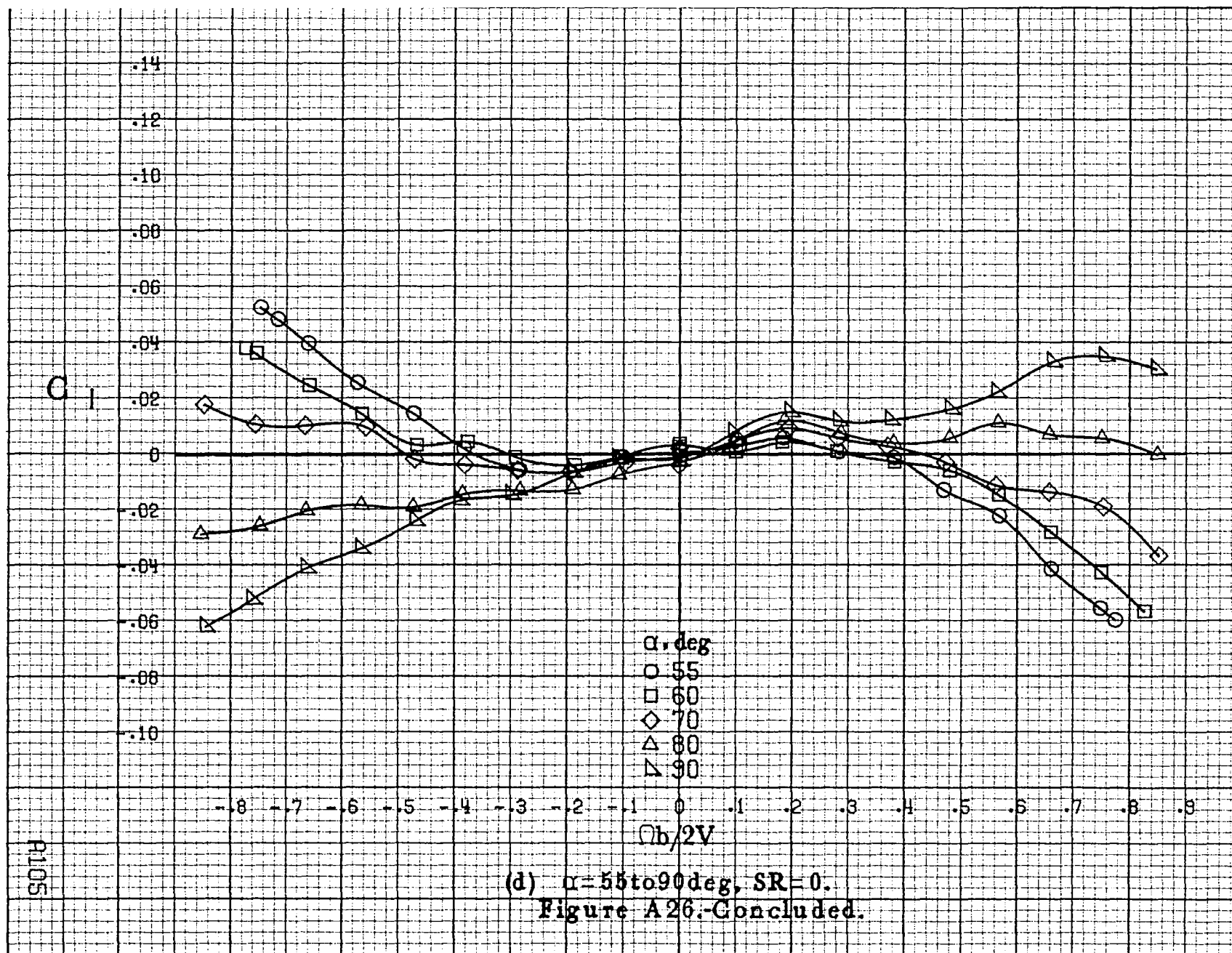


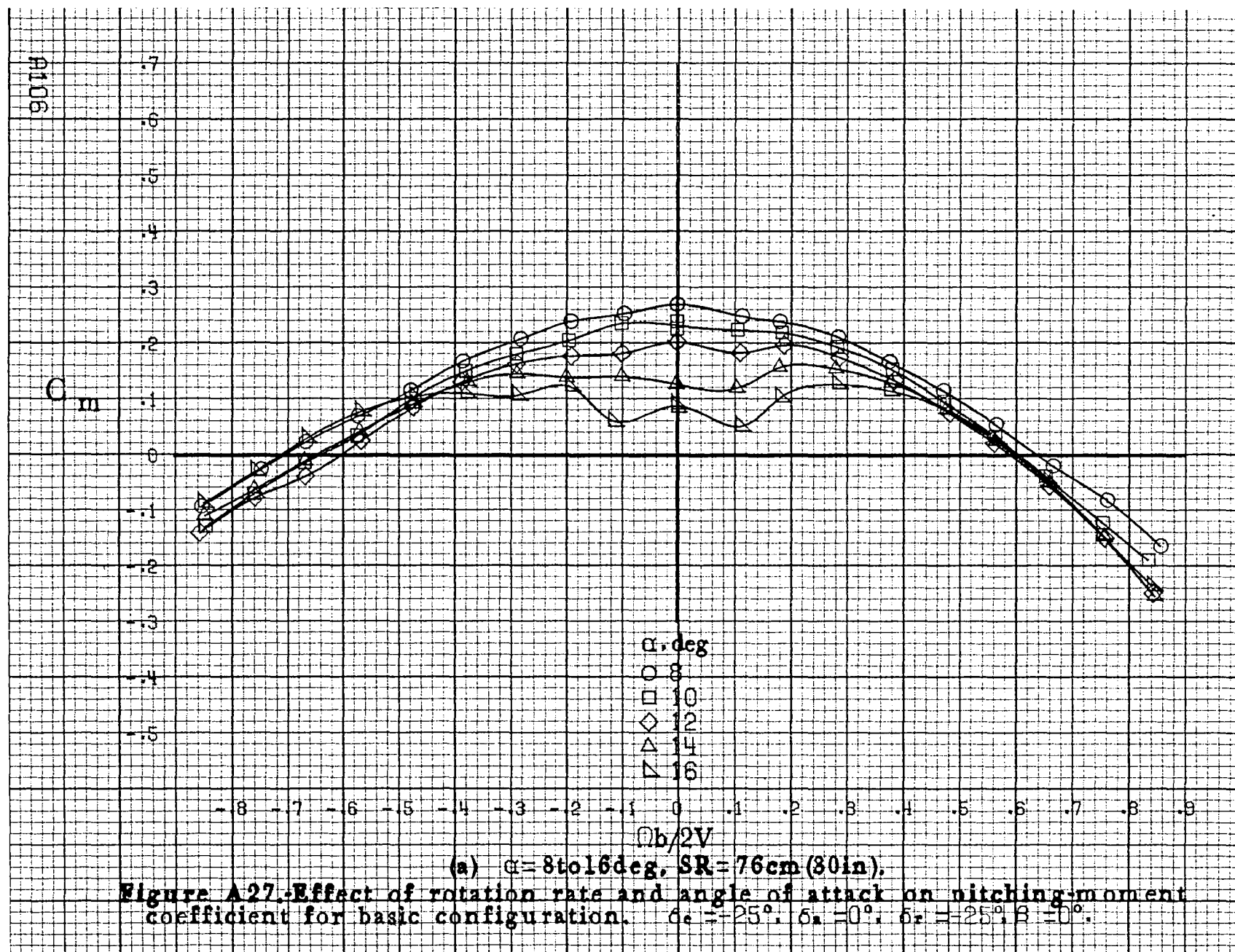
(a) $\alpha = 8$ to 16° , $SR = 76\text{cm (30 in.)}$.

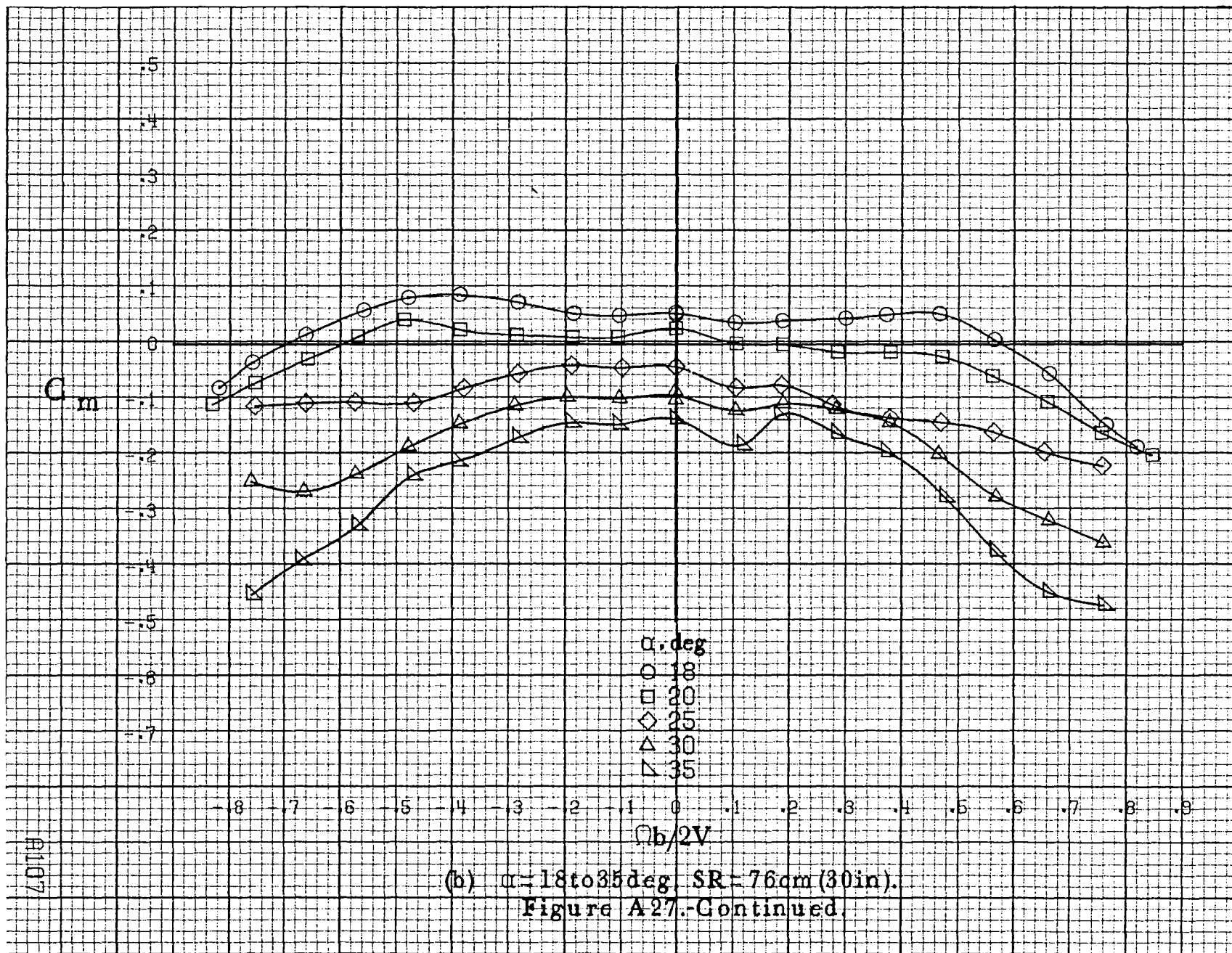
Figure A26.-Effect of rotation rate and angle of attack on rolling-moment coefficient for basic configuration. $\delta_e = -25^\circ$; $\delta_a = 0^\circ$; $\delta_r = 25^\circ$; $\beta = 0^\circ$.

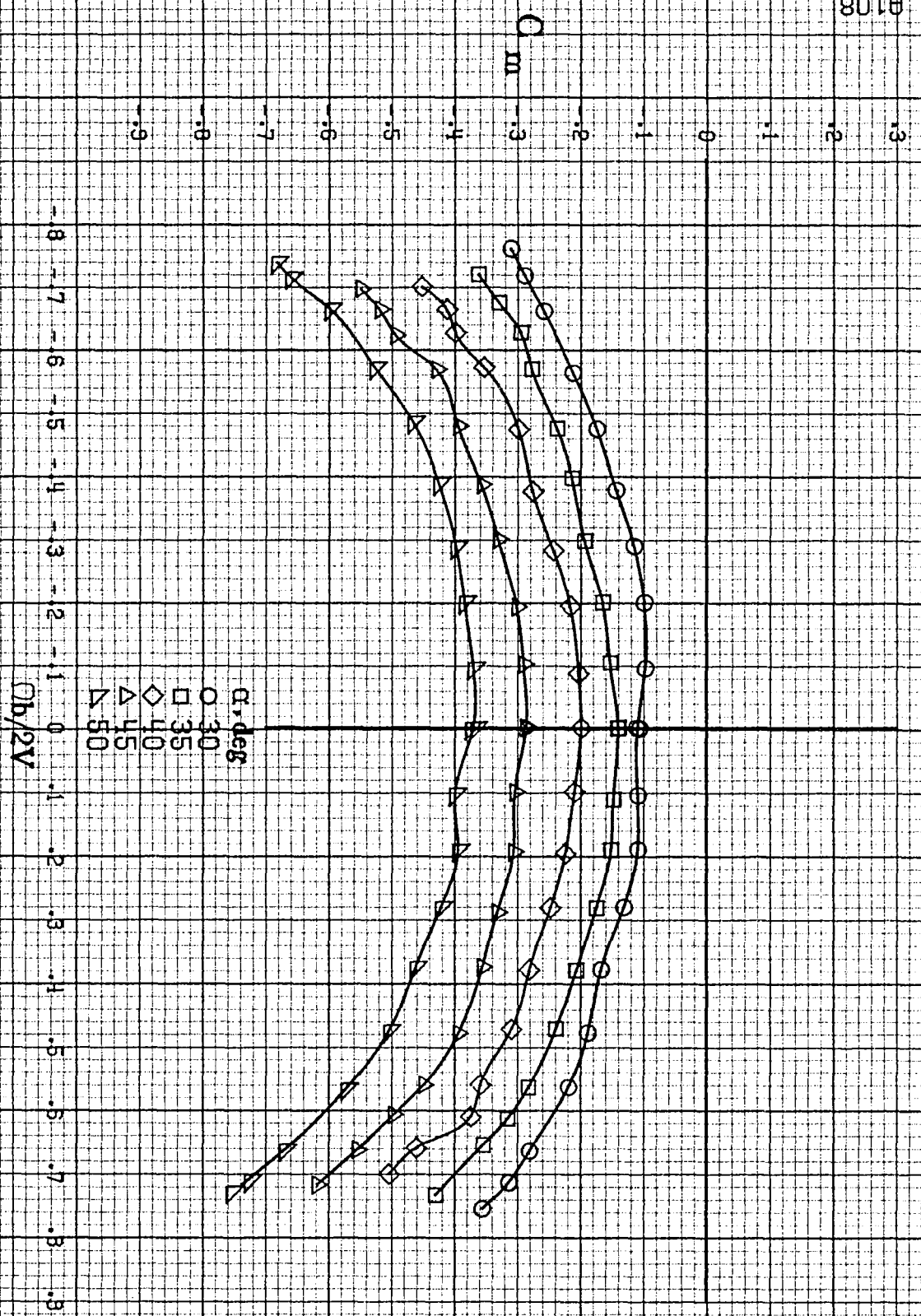




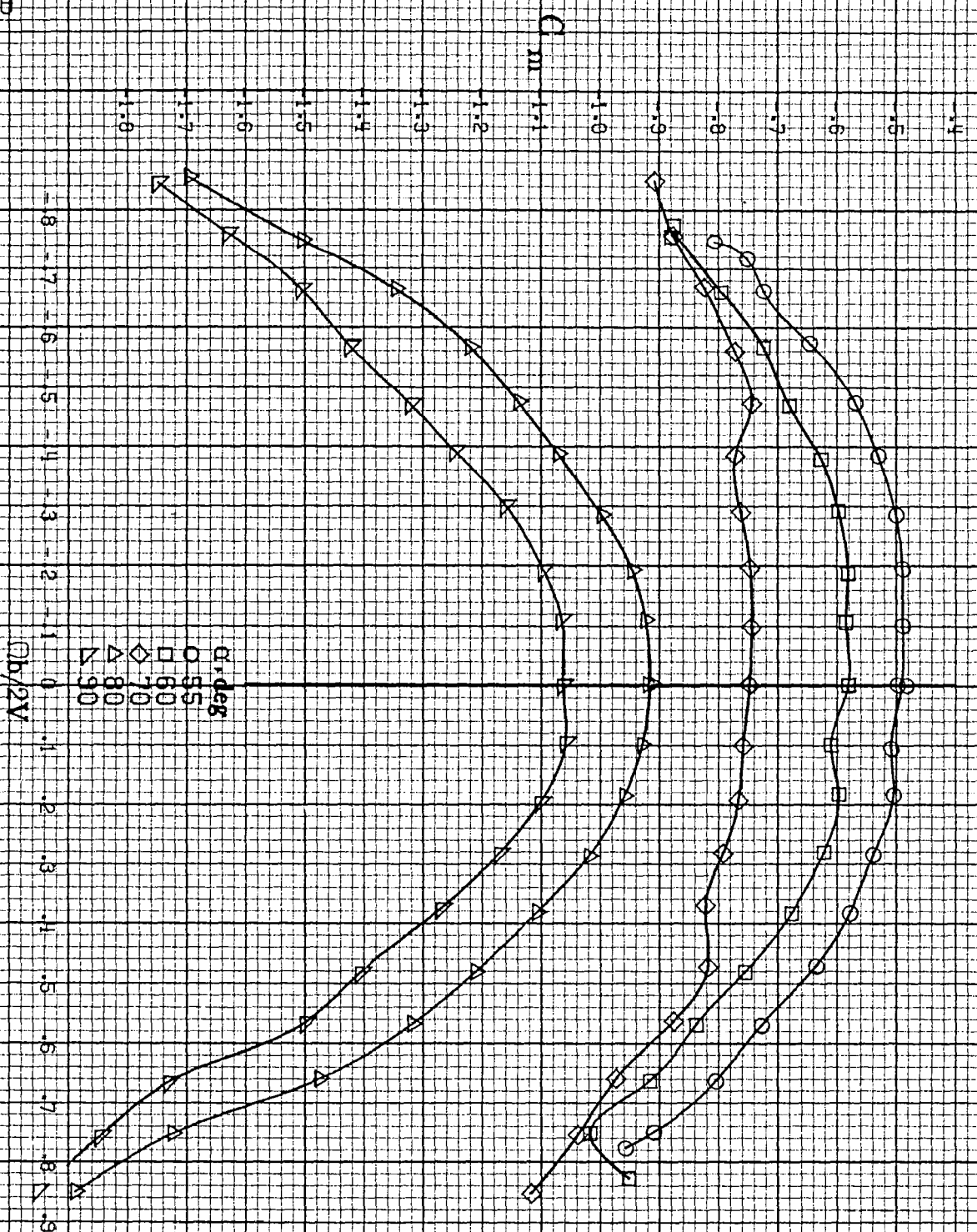




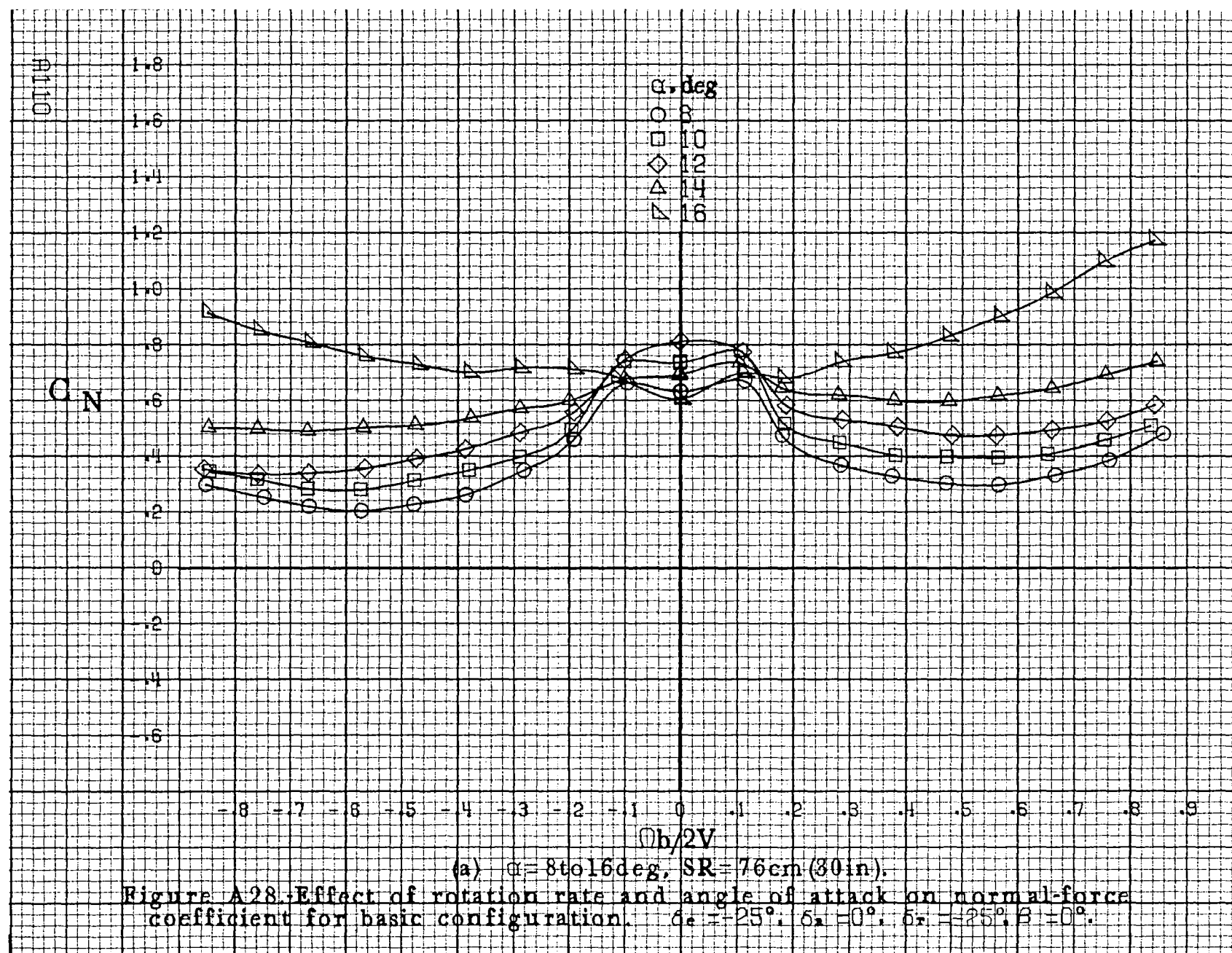


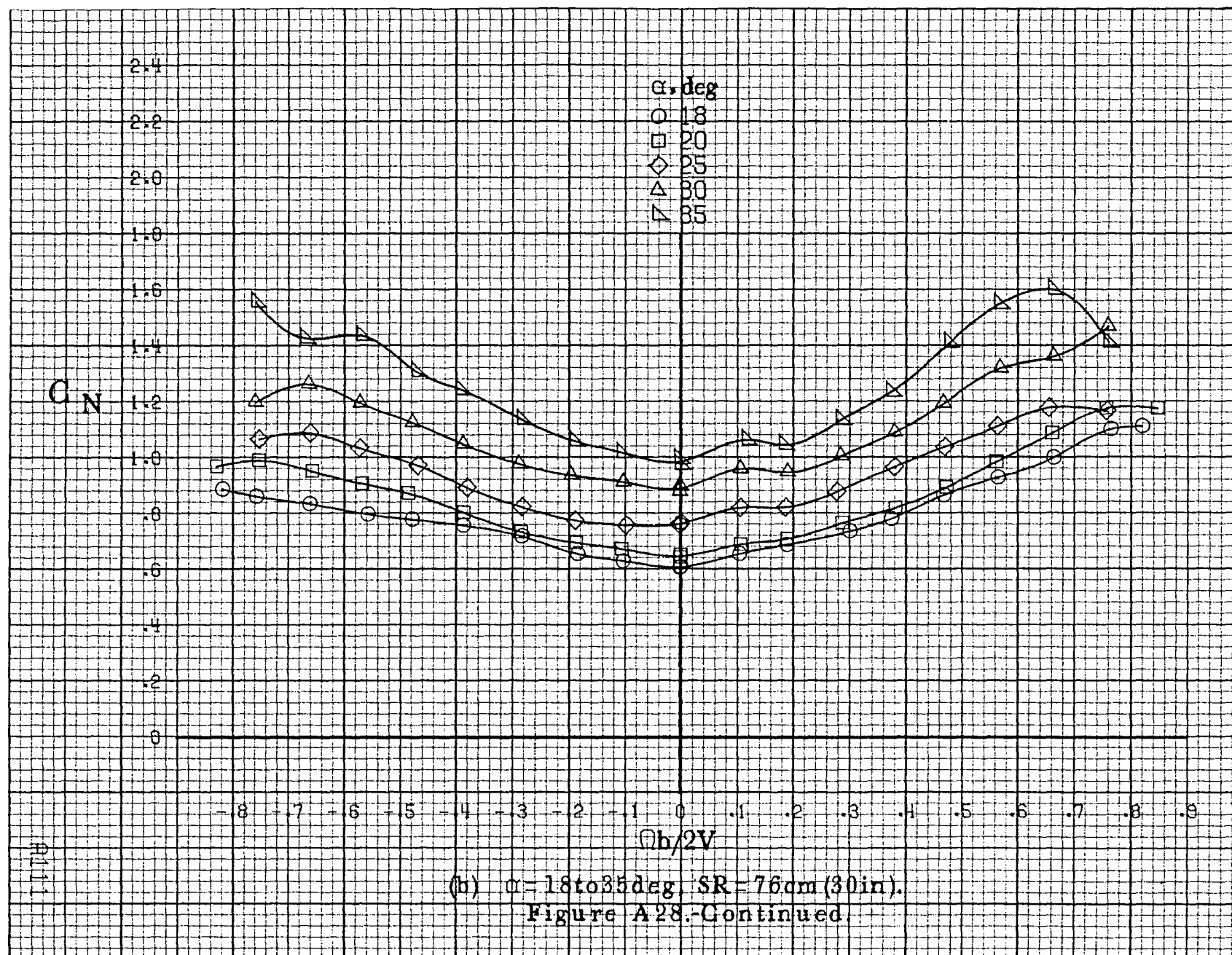


(c) $\alpha = 80$ to 50° , $SR = 0$.
Figure A27.-Continued.

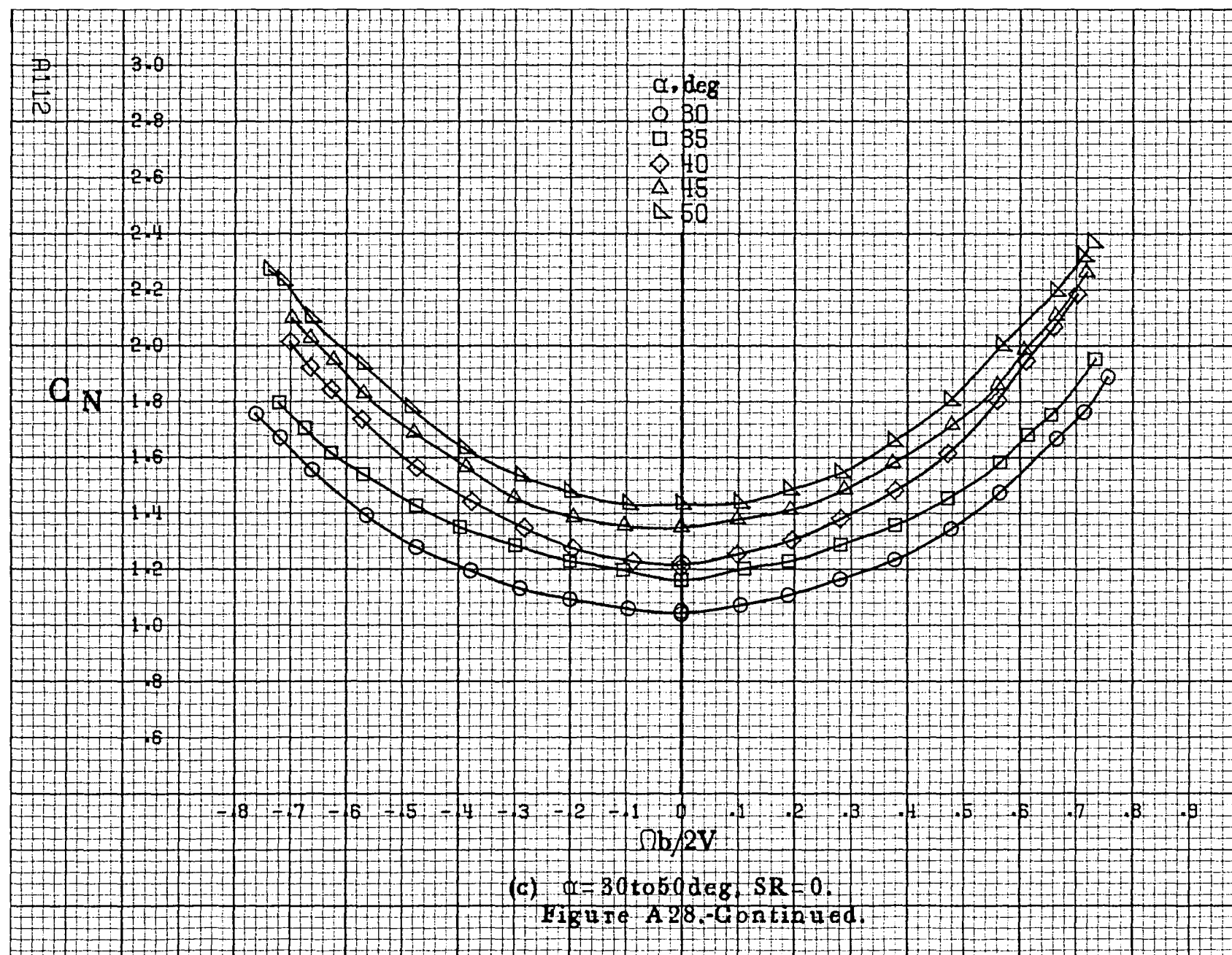


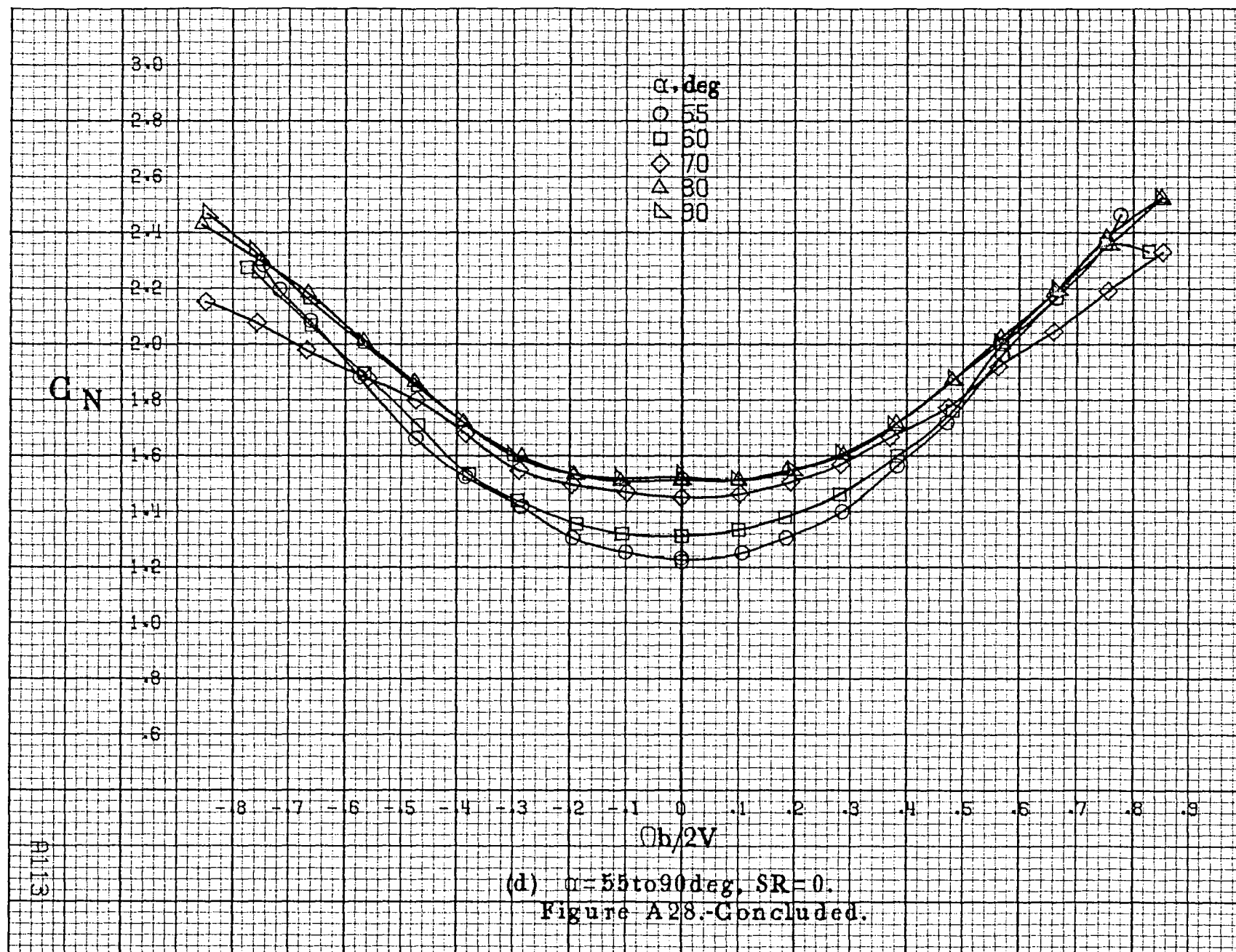
(d) $\alpha = 55$ to 90 deg, $SR = 0$.
Figure A27-C concluded.

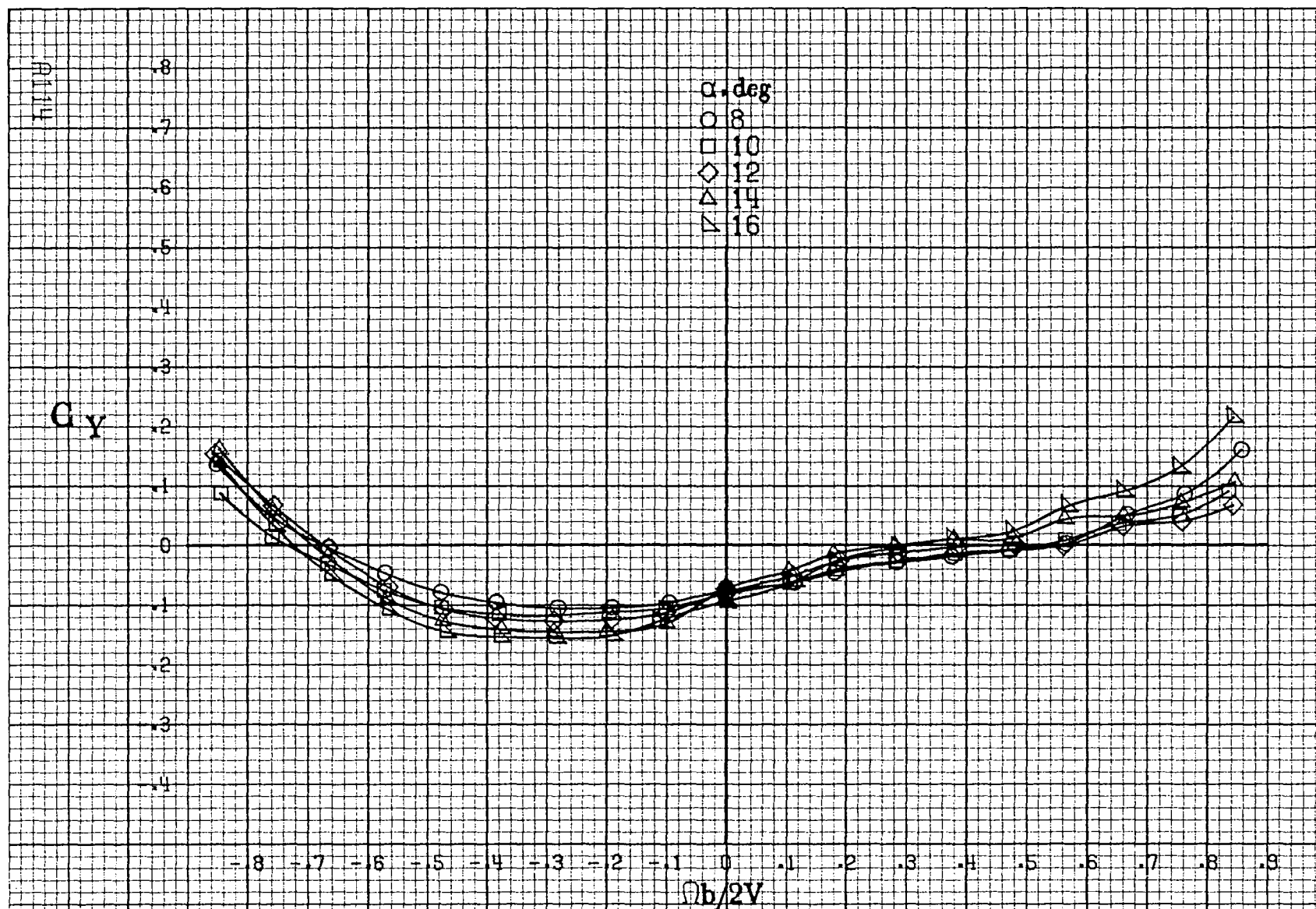




(b) $\alpha = 18$ to 35° , $SR = 76\text{cm}$ (30 in).
Figure A28.-Continued.

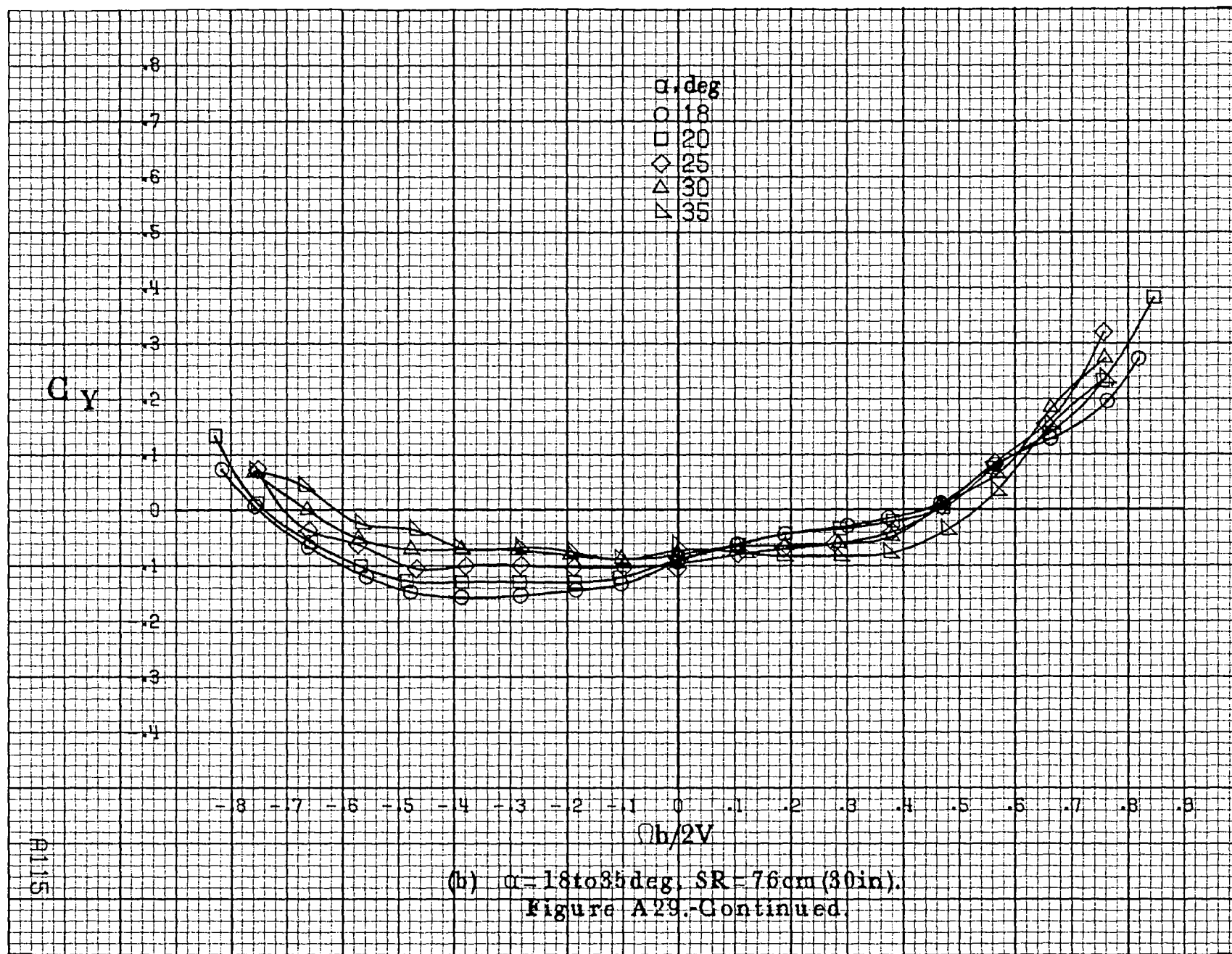


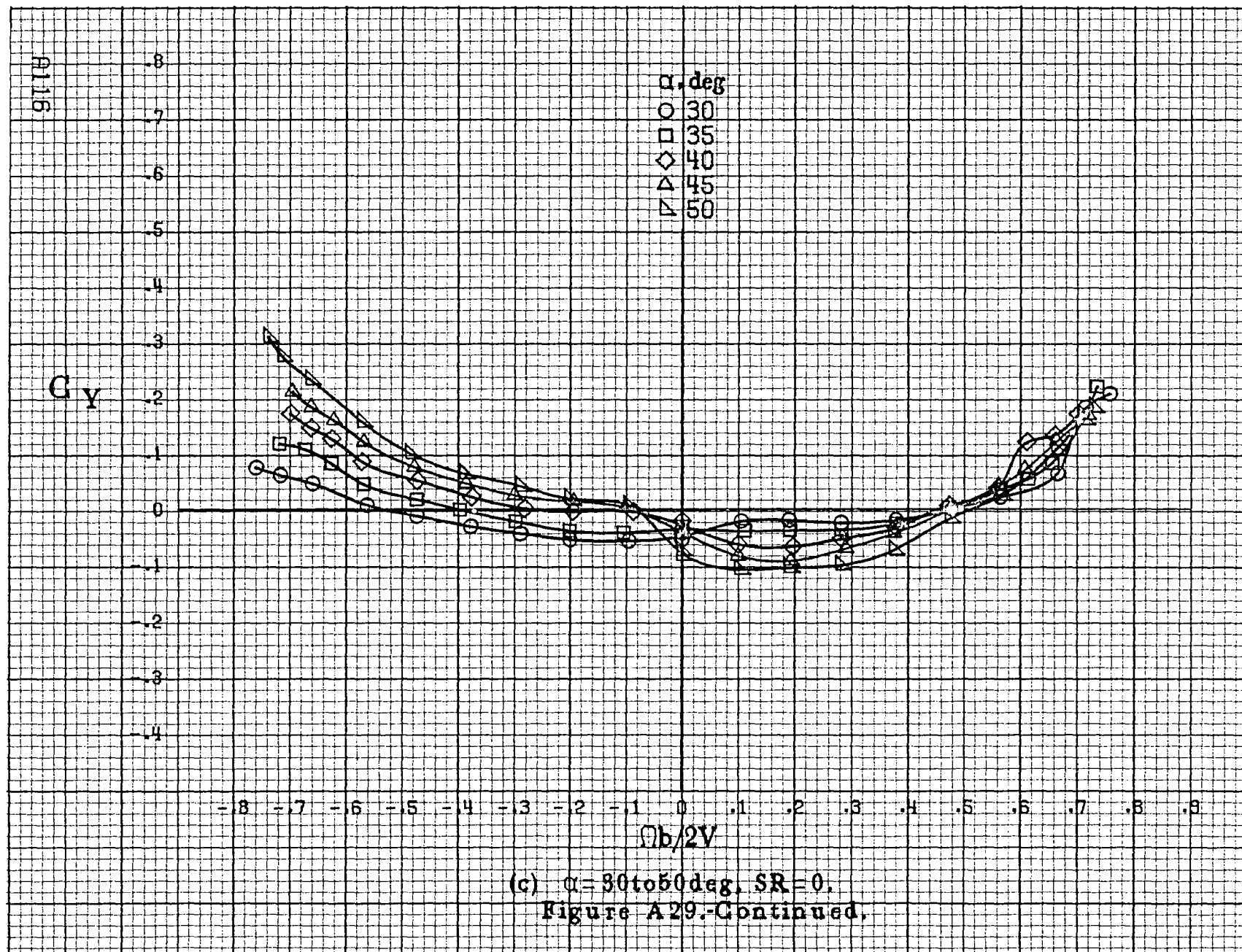


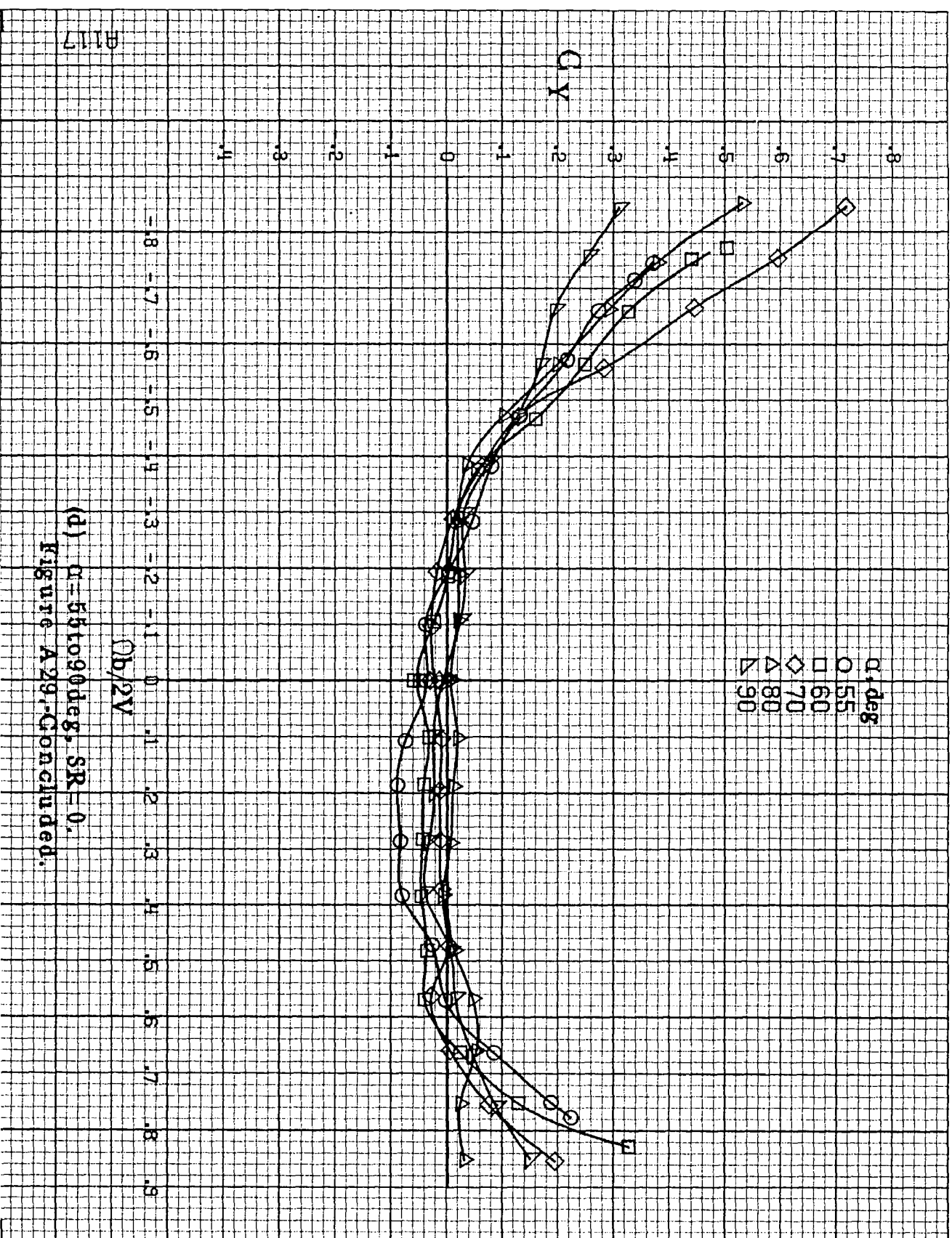


(a) $\alpha = 8 \text{ to } 16 \text{ deg}$, $SR = 76 \text{ cm (30 in)}$.

Figure A29. Effect of rotation rate and angle of attack on side-force coefficient for basic configuration. $\delta_a = -25^\circ$, $\delta_s = 0^\circ$, $\delta_r = 25^\circ$, $\beta = 0^\circ$.

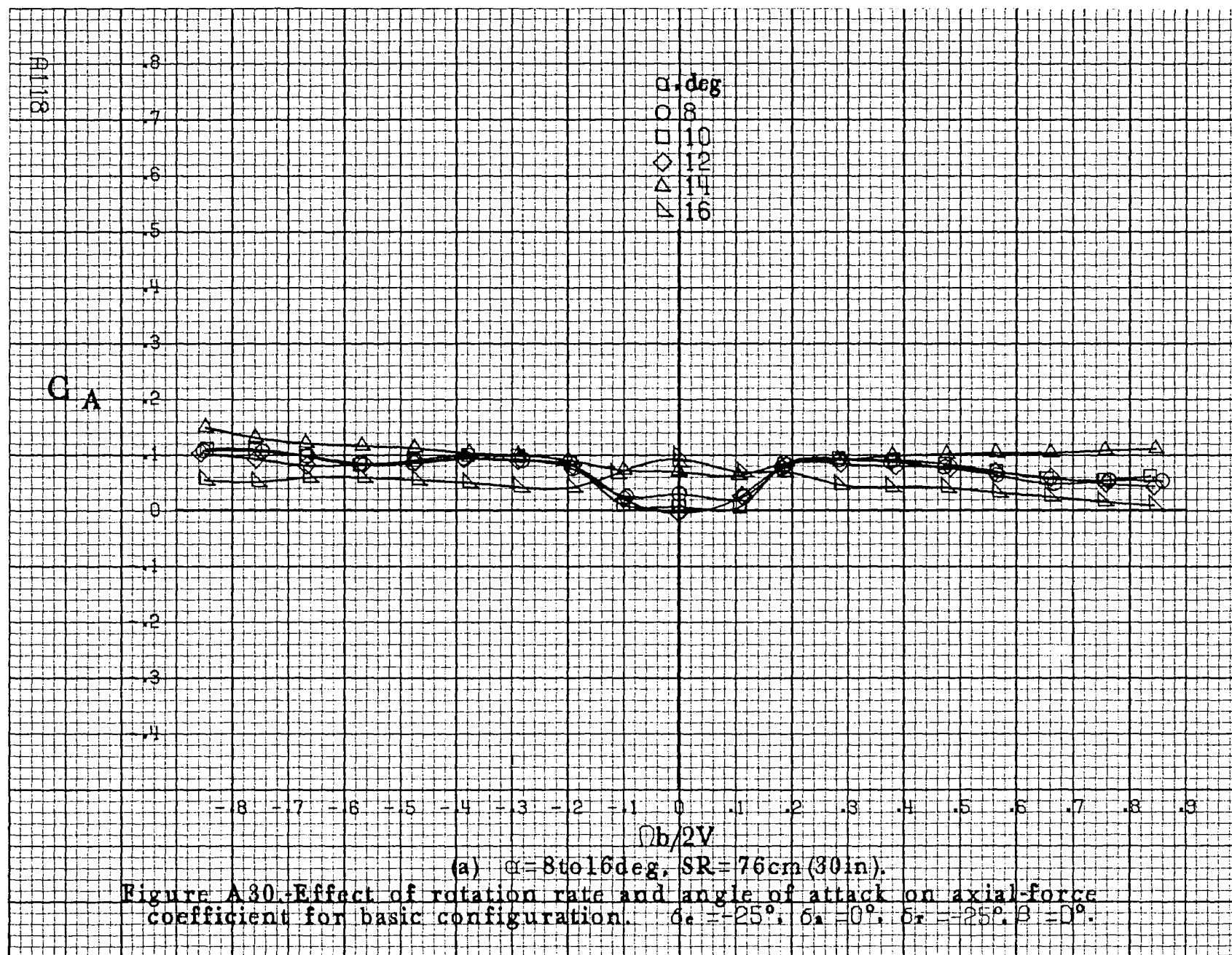


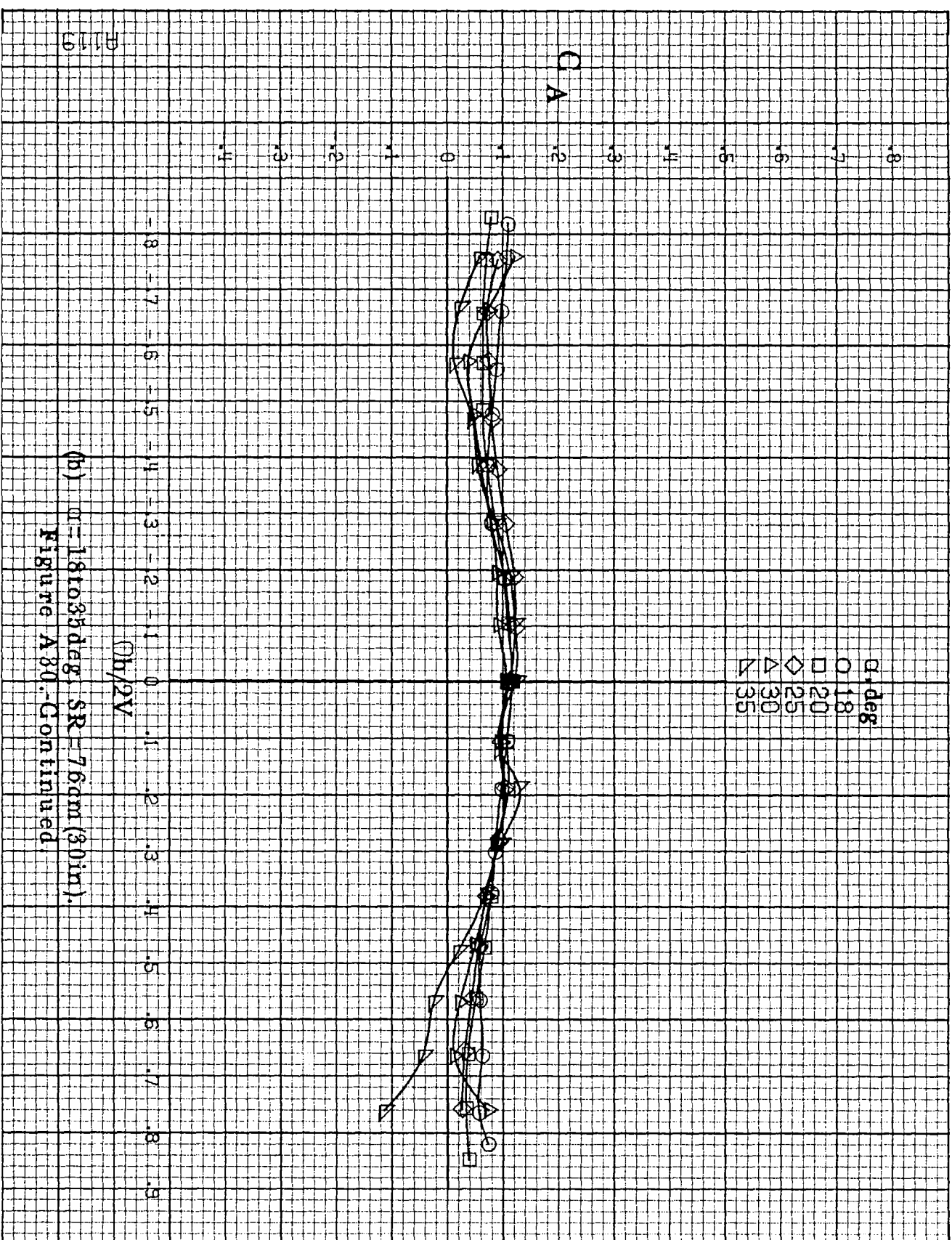




(d) $\alpha = 55$ to 90 deg, $SR = 0$.
Figure A29.-Concluded.

A1117





(b) $\alpha = 18$ to 35 deg, $SR = 7.6$ cm (3.0 in).
Figure A80.-Continued

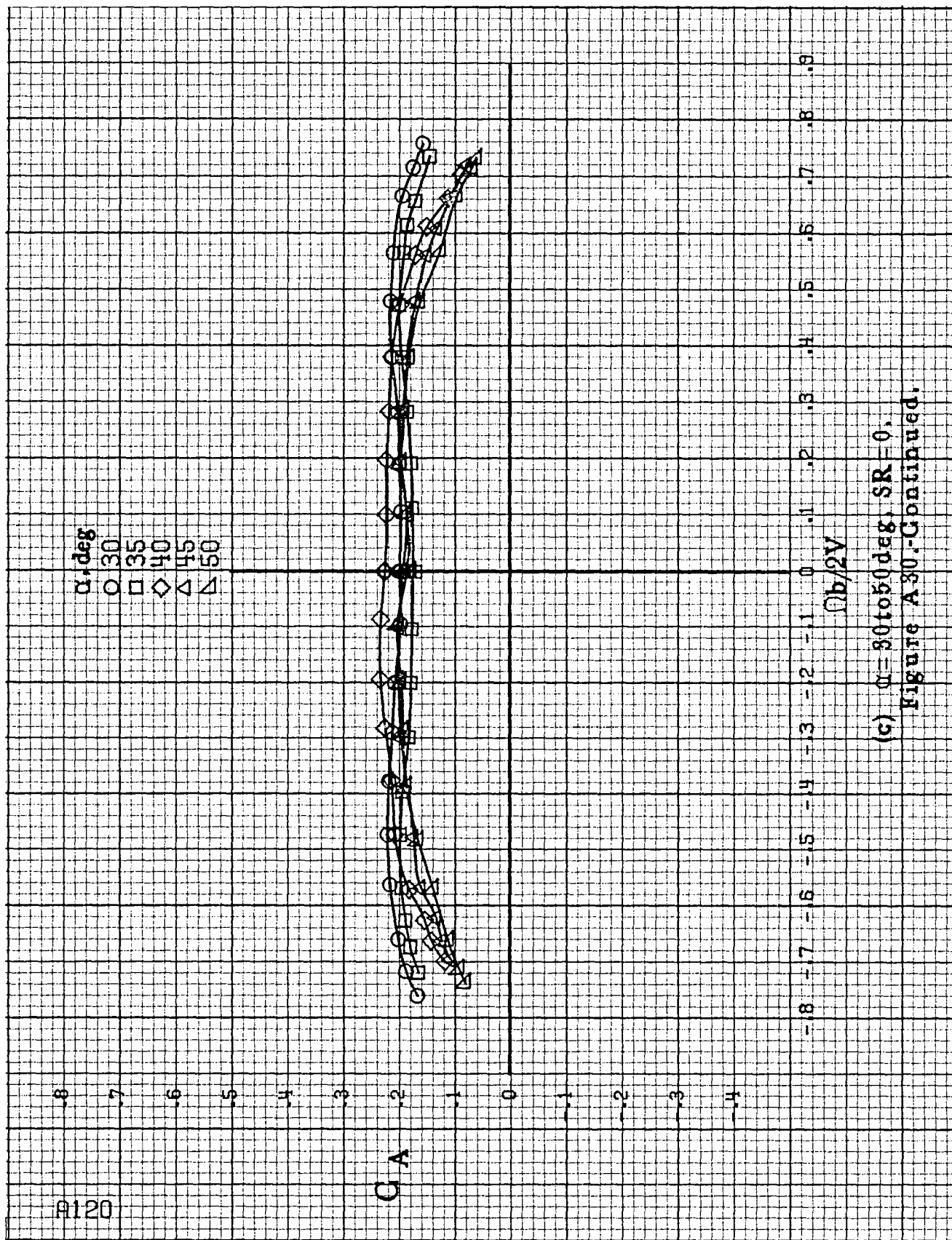
8120

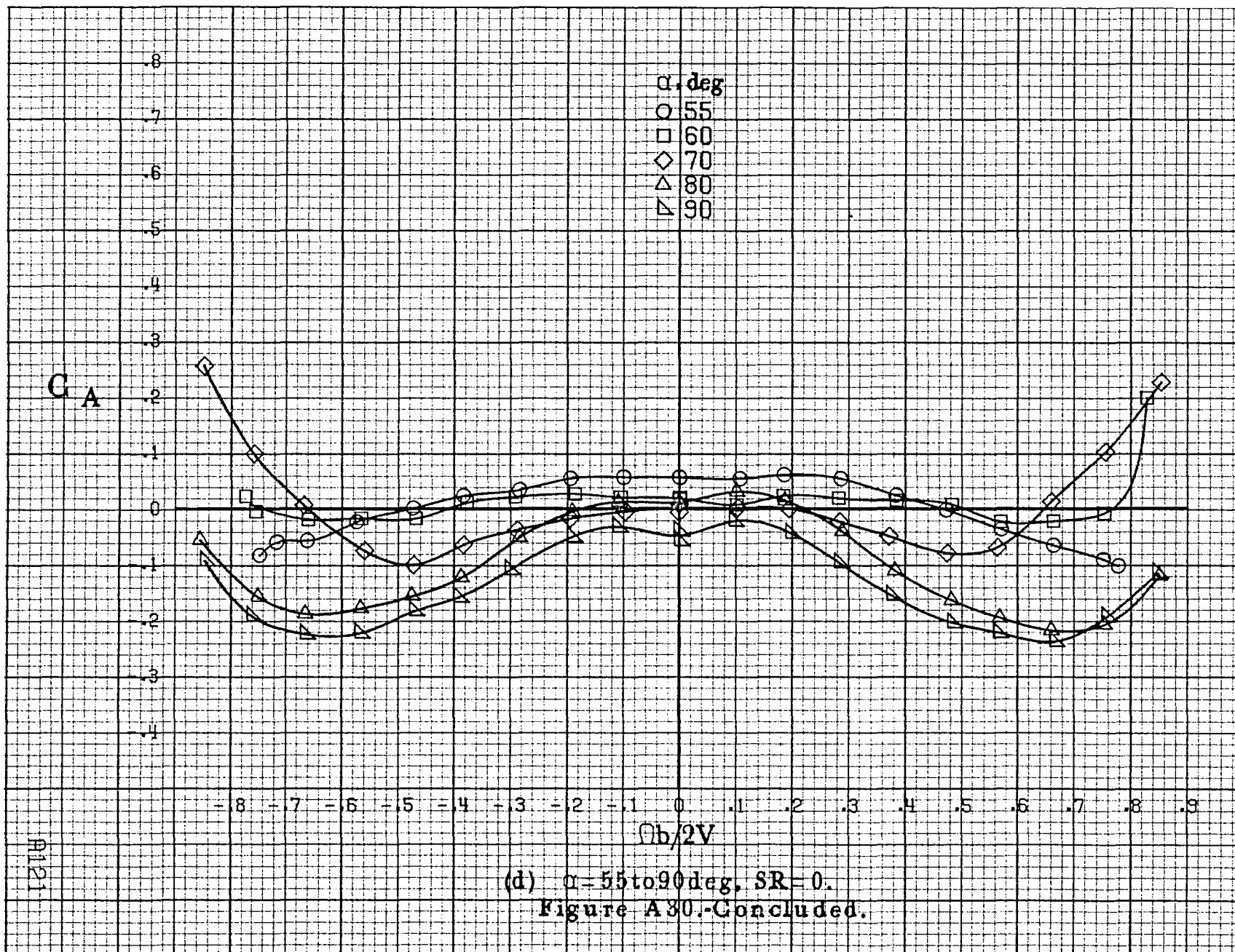
α, deg
 O 30
 □ 35
 ◇ 40
 △ 45
 ▽ 50

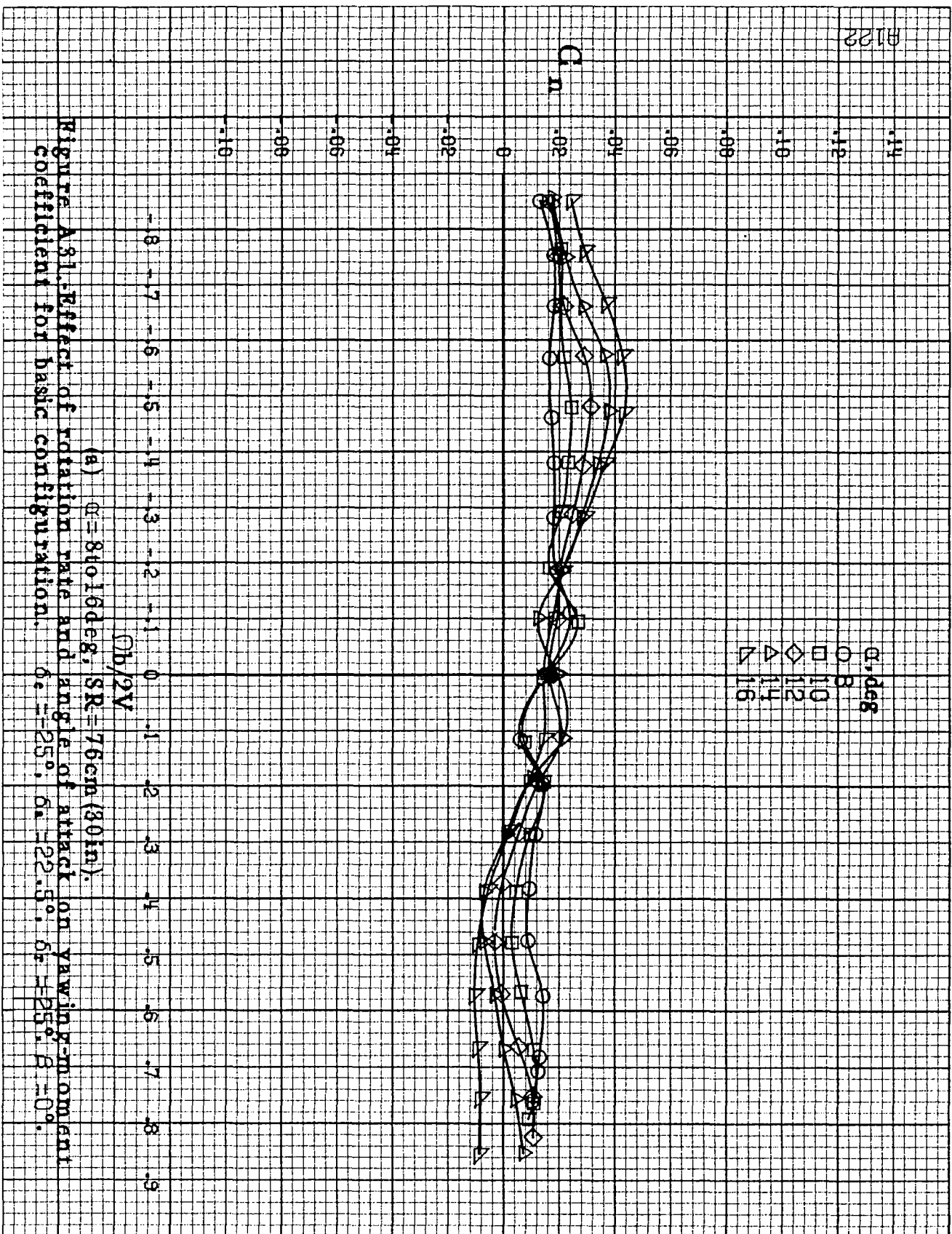
CA

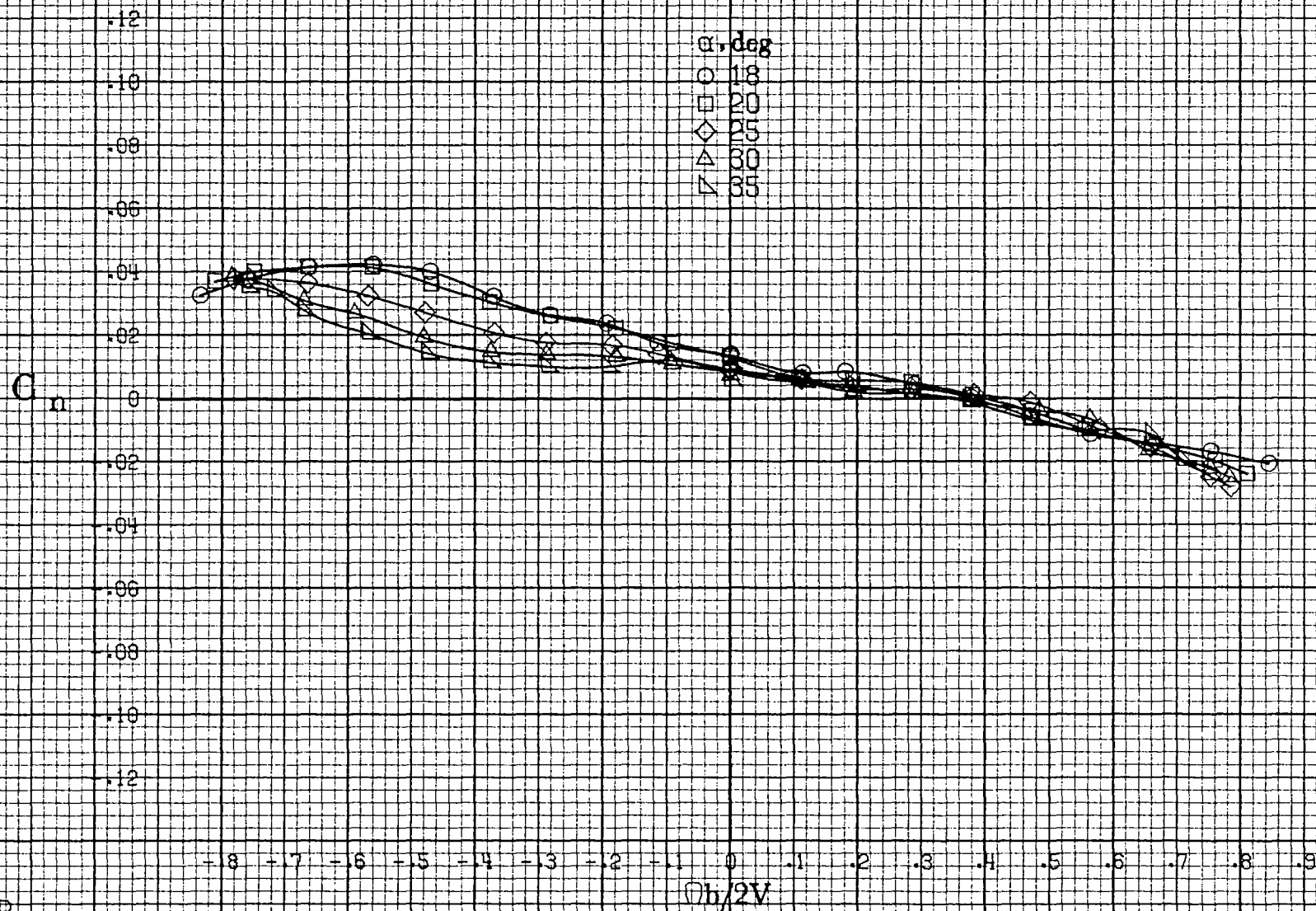
$\Omega b/2V$

(c) $\alpha = 30 \text{ to } 50 \text{ deg}$, $SR = 0$.
 Figure A30.-Continued.

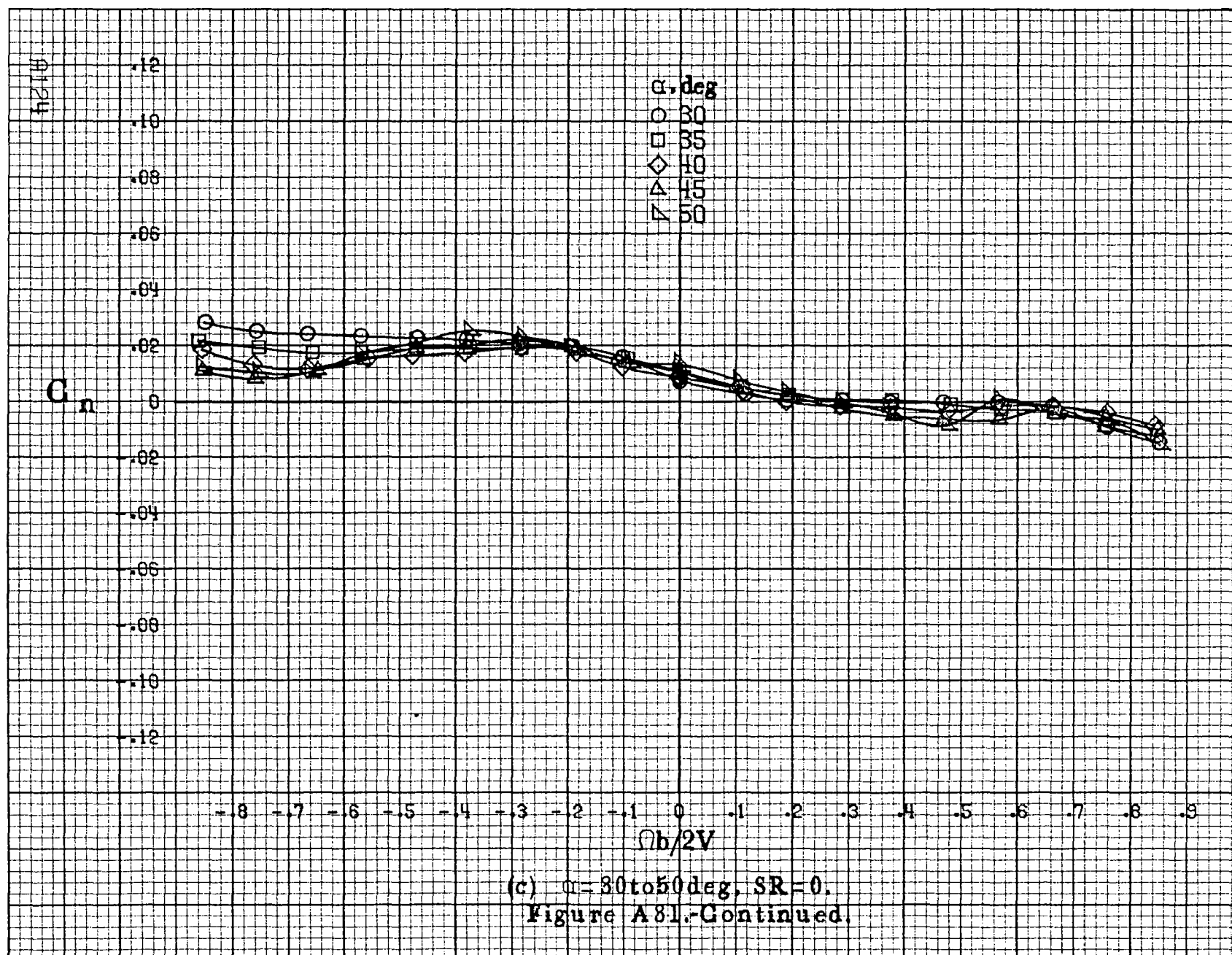


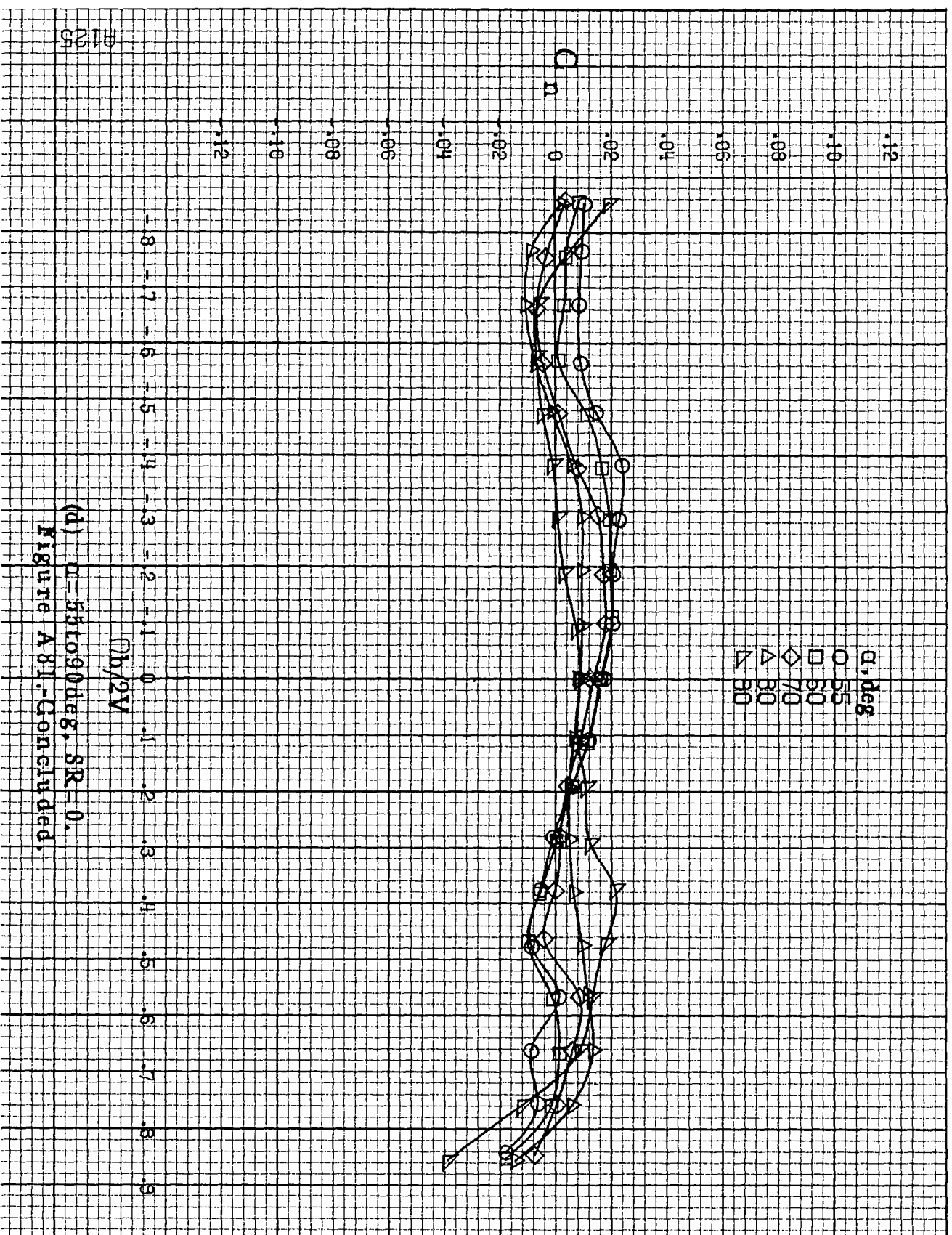






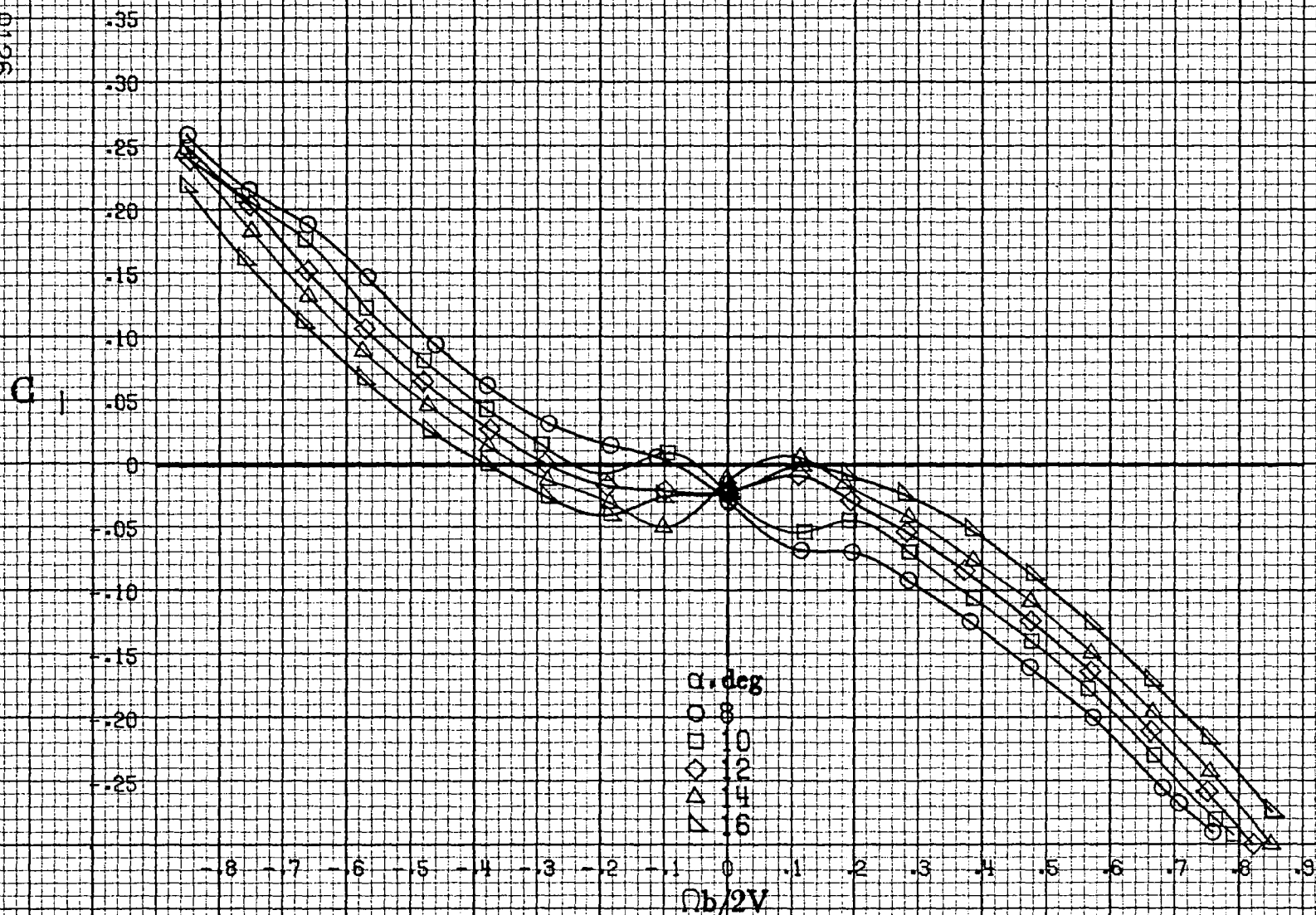
(b) $\alpha = 18$ to 35° , SR = 76 cm (30 in).
Figure A31.-Continued.





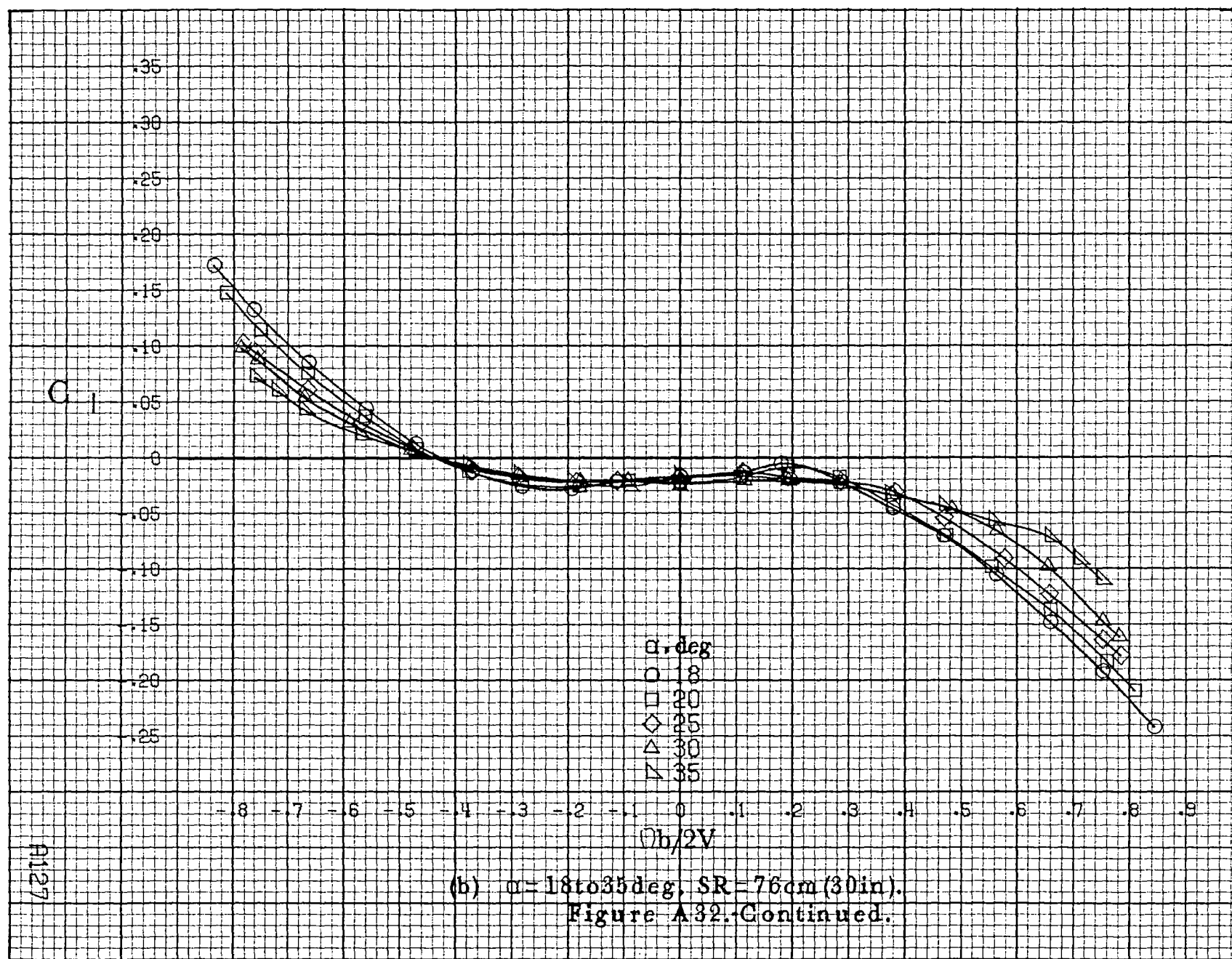
(d) $\alpha = 55$ to 90 deg, $SR = 0$.
 Figure A81.-Concluded.

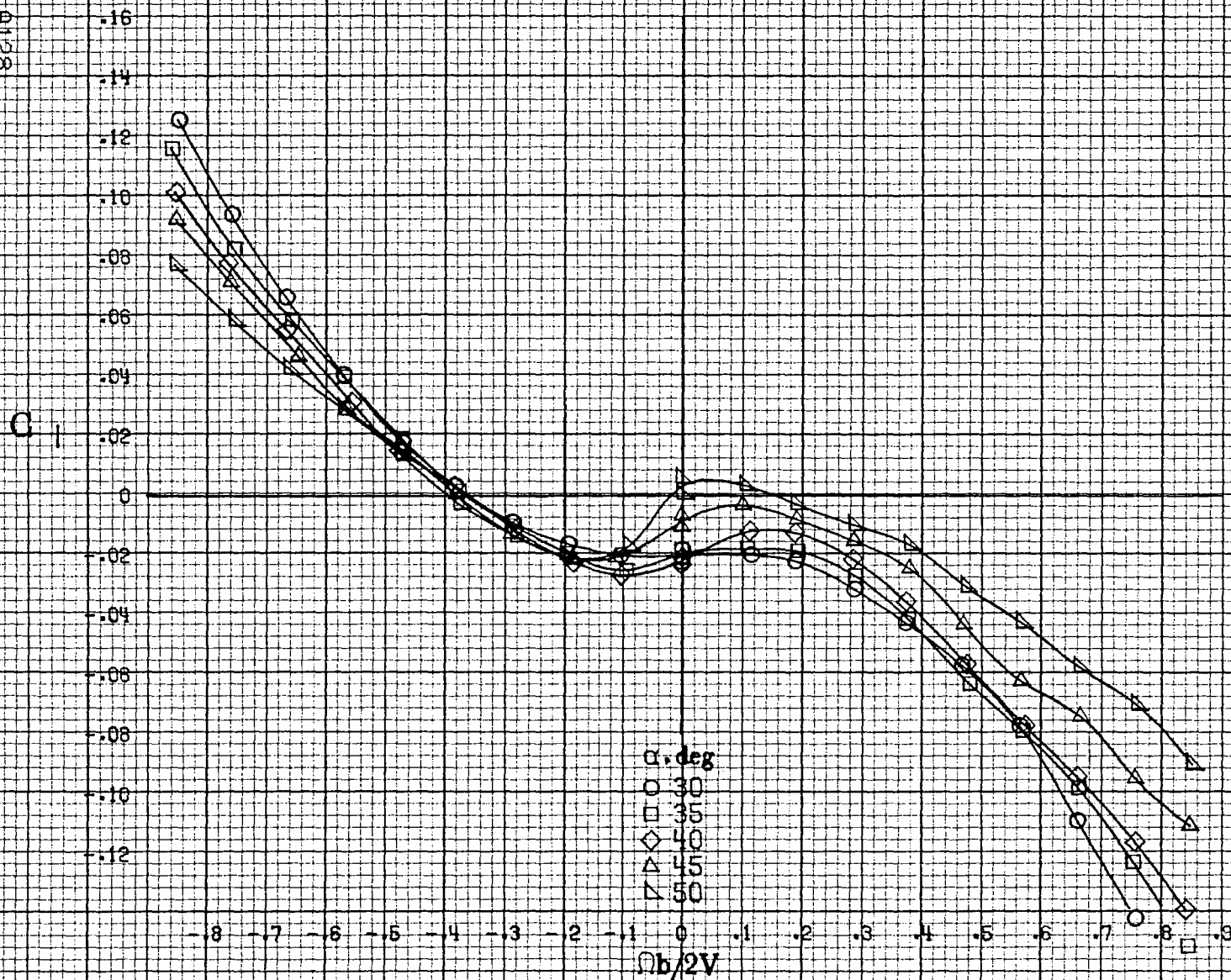
A125



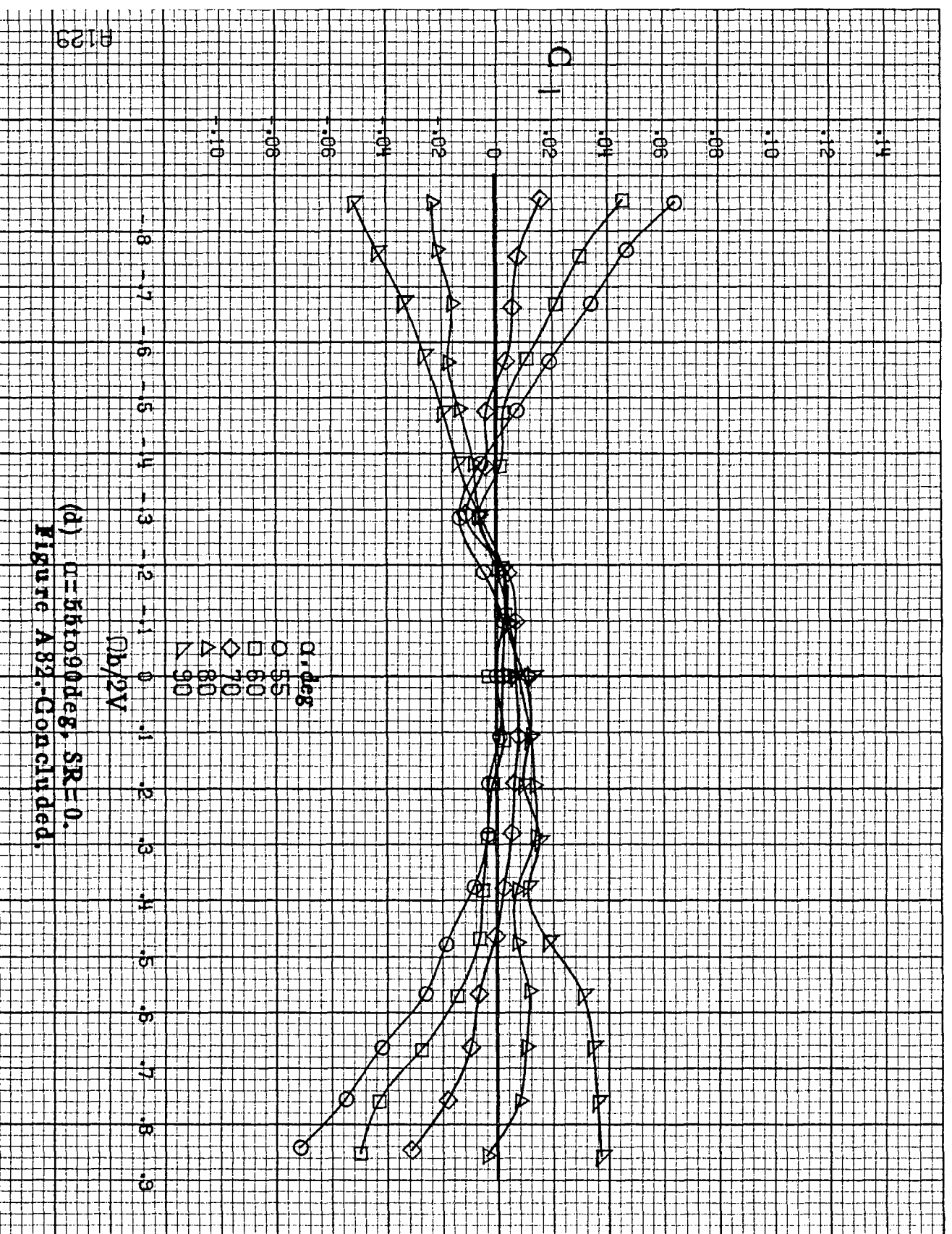
(a) $\alpha = 8$ to 16° , $SR = 76 \text{ cm (30 in.)}$.

Figure A32: Effect of rotation rate and angle of attack on rolling-moment coefficient for basic configuration. $\delta_a = -25^\circ$, $\delta_s = 22.5^\circ$, $\delta_r = 25^\circ$, $\beta = 0^\circ$.





(c) $\alpha = 30$ to 50° , $SR = 0$.
Figure A32.-Continued.



P130

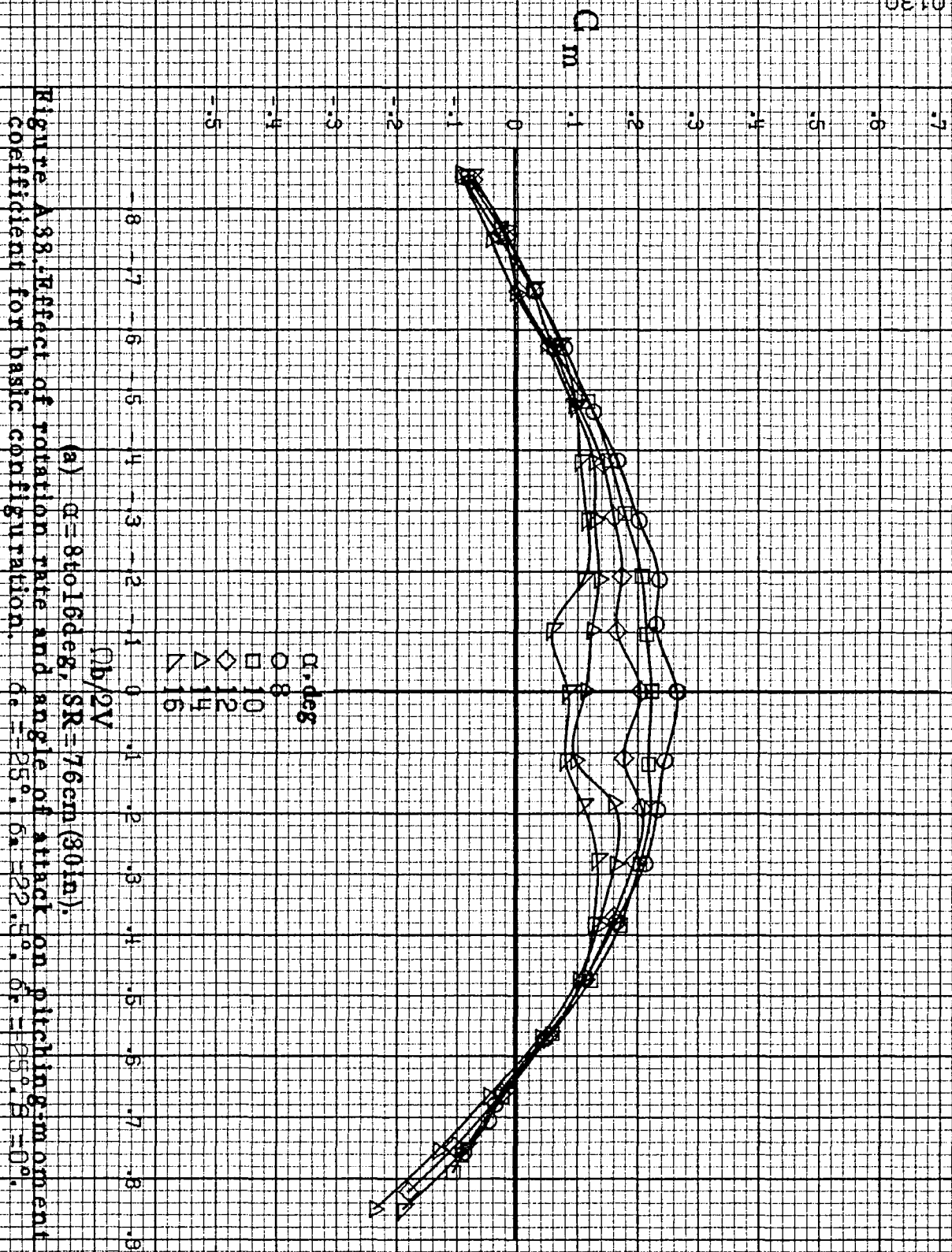
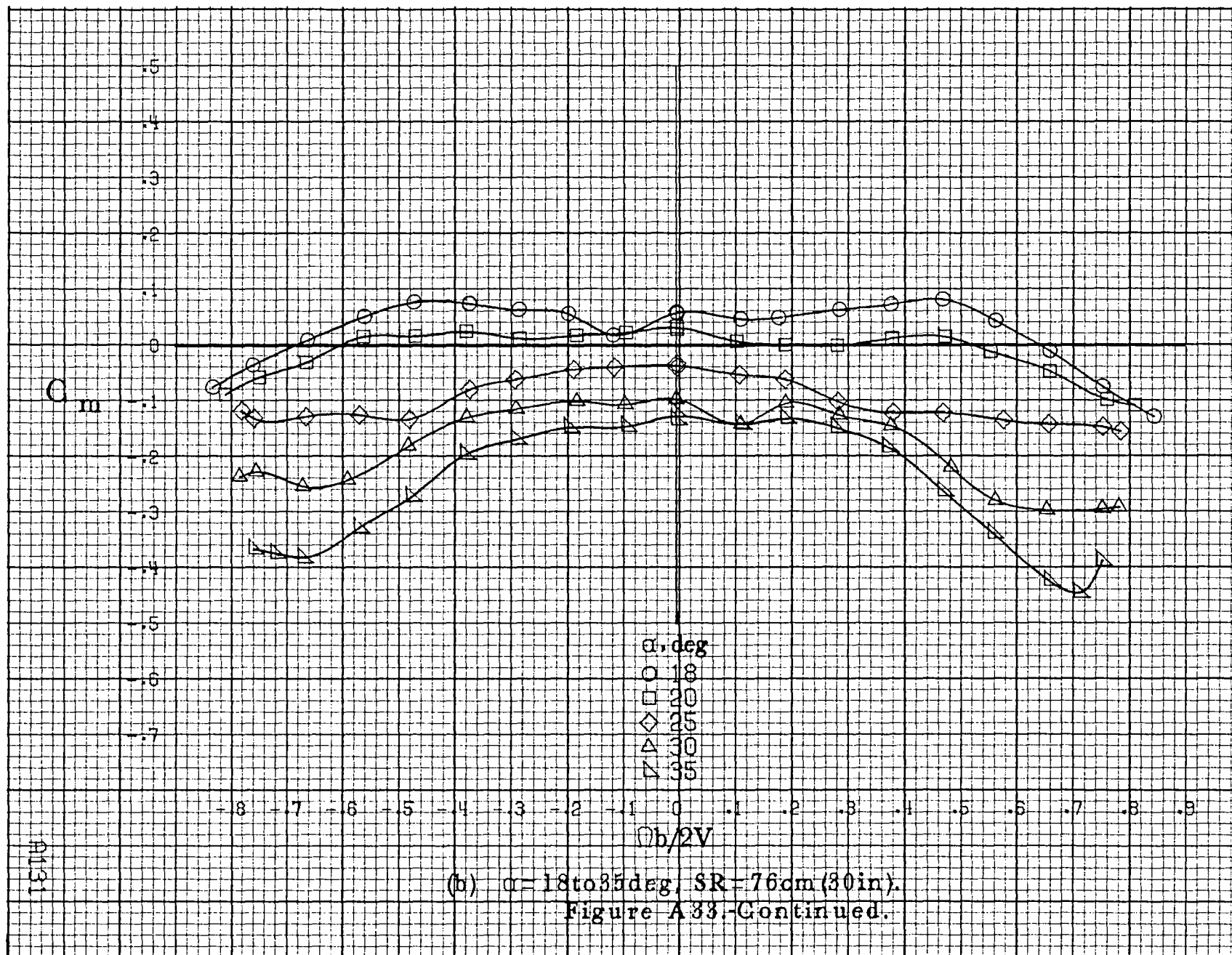


Figure A38. Effect of rotation rate and angle of attack on pitching moment coefficient for basic configuration. $\alpha_a = -25^\circ$, $\alpha_a = -22.5^\circ$, $\alpha_a = -20^\circ$, $\alpha_a = -17.5^\circ$, $\alpha_a = -15^\circ$, $\alpha_a = -12.5^\circ$, $\alpha_a = -10^\circ$, $\alpha_a = -7.5^\circ$, $\alpha_a = -5^\circ$, $\alpha_a = -2.5^\circ$, $\alpha_a = 0^\circ$.



C_m

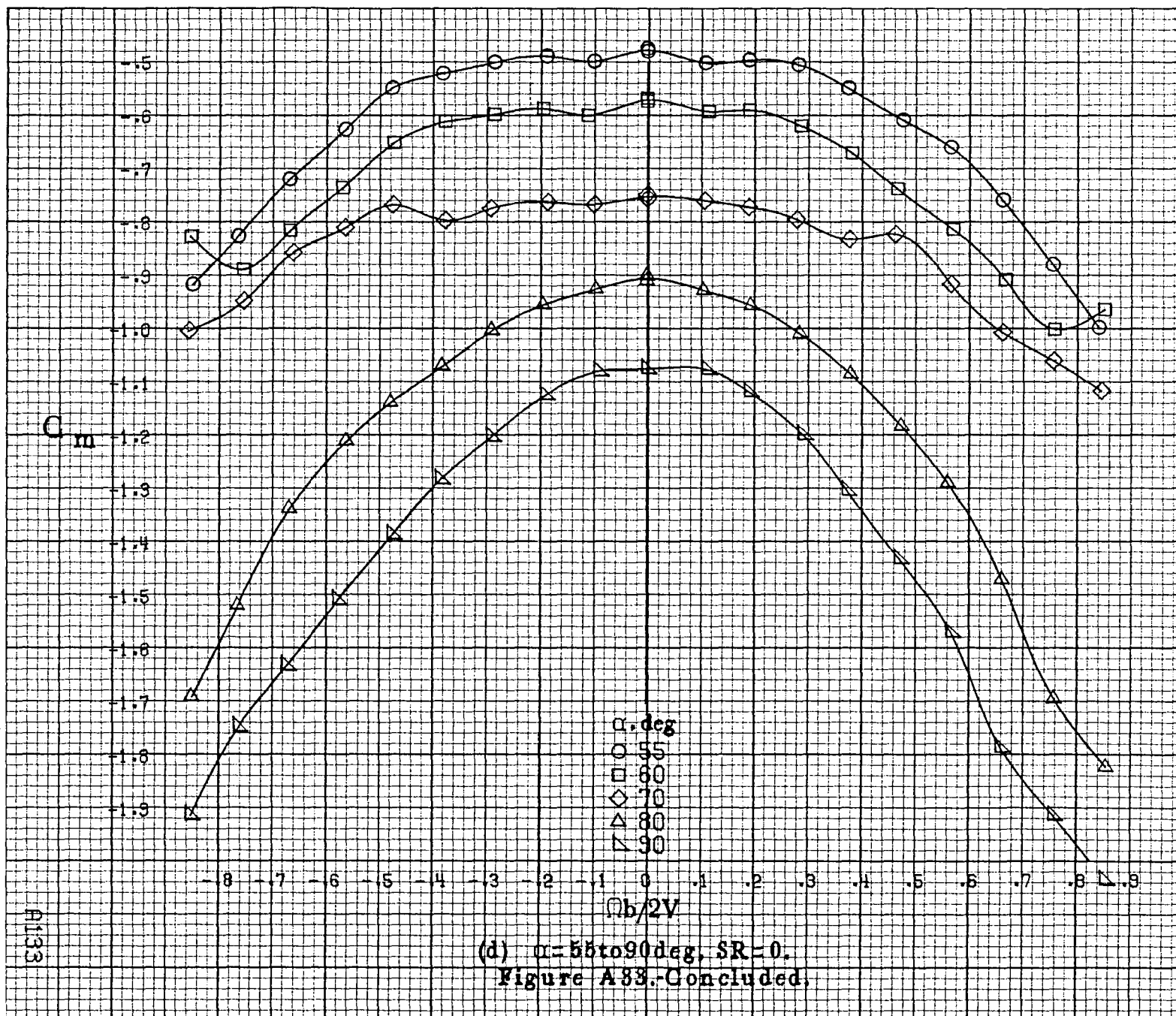
.2
 .1
 0
 -.1
 -.2
 -.3
 -.4
 -.5
 -.6
 -.7
 -.8
 -.9
 -1.0

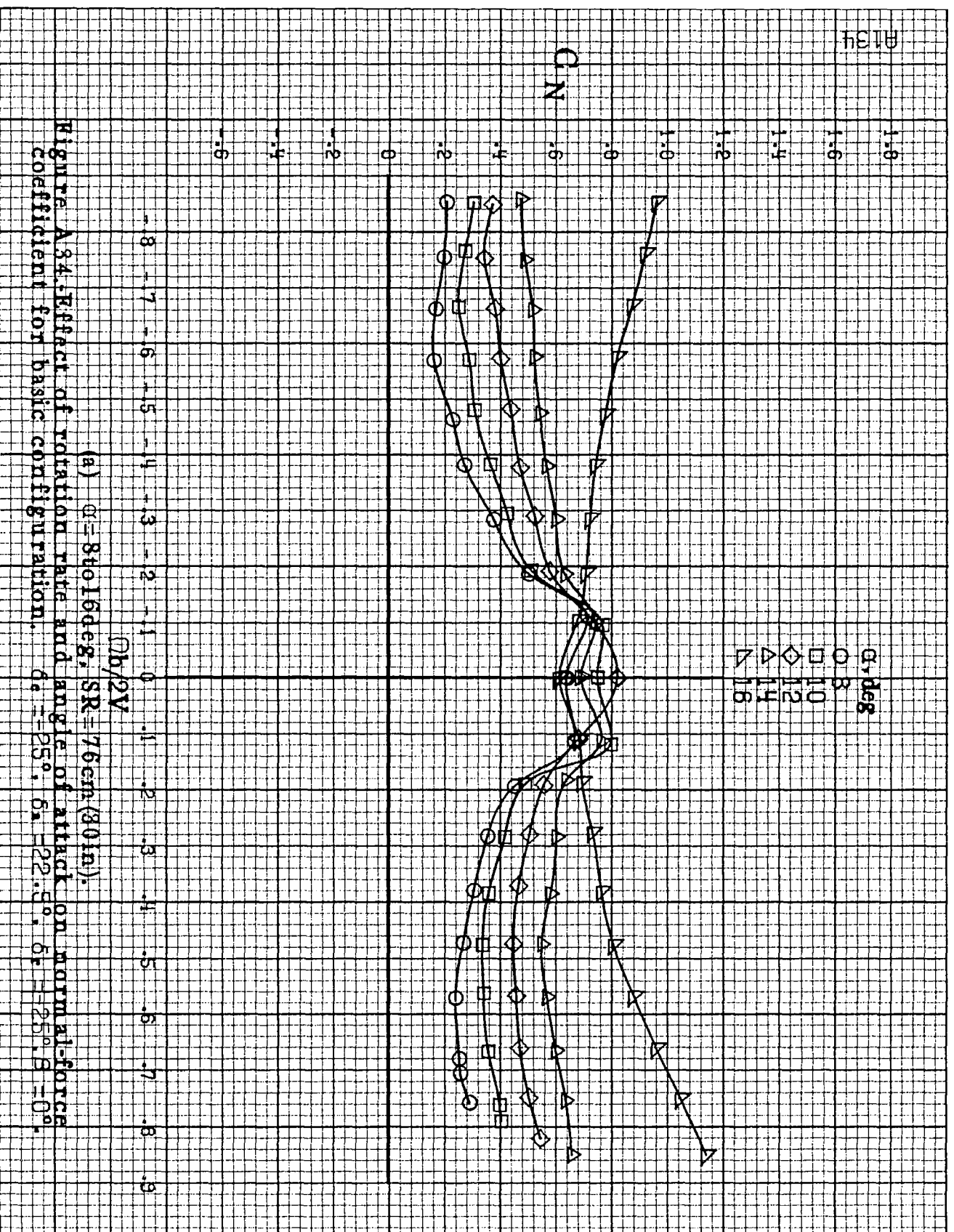
α , deg
 ○ 30
 □ 35
 ◇ 40
 △ 45
 ▴ 50

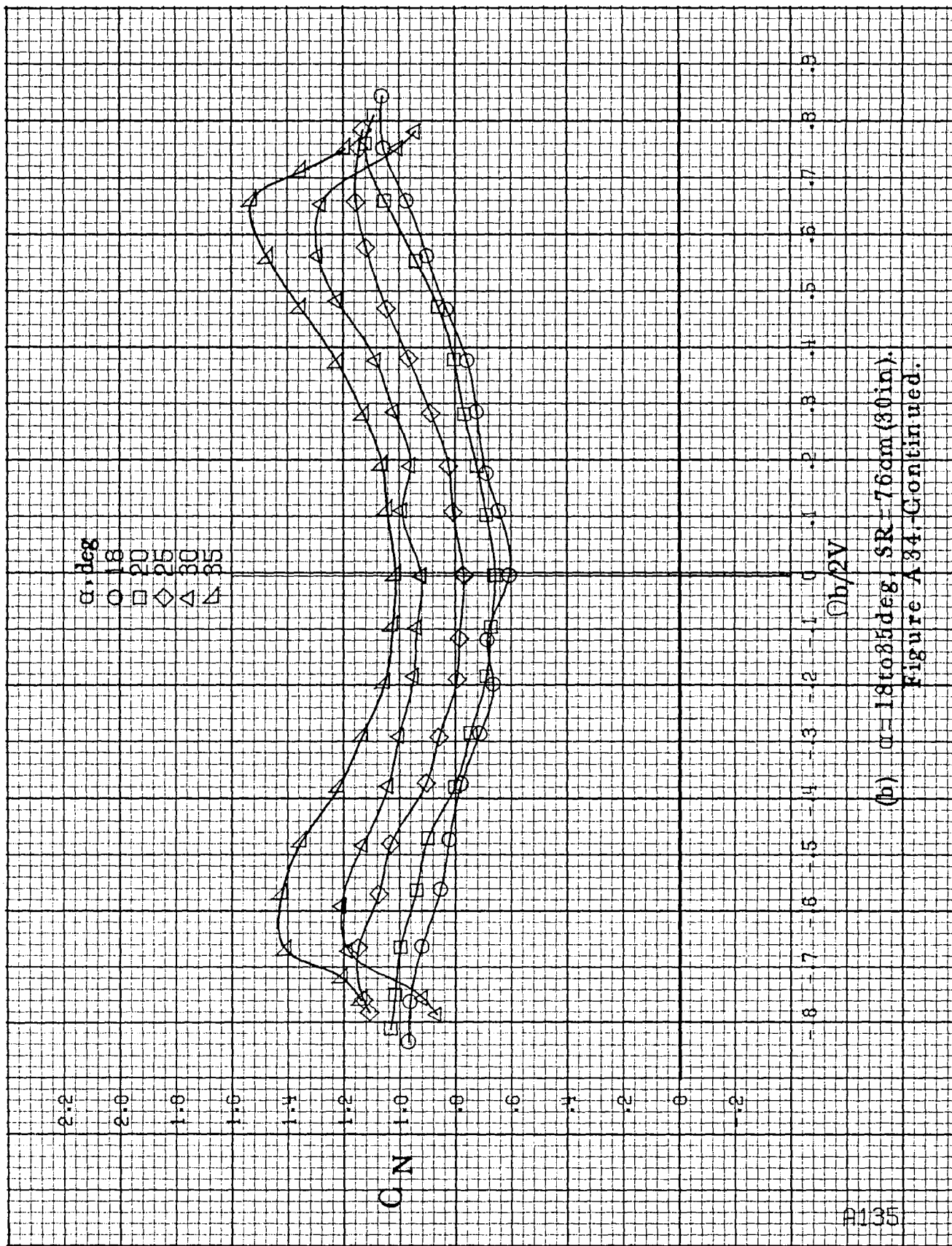
 $\Omega b/2V$

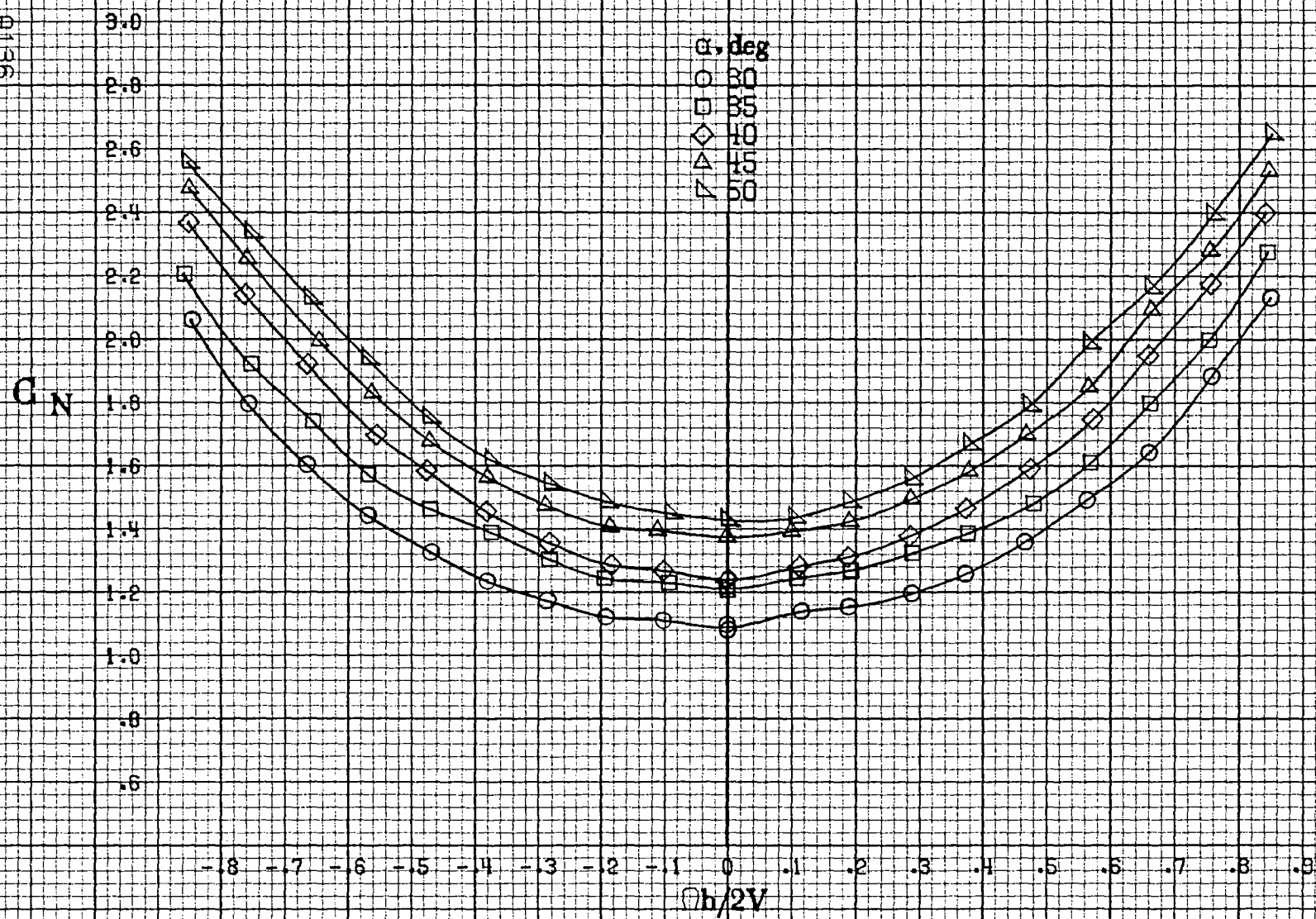
-.8 -.7 -.6 -.5 -.4 -.3 -.2 -.1 0 .1 .2 .3 .4 .5 .6 .7 .8 .9

(c) $\alpha=30$ to 50 deg, $SR=0$.
 Figure A88.-Continued.

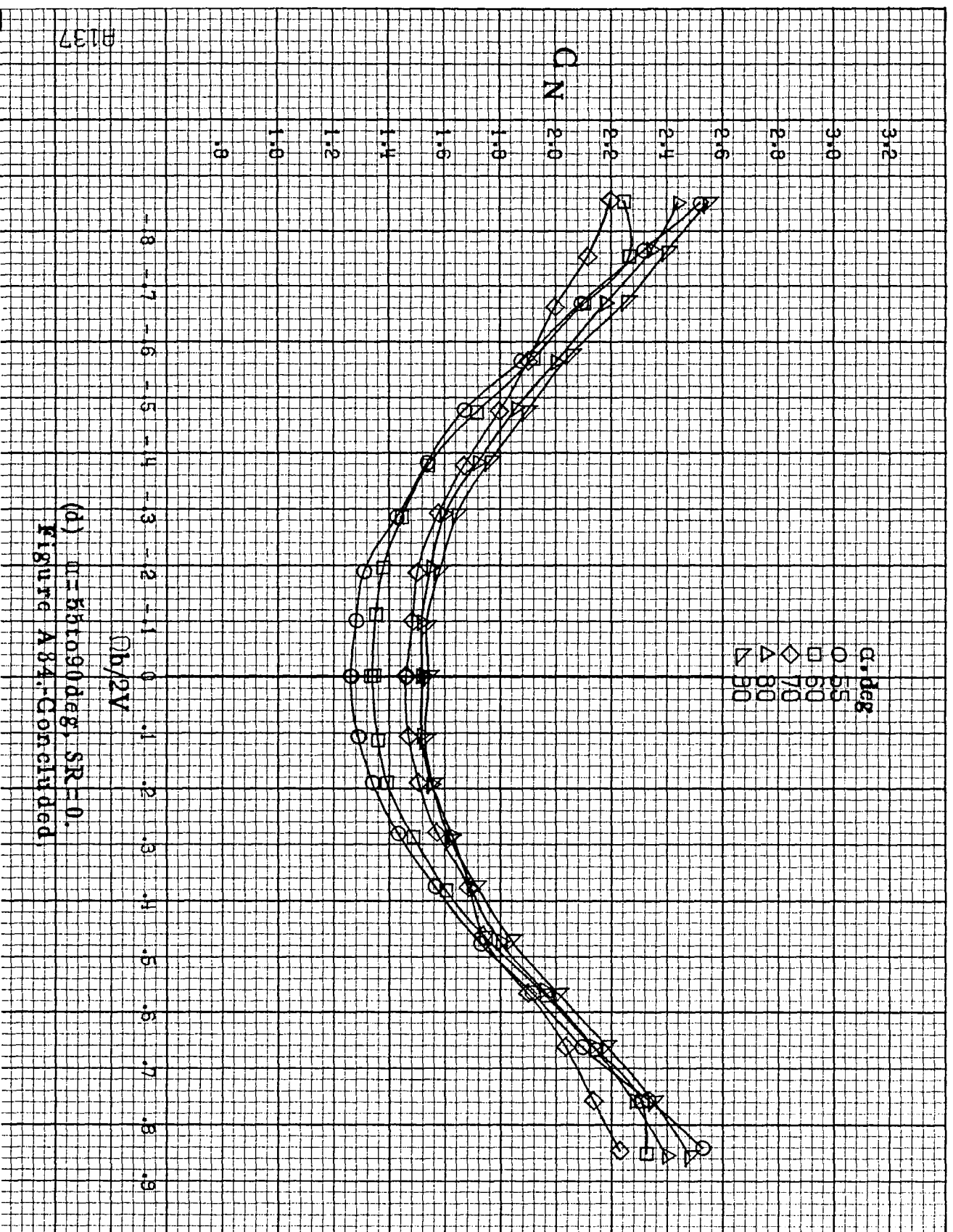




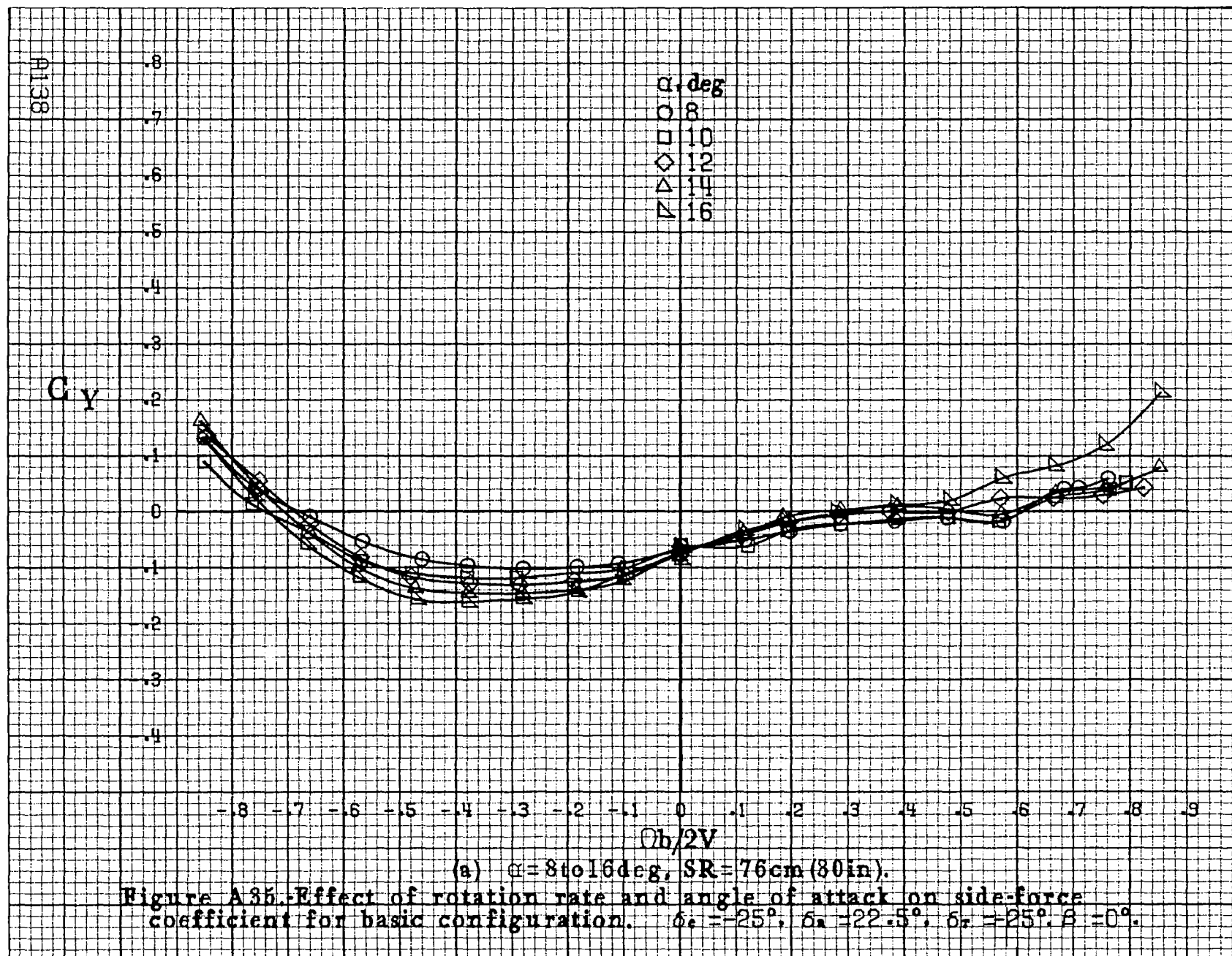


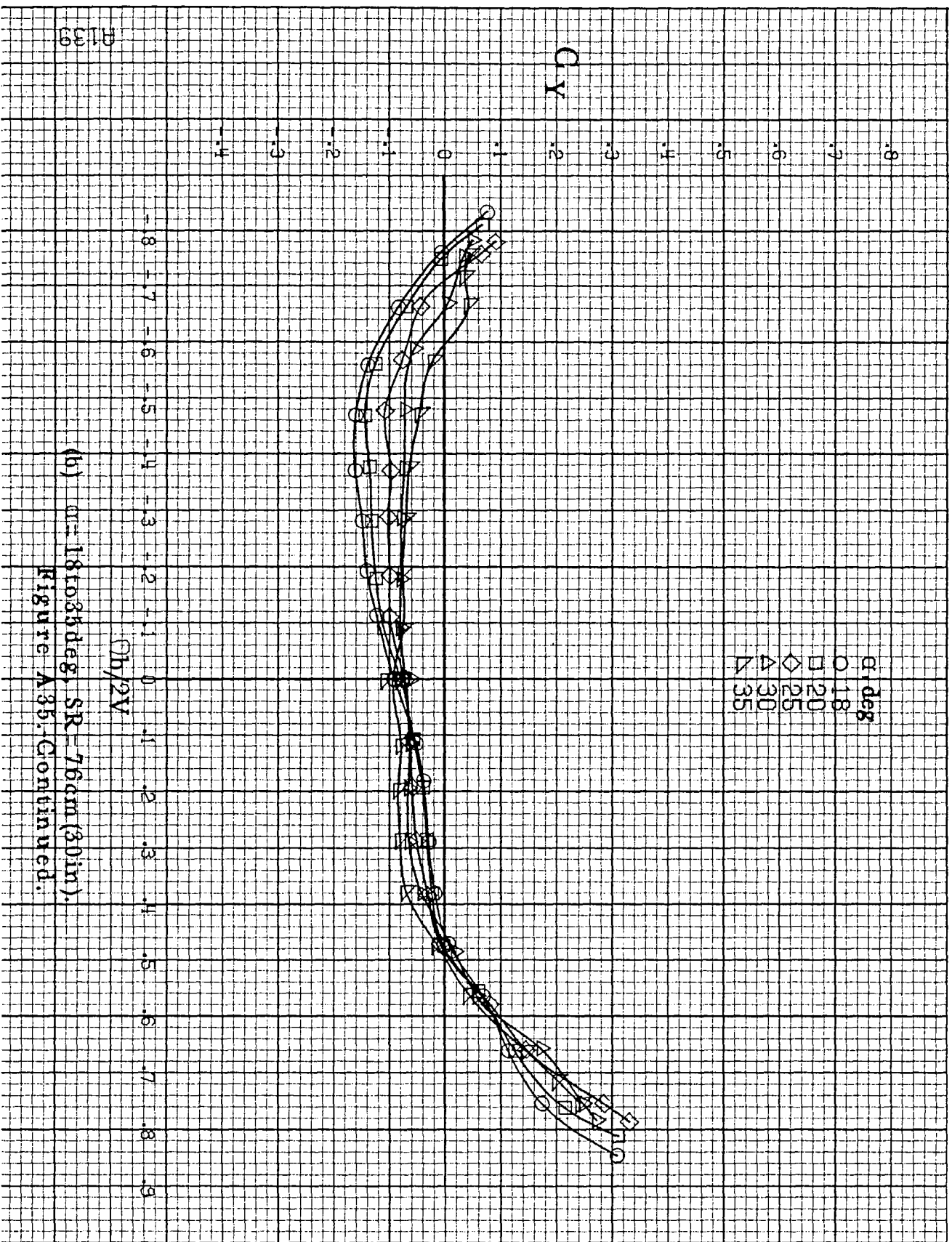


(c) $\alpha=30$ to 50 deg, $SR=0$.
Figure A84-Continued.

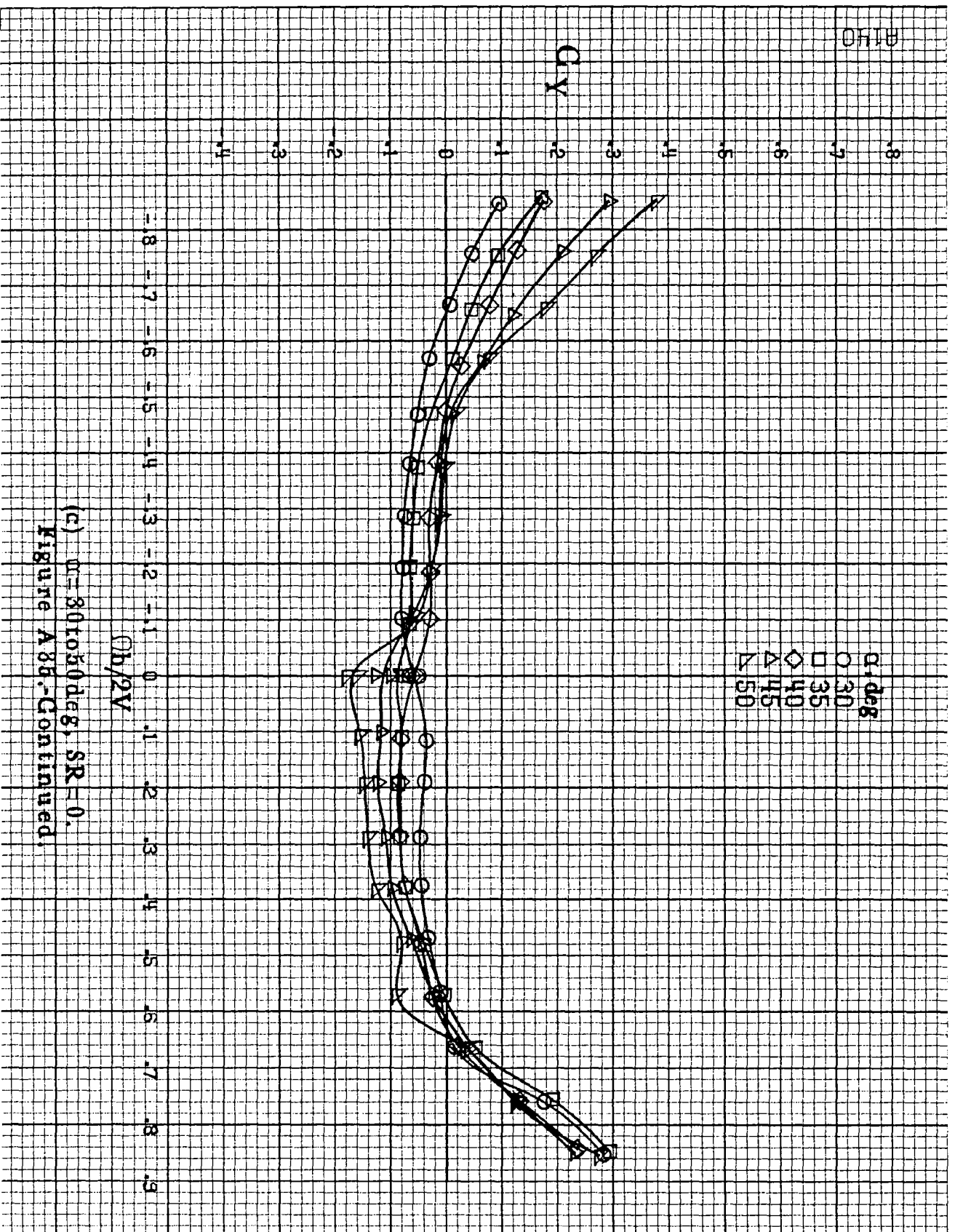


(d) $\alpha = 55$ to 90 deg, $SR = 0$.
Figure A84. Continued.

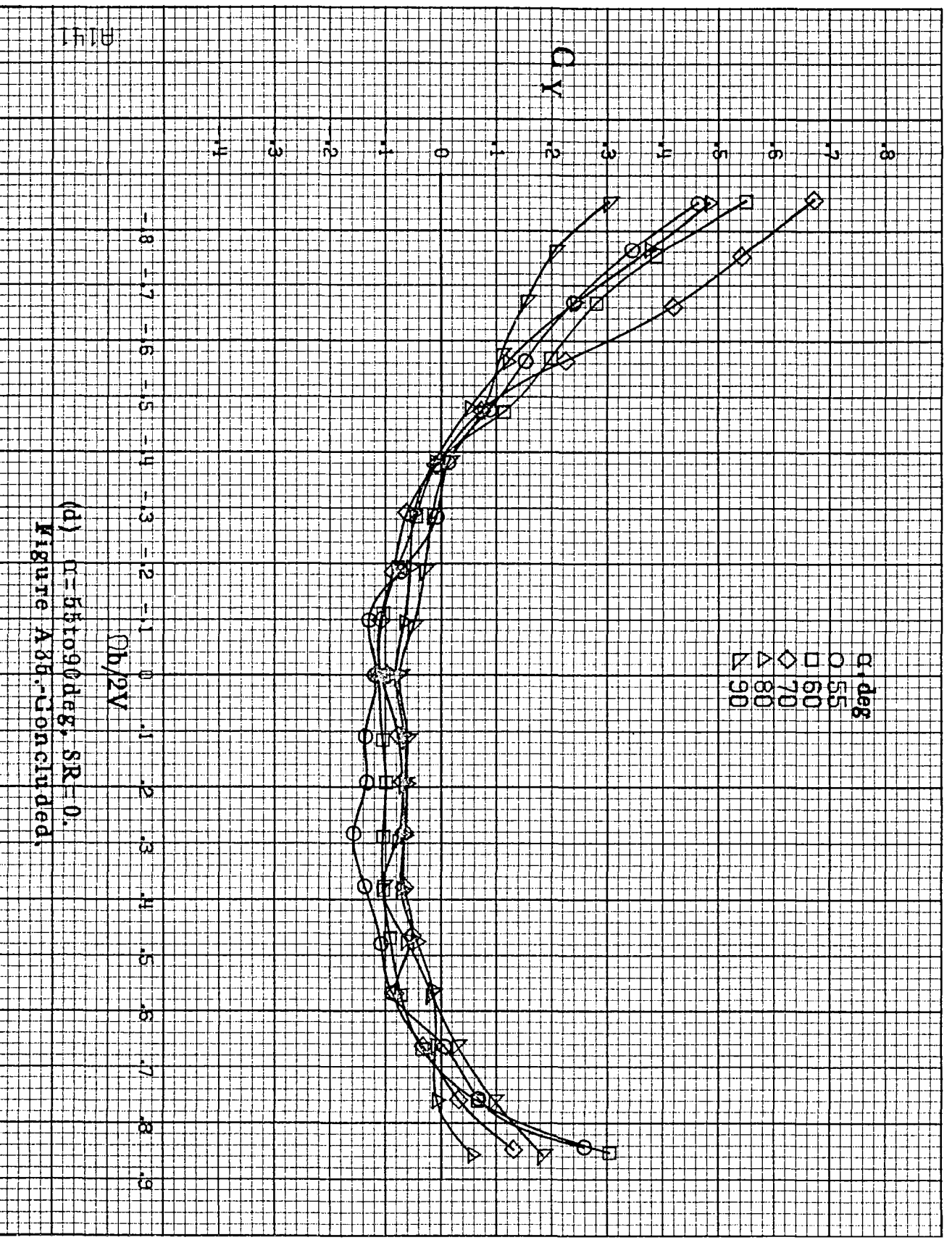




(b) $\alpha = 18$ to 35 deg, $SR = 76$ cm (30 in).
 Figure A35. Continued.



(c) $\alpha = 30$ to 50 deg, $SR = 0$.
Figure A88-Continued.



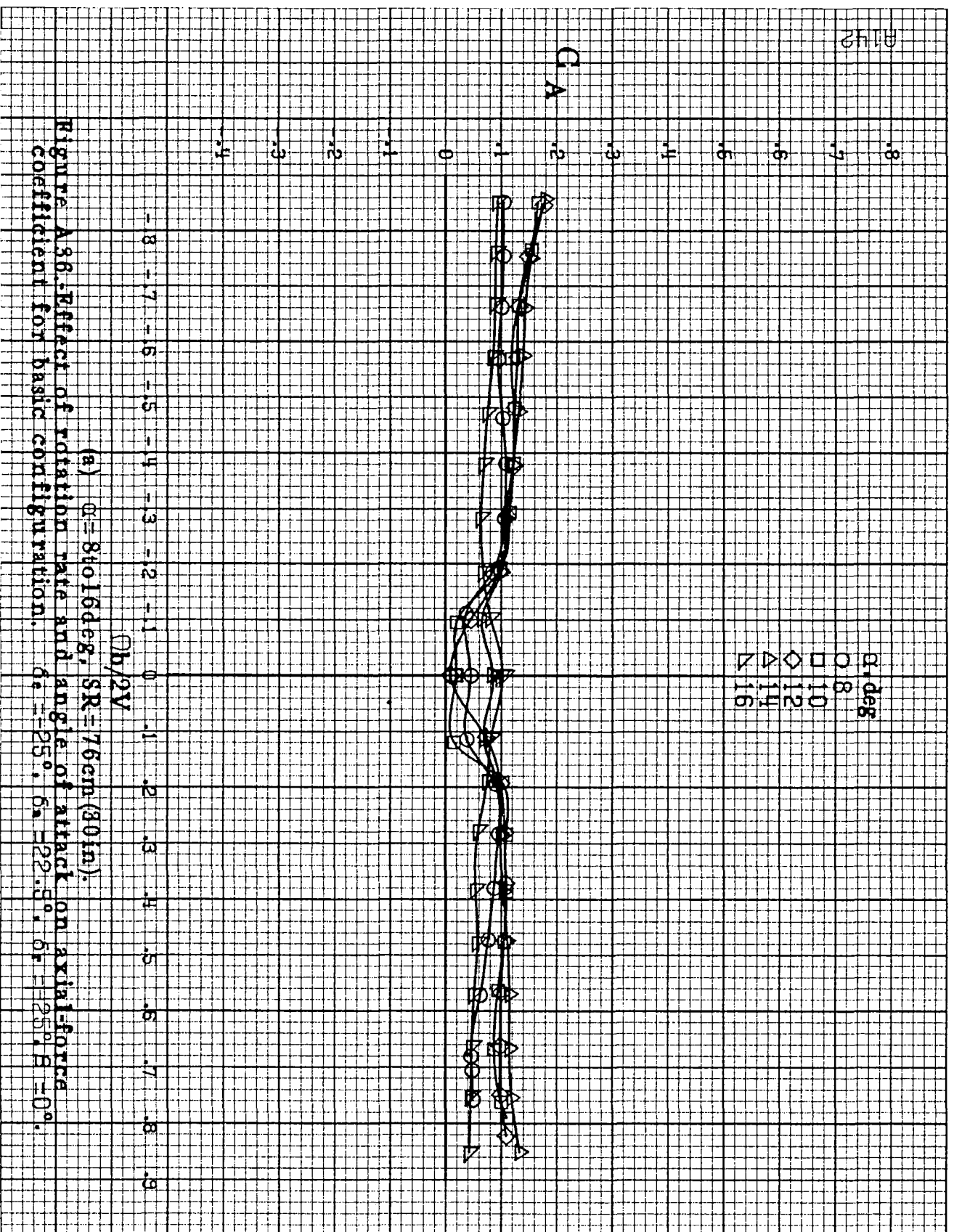
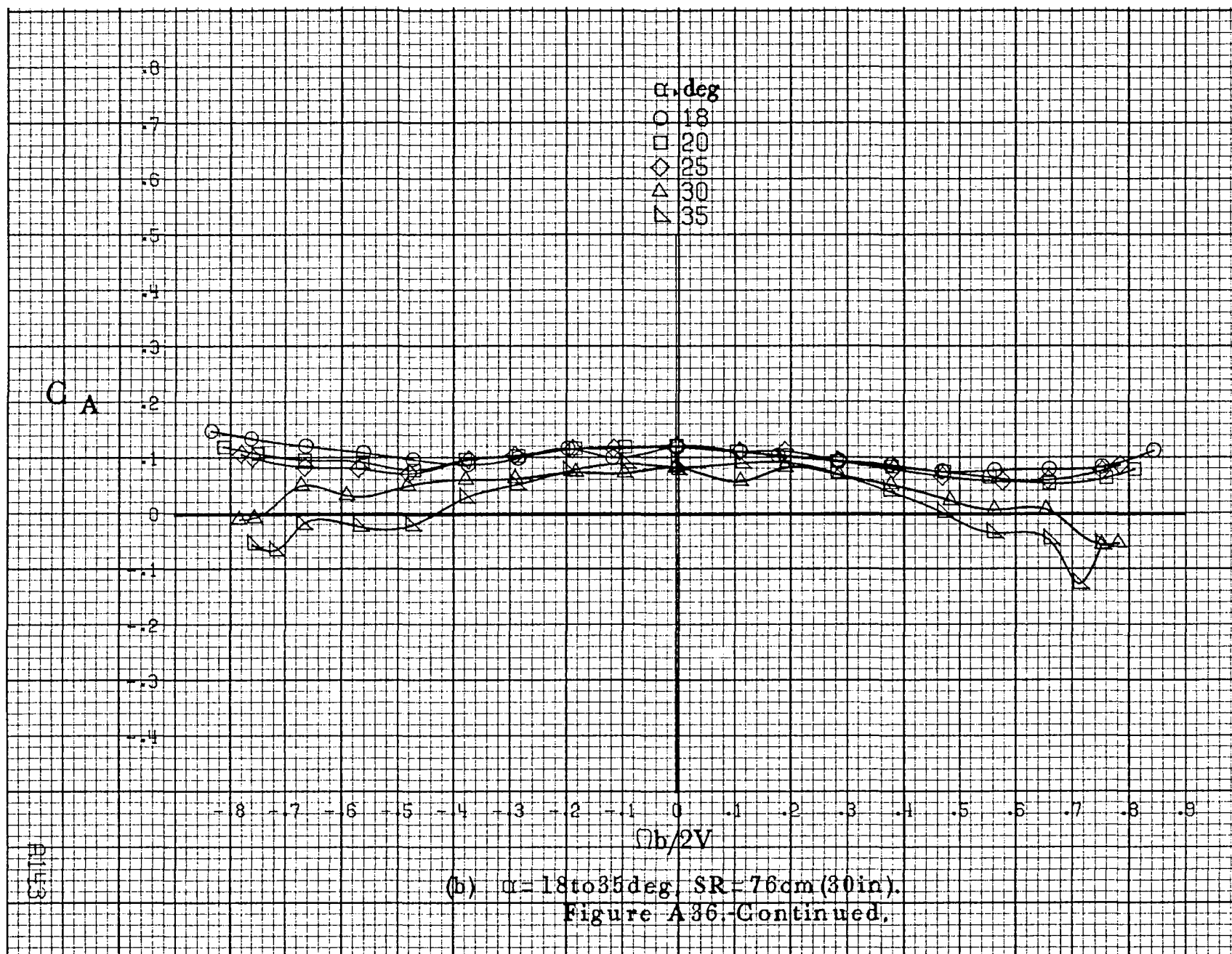
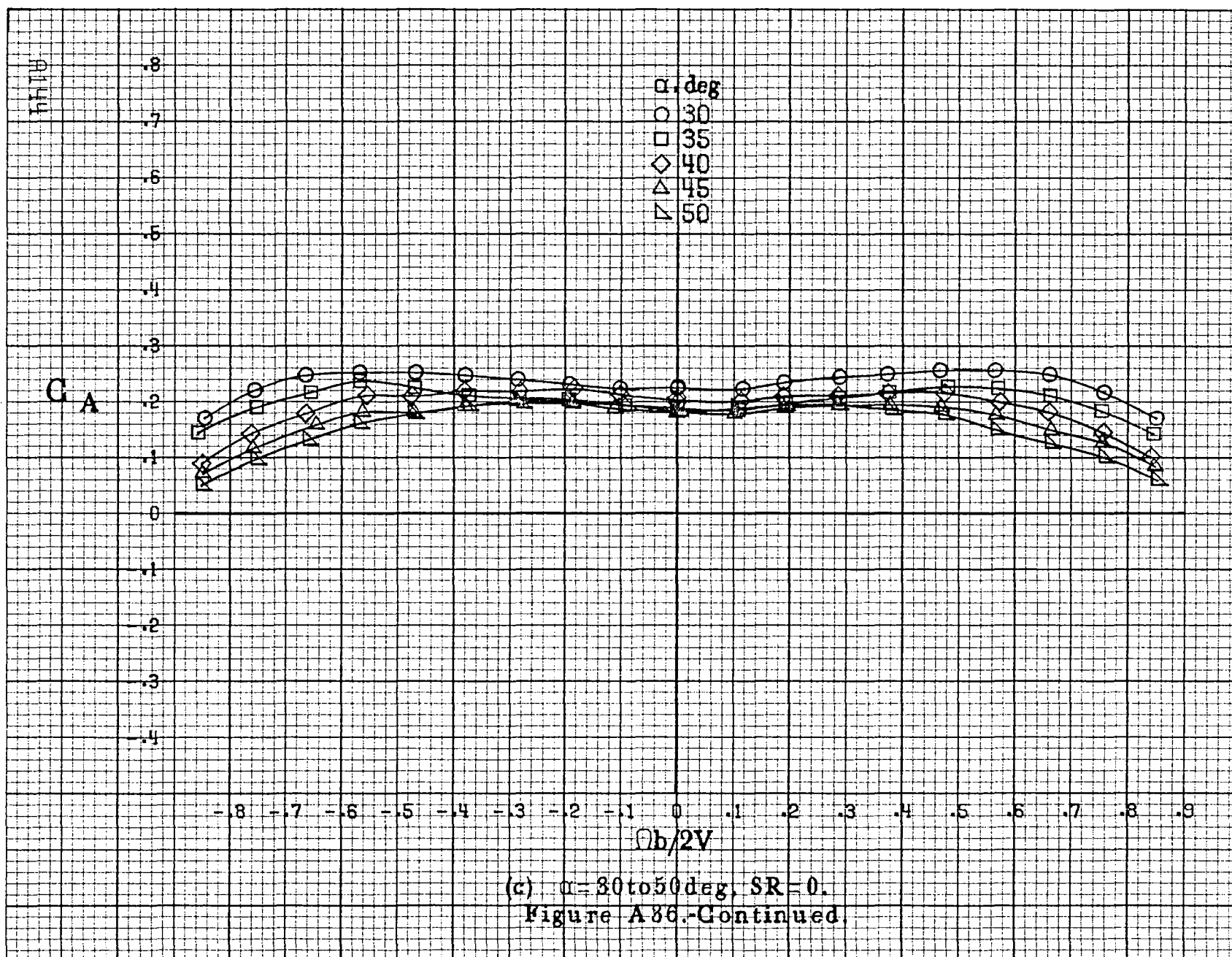
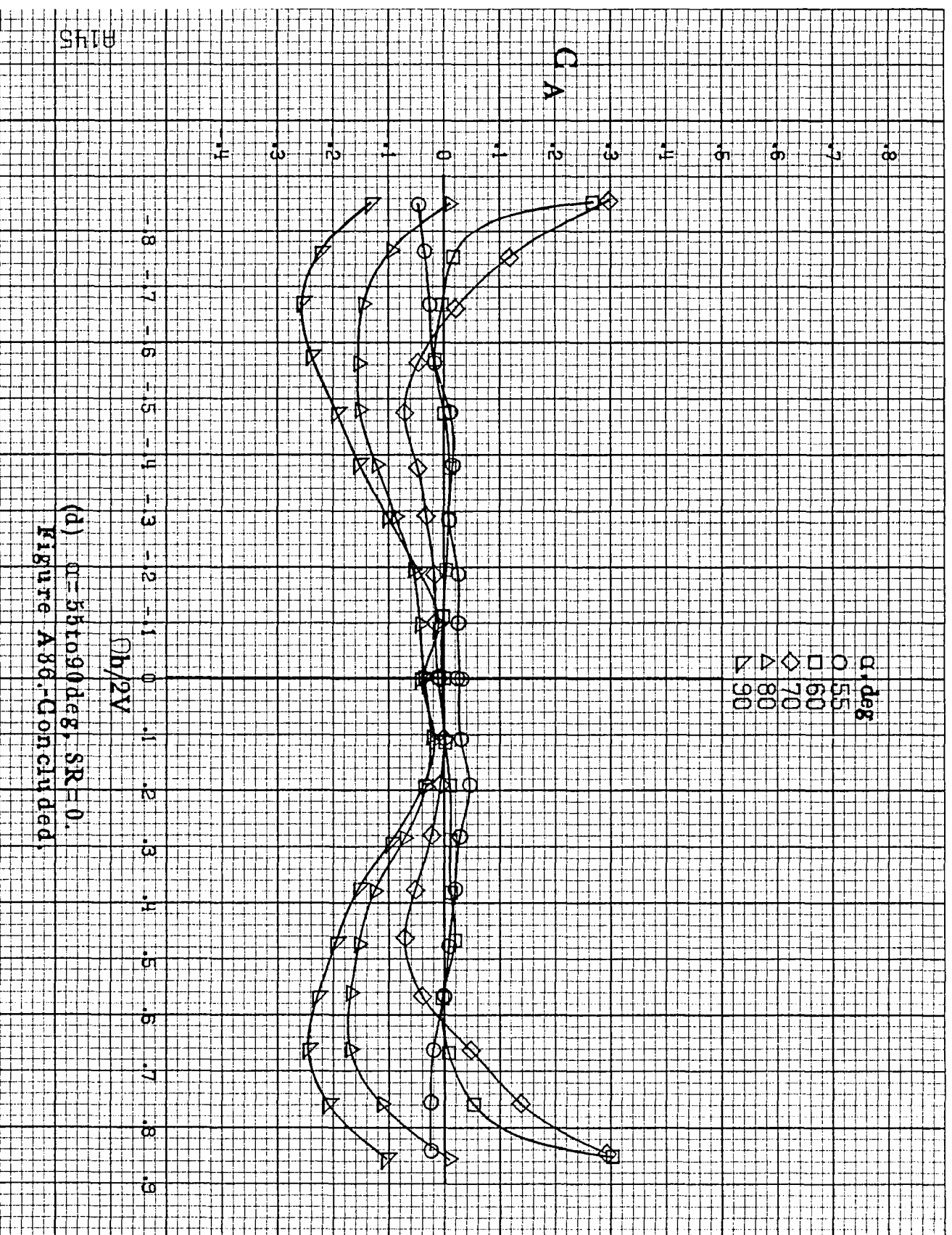


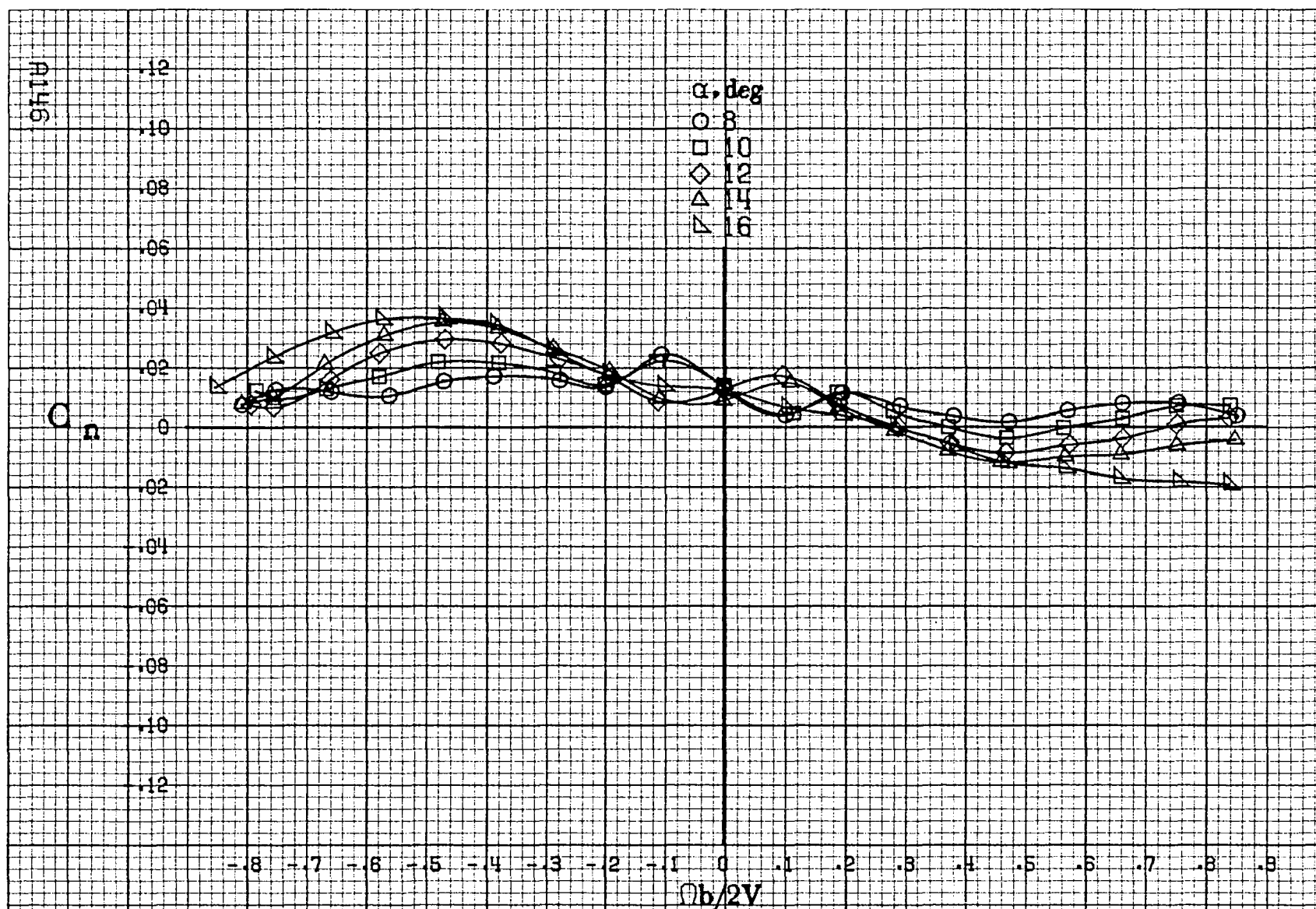
Figure A3.6: Effect of rotation rate and angle of attack on axial force coefficient for basic configuration. $\alpha = 25^\circ$, $\alpha_a = 22.5^\circ$, $\alpha_r = 25^\circ$, $\beta = 0^\circ$.





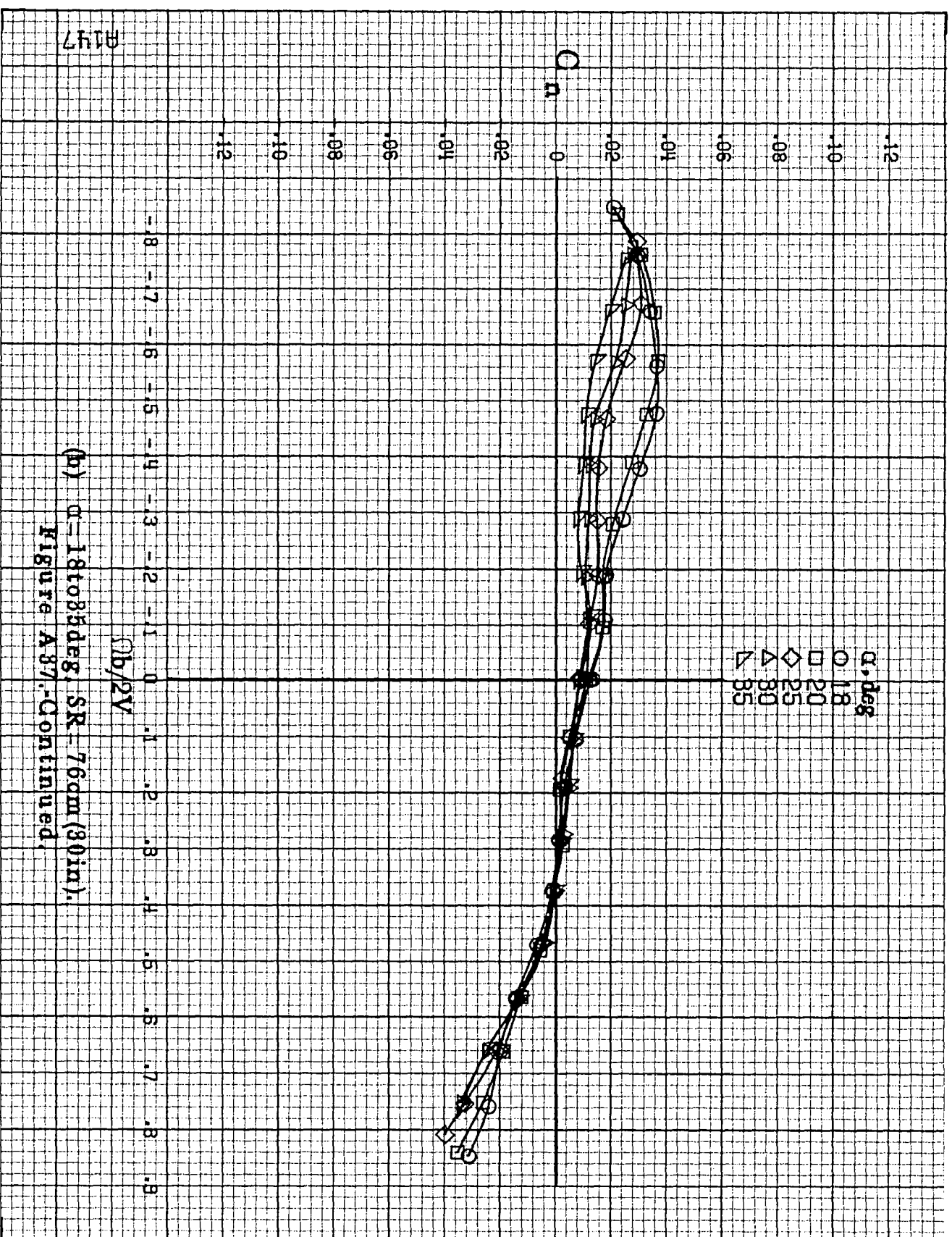


(d) $\alpha = 55$ to 90° deg, $SR = 0$.
Figure A86-Concluded.

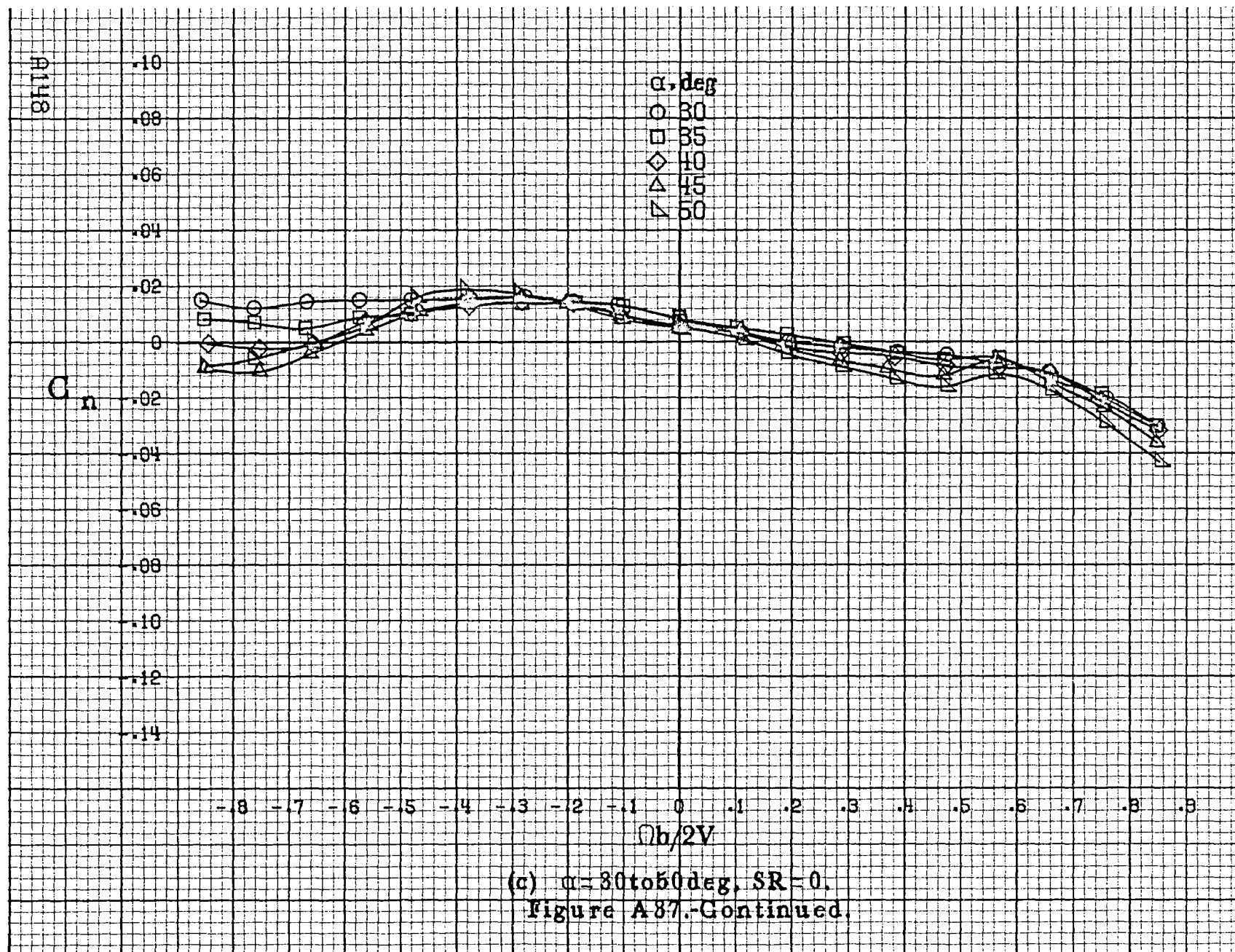


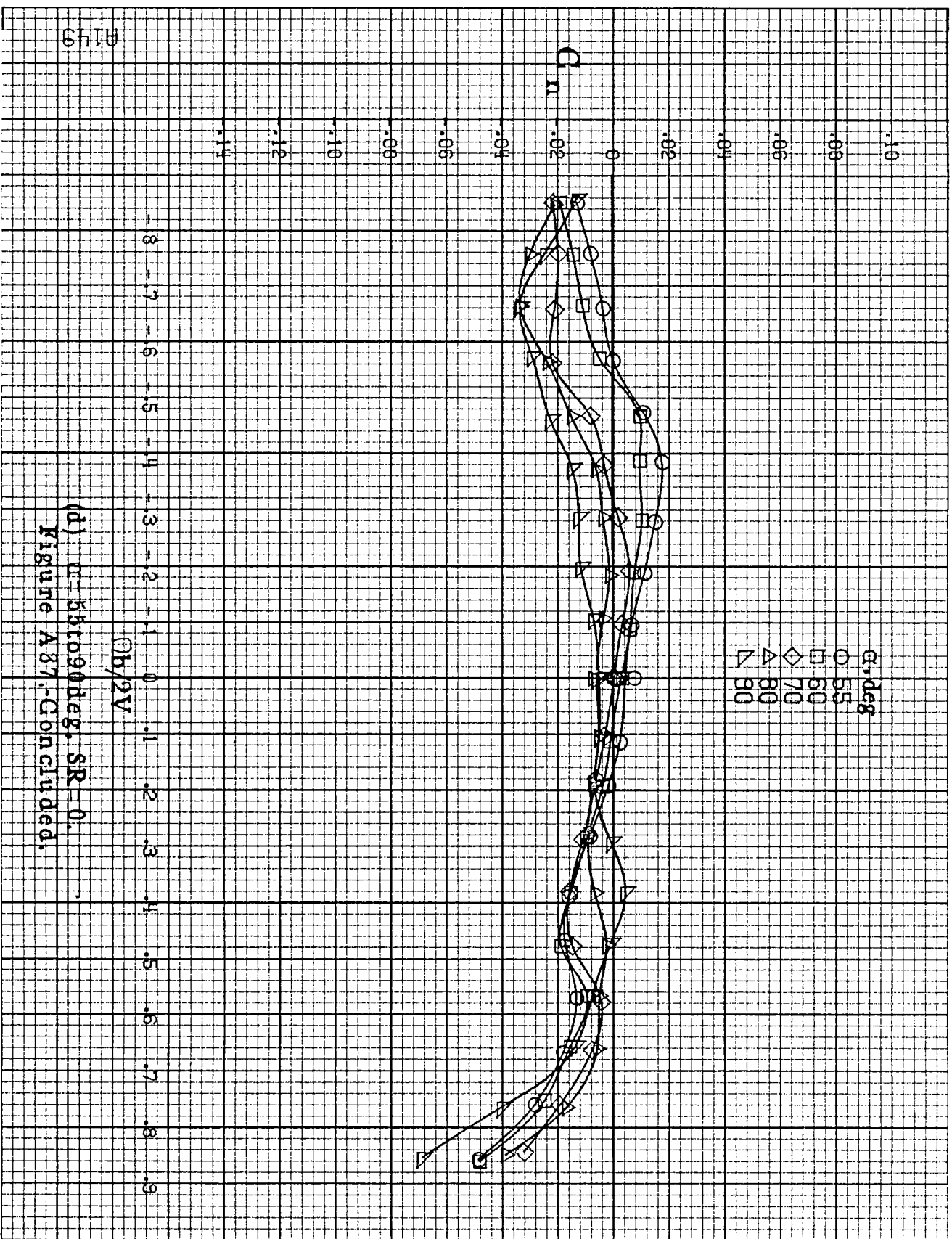
(a) $\alpha = 8$ to 16° , $SR = 76\text{cm (30in)}$.

Figure A37. Effect of rotation rate and angle of attack on yawing-moment coefficient for basic configuration. $\delta_a = \pm 25^\circ$, $\delta_n = -22.5^\circ$, $\delta_r = \pm 25^\circ$, $\beta = 0^\circ$.

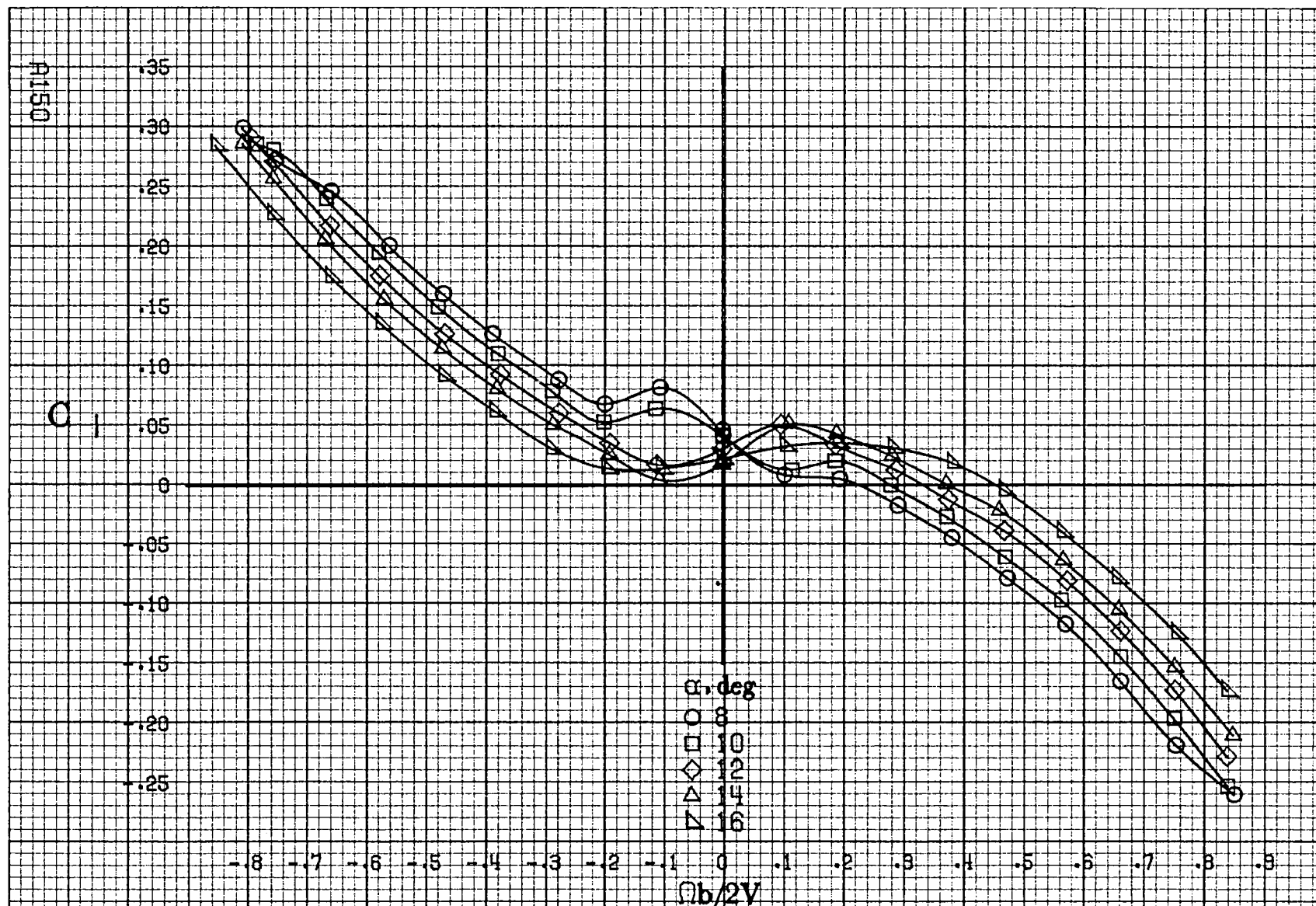


(b) $\alpha=18$ to 35 deg, SR = 76 cm (30 in).
Figure A37.-Continued.



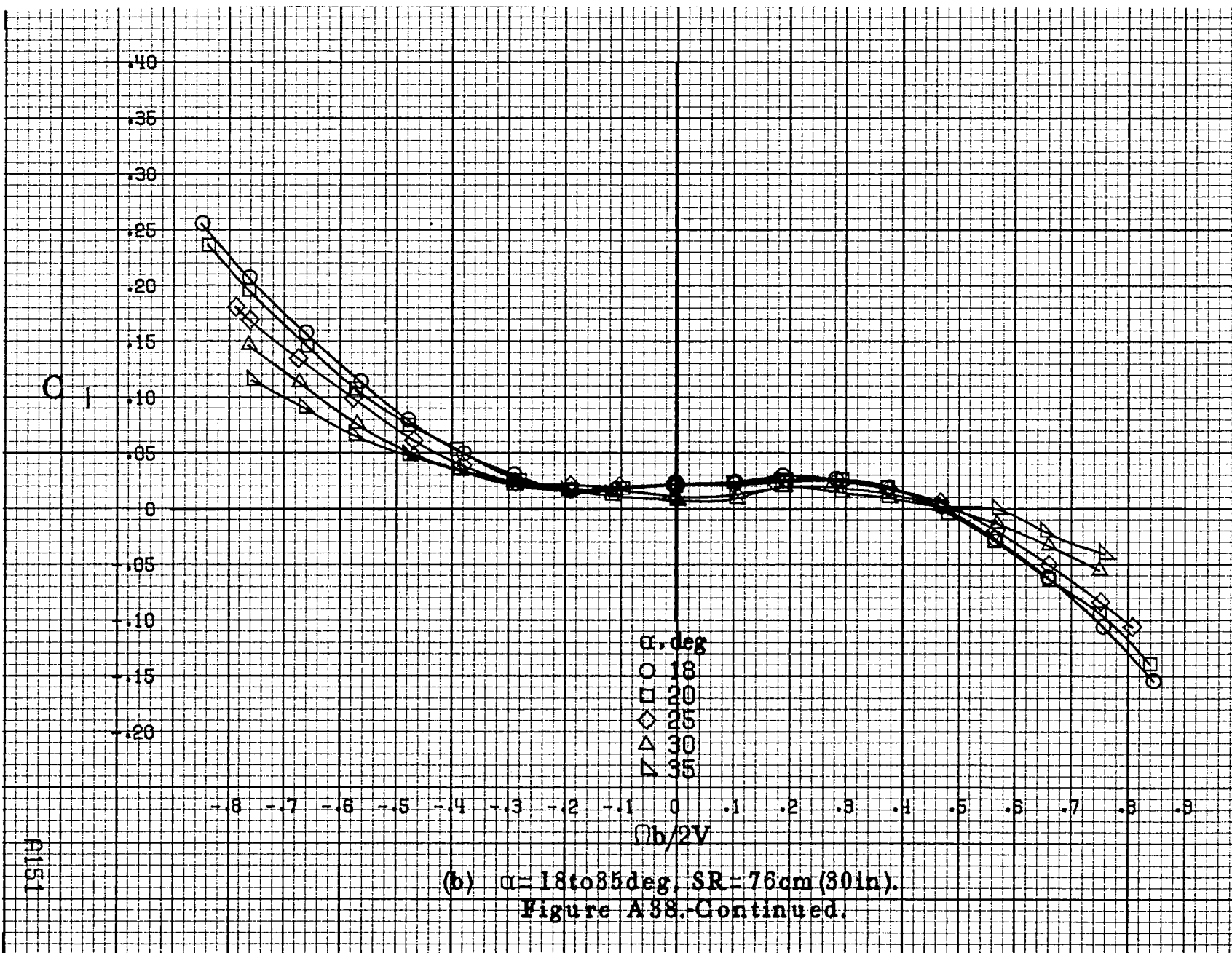


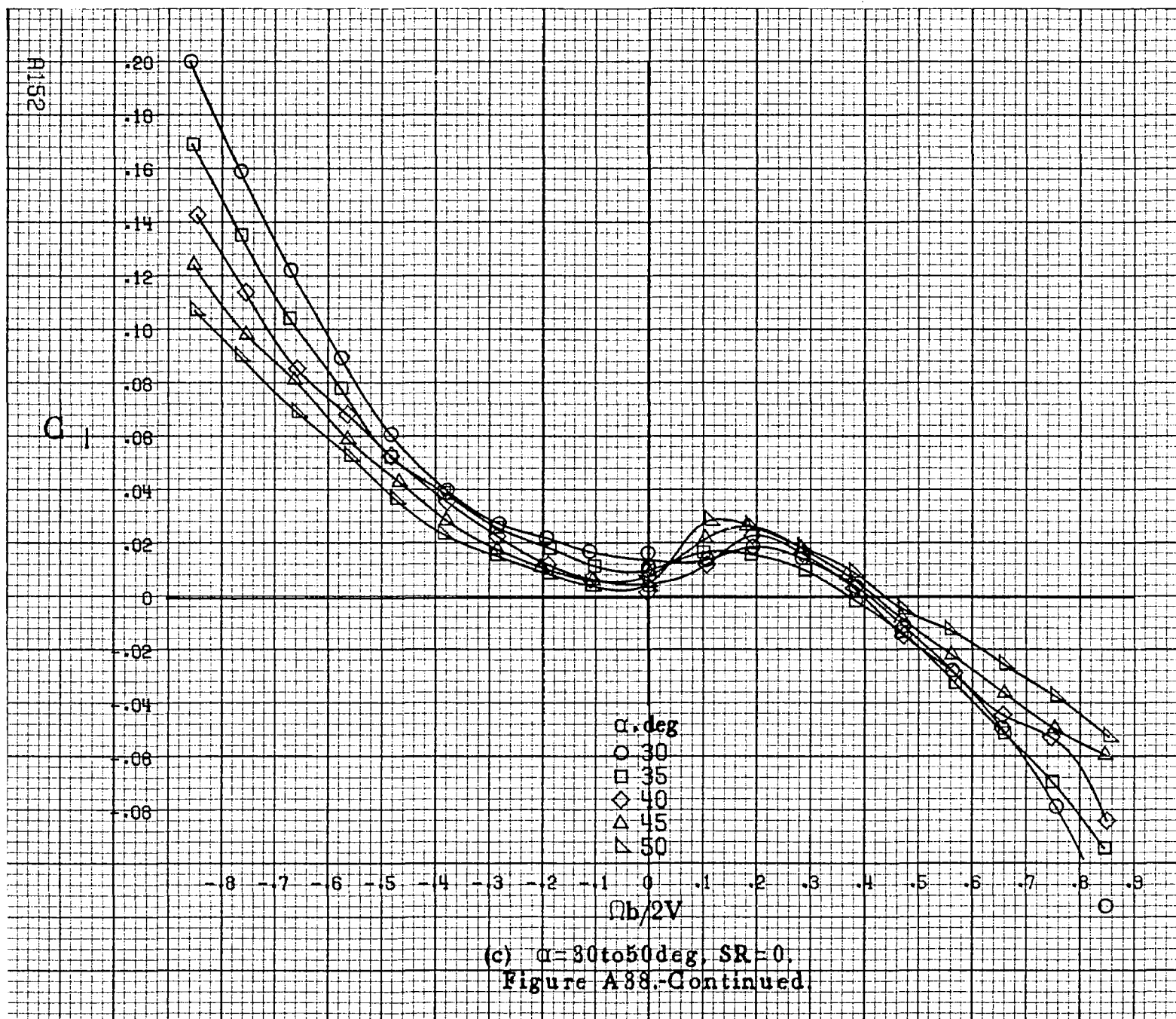
(d) $\alpha = 55$ to 90° deg, $SR = 0$.
 Figure A87.-Concluded.

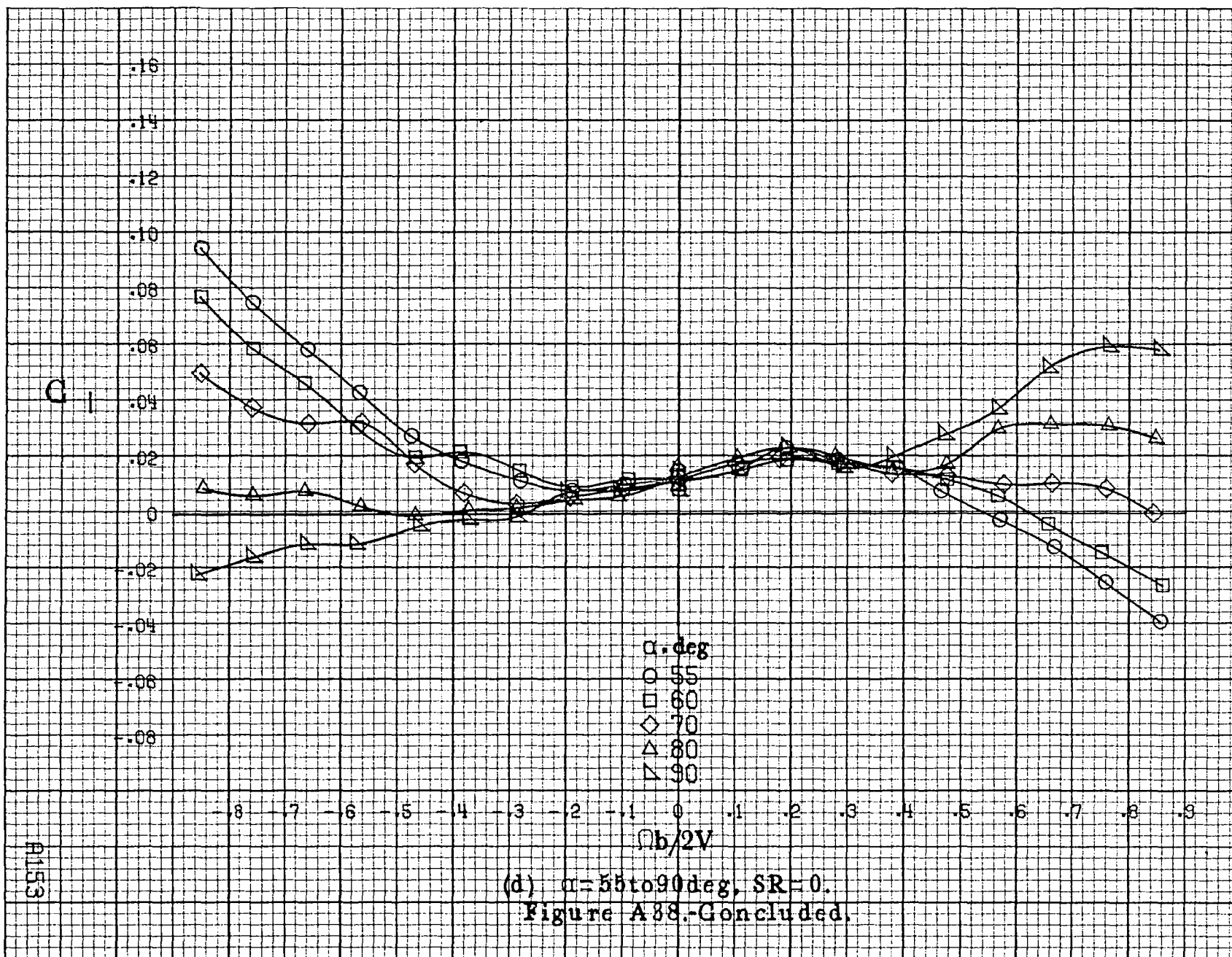


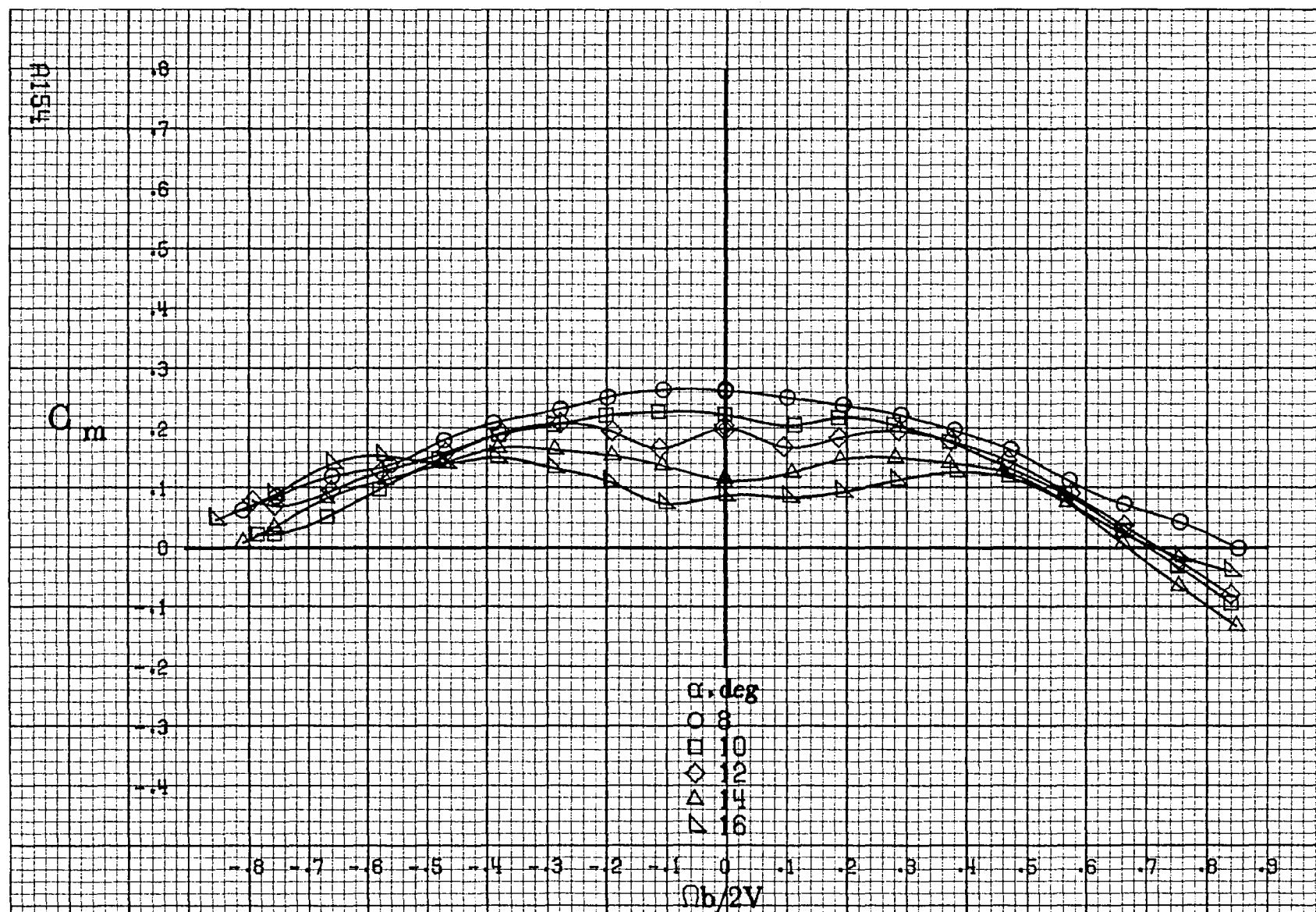
(a) $\alpha = 8$ to 16° , $SR = 76\text{cm} (30\text{in})$.

Figure A38. Effect of rotation rate and angle of attack on rolling-moment coefficient for basic configuration. $\delta_e = -25^\circ$, $\delta_n = -22.5^\circ$, $\delta_r = -25^\circ$, $\beta = 0^\circ$.



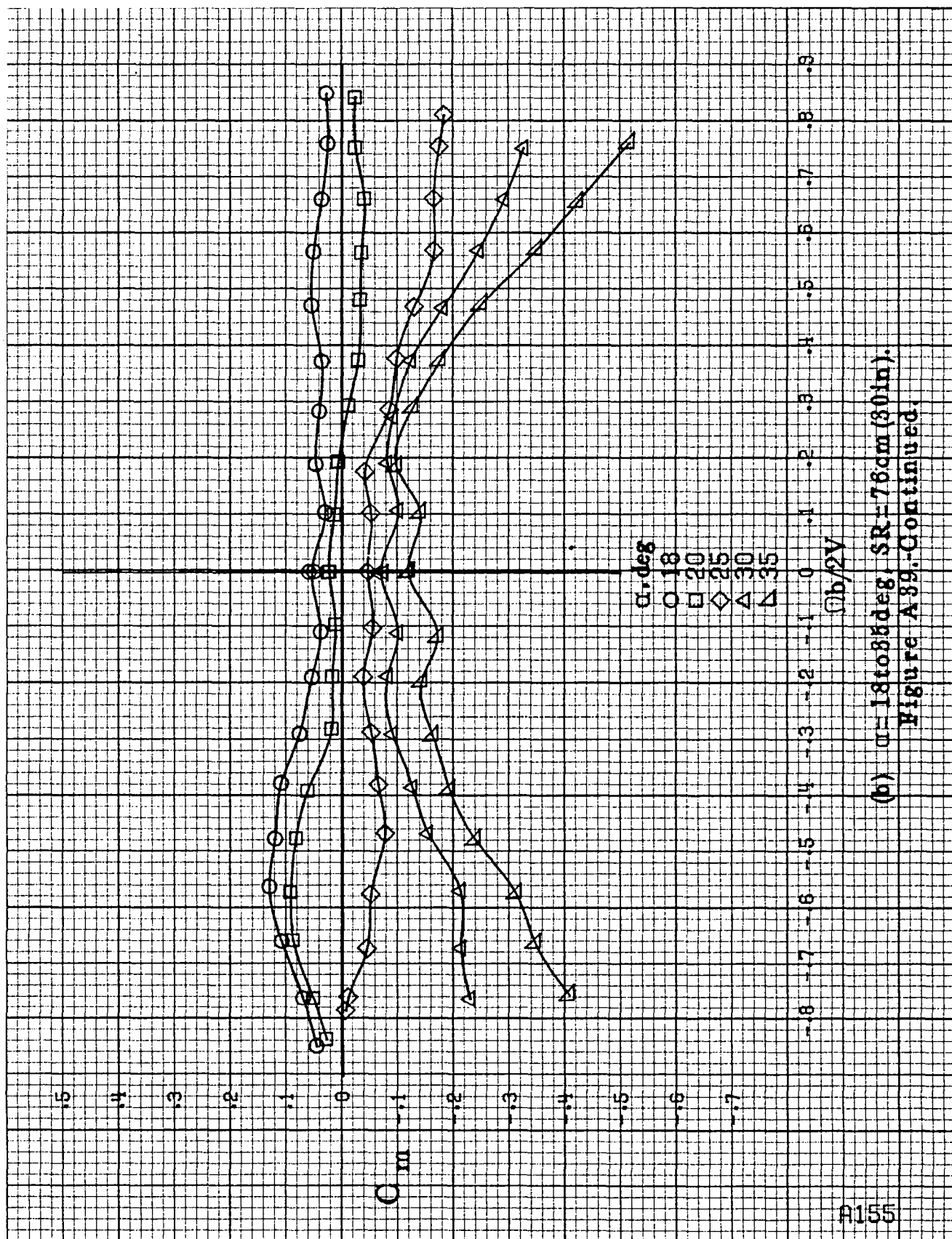




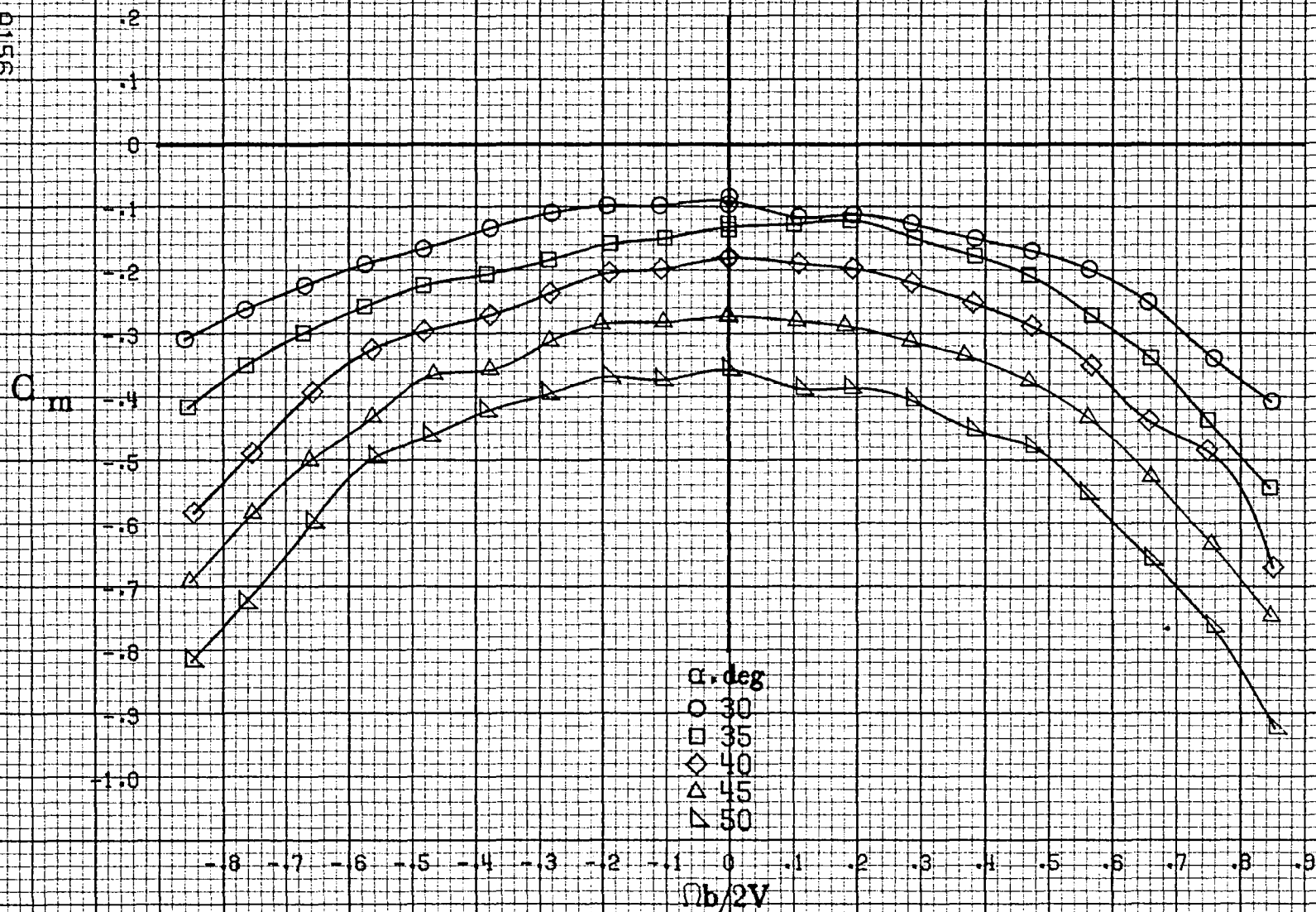


(a) $\alpha = 8$ to 16 deg, $SR = 76$ cm (30 in).

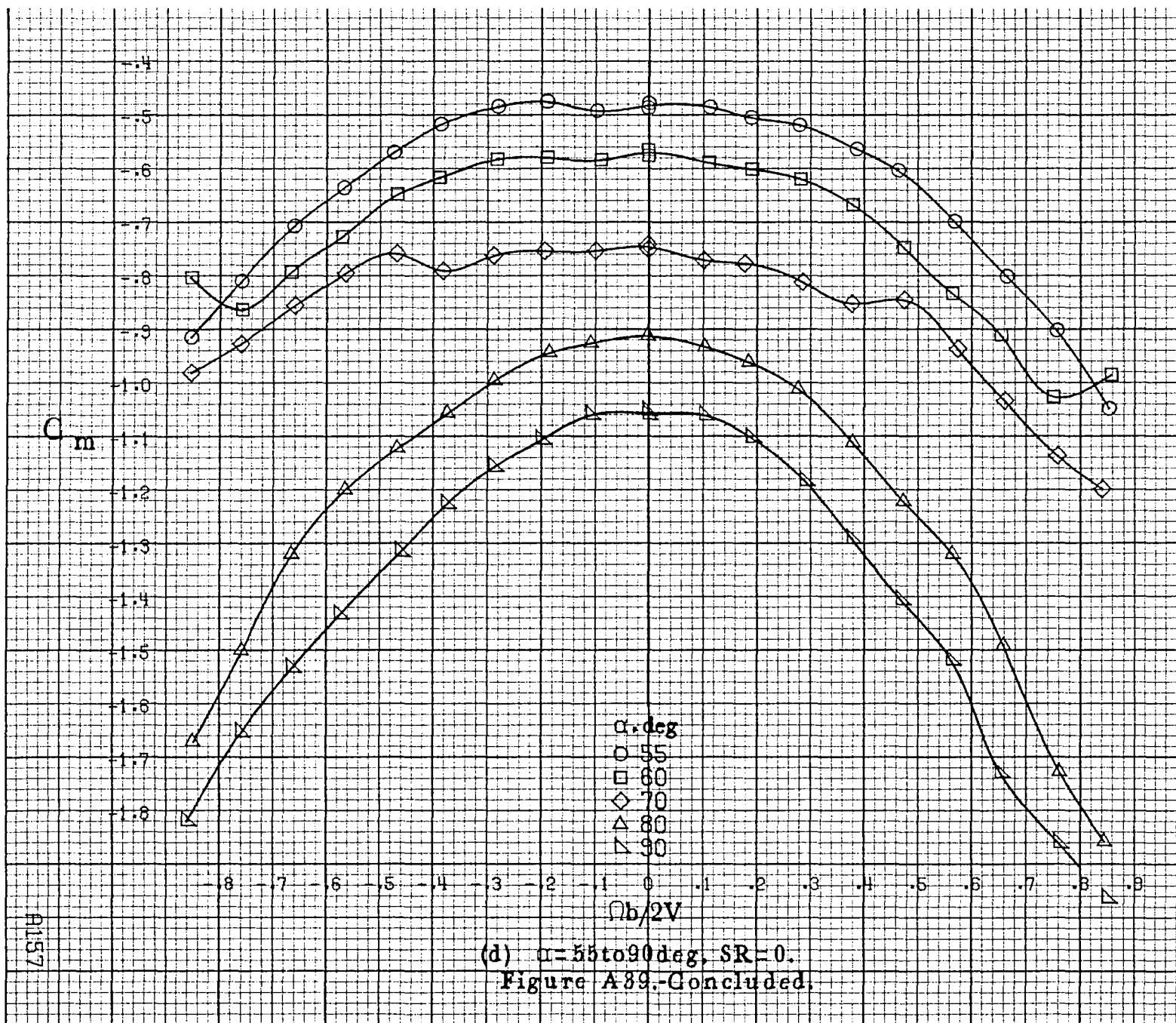
Figure A39. Effect of rotation rate and angle of attack on pitching-moment coefficient for basic configuration. $\delta_e = -25^\circ$, $\delta_a = -22.5^\circ$, $\delta_r = -25^\circ$, $\beta = 0^\circ$.

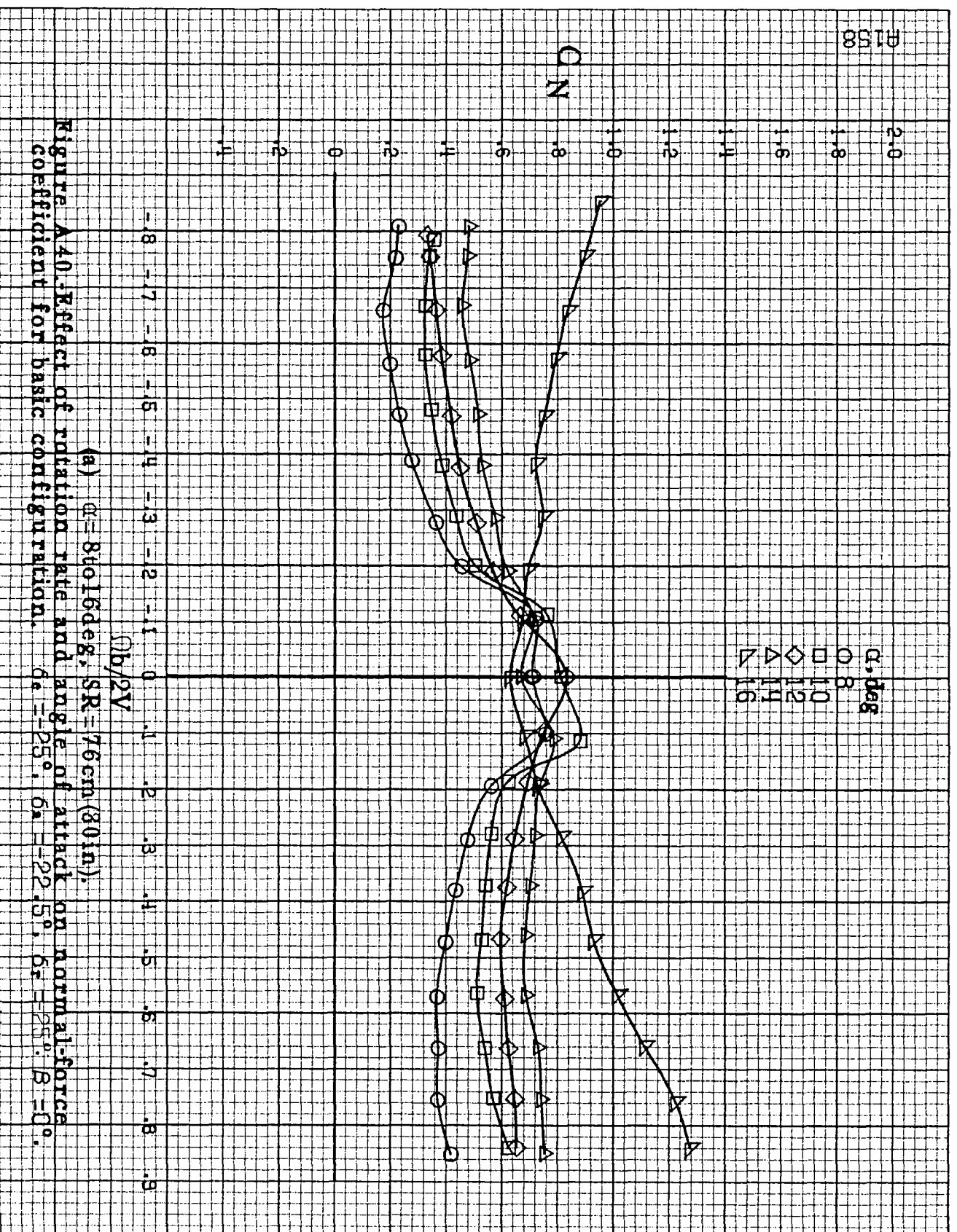


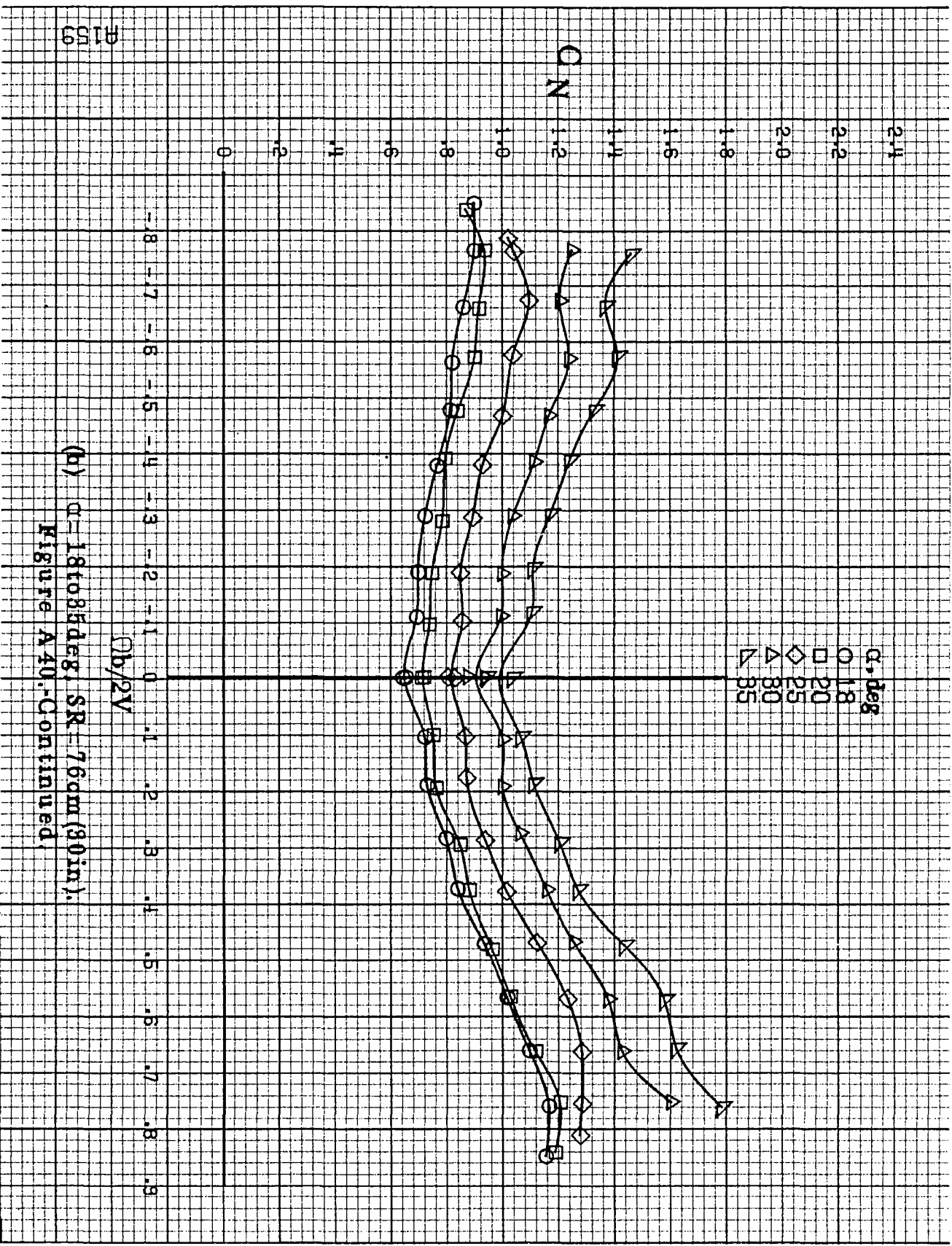
(b) $\alpha = 18$ to 35° , $SR = 76 \text{ cm (30 in.)}$.
Figure A39.-Continued.



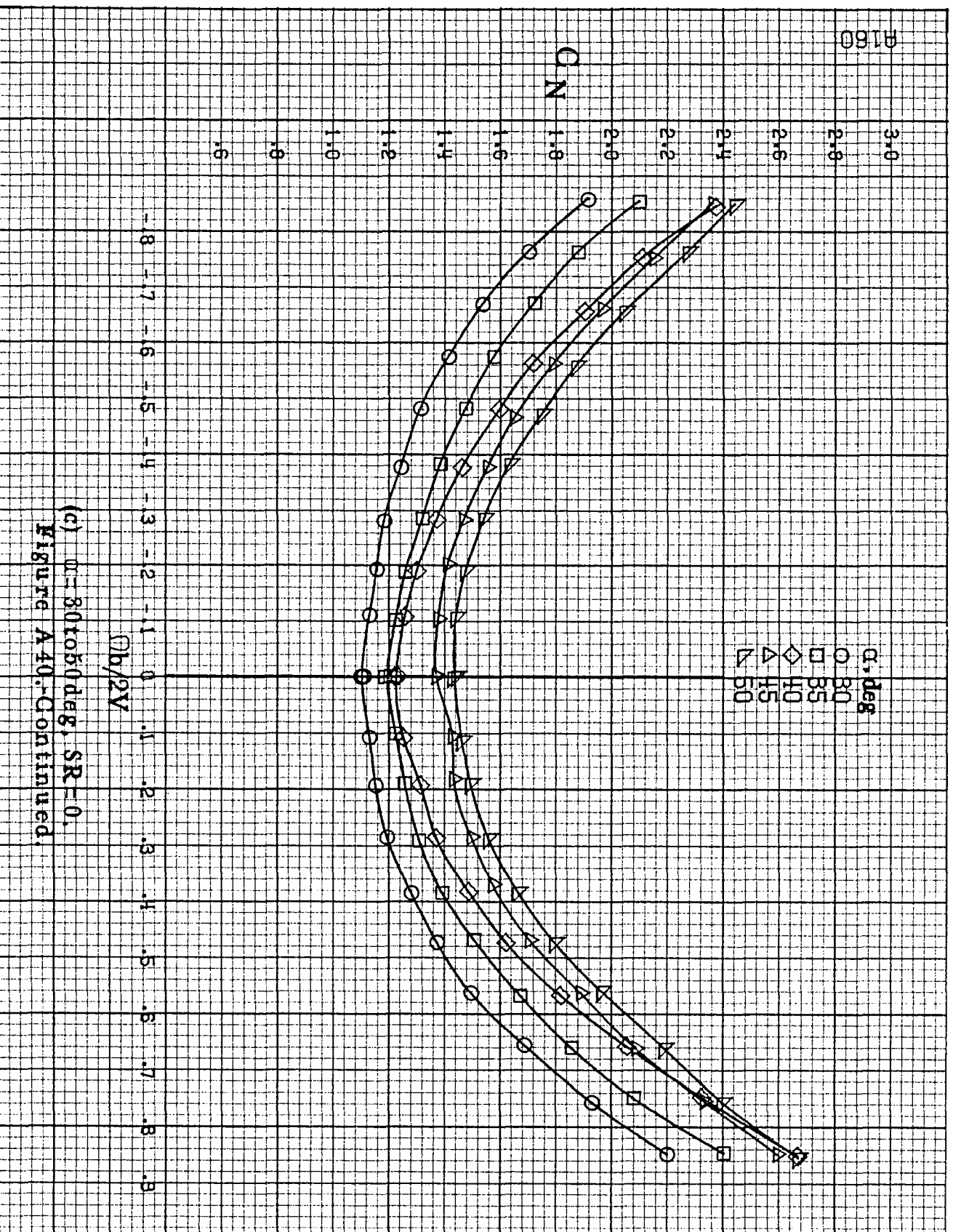
(c) $\alpha = 30$ to 50° , $SR = 0$.
Figure A89.-Continued.



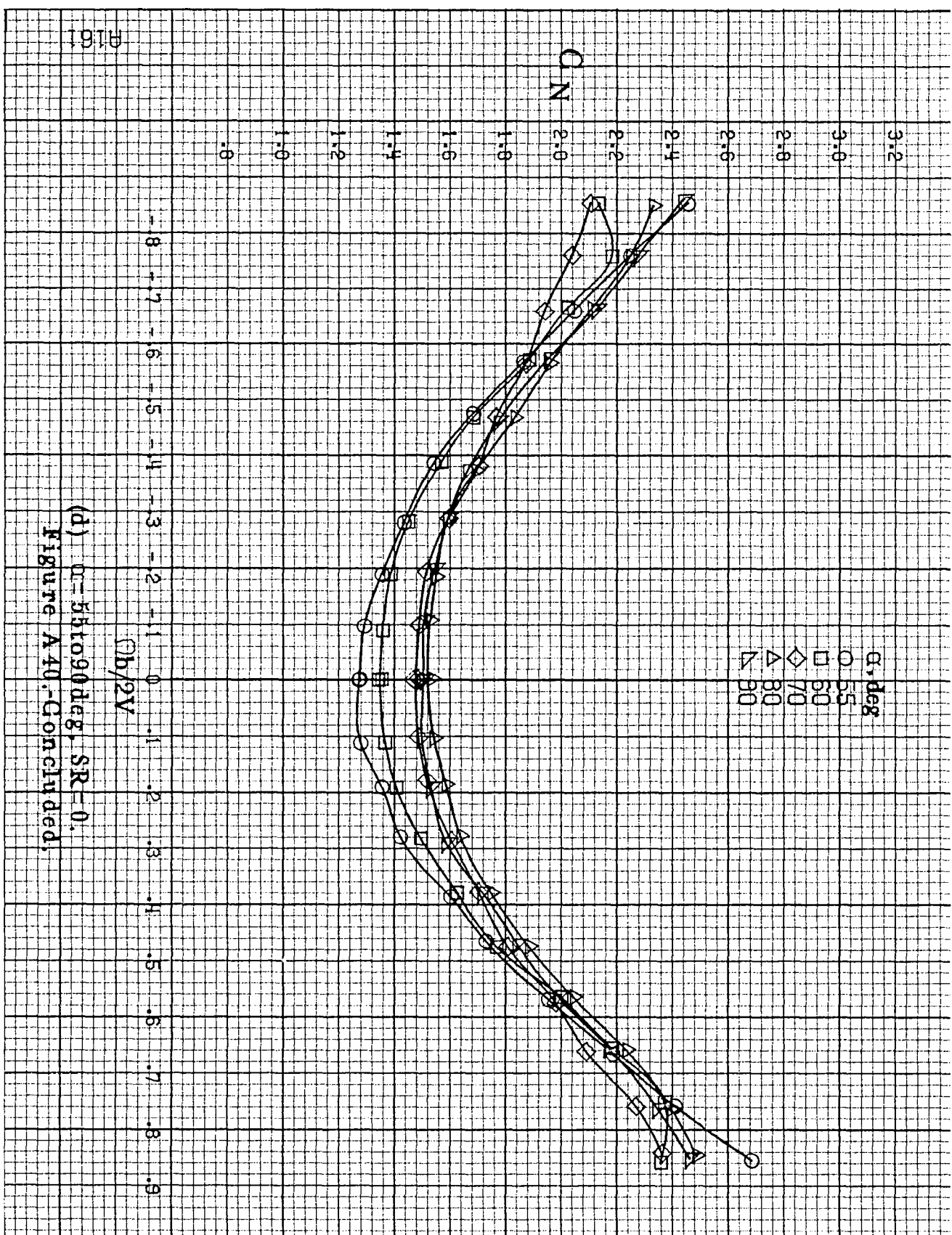




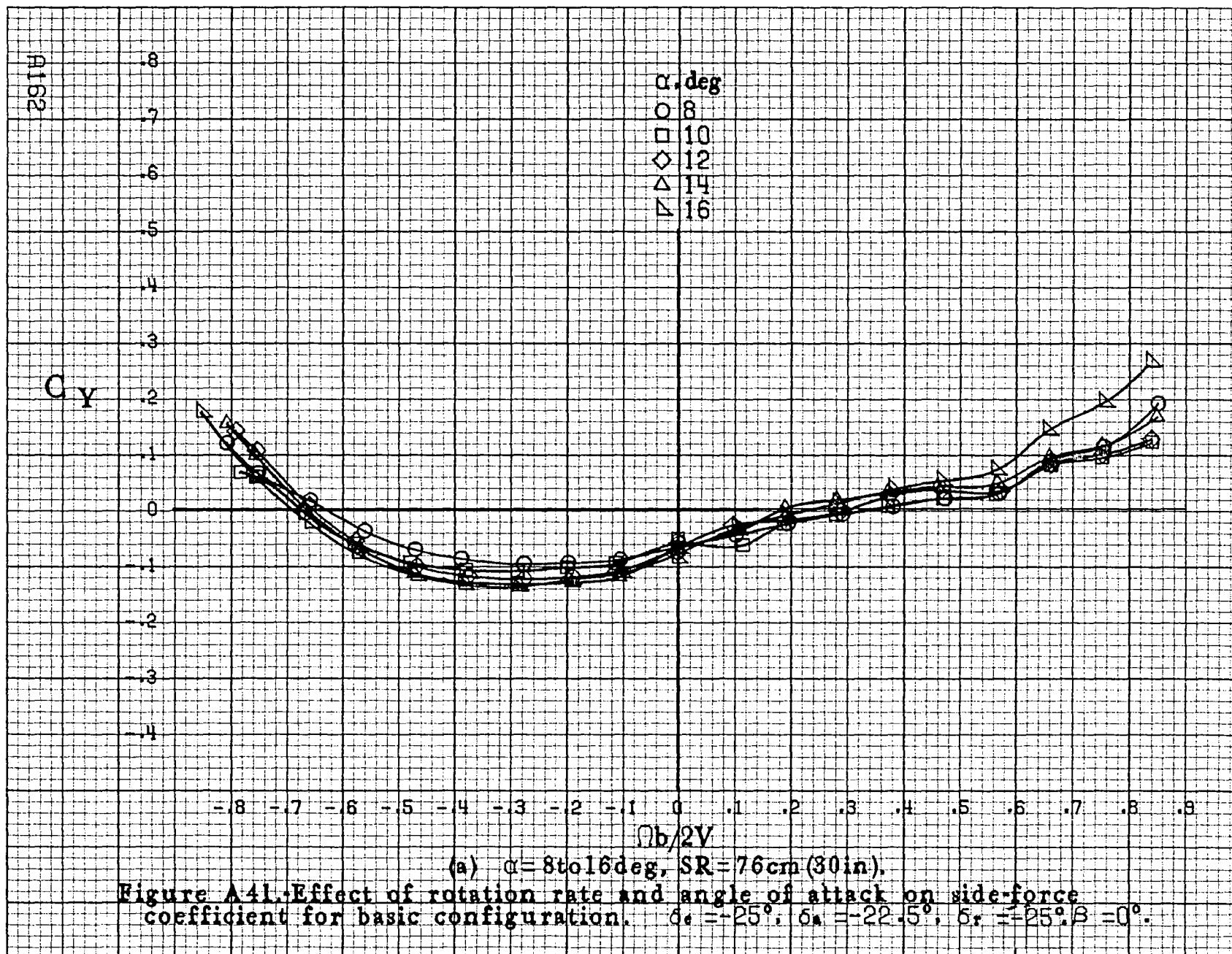
(b) $\alpha = 18$ to 35 deg, SR = 76 cm (30 in.).
Figure A40.-Continued.

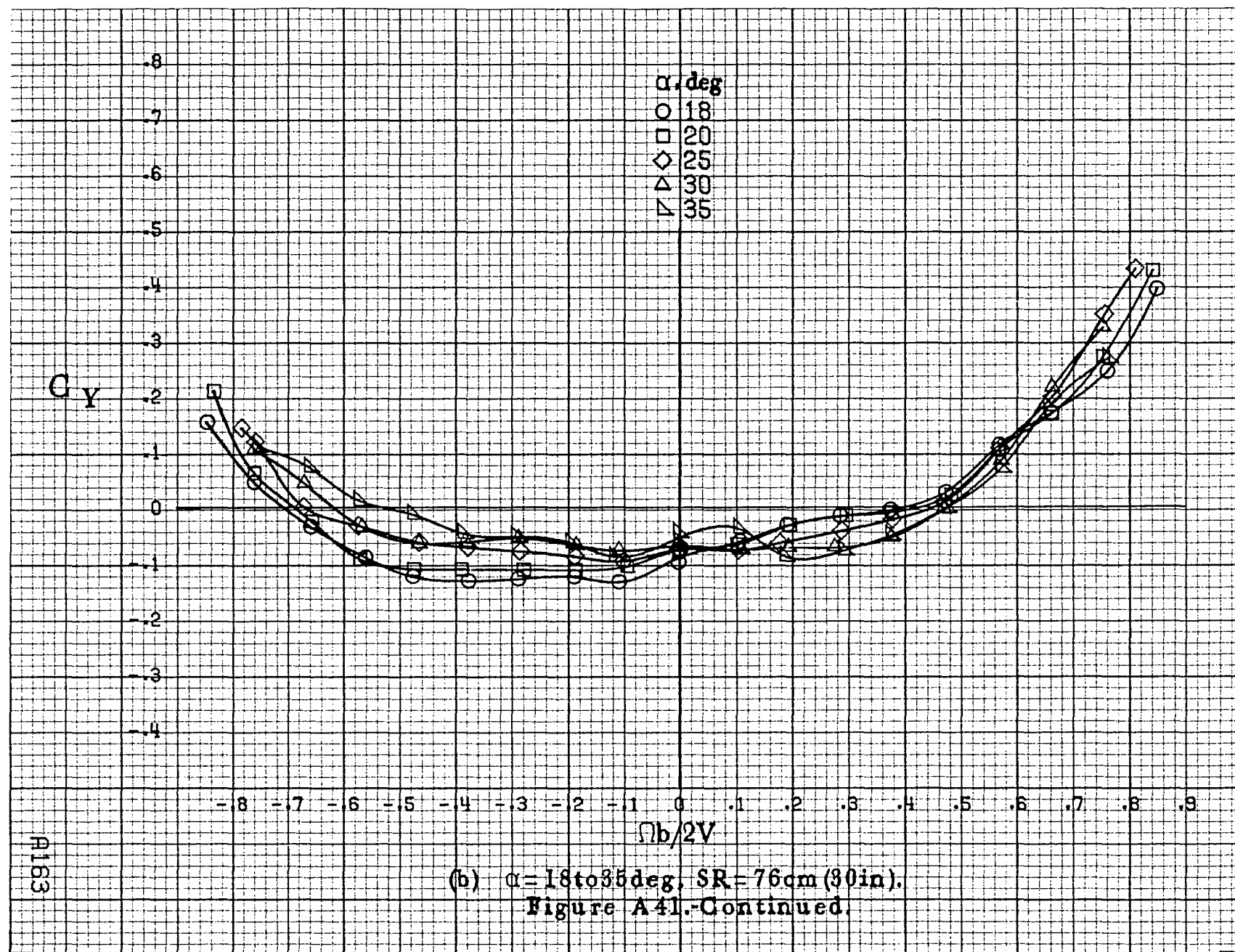


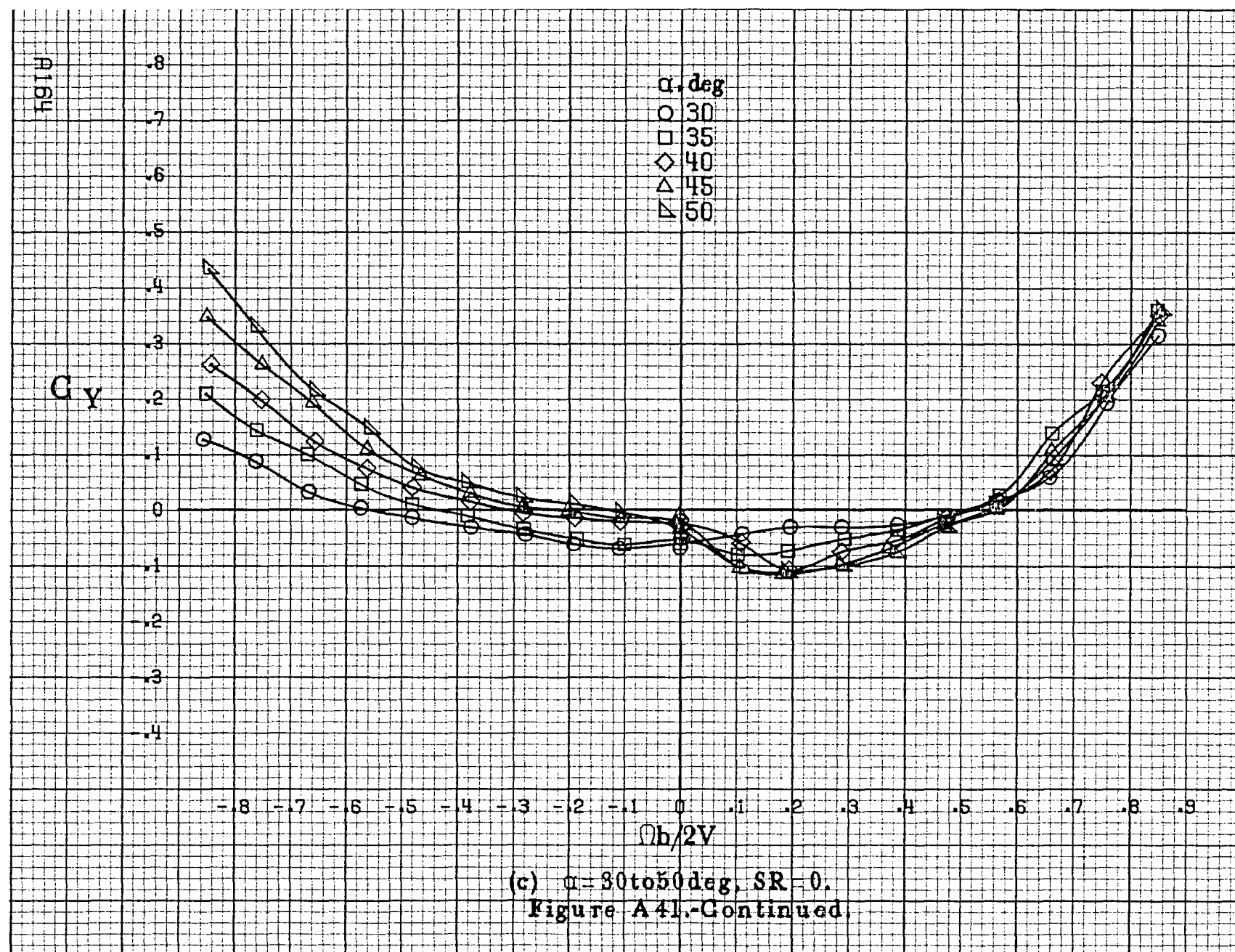
(c) $\alpha=30$ to 50 deg, $SR=0$,
Figure A40.-Continued.

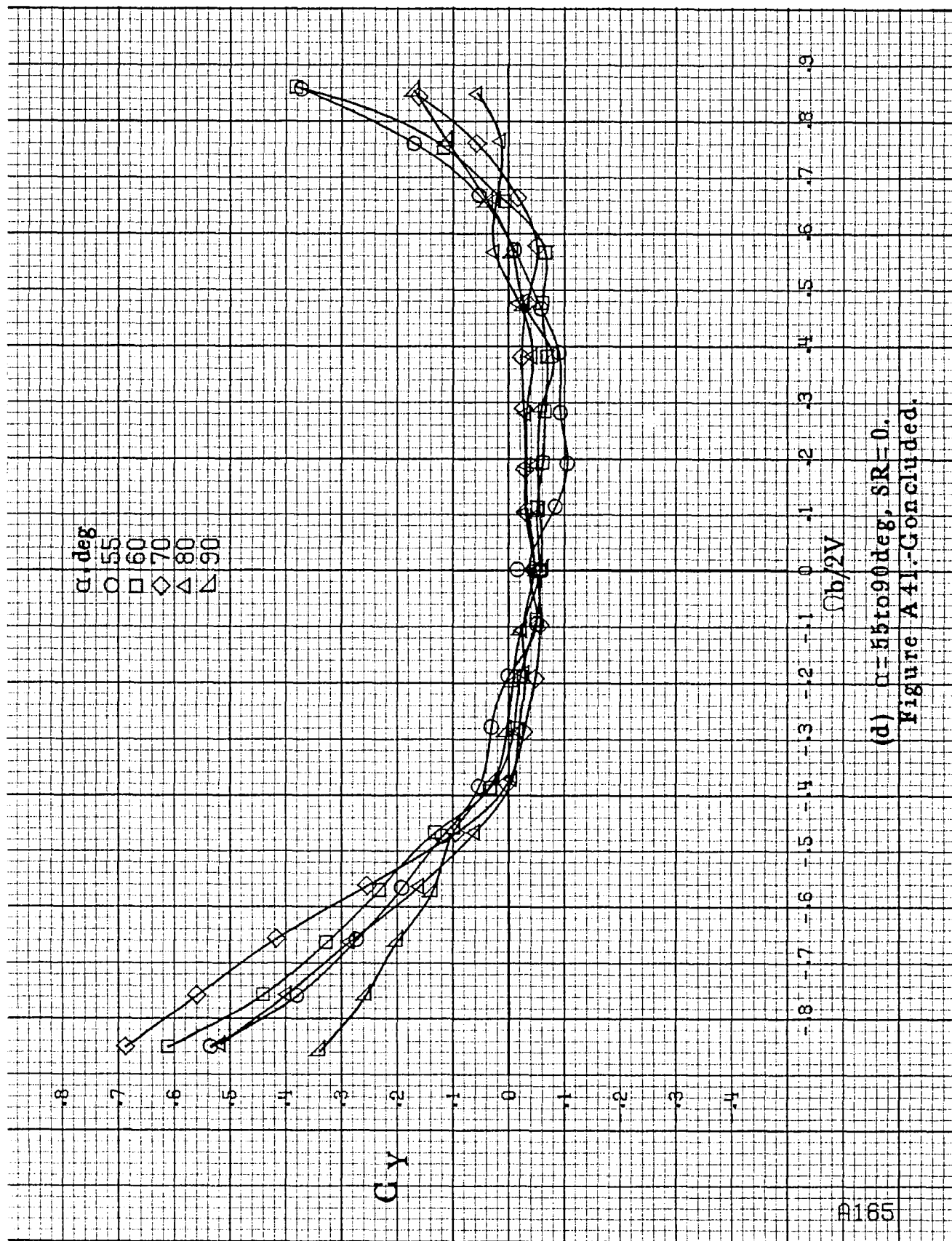


(d) $\alpha=55$ to 90 deg, $SR=0$,
Figure A 40.-Concluded.

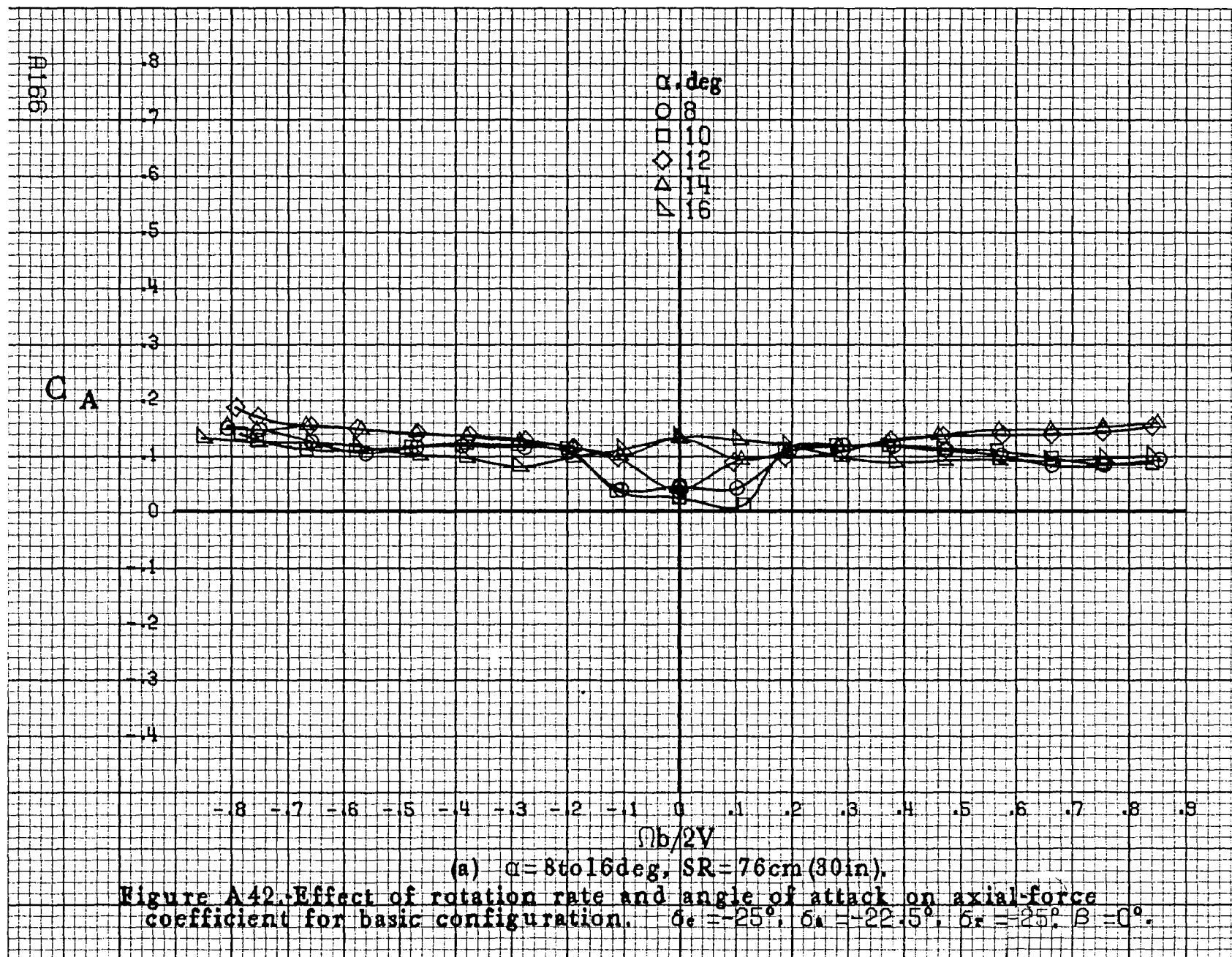


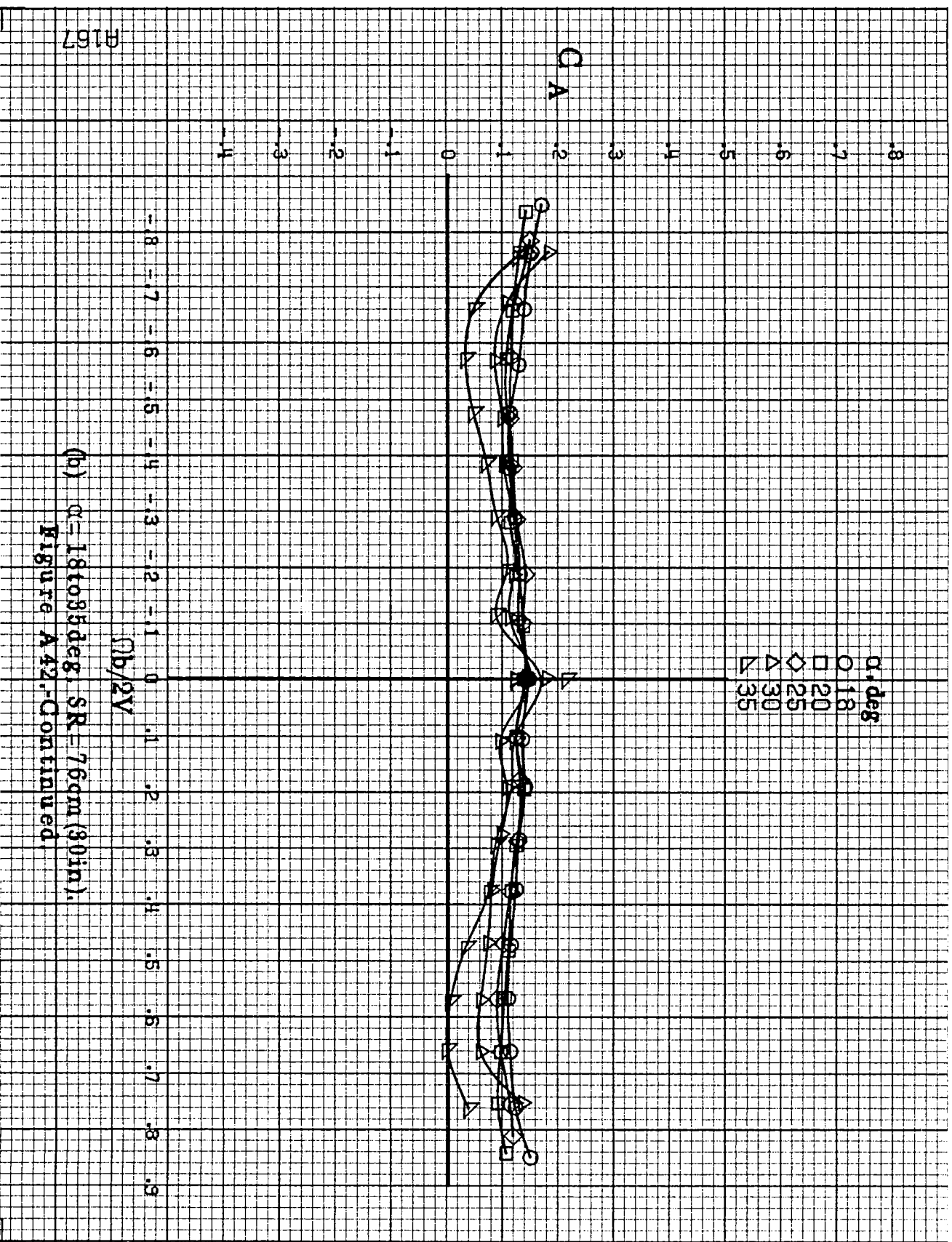






(d) $\alpha=55$ to 90° deg, $SR=0$.
Figure A41.-Concluded.

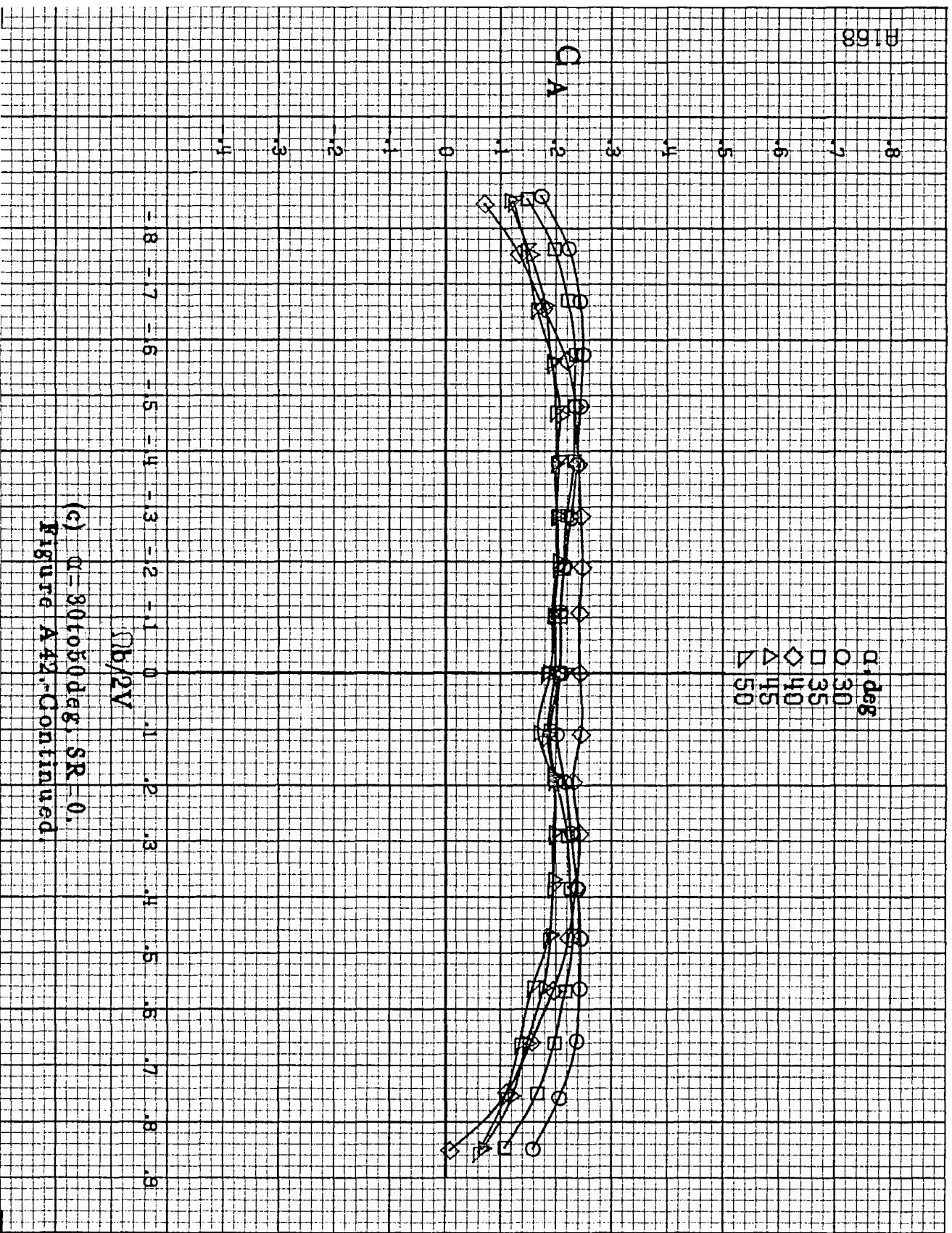


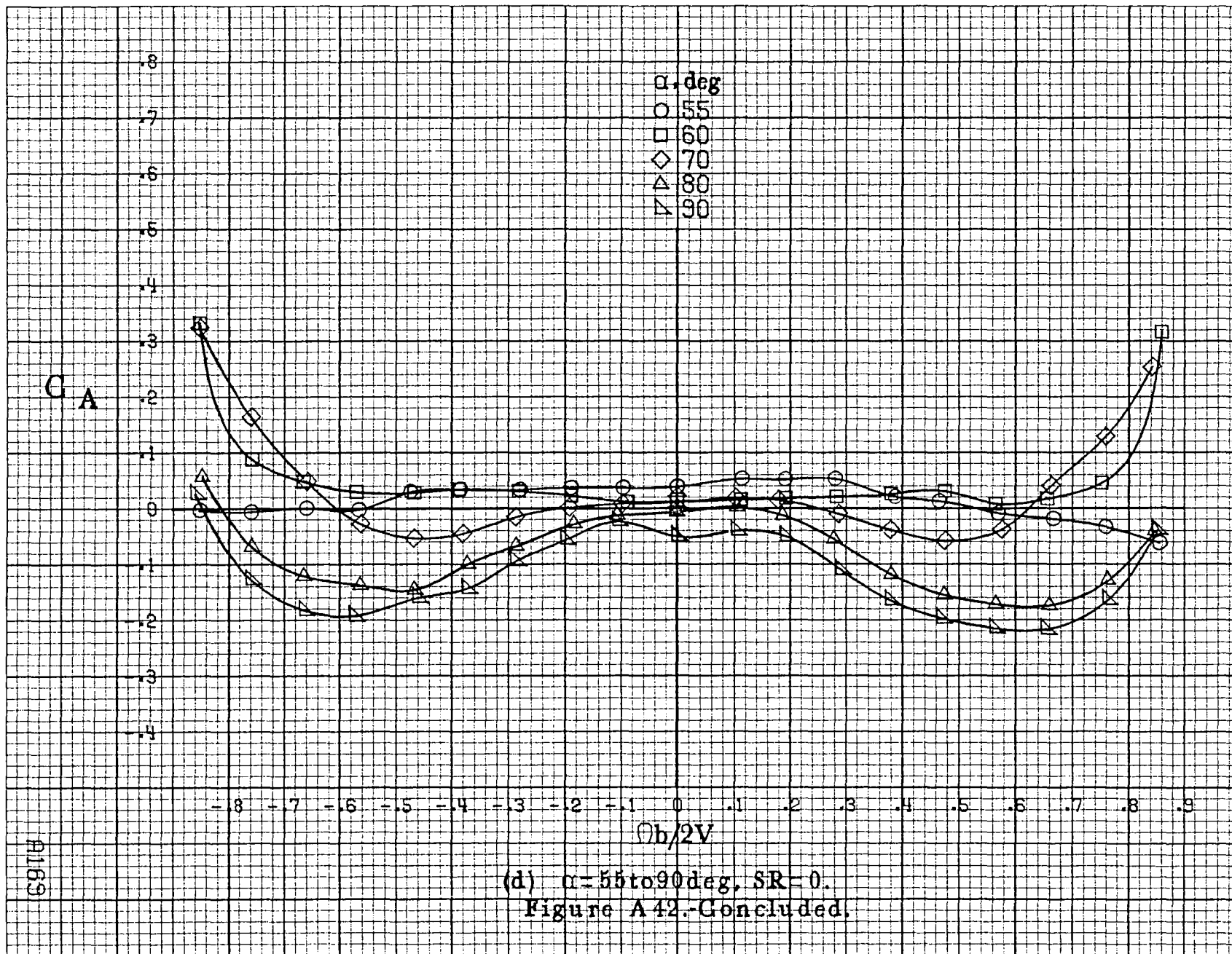


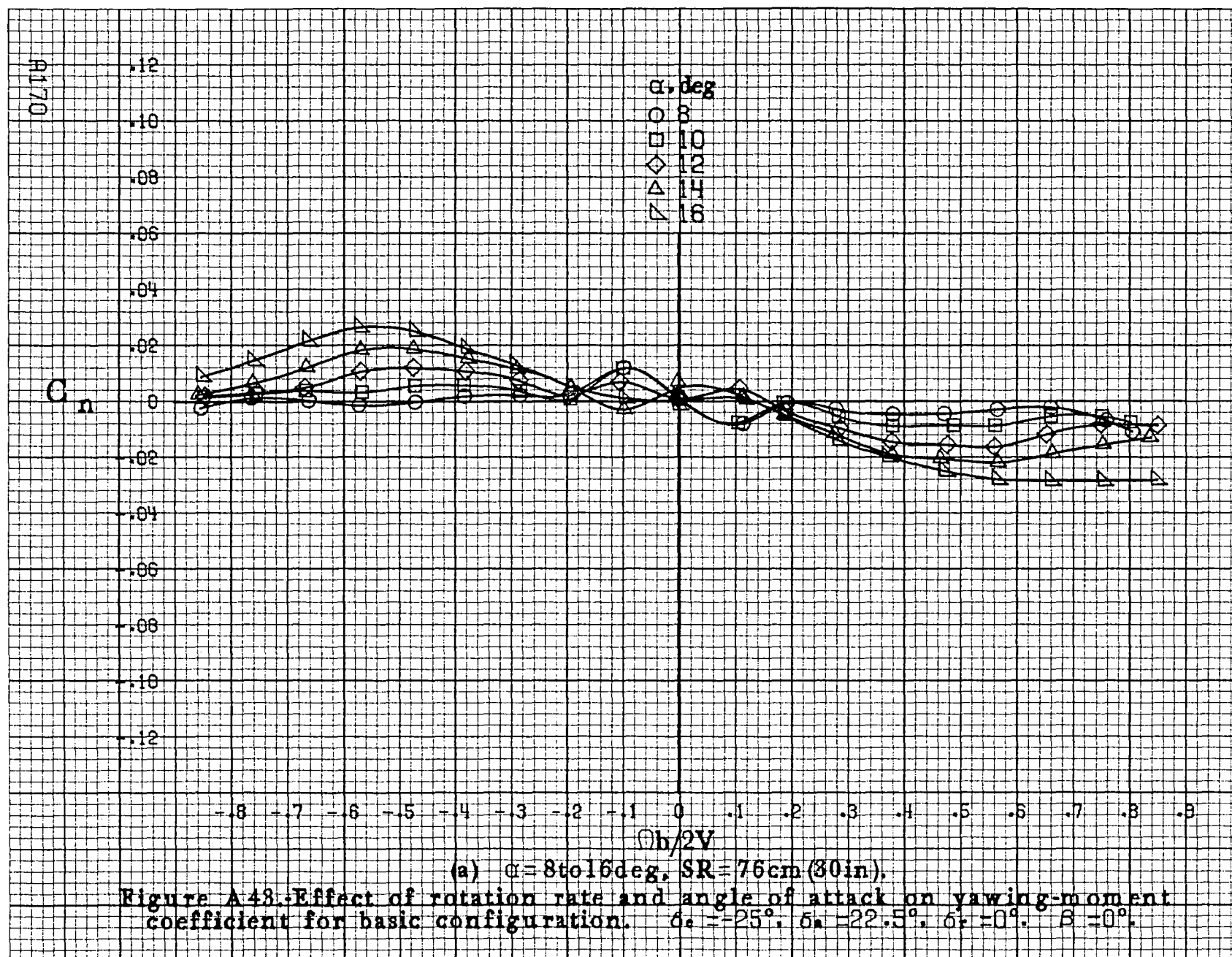
(b) $\alpha = 18$ to 35° , $SR = 76 \mu m (30 in.)$.

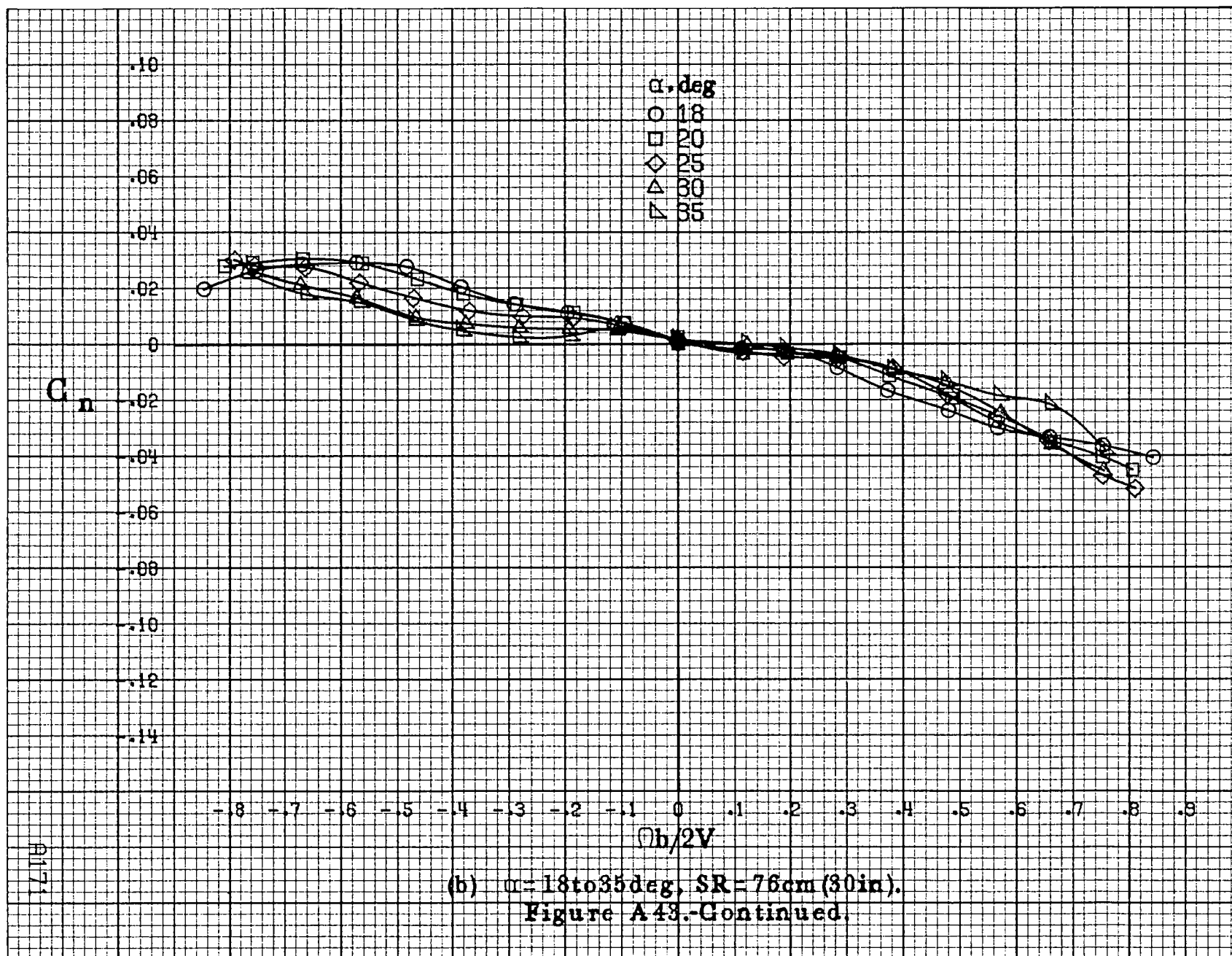
Figure A42.-Continued.

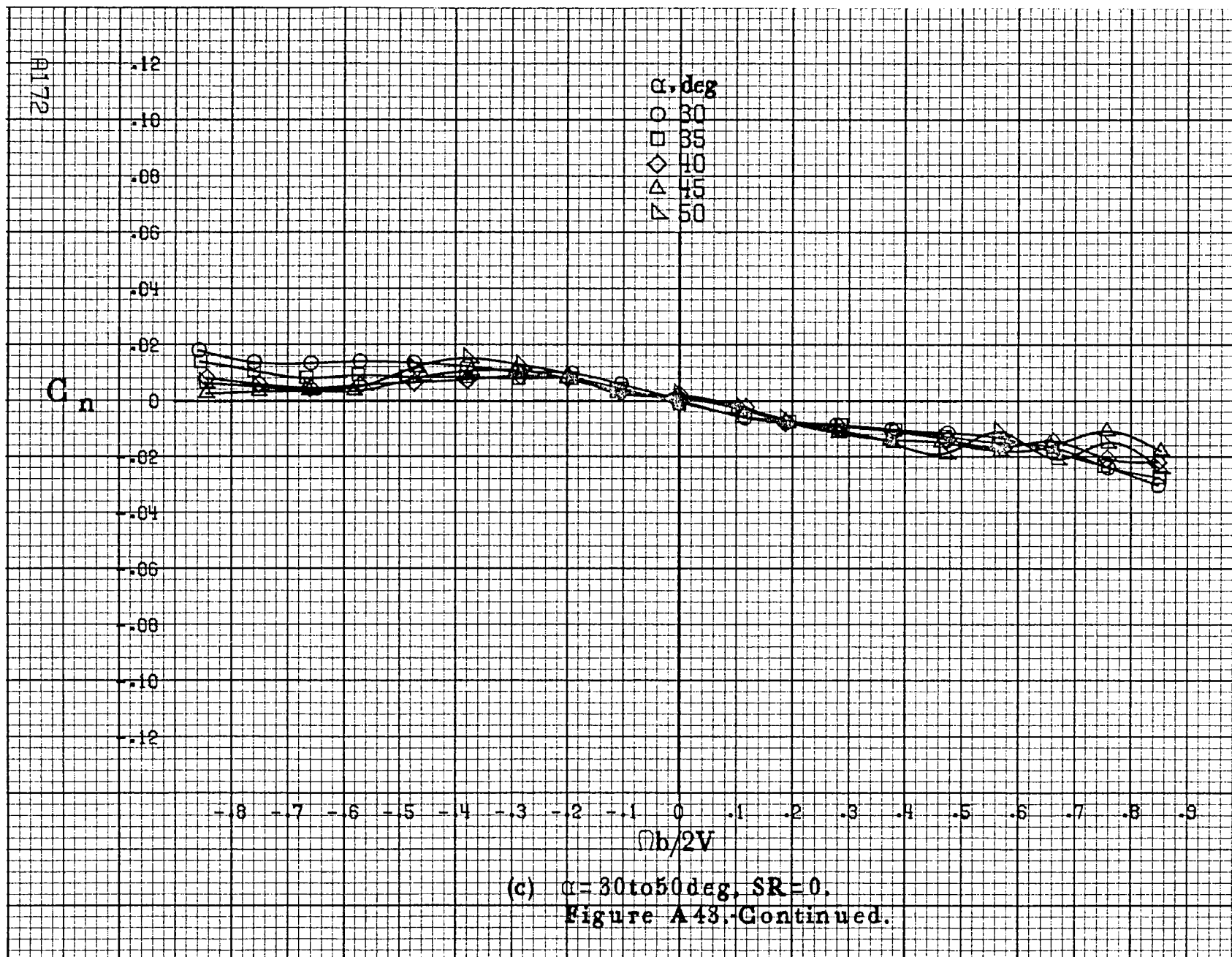
A167

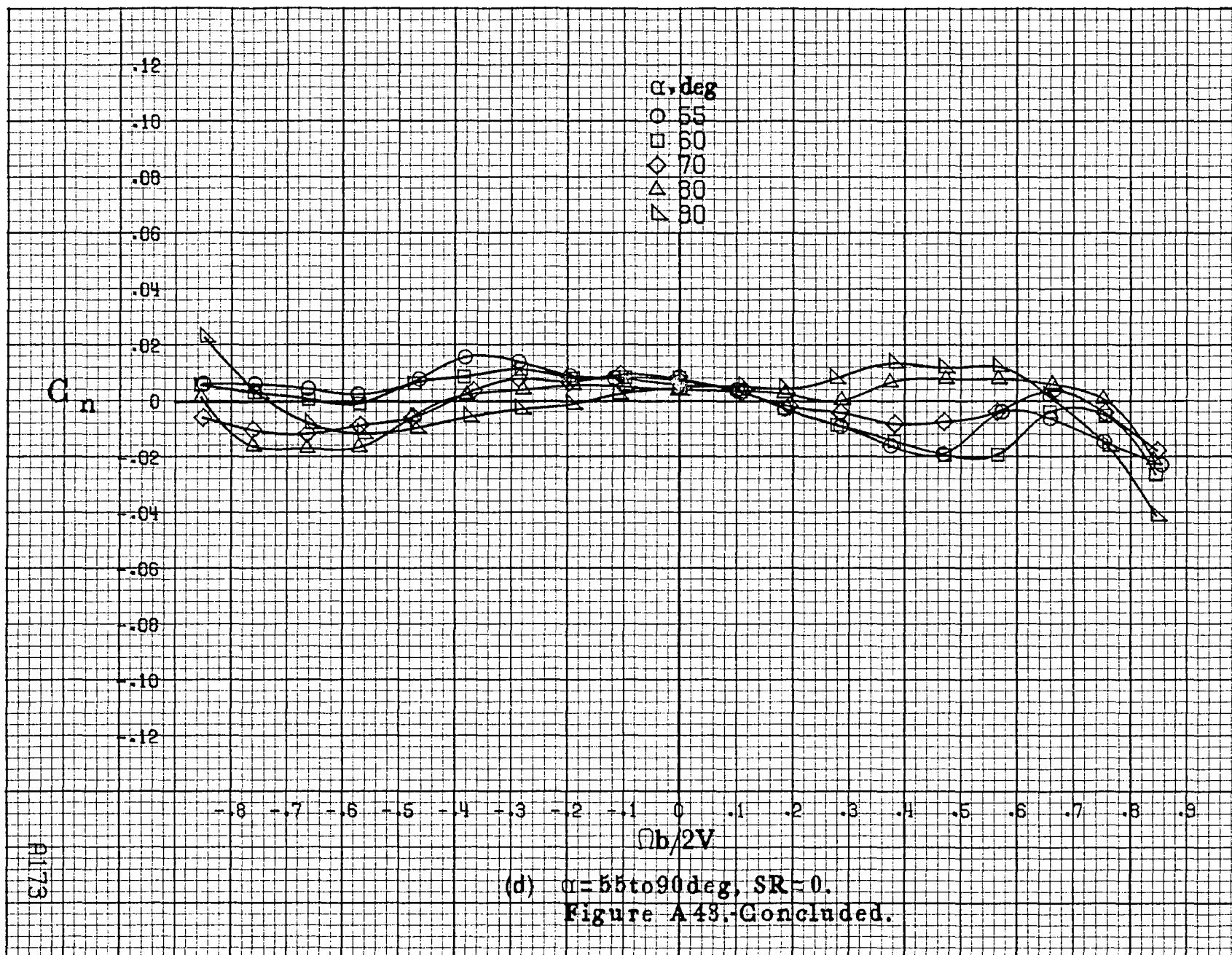


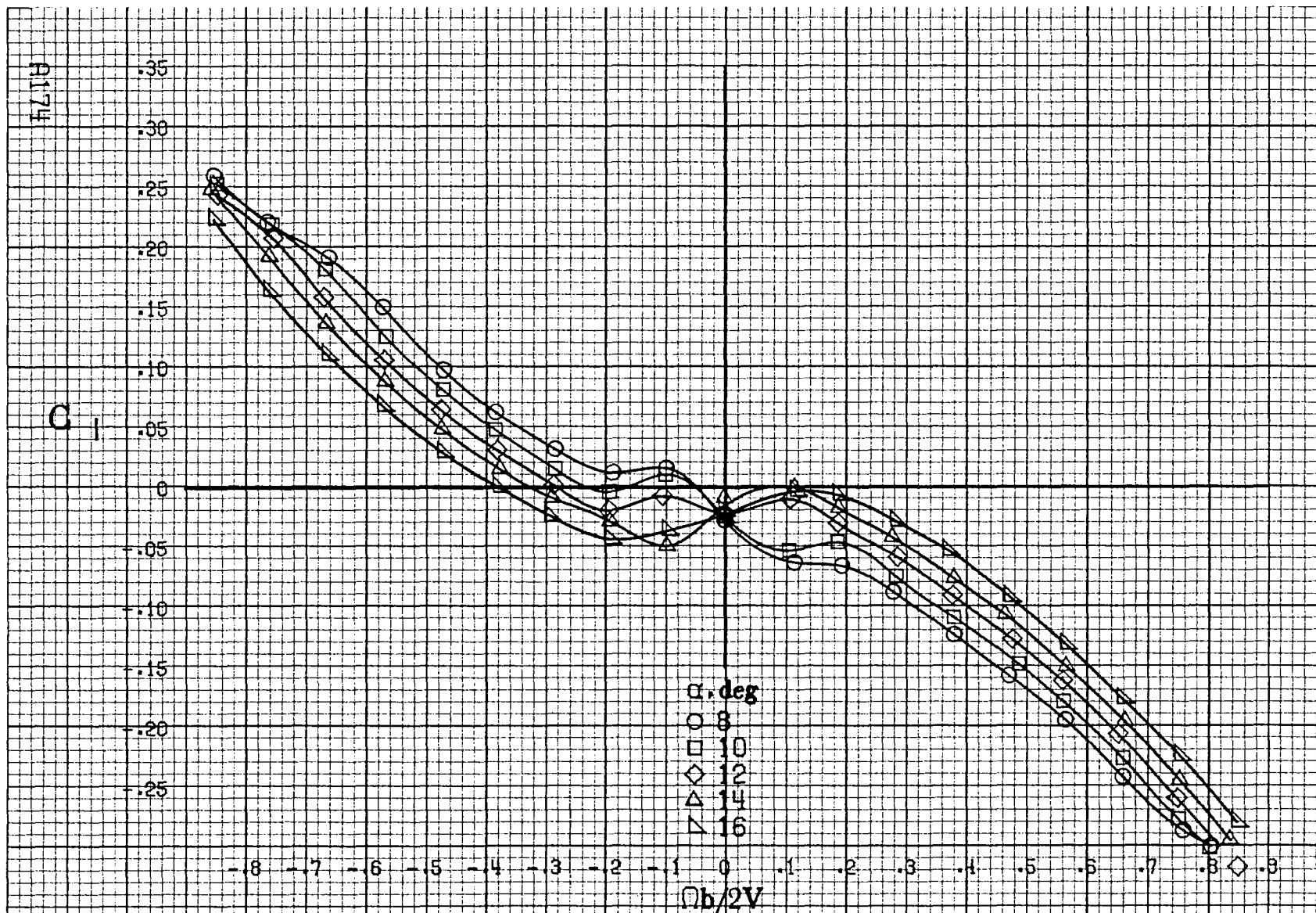






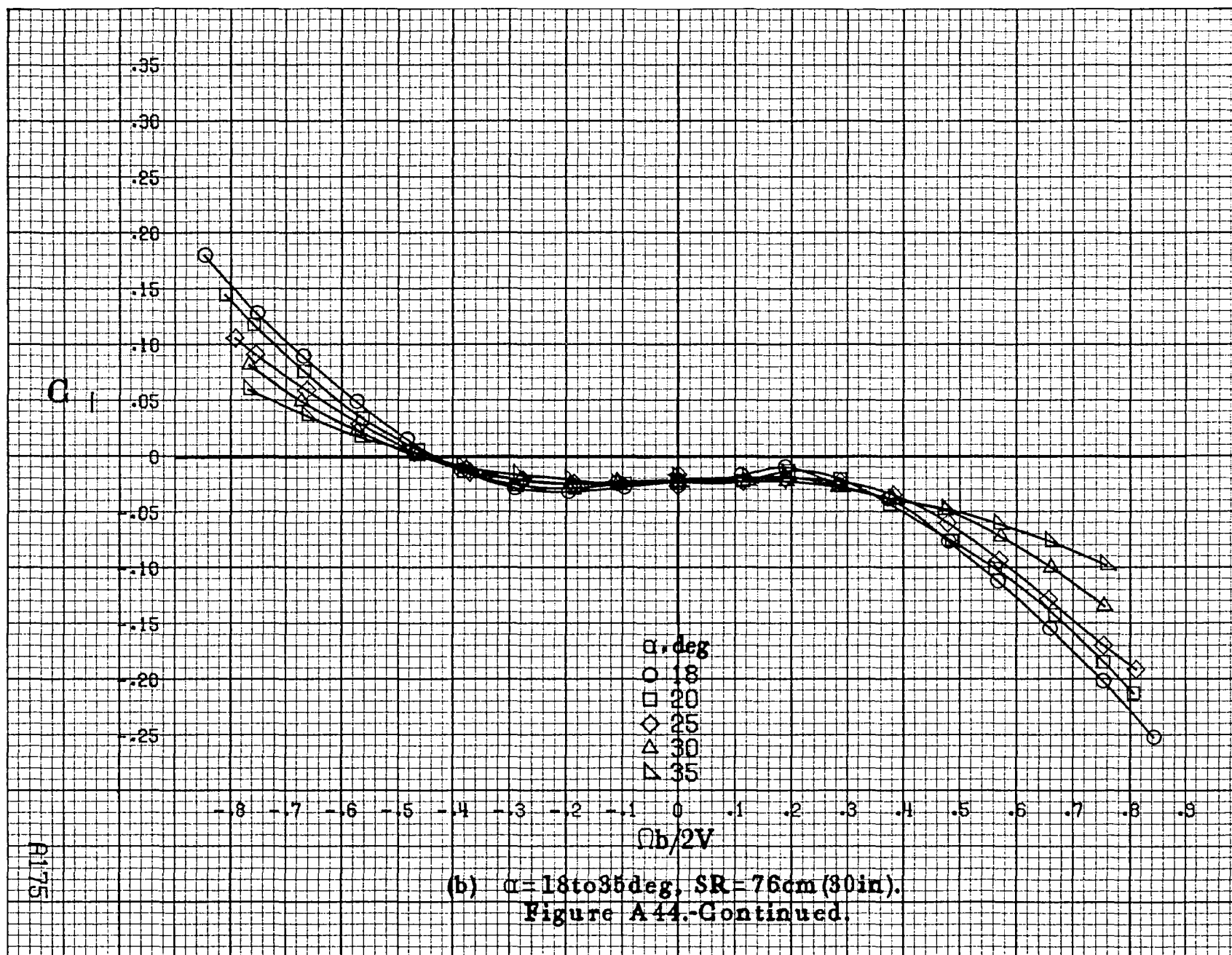


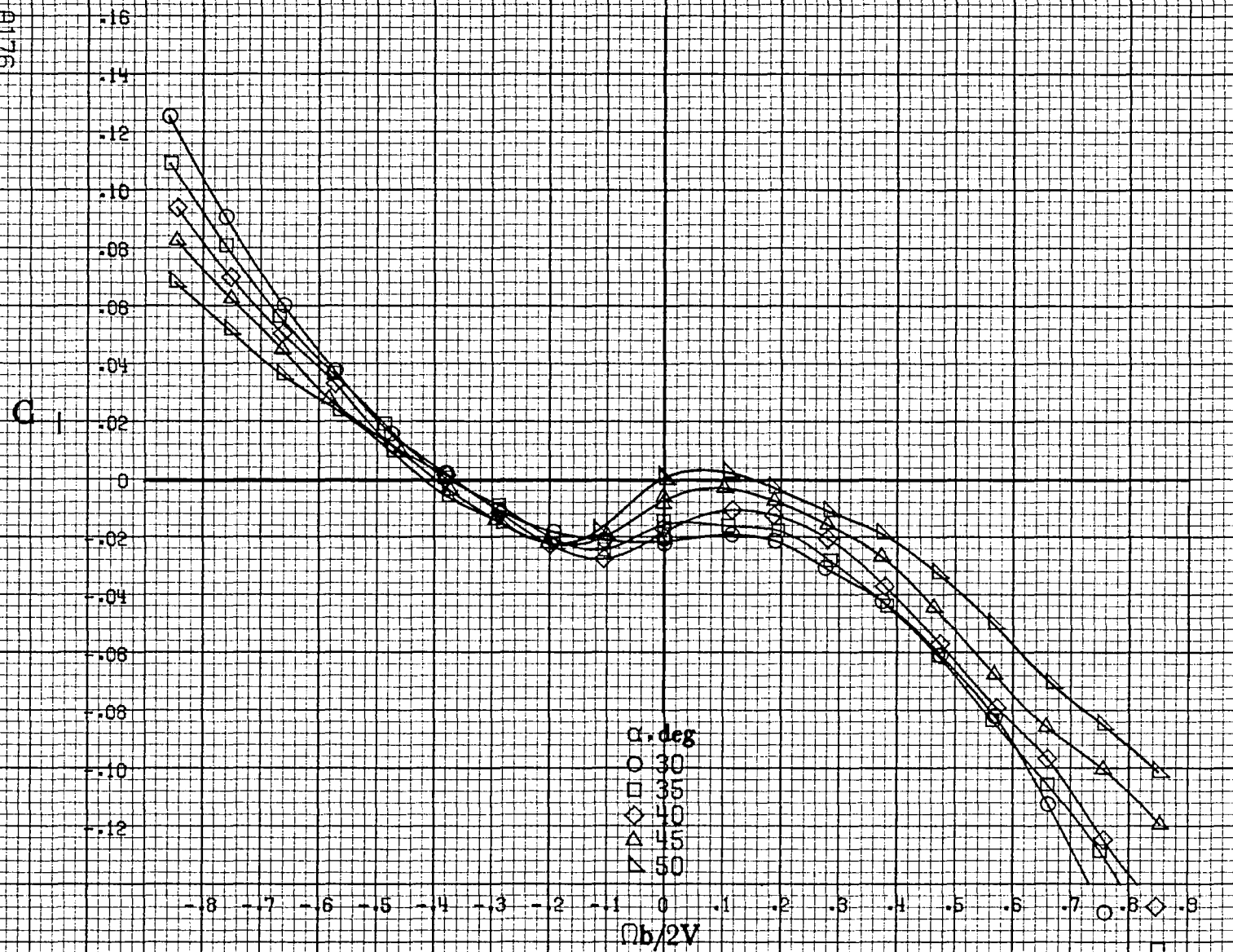




(a) $\alpha = 8$ to 16 deg, $SR = 76$ cm (30 in).

Figure A44.-Effect of rotation rate and angle of attack on rolling-moment coefficient for basic configuration. $\delta_r = \pm 25^\circ$, $\delta_r = \pm 22.5^\circ$, $\delta_r = 0^\circ$, $\beta = 0^\circ$.





(c) $\alpha = 30$ to 50° , $SR = 0$.
Figure A44. Continued.

C₁

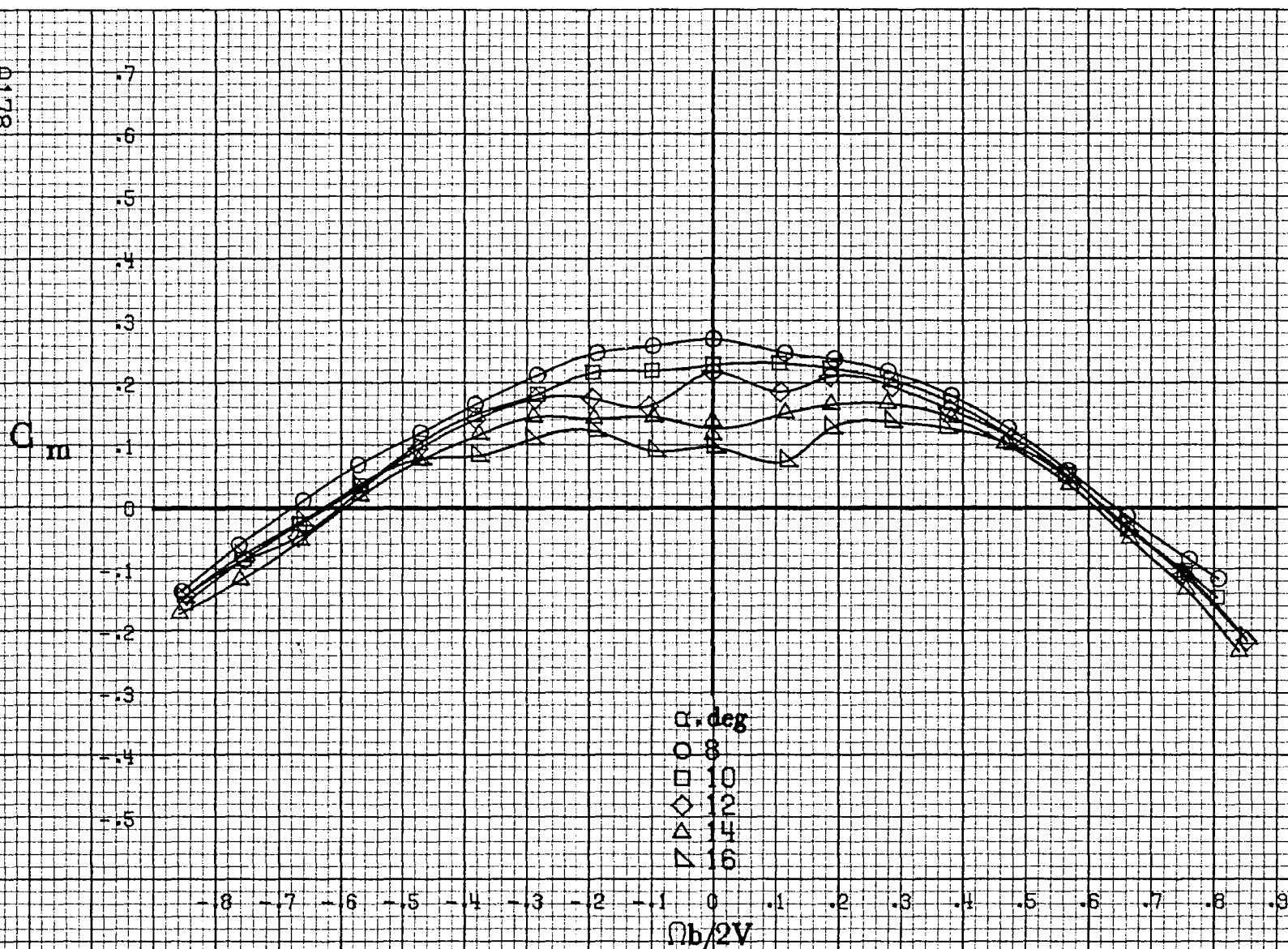
.14
.12
.10
.08
.06
.04
0
-.02
-.04
-.06
-.08
-.10

α, deg
○ 55
□ 60
◇ 70
△ 80
▽ 90

$\Omega b/2V$

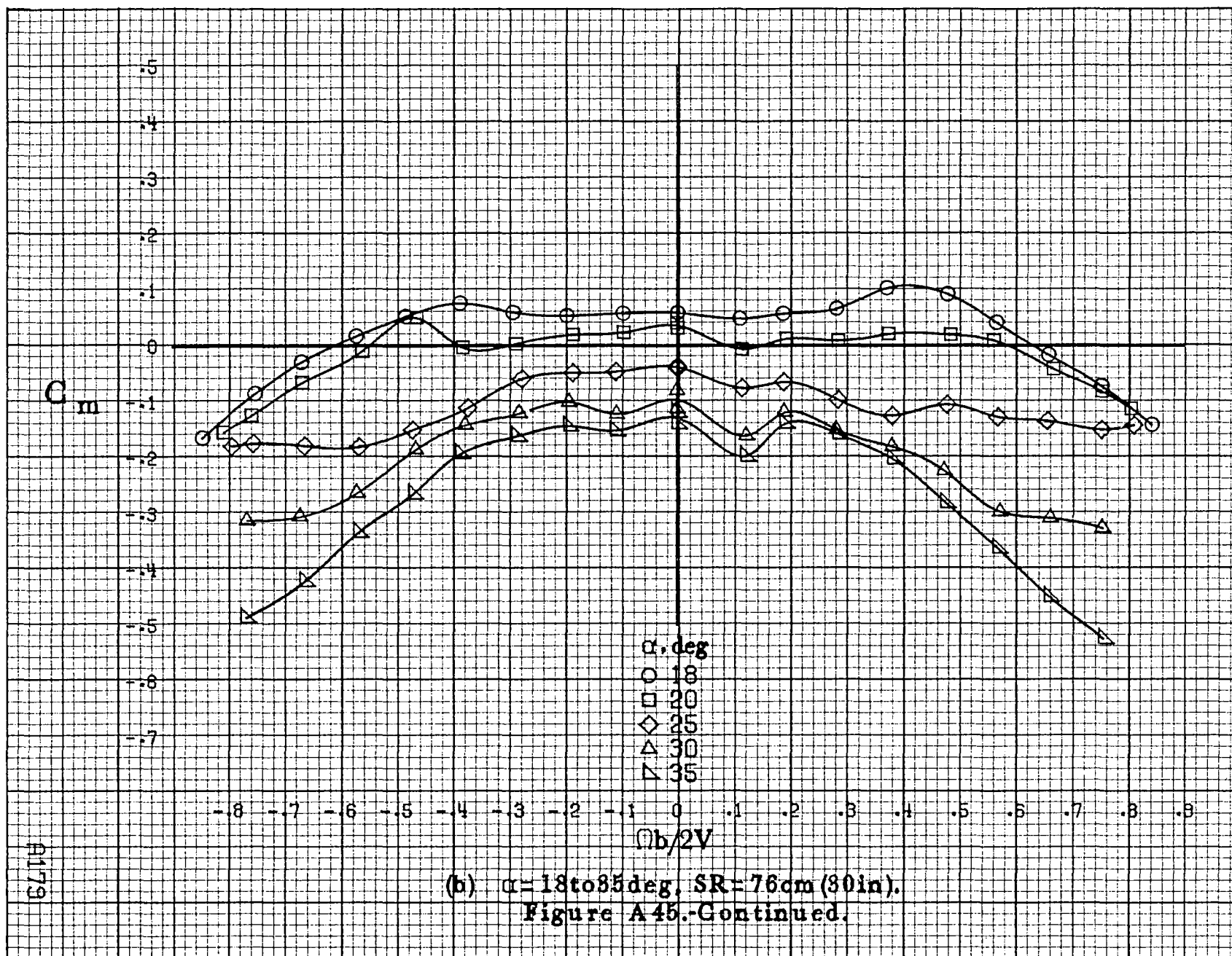
-.8 -.7 -.6 -.5 -.4 -.3 -.2 -.1 0 .1 .2 .3 .4 .5 .6 .7 .8 .9

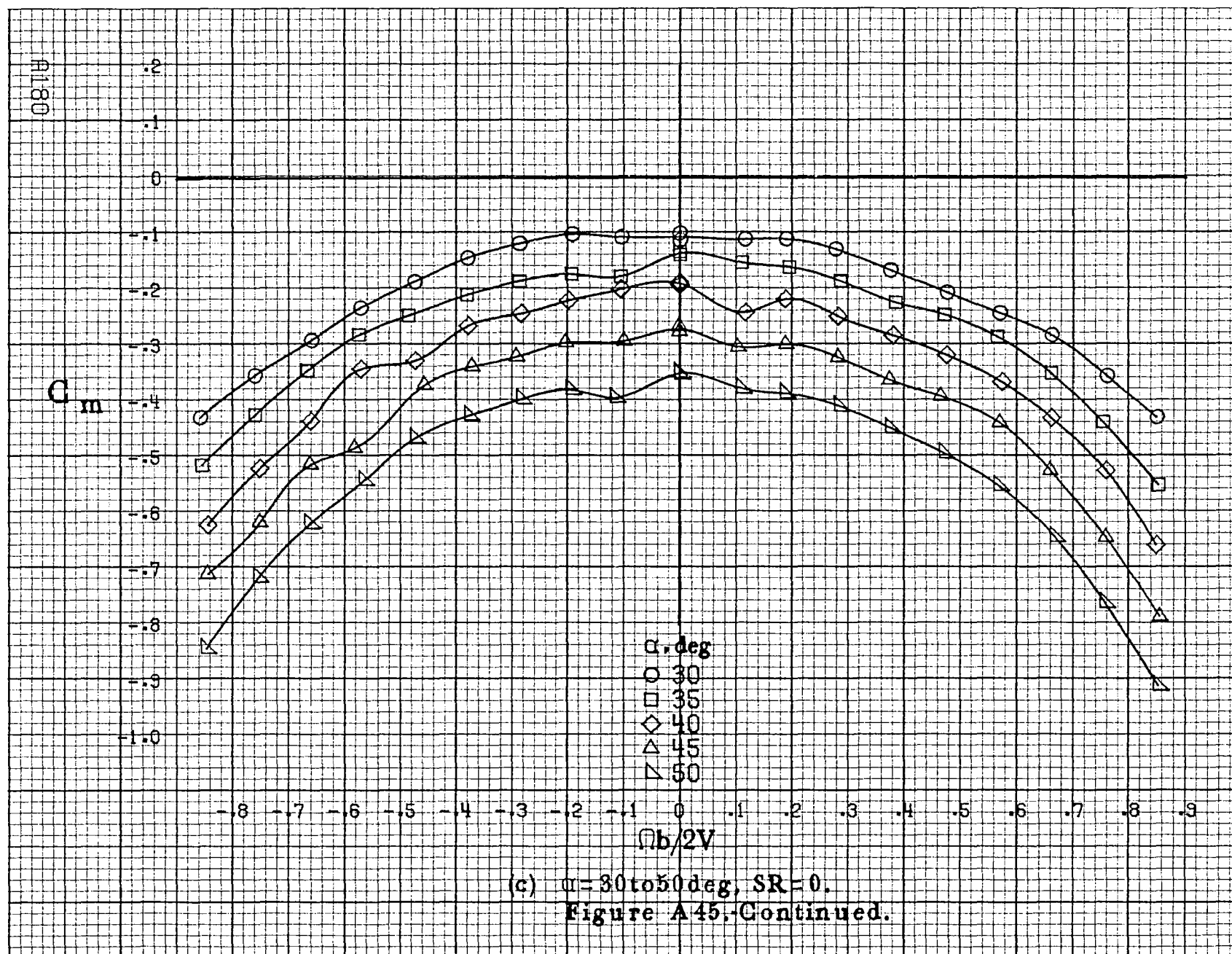
(d) $\alpha=55$ to 90 deg, $SR=0$.
Figure A44-Concluded.

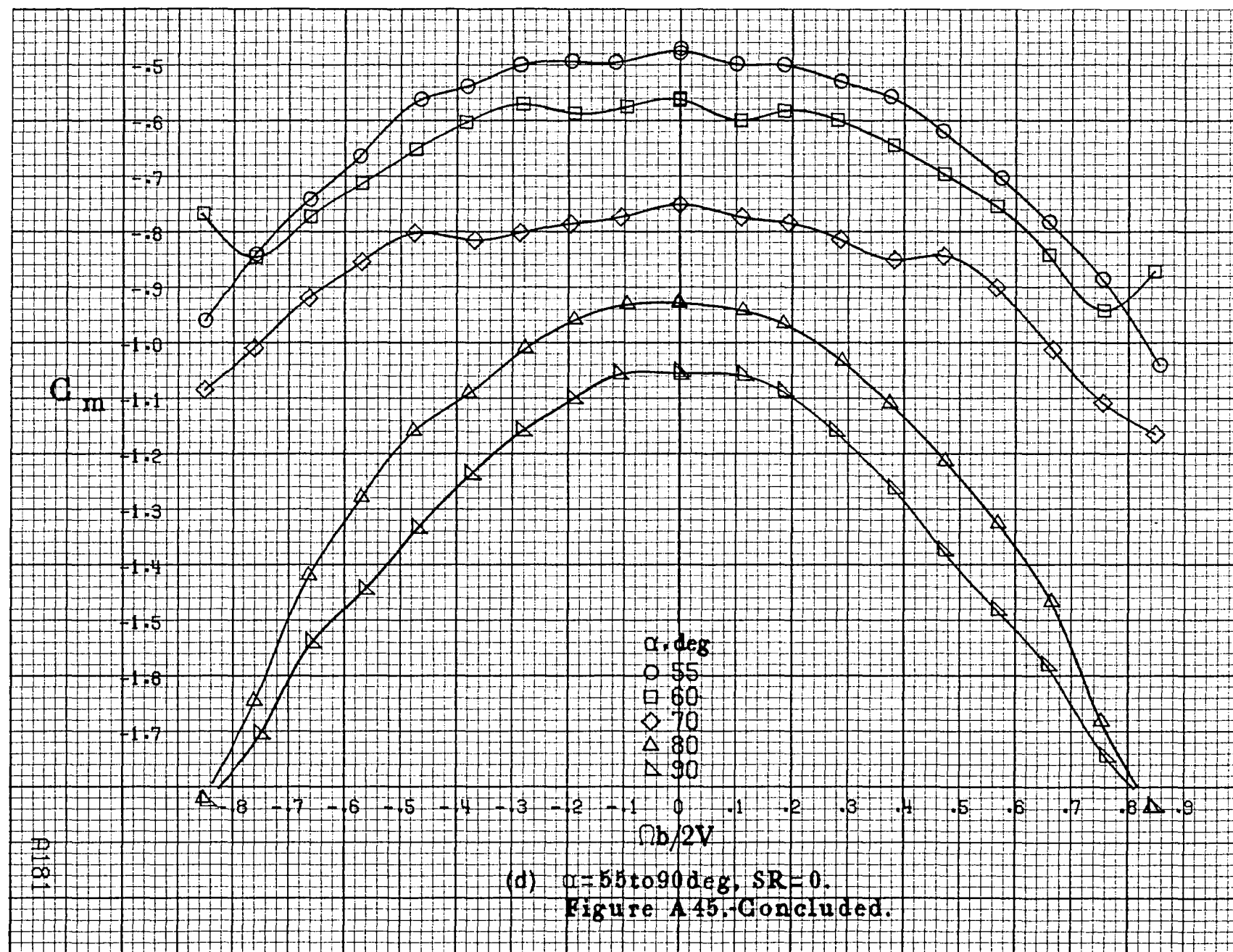


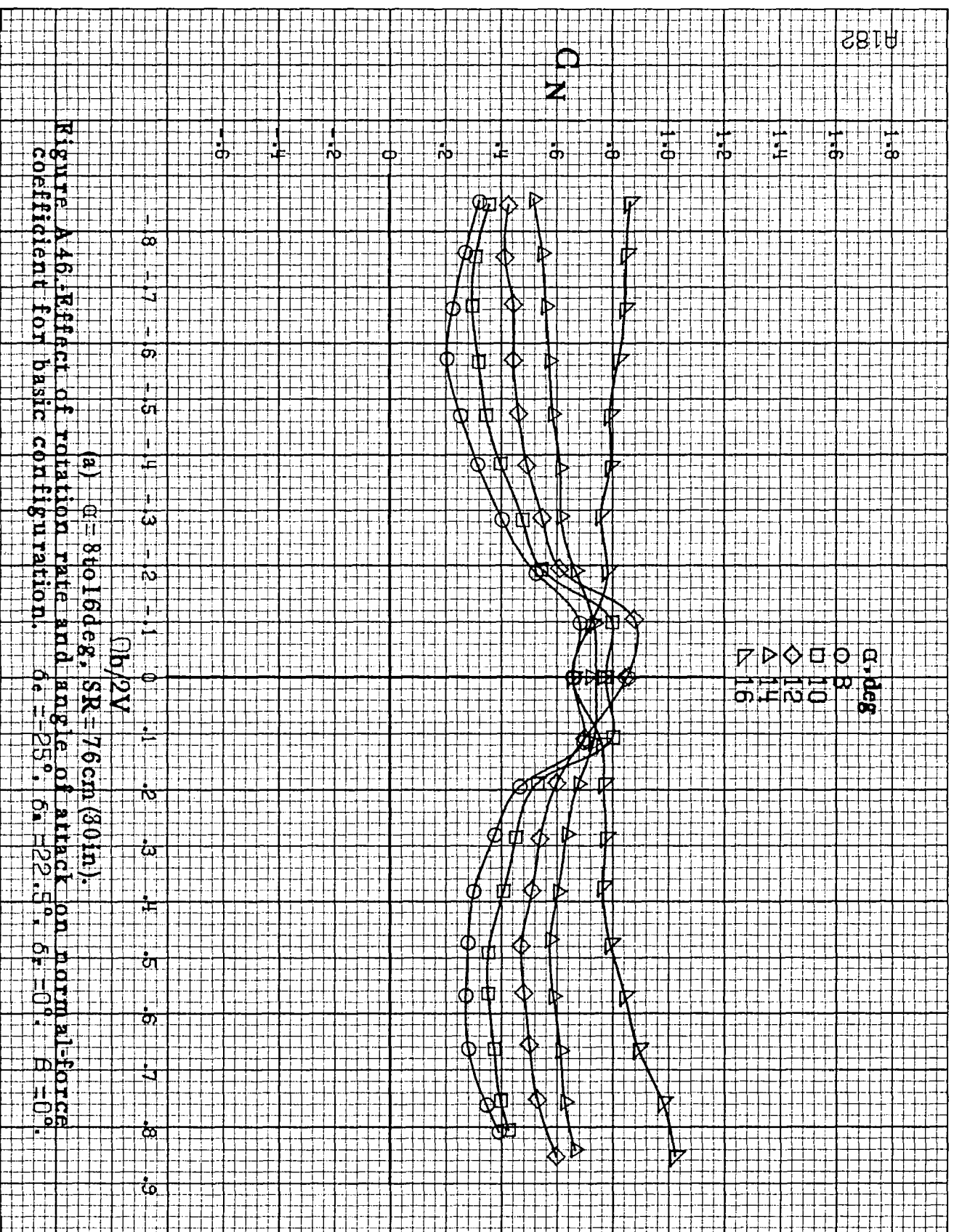
(a) $\alpha = 8$ to 16° , $SR = 76\text{cm} (30\text{in})$.

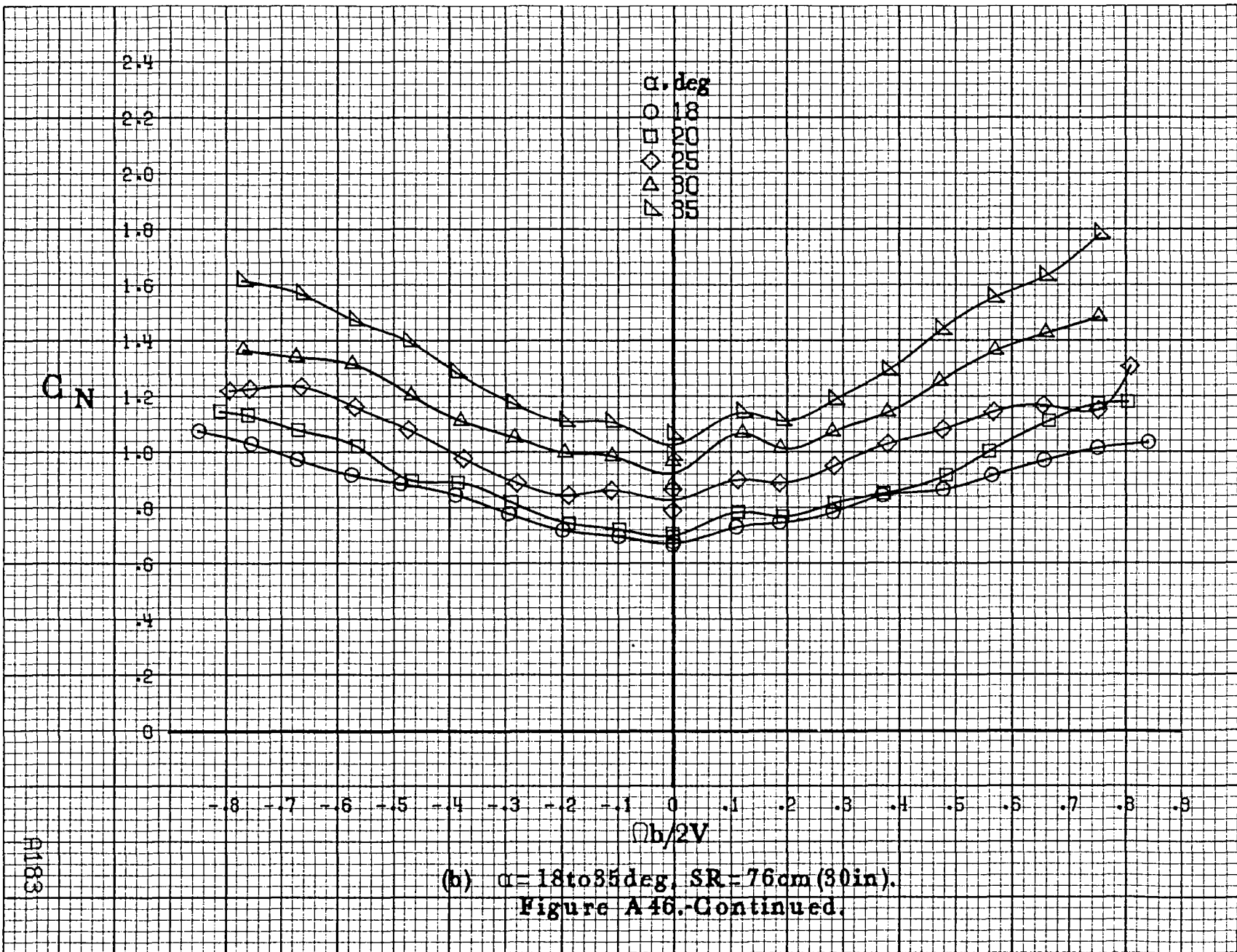
Figure A45.-Effect of rotation rate and angle of attack on pitching-moment coefficient for basic configuration. $\delta_e = -25^\circ$, $\delta_a = 22.5^\circ$, $\delta_r = 0^\circ$, $\delta = 0^\circ$.

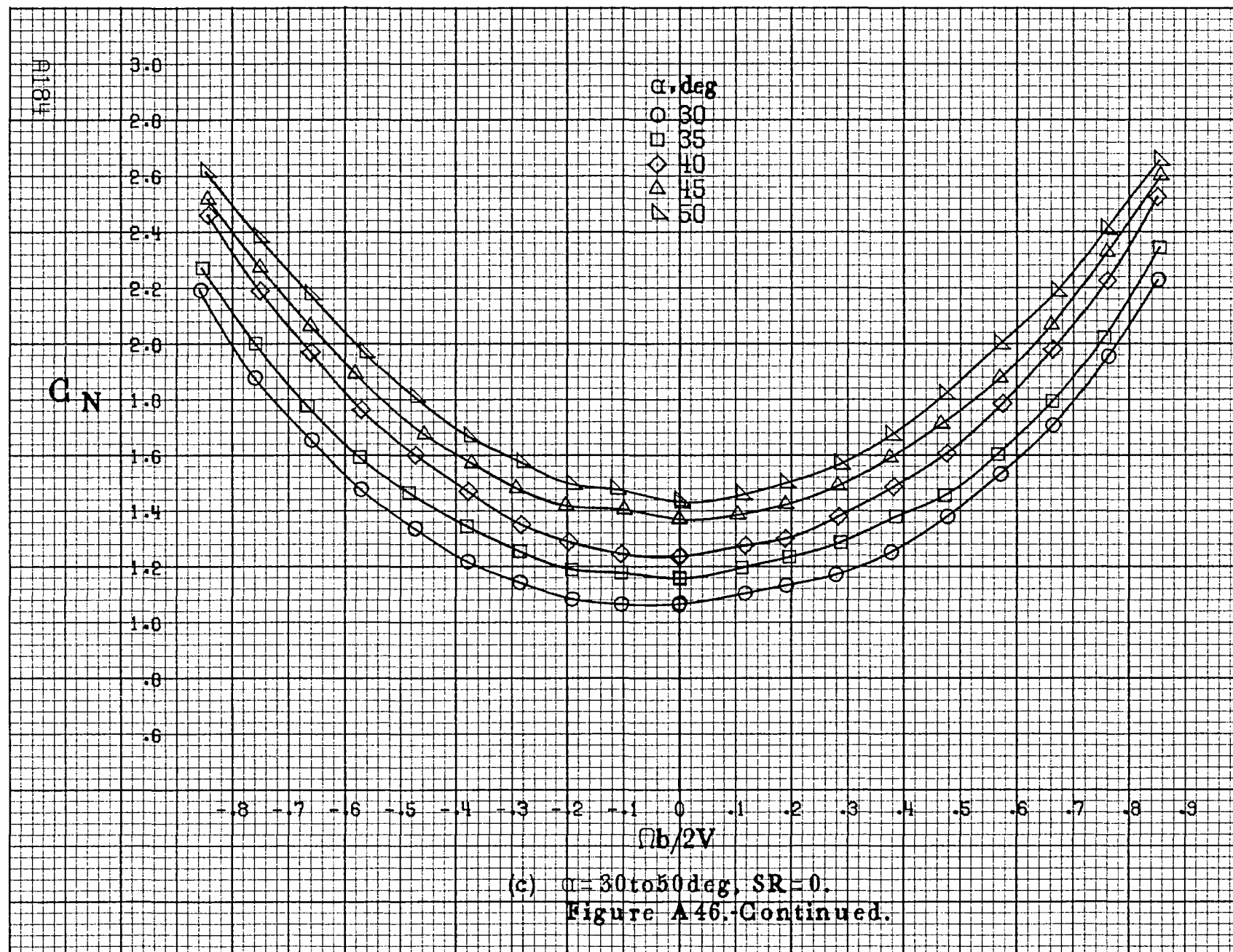


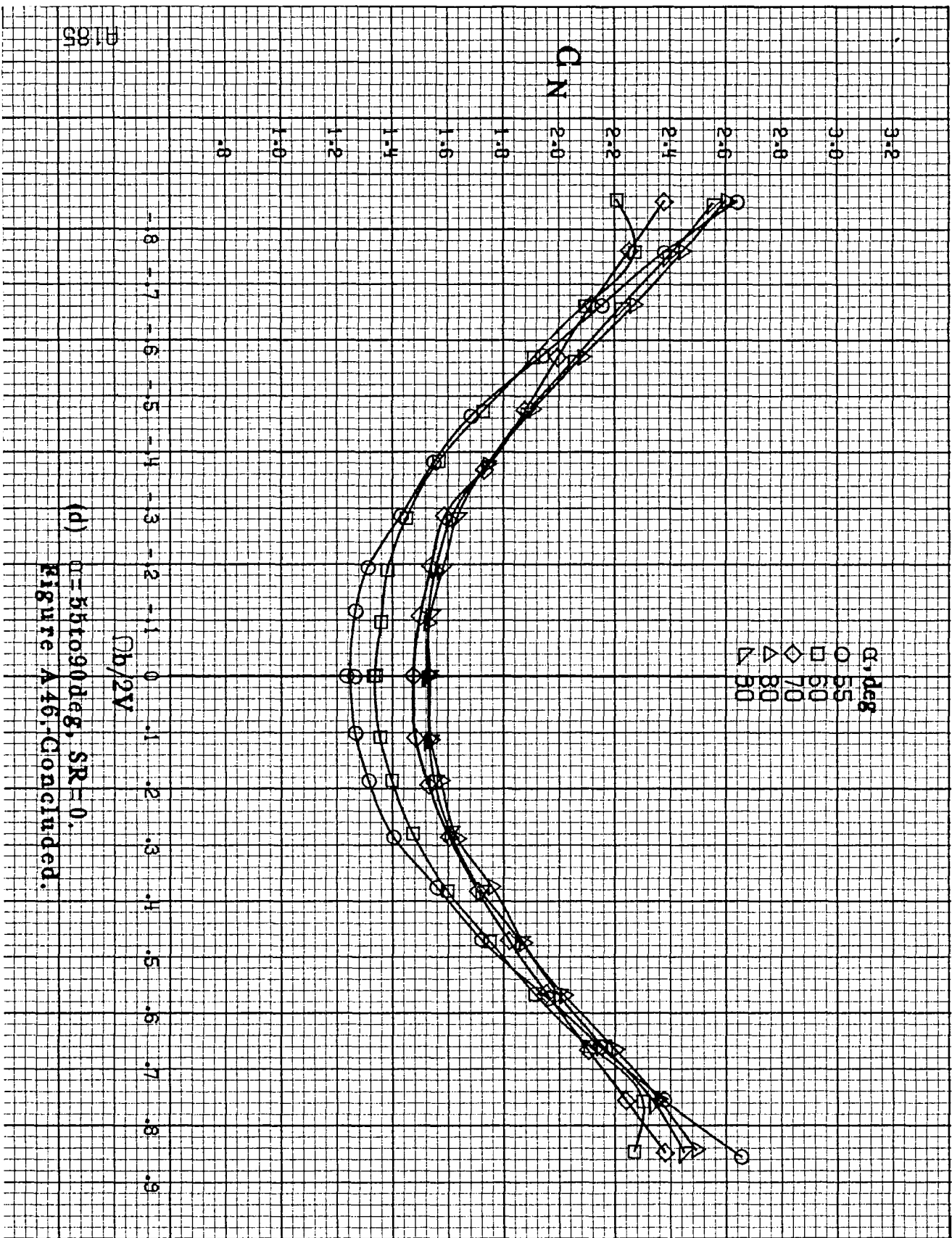




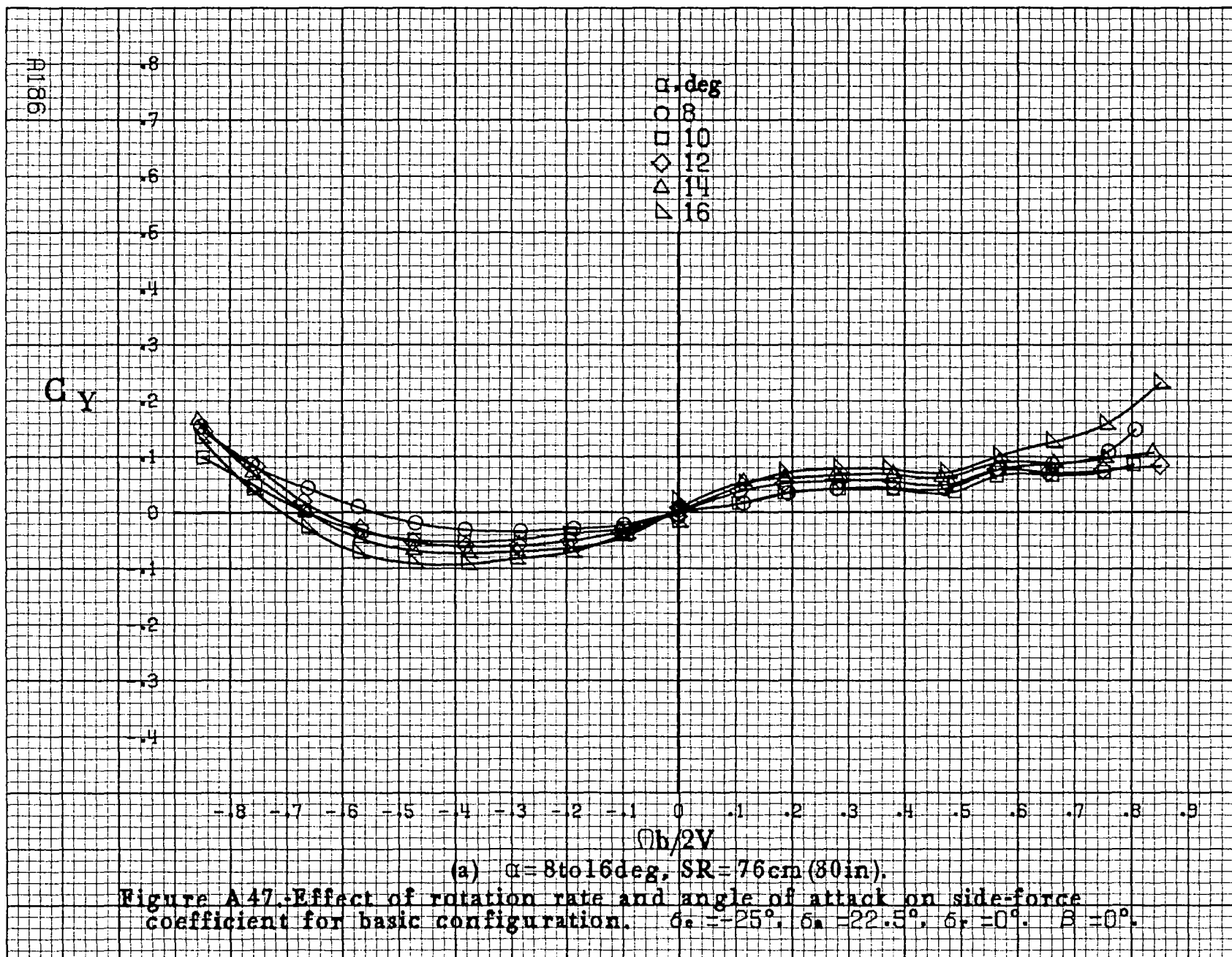


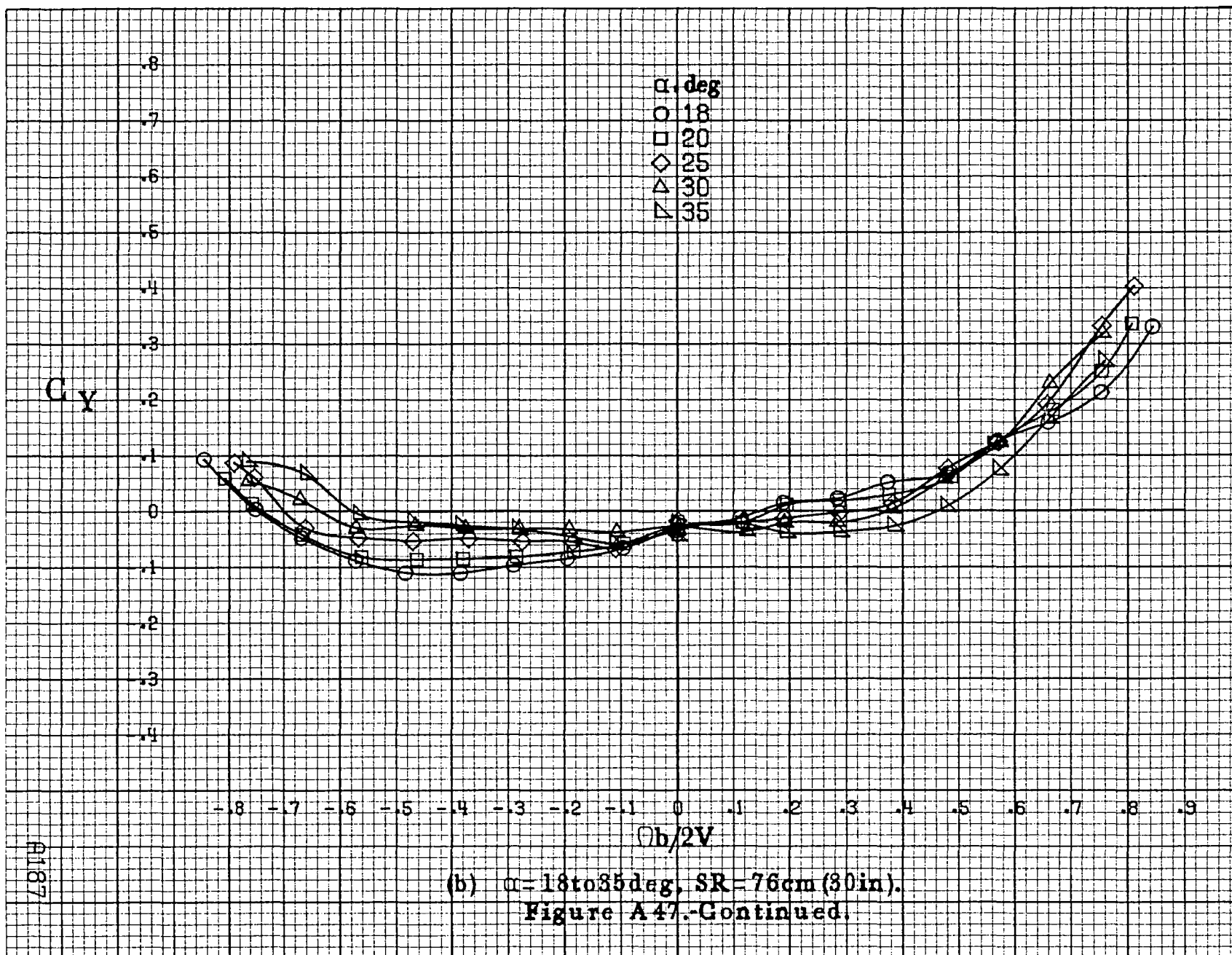




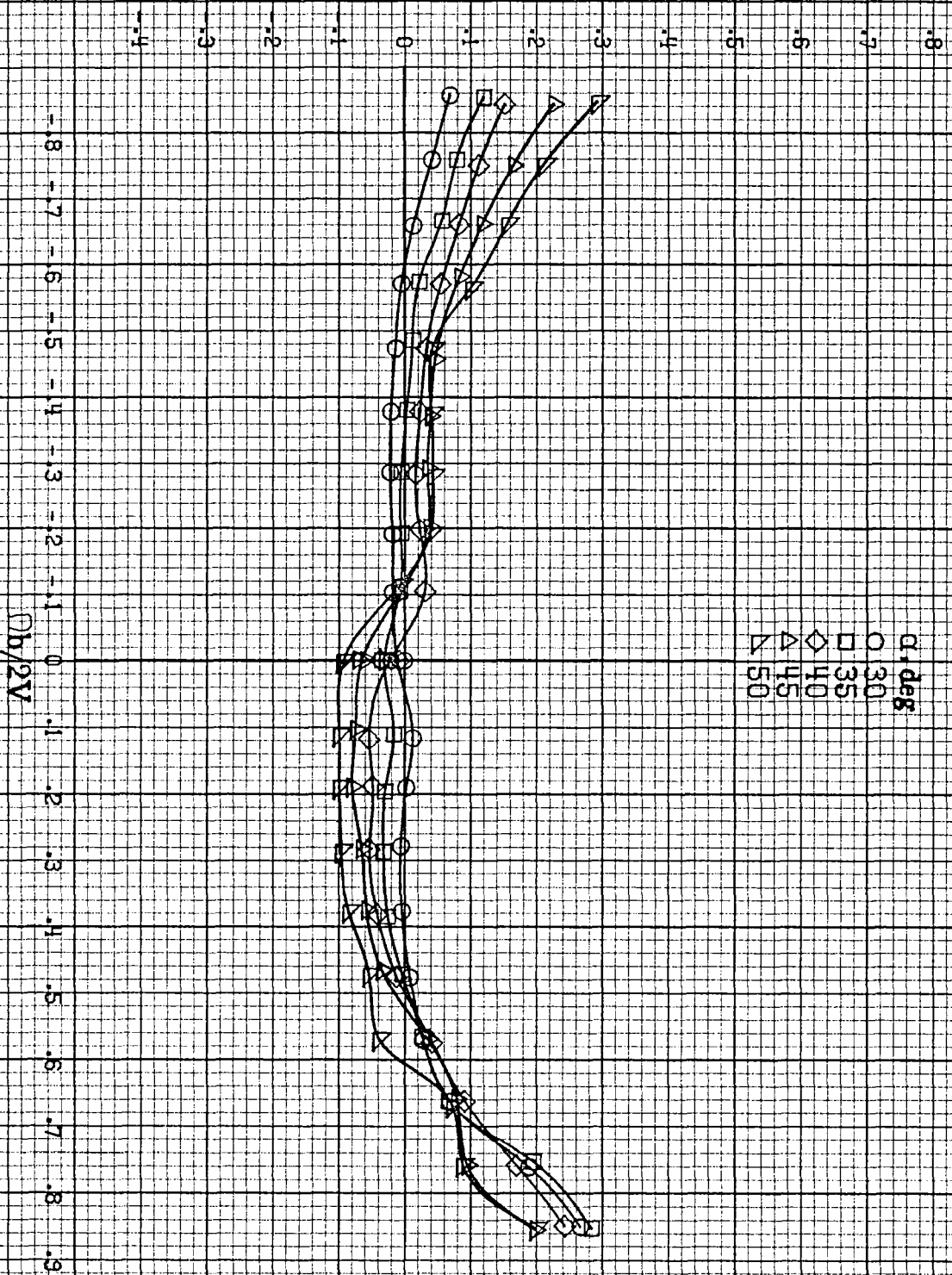


(d) $\alpha = 55$ to 90° , $SR = 0$.
Figure A46, Concluded.



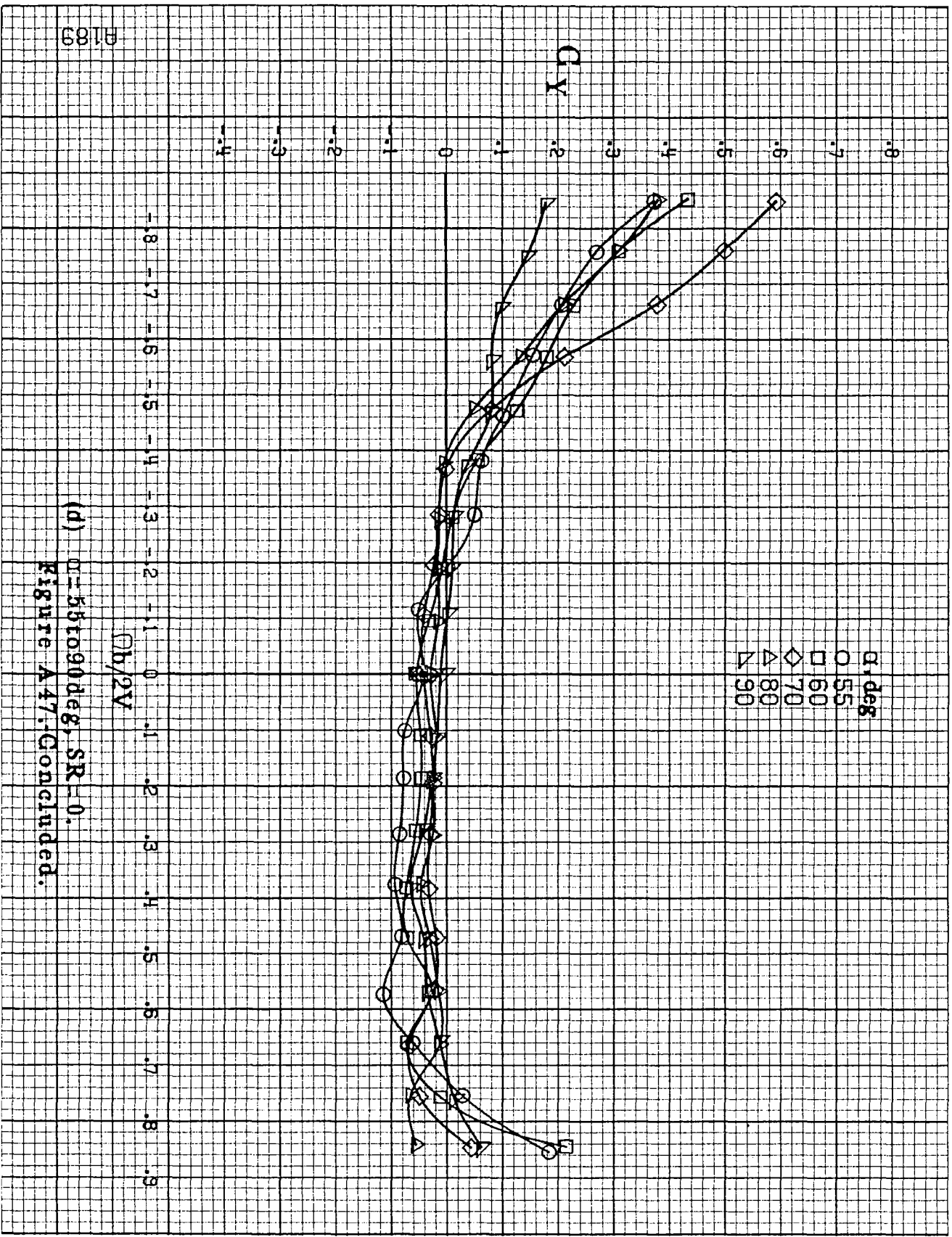


C_Y

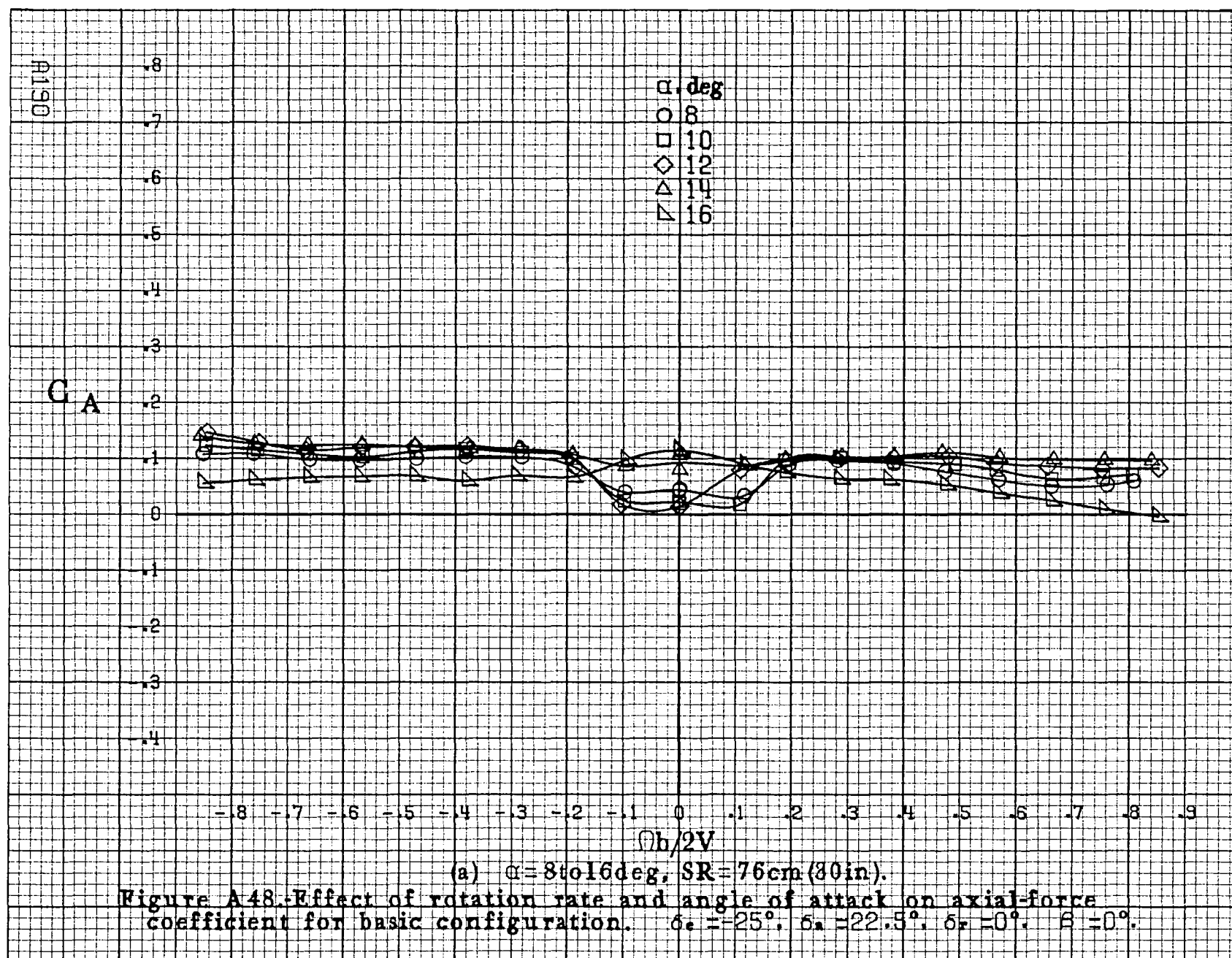


(c) $\alpha = 30$ to 50 deg, $SR = 0$.

Figure A47: Continued.

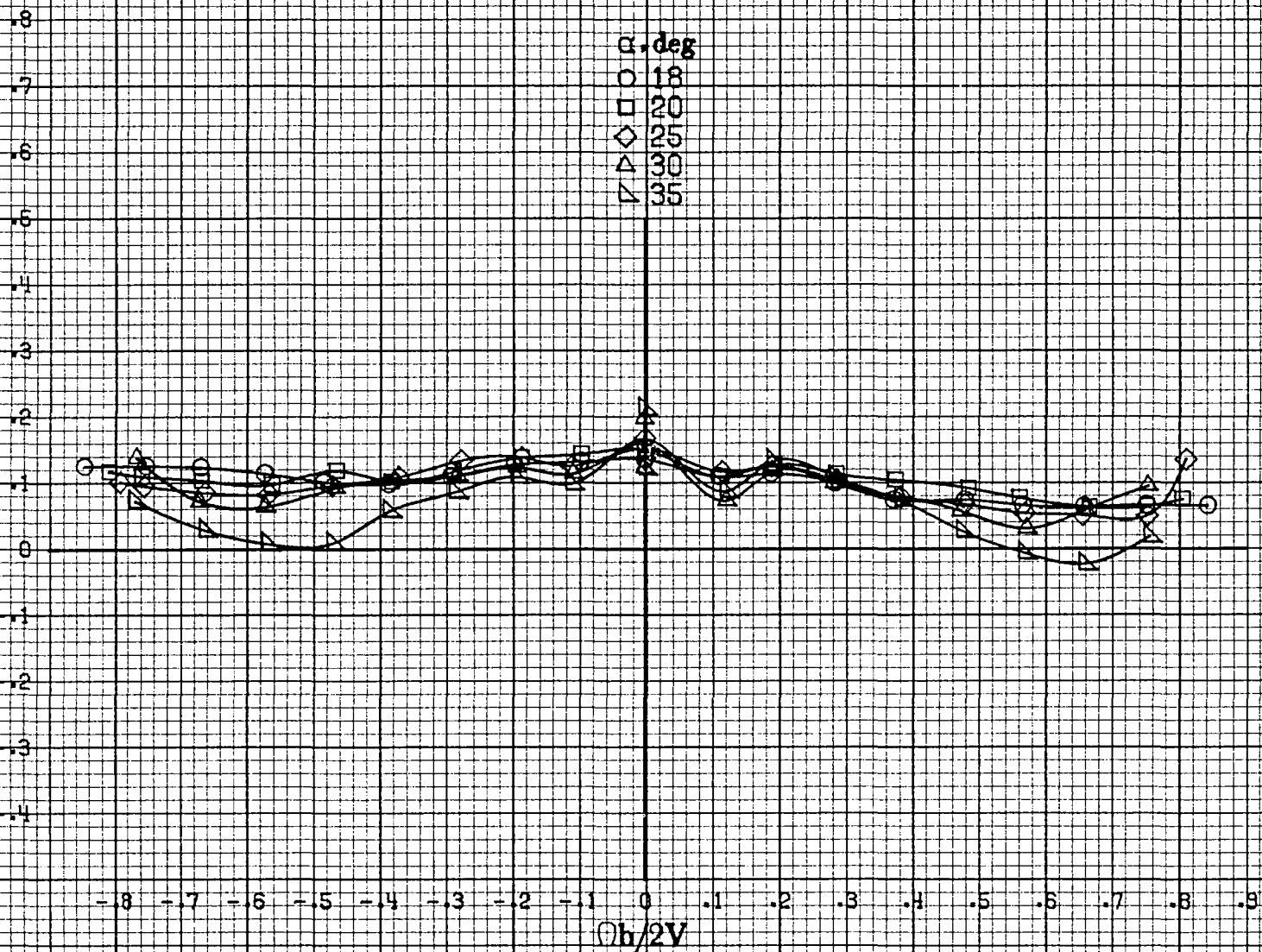


(d) $\alpha = 55$ to 90° , $SR = 0$.
 Figure A47: Concluded.

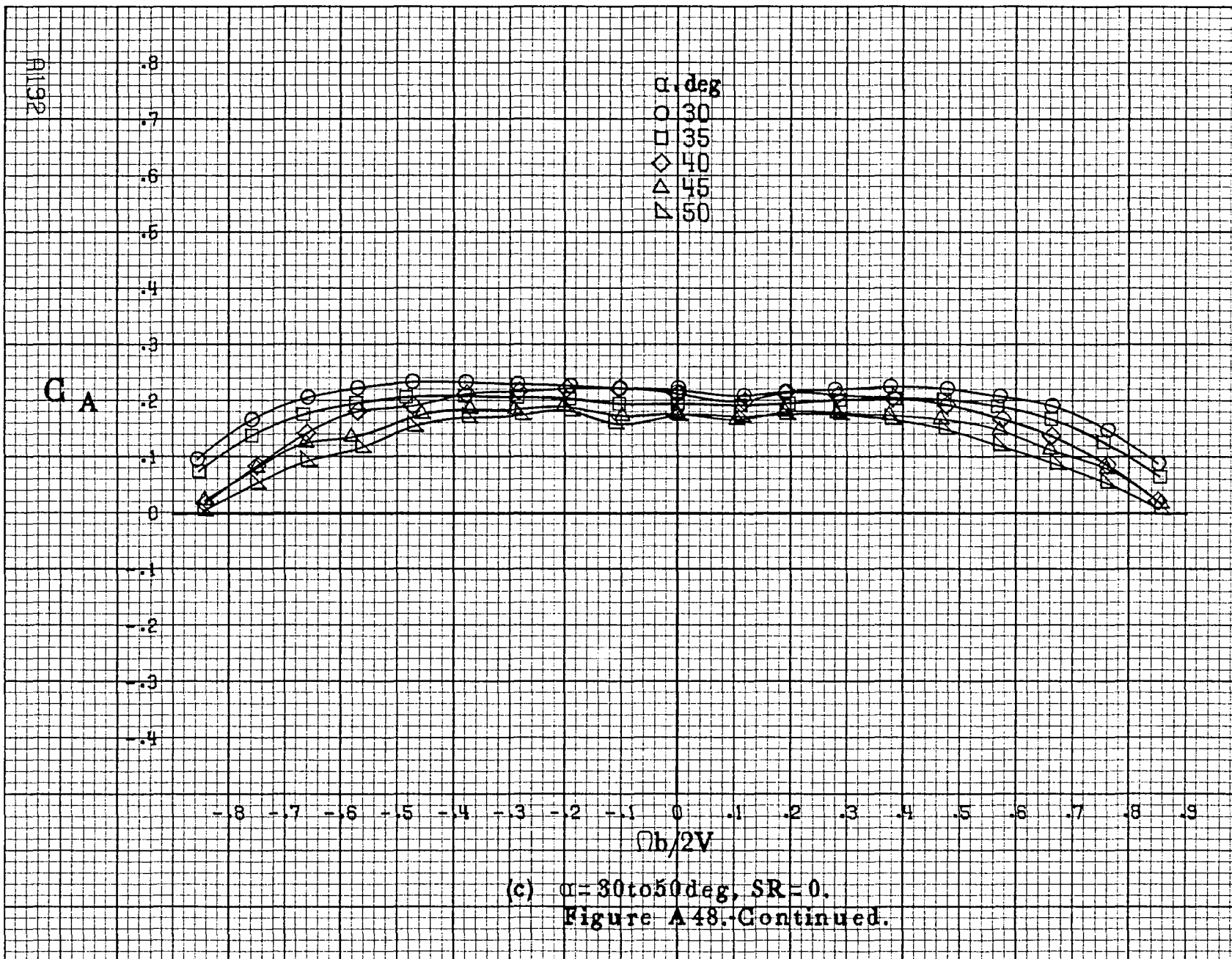


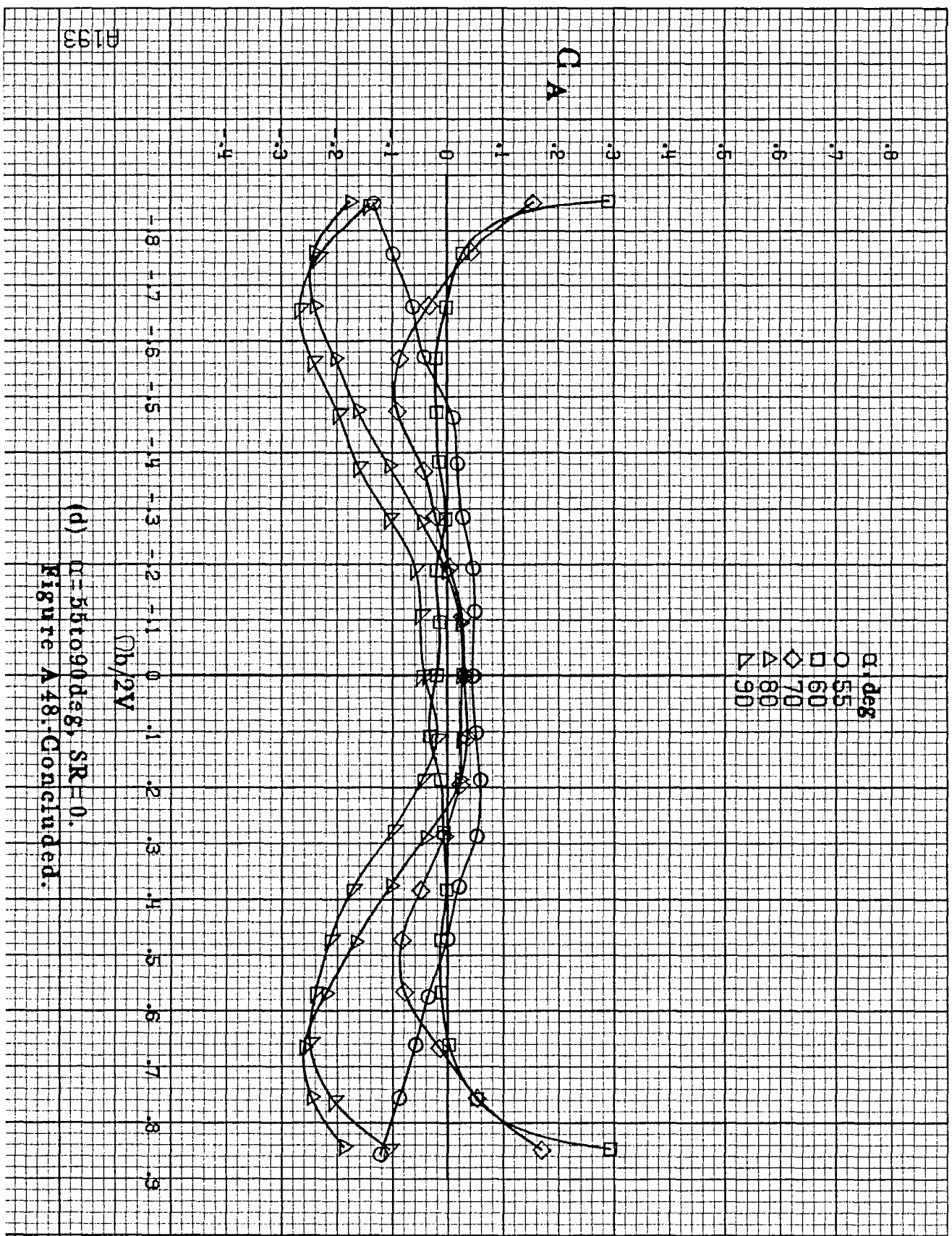
C_A

α, deg
 ○ 18
 □ 20
 ◇ 25
 △ 30
 ▽ 35

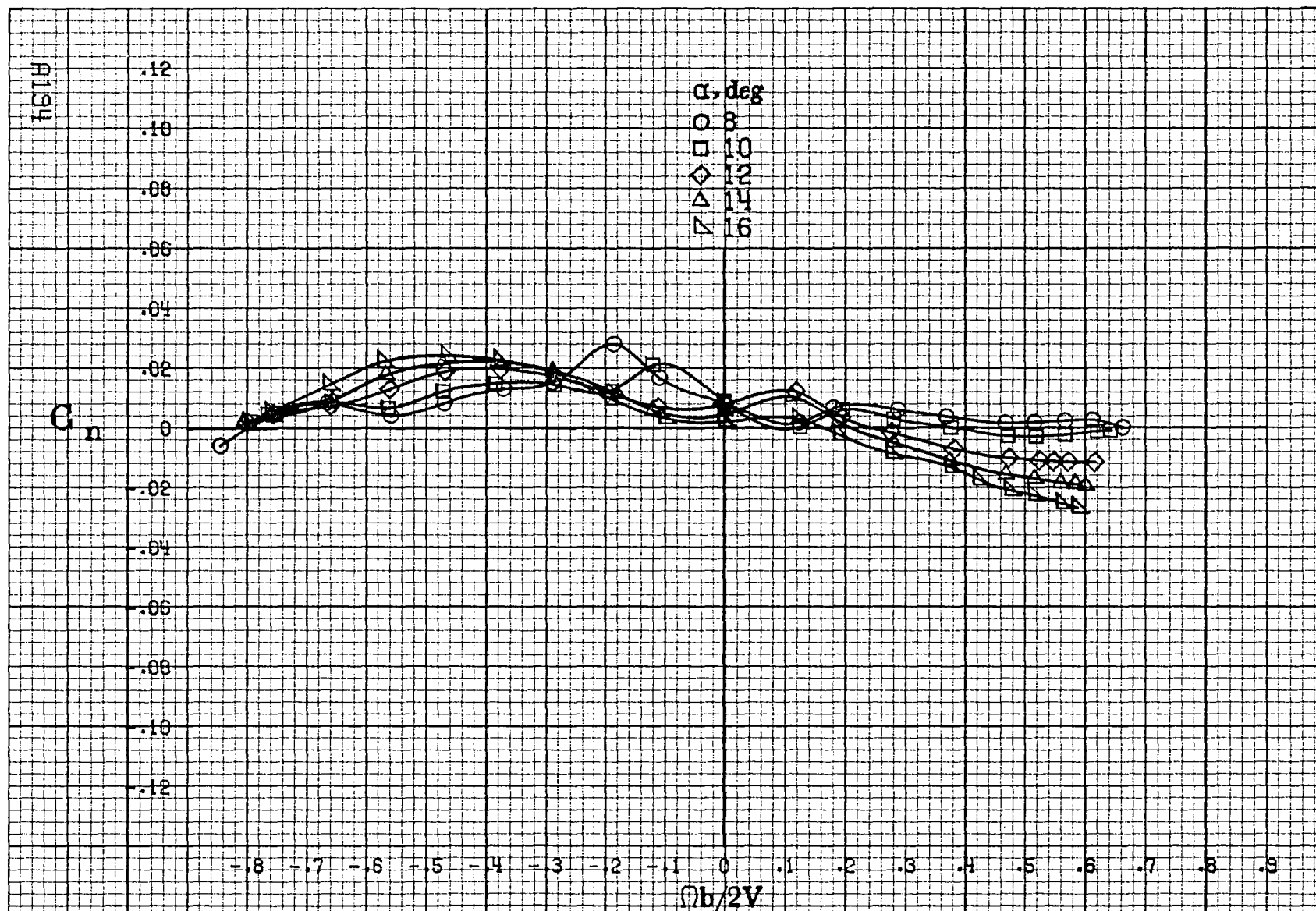


(b) $\alpha = 18 \text{ to } 35 \text{ deg}$, $SR = 76 \text{ cm (30 in)}$.
 Figure A48.-Continued.



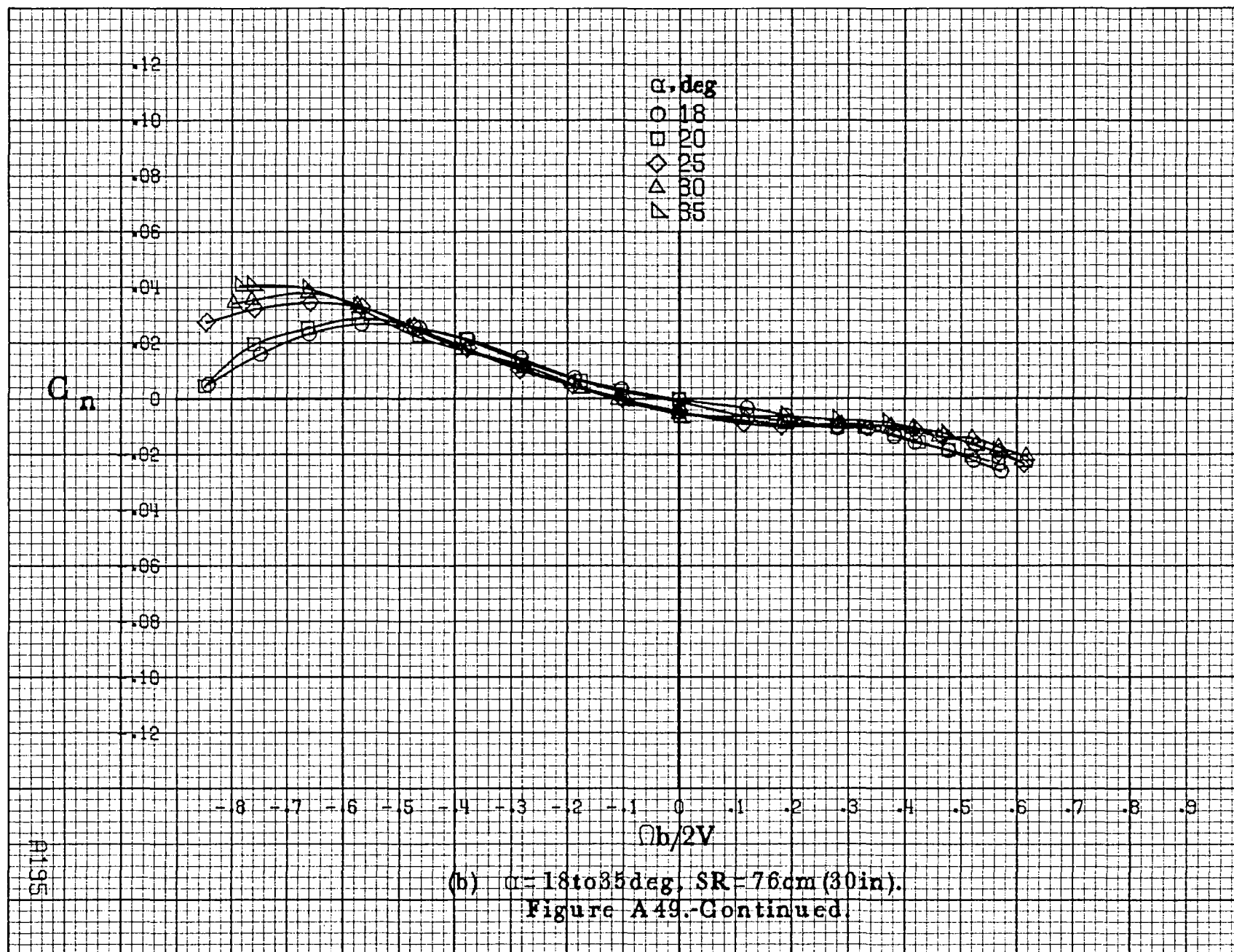


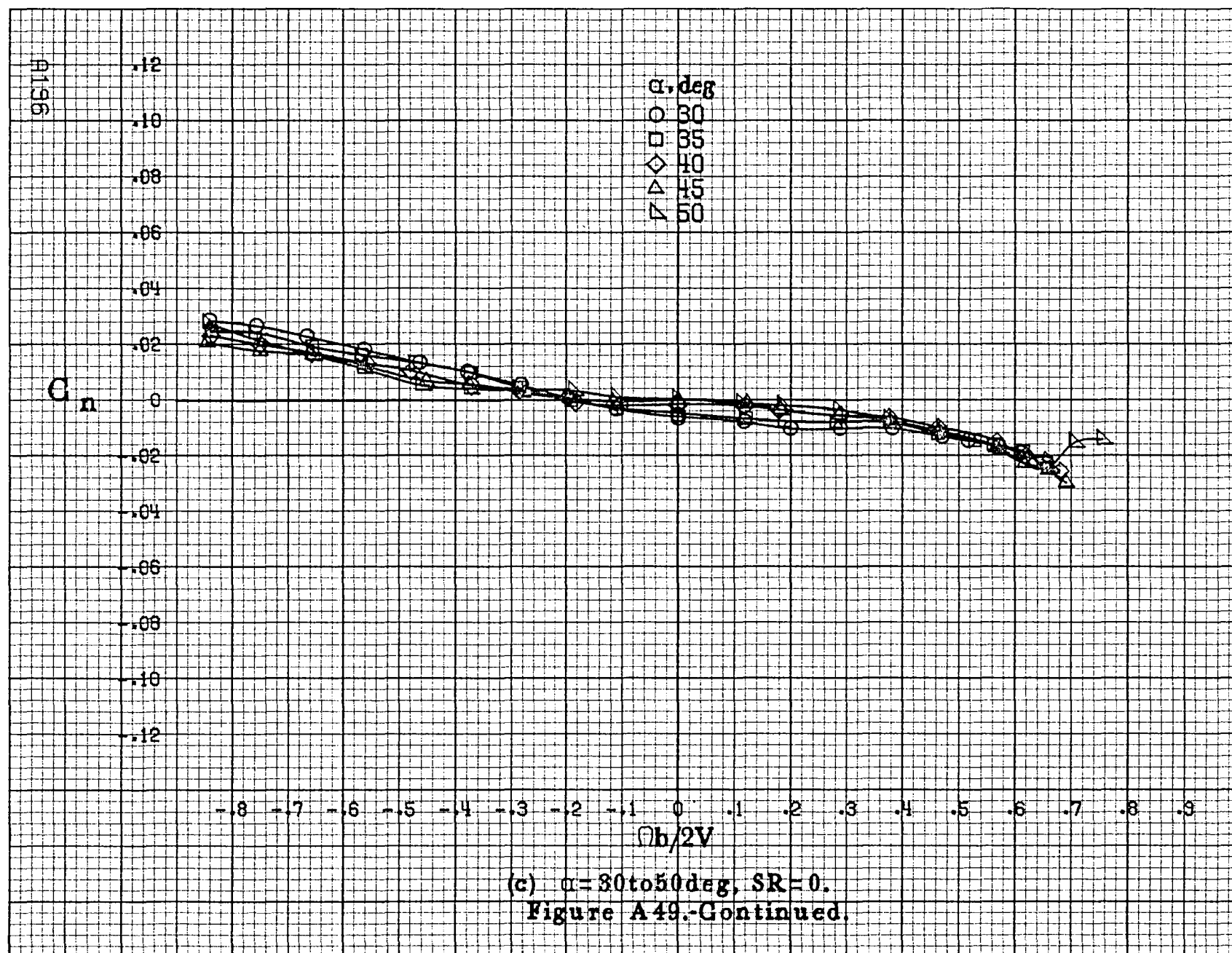
(d) $\alpha = 55$ to 90 deg, $SR = 0$.
 Figure A48: Concluded.

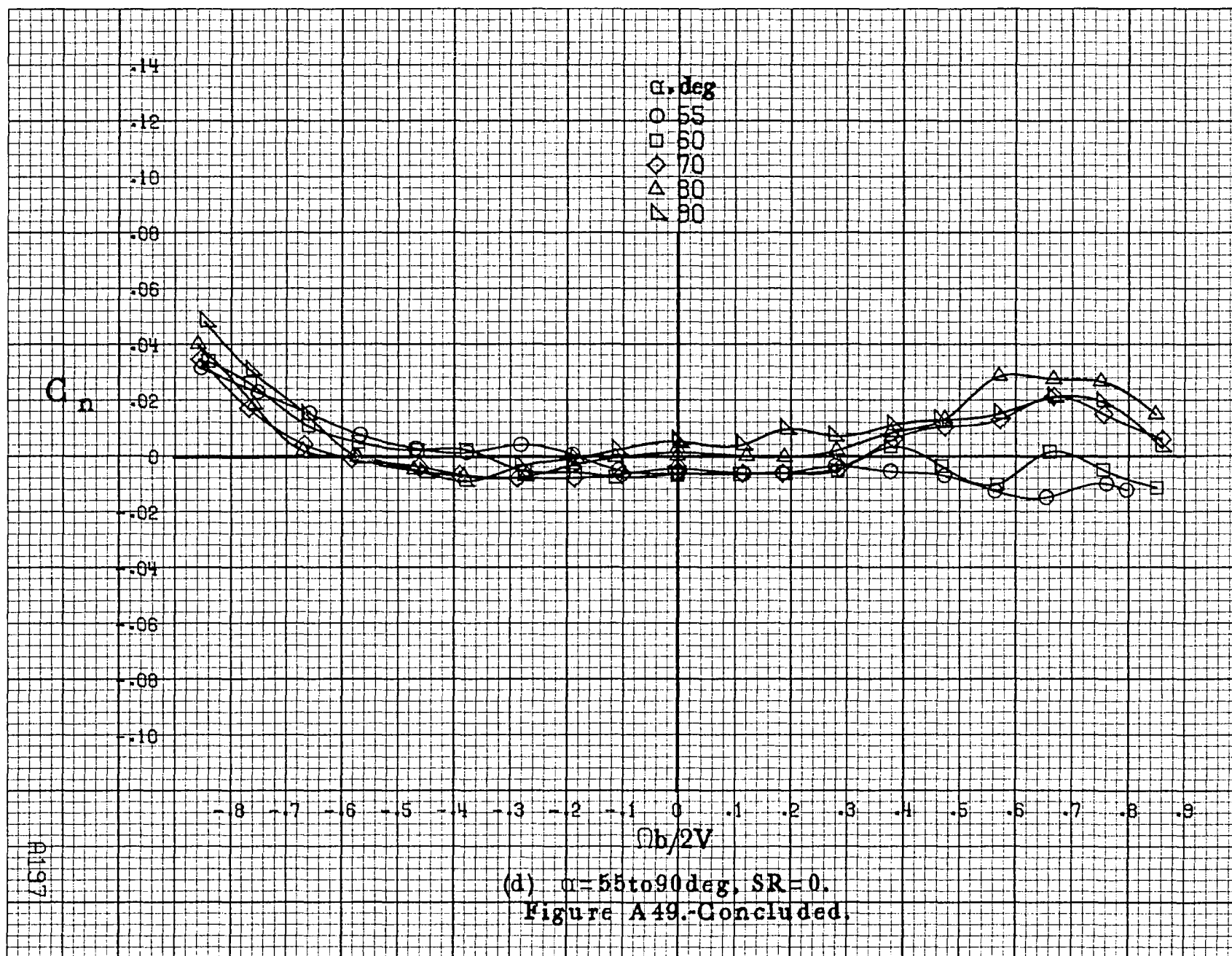


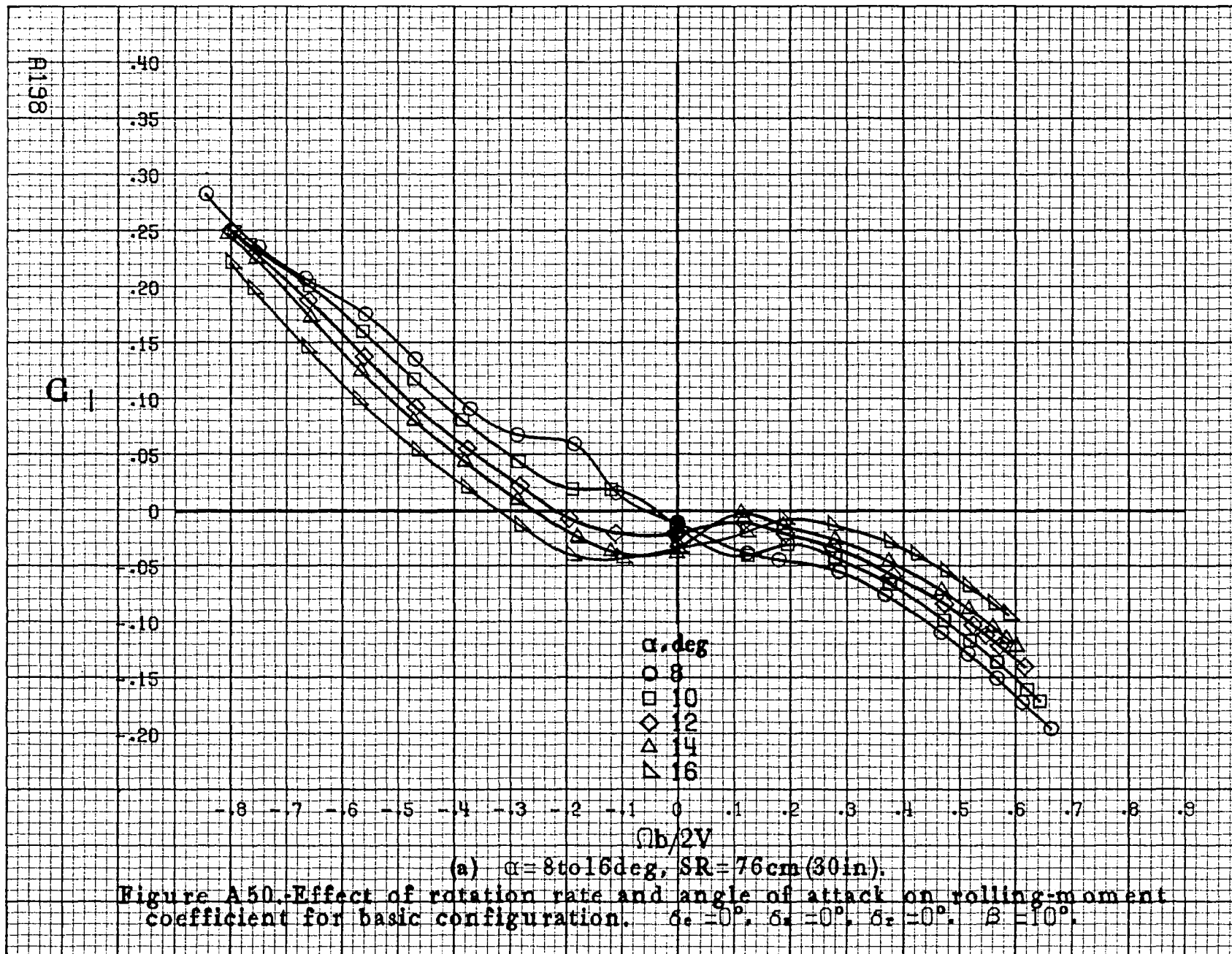
(a) $\alpha = 8$ to 16 deg, $SR = 76 \text{ cm (30 in.)}$.

Figure A49.-Effect of rotation rate and angle of attack on yawing-moment coefficient for basic configuration. $\delta_a = 0^\circ$, $\delta_e = 0^\circ$, $\delta_r = 0^\circ$. $\beta = 10^\circ$.



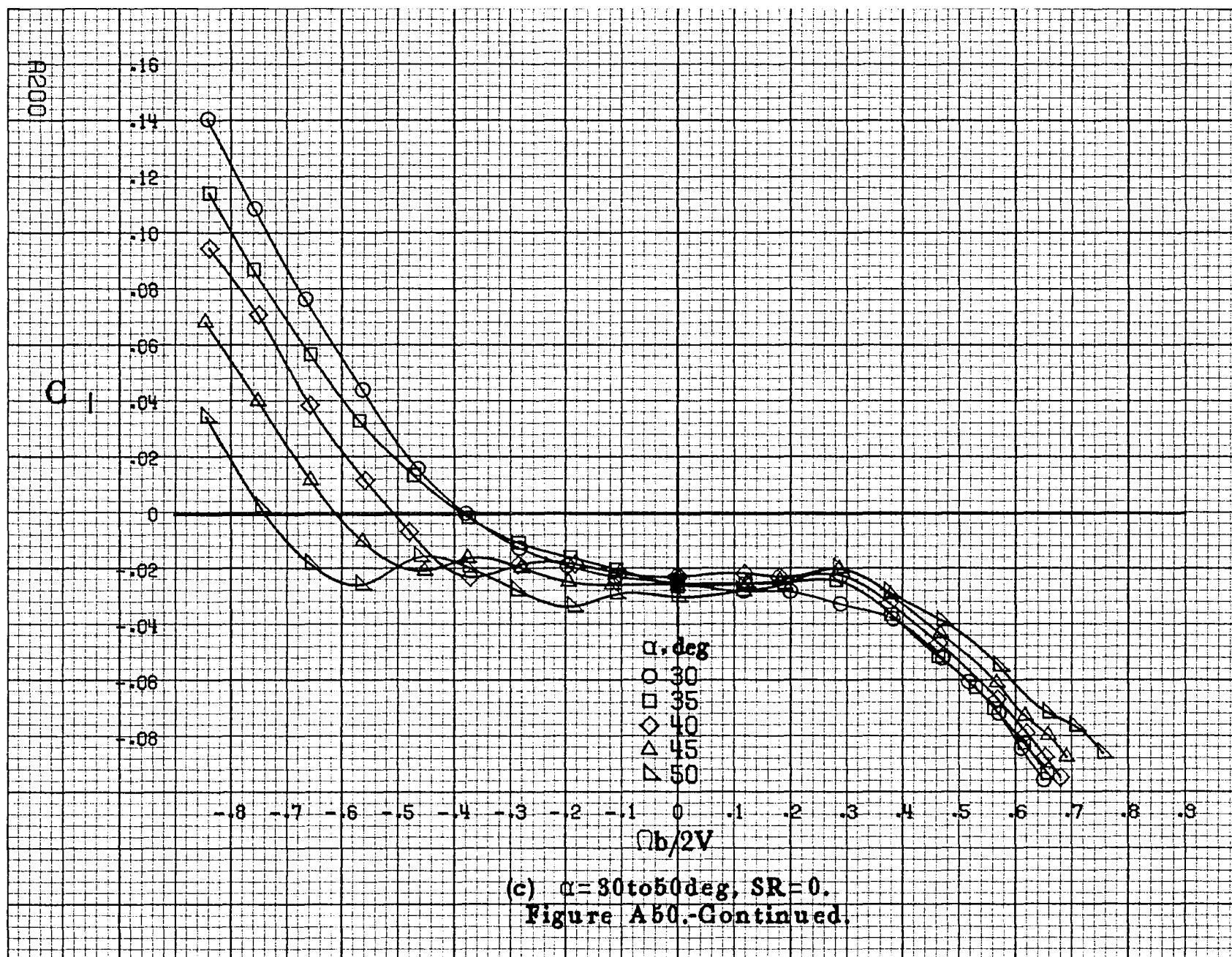


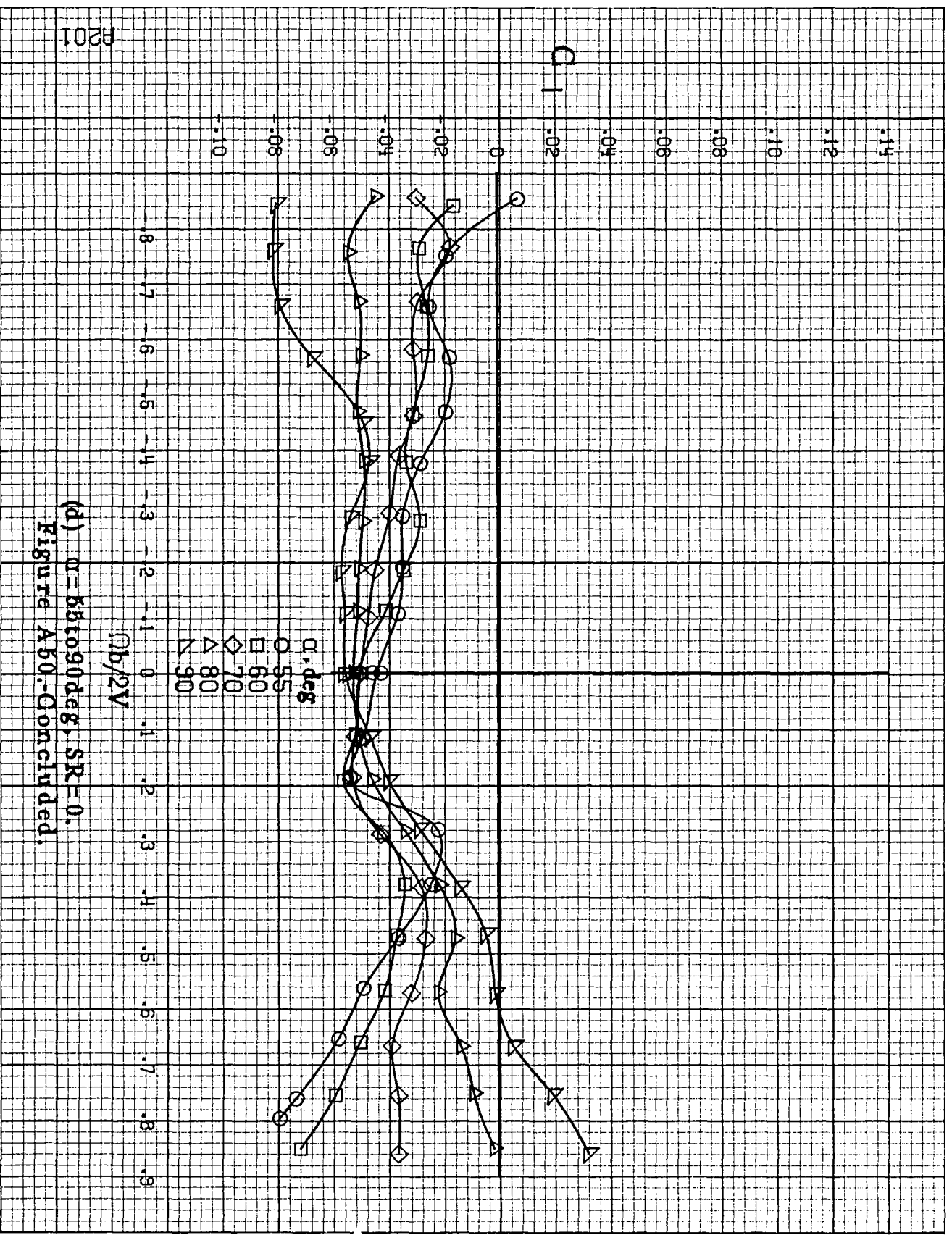




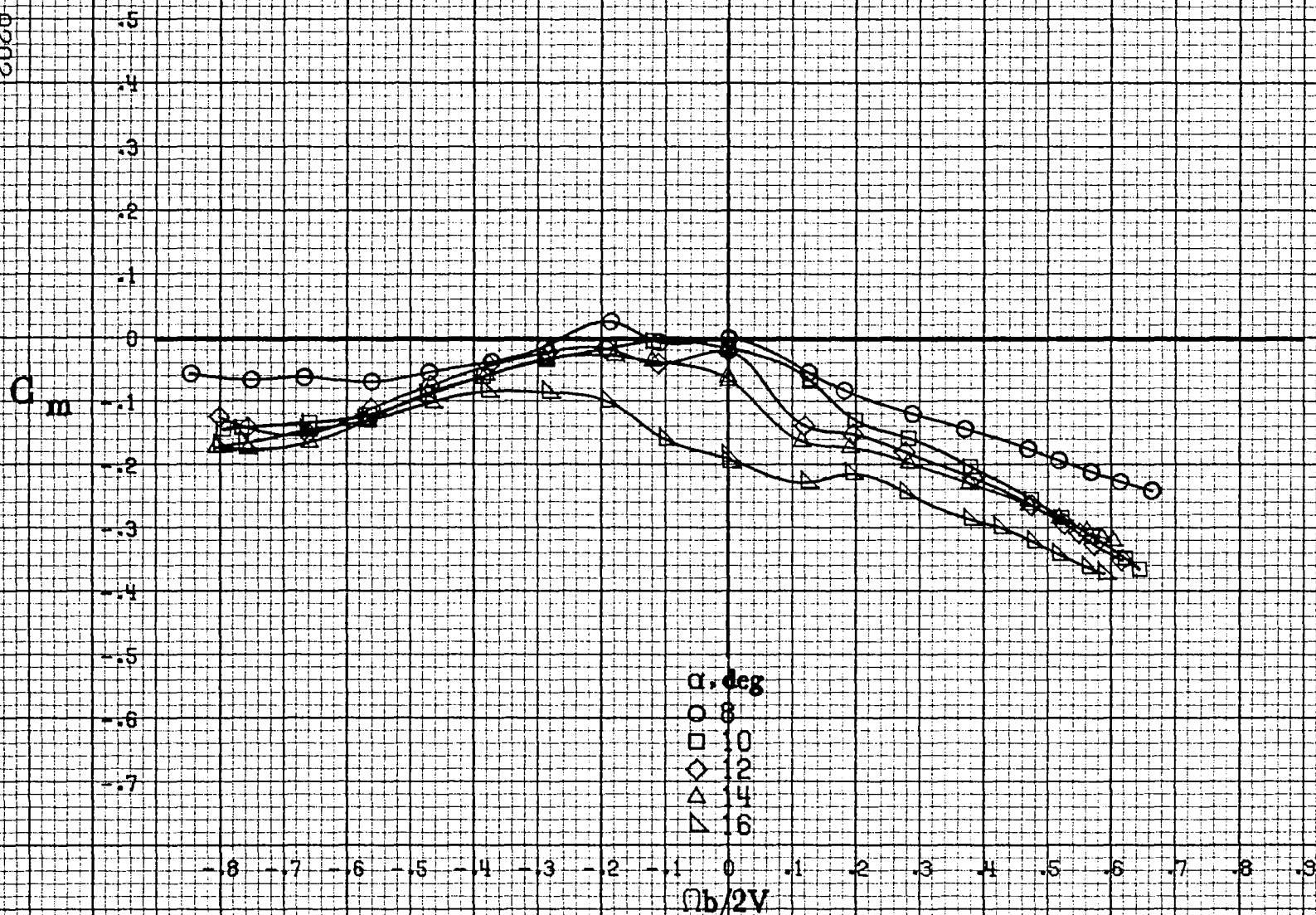


(b) $\alpha = 18.035 \text{ deg}$, $SR = 76 \text{ cm (30 in.)}$.
Figure A50.-Continued.



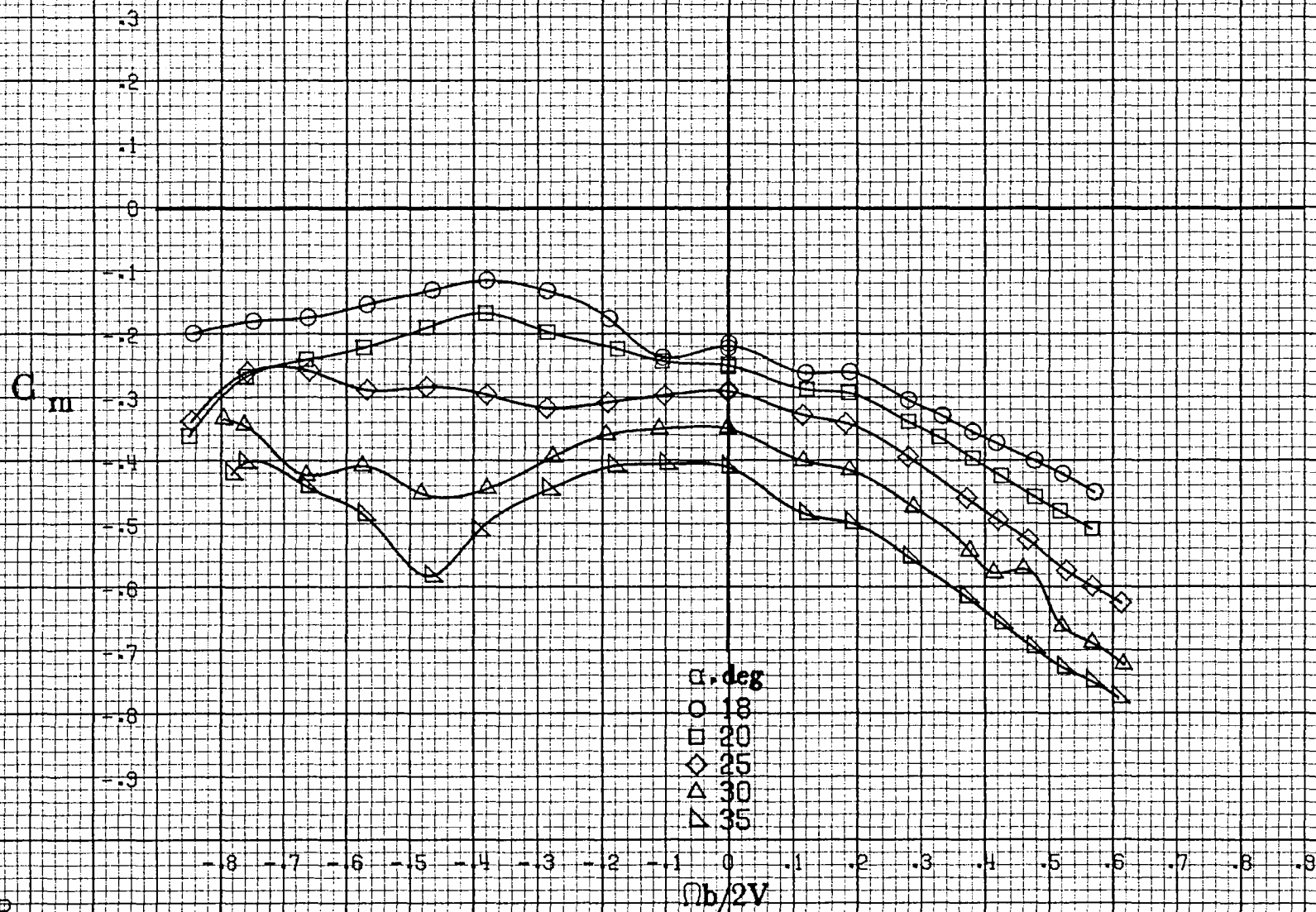


(d) $\alpha = 55$ to 90 deg, $SR = 0$.
Figure A50-Concluded.

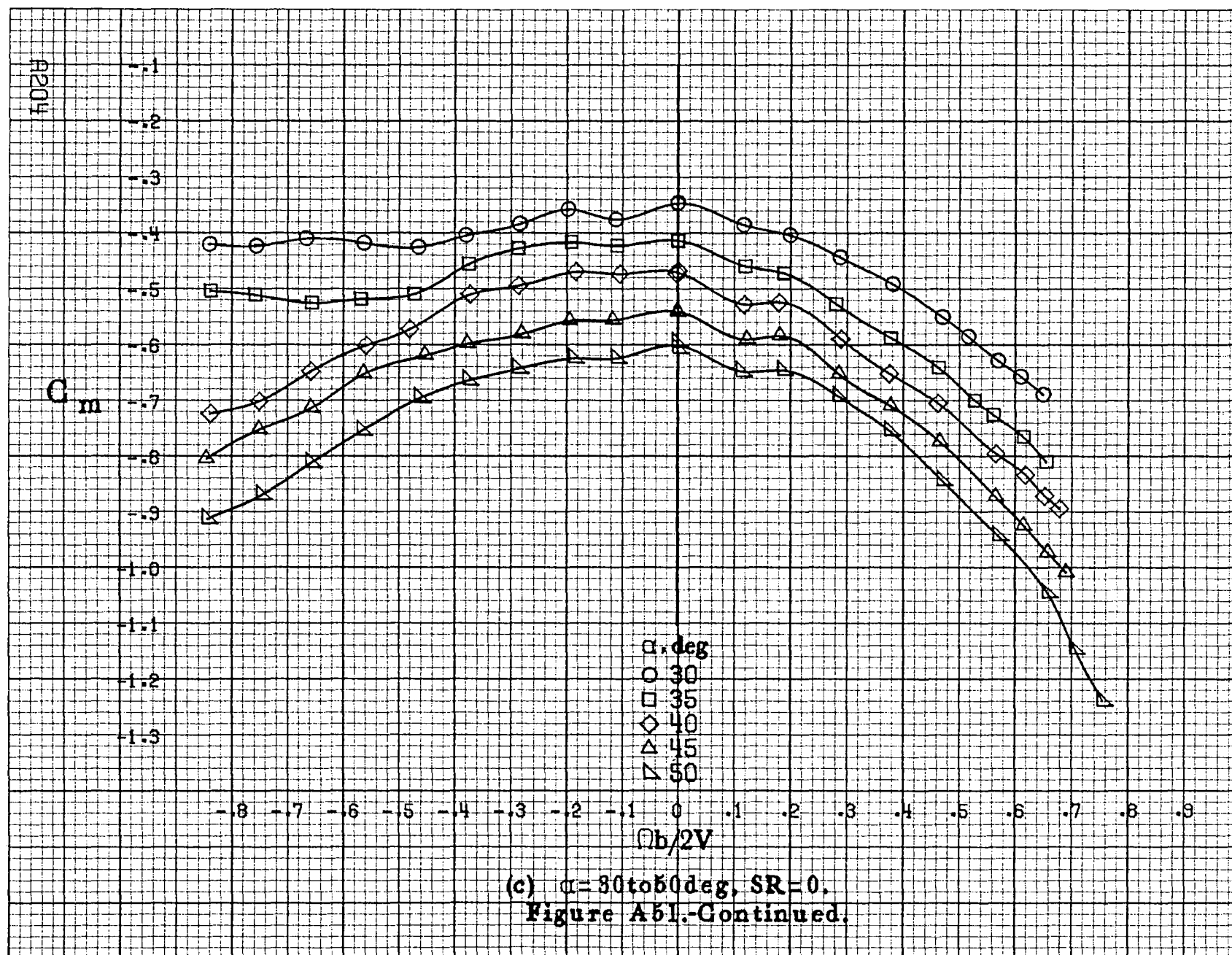


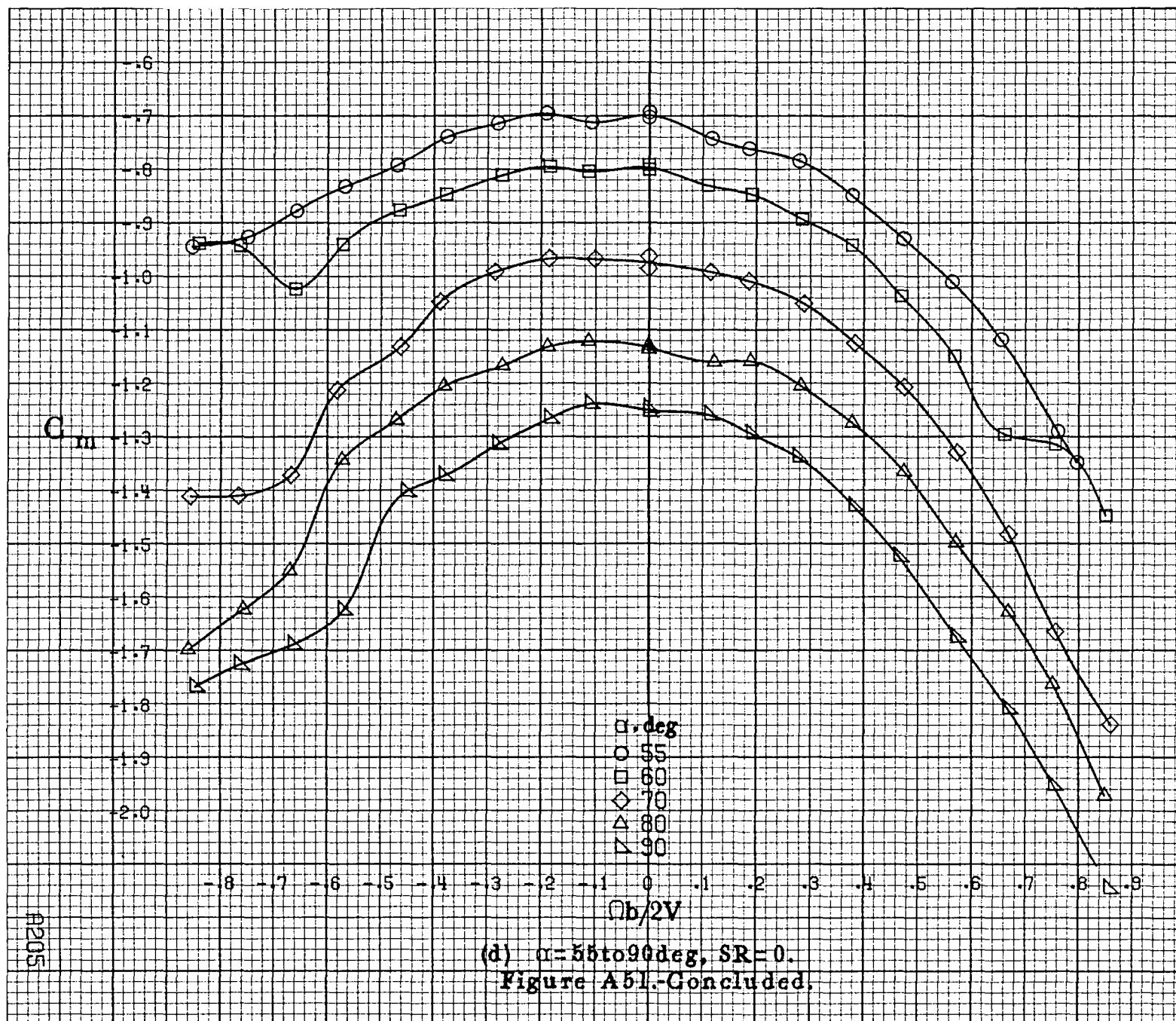
(a) $\alpha=8$ to 16° , $SR=76$ cm (30 in).

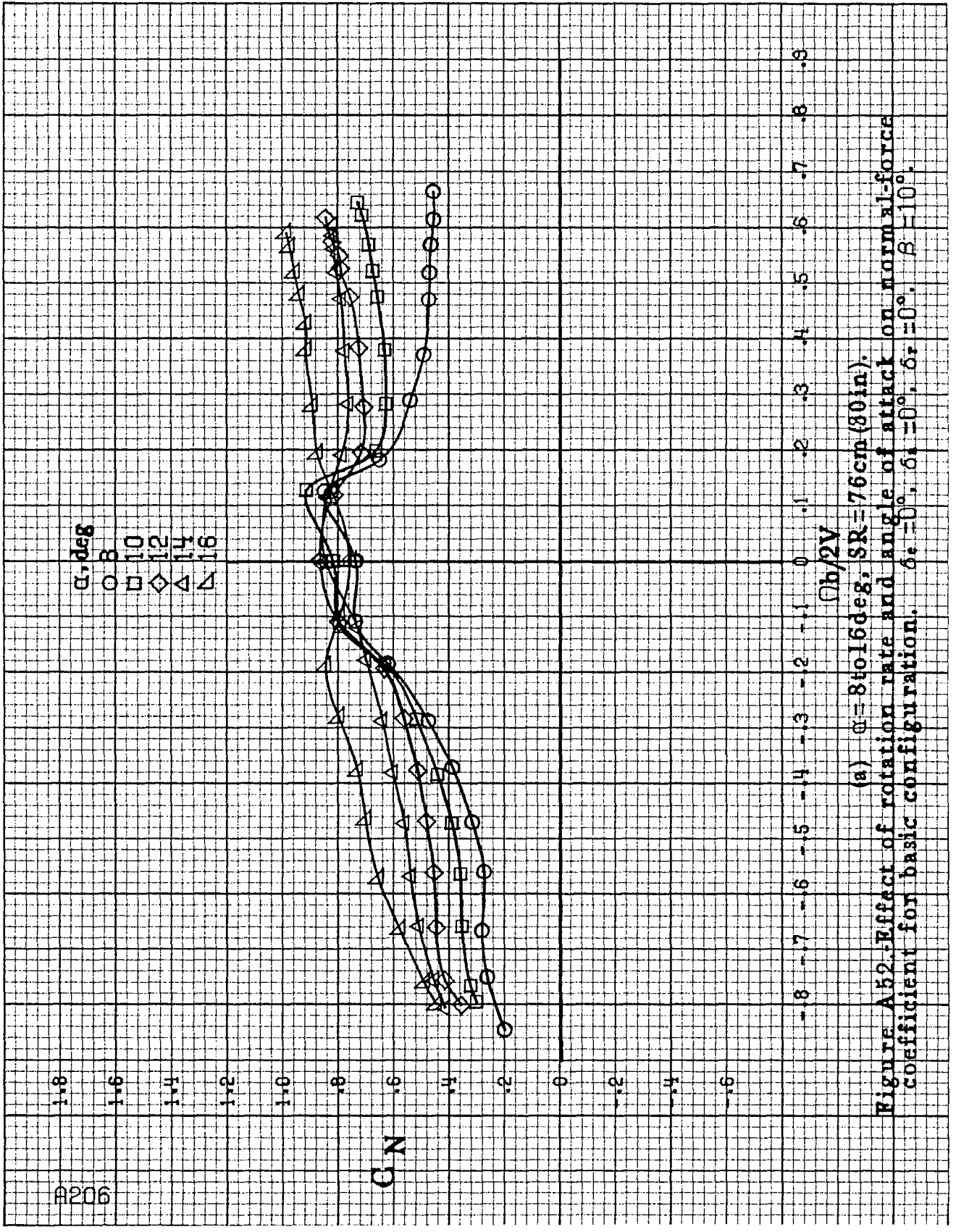
Figure A51. Effect of rotation rate and angle of attack on pitching-moment coefficient for basic configuration. $\delta_e=0^\circ$, $\delta_a=0^\circ$, $\delta_r=0^\circ$, $\beta=10^\circ$.

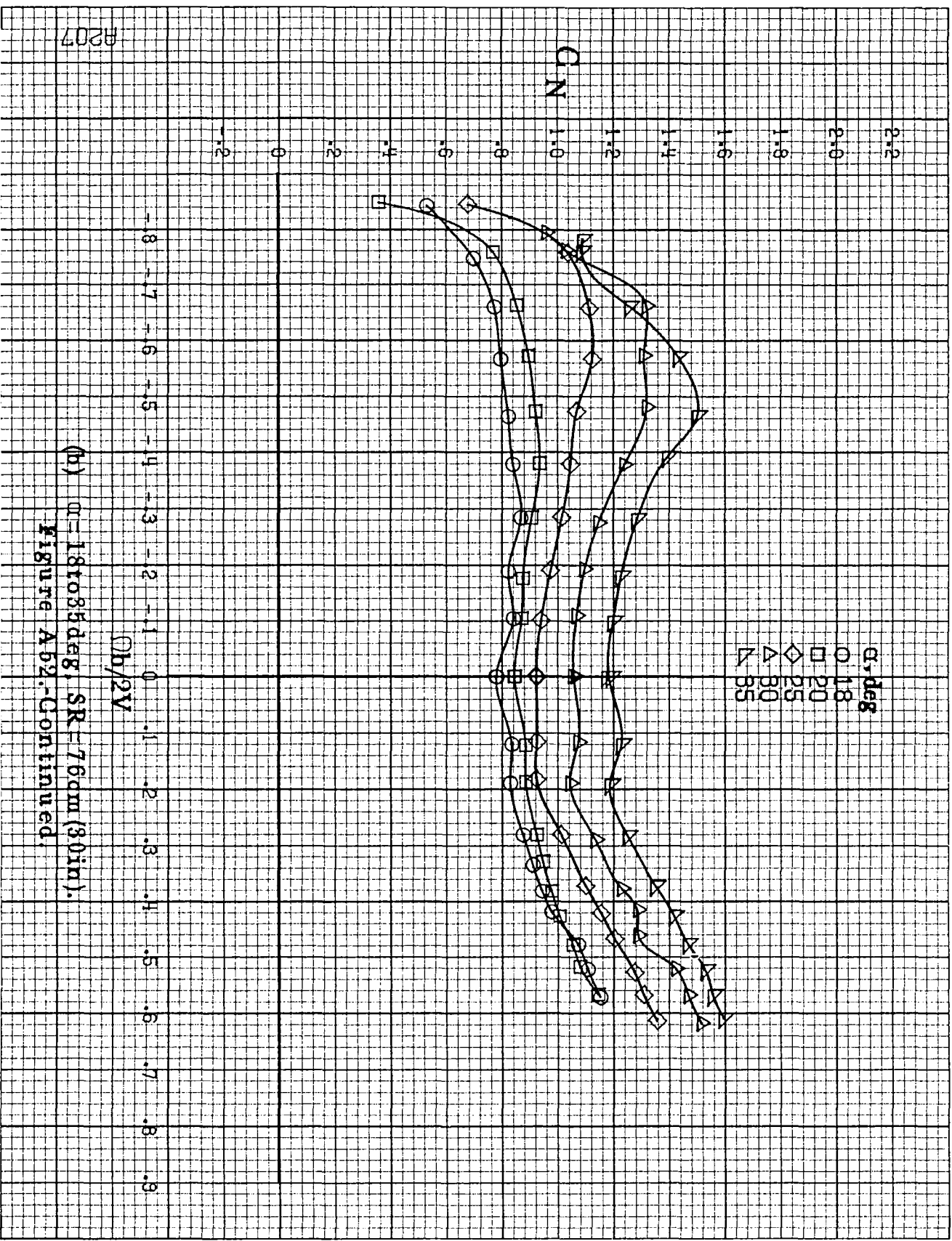


(b) $\alpha = 18$ to 35° , $SR = 76\text{cm}$ (30in).
Figure A51.-Continued.

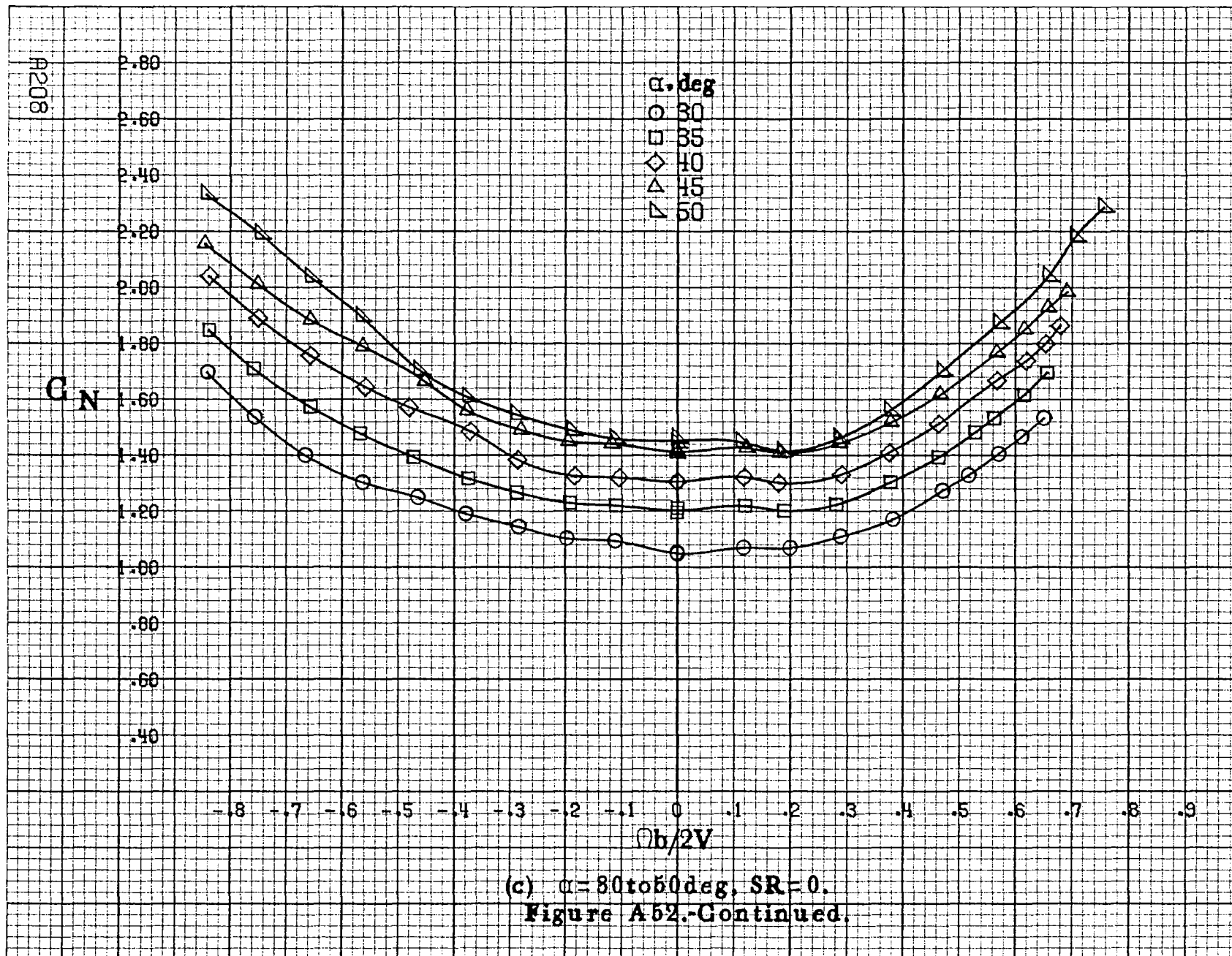


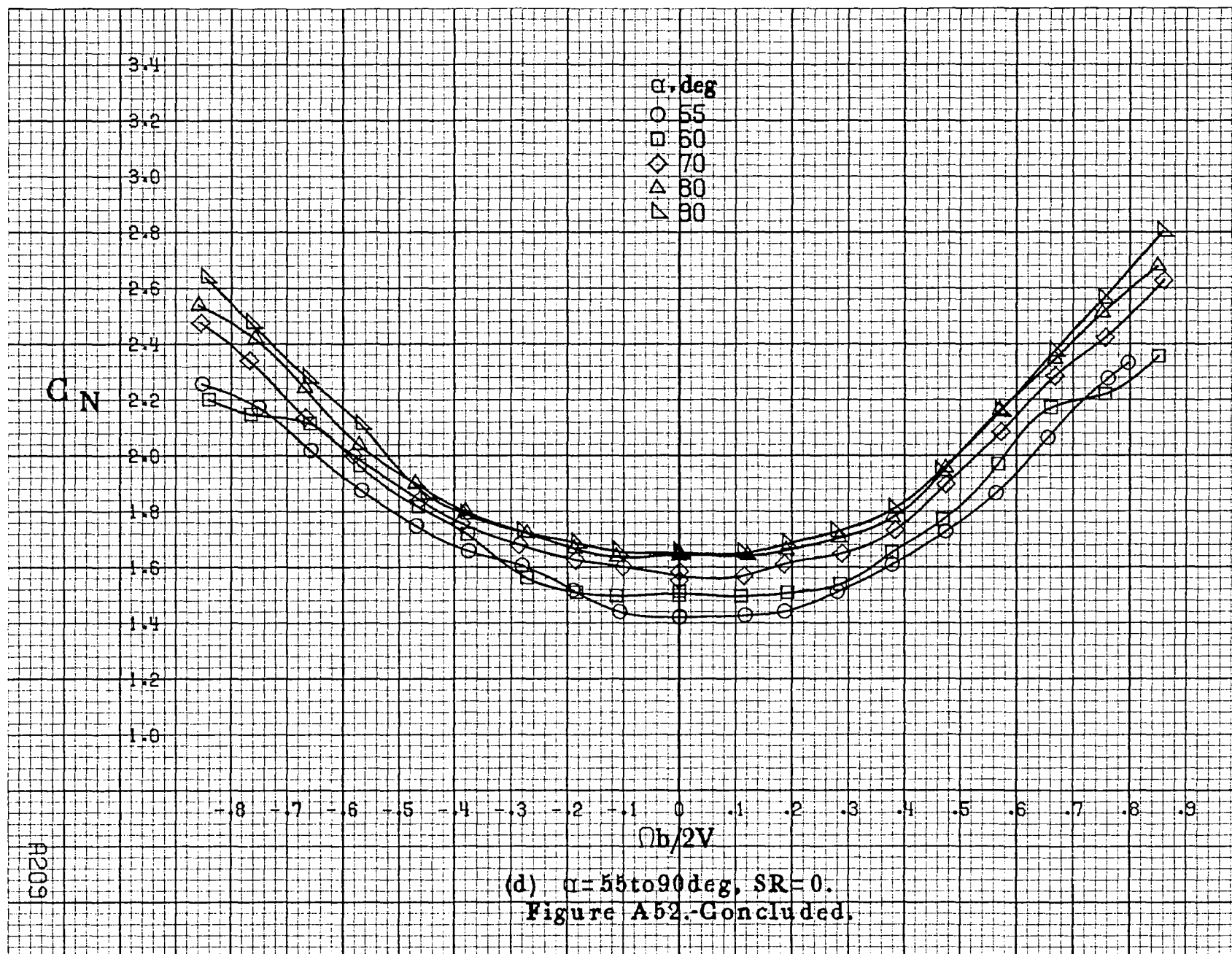


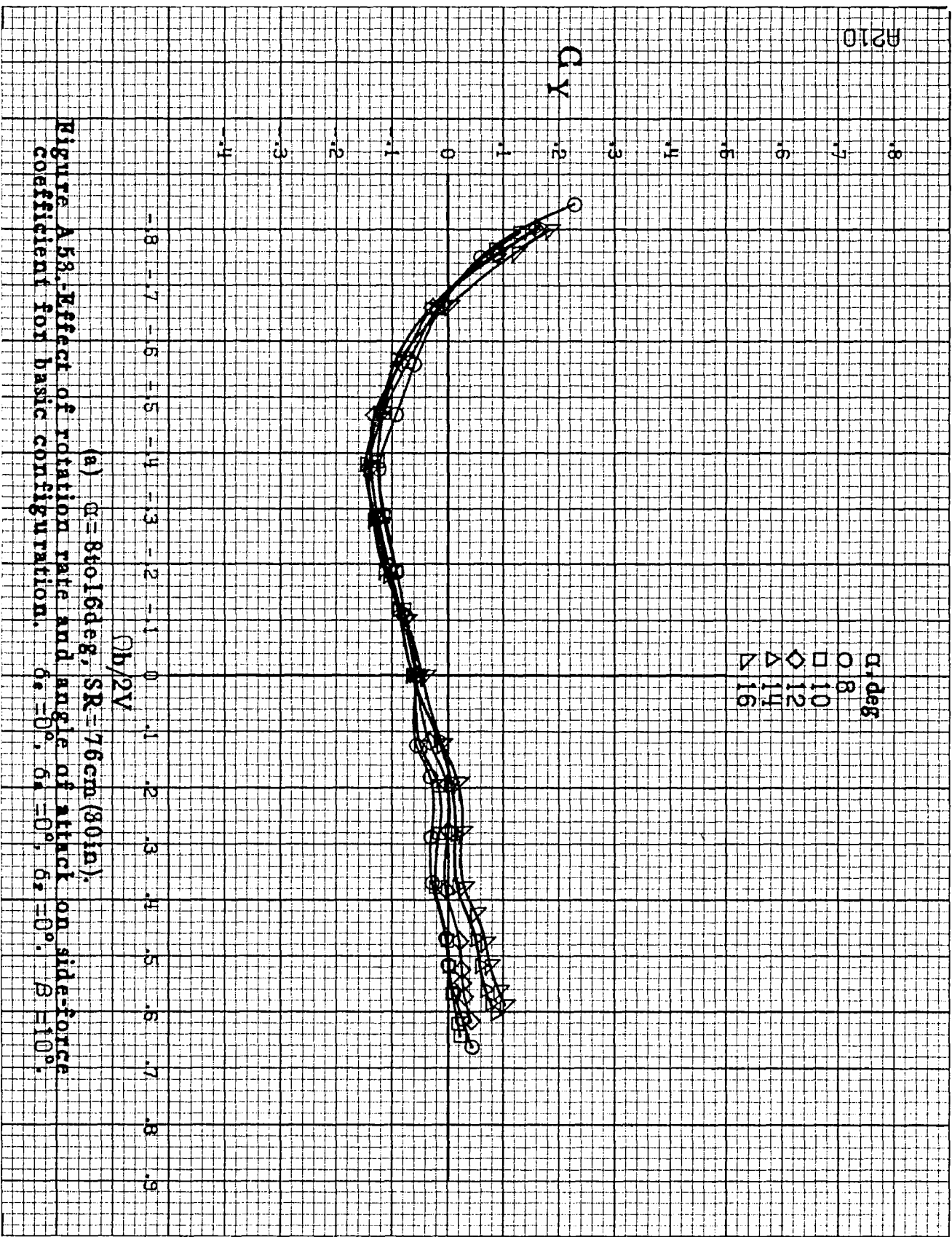


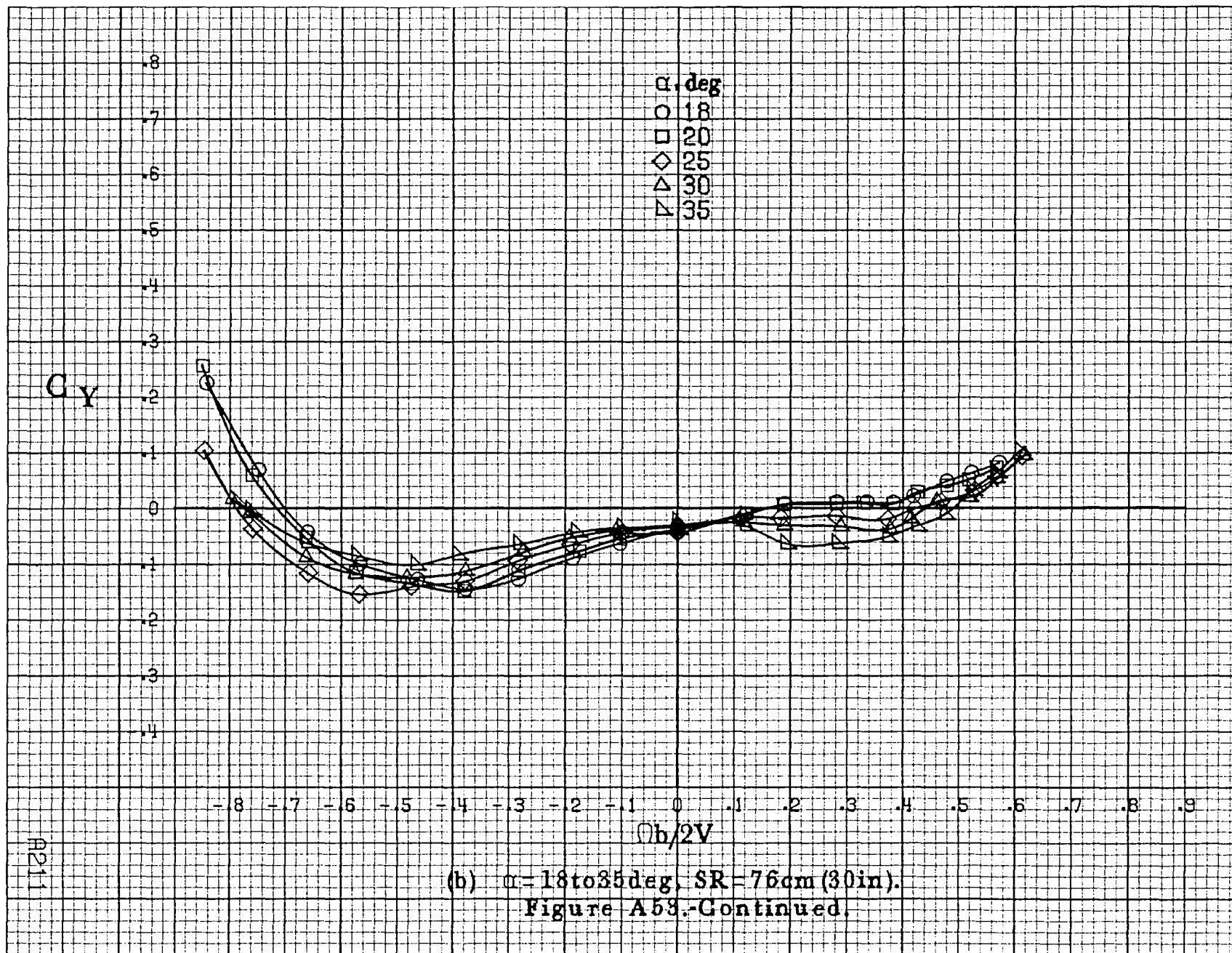


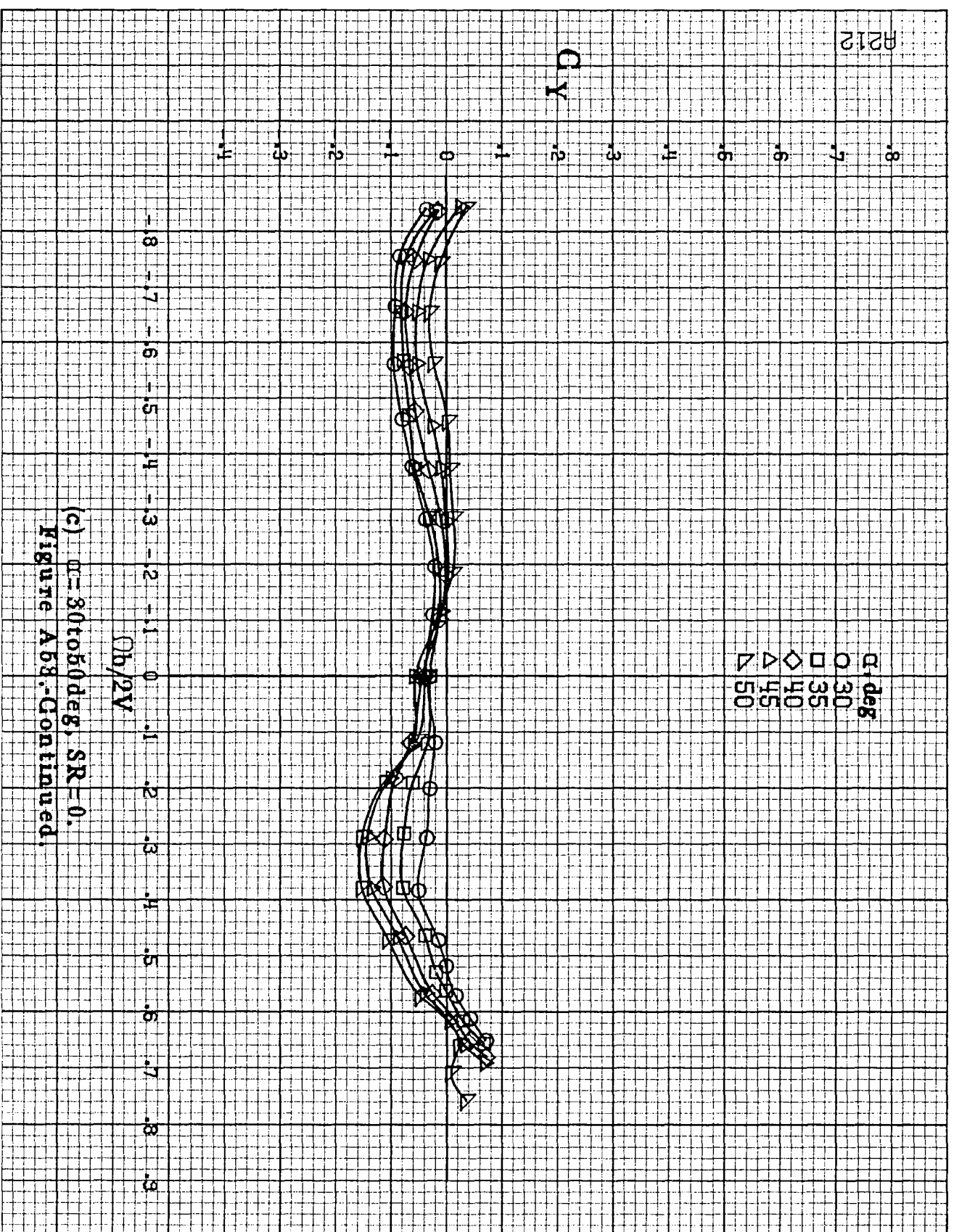
(b) $\alpha = 18$ to 35 deg, $SR = 76$ cm (30 in).
Figure A52.-Continued.

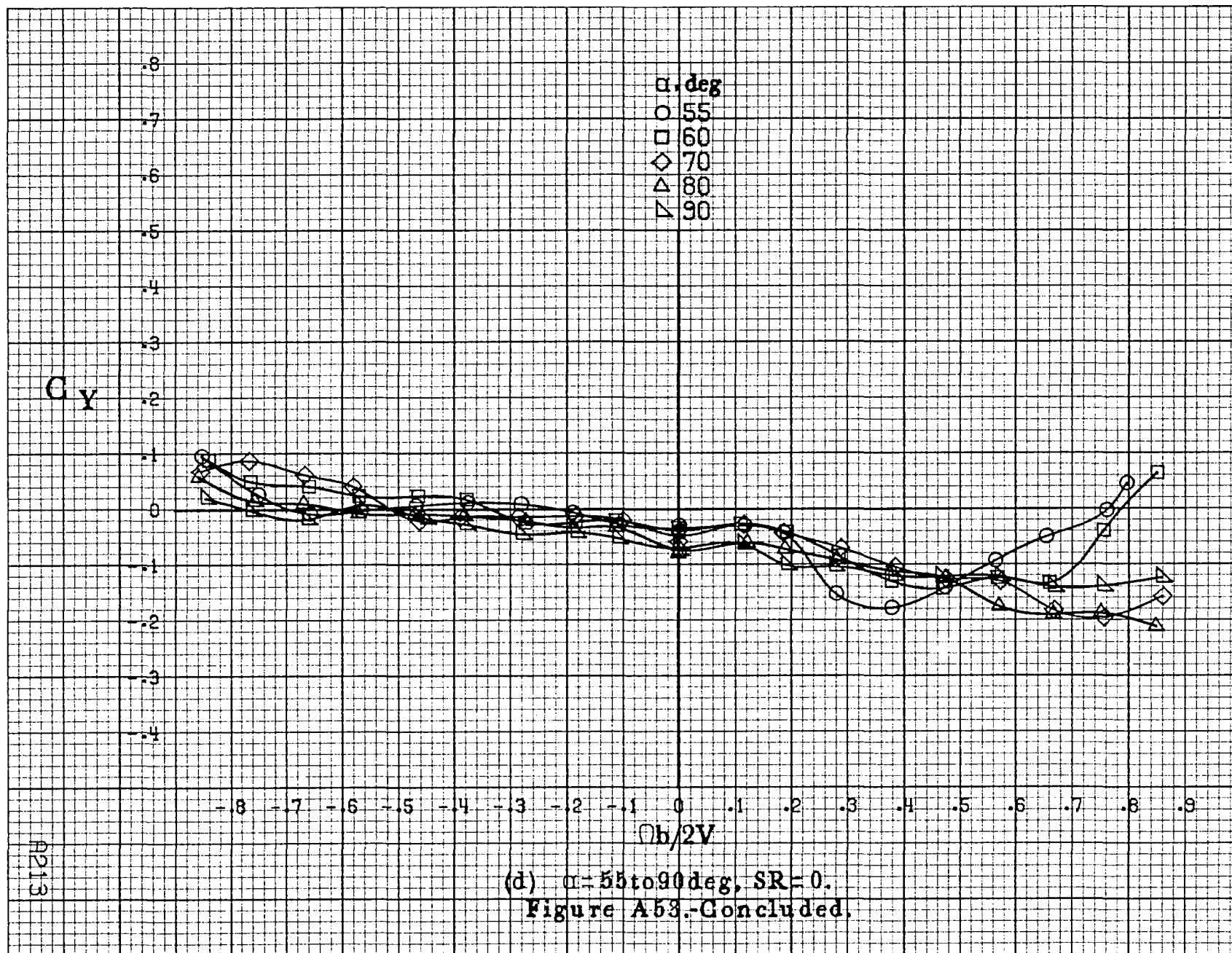












C_A

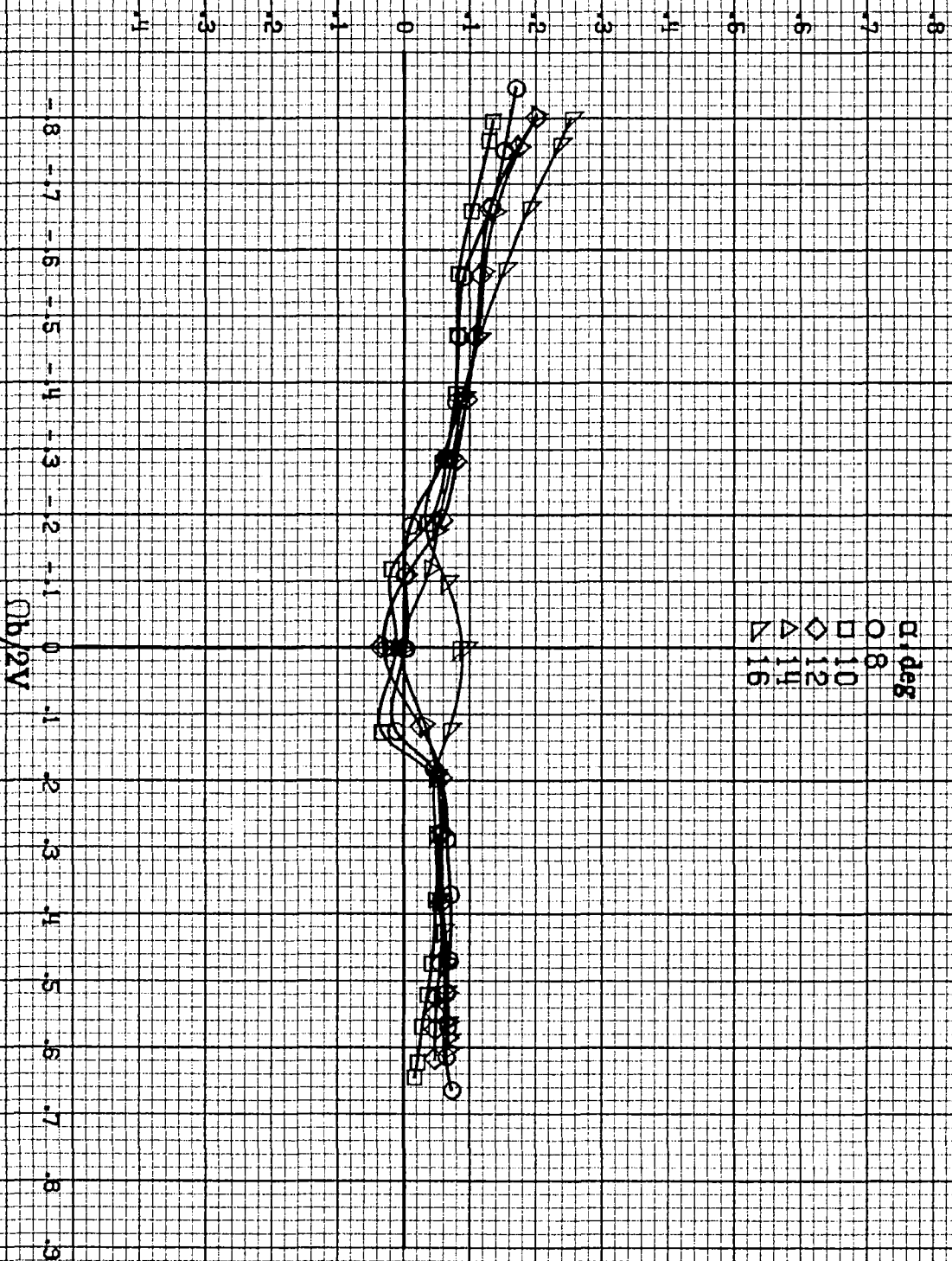
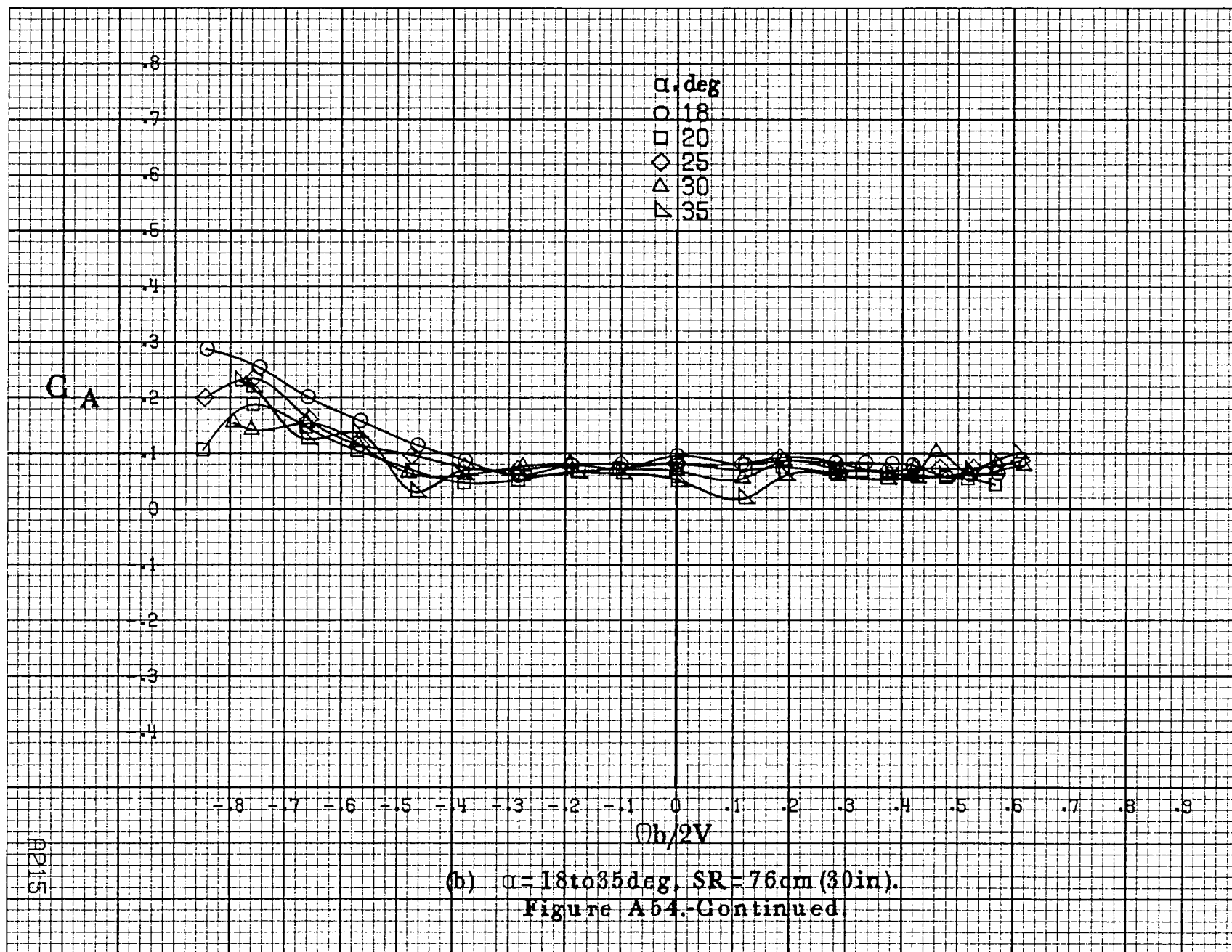
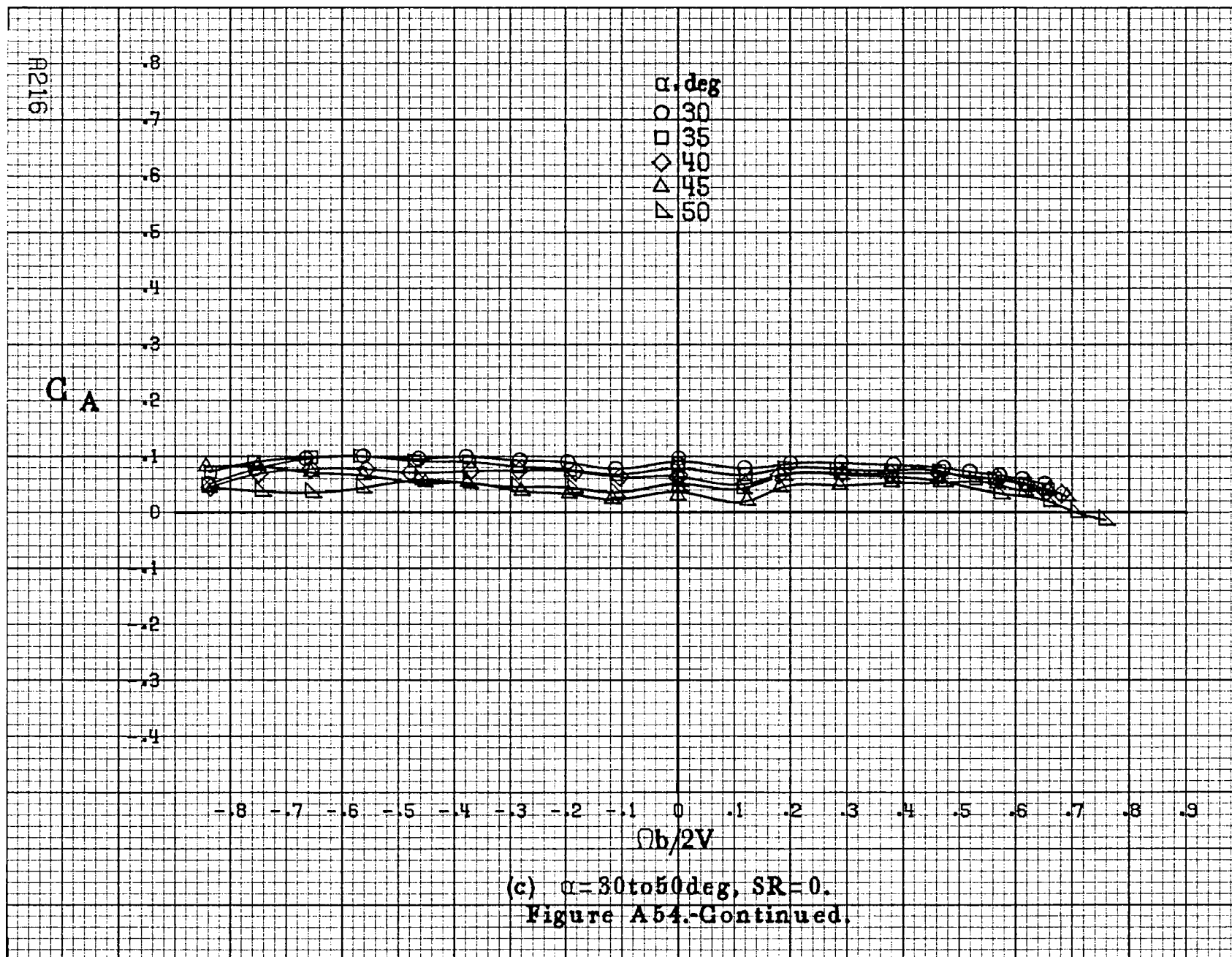
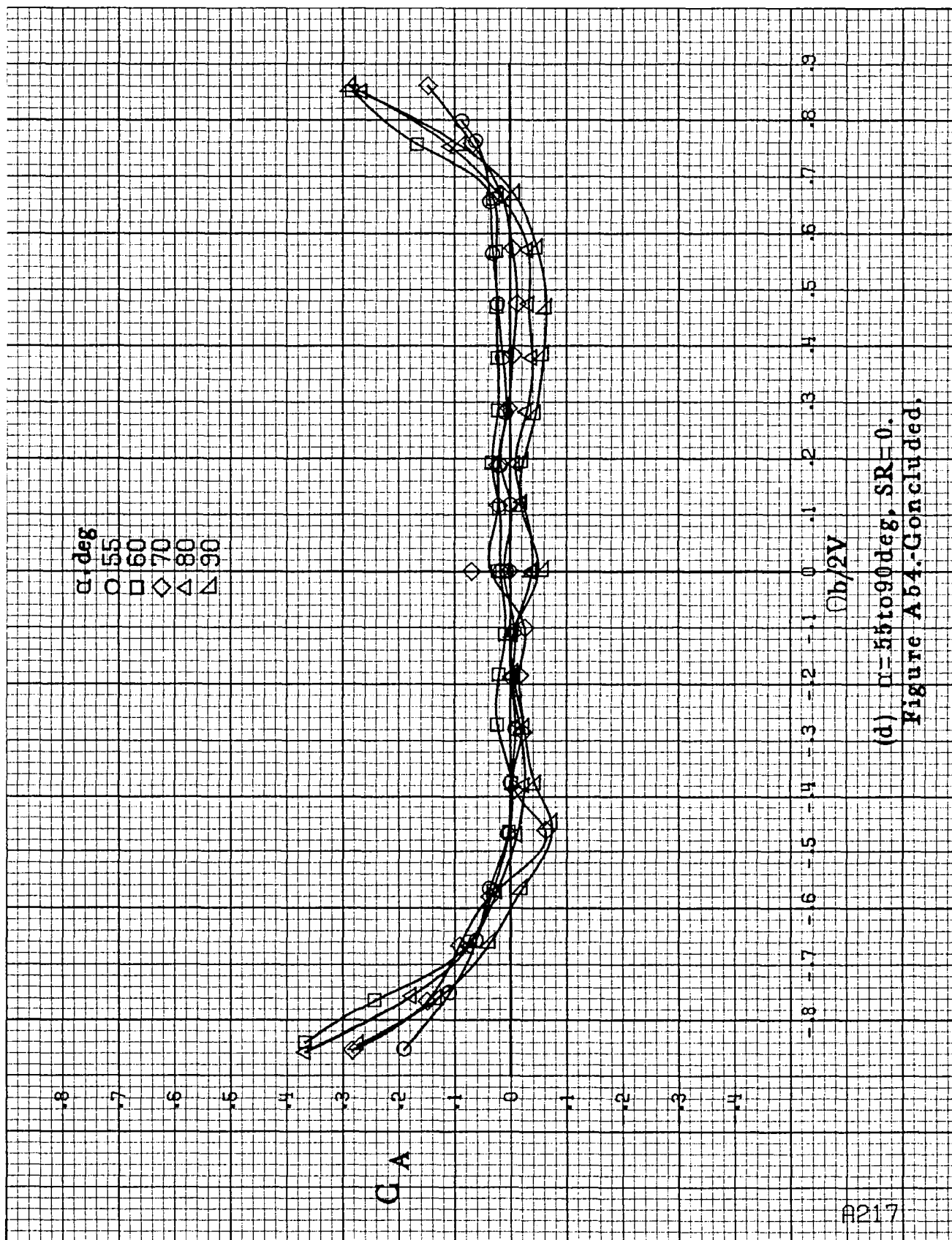


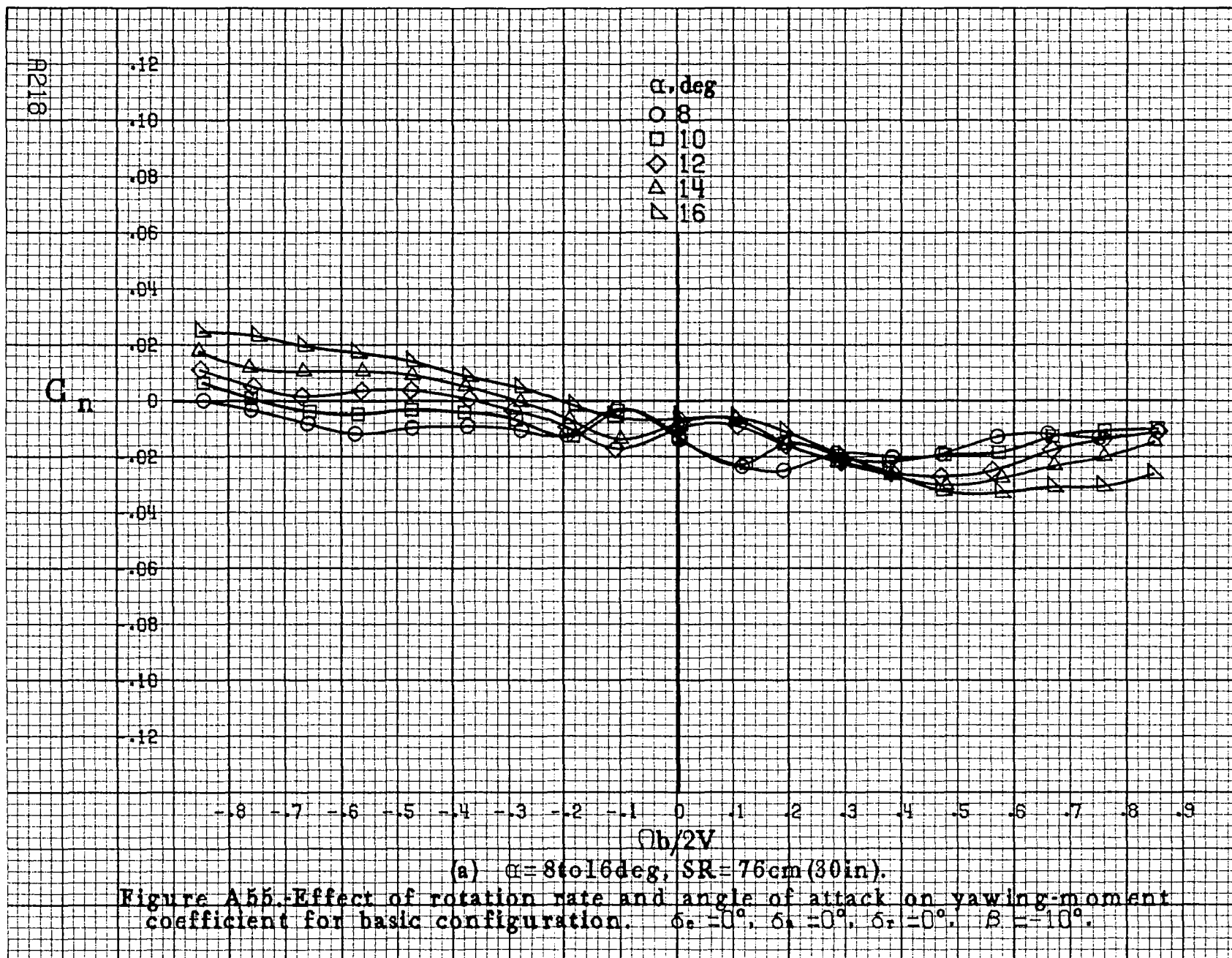
Figure A5.4. Effect of rotation rate and angle of attack on axial force coefficient for basic configuration. $\alpha=8^\circ, 10^\circ, 12^\circ, 14^\circ, 16^\circ$. $Re=10^6$, $SR=76$ cm (30 in.).

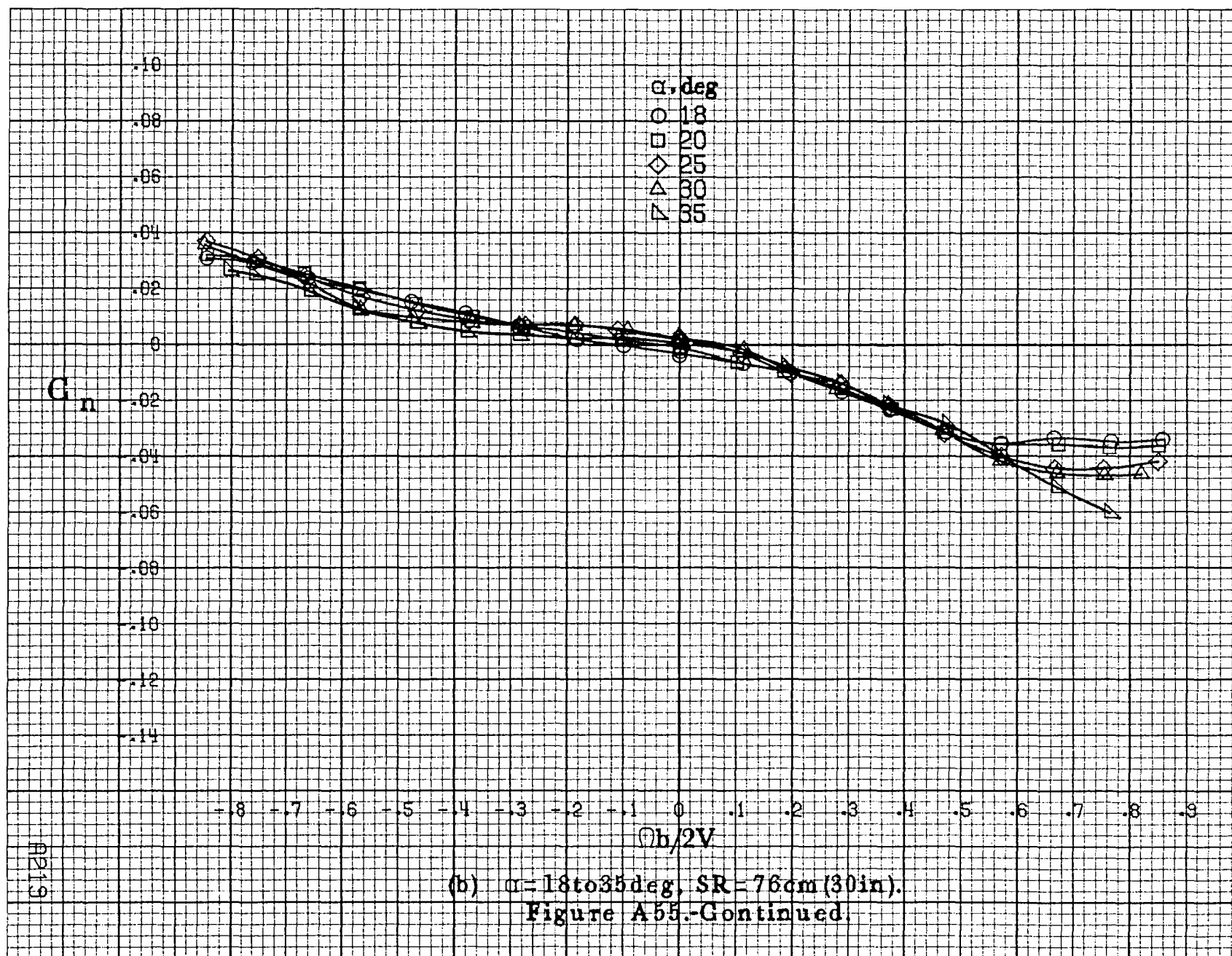


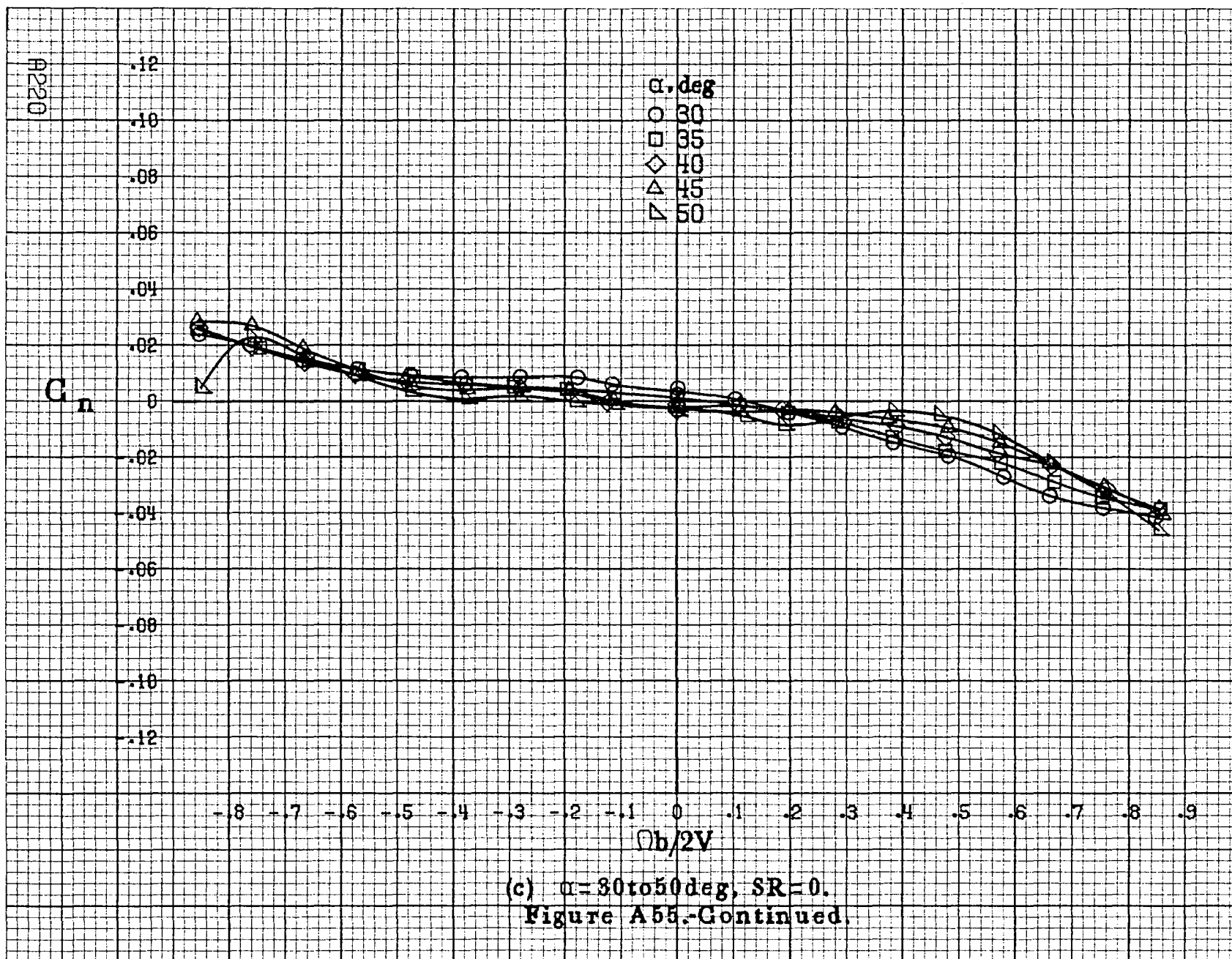


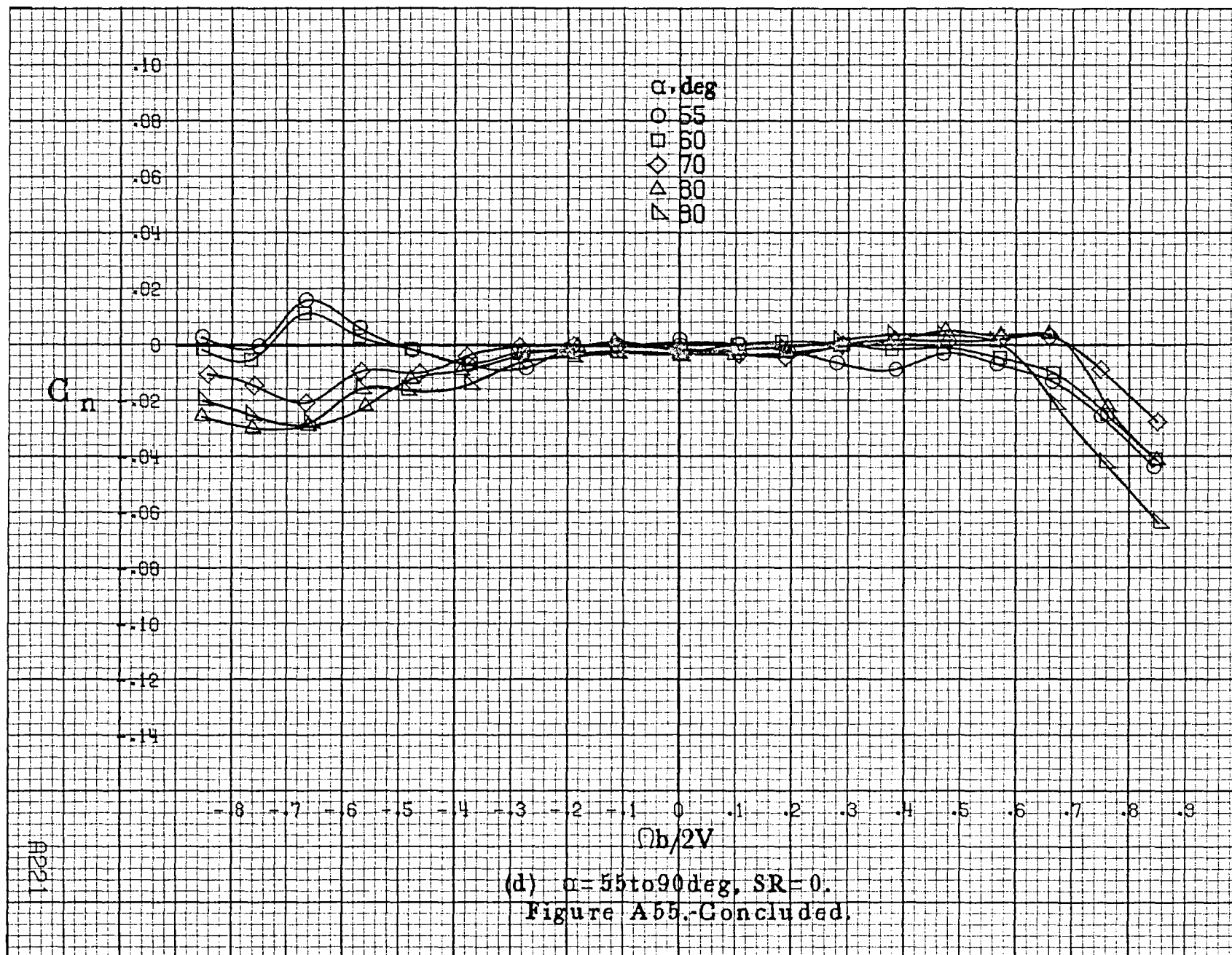


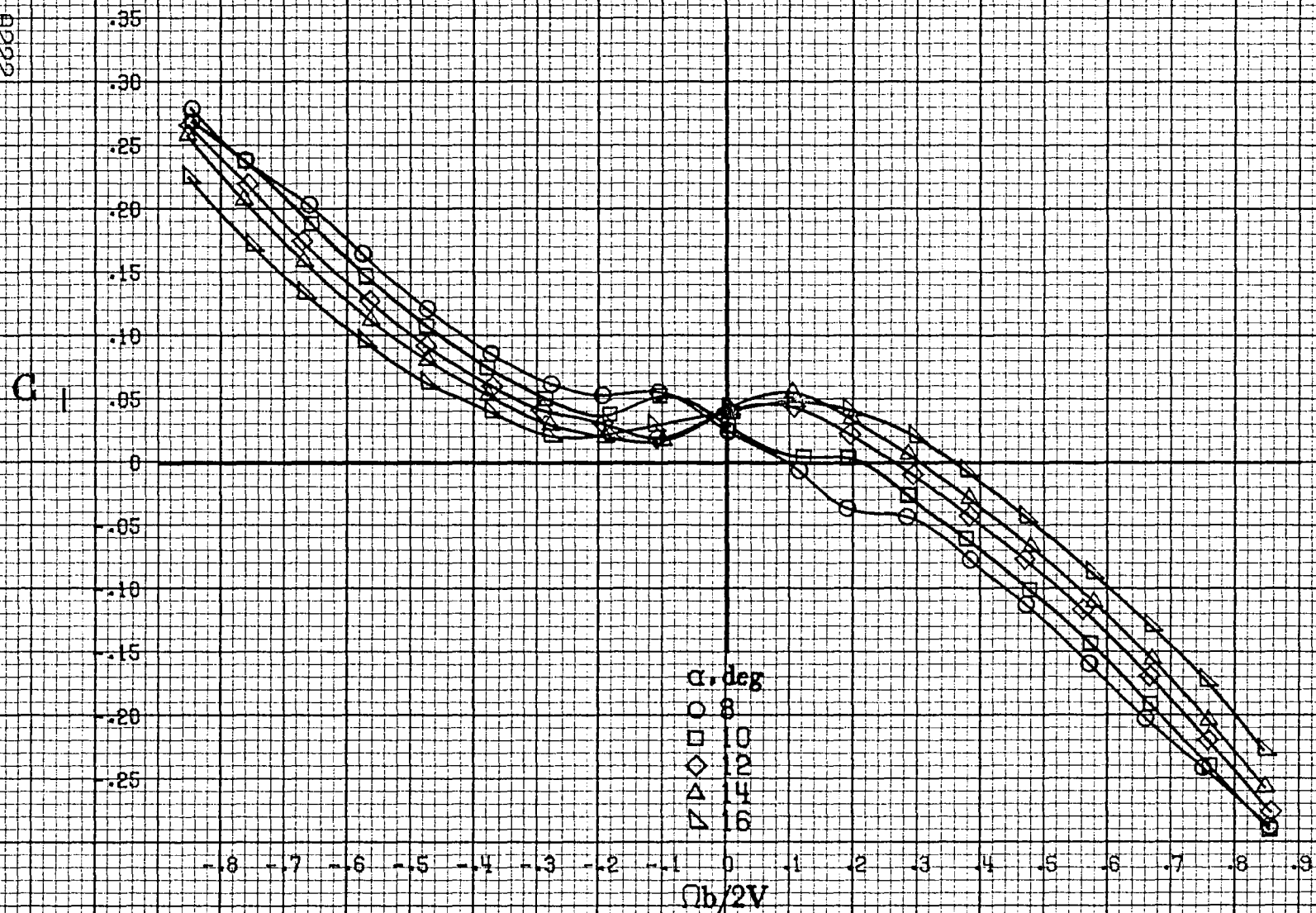
(d) $\alpha = 55$ to 90° , $SR = 0$.
Figure A 54.-Concluded.











(a) $\alpha = 8$ to 16° , $SR = 76 \text{ cm (30 in.)}$.

Figure A56.-Effect of rotation rate and angle of attack on rolling-moment coefficient for basic configuration. $\delta_e = 0^\circ$, $\delta_a = 0^\circ$, $\delta_r = 0^\circ$, $B = 10^\circ$.

C_{II}

-0.35
-0.30
-0.25
-0.20
-0.15
-0.10
-0.05
0
-0.05
-0.10
-0.15
-0.20
-0.25

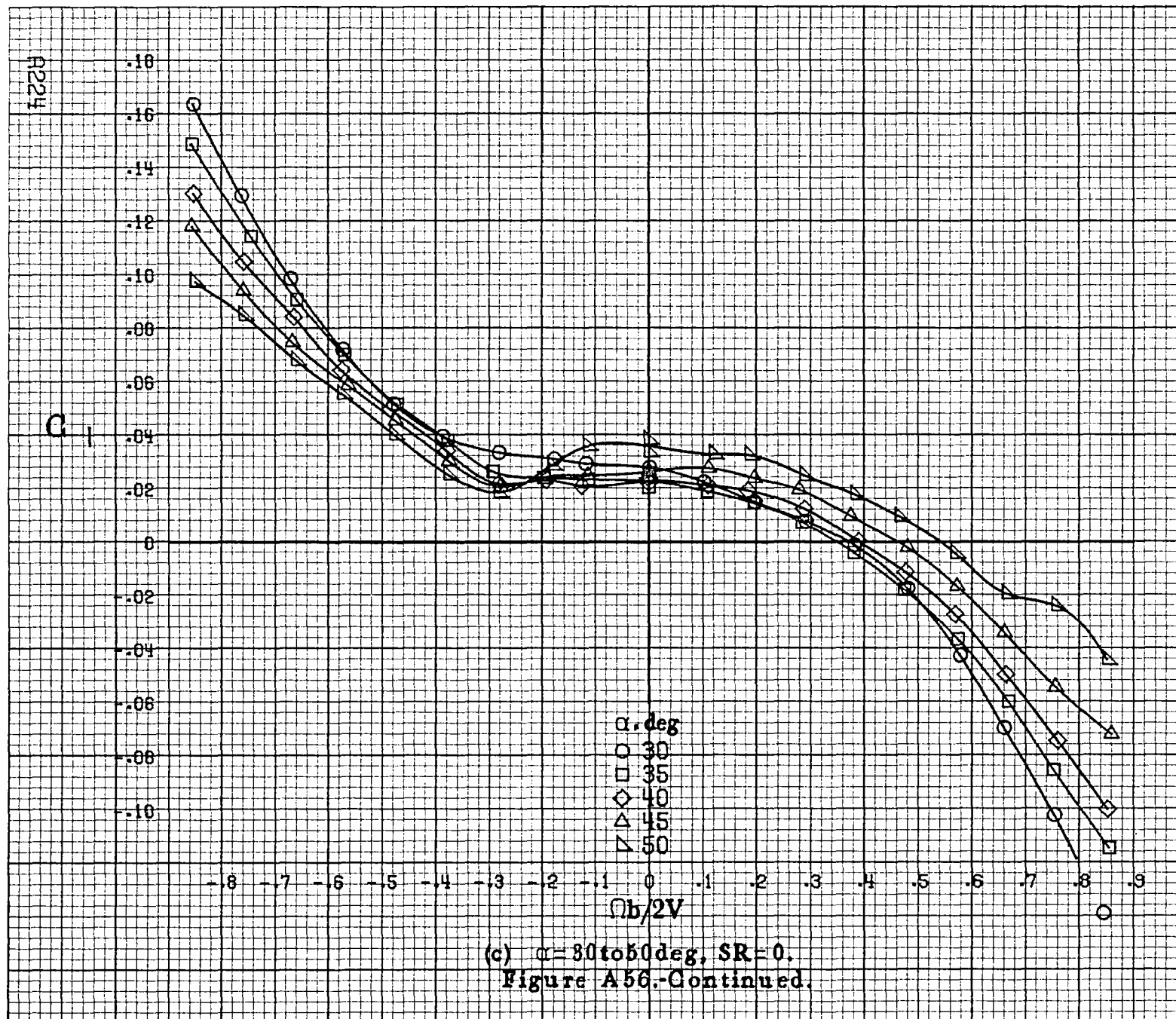
α, deg
○ 18
□ 20
◇ 25
△ 30
▽ 35

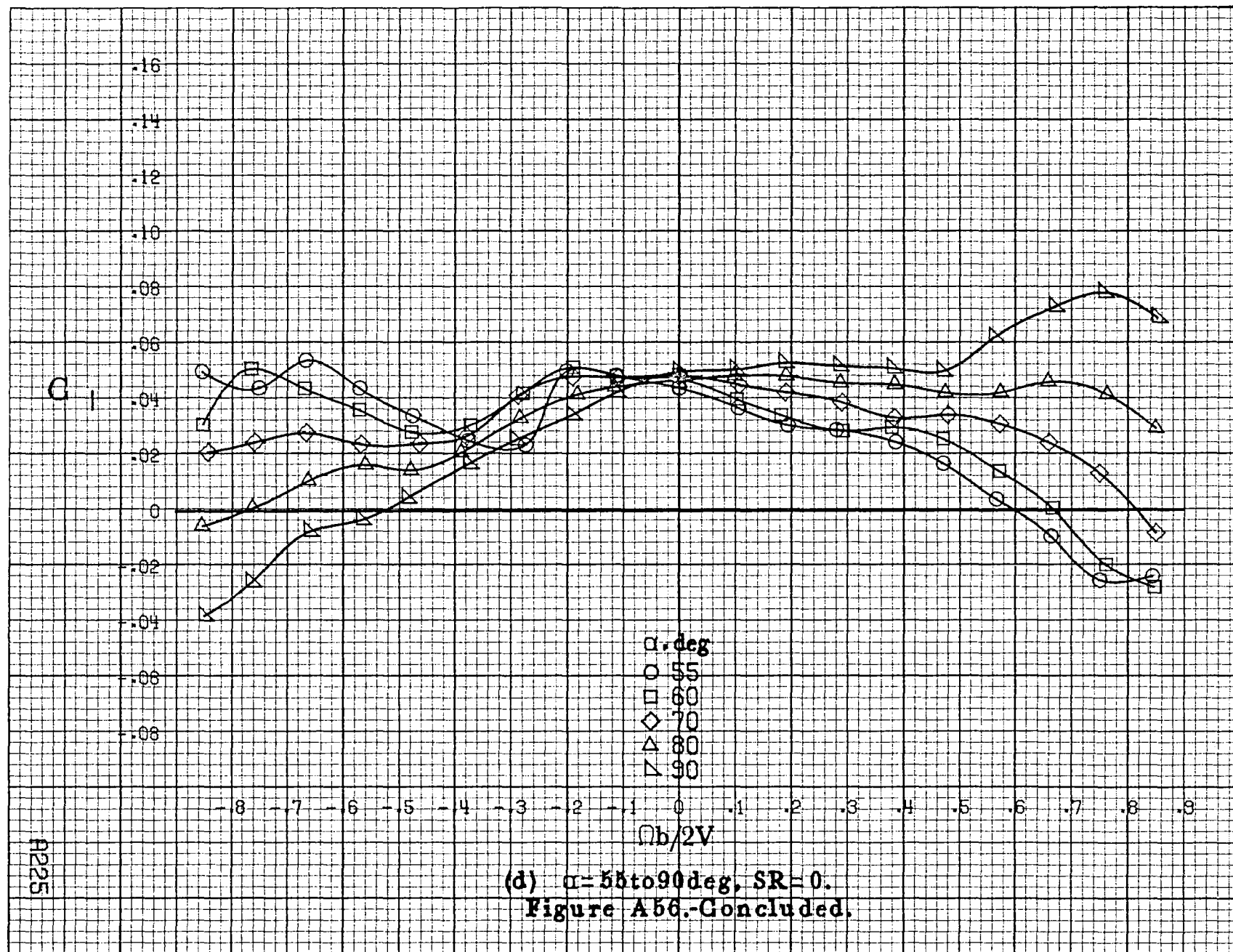
$\Omega b/2V$

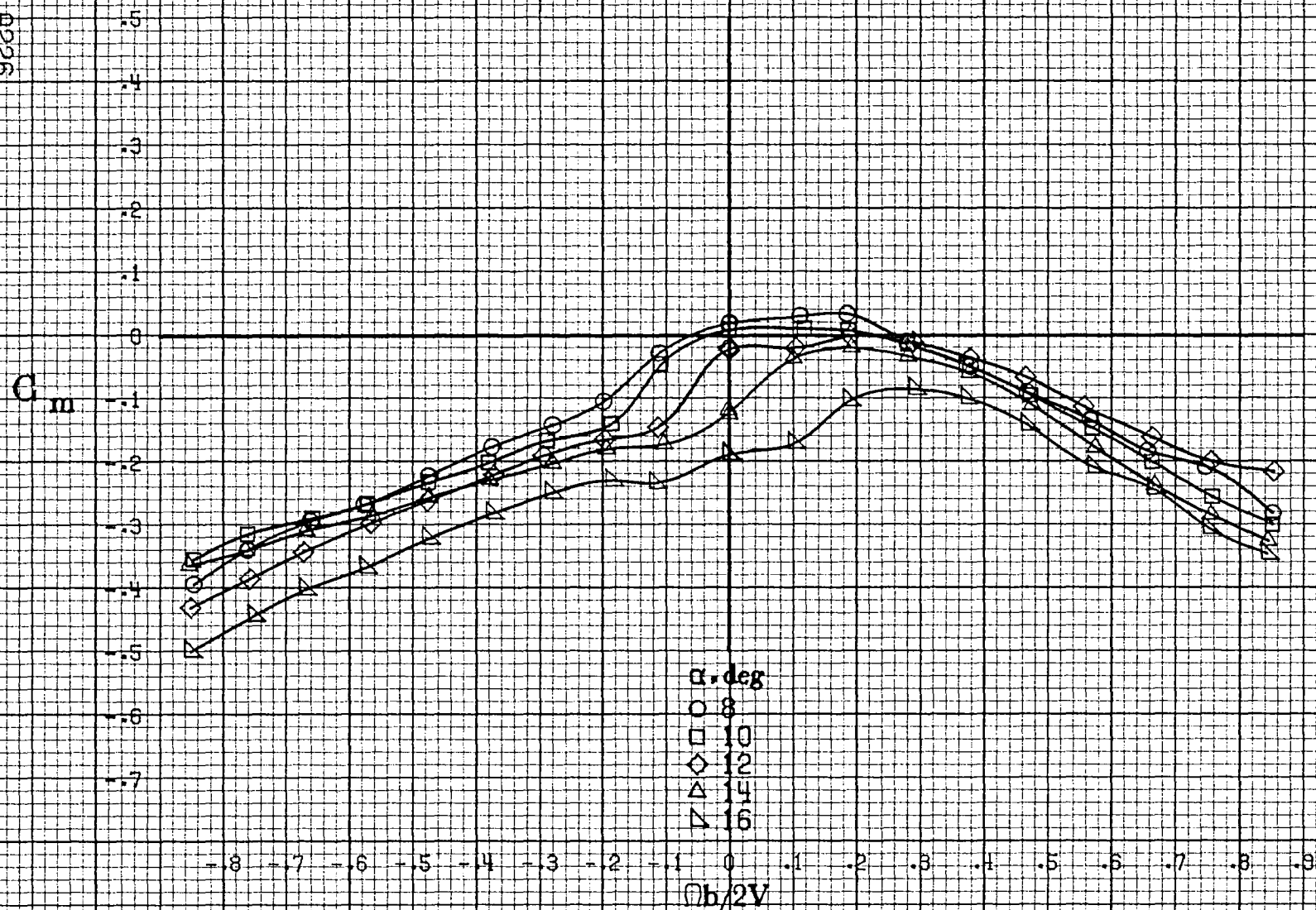
-0.8 -0.7 -0.6 -0.5 -0.4 -0.3 -0.2 -0.1 0 0.1 0.2 0.3 0.4 0.5 0.6 0.7 0.8 0.9

(b) $\alpha = 18 \text{ to } 35 \text{ deg}$, $SR = 76 \text{ cm (30 in.)}$.
Figure A56-Continued.

R2223

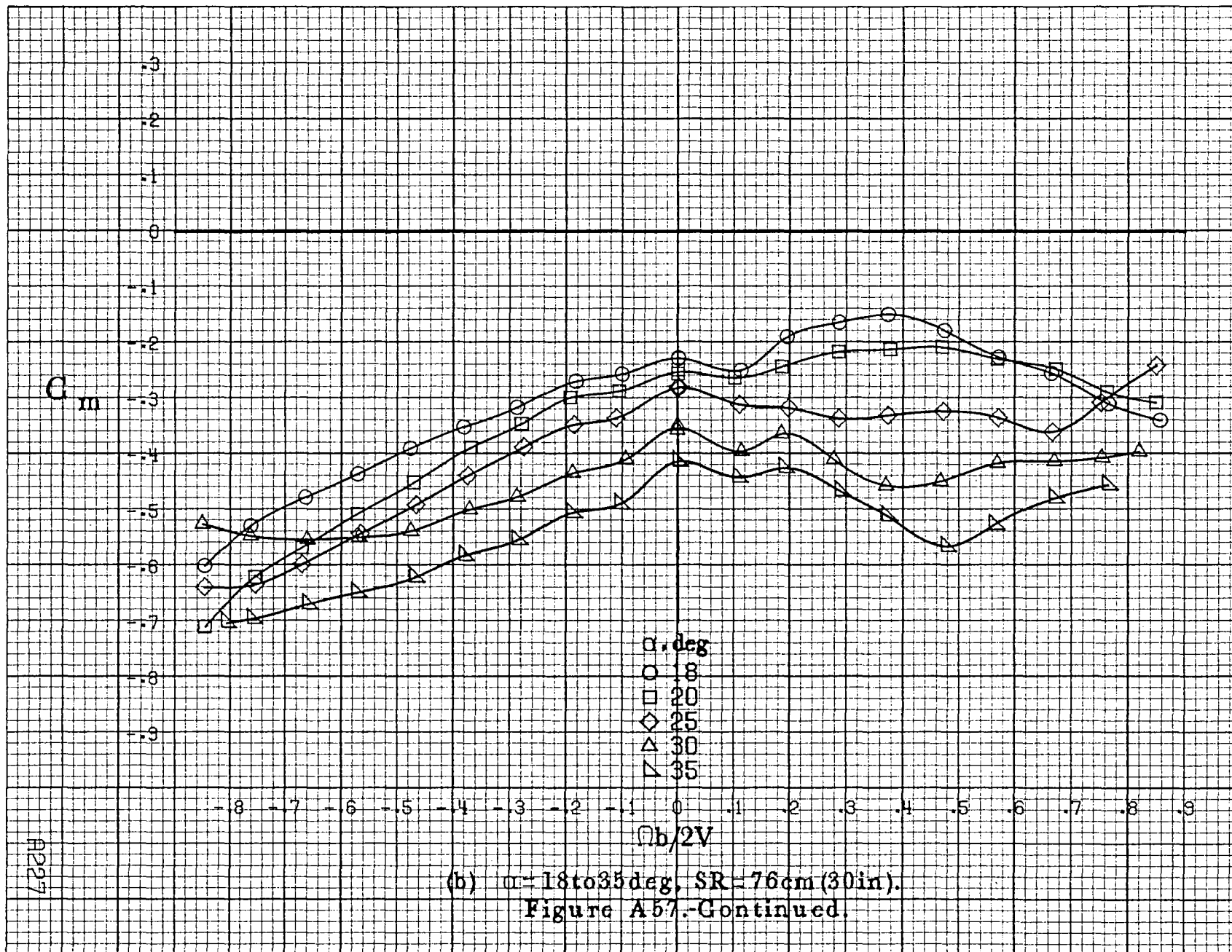


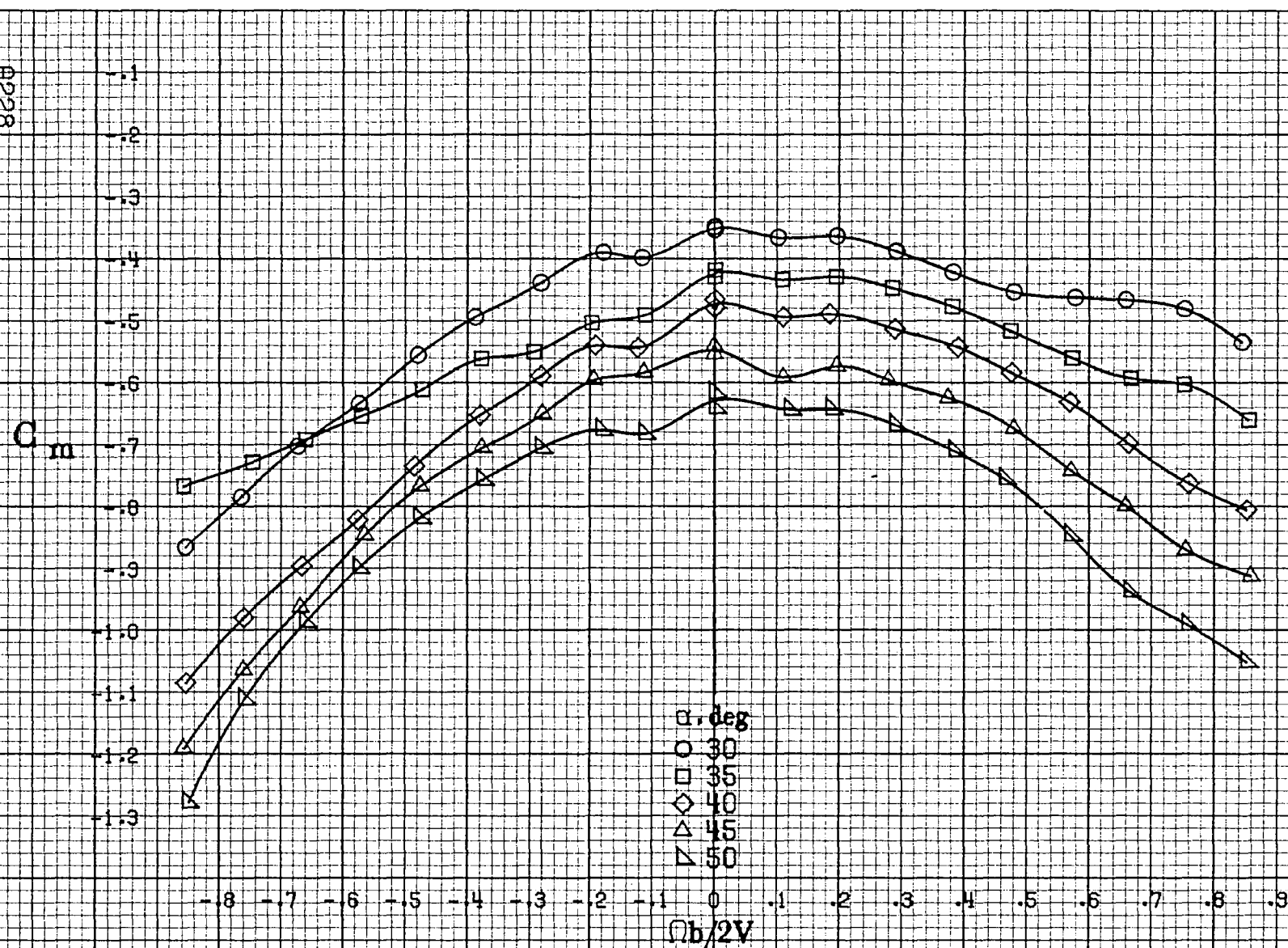




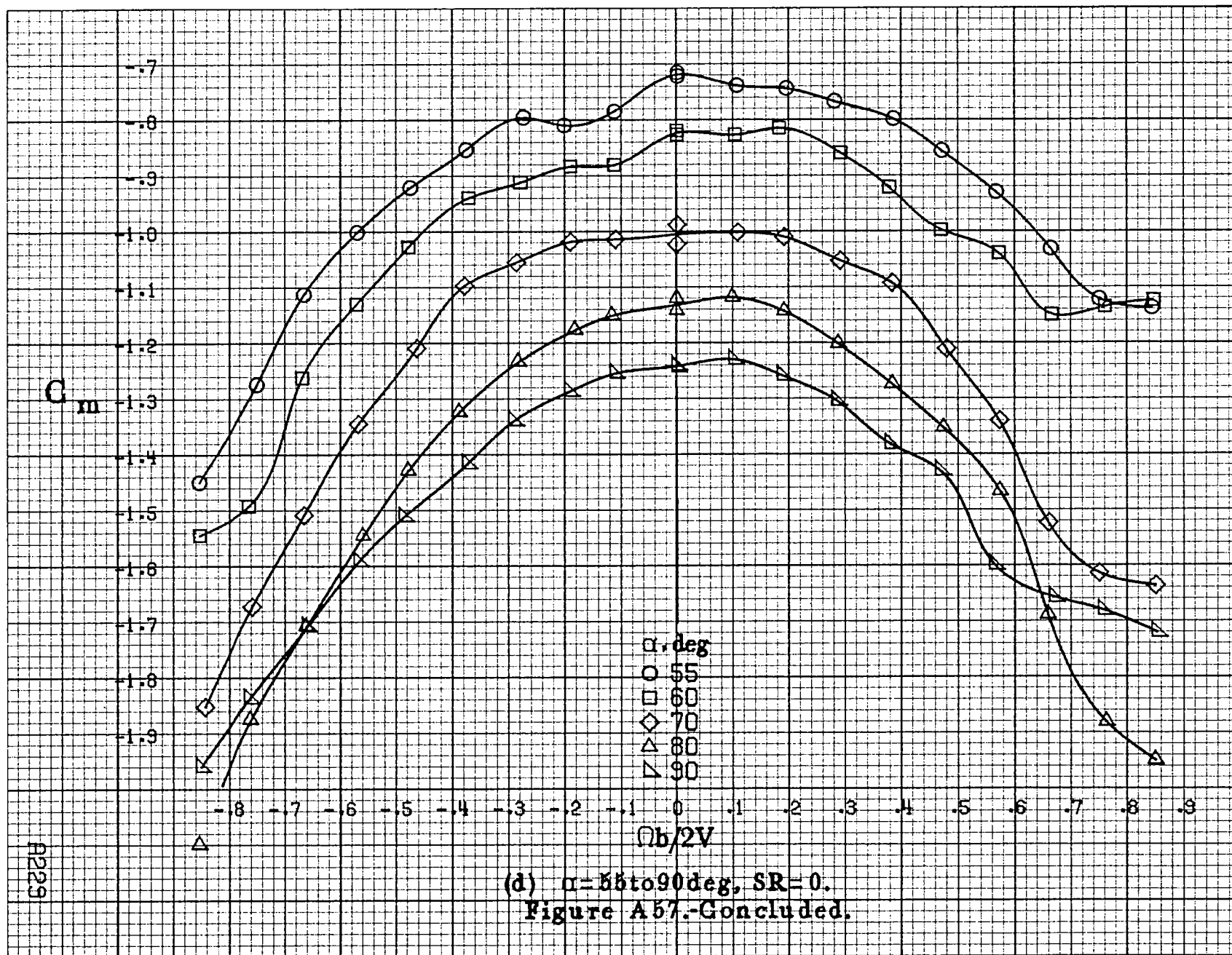
(a) $\alpha = 8$ to 16° , $SR = 76\text{ cm (30 in.)}$.

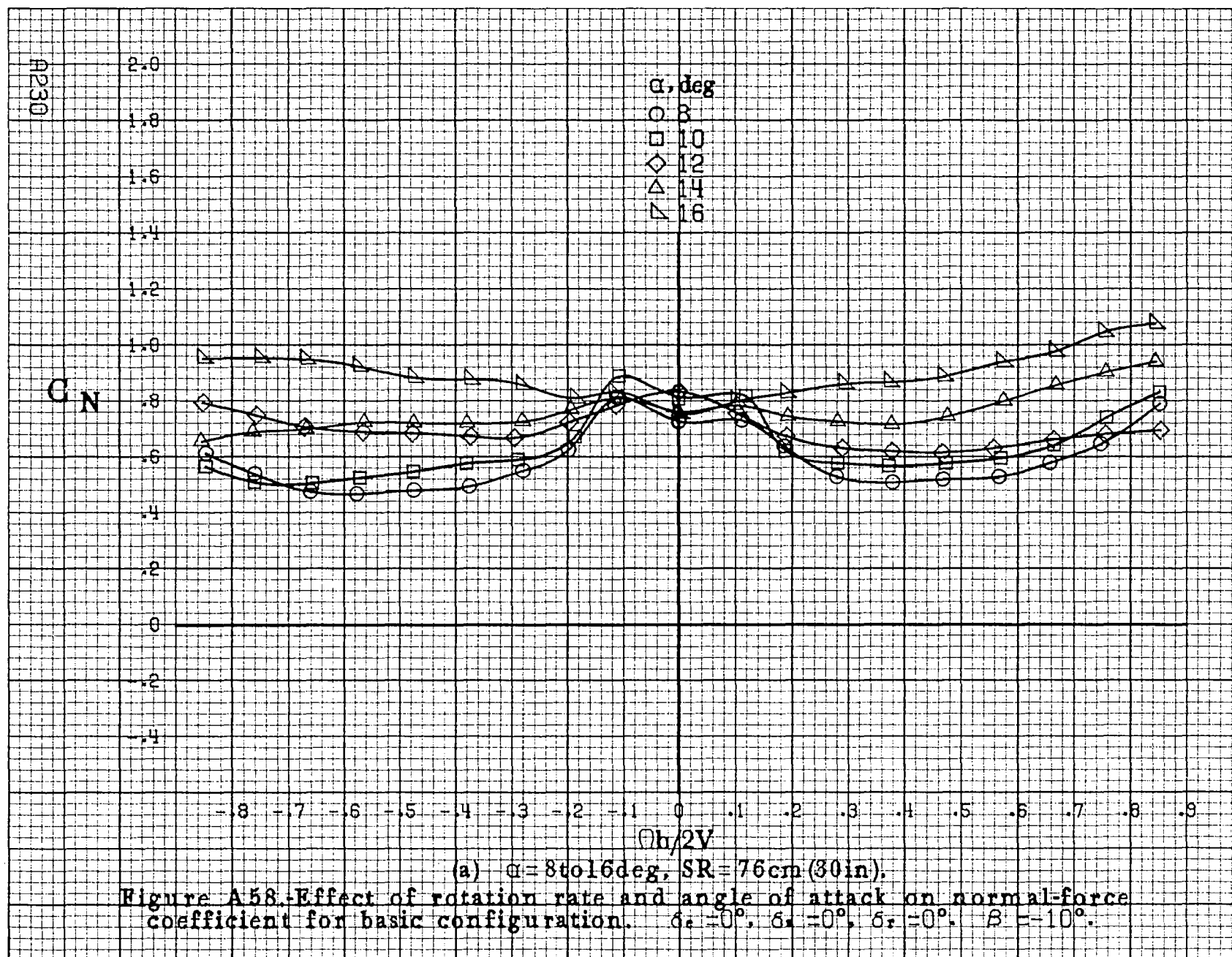
Figure A57.-Effect of rotation rate and angle of attack on pitching-moment coefficient for basic configuration. $\delta_a = 0^\circ$, $\delta_s = 0^\circ$, $\delta_r = 0^\circ$, $\beta = -10^\circ$.

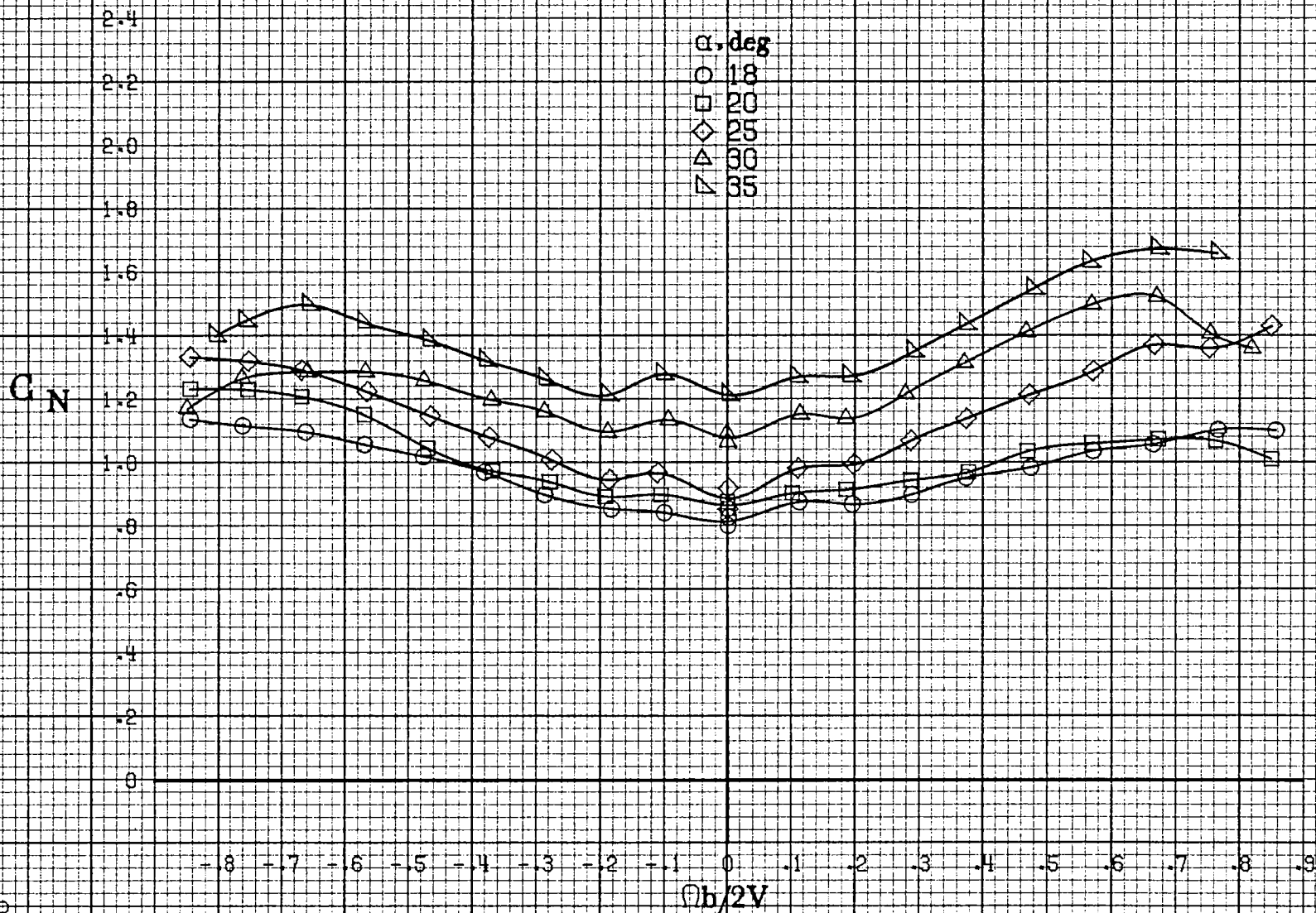




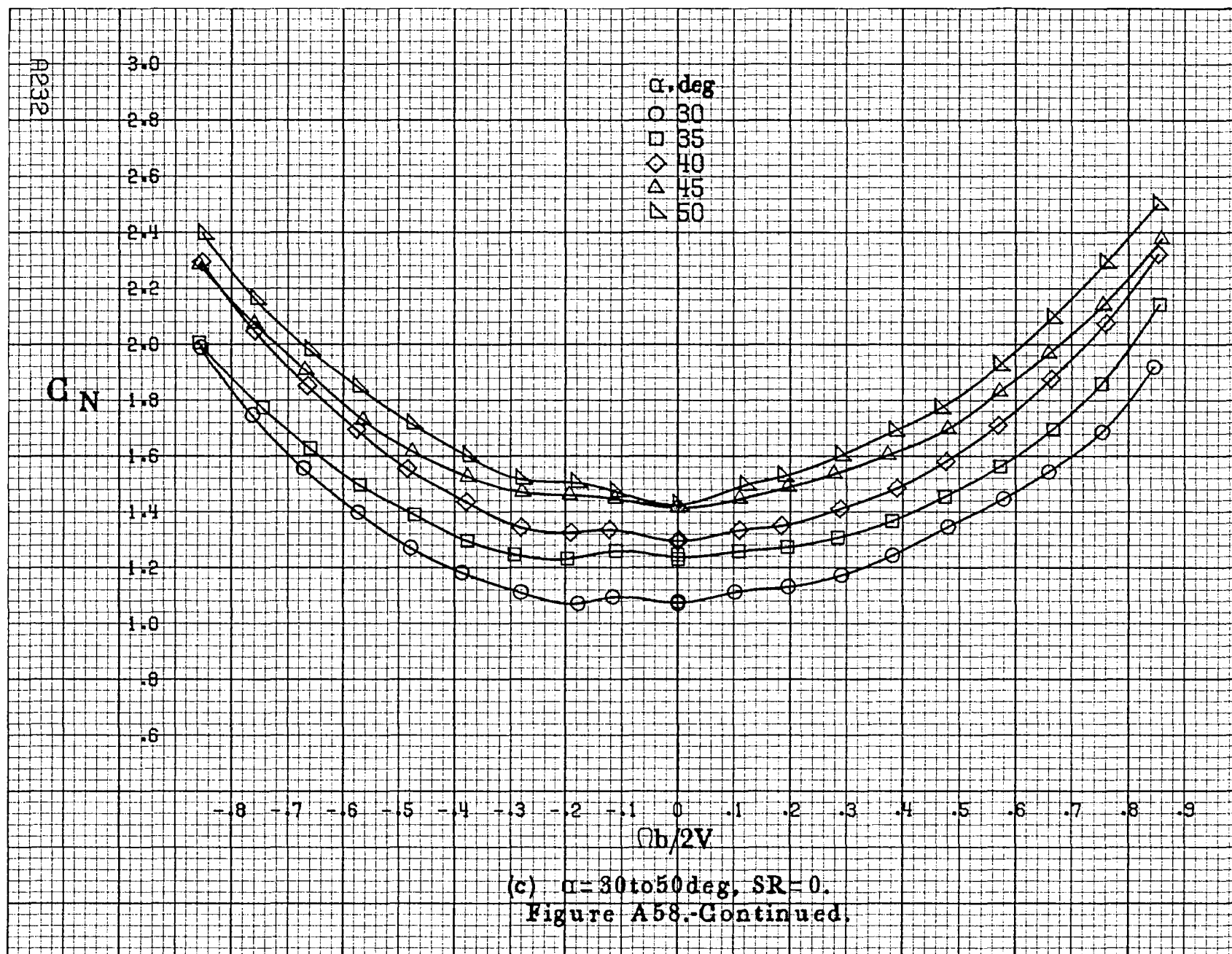
(c) $\alpha = 30$ to 50° , $SR = 0$.
Figure A57.-Continued.

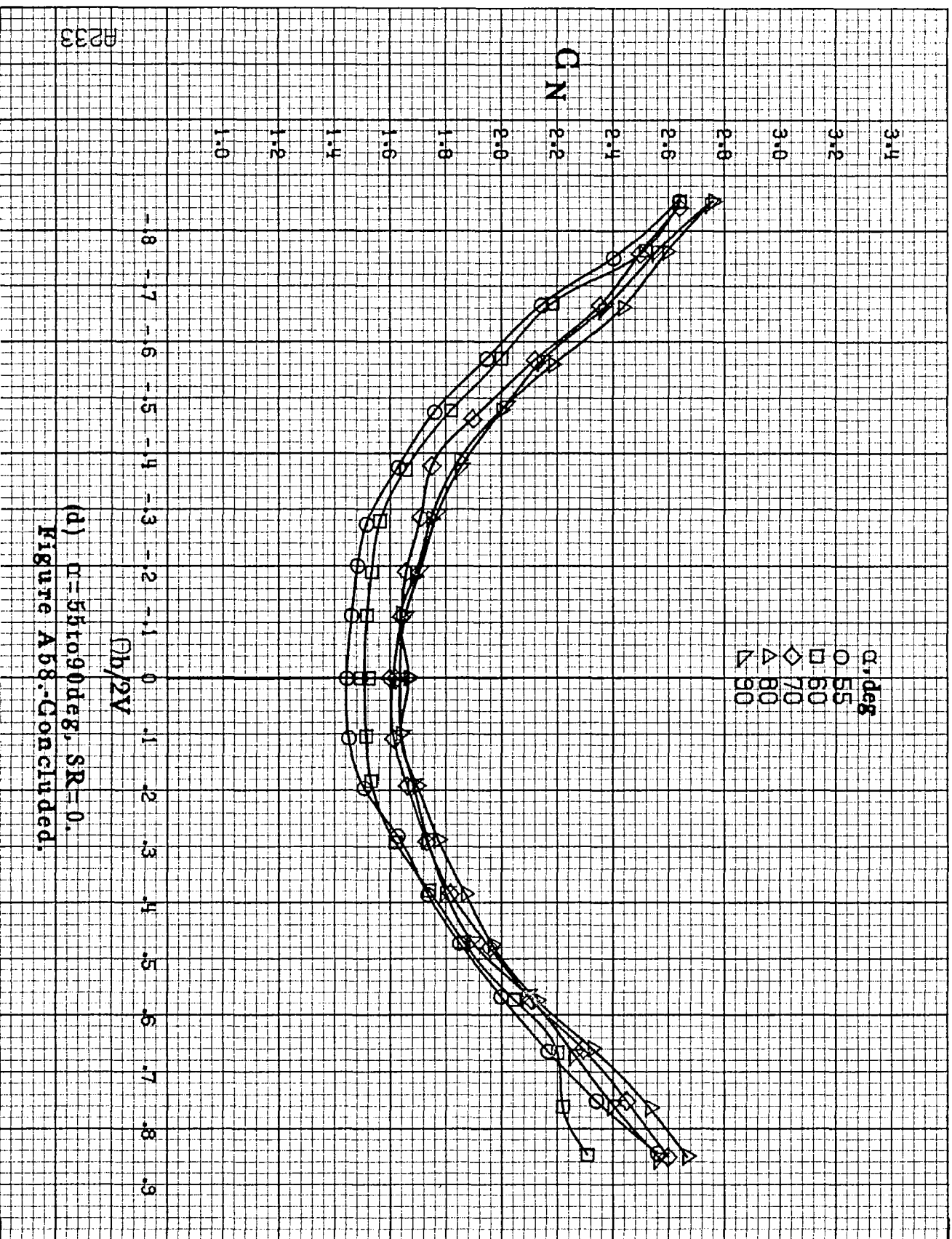






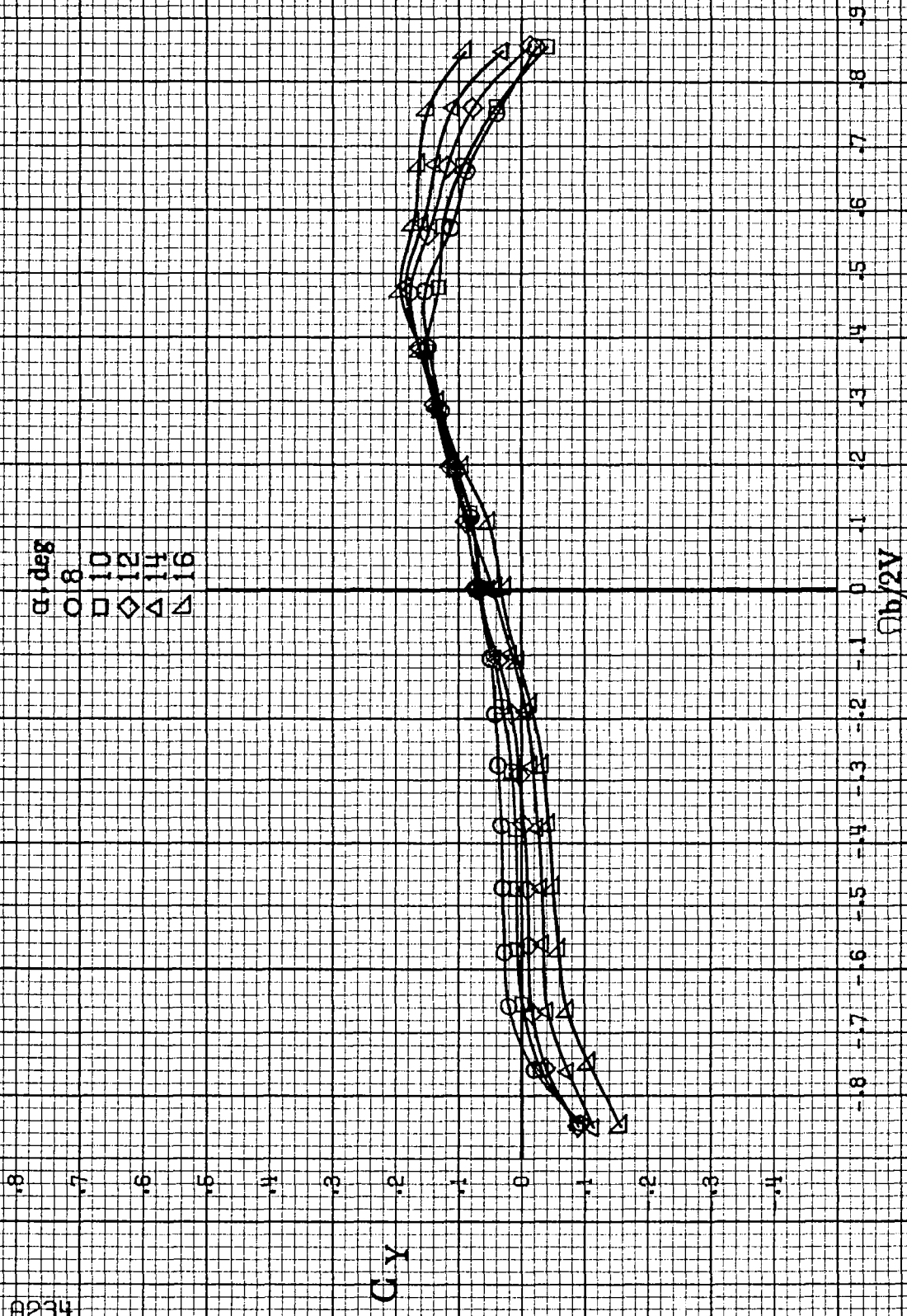
(b) $\alpha = 18$ to 35° , $SR = 76\text{cm}$ (30 in).
Figure A58.-Continued.



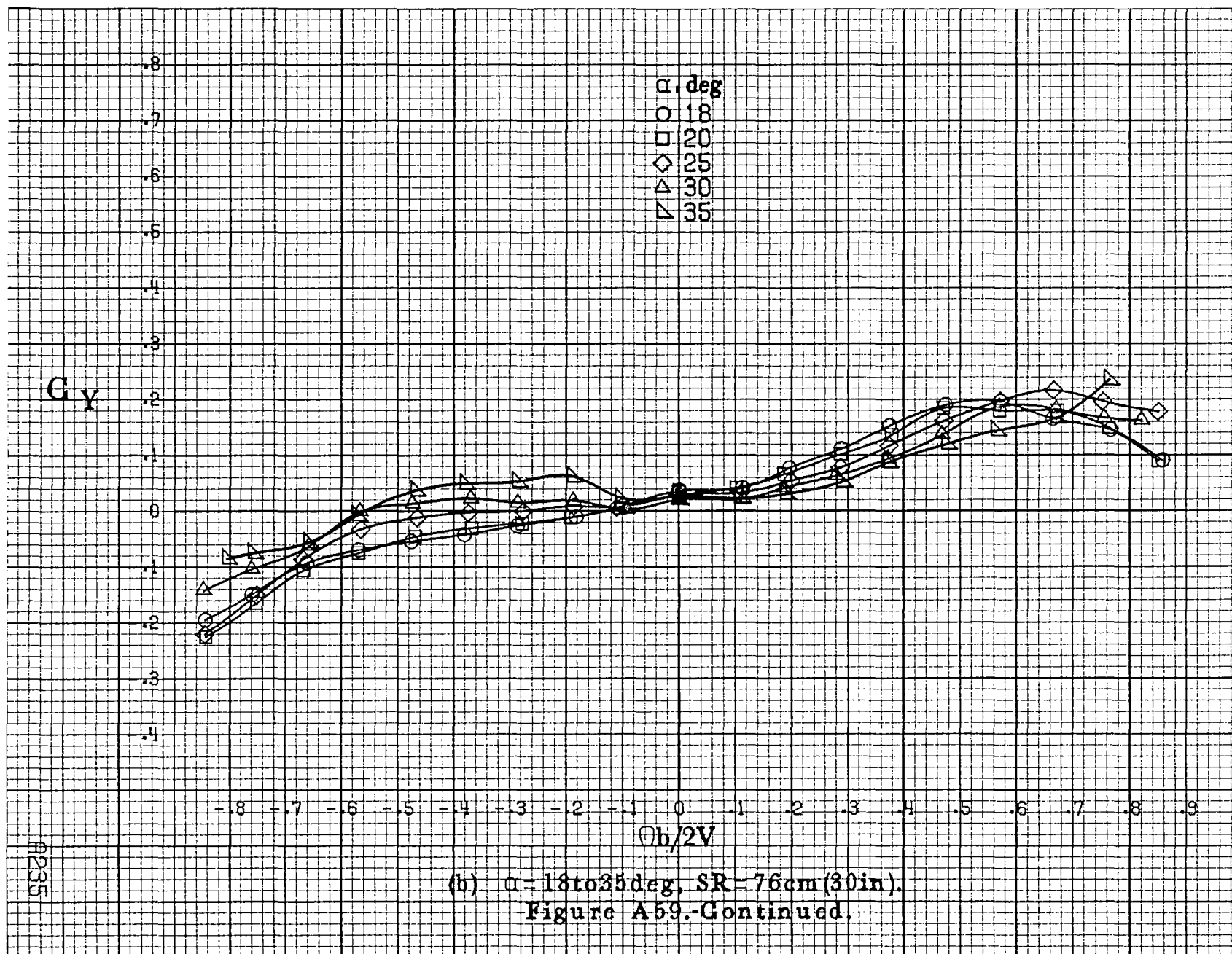


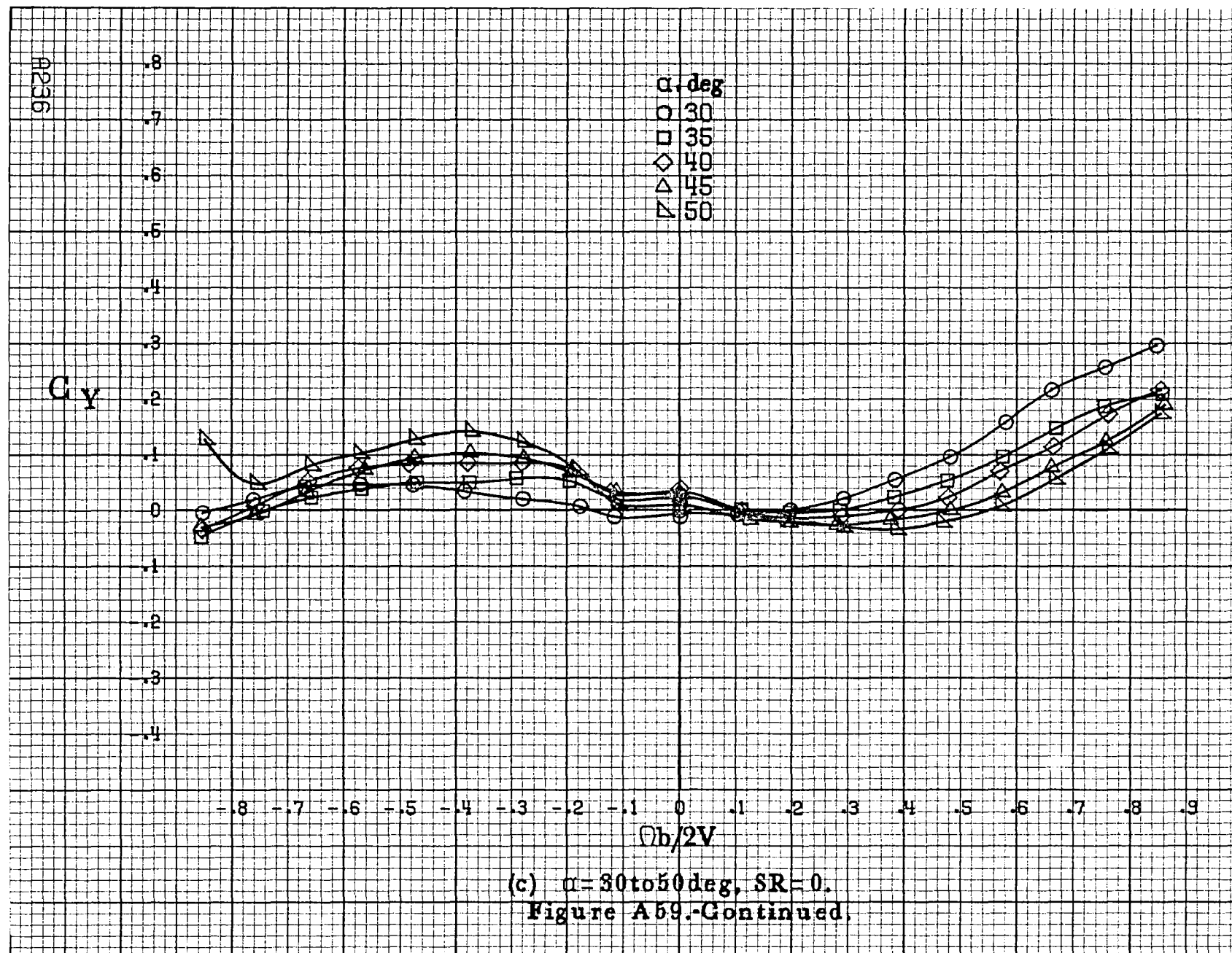
(d) $\alpha=55$ to 90° deg, $SR=0$.
Figure A58.-Concluded.

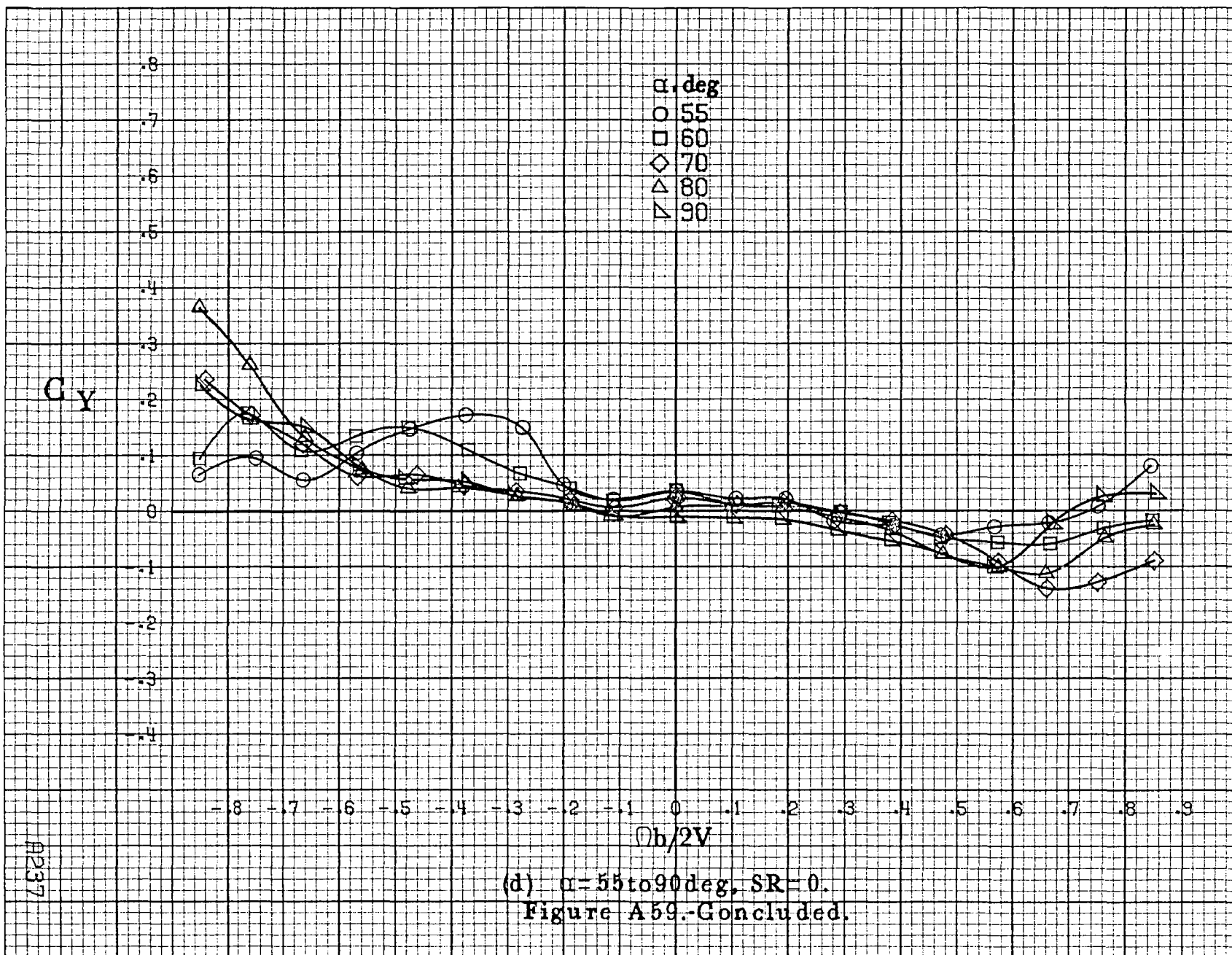
A234

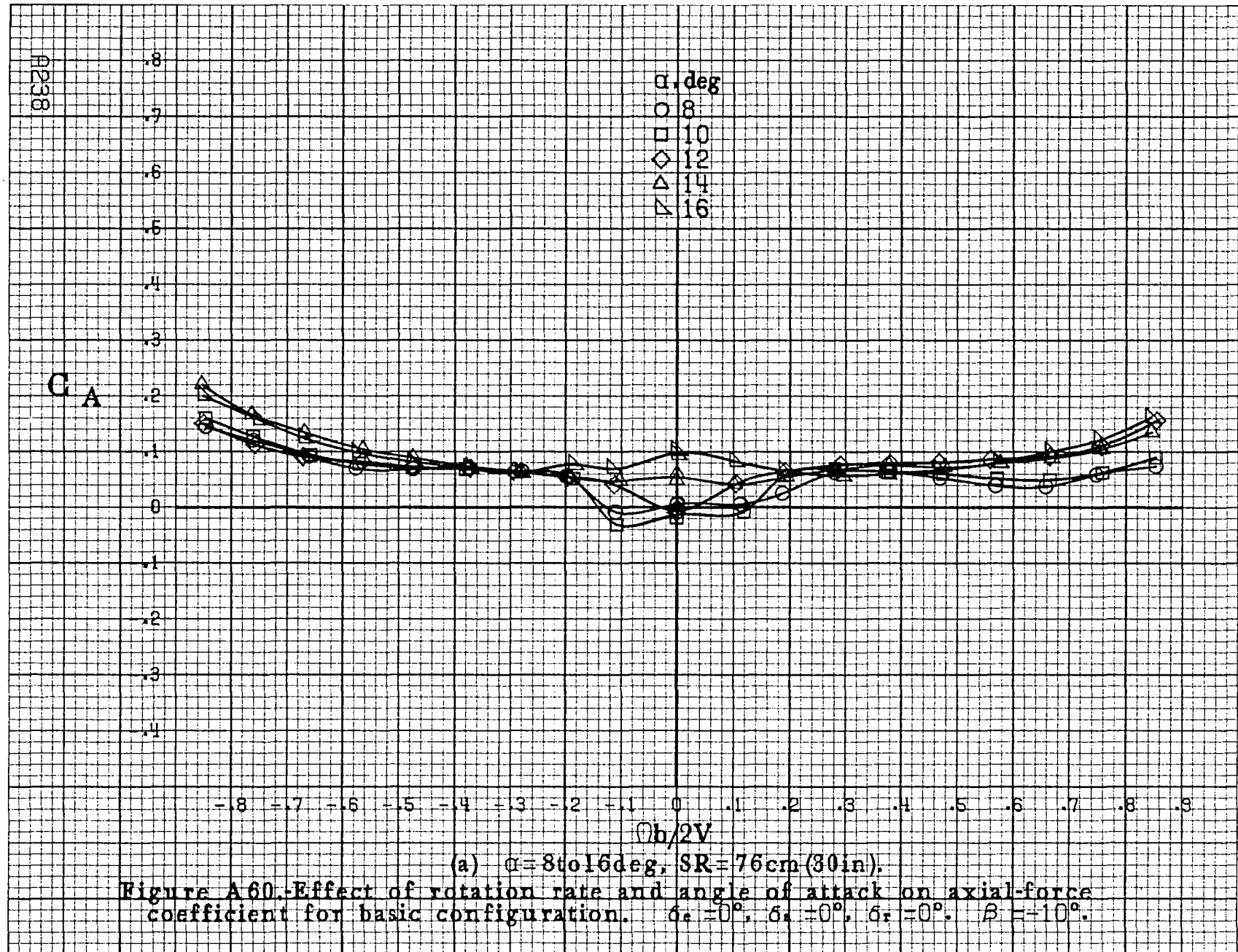


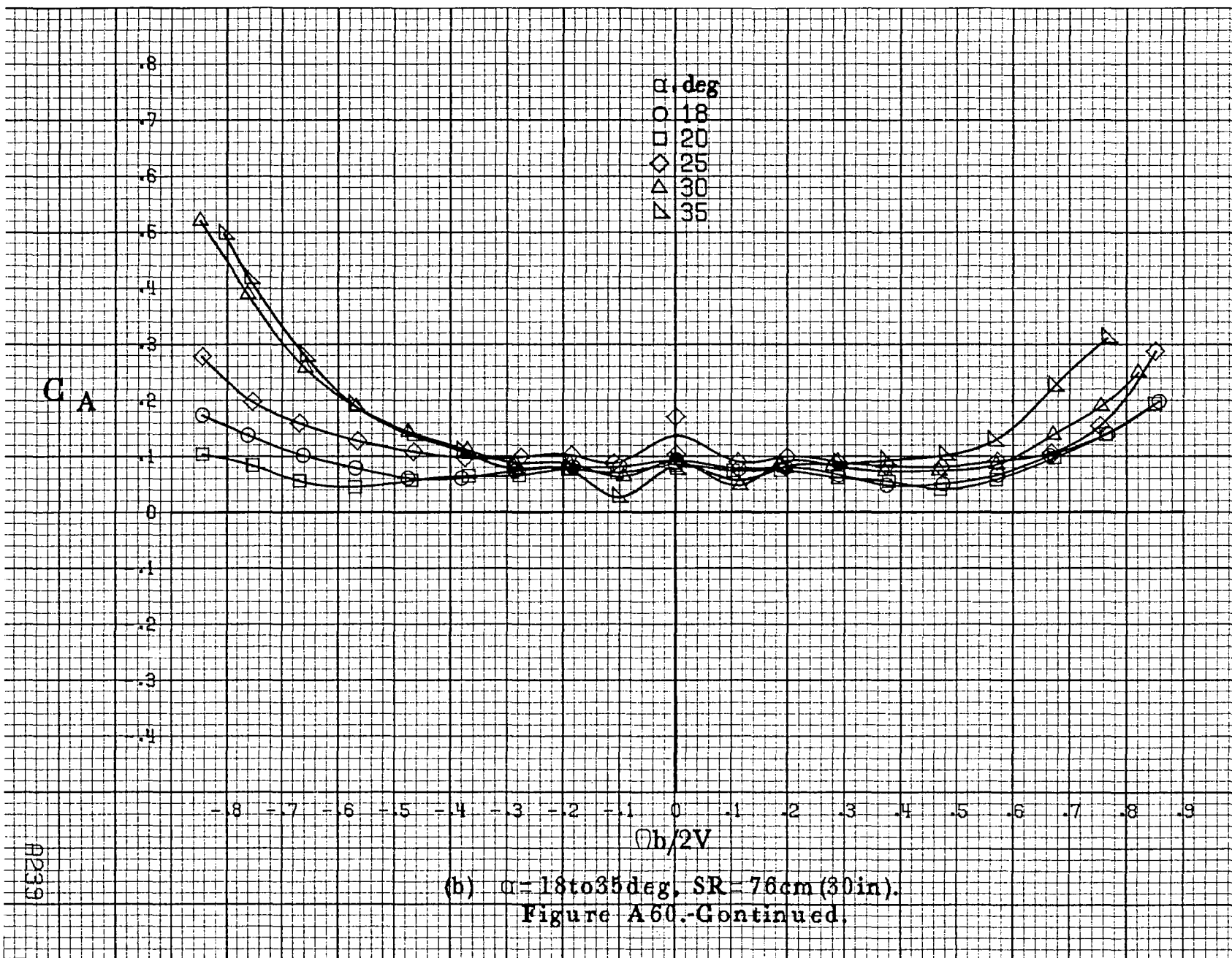
(a) $\alpha=8$ to 16° , $SR=76$ cm (30 in).
 Figure A59.-Effect of rotation rate and angle of attack on side-force coefficient for basic configuration. $\delta_a=0^\circ$, $\delta_h=0^\circ$, $\delta_r=0^\circ$, $B=-10^\circ$.

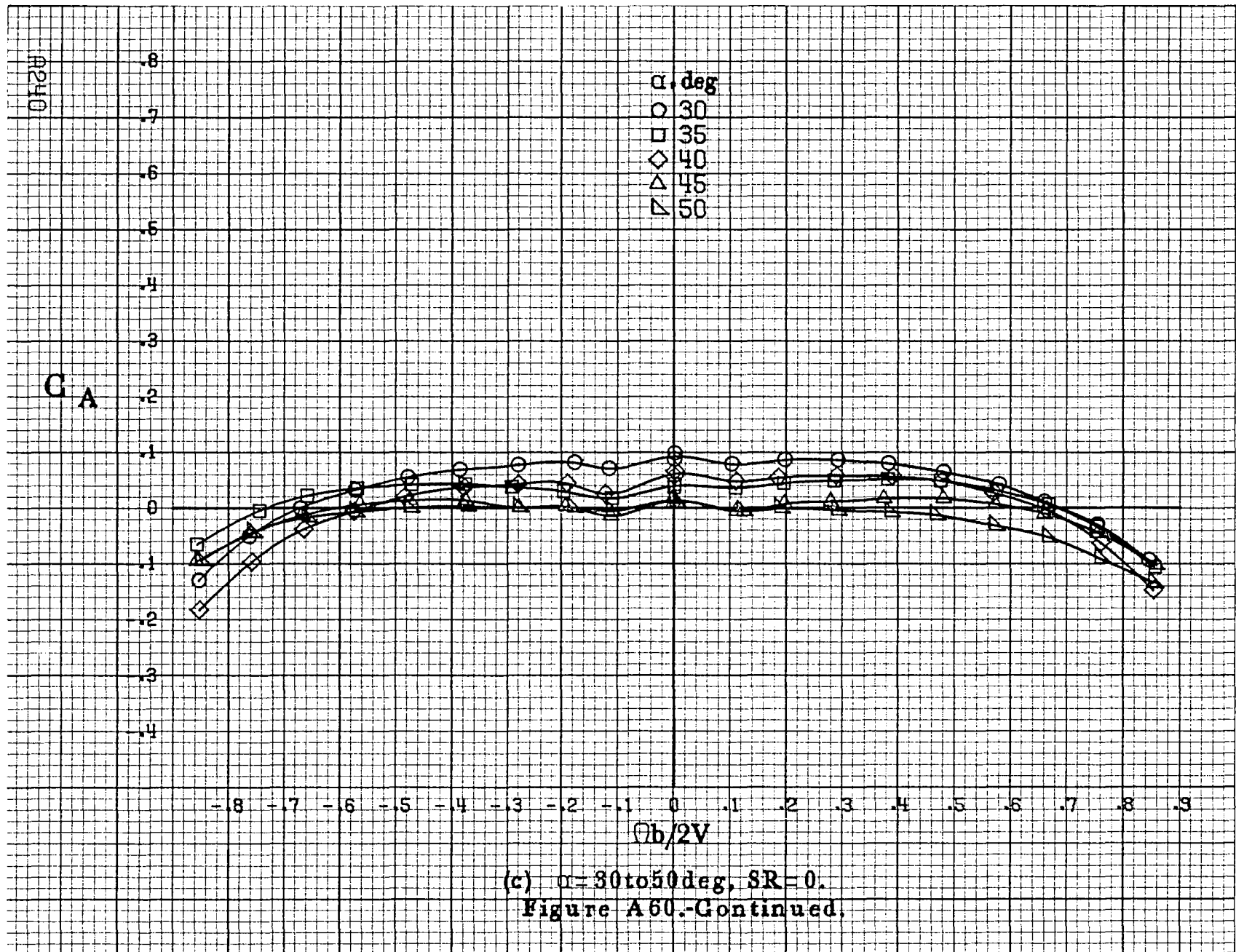


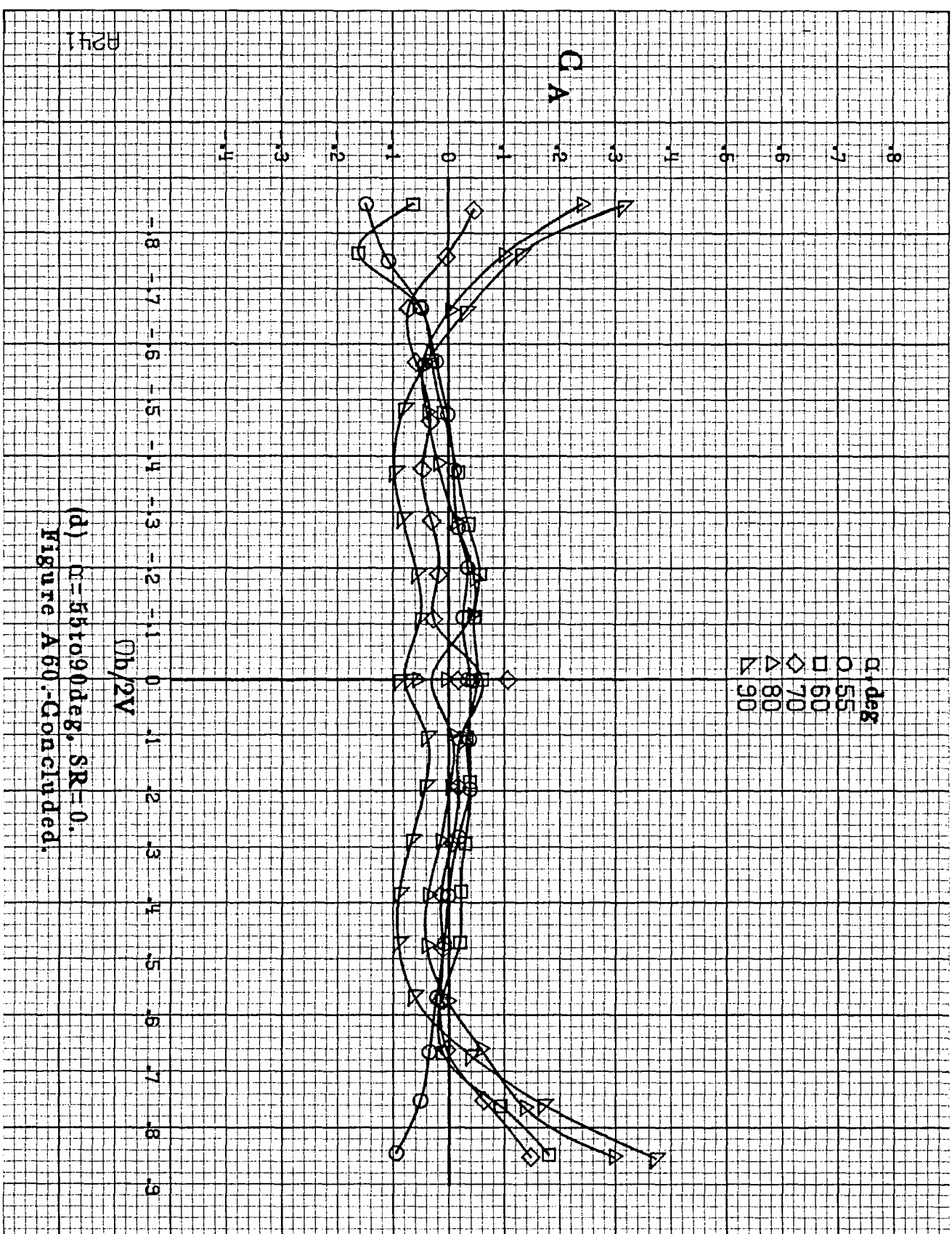


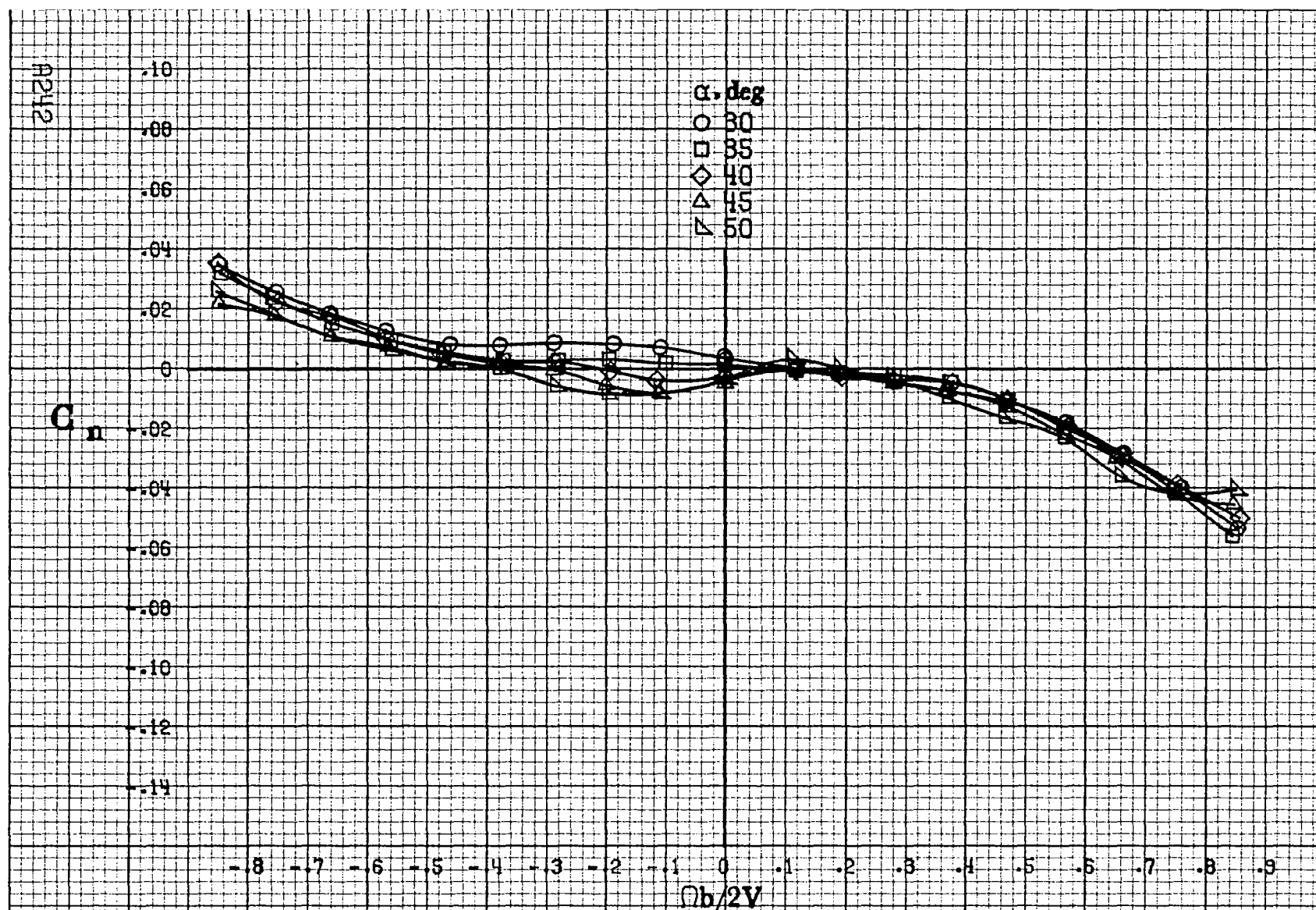






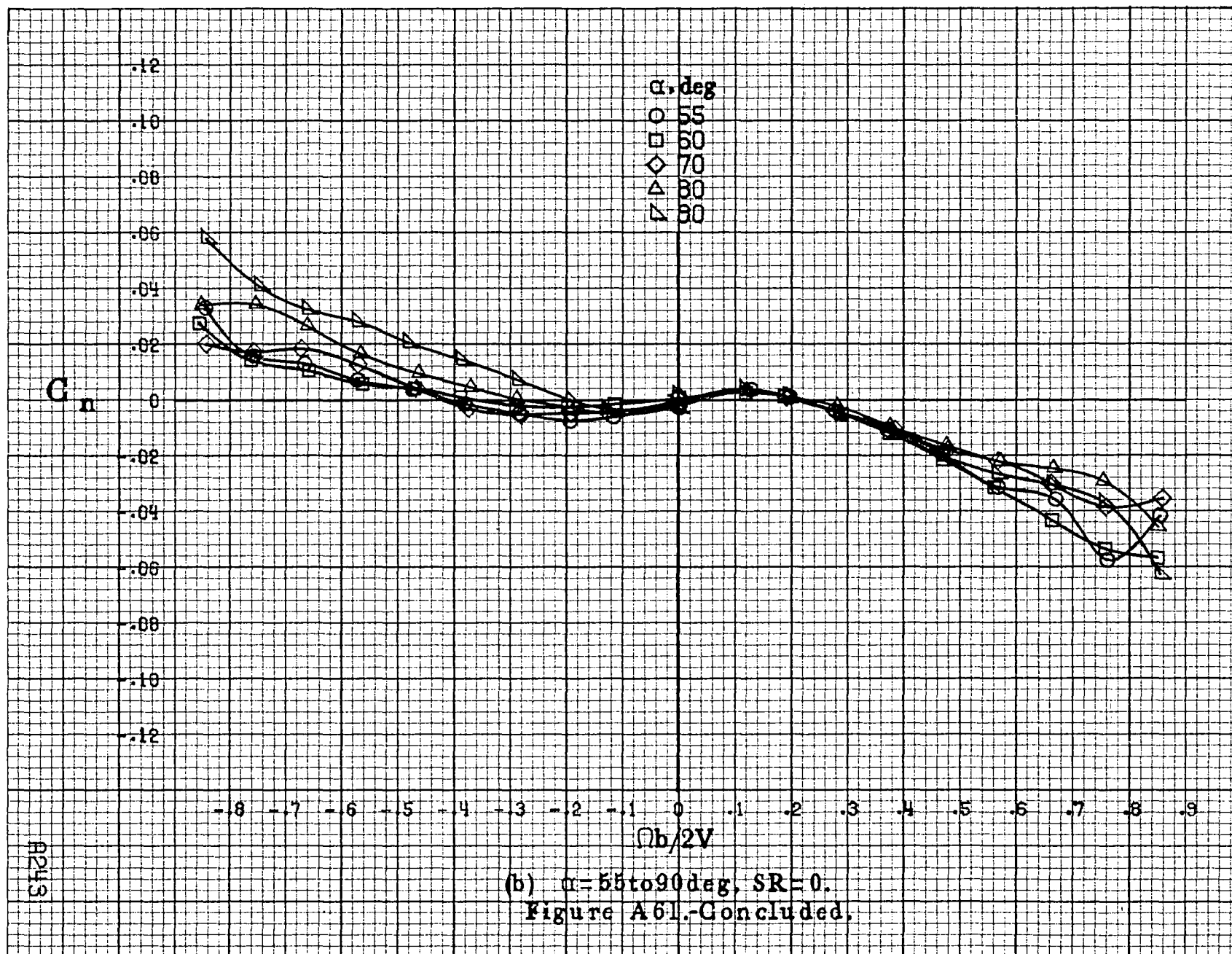


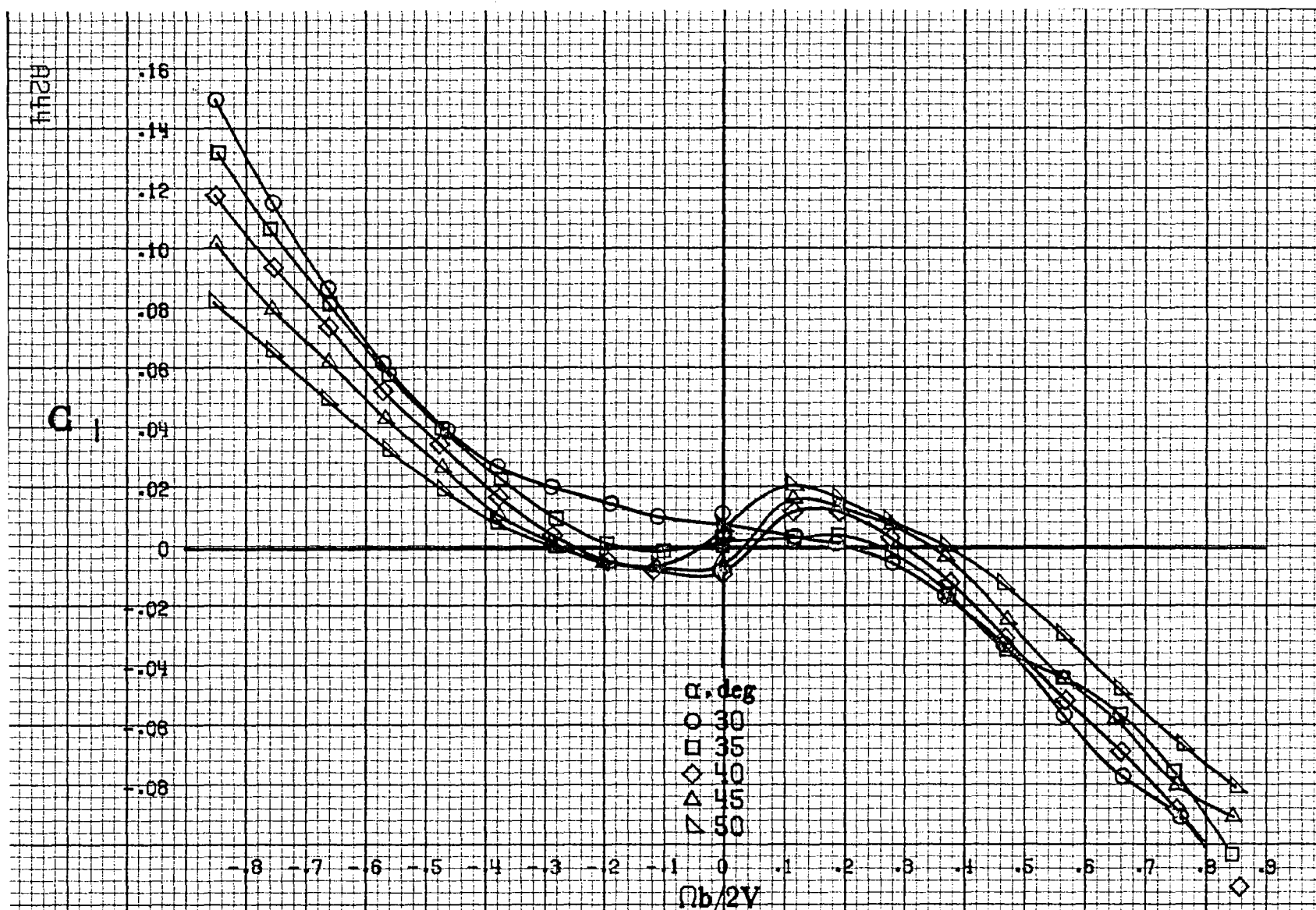




(a) $\alpha = 30$ to 50 deg, $SR = 0$.

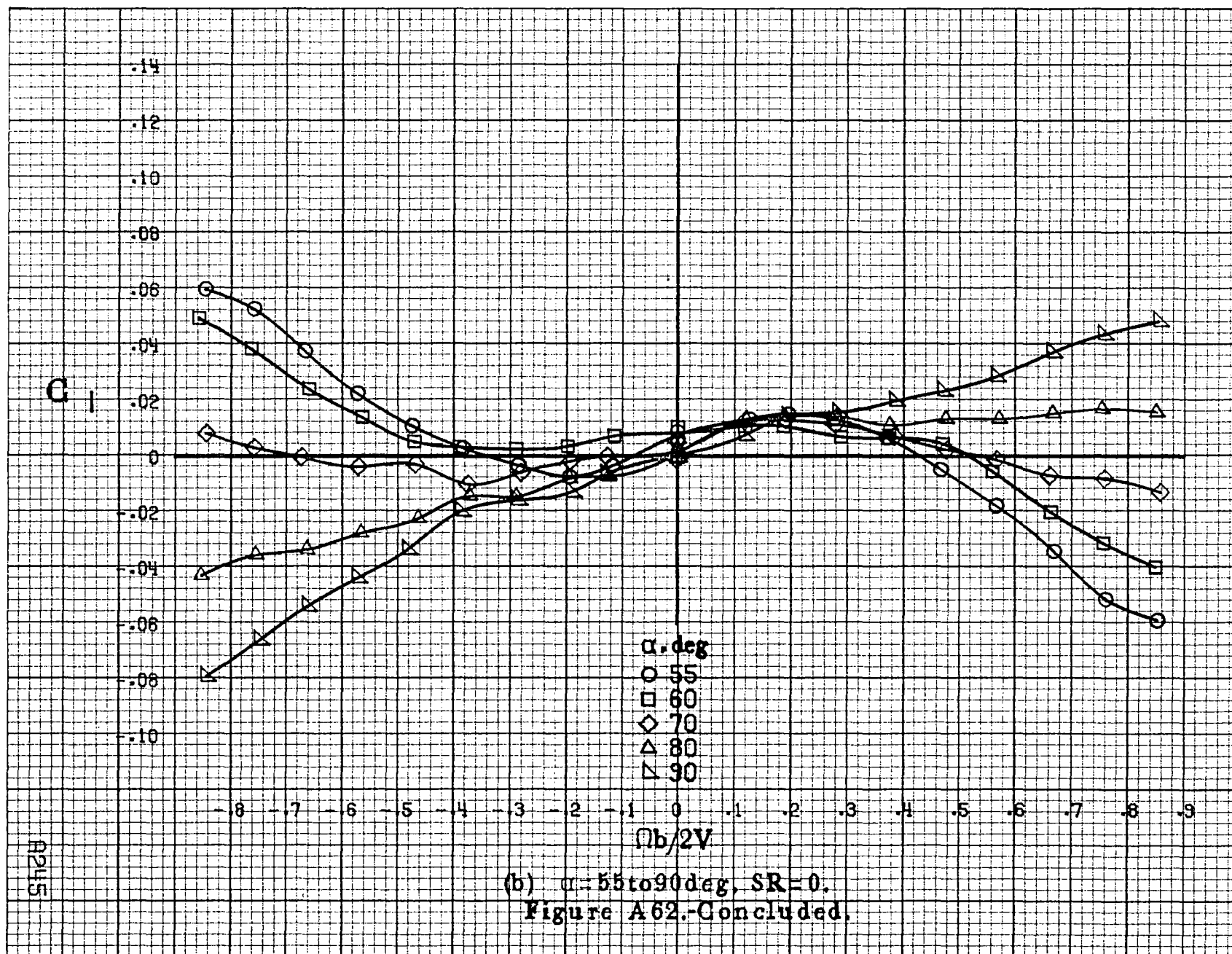
Figure A61.-Effect of rotation rate and angle of attack on yawing-moment coefficient for configuration having rounded fuselage bottom aft of wing TR. $\delta_e = 0^\circ$, $\delta_a = 0^\circ$, $\delta_r = 0^\circ$, $\beta = 0^\circ$.

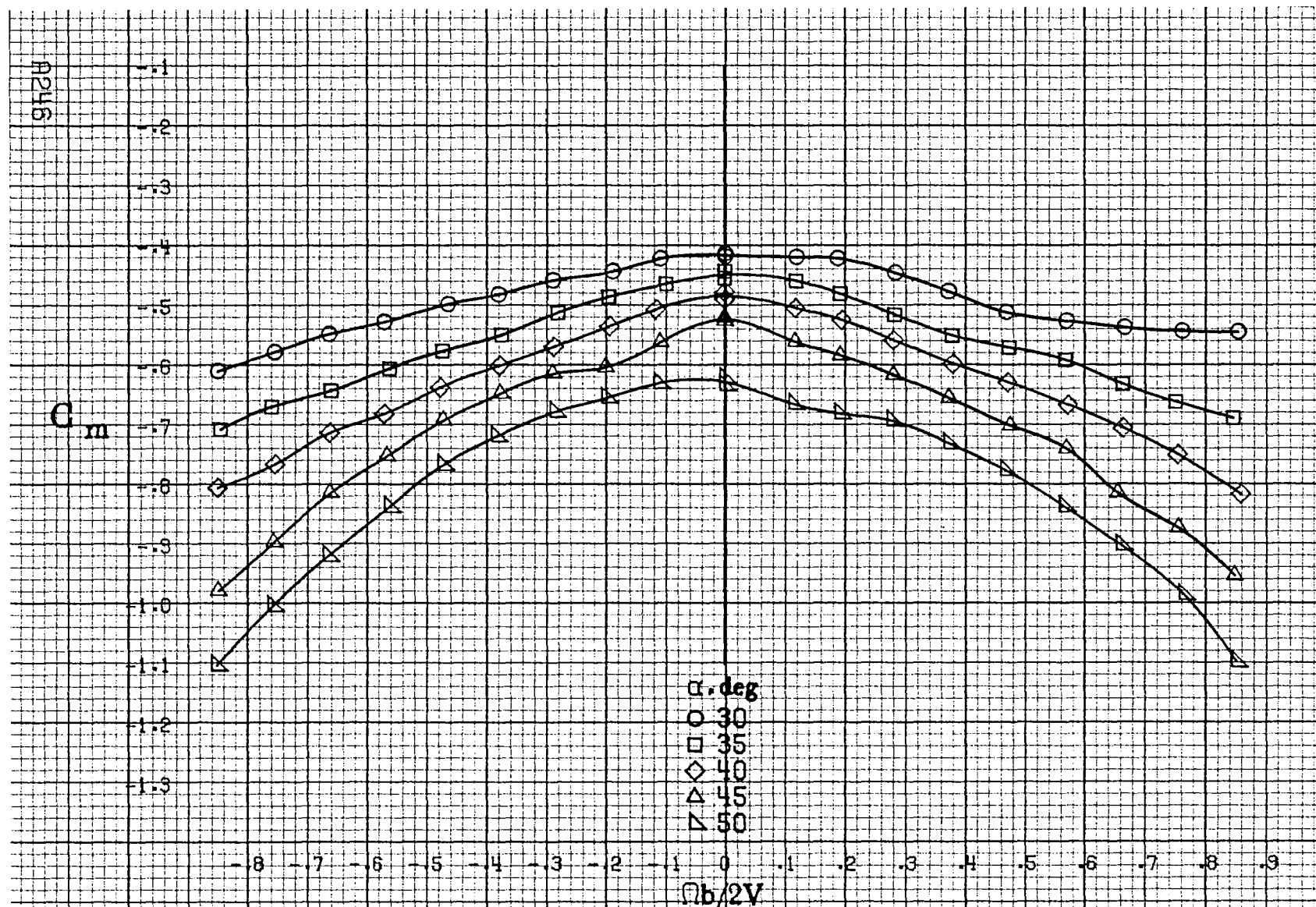




(a) $\alpha = 30$ to 50 deg, $SR = 0$.

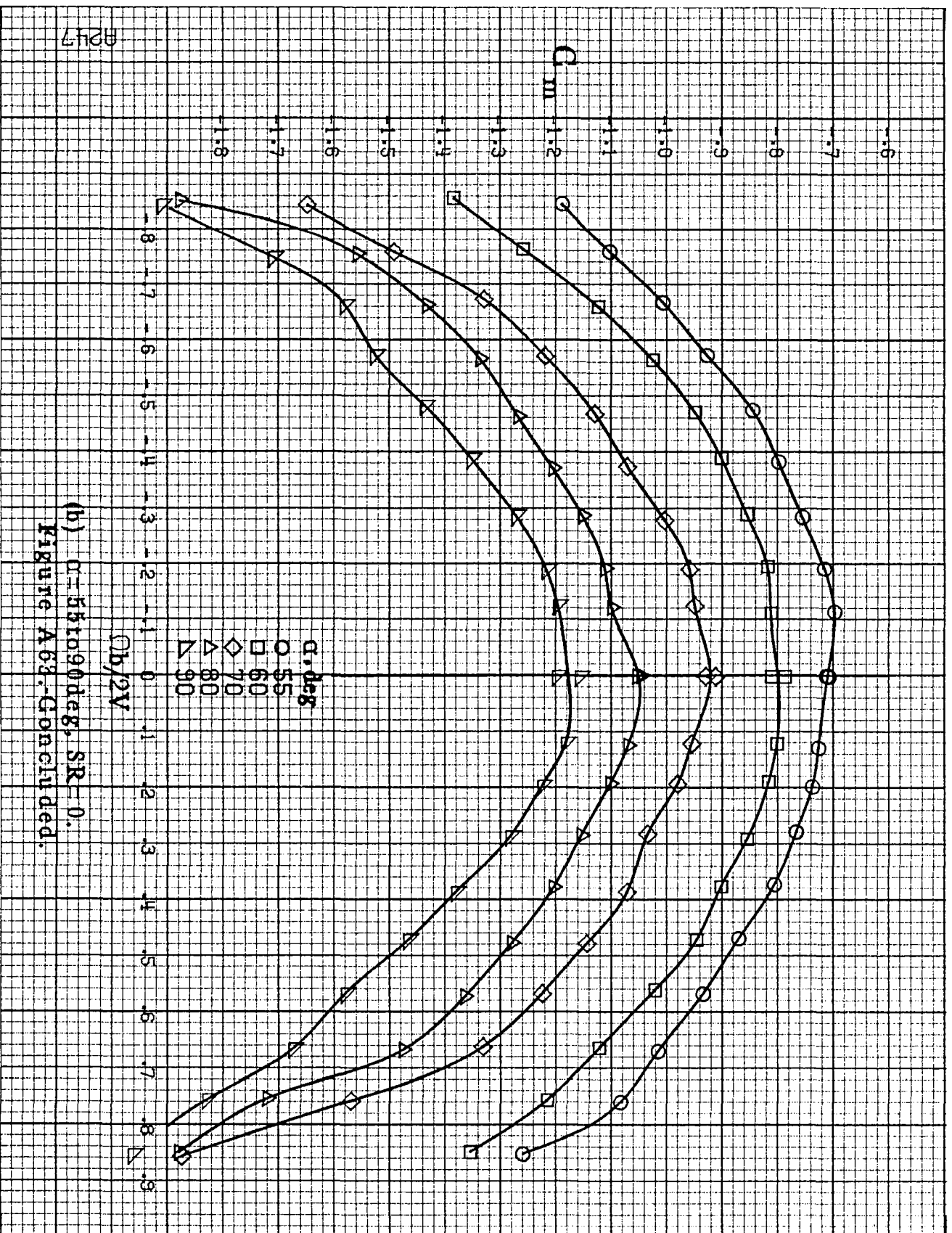
Figure A62.-Effect of rotation rate and angle of attack on rolling-moment coefficient for configuration having rounded fuselage bottom aft of wing T.E. $\delta_c = 0^\circ$, $\delta_s = 0^\circ$, $\delta_r = 0^\circ$, $\beta = 0^\circ$.



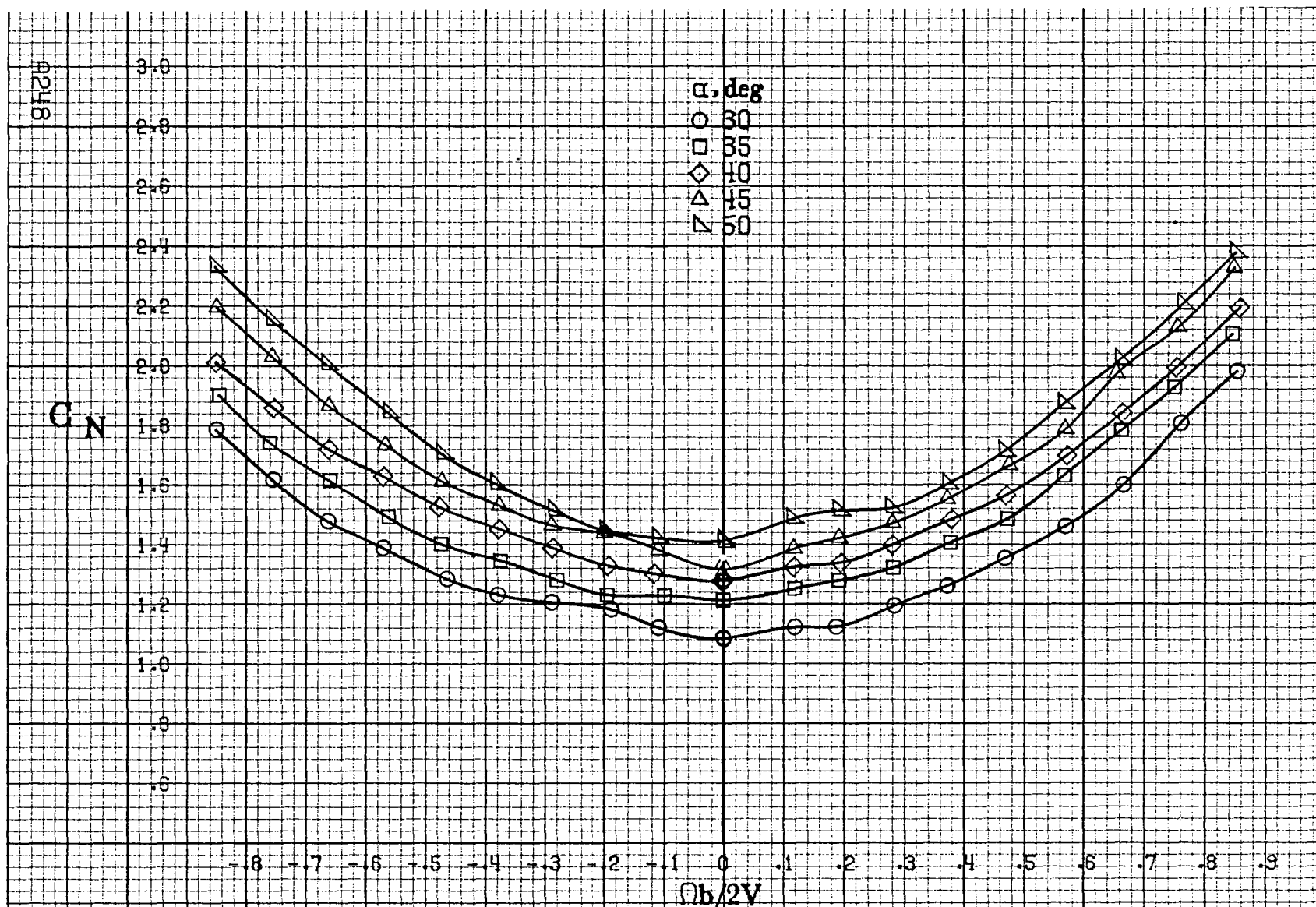


(a) $\alpha=30$ to 50° , $SR=0$.

Figure A68: Effect of rotation rate and angle of attack on pitching-moment coefficient for configuration having rounded fuselage bottom aft of wing TR. $\delta_e=0^\circ$, $\delta_s=0^\circ$, $\delta_r=0^\circ$, $\beta=0^\circ$.

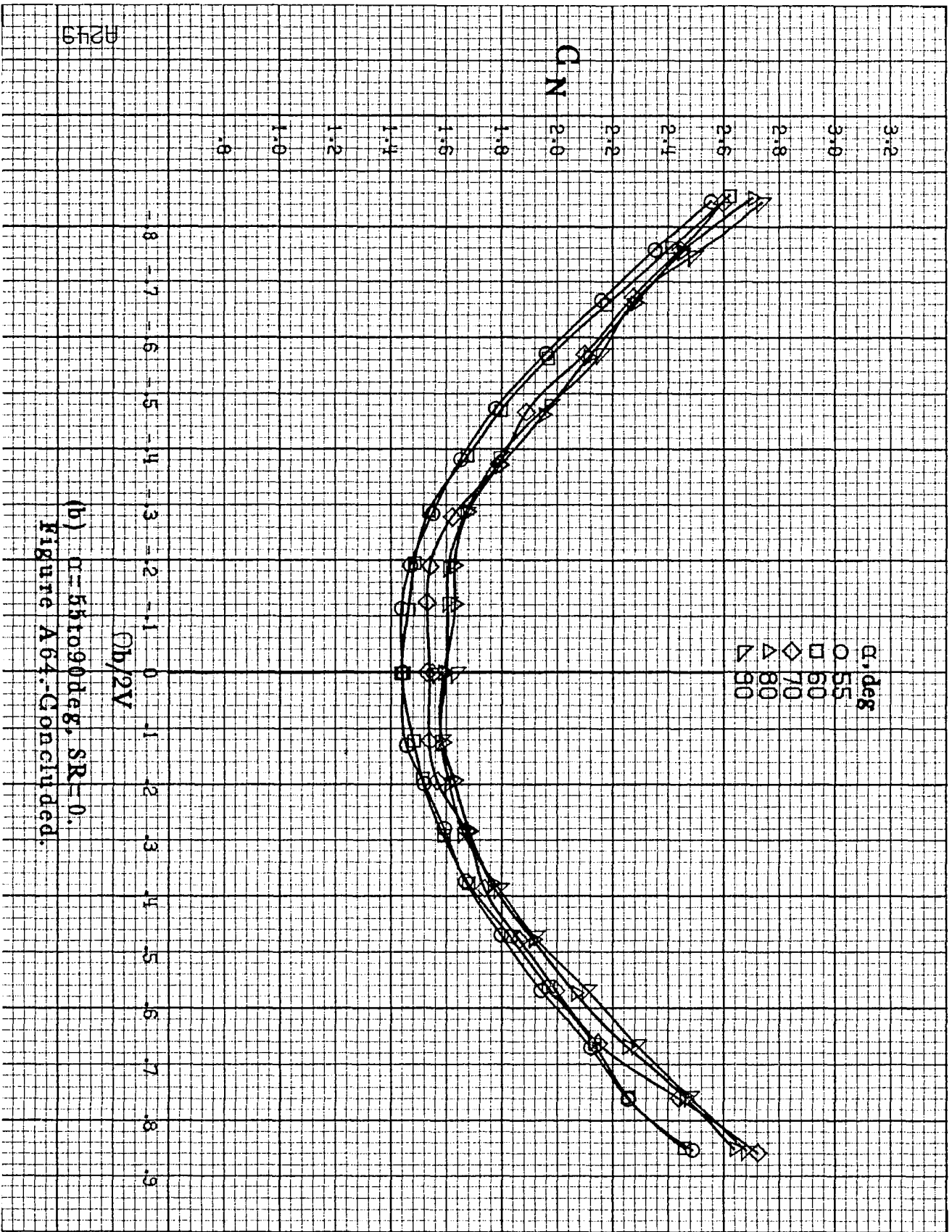


(b) $\alpha=55$ to 90° , $SR=0$.
Figure A63-Continued.

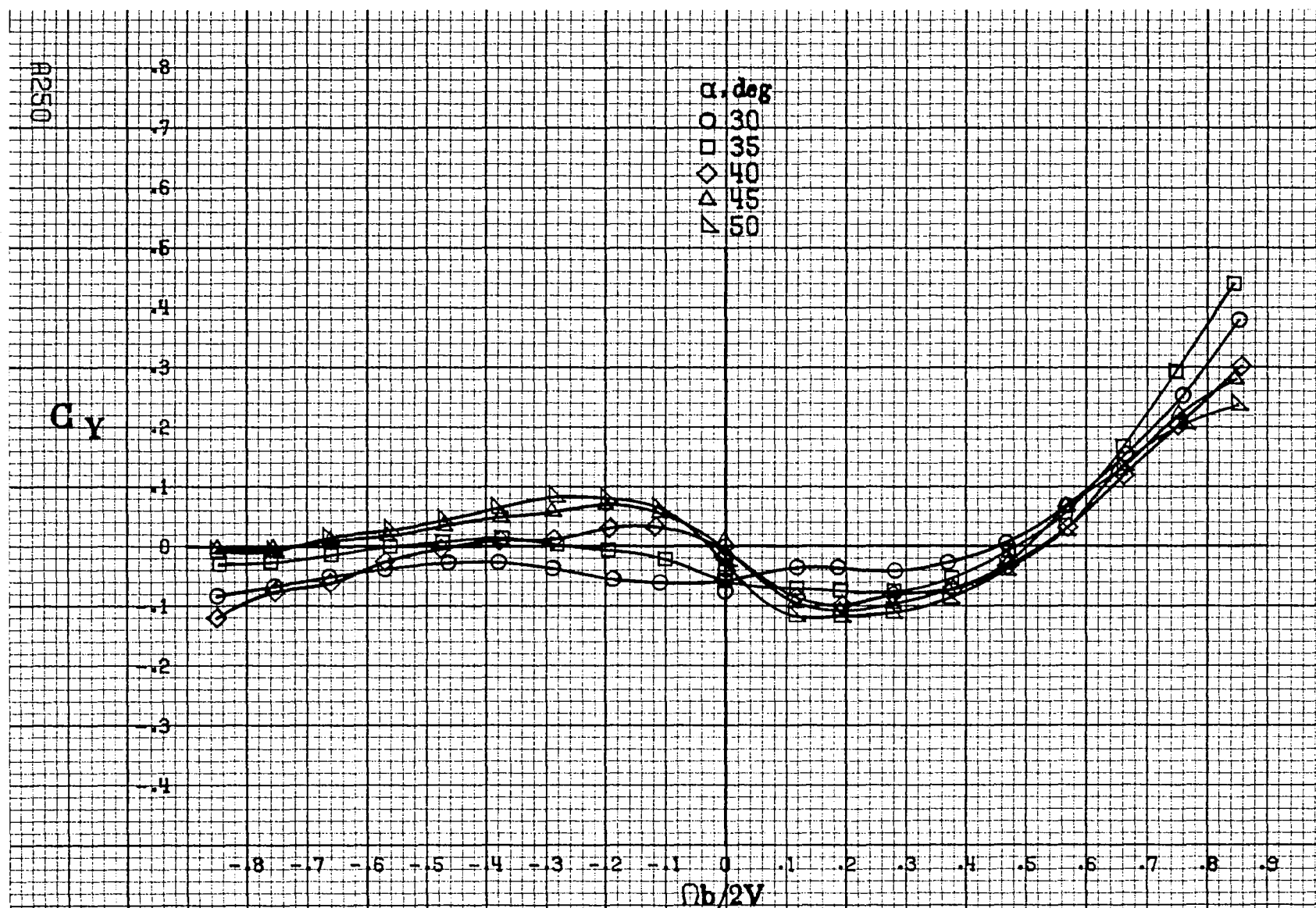


(a) $\alpha = 30$ to 50° , $SR = 0$.

Figure A64. Effect of rotation rate and angle of attack on normal-force coefficient for configuration having rounded fuselage bottom aft of wing T.E. $\delta_e = 0^\circ$, $\delta_a = 0^\circ$, $\delta_r = 0^\circ$, $\beta = 0^\circ$.

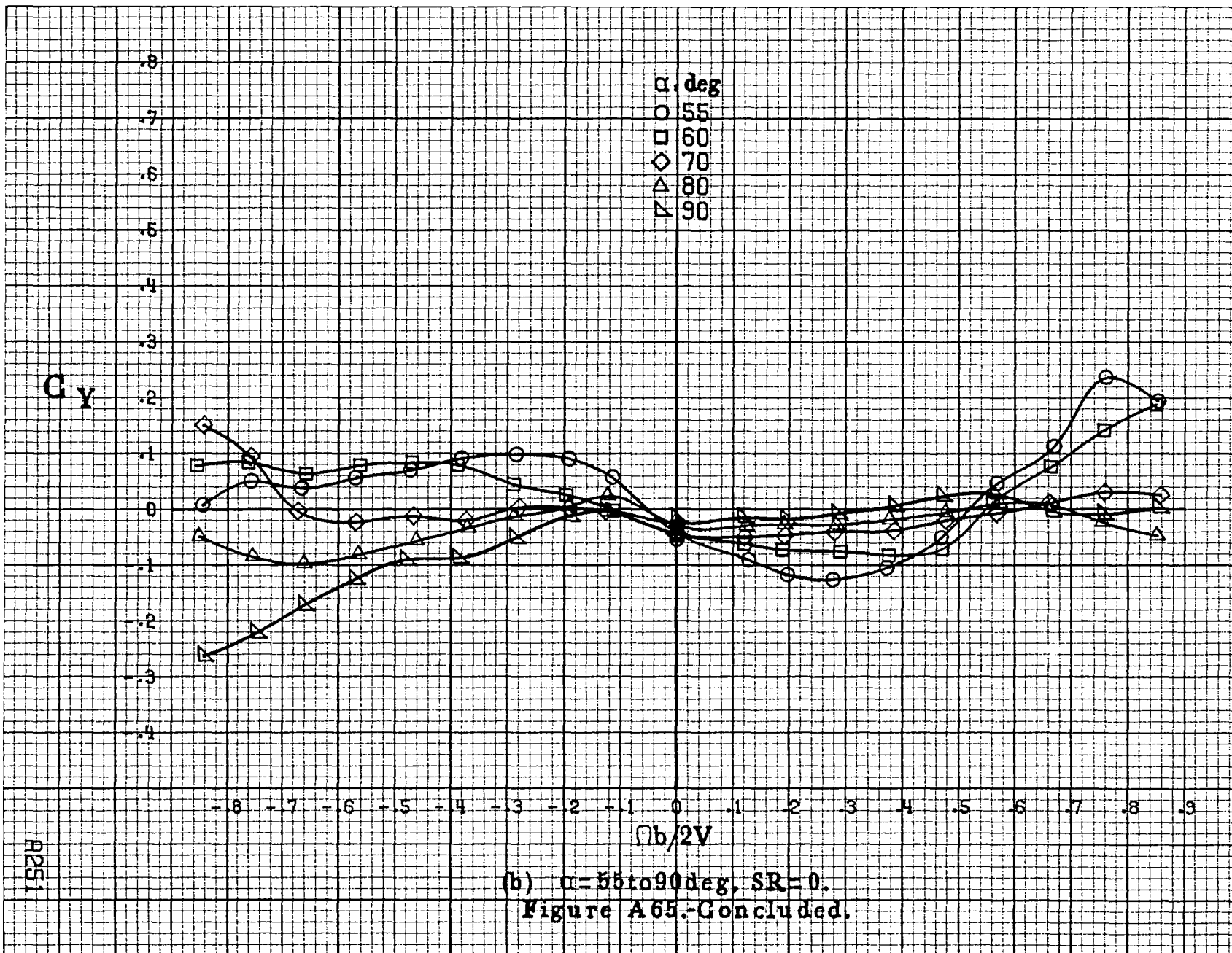


(b) $\alpha = 55$ to 90° , $SR = 0$.
Figure A64.-Concluded.



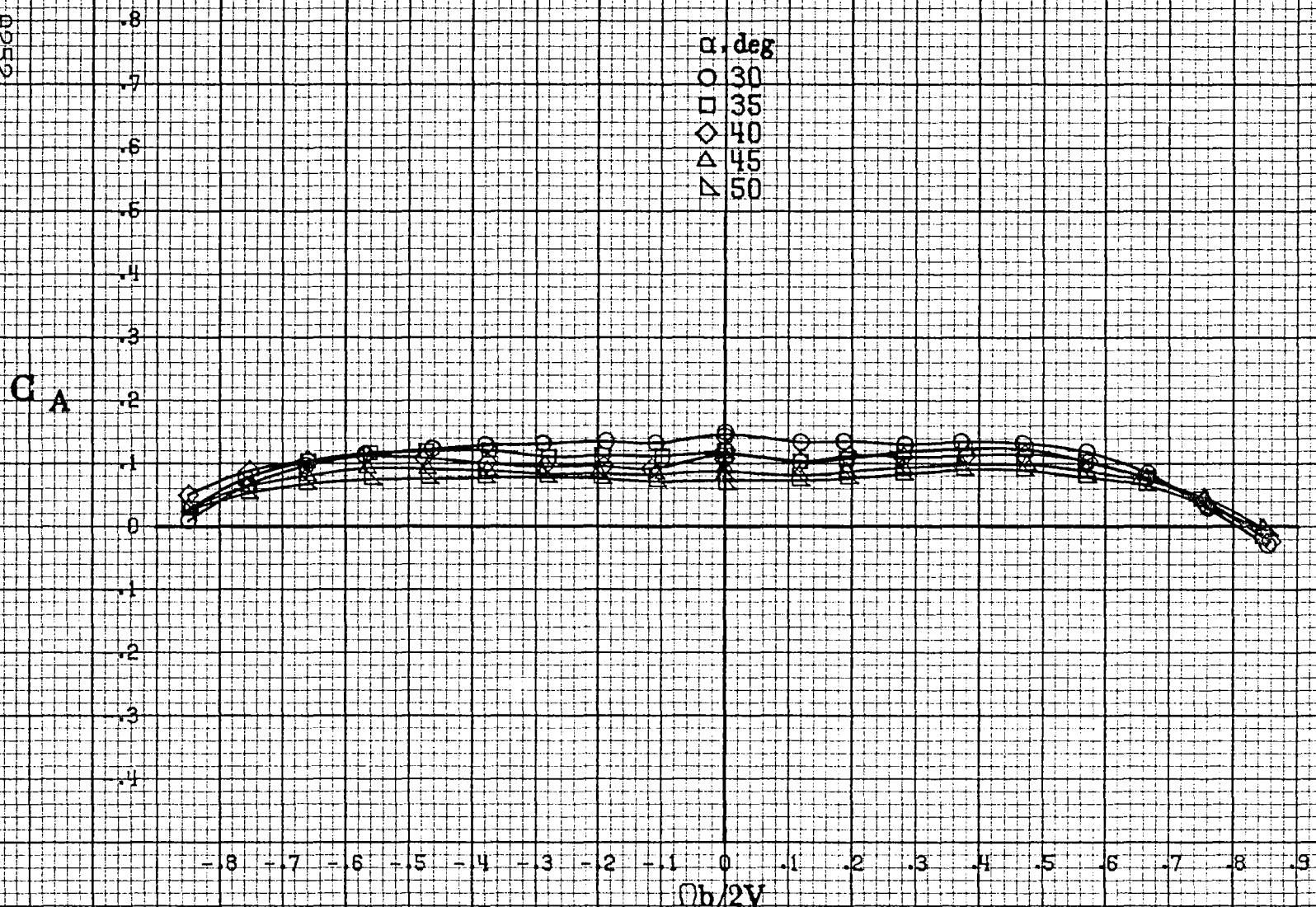
(a) $\alpha=30$ to 50 deg, $SR=0$.

Figure A65.-Effect of rotation rate and angle of attack on side-force coefficient for configuration having rounded fuselage bottom aft of wing I.E. $\delta_1 = 0^\circ$, $\delta_2 = 0^\circ$, $\delta_3 = 0^\circ$, $\beta = 0^\circ$.



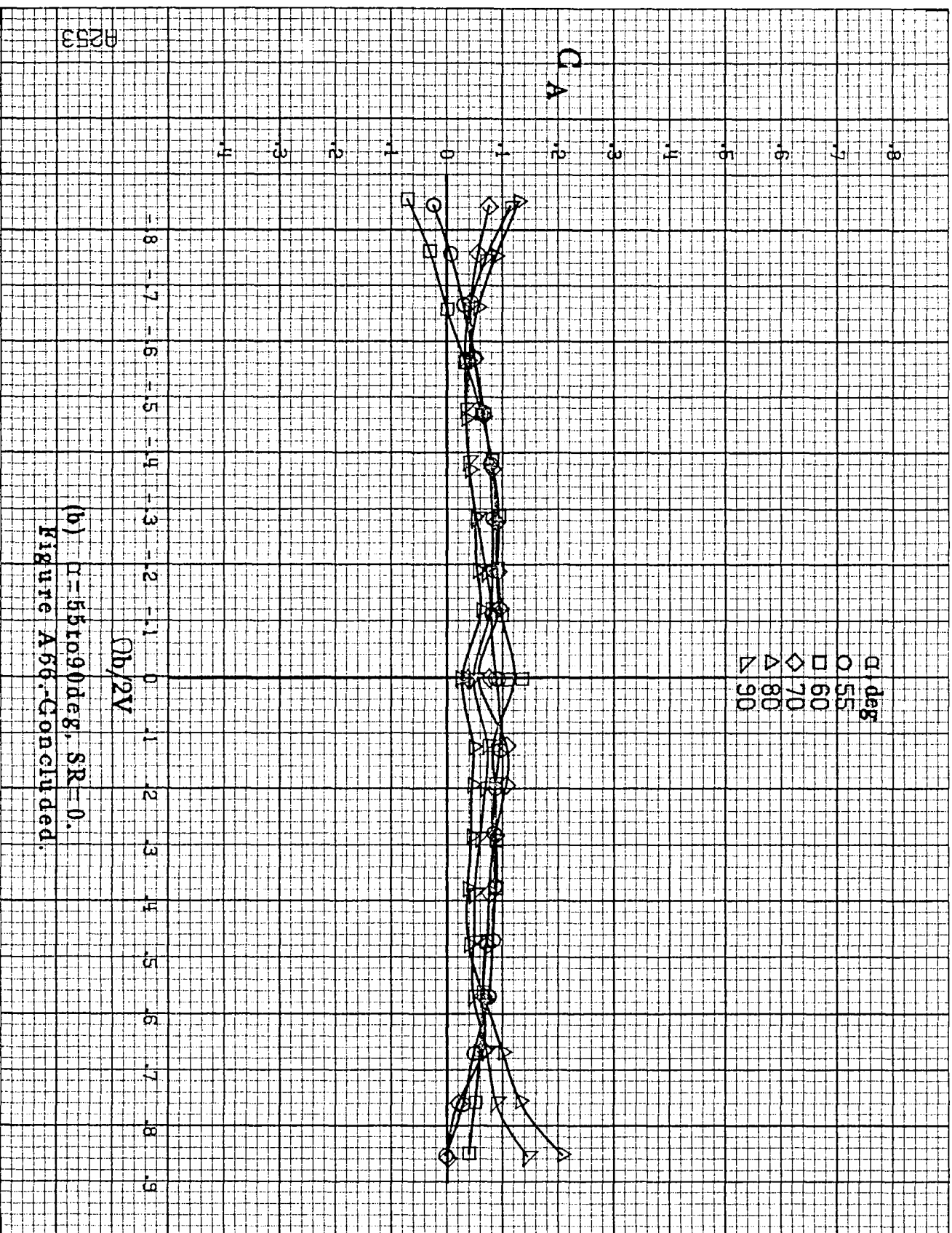
(b) $\alpha=55$ to 90° , $SR=0$.
Figure A65.-Concluded.

A252



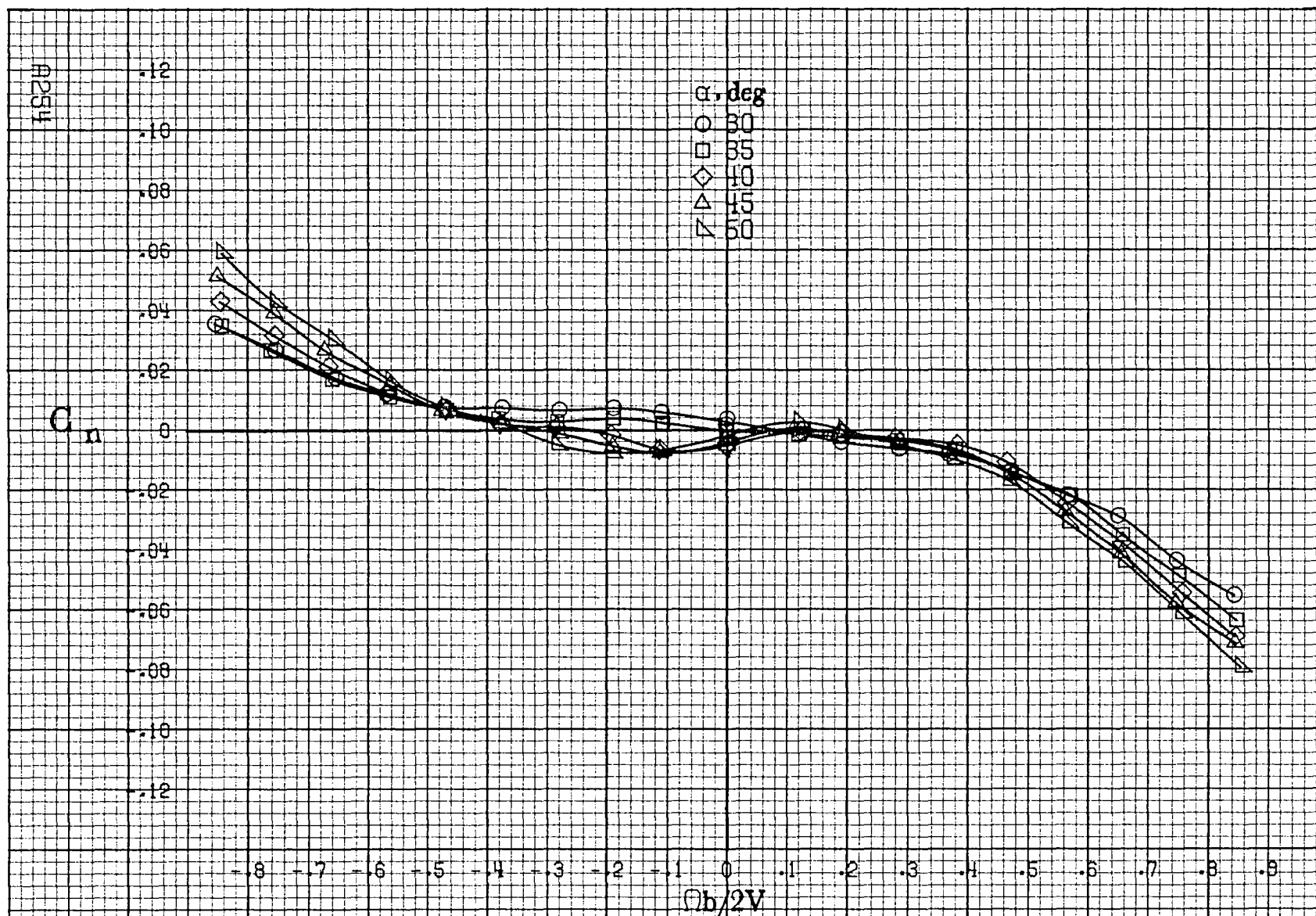
(a) $\alpha = 30$ to 50° , $SR = 0$.

Figure A66.-Effect of rotation rate and angle of attack on axial-force coefficient for configuration having rounded fuselage bottom aft of wing T.E. $\delta_e = 0^\circ$, $\delta_a = 0^\circ$, $\delta_r = 0^\circ$. $\beta = 0^\circ$.



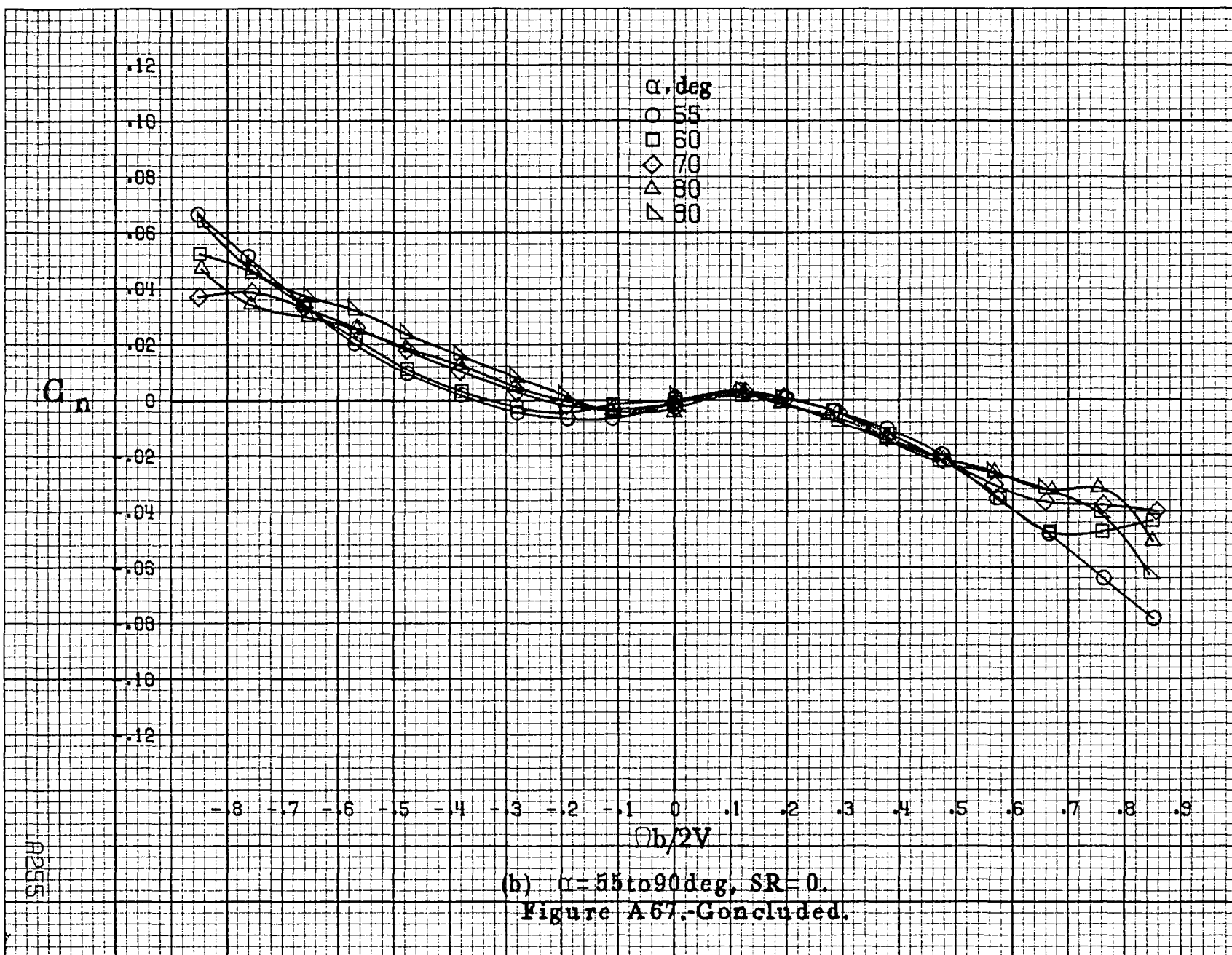
(b) $\alpha = 55$ to 90 deg, $SR = 0$.
Figure A66-Continued.

B253



(a) $\alpha = 30$ to 50° , $SR = 0$.

Figure A67.-Effect of rotation rate and angle of attack on yawing-moment coefficient for configuration having rounded fuselage bottom aft of engine cowlings. $\delta_e = 0^\circ$, $\delta_a = 0^\circ$, $\delta_r = 0^\circ$, $\beta = 0^\circ$.



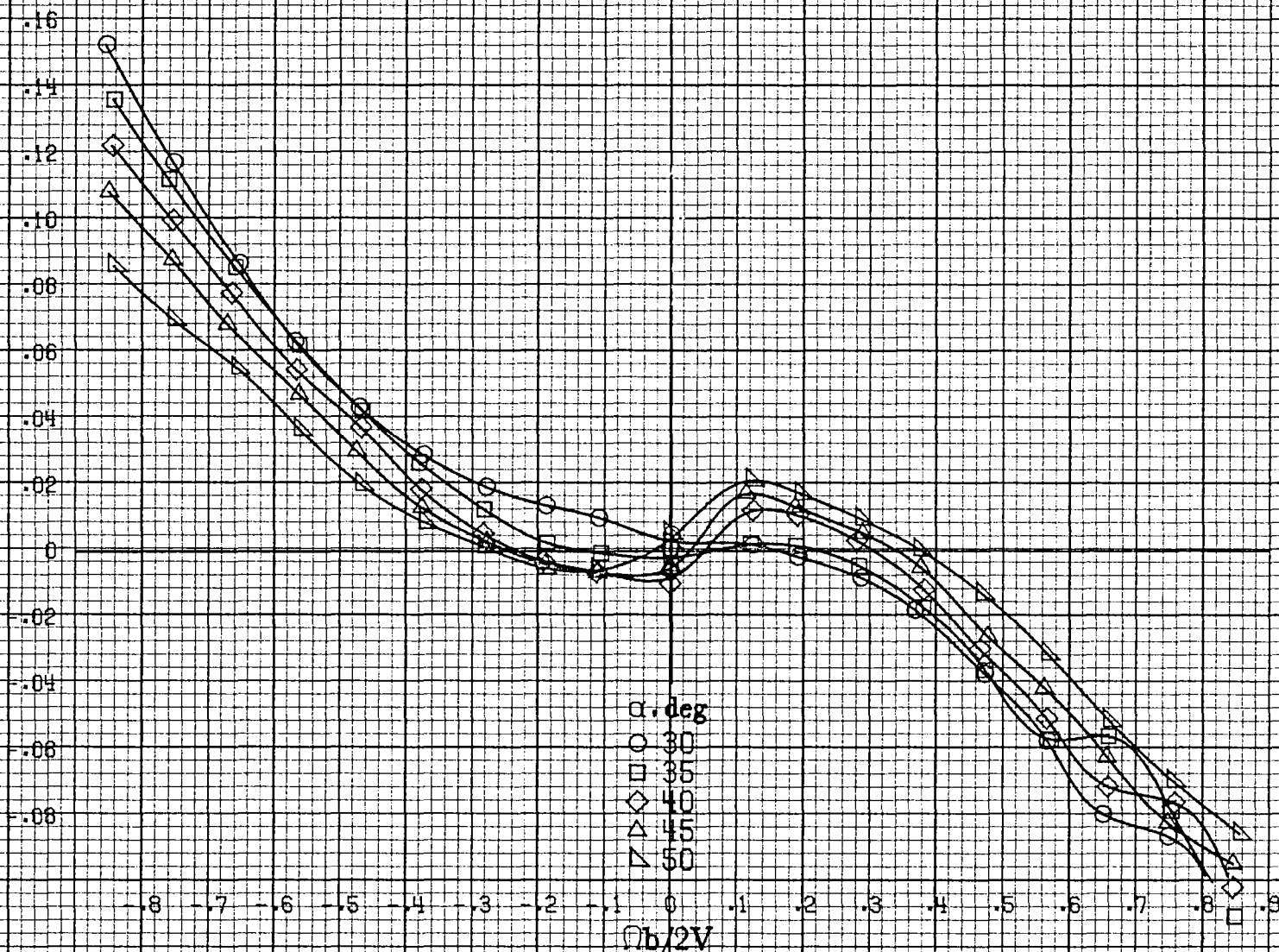
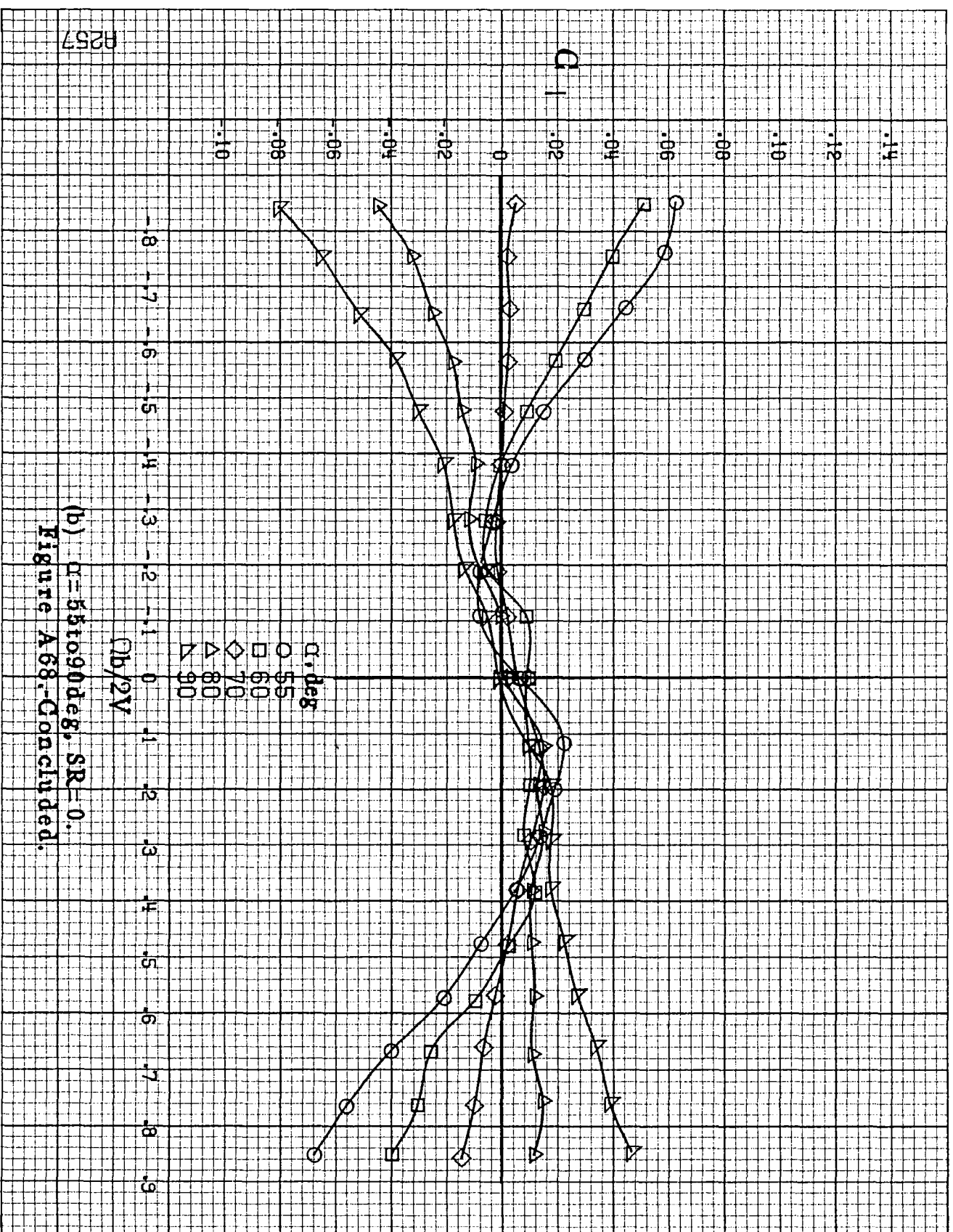
C_l (a) $\alpha = 30$ to 50 deg, $SR = 0$.

Figure A68.-Effect of rotation rate and angle of attack on rolling-moment coefficient for configuration having rounded fuselage bottom aft of engine cowl. $\delta_e = 0^\circ$, $\delta_a = 0^\circ$, $\delta_r = 0^\circ$, $\beta = 0^\circ$.



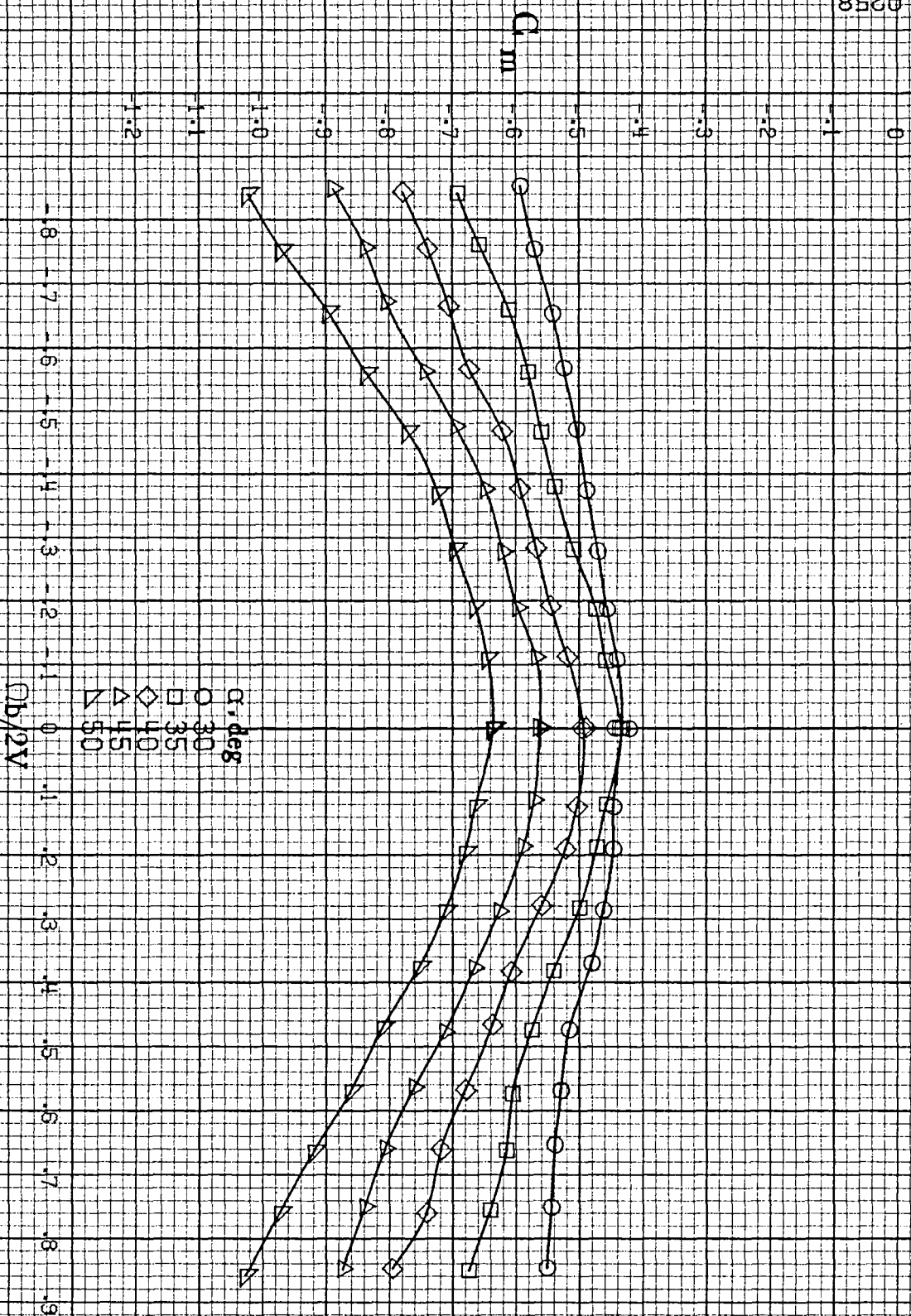
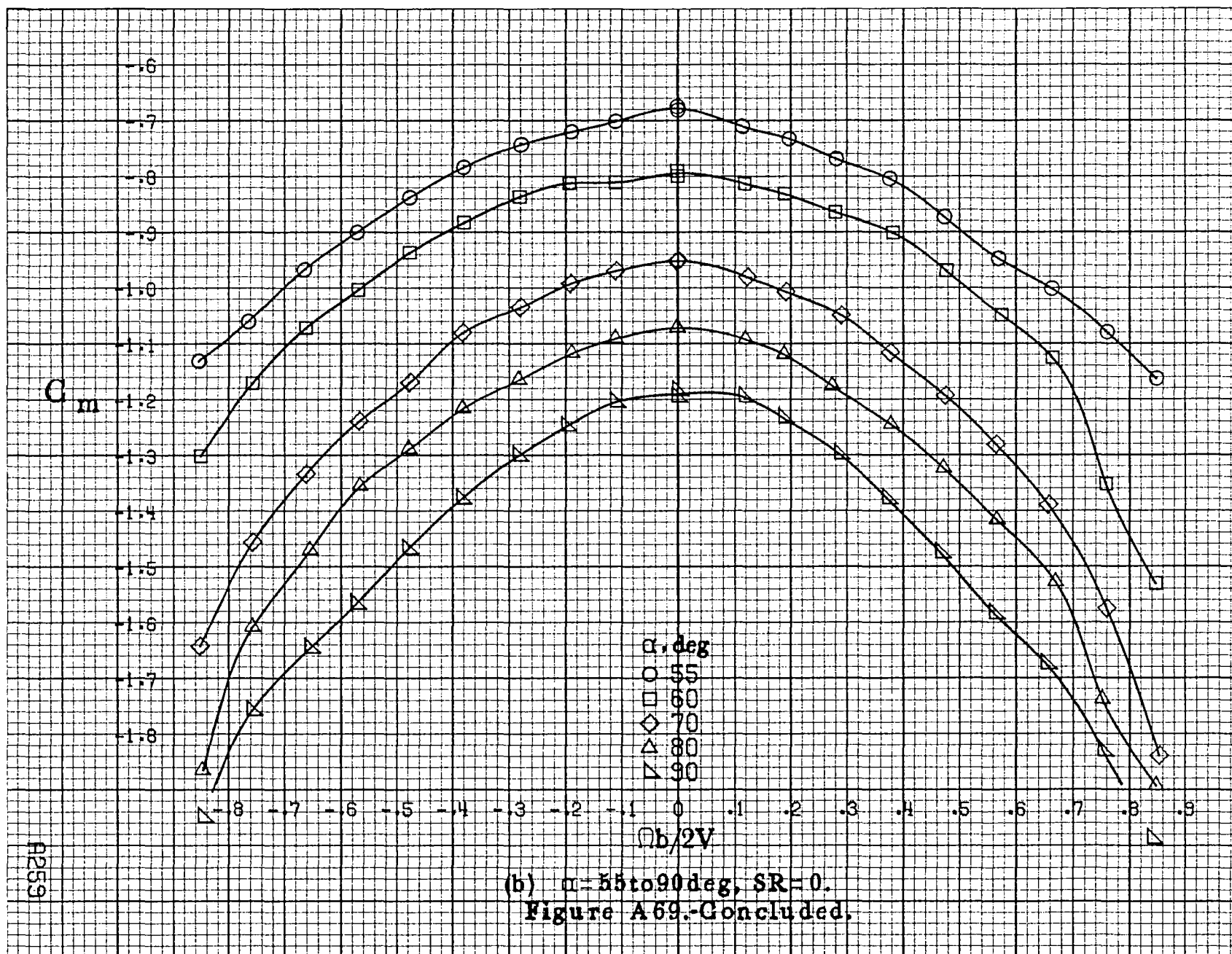
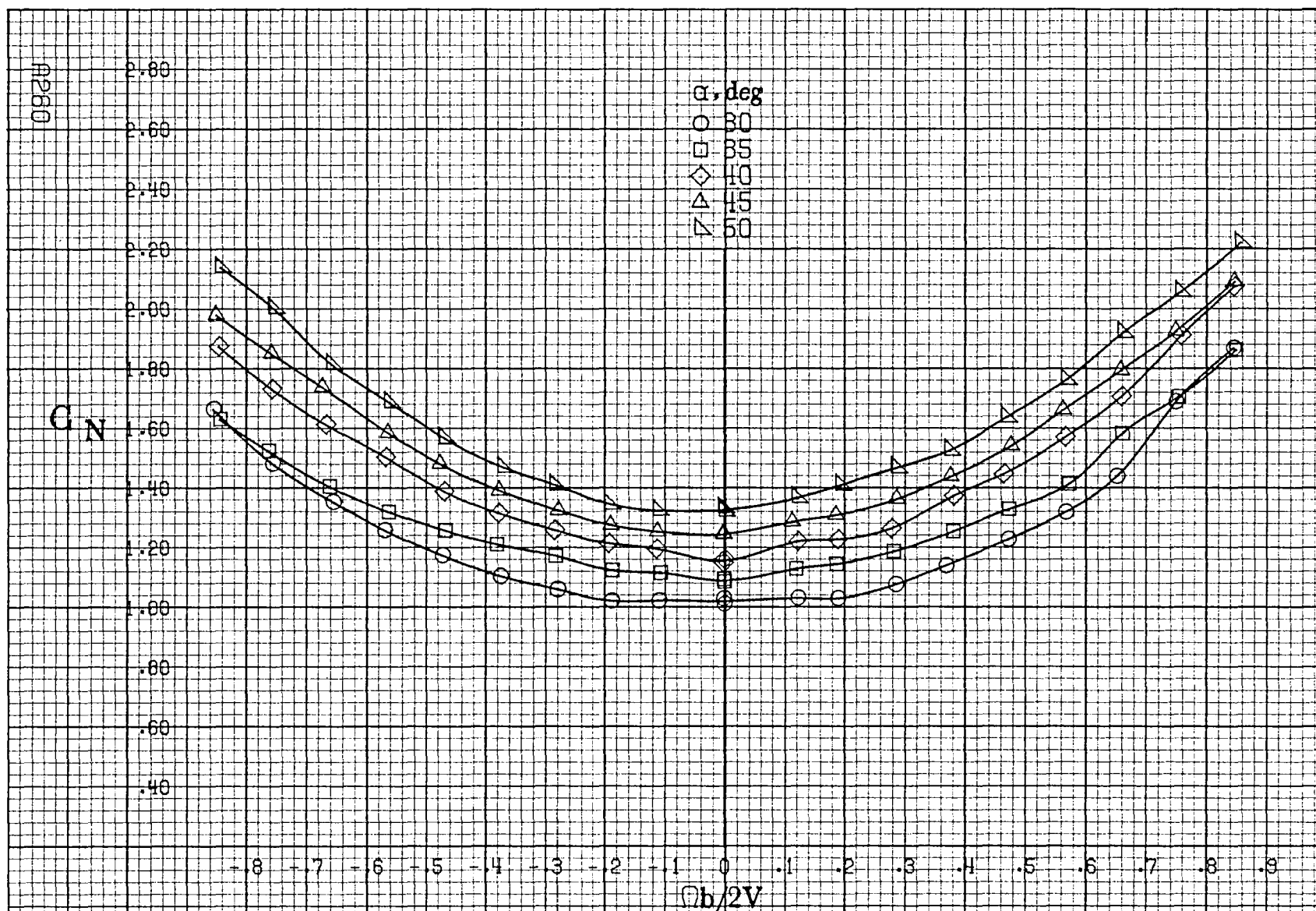


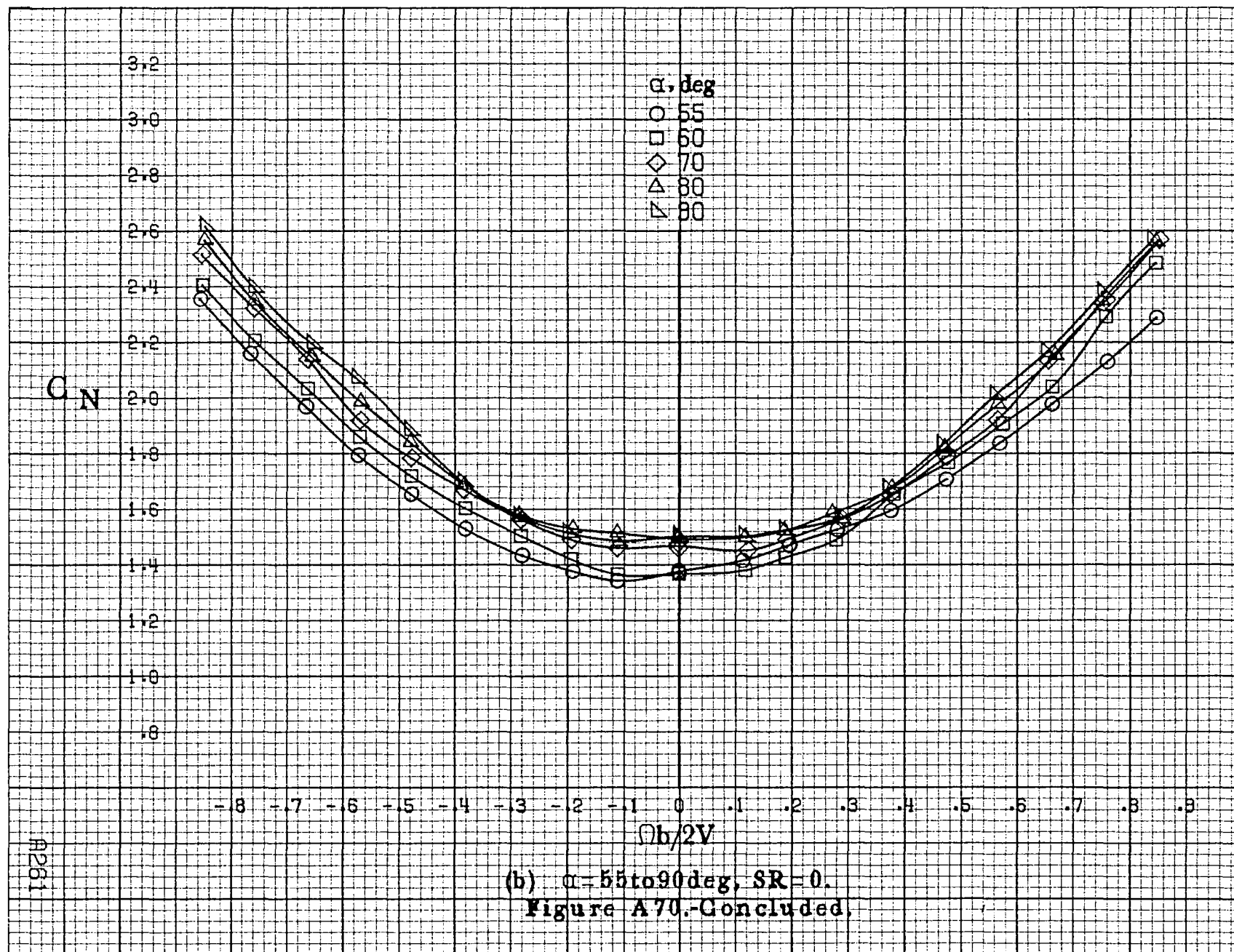
Figure A69. Effect of rotation rate and angle of attack on pitching-moment coefficient for configuration having rounded fuselage bottom aft of engine cowlings. $\alpha = 30^\circ, 35^\circ, 40^\circ, 45^\circ, 50^\circ$. $SR = 0$.

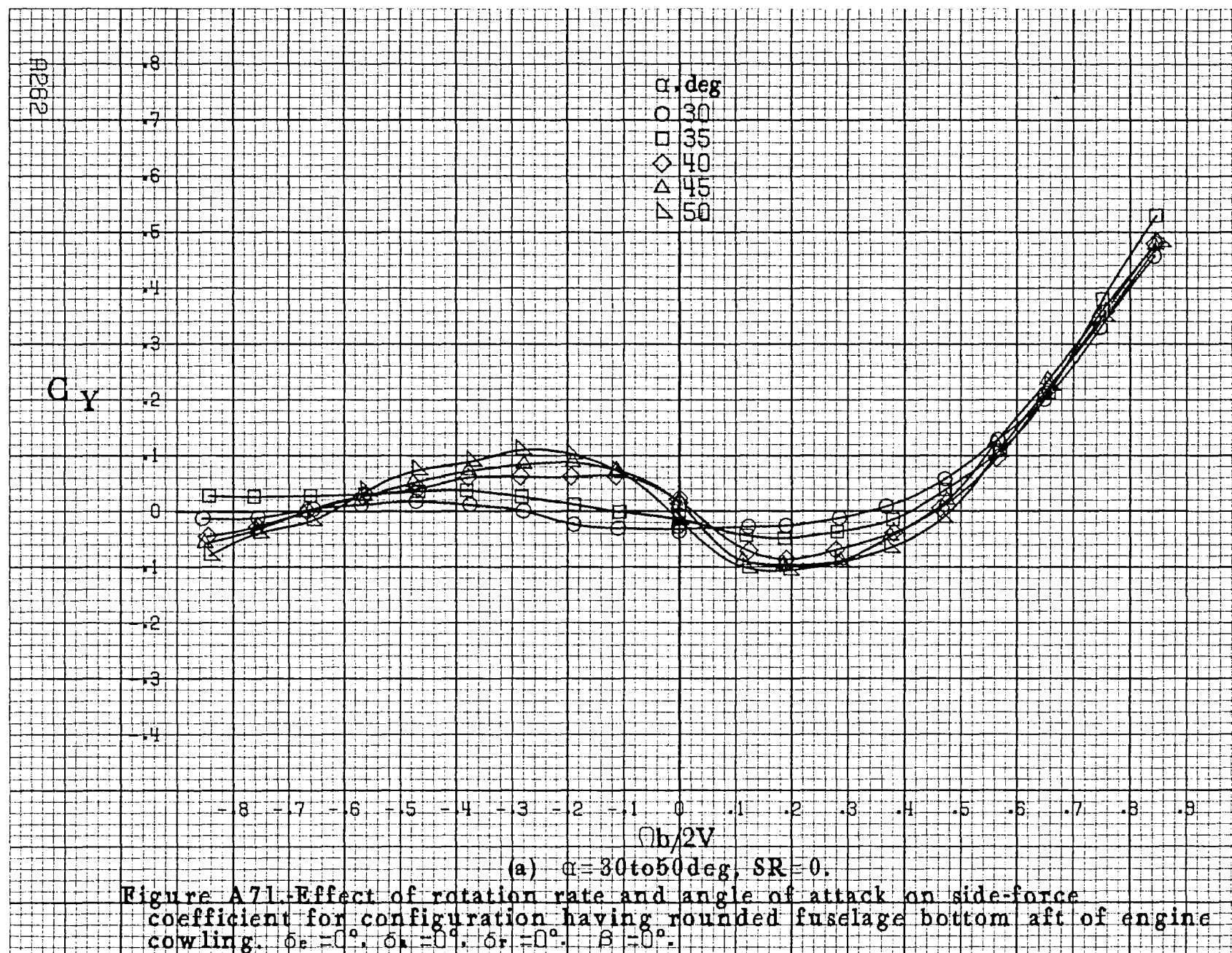


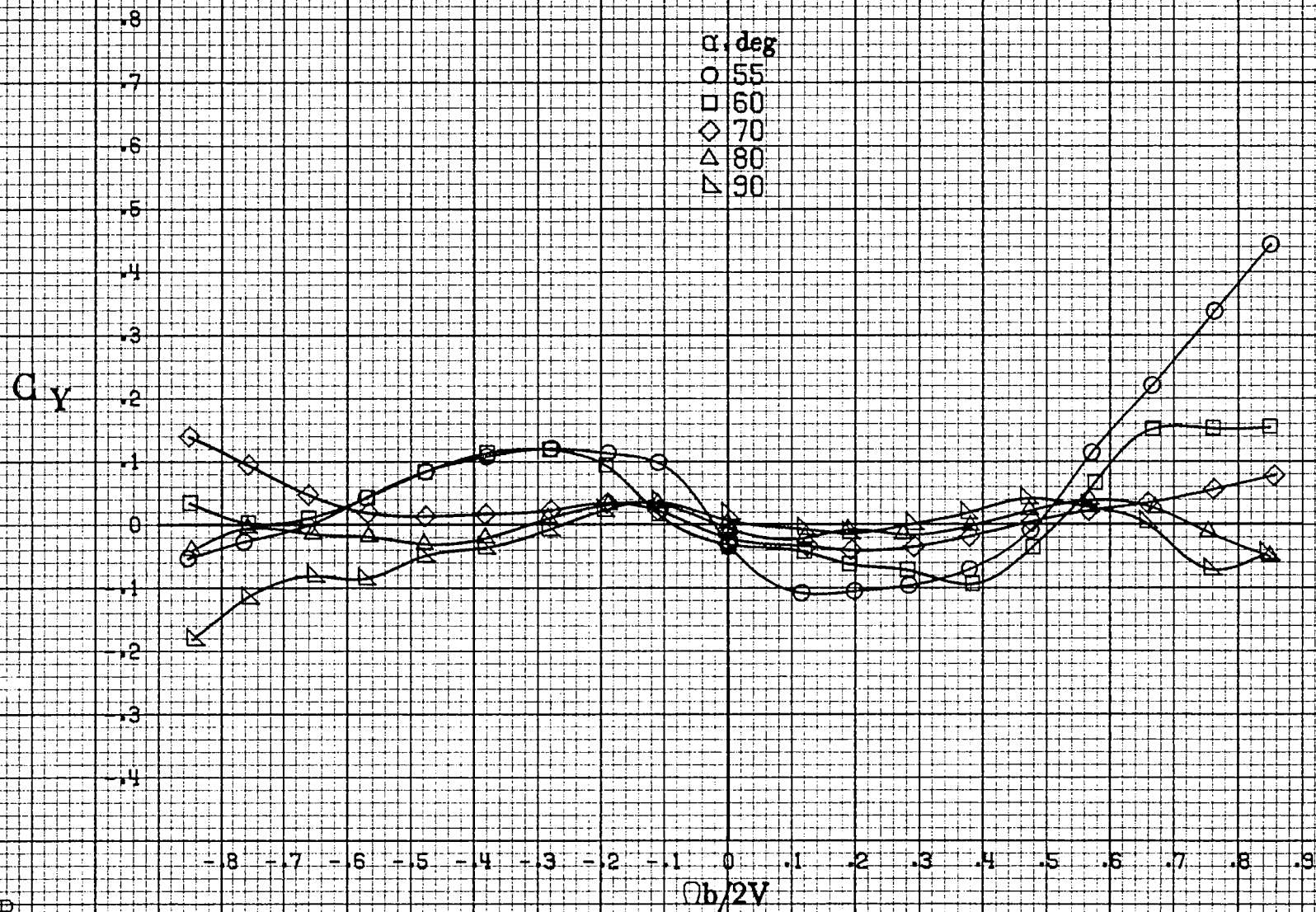


(a) $\alpha = 30$ to 50 deg, $SR = 0$.

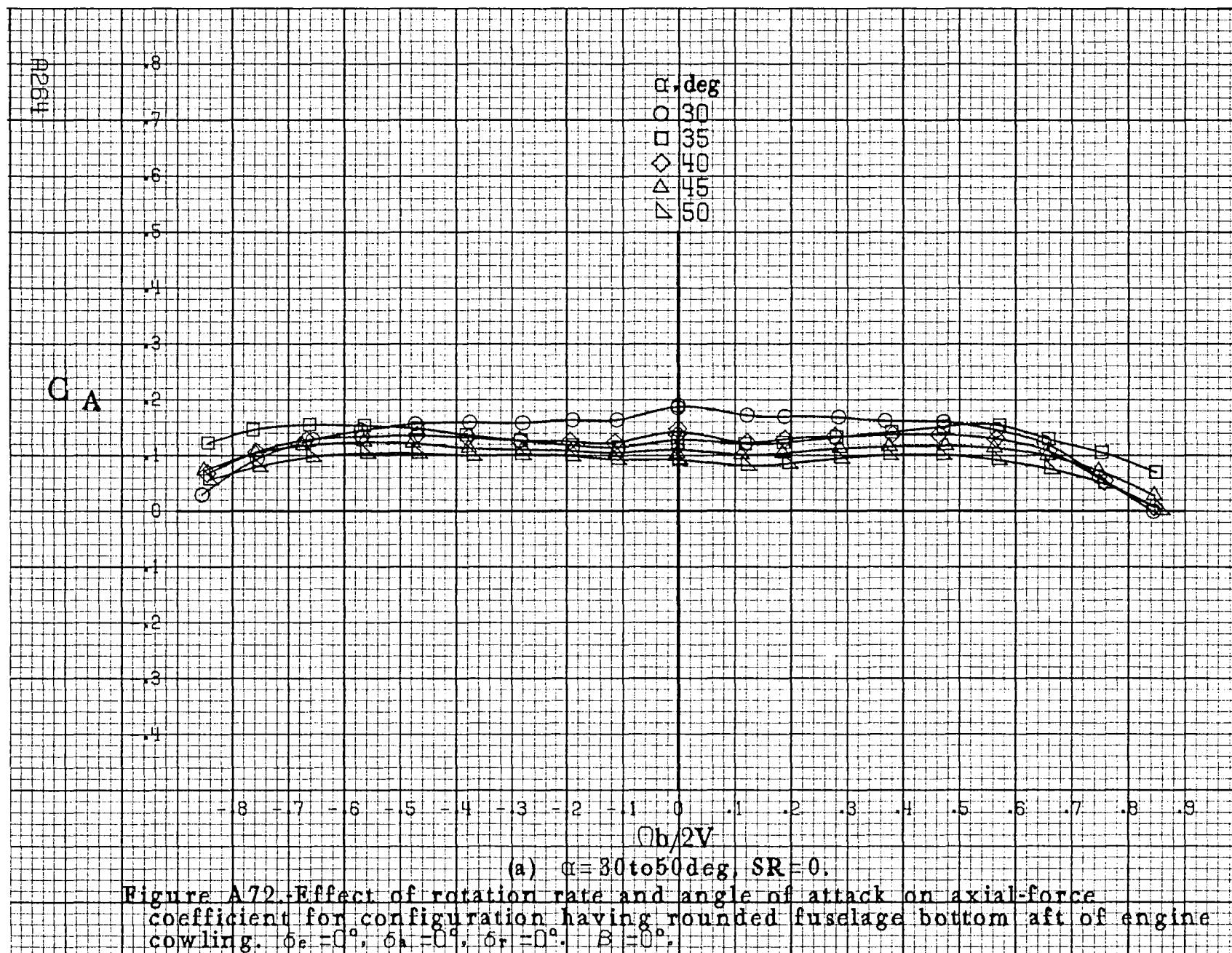
Figure A70.-Effect of rotation rate and angle of attack on normal-force coefficient for configuration having rounded fuselage bottom aft of engine cowlings. $\delta_e = 0^\circ$, $\delta_a = 0^\circ$, $\delta_r = 0^\circ$, $\beta = 0^\circ$.

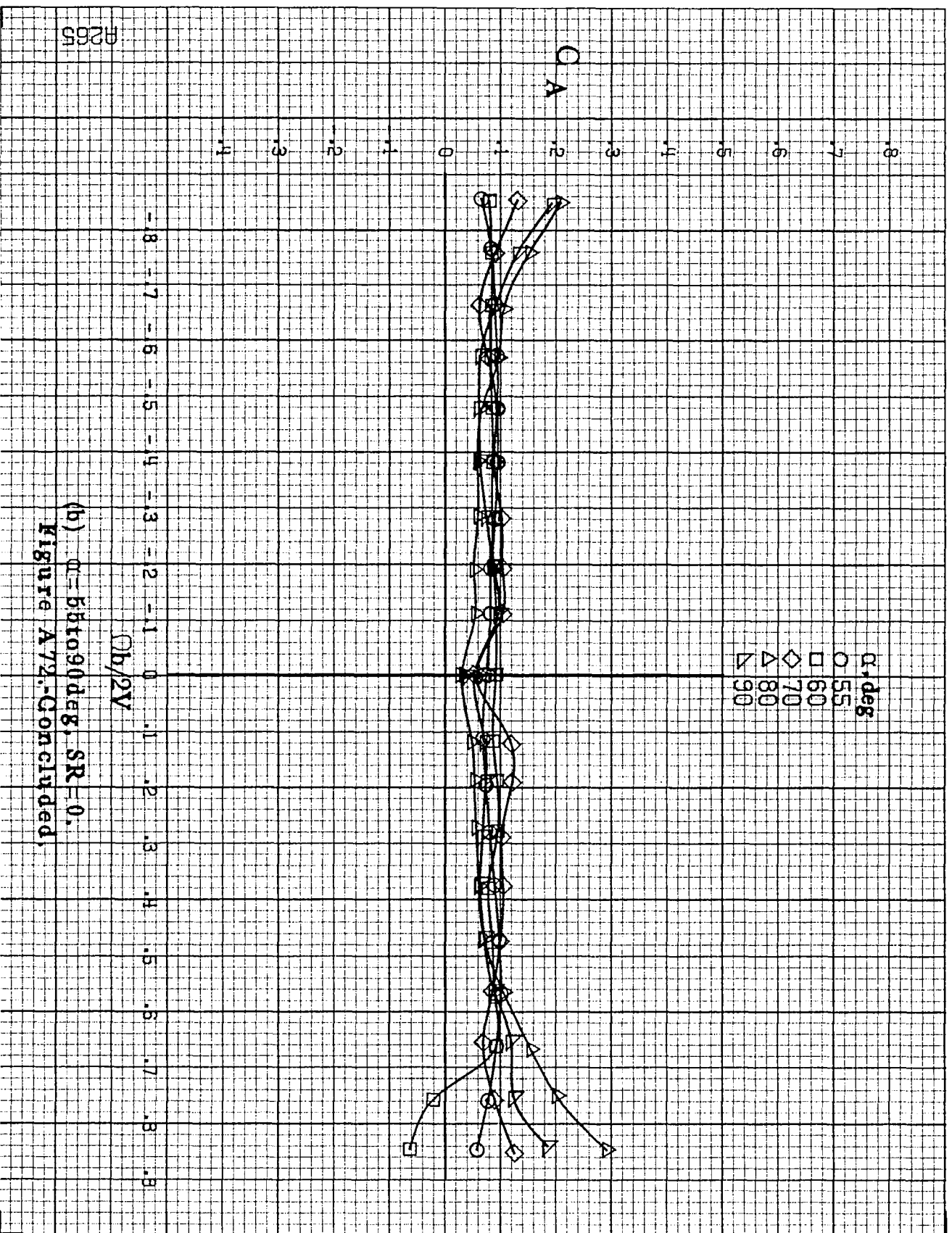






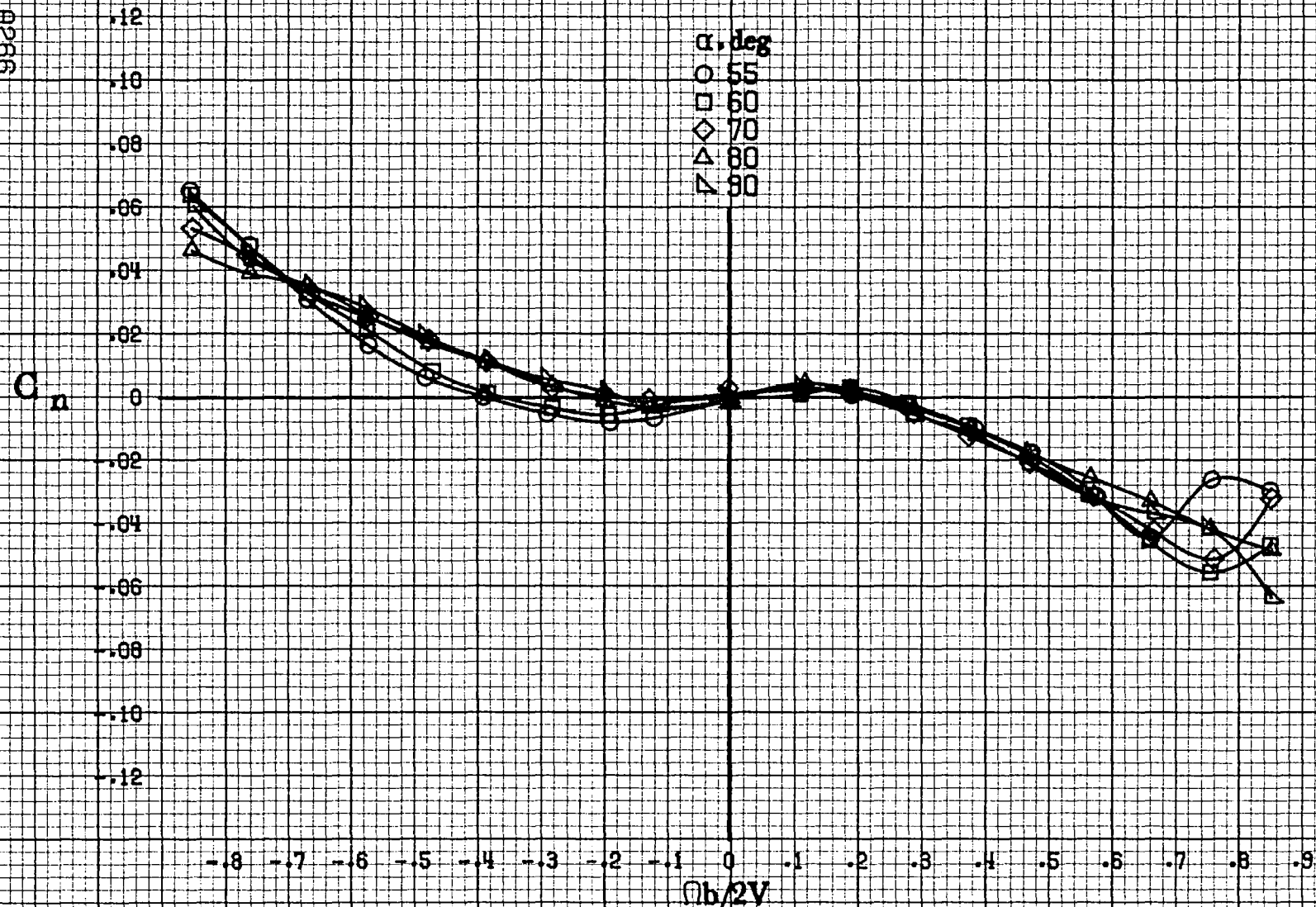
(b) $\alpha = 55$ to 90° , $SR = 0$.
Figure A71.-Concluded.





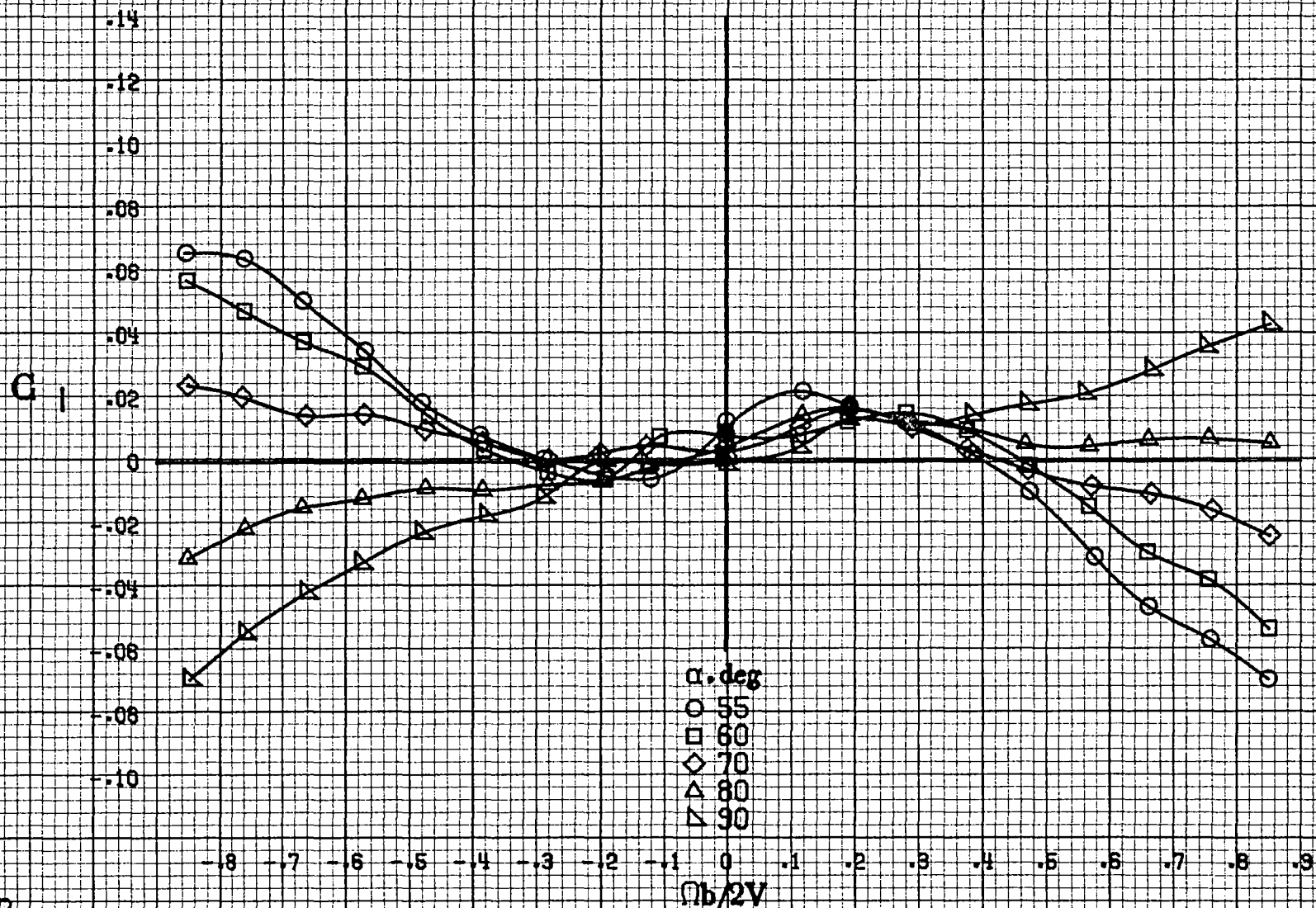
(b) $\alpha = 55$ to 90 deg, $SR = 0$,
Figure A72.-Concluded,

R2265



$\alpha = 55$ to 90 deg, $SR = 0$.

Figure A73.-Effect of rotation rate and angle of attack on yawing-moment coefficient for configuration having rounded fuselage bottom aft of engine cowlings and wing fairings removed. $\delta_e = 0^\circ$, $\delta_a = 0^\circ$, $\delta_r = 0^\circ$, $\beta = 0^\circ$.



$\alpha = 55$ to 90° , $SR = 0$.

Figure A74. Effect of rotation rate and angle of attack on rolling-moment coefficient for configuration having rounded fuselage bottom aft of engine cowl and wing fairings removed. $\delta_s = 0^\circ$, $\delta_a = 0^\circ$, $\delta_r = 0^\circ$, $\beta = 0^\circ$.

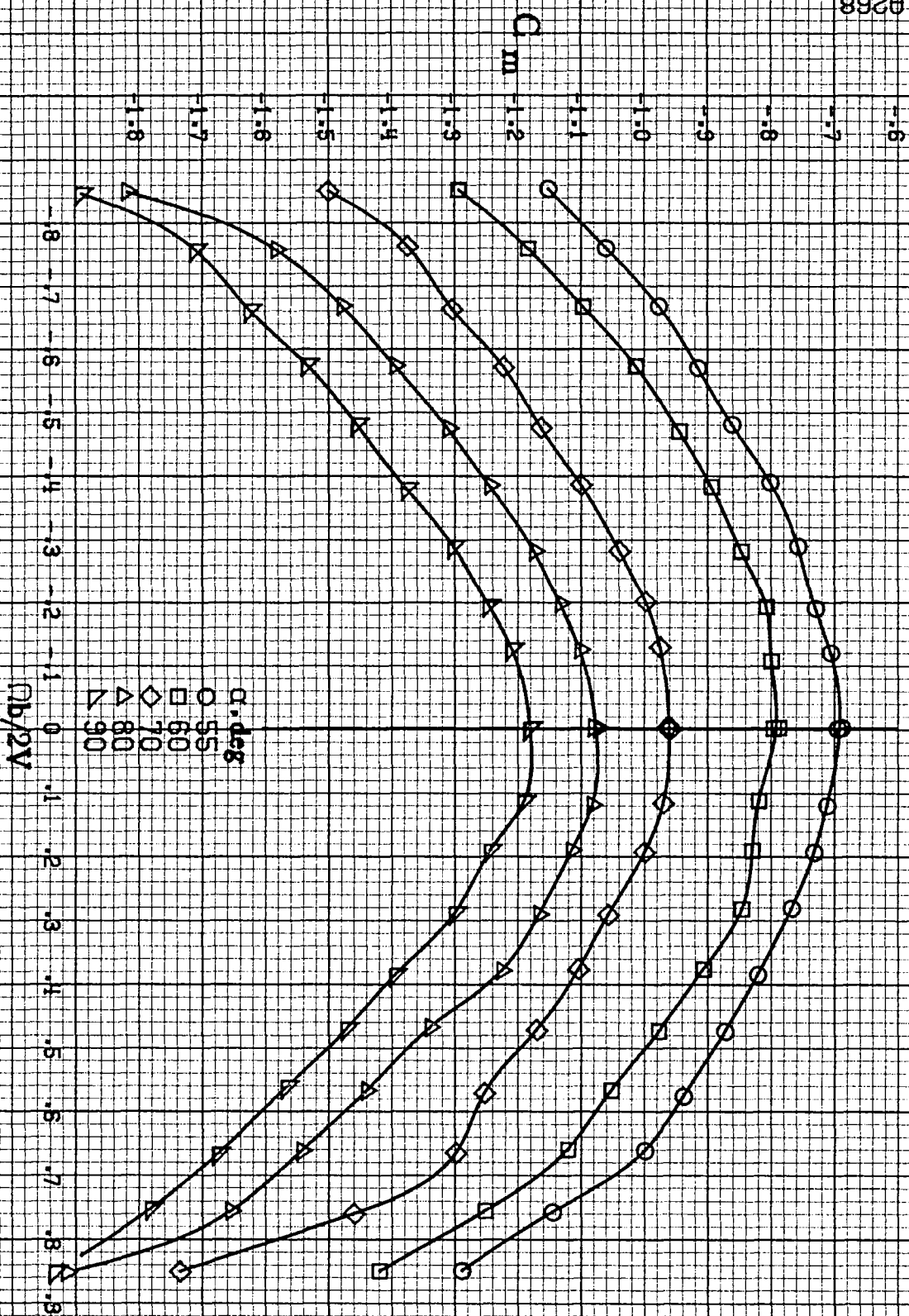
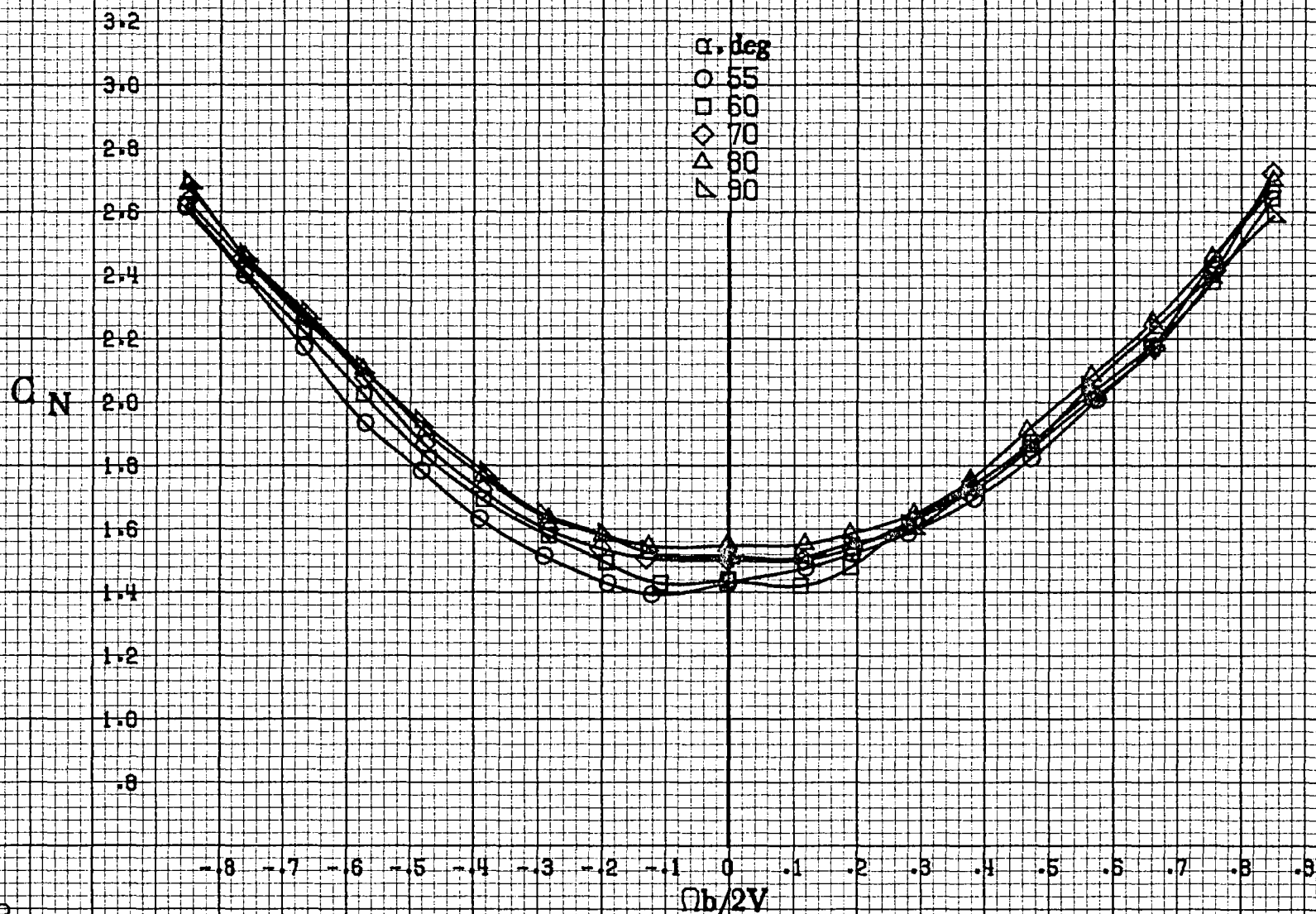


Figure A75.-Effect of rotation rate and angle of attack on pitching-moment coefficient for configuration having rounded fuselage bottom aft of engine cowl and wing fairings removed. $\alpha = 55$ to 90° , $SR = 0$.



$\alpha = 55$ to 90° , $SR = 0$.

Figure A76. Effect of rotation rate and angle of attack on normal-force coefficient for configuration having rounded fuselage bottom aft of engine cowl and wing fairings removed. $\delta_e = 0^\circ$, $\delta_a = 0^\circ$, $\delta_r = 0^\circ$, $\beta = 0^\circ$.

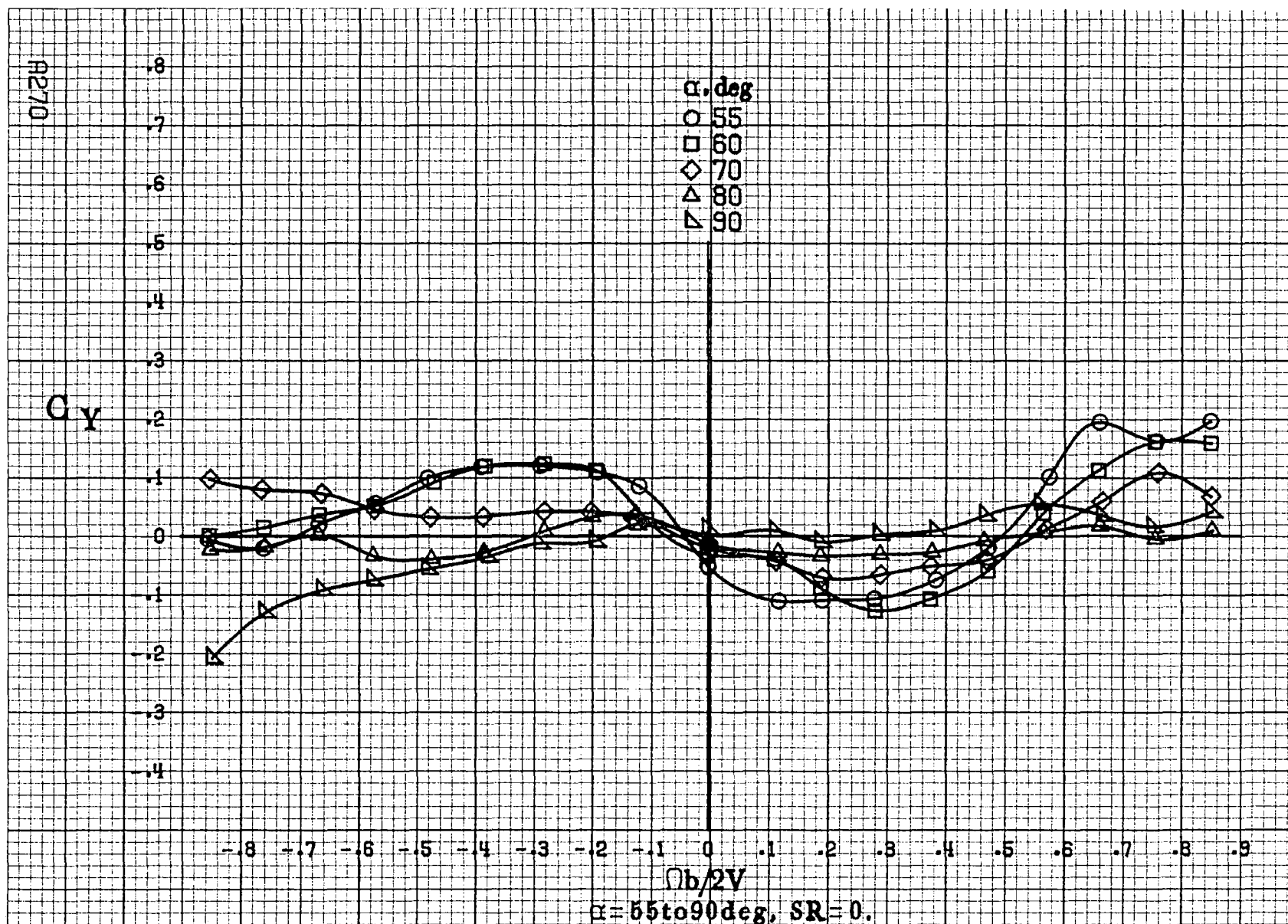
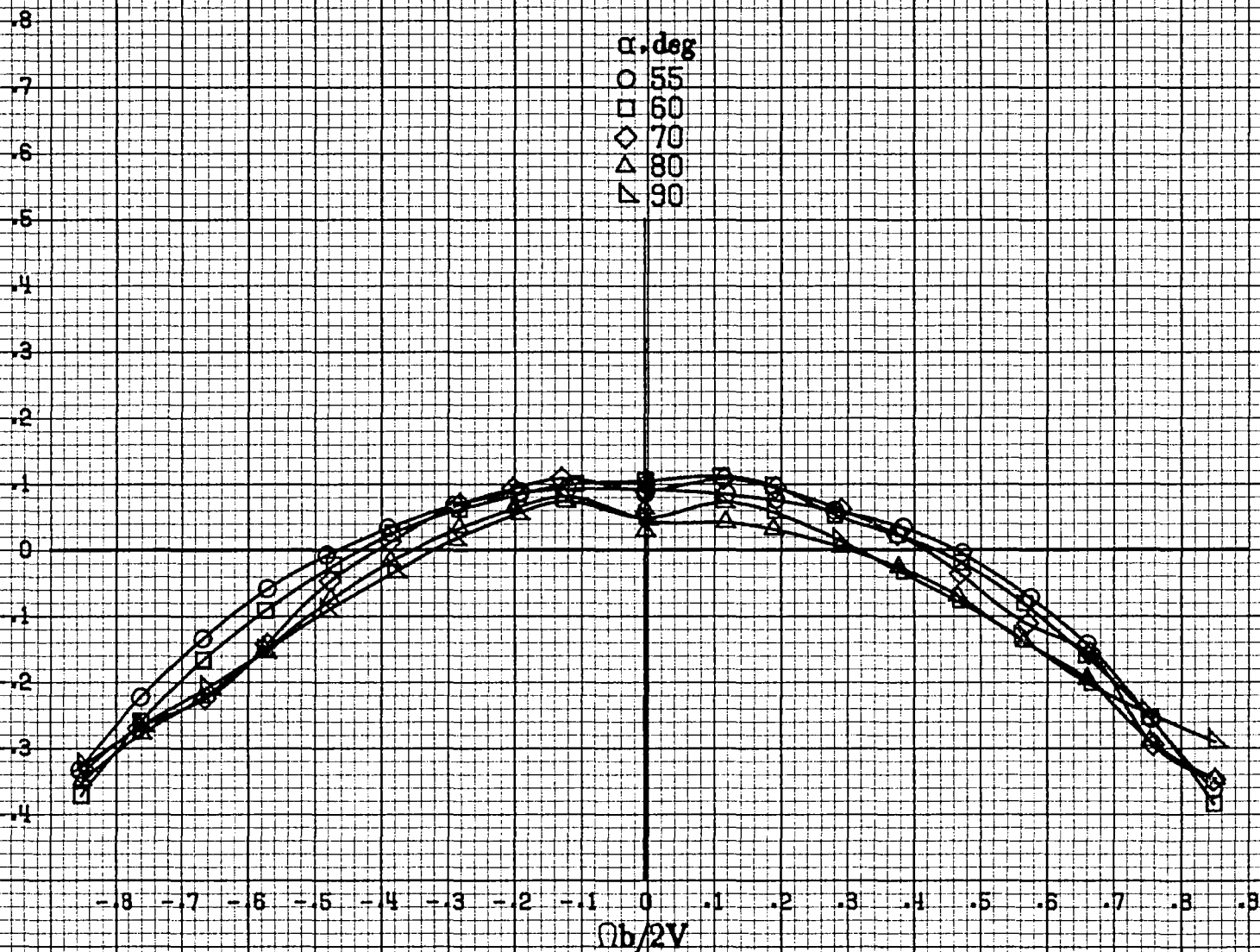


Figure A77.-Effect of rotation rate and angle of attack on side-force coefficient for configuration having rounded fuselage bottom aft of engine cowlings and wing fairings removed. $\delta_s = 0^\circ$, $\delta_a = 0^\circ$, $\delta_r = 0^\circ$, $\beta = 0^\circ$.

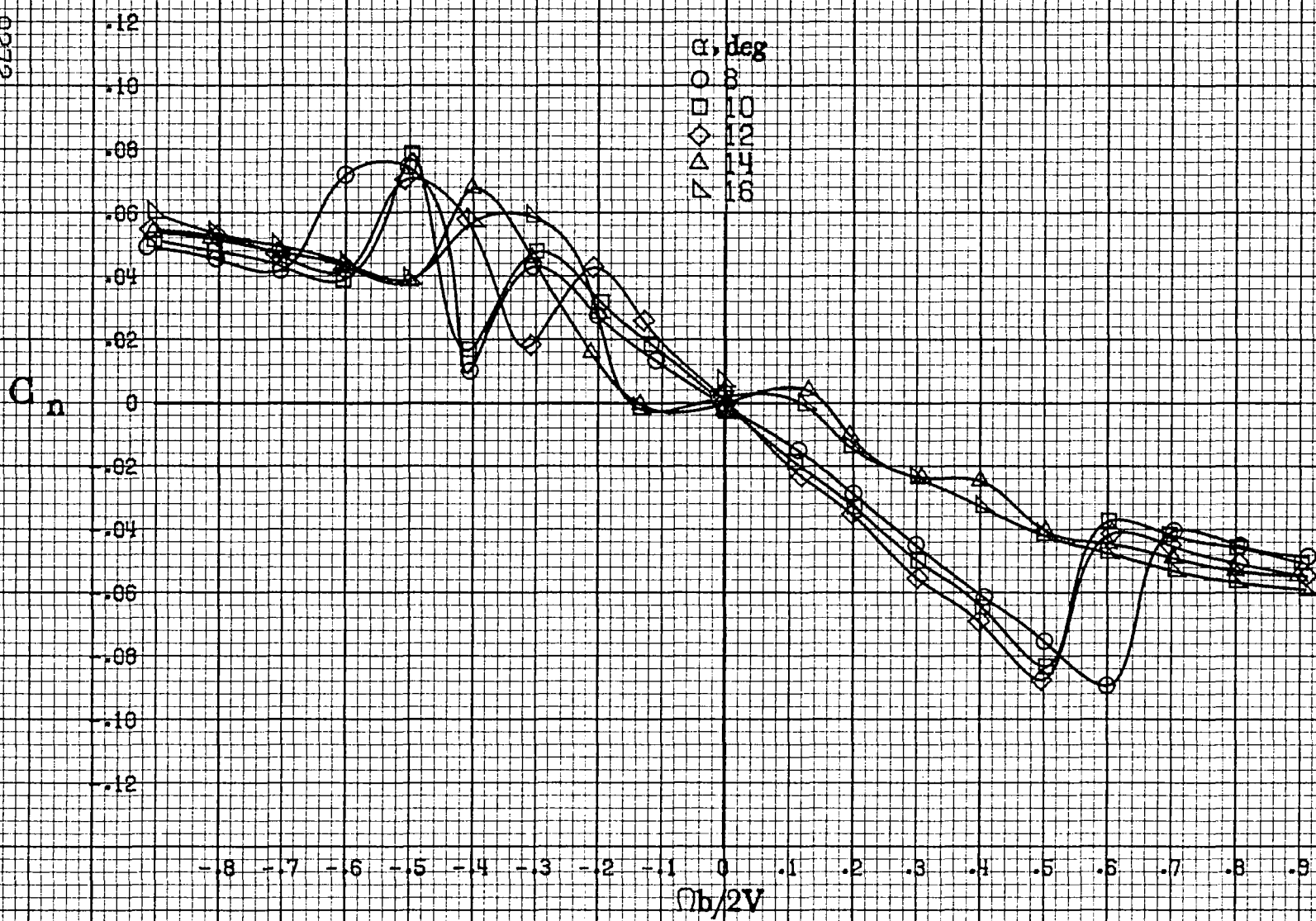
C_A



$\alpha=55\text{to}90\text{deg}, SR=0.$

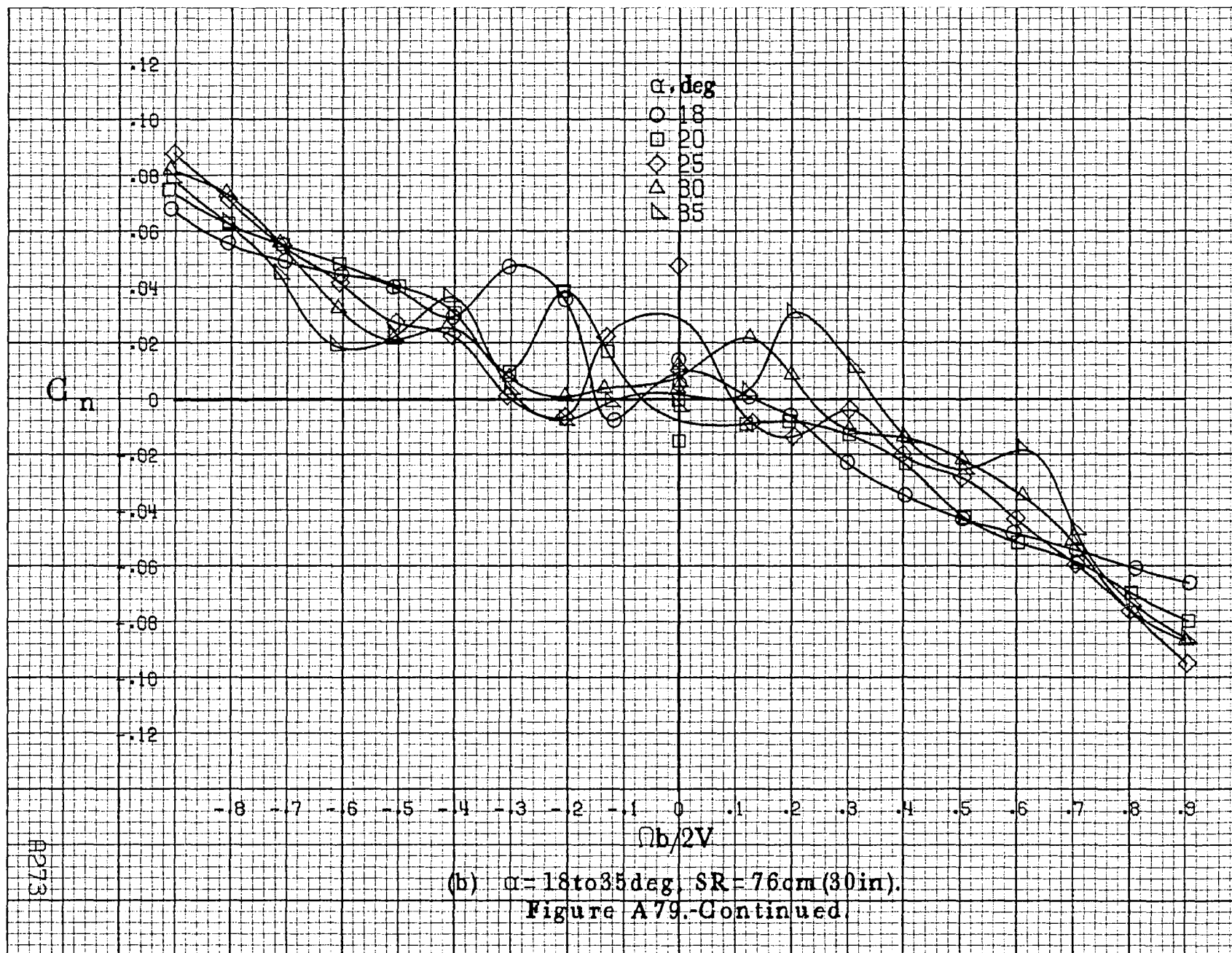
Figure A78.-Effect of rotation rate and angle of attack on axial-force coefficient for configuration having rounded fuselage bottom aft of engine cowl and wing fairings removed. $\delta_s=0^\circ$, $\delta_a=0^\circ$, $\delta_r=0^\circ$, $\beta=0^\circ$.

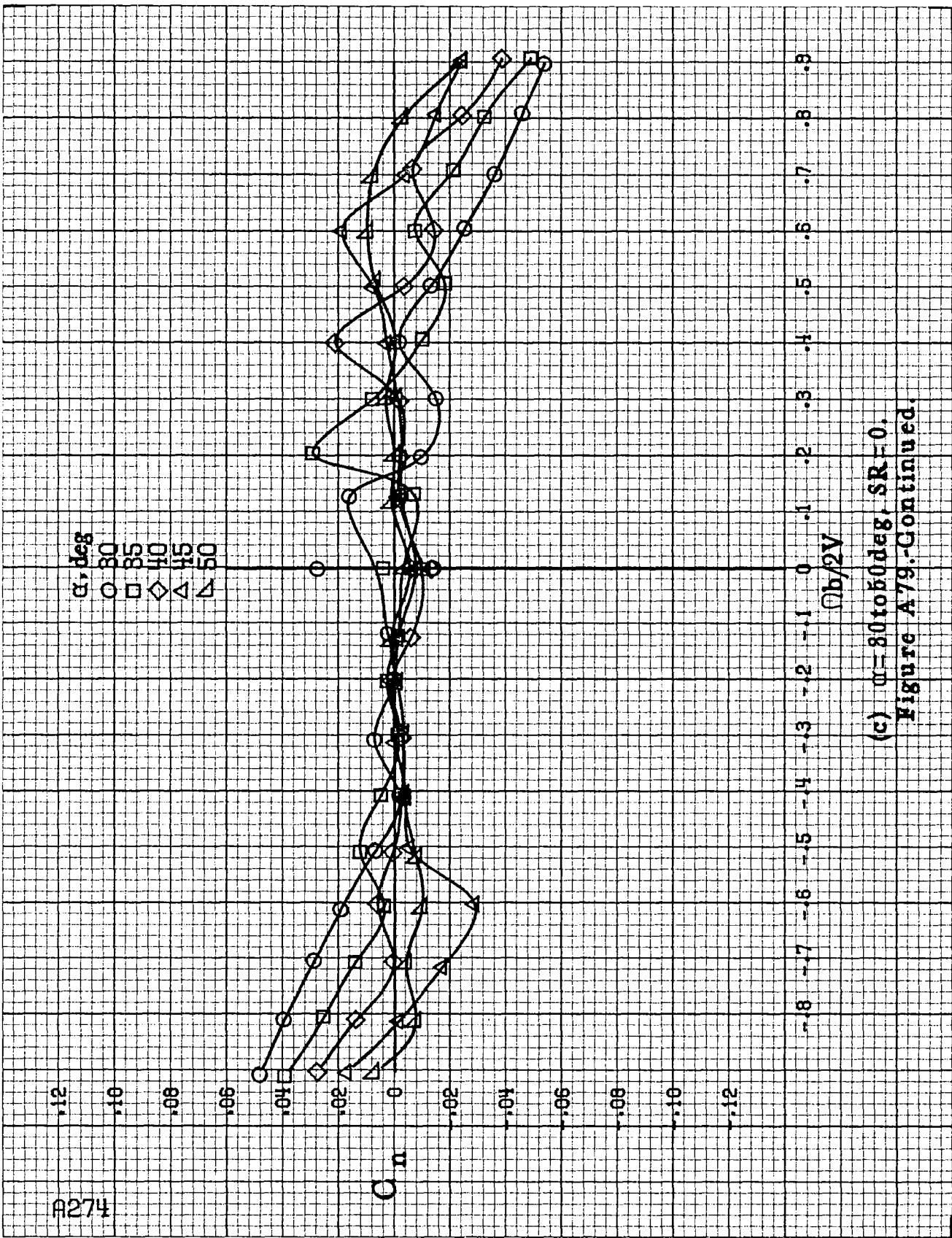
A272



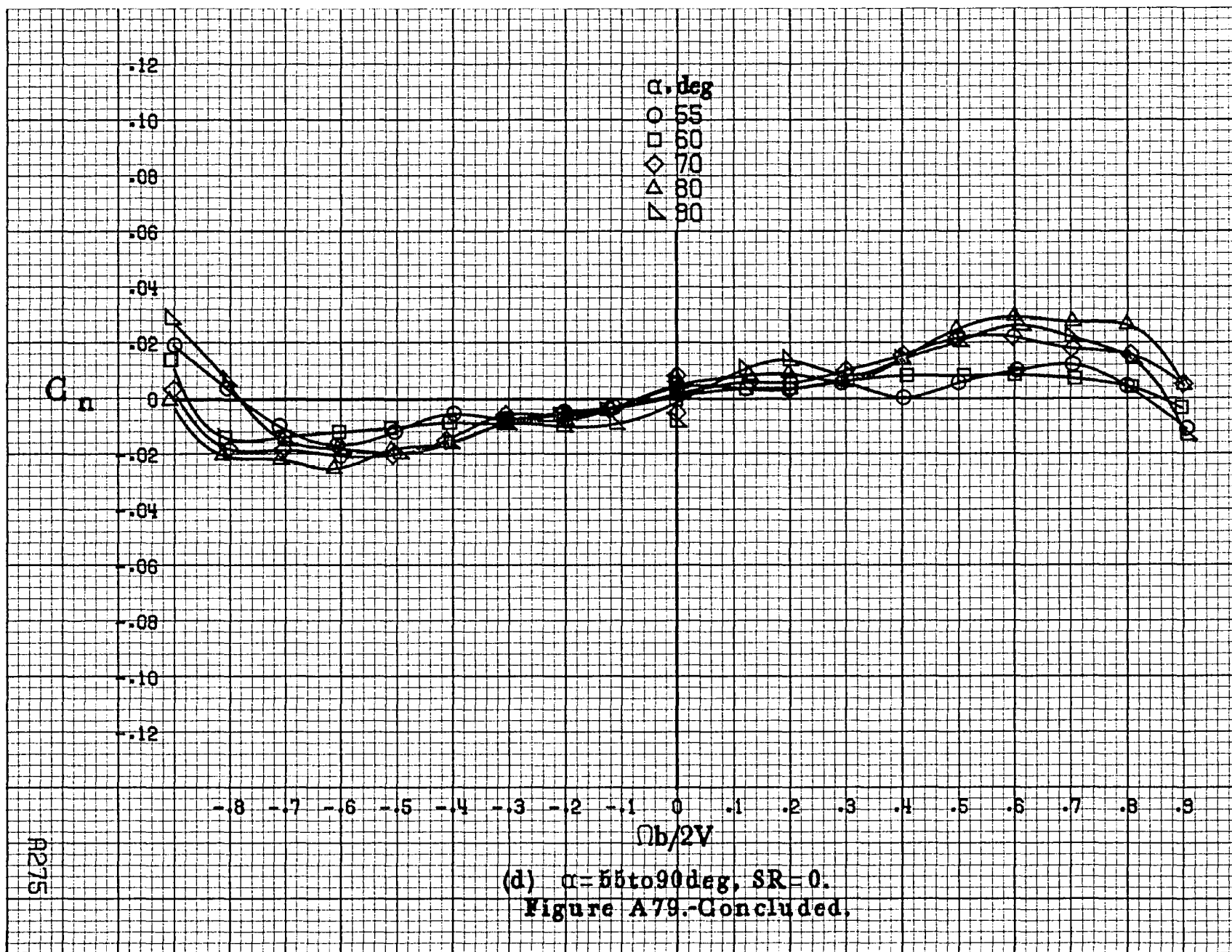
(a) $\alpha = 8$ to 16° , $SR = 76\text{cm (30in)}$.

Figure A79.-Effect of rotation rate and angle of attack on yawing-moment coefficient for configuration having full-span LE wing droop. $\delta_e = 0^\circ$, $\delta_a = 0^\circ$, $\delta_r = 0^\circ$, $\beta = 0^\circ$.

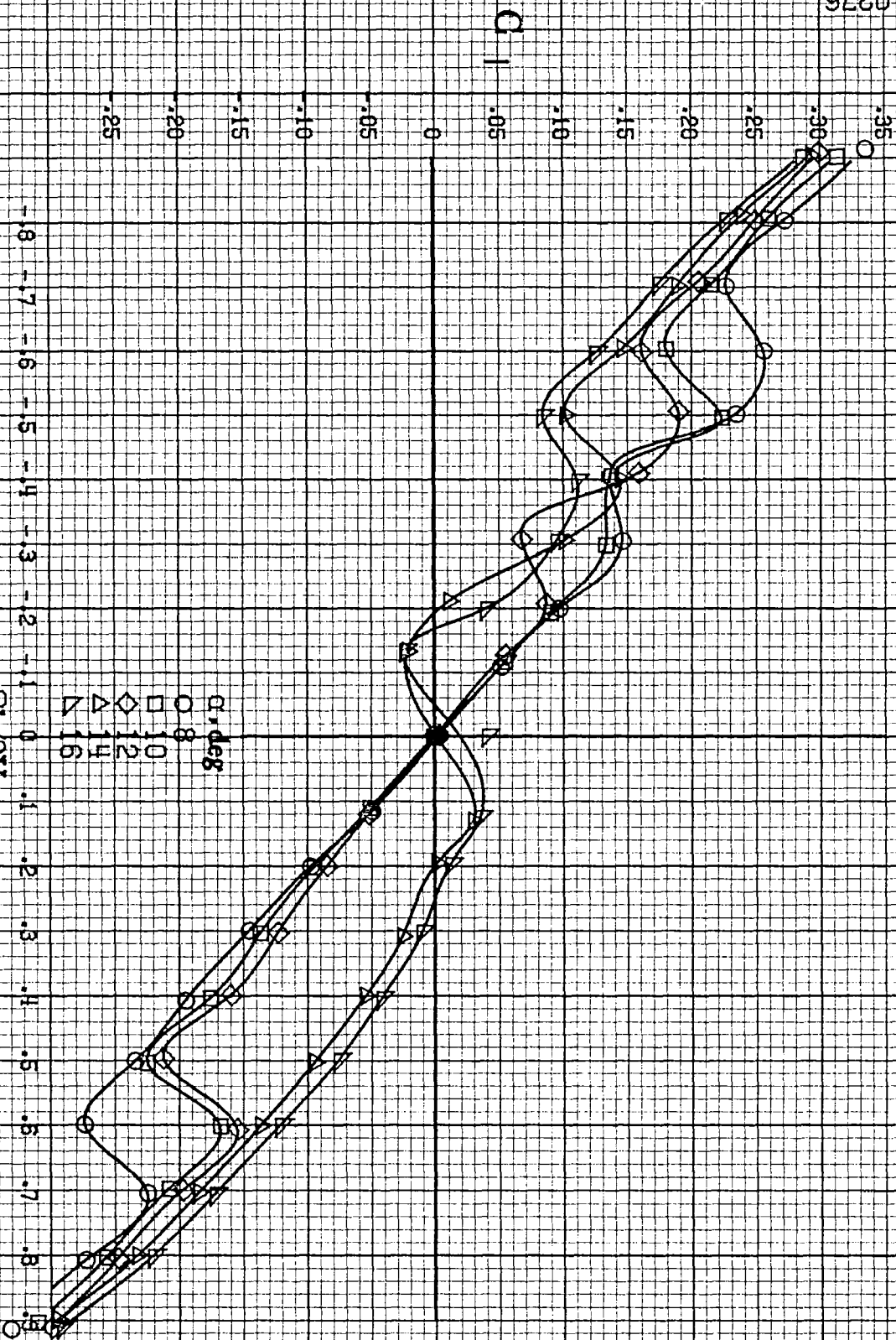




(c) $\alpha=30$ to 50 deg, $SR=0$.
 Figure A79.-Continued.

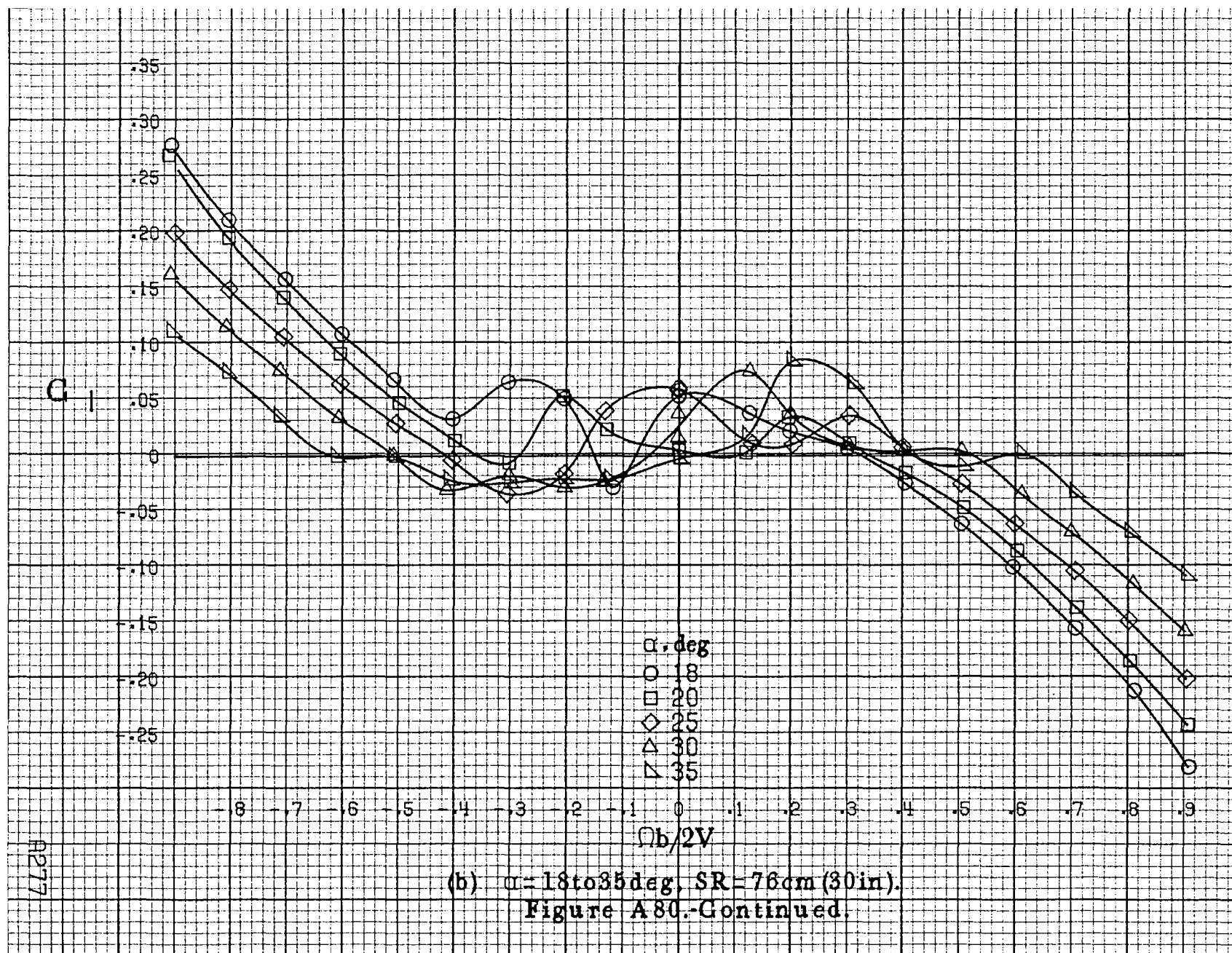


A276



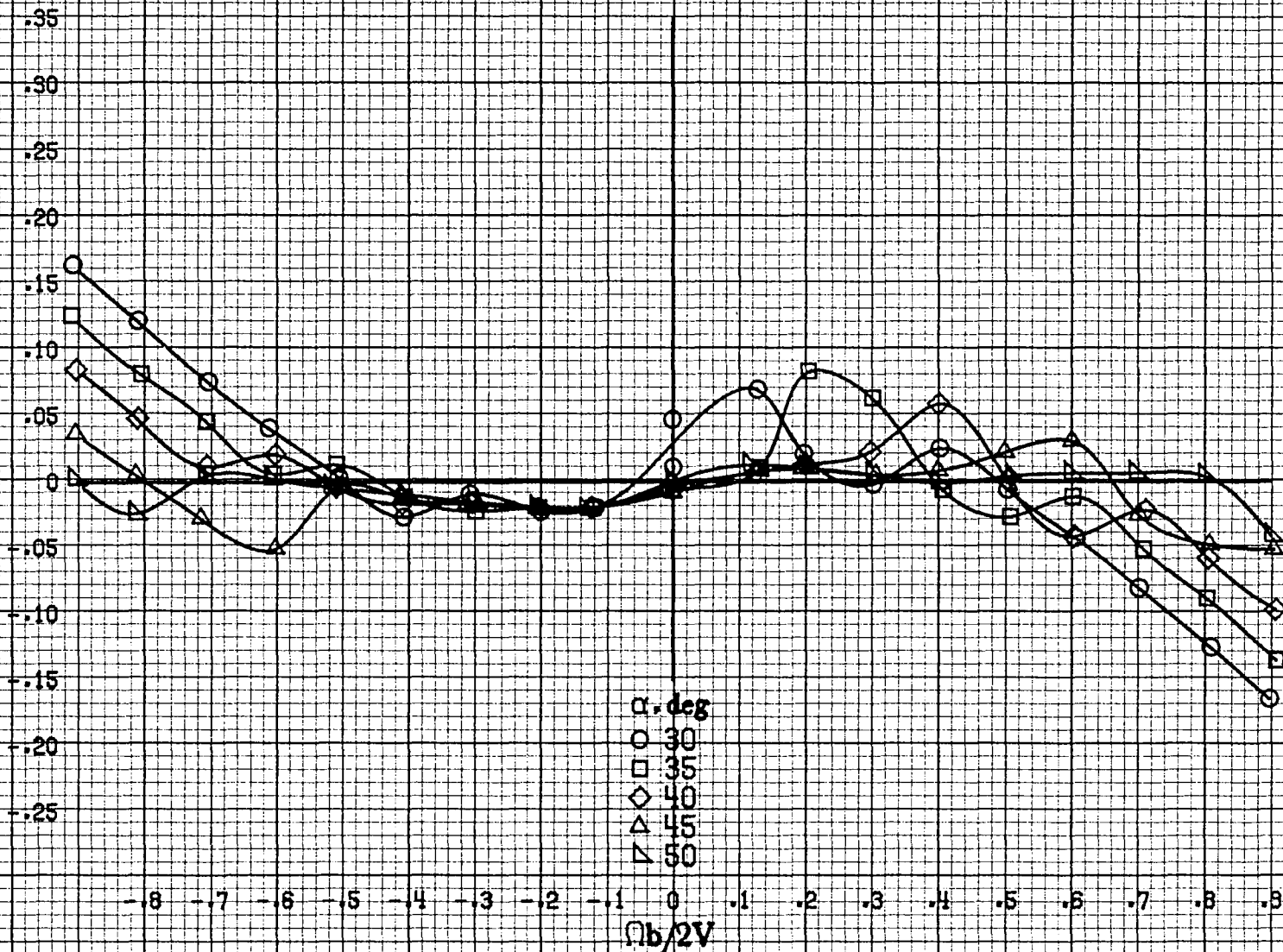
(a) $\omega = 840.16 \text{ deg}$, $SR = 76 \text{ cm (30 in)}$.

Figure A80. Effect of rotation rate and angle of attack on rolling-moment coefficient for configuration having full-span LE wing droop. $\delta_r = 0^\circ$, $\delta_a = 0^\circ$.

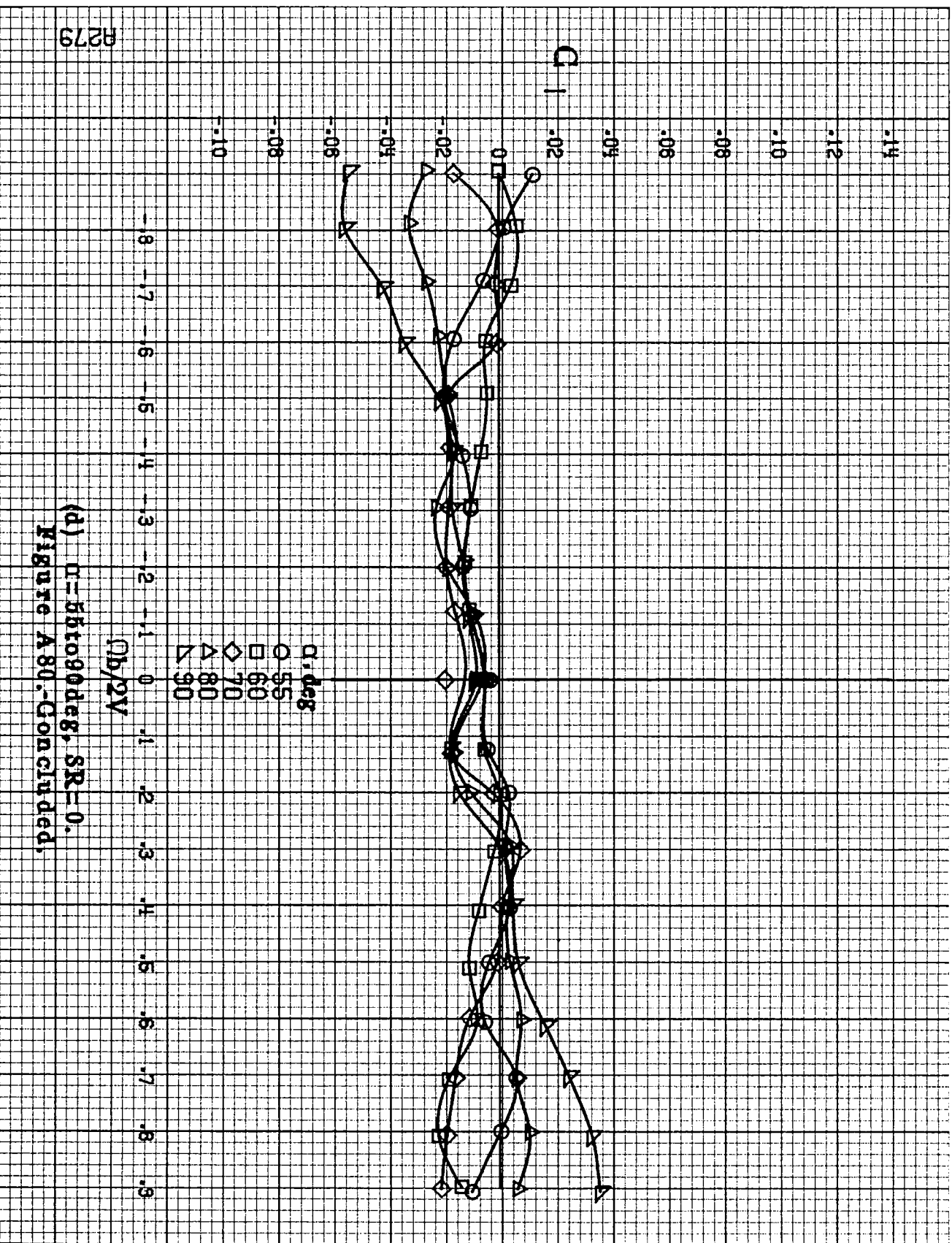


A278

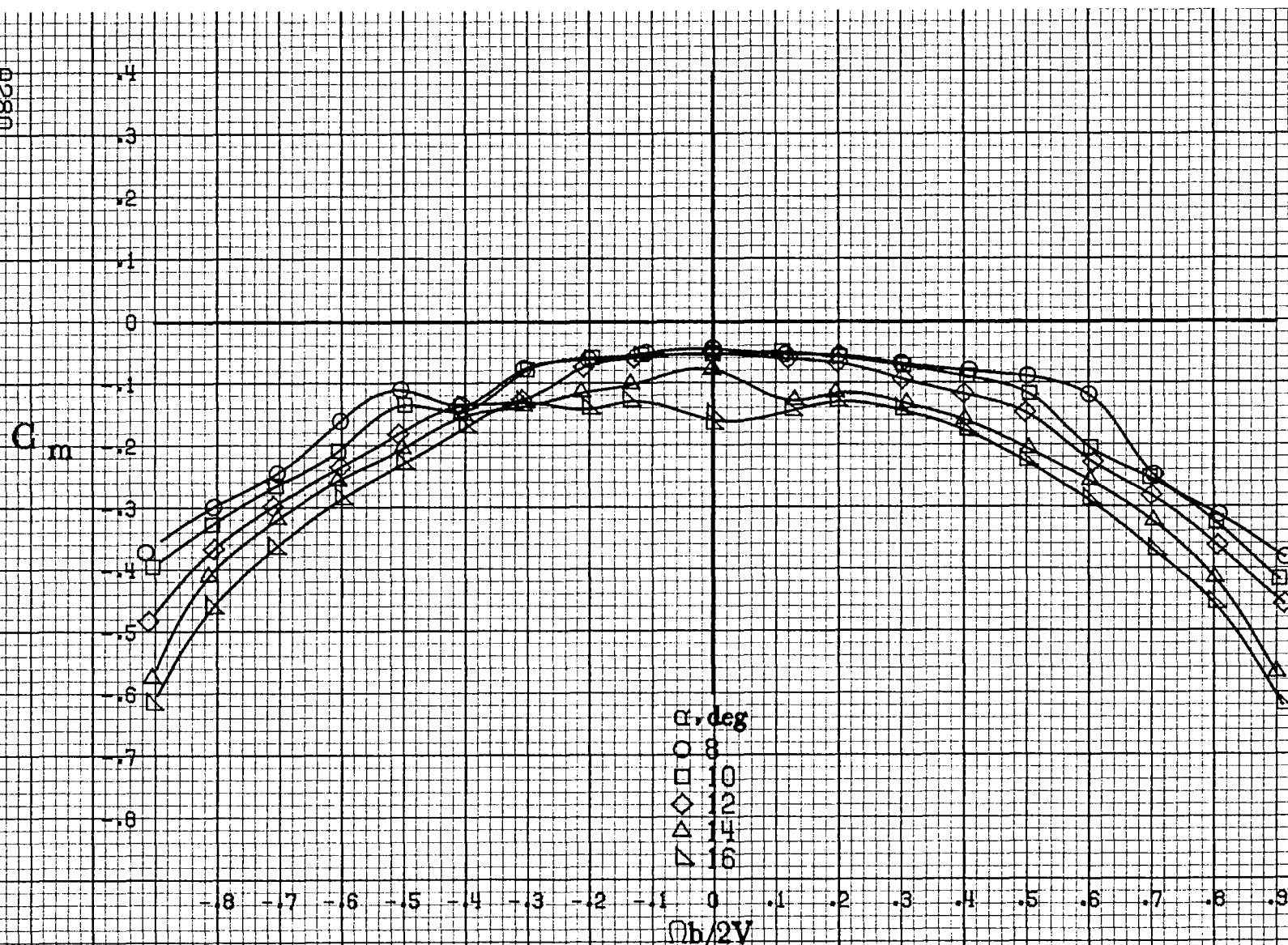
C_1



(c) $\alpha = 30$ to 50° , $SR = 0$.
Figure A80.-Continued.

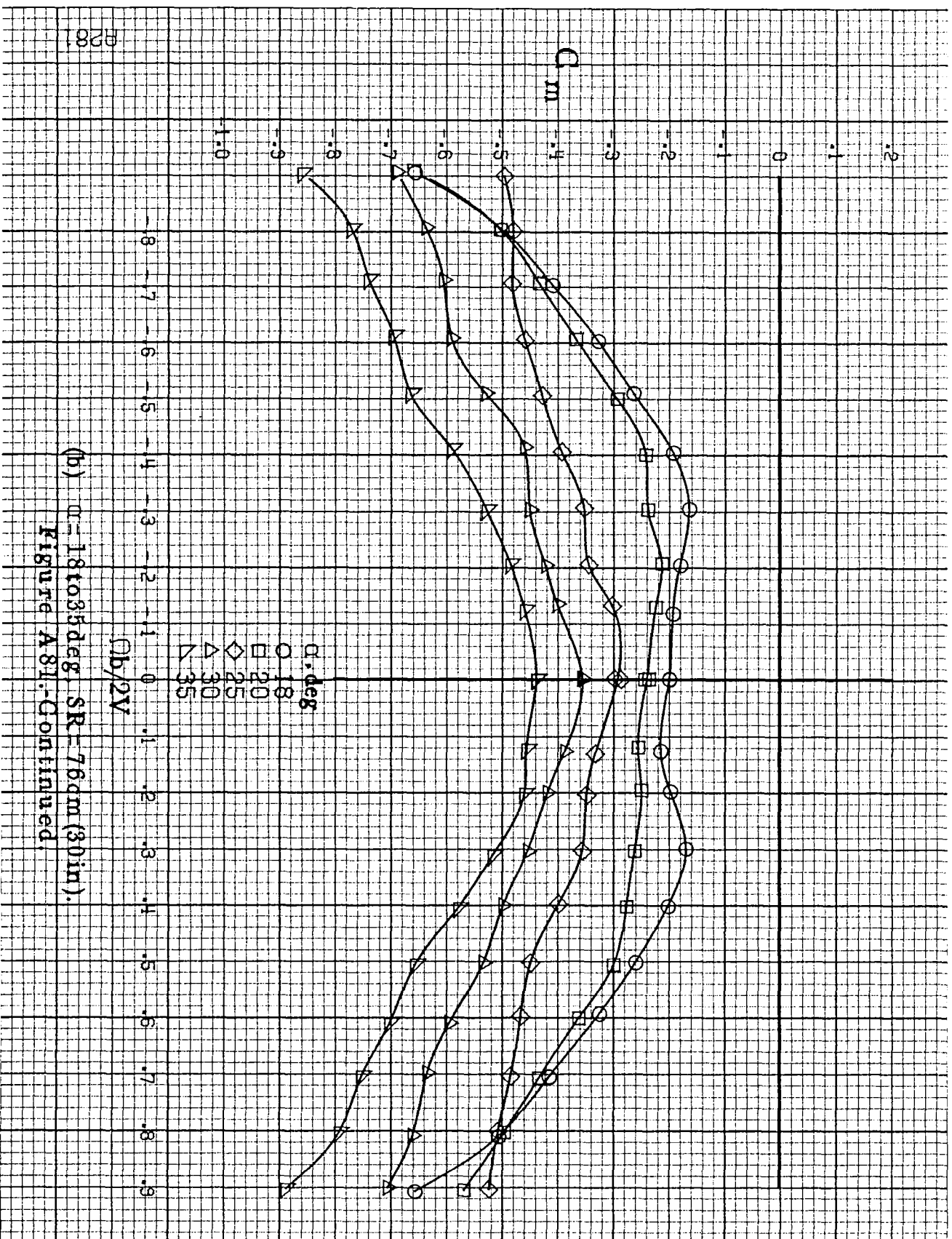


(d) $\alpha = 55$ to 90 deg, $SR = 0$.
Figure A80.-Concluded.



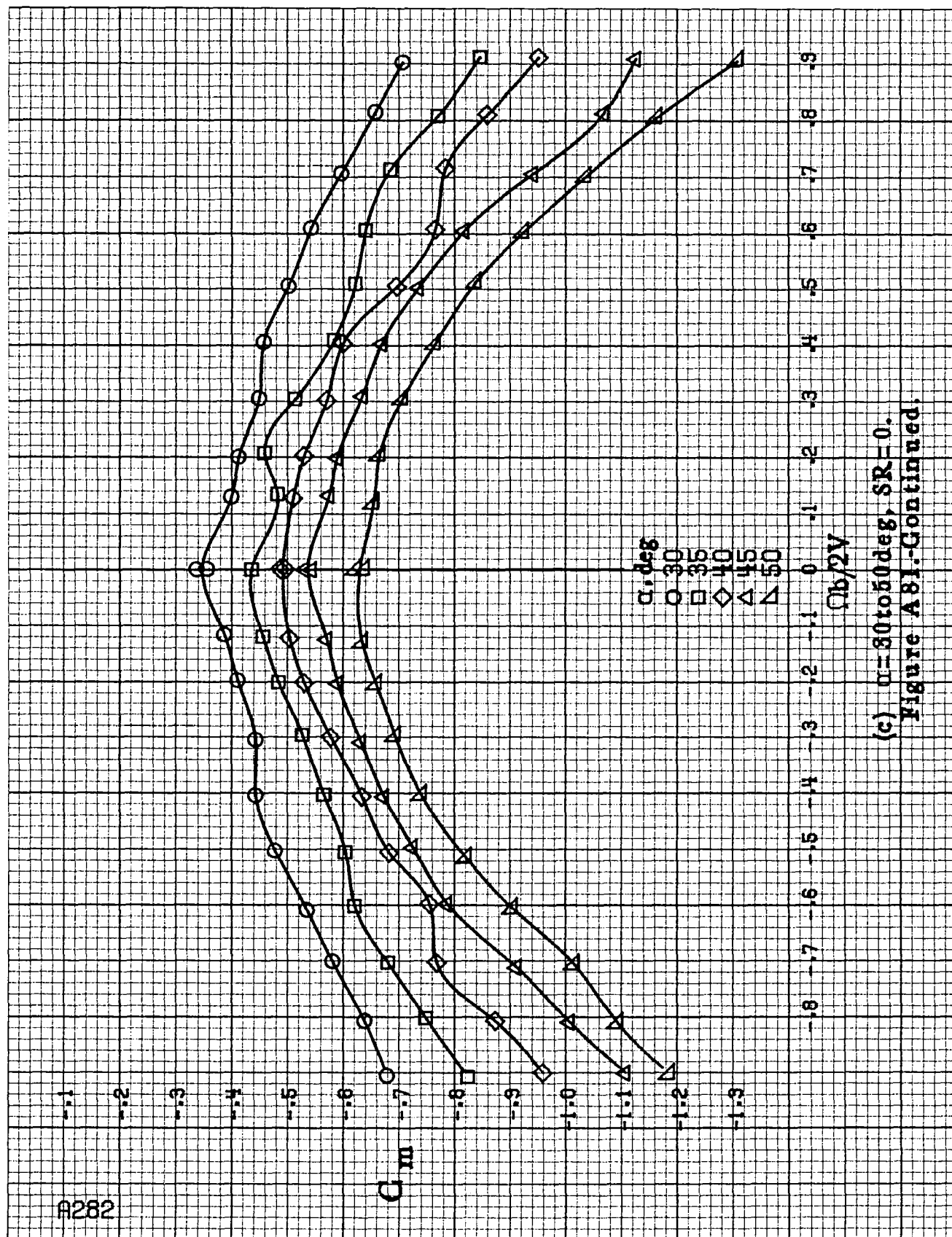
(a) $\alpha = 8$ to 16° , $SR = 76\text{ cm (30 in.)}$.

Figure A81. Effect of rotation rate and angle of attack on pitching moment coefficient for configuration having full-span LE wing droop. $\delta_e = 0^\circ$, $\delta_a = 0^\circ$, $\delta_r = 0^\circ$, $\beta = 0^\circ$.

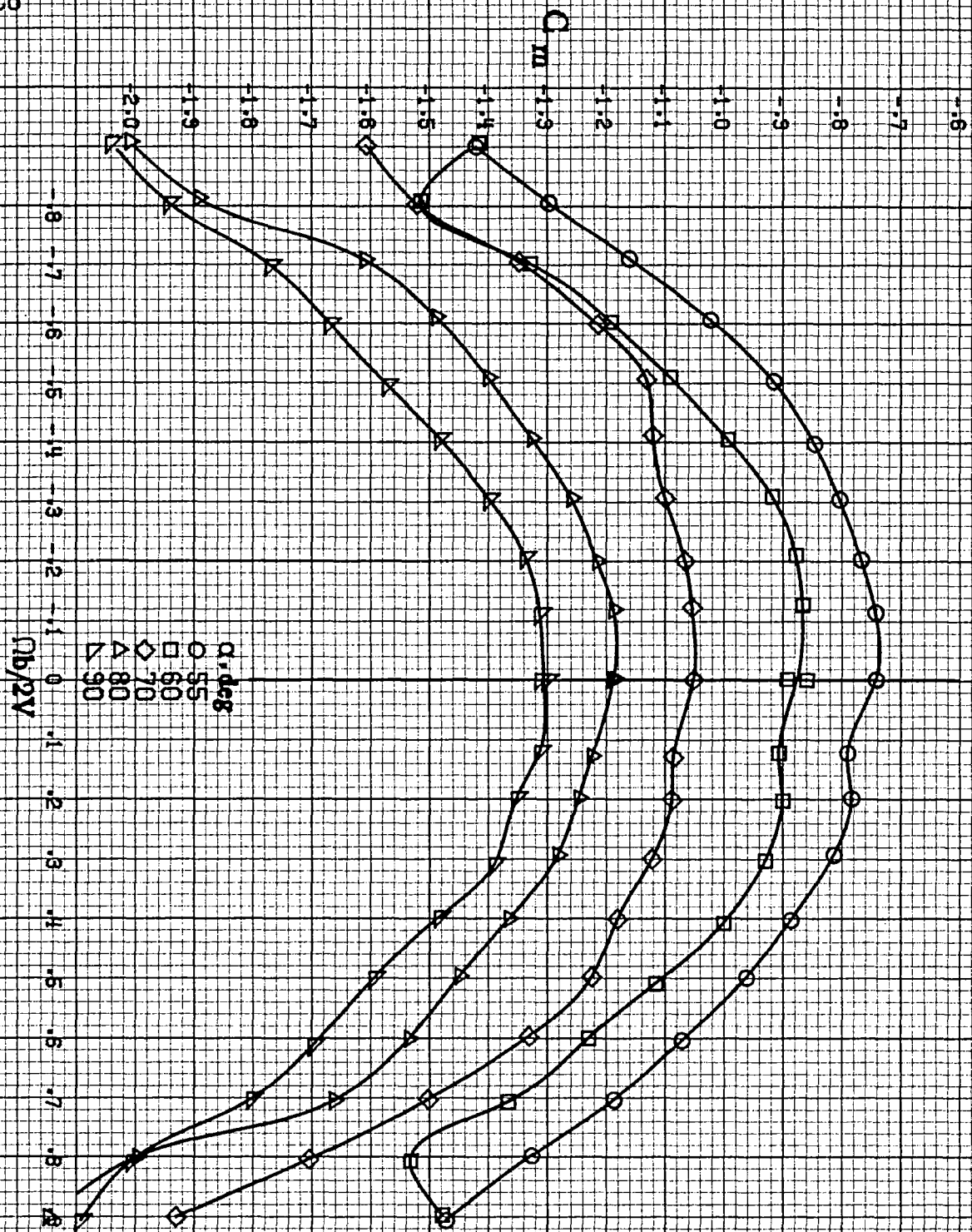


(b) $\omega = 181035 \text{ deg}$ SR = 76 cm (30 in).
 Figure A81-Continued.

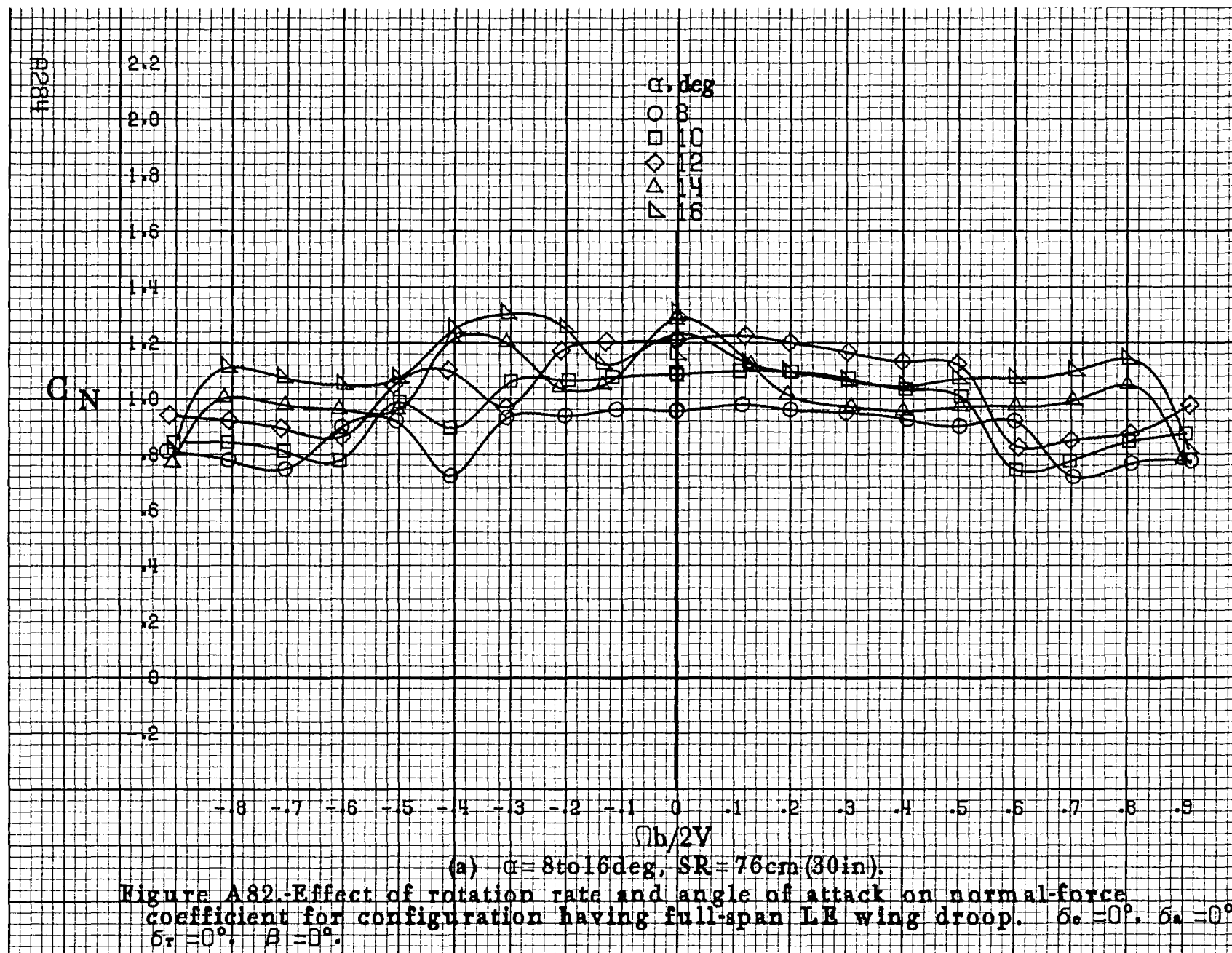
A282

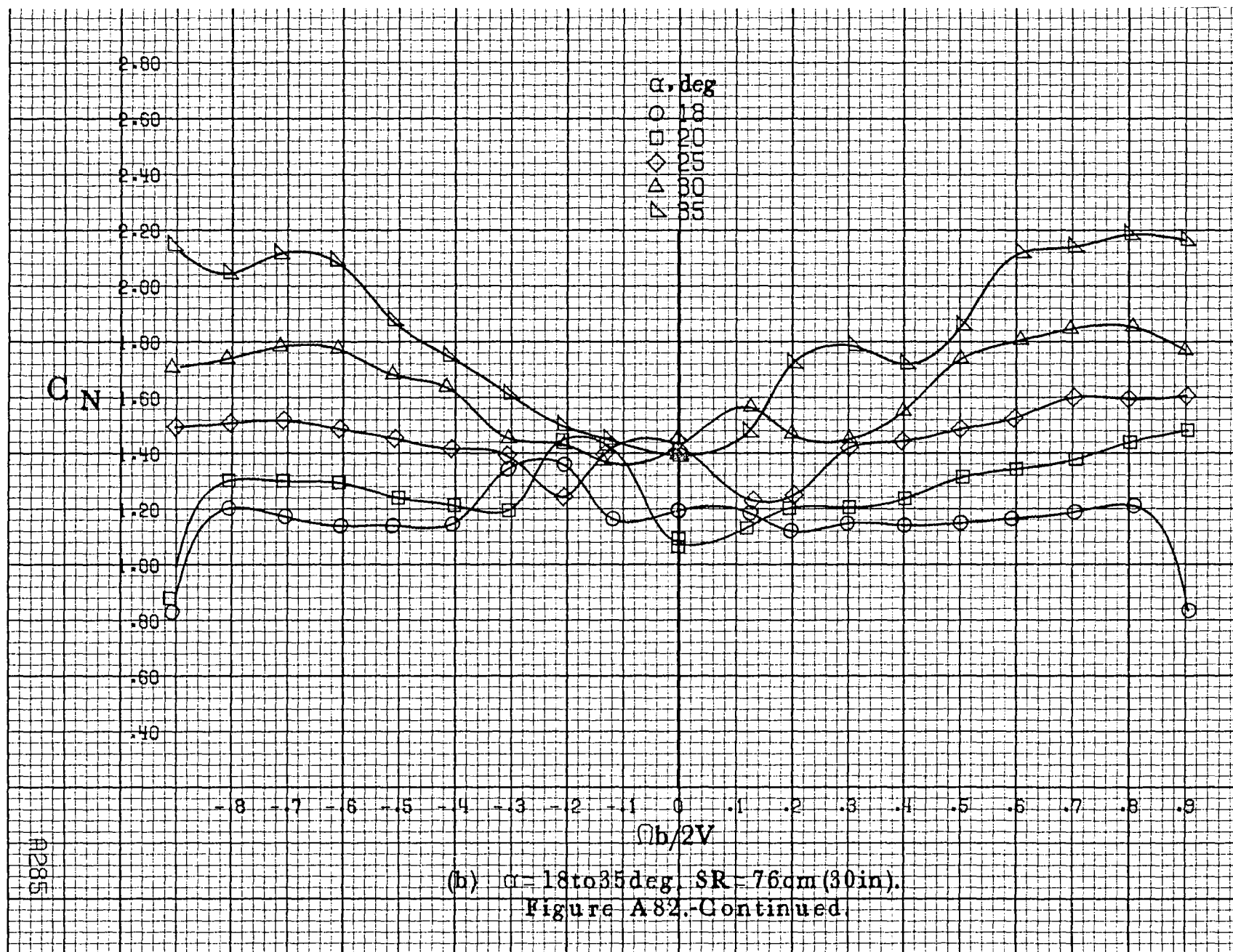


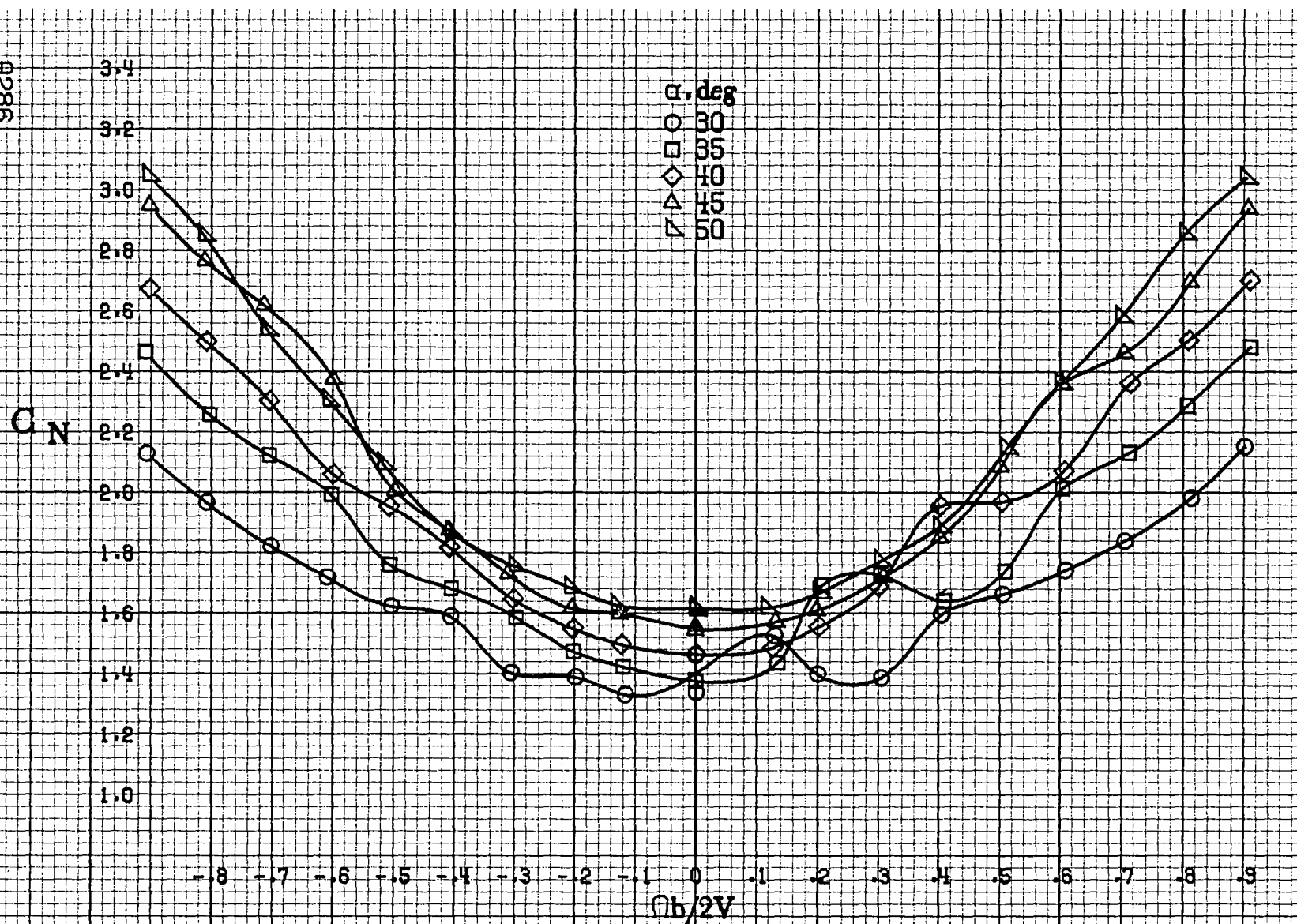
(c) $\alpha = 30$ to 50° , $SR = 0$.
Figure A81-Continued.



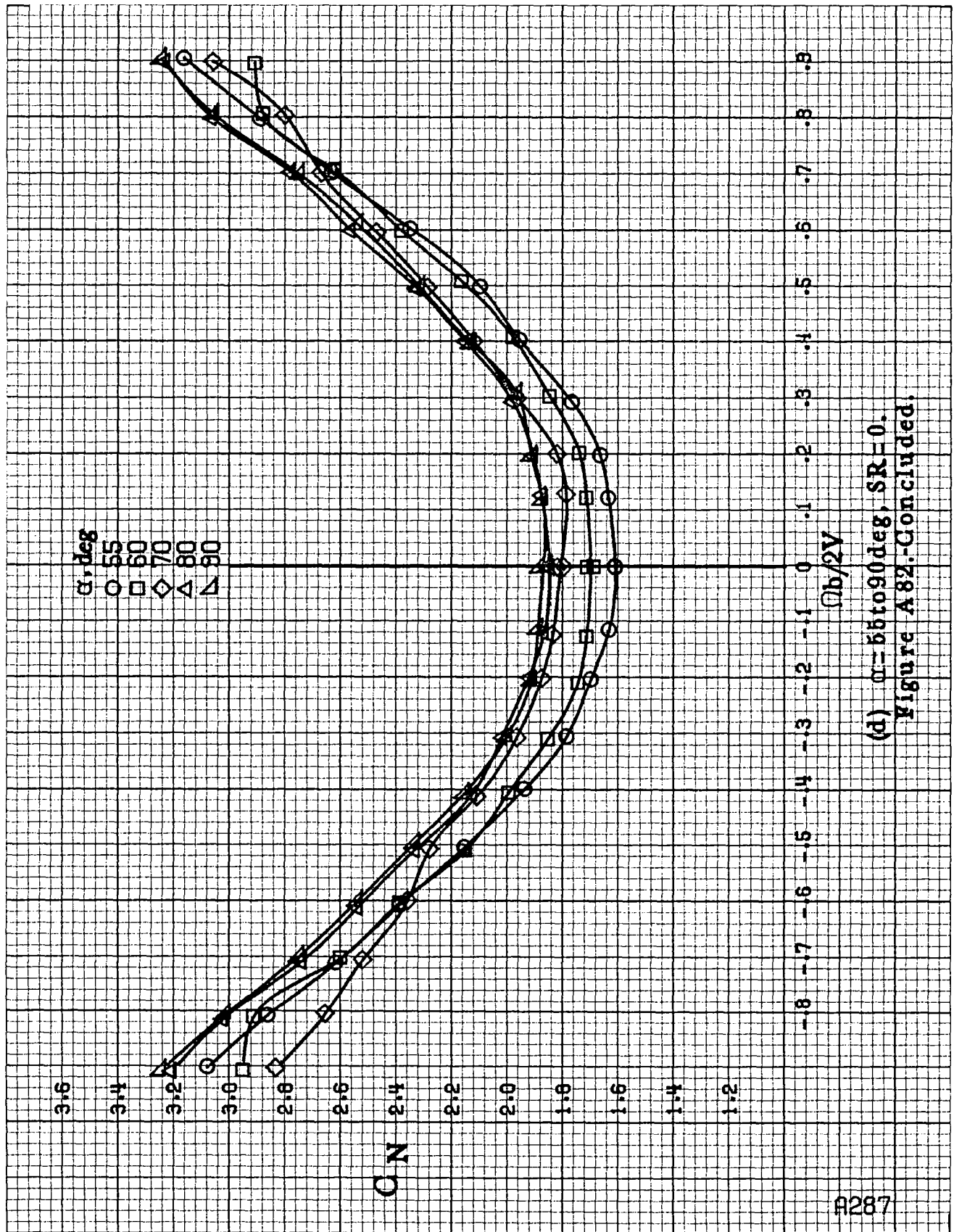
(d) $\alpha=55$ to 90° , $SR=0$.
Figure A81.-Concluded.



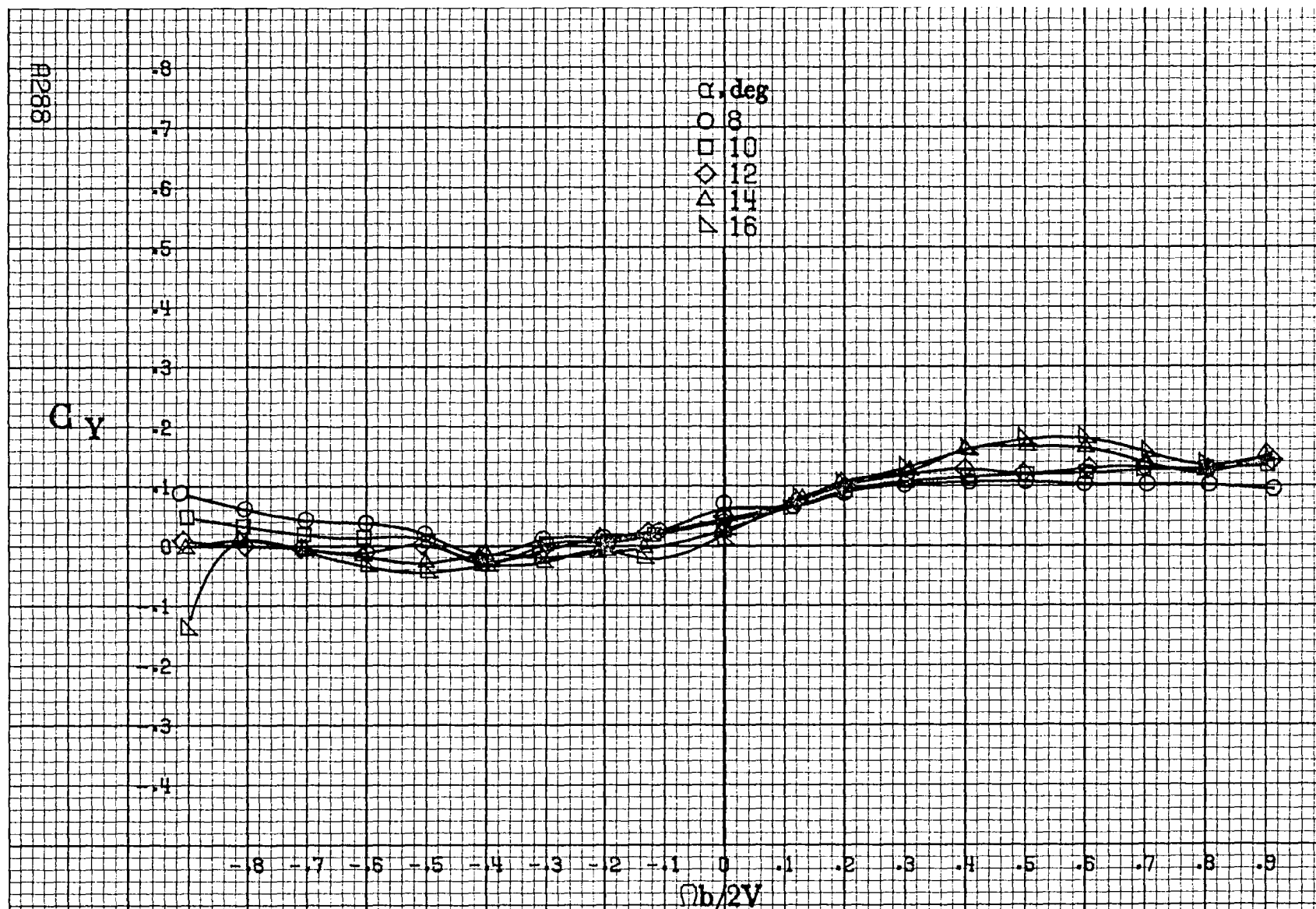




(c) $\alpha = 30$ to 50 deg, $SR = 0$.
Figure A82.-Continued.

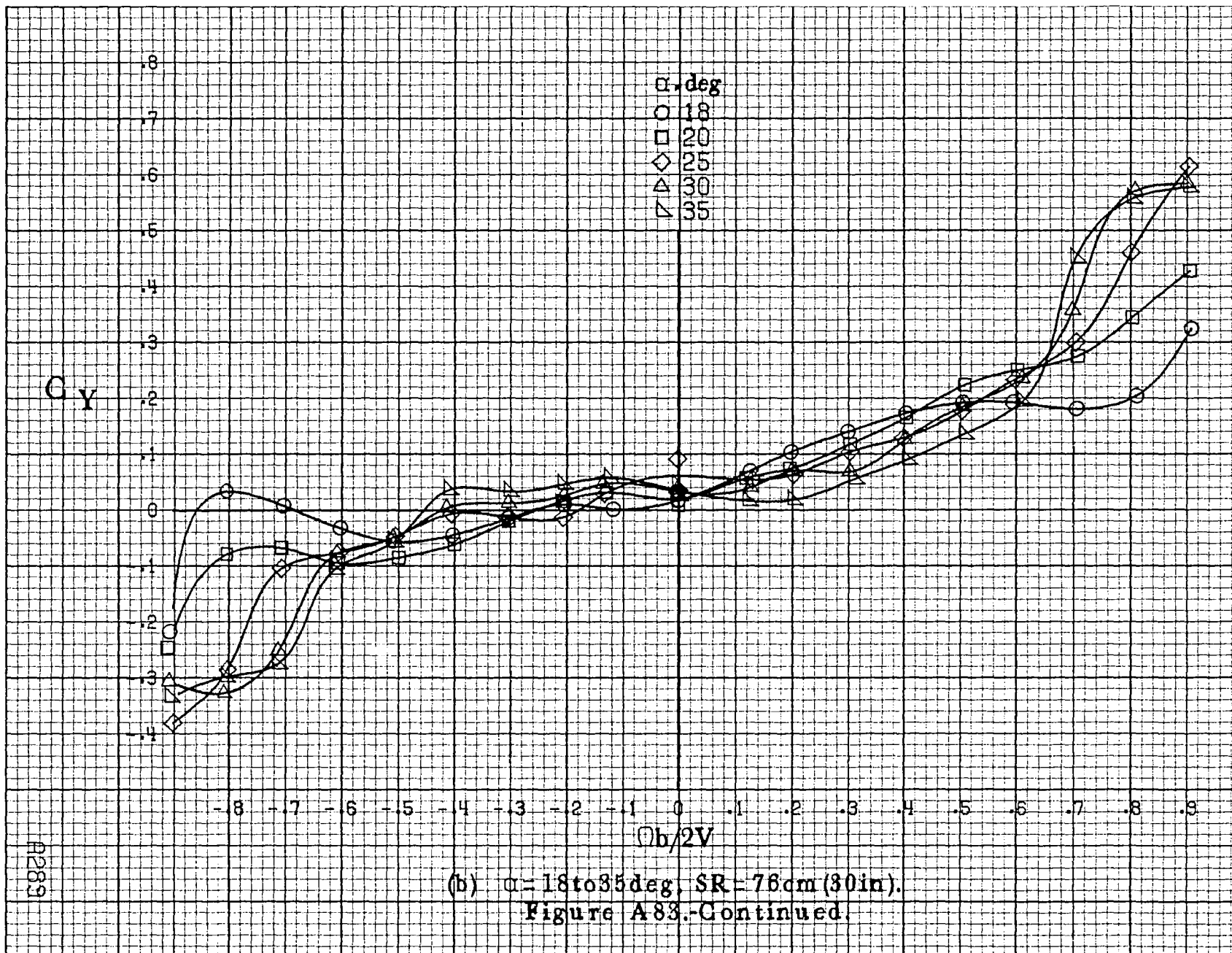


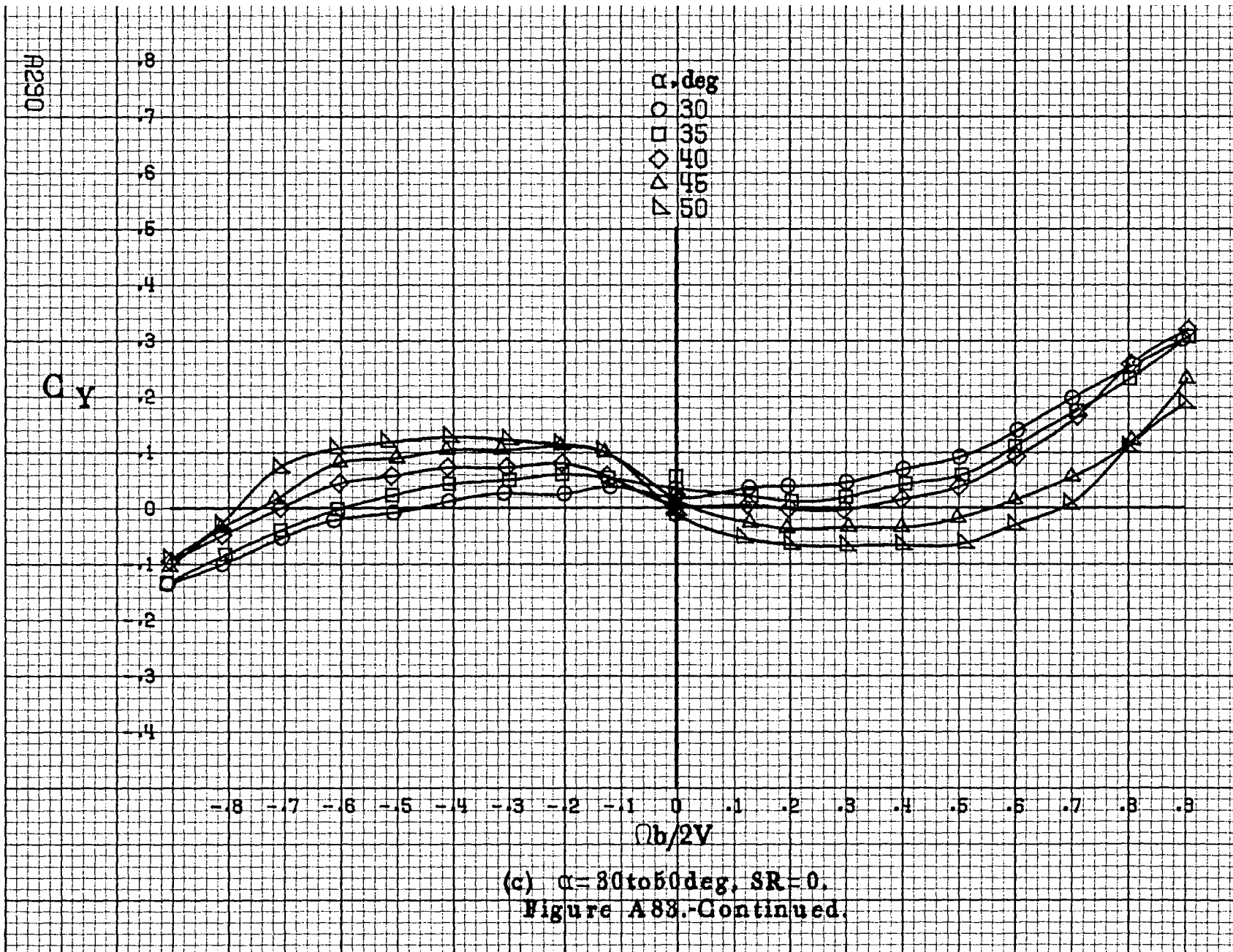
(d) $\alpha=55$ to 90 deg, $SR=0$.
Figure A82.-Concluded.

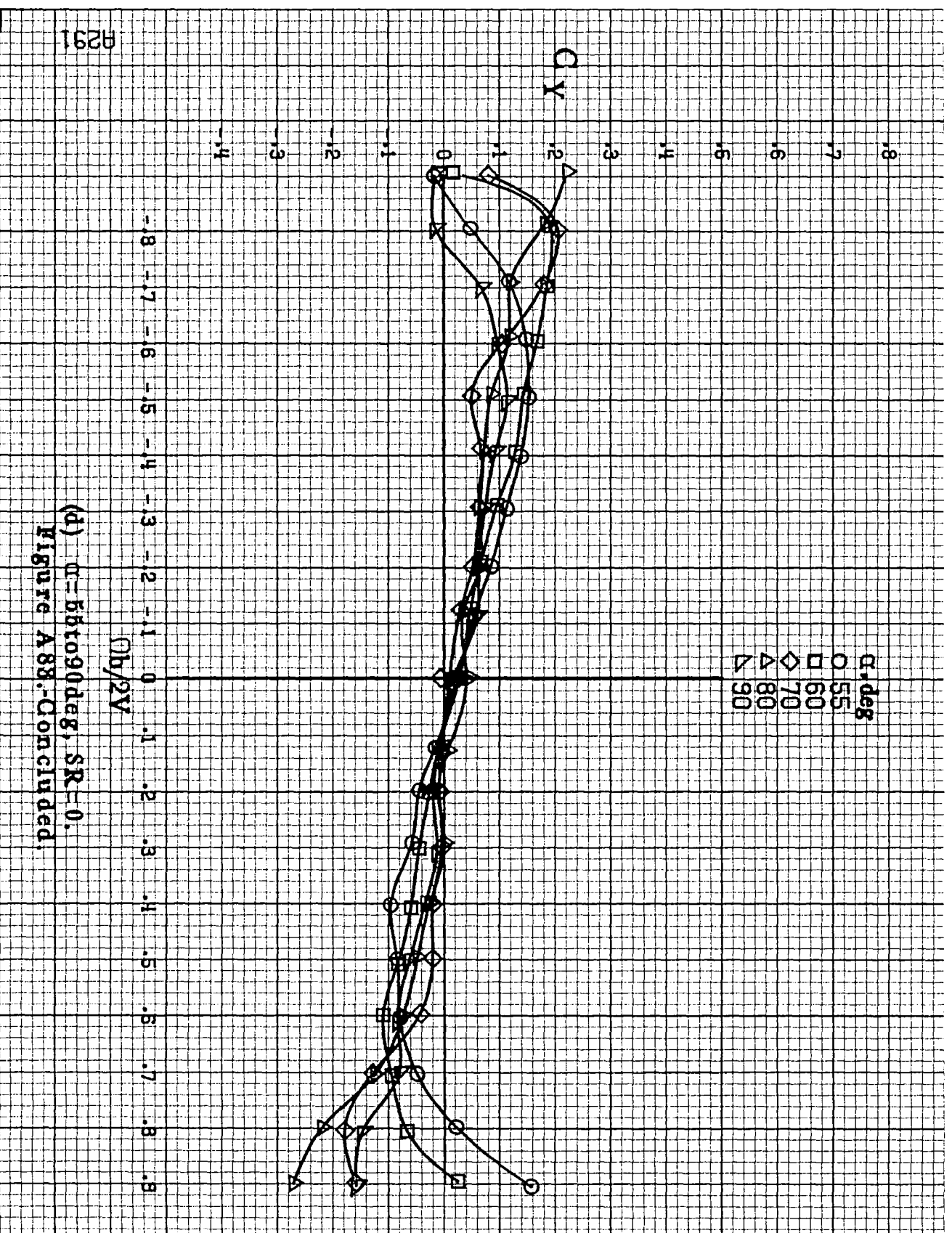


(a) $\alpha = 8$ to 16° , $SR = 76\text{cm (30in)}$.

Figure A83. Effect of rotation rate and angle of attack on side-force coefficient for configuration having full-span LE wing droop. $\delta_r = 0^\circ$, $\delta_a = 0^\circ$, $\delta_s = 0^\circ$, $\beta = 0^\circ$.







A292

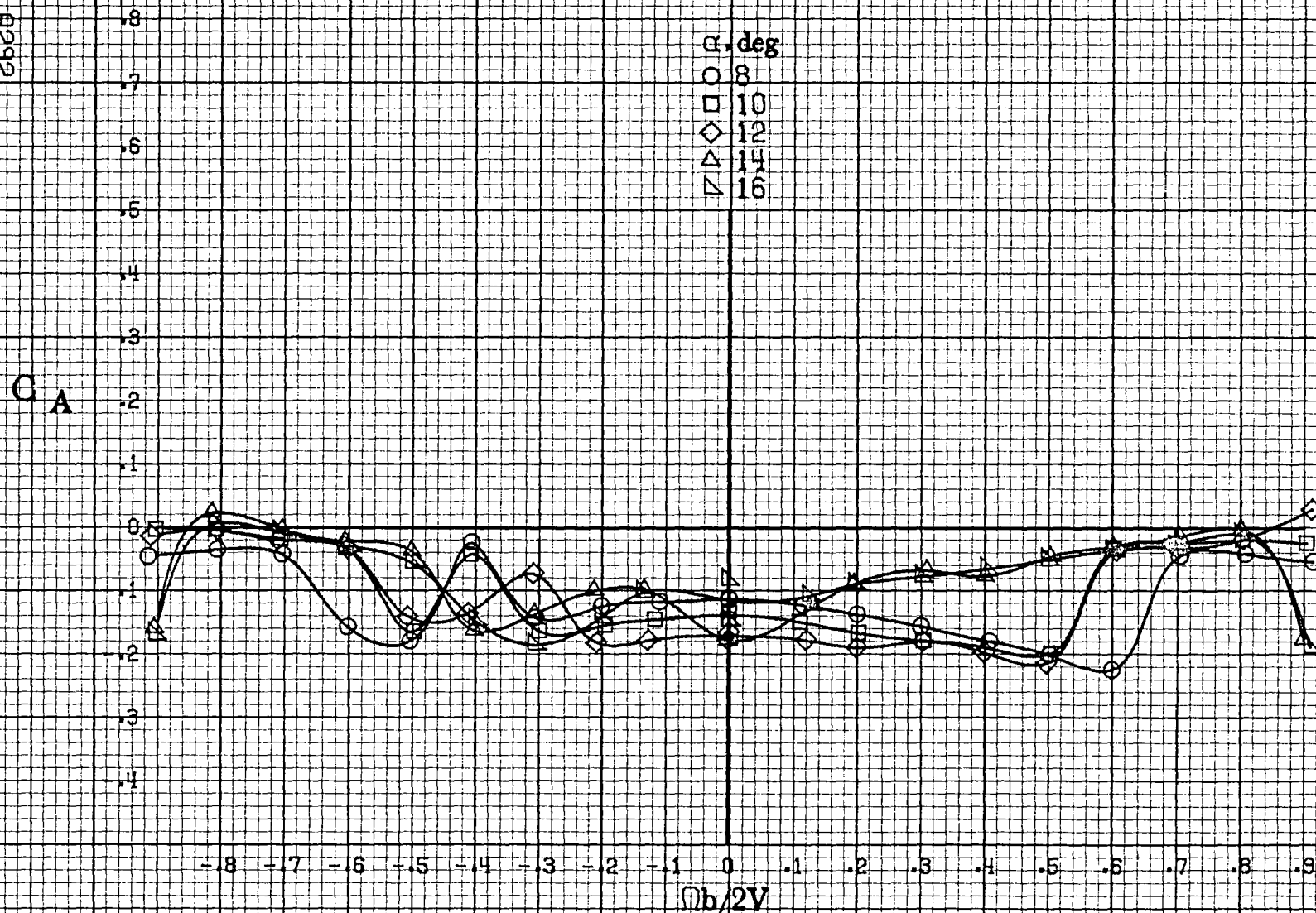
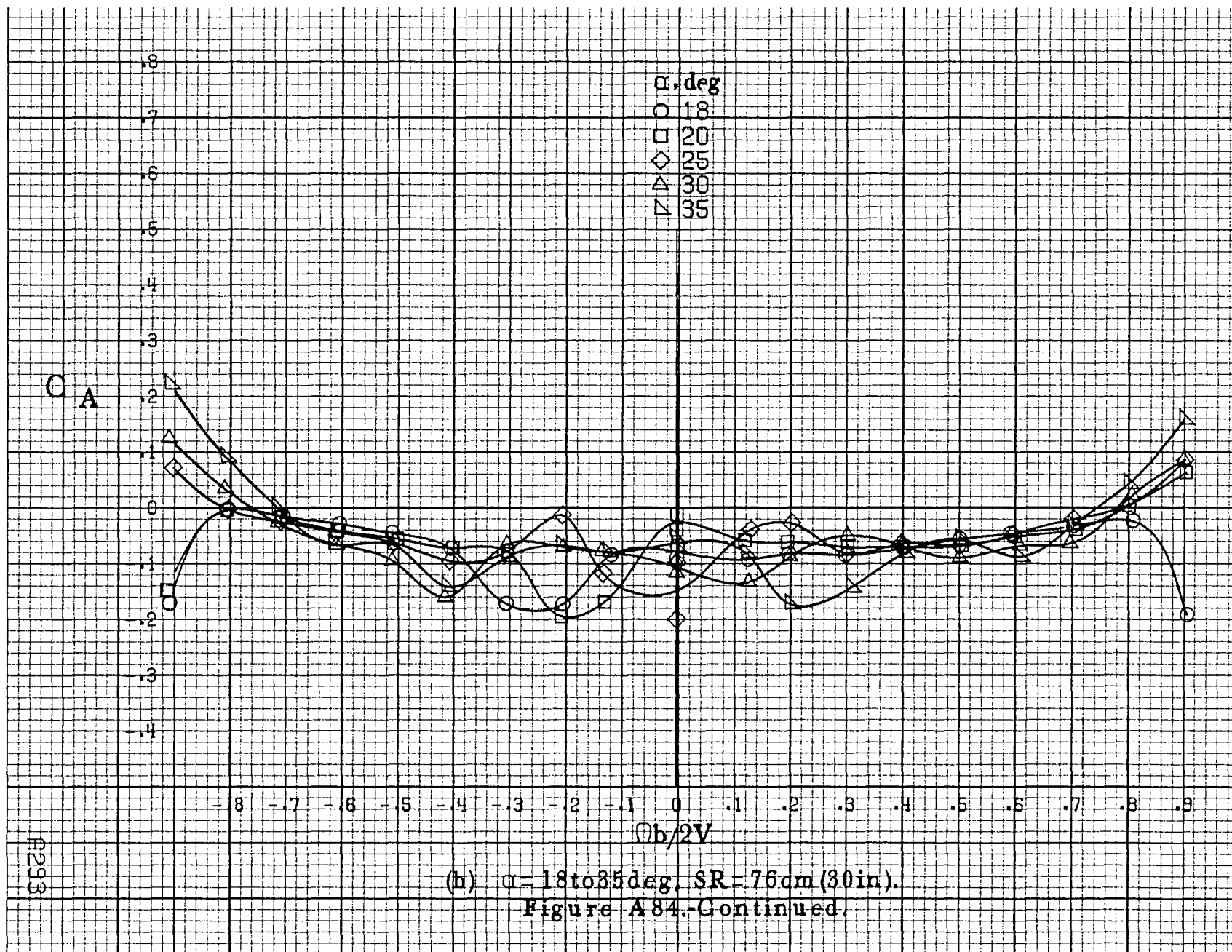
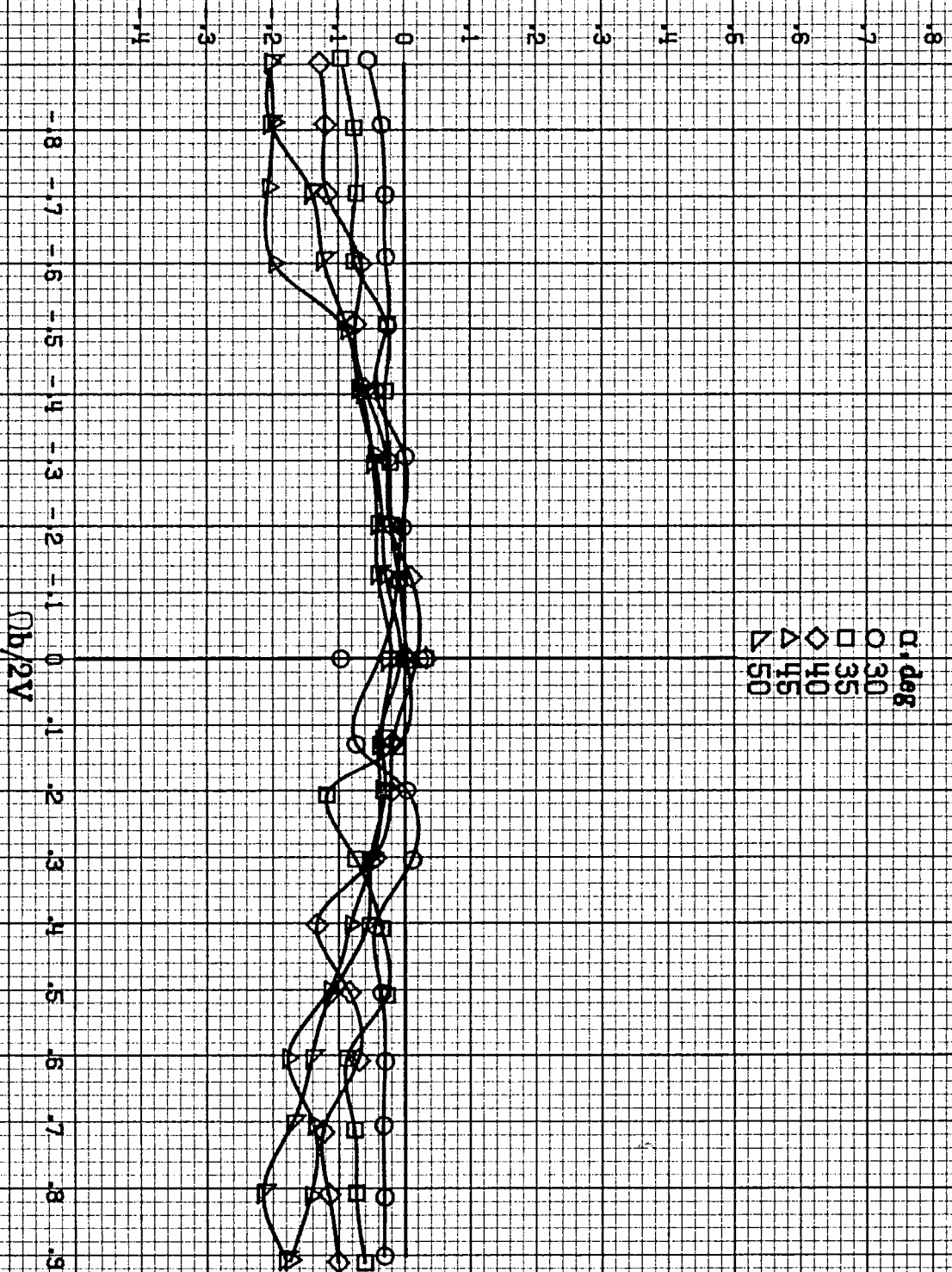
(a) $\alpha = 8$ to 16 deg, $SR = 76$ cm (30 in).

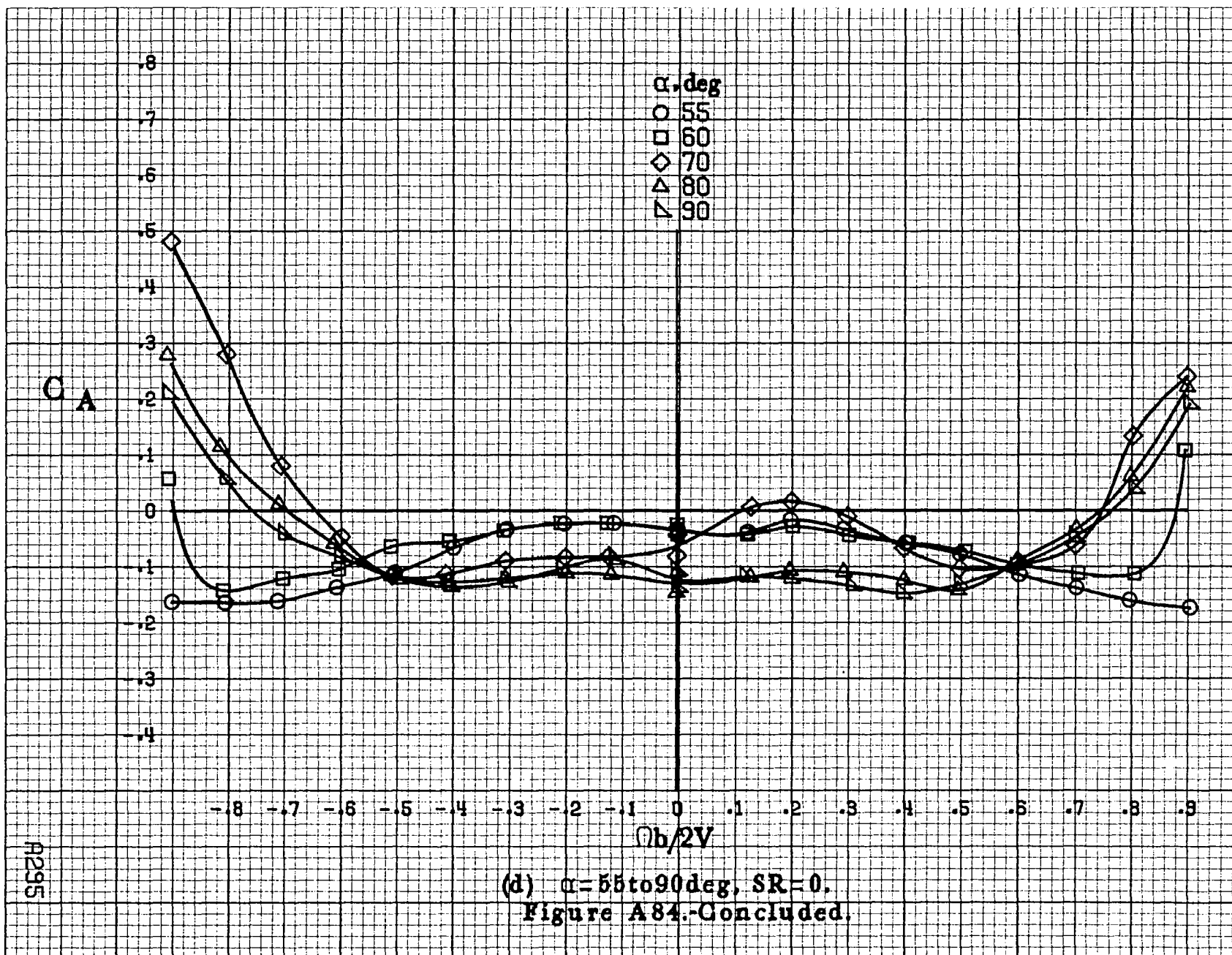
Figure A84. Effect of rotation rate and angle of attack on axial-force coefficient for configuration having full-span LE wing droop. $\delta_e = 0^\circ$, $\delta_a = 0^\circ$, $\delta_r = 0^\circ$, $\beta = 0^\circ$.

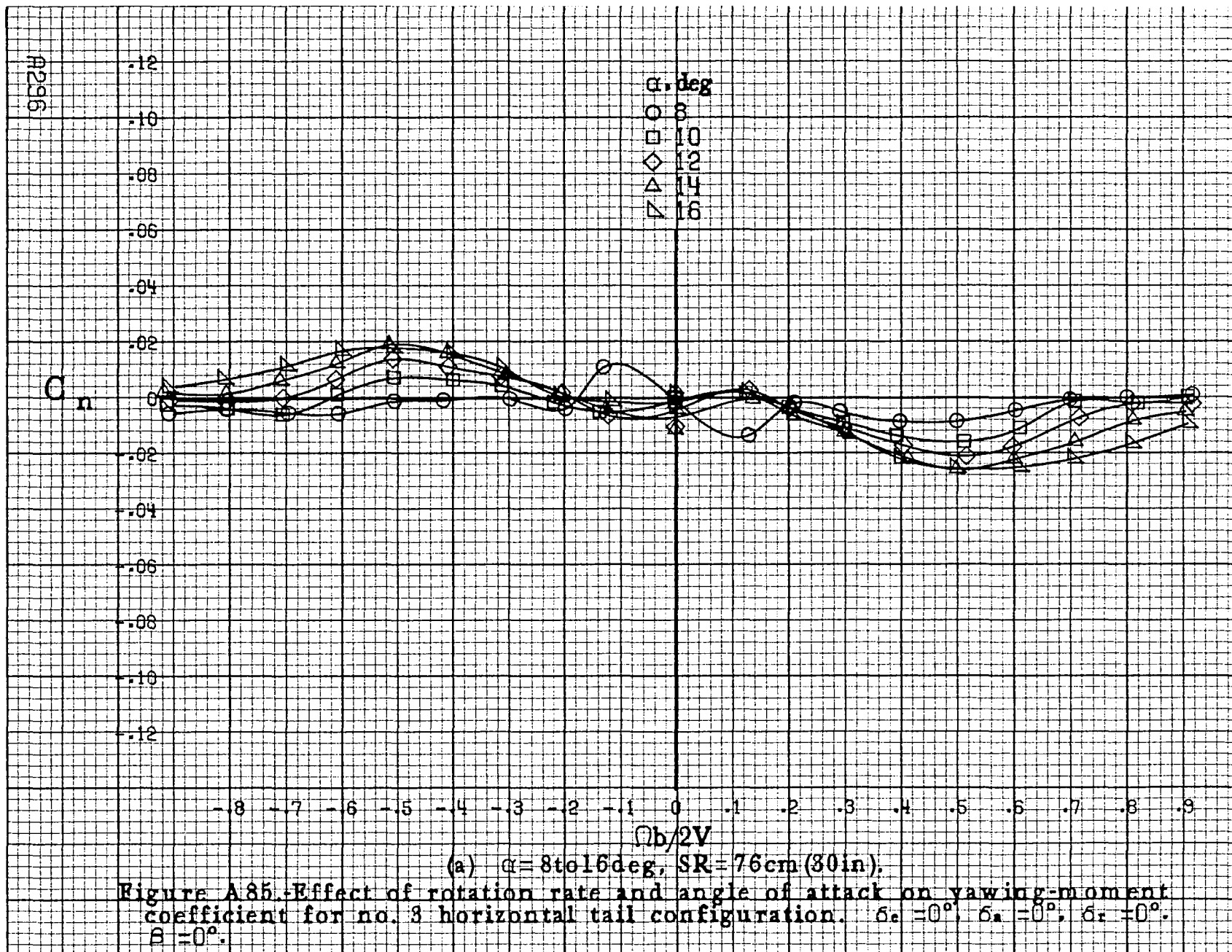


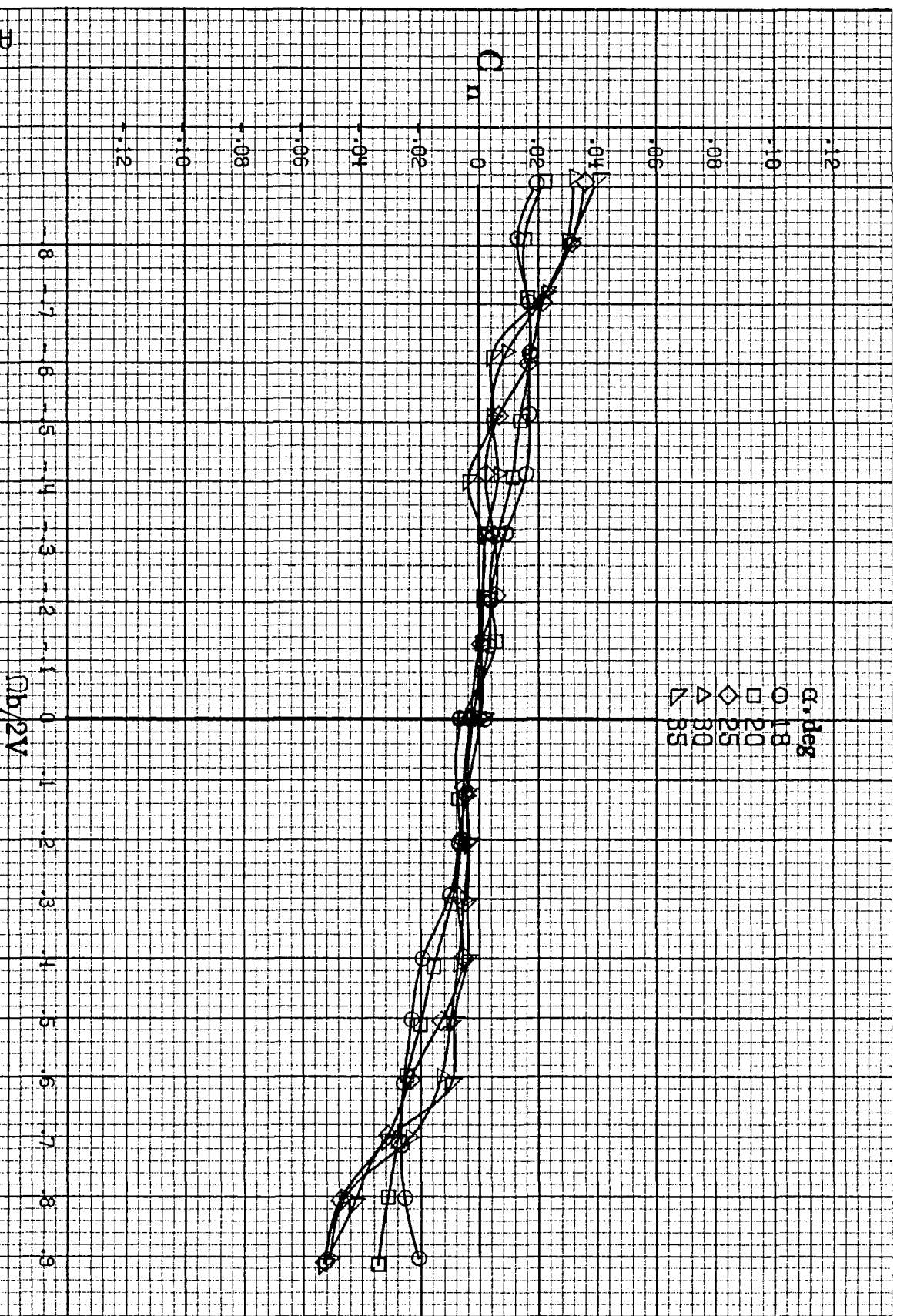
C_A



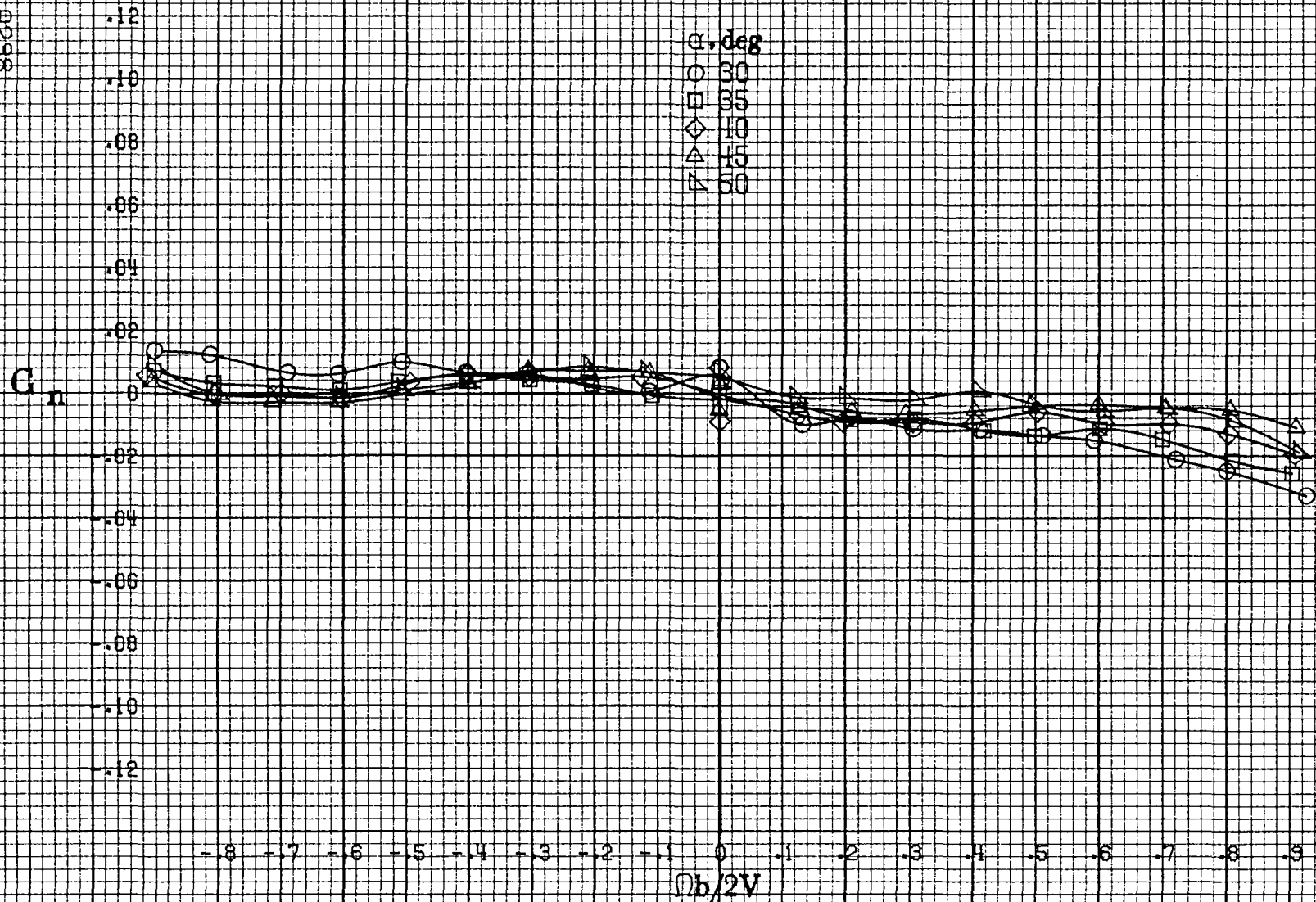
(c) $\alpha = 30$ to 50 deg, $SR = 0$.
Figure A84.-Continued.



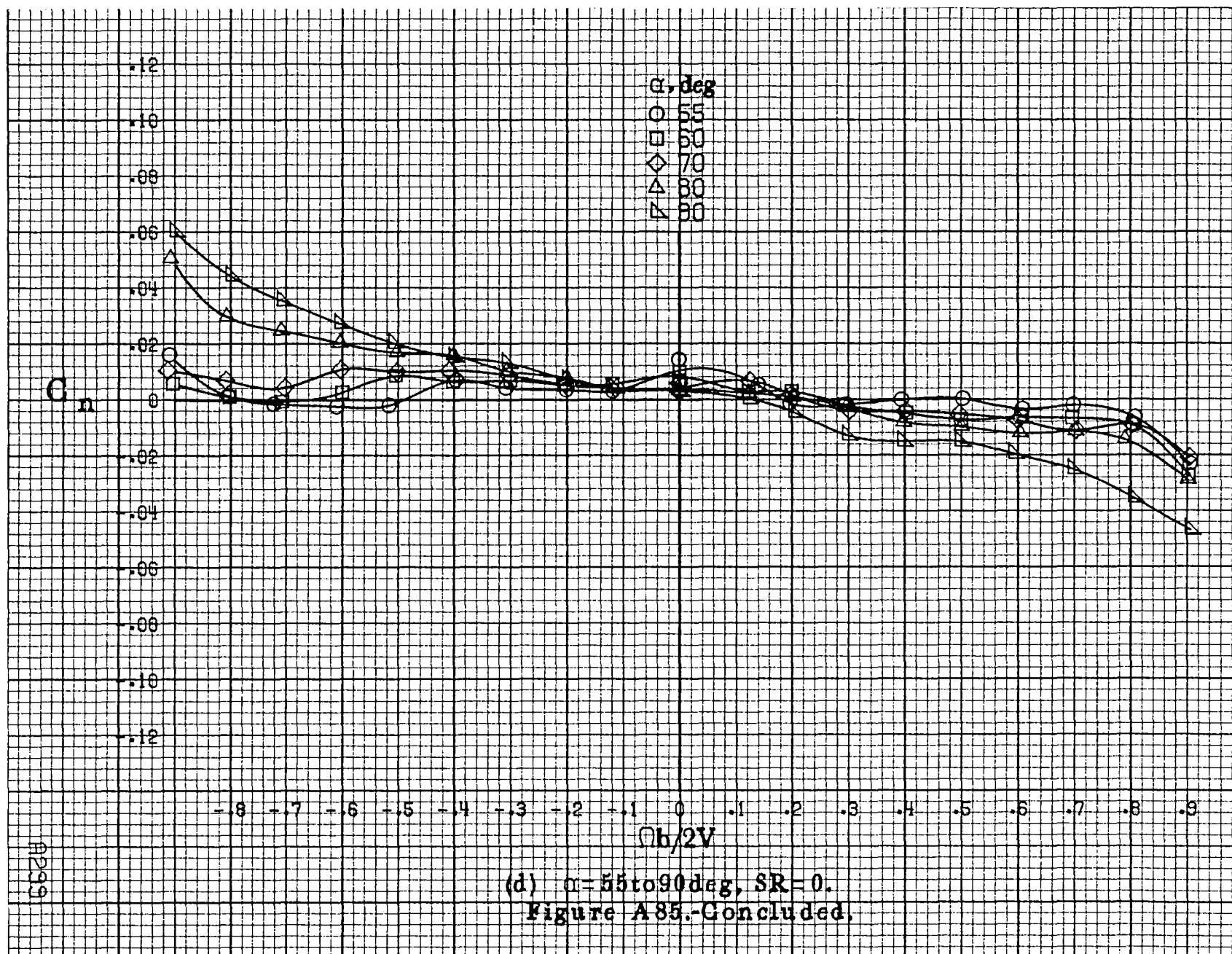


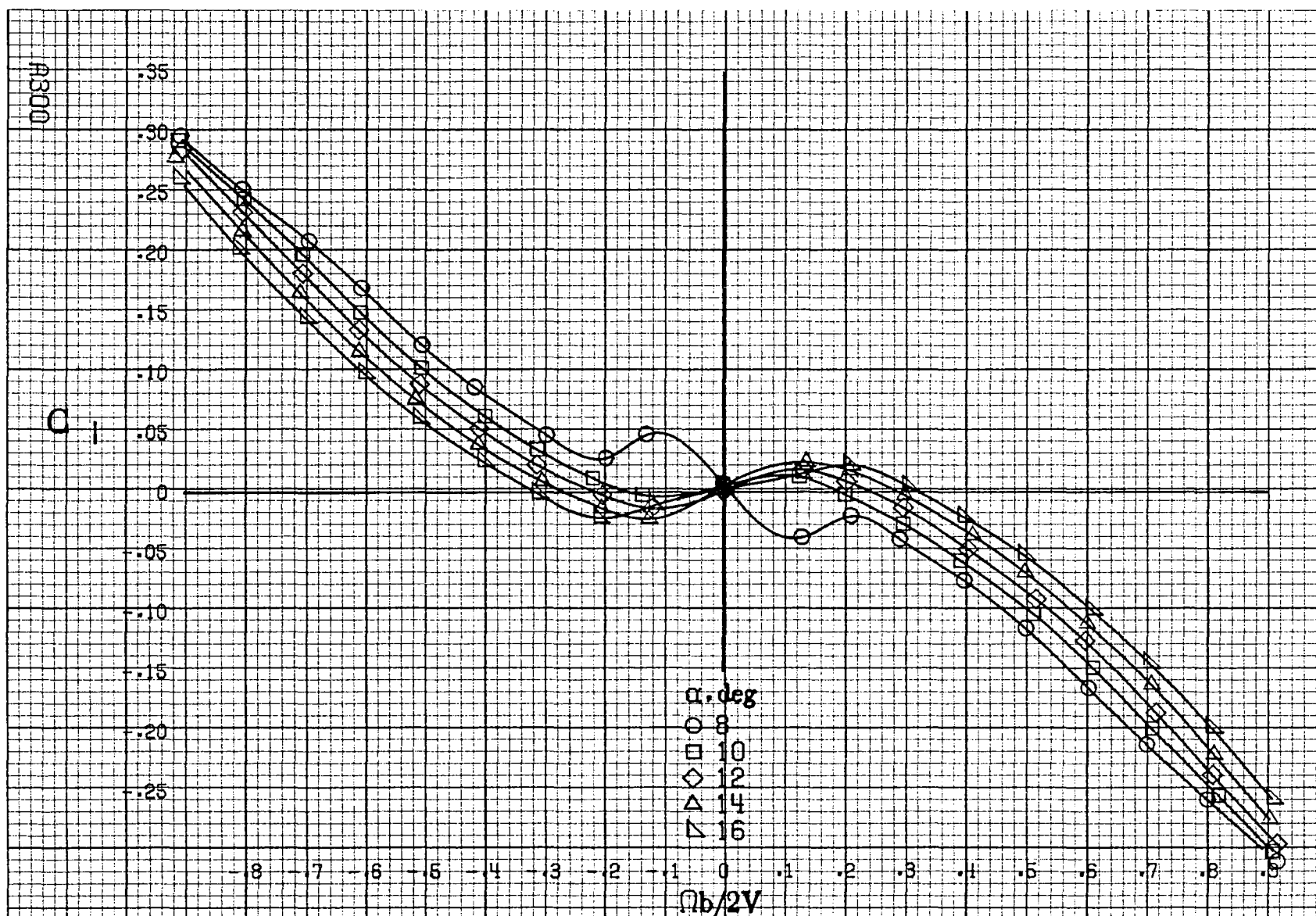


(b) $\alpha = 18$ to 35 deg, $SR = 7.6$ cm (30 in.).
Figure A85.-Continued.



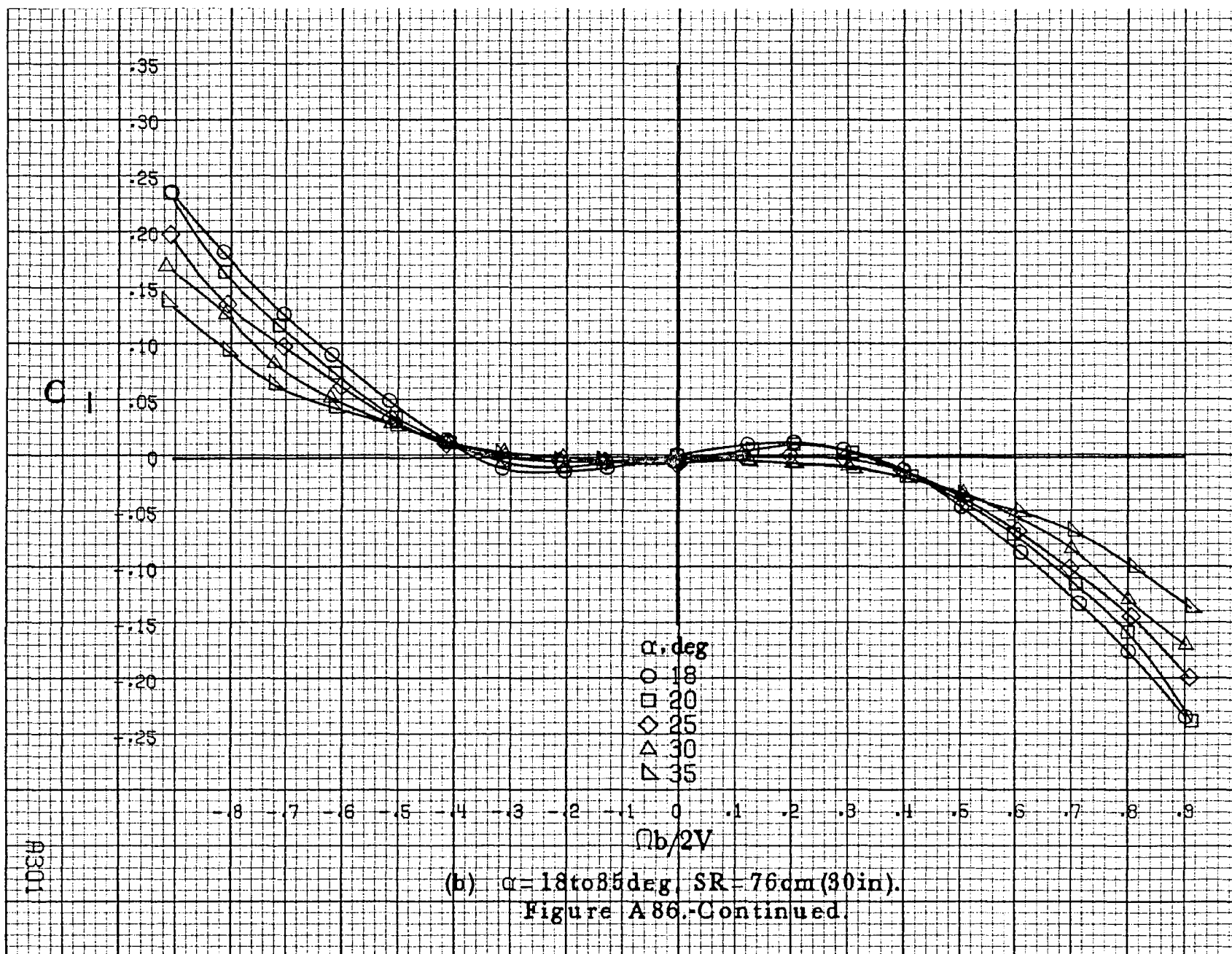
(c) $\alpha = 30$ to 50 deg, $SR = 0$.
Figure A 85.-Continued.



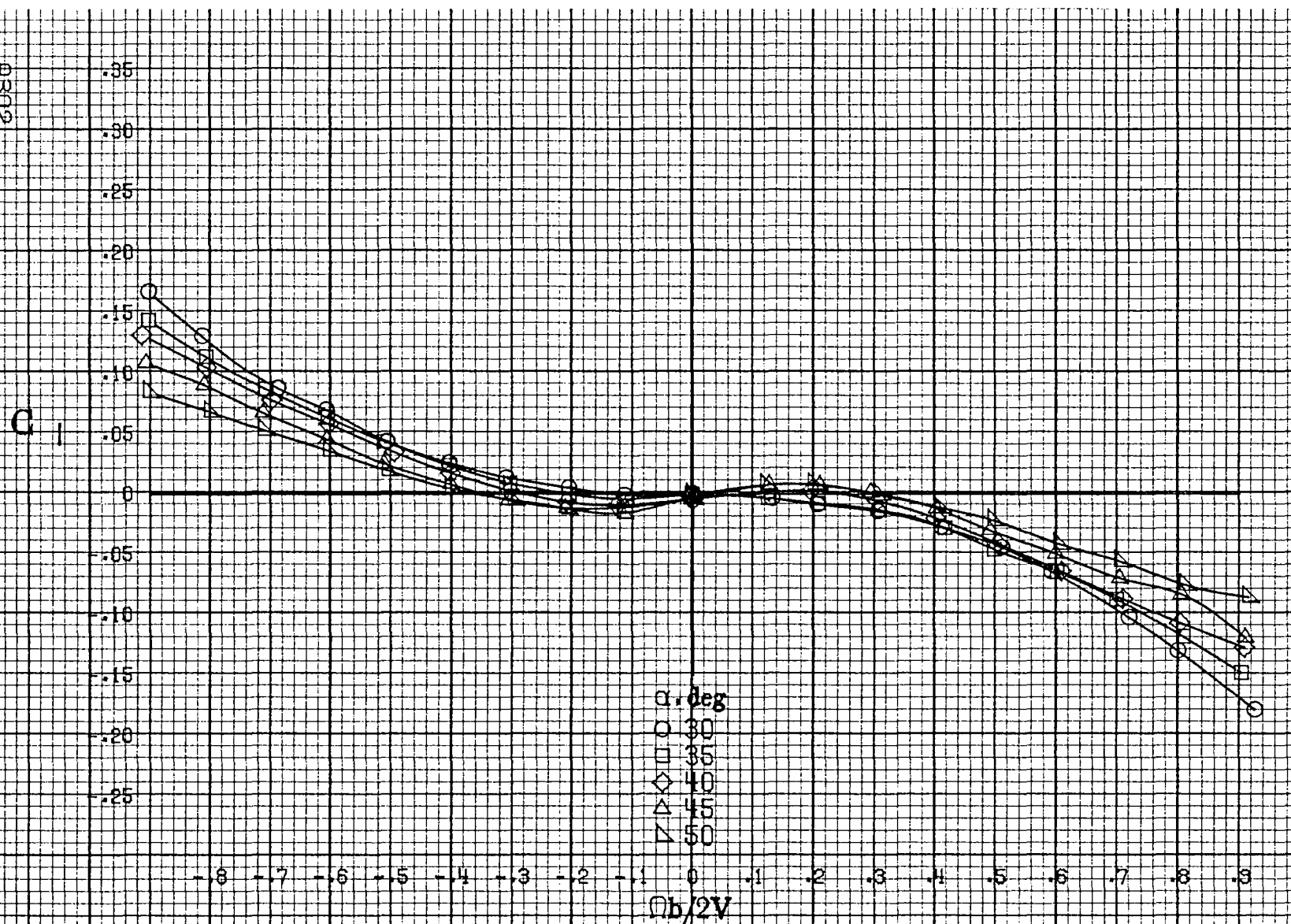


(a) $\alpha=8$ to 16° , $SR=76\text{cm}(30\text{in})$.

Figure A86.-Effect of rotation rate and angle of attack on rolling-moment coefficient for no. 3 horizontal tail configuration. $\delta_e = 0^\circ$, $\delta_a = 0^\circ$, $\delta_r = 0^\circ$. $B = 0^\circ$.



A802



(c) $\alpha=30$ to 50 deg, $SR=0$.
Figure A86.-Continued.

0.1

.14
.12
.10
.08
.06
.04
.02
0
-.02
-.04
-.06
-.08
-.10

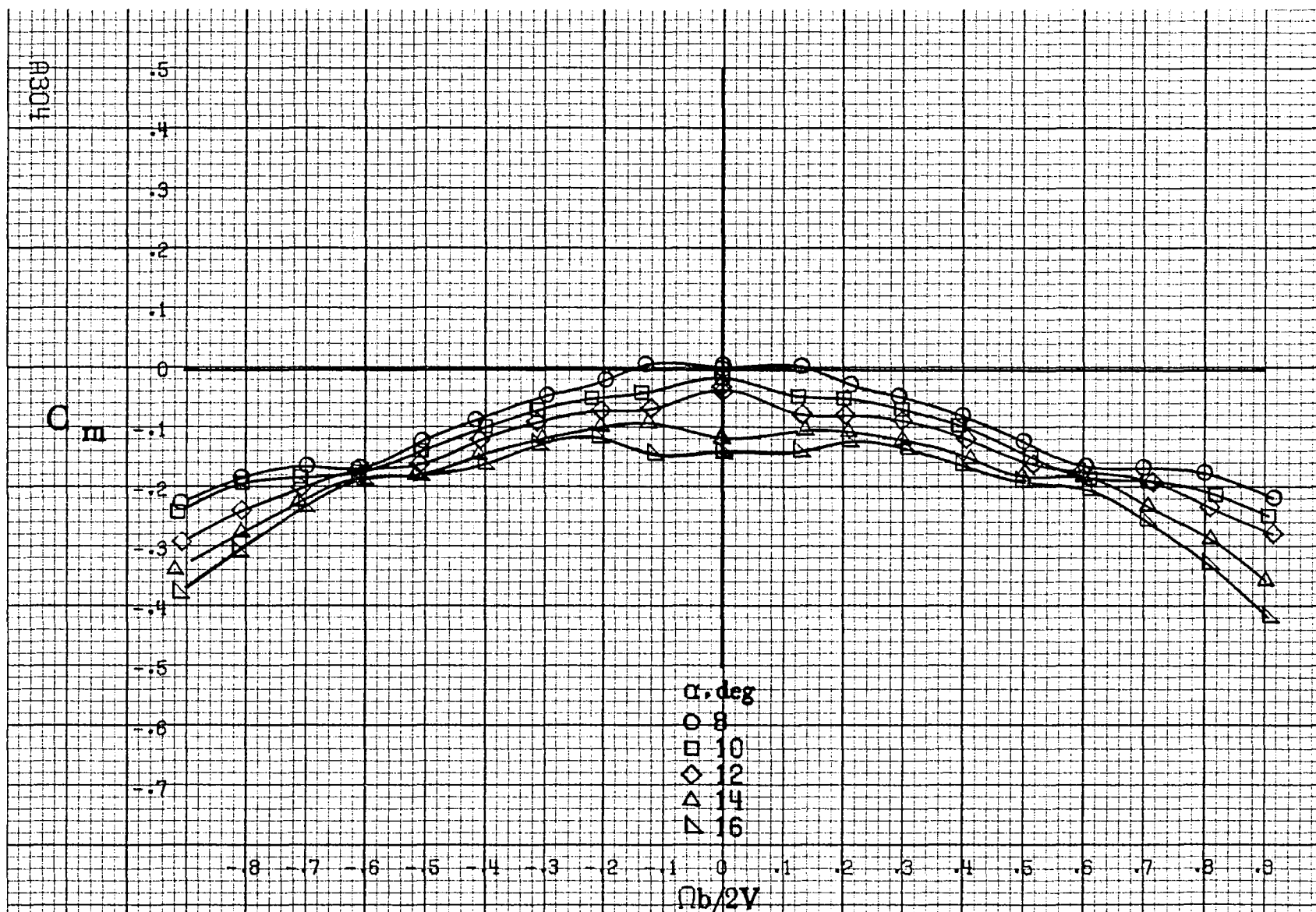
α, deg
○ 55
□ 60
◇ 70
△ 80
▽ 90

-0.8 -0.7 -0.6 -0.5 -0.4 -0.3 -0.2 -0.1 0 0.1 0.2 0.3 0.4 0.5 0.6 0.7 0.8 0.9

$Qb/2V$

(d) $\alpha=55\text{to}90\text{deg}, SR=0.$
Figure A86.-Concluded,

A803



(a) $\alpha=8$ to 16° , $SR=76\text{cm}(30\text{in})$.
 Figure A87. Effect of rotation rate and angle of attack on pitching-moment coefficient for no. 3 horizontal tail configuration. $\delta_a=0^\circ$, $\delta_s=0^\circ$, $\delta_r=0^\circ$, $\beta=0^\circ$.

C_m

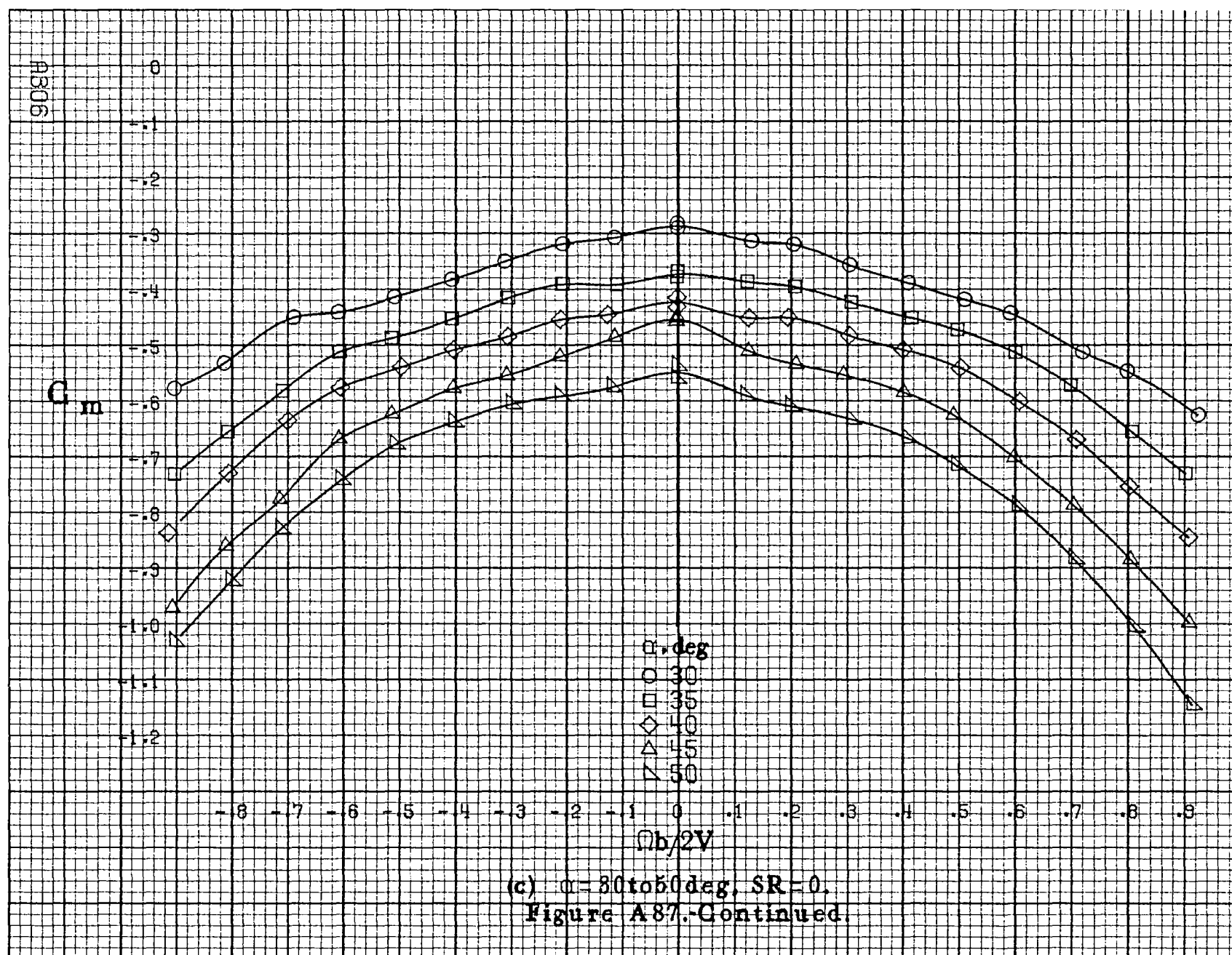
.3
.2
.1
0
-.1
-.2
-.3
-.4
-.5
-.6
-.7
-.8
-.9

α , deg
○ 18
□ 20
◇ 25
△ 30
▽ 35

-.8 -.7 -.6 -.5 -.4 -.3 -.2 -.1 0 .1 .2 .3 .4 .5 .6 .7 .8 .9
 $b/2V$

(b) $\alpha=18$ to 35 deg, $SR=76$ cm (30 in).
Figure A87-Continued.

A305



C_m

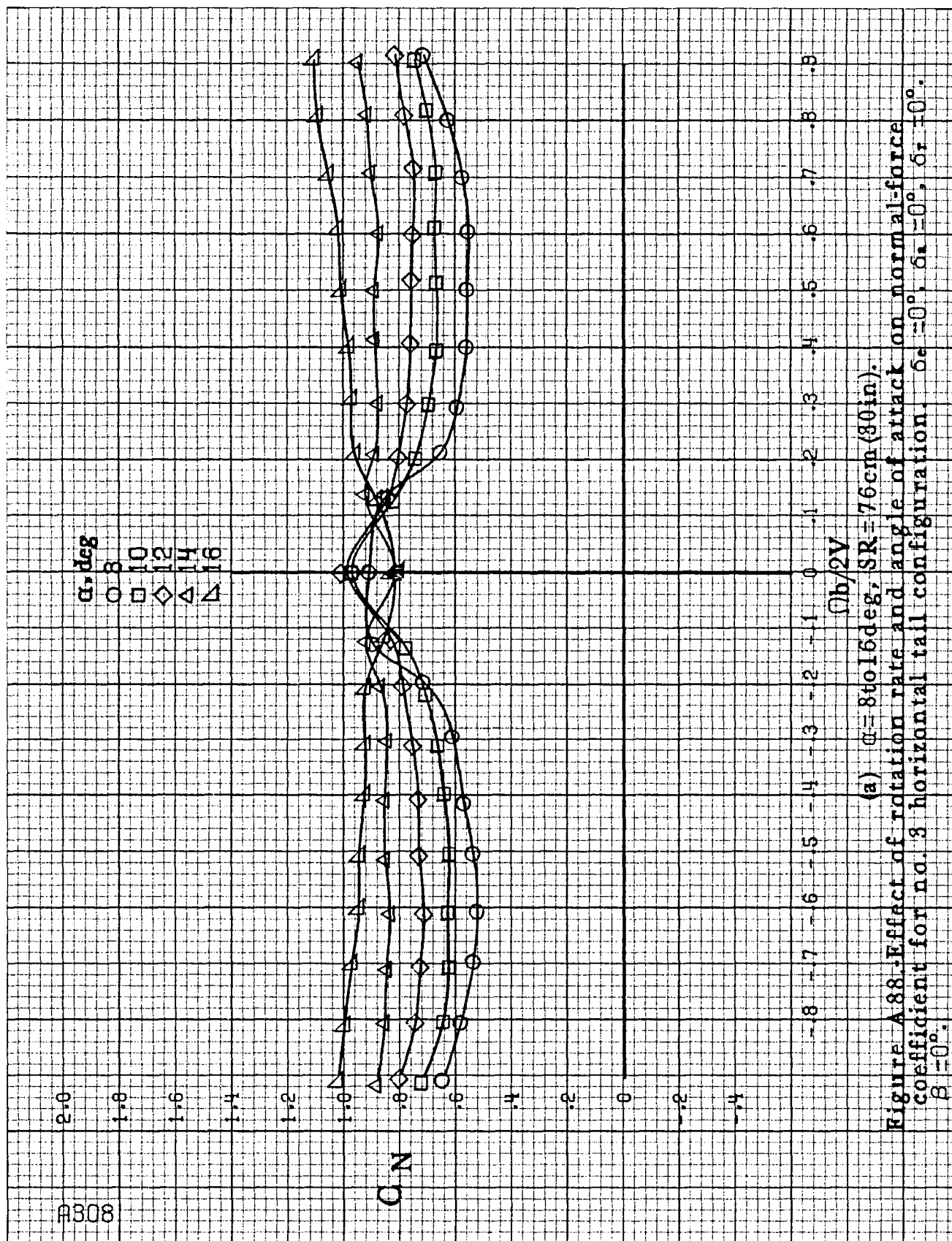
-0.5
-0.6
-0.7
-0.8
-0.9
-1.0
-1.1
-1.2
-1.3
-1.4
-1.5
-1.6
-1.7

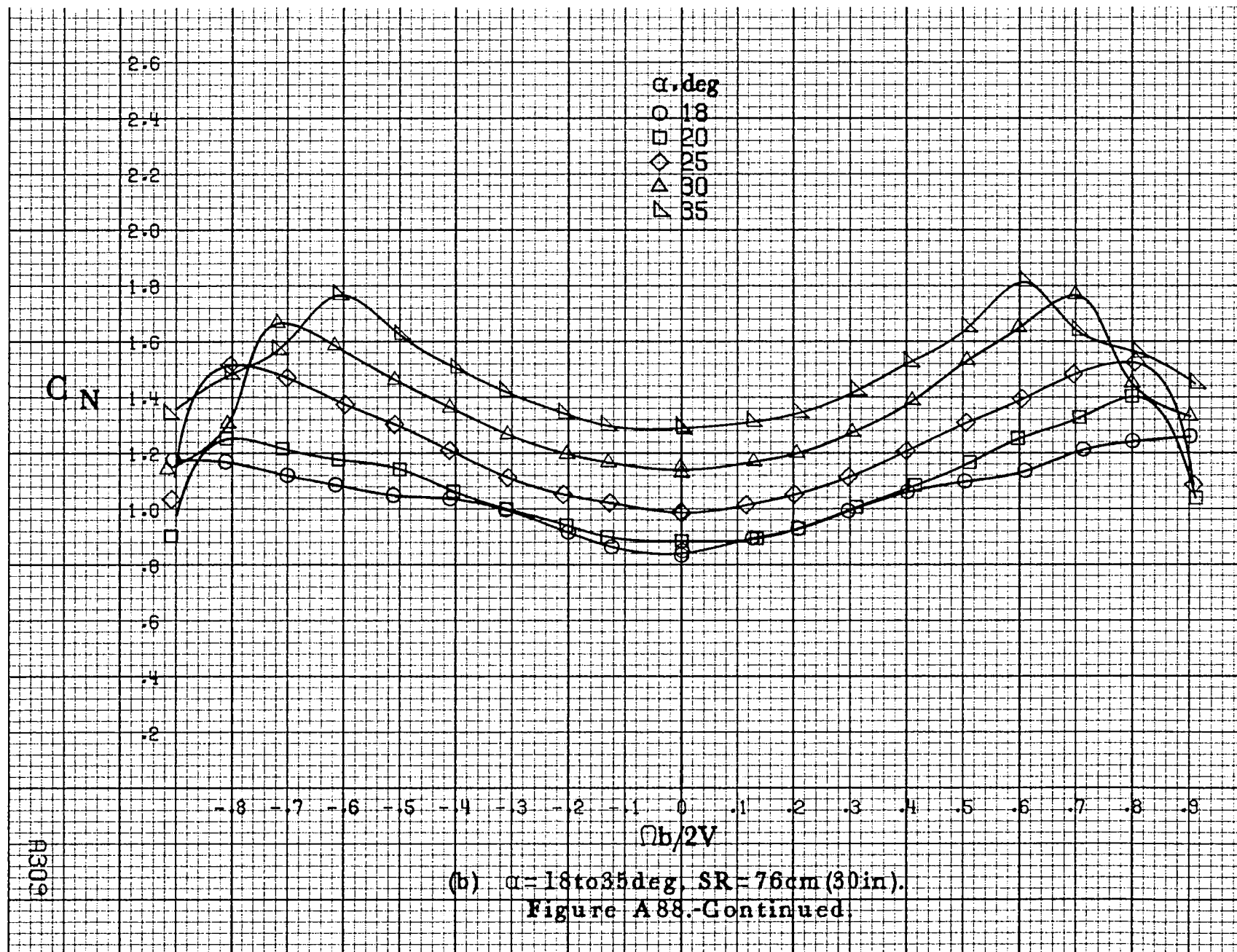
α, deg
○ 55
□ 60
◇ 70
△ 80
▽ 90

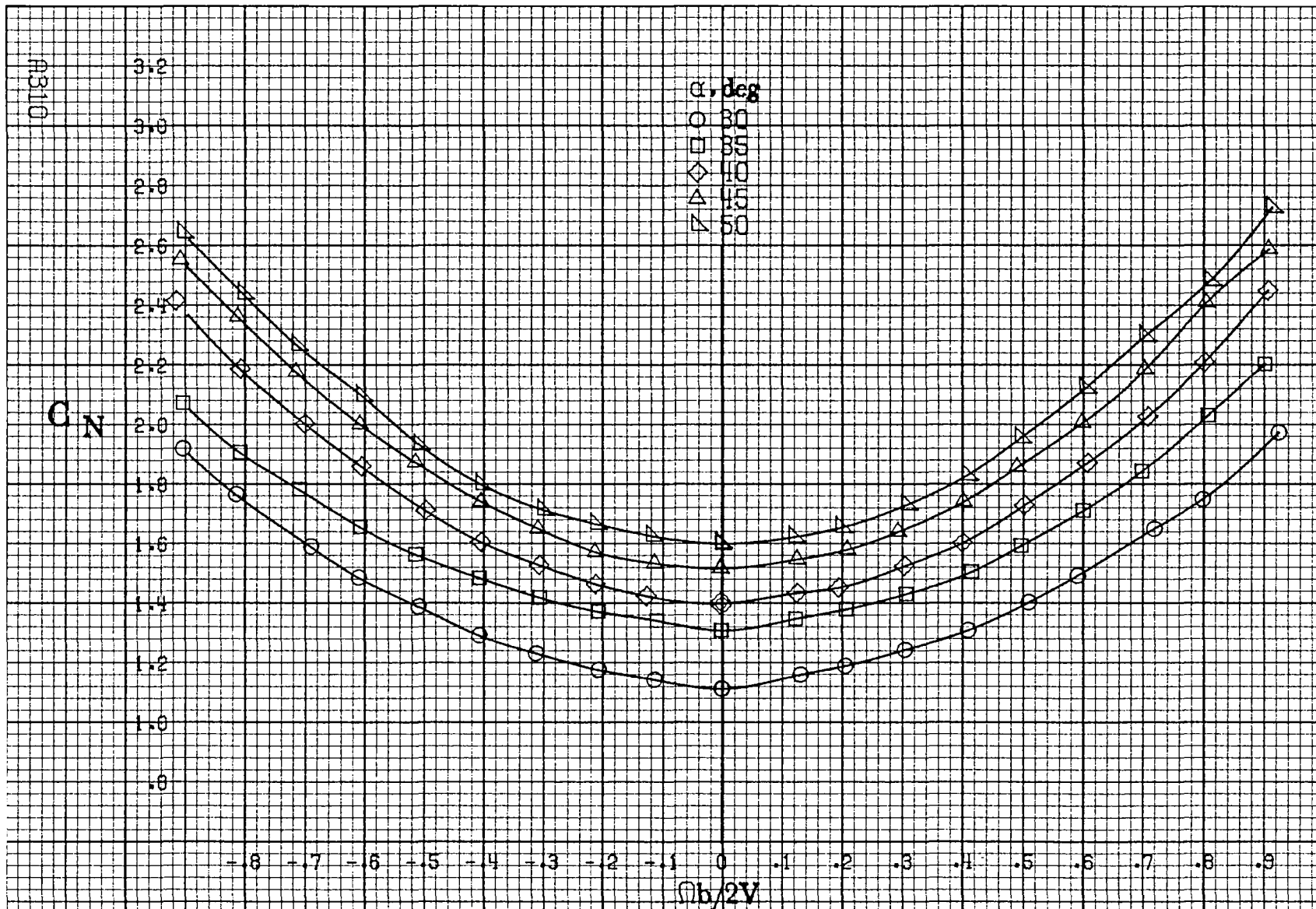
-0.8 -0.7 -0.6 -0.5 -0.4 -0.3 -0.2 -0.1 0 0.1 0.2 0.3 0.4 0.5 0.6 0.7 0.8 0.9
 $\Omega b/2V$

(d) $\alpha=55\text{to}90\text{deg}$, $SR=0$.
Figure A87.-Concluded.

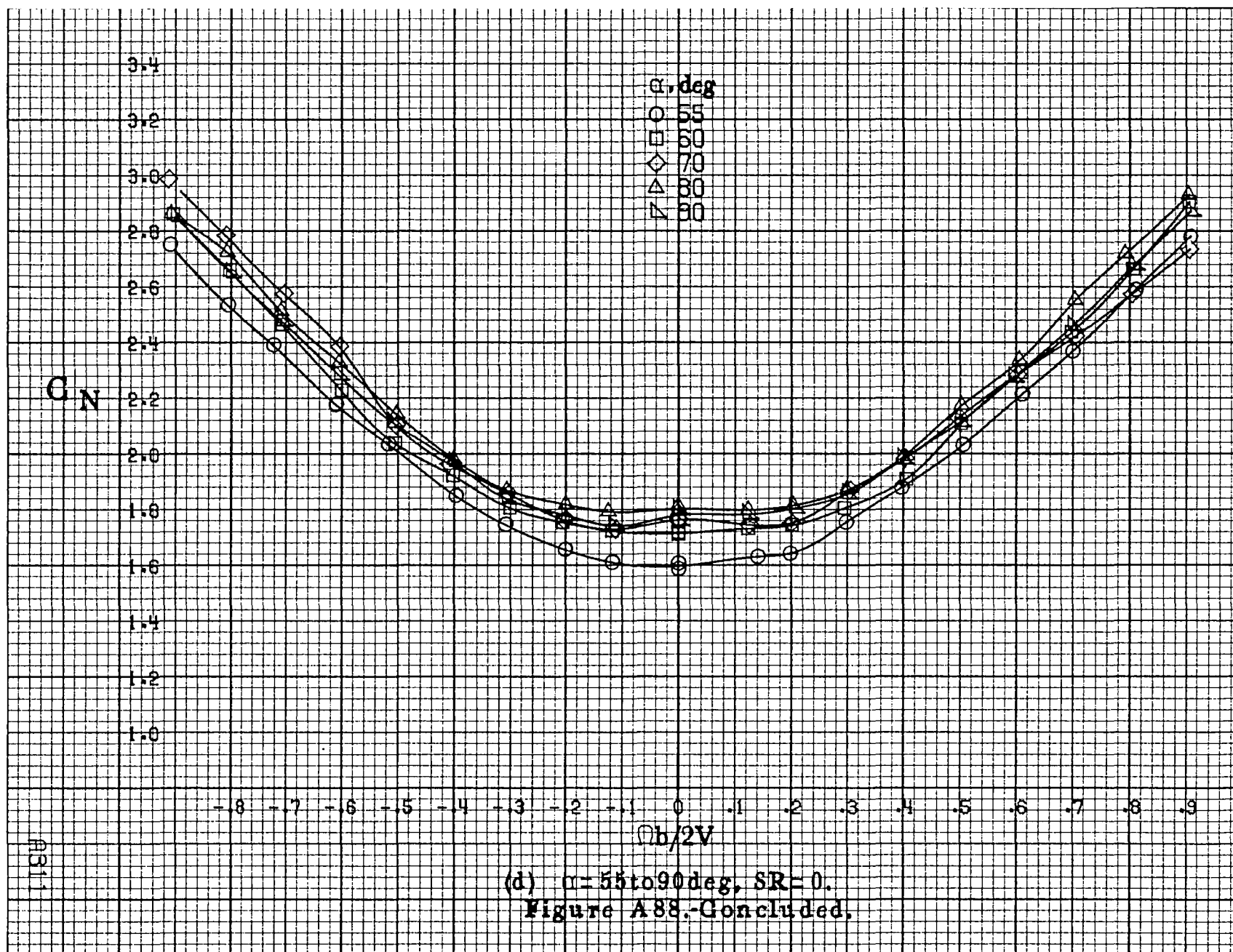
HR307

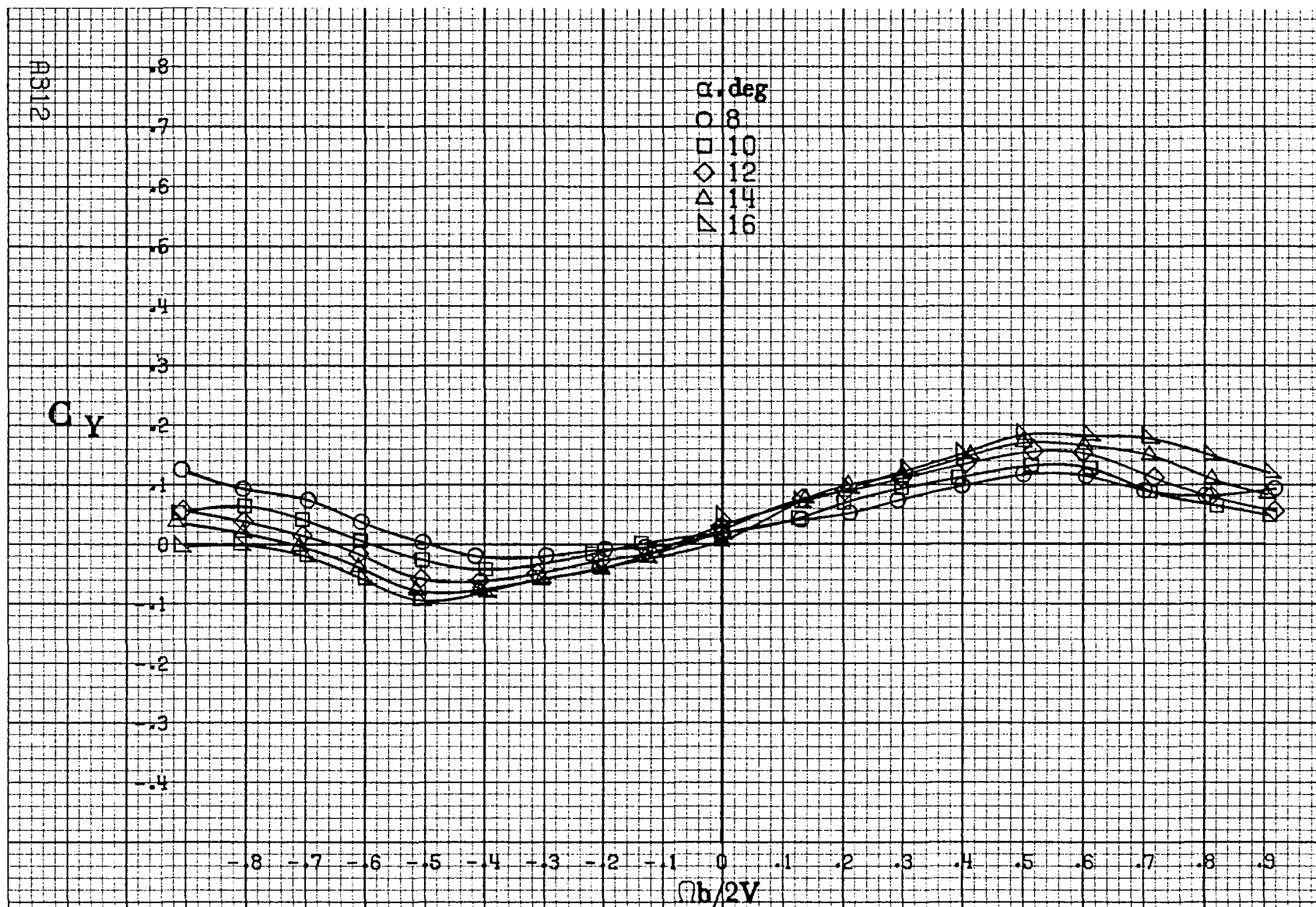






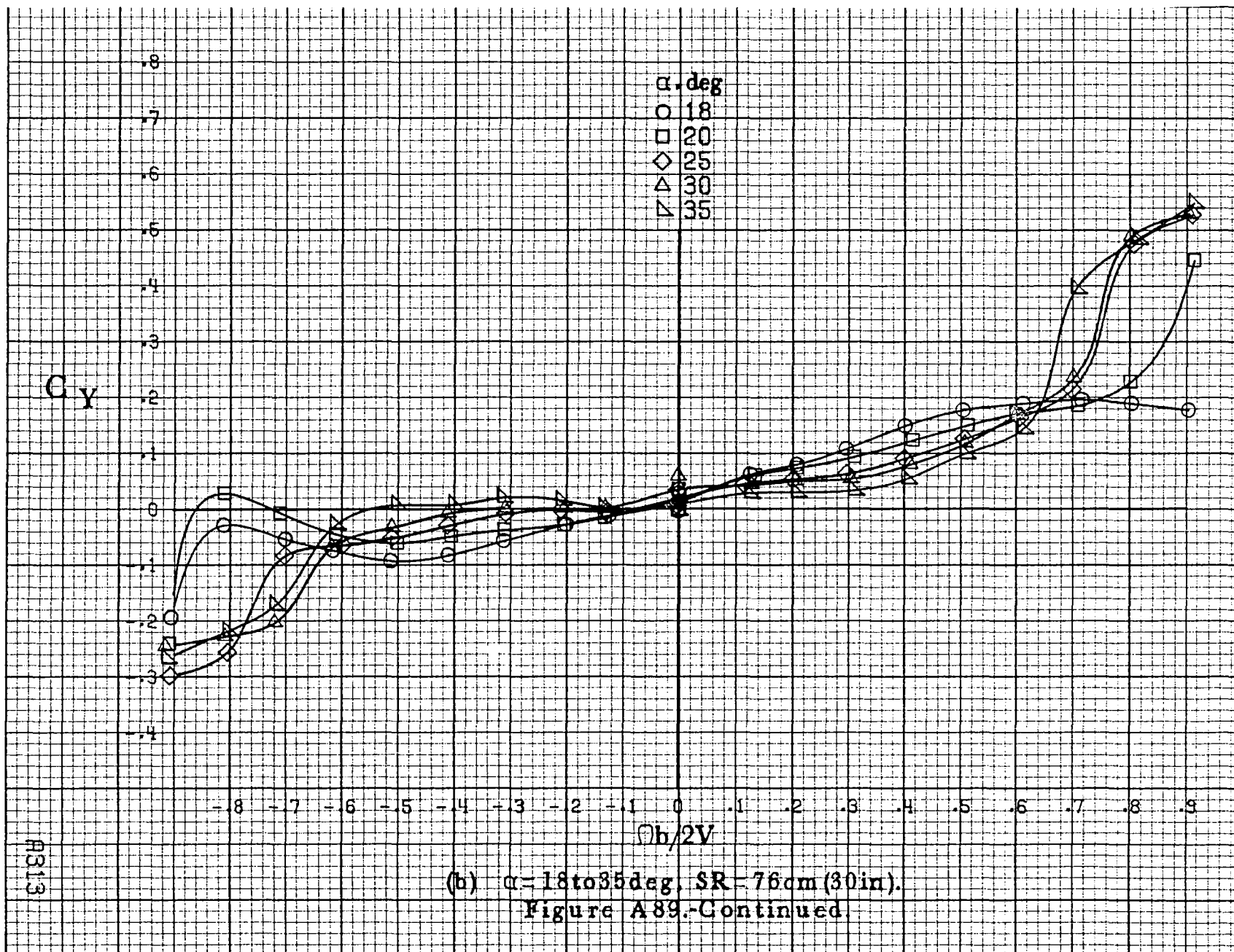
(c) $\alpha = 30$ to 50 deg, $SR = 0$.
Figure A88.-Continued.

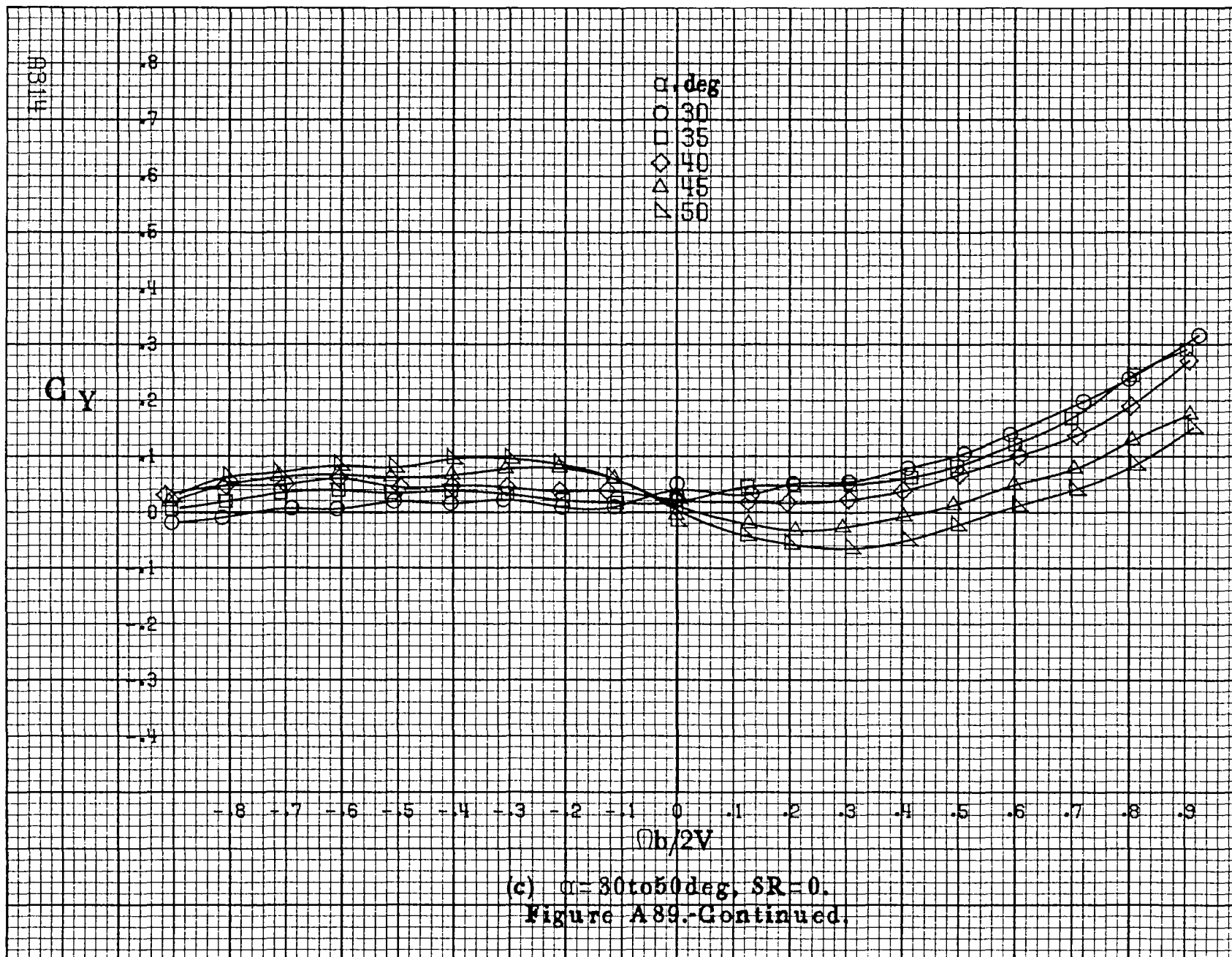


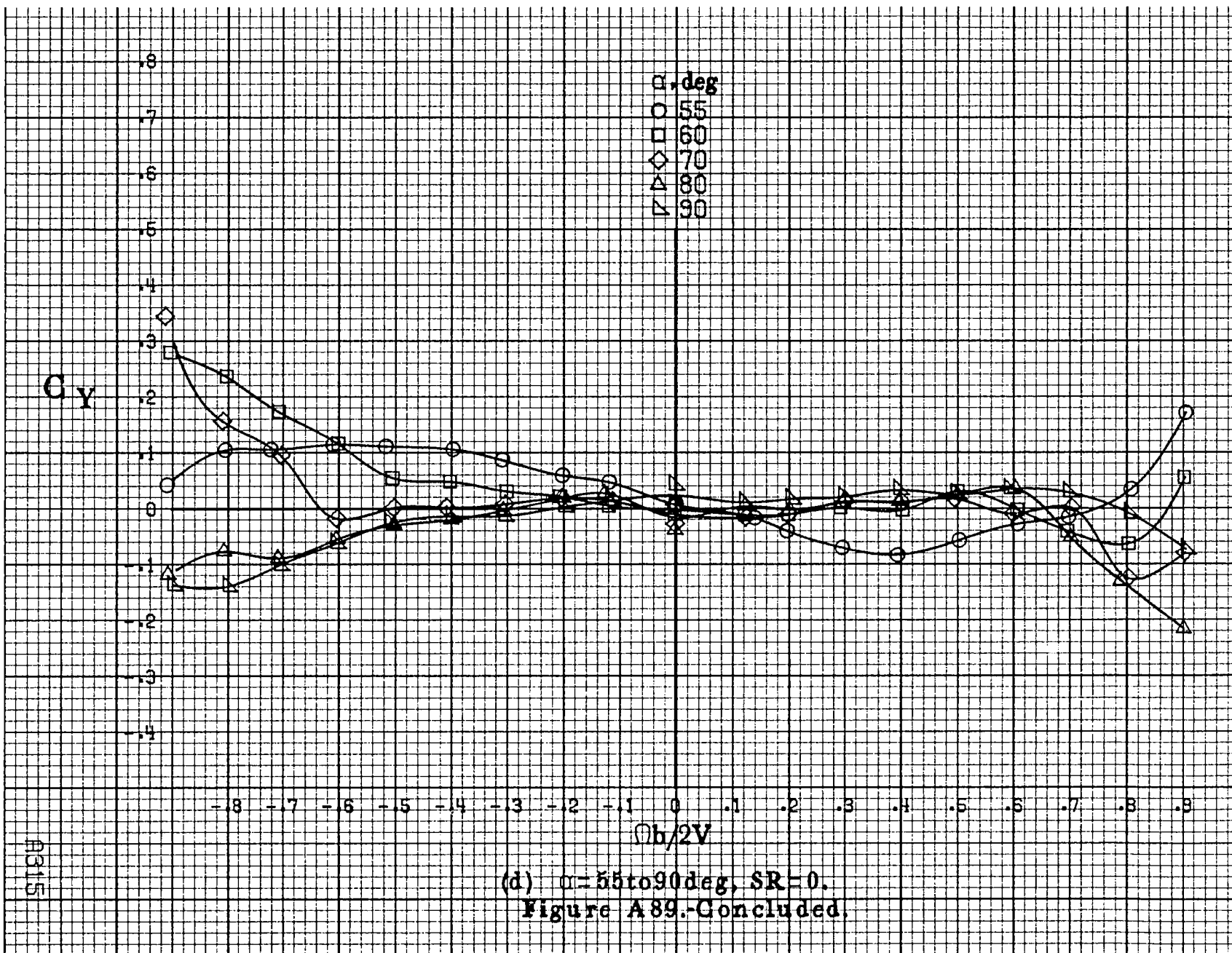


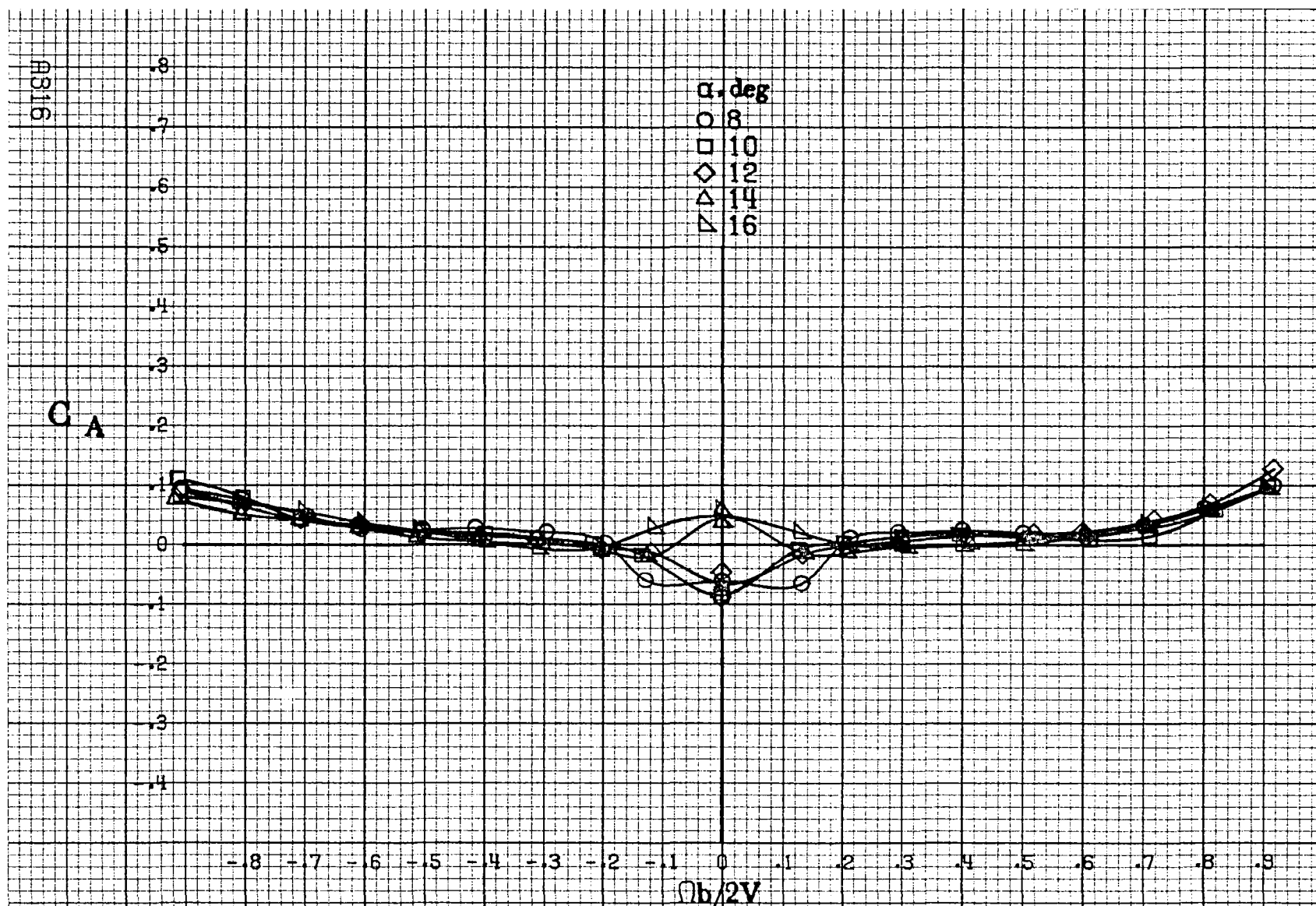
(a) $\alpha = 8 \text{ to } 16^\circ$, $SR = 76 \text{ cm (30 in.)}$.

Figure A89. Effect of rotation rate and angle of attack on side-force coefficient for no. 3 horizontal tail configuration. $\delta_e = 0^\circ$, $\delta_a = 0^\circ$, $\delta_r = 0^\circ$, $\beta = 0^\circ$.



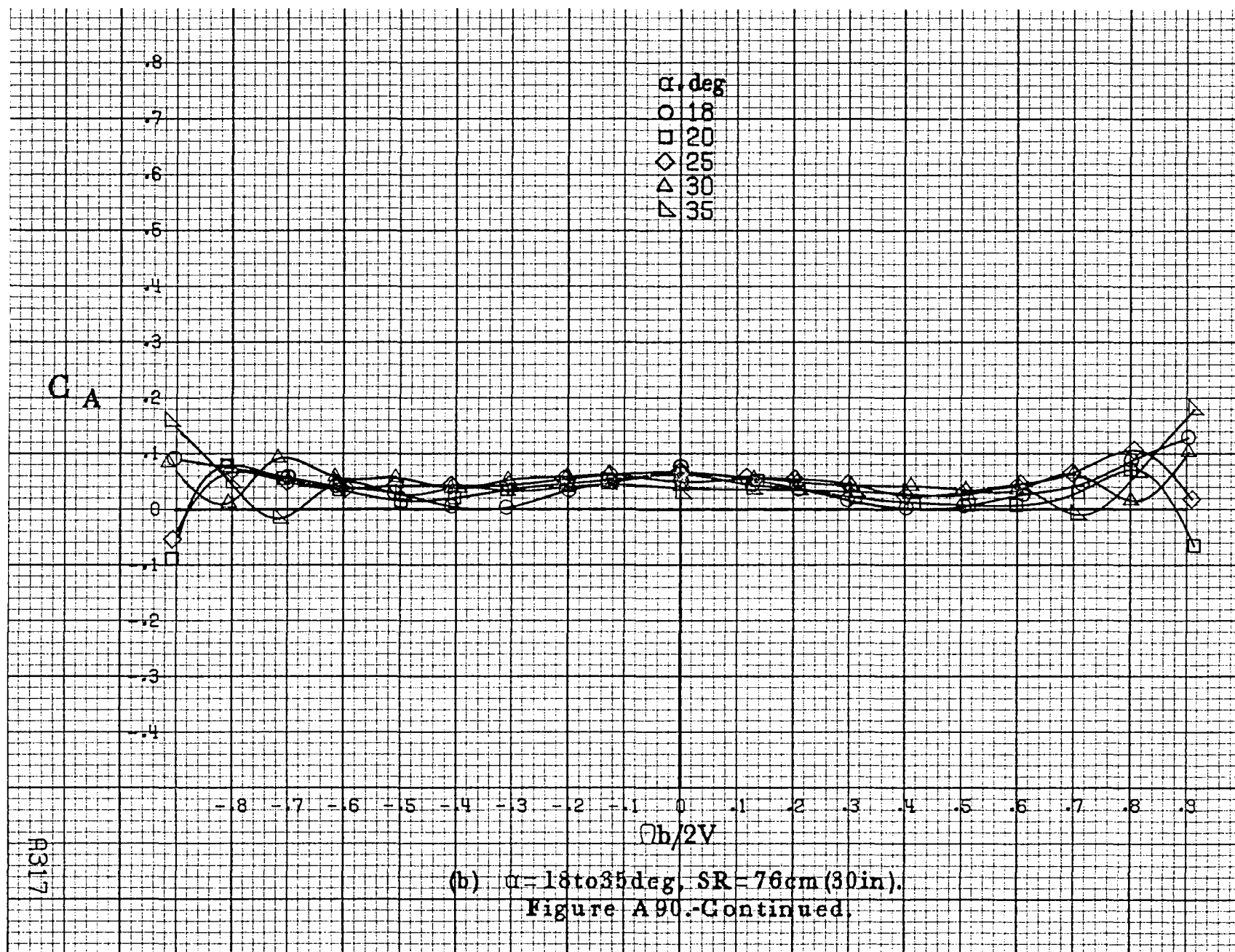


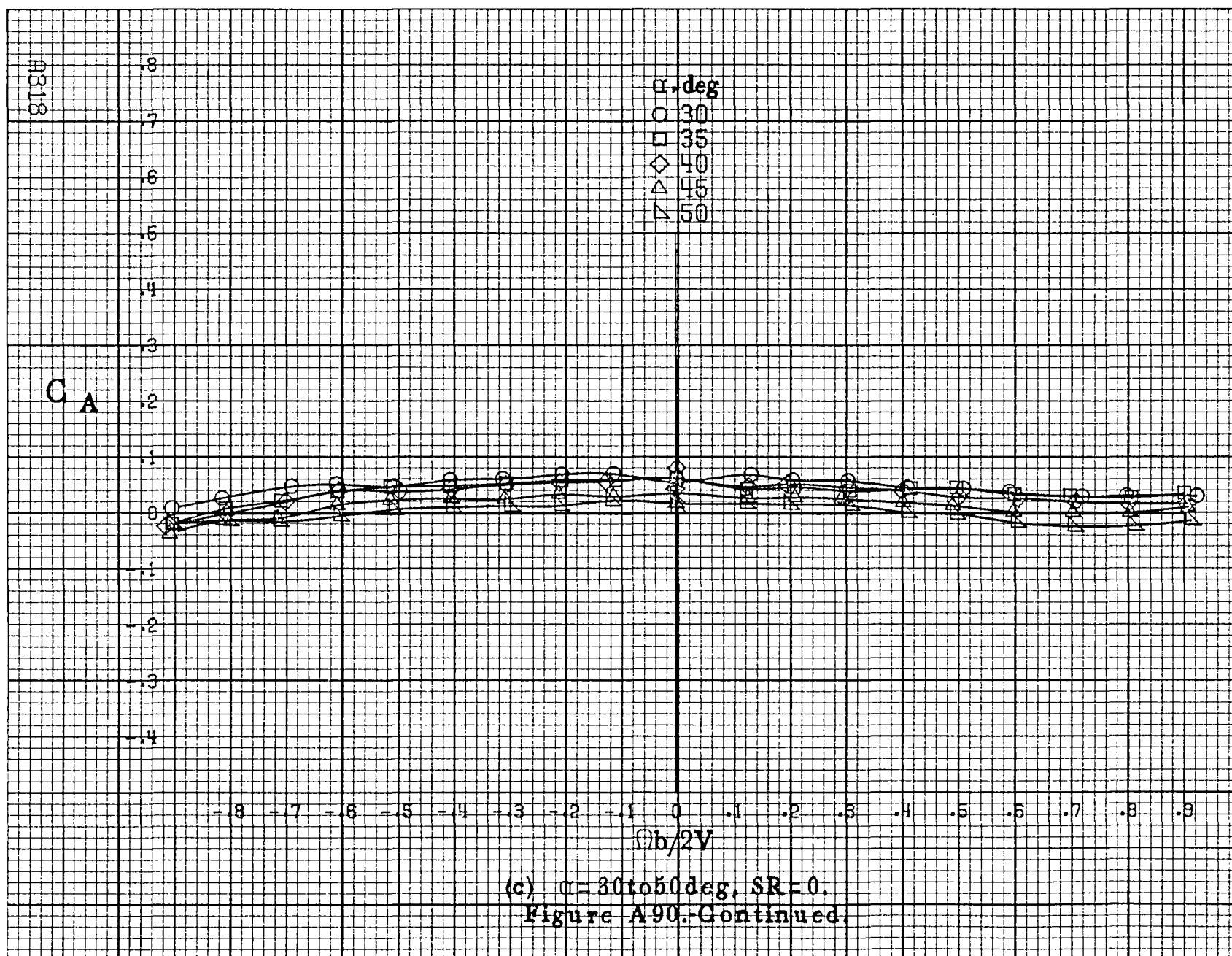




(a) $\alpha=8$ to 16° , $SR=76\text{cm}(80\text{in})$.

Figure A90. Effect of rotation rate and angle of attack on axial-force coefficient for no. 3 horizontal tail configuration. $\delta_e=0^\circ$, $\delta_a=0^\circ$, $\delta_r=0^\circ$. $B=0^\circ$.





C_A

α, deg

- 55
- 60
- ◇ 70
- △ 80
- ▽ 90

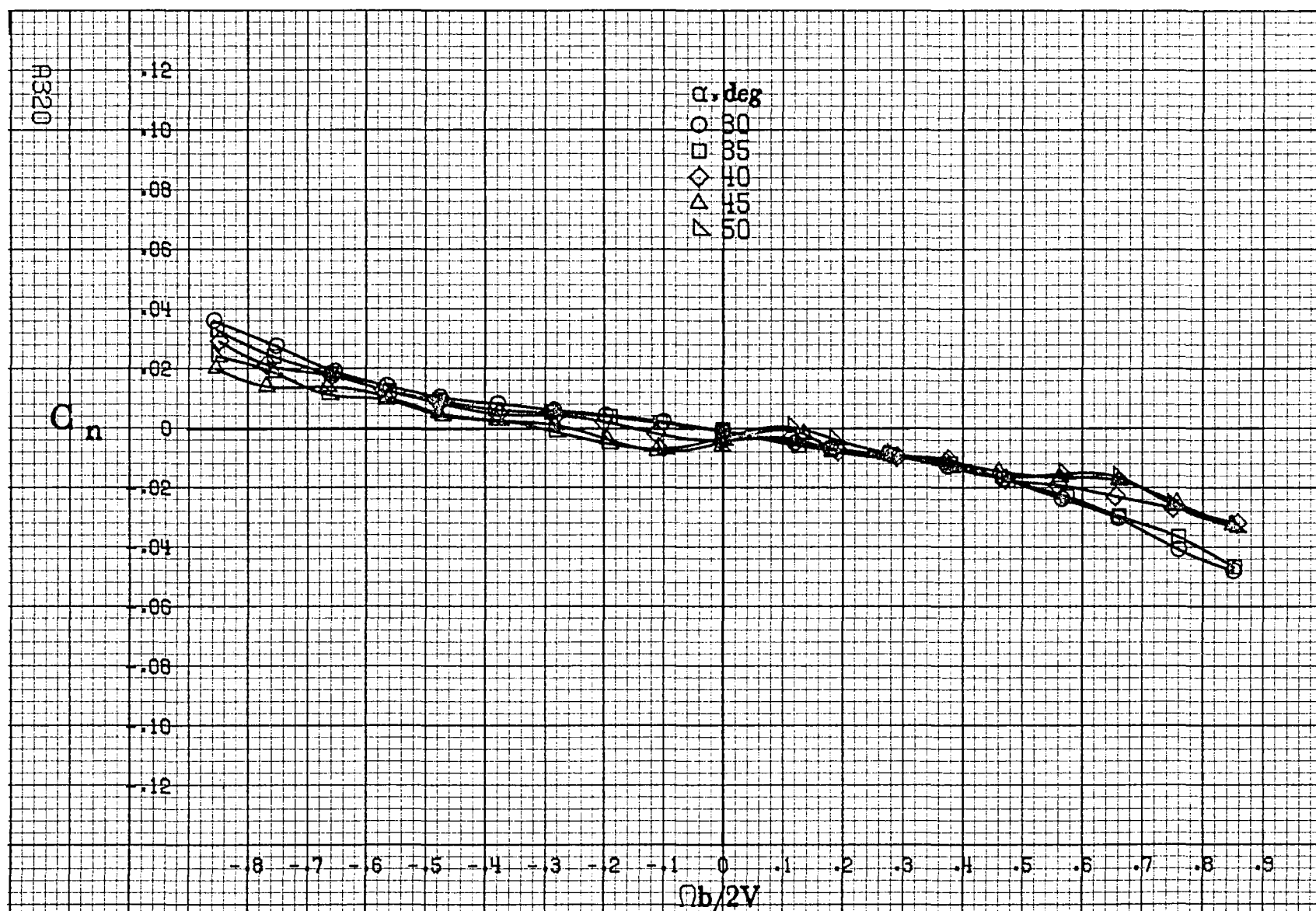
.8
.7
.6
.5
.4
.3
.2
.1
0
-.1
-.2
-.3
-.4

-.8 -.7 -.6 -.5 -.4 -.3 -.2 -.1 0 .1 .2 .3 .4 .5 .6 .7 .8 .9

$\Omega b/2V$

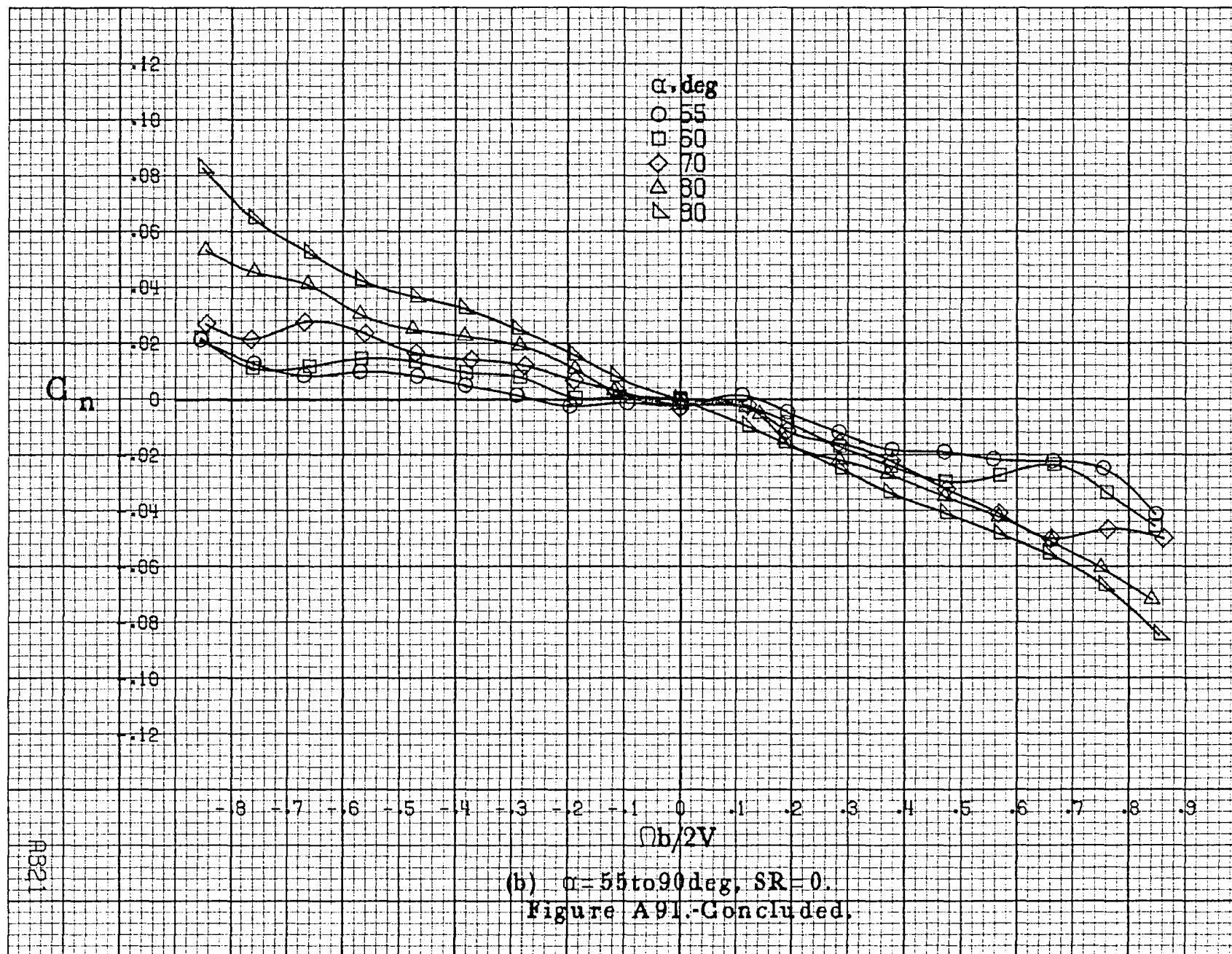
(d) $\alpha=55$ to 90 deg, $SR=0$.
Figure A90.-Concluded.

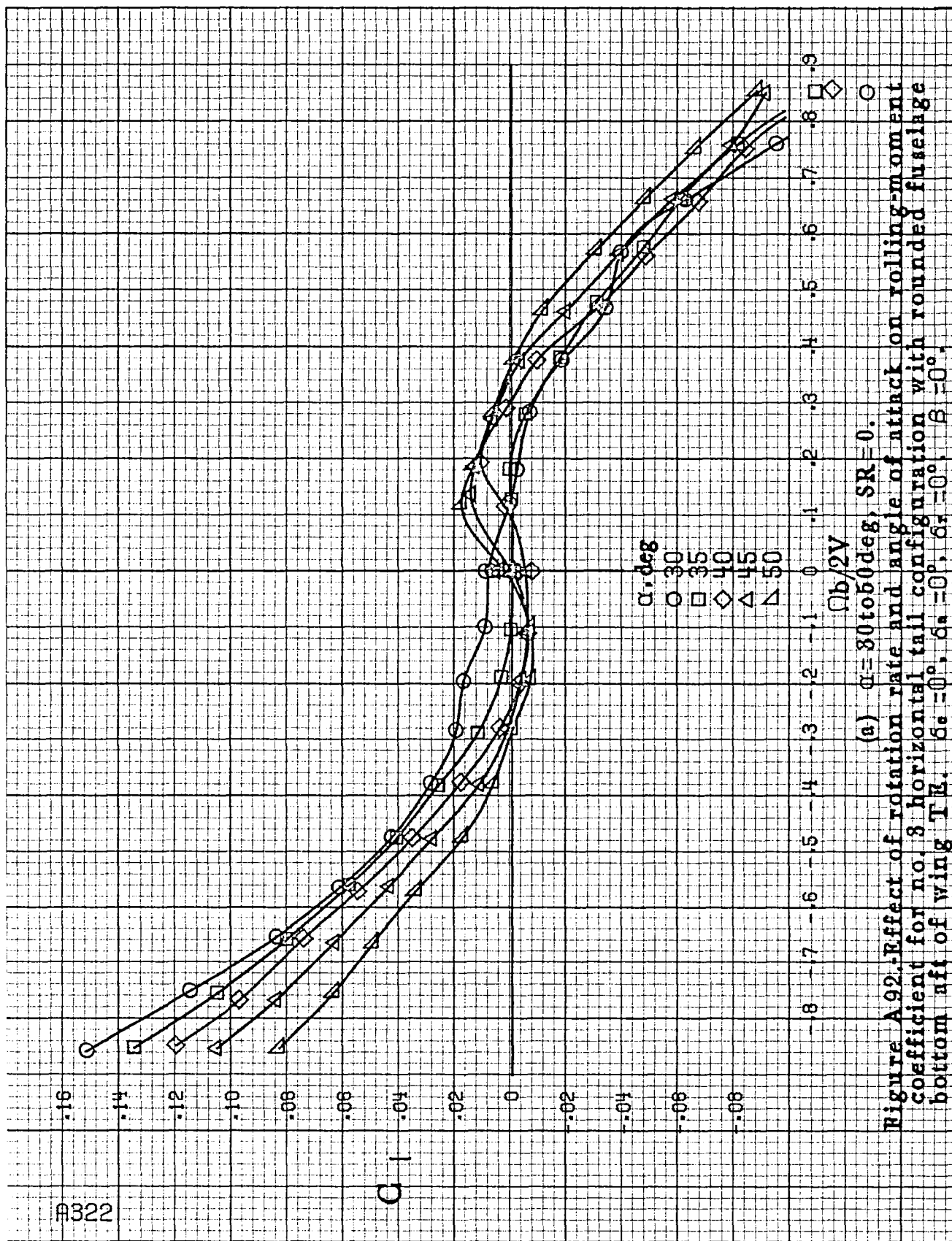
A9319

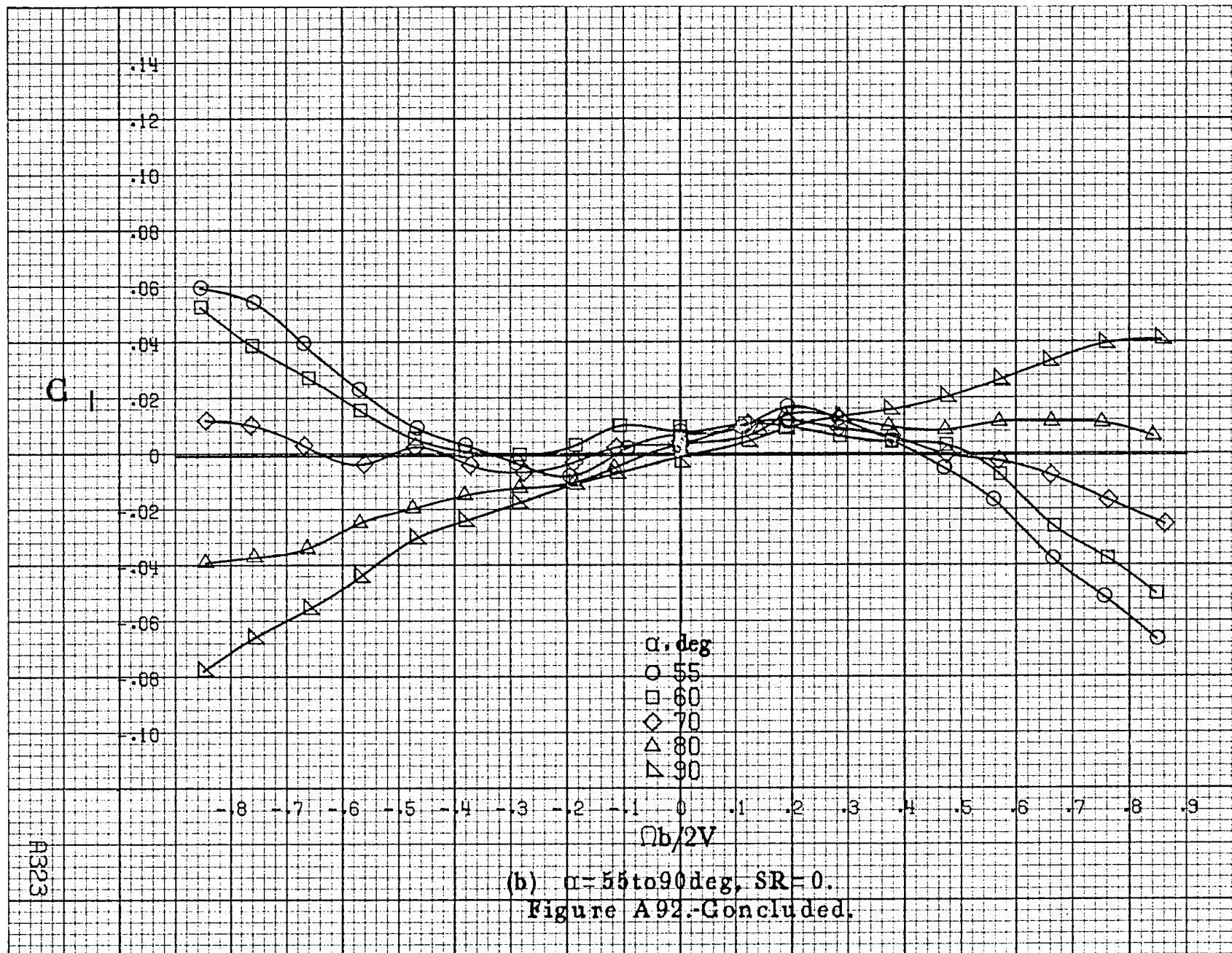


(a) $\alpha = 30$ to 50 deg, $SR = 0$.

Figure A91.-Effect of rotation rate and angle of attack on yawing-moment coefficient for no. 3 horizontal tail configuration with rounded fuselage bottom aft of wing T.E. $\delta_e = 0^\circ$, $\delta_a = 0^\circ$, $\delta_r = 0^\circ$, $\beta = 0^\circ$.







A9324

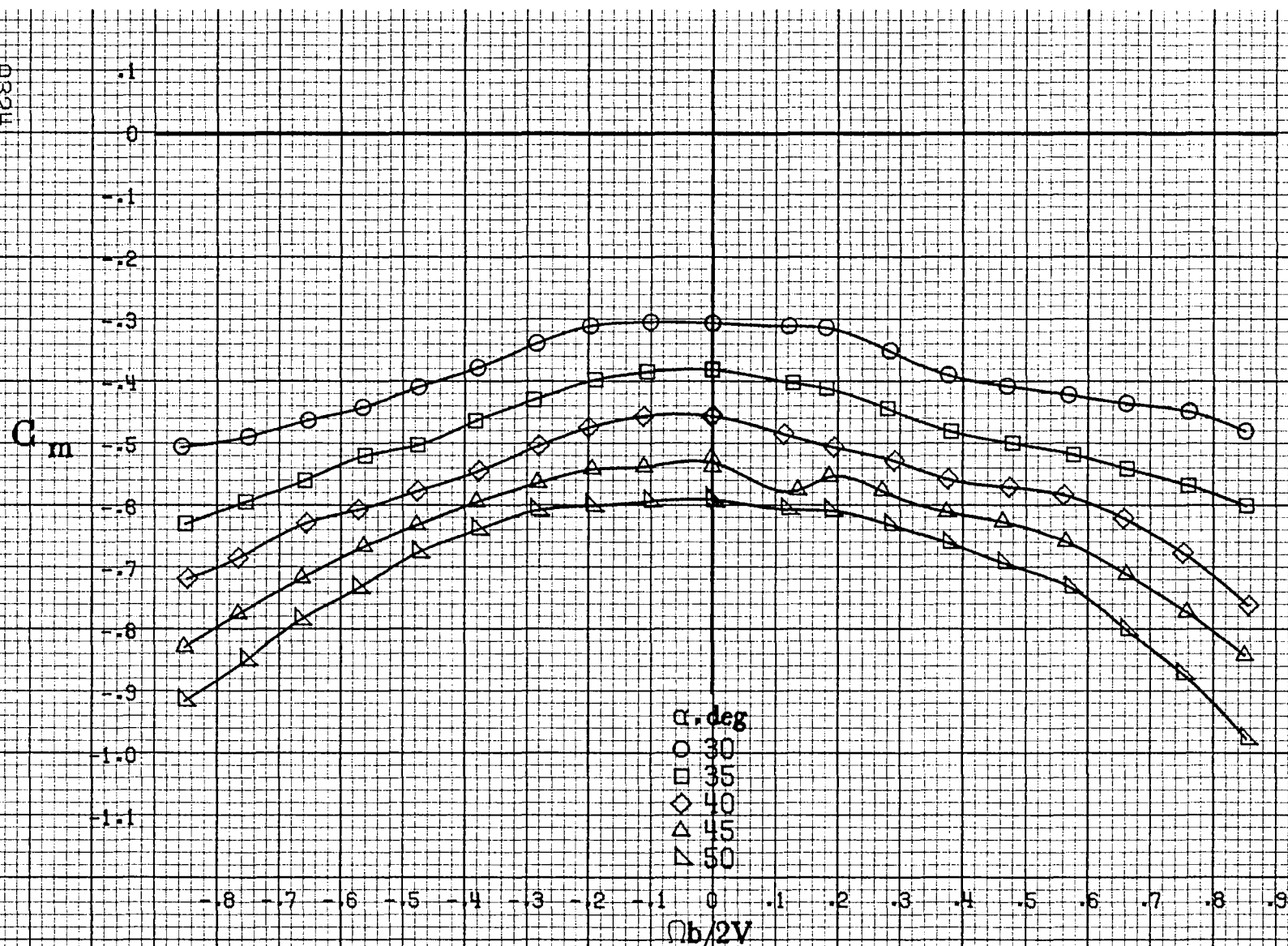
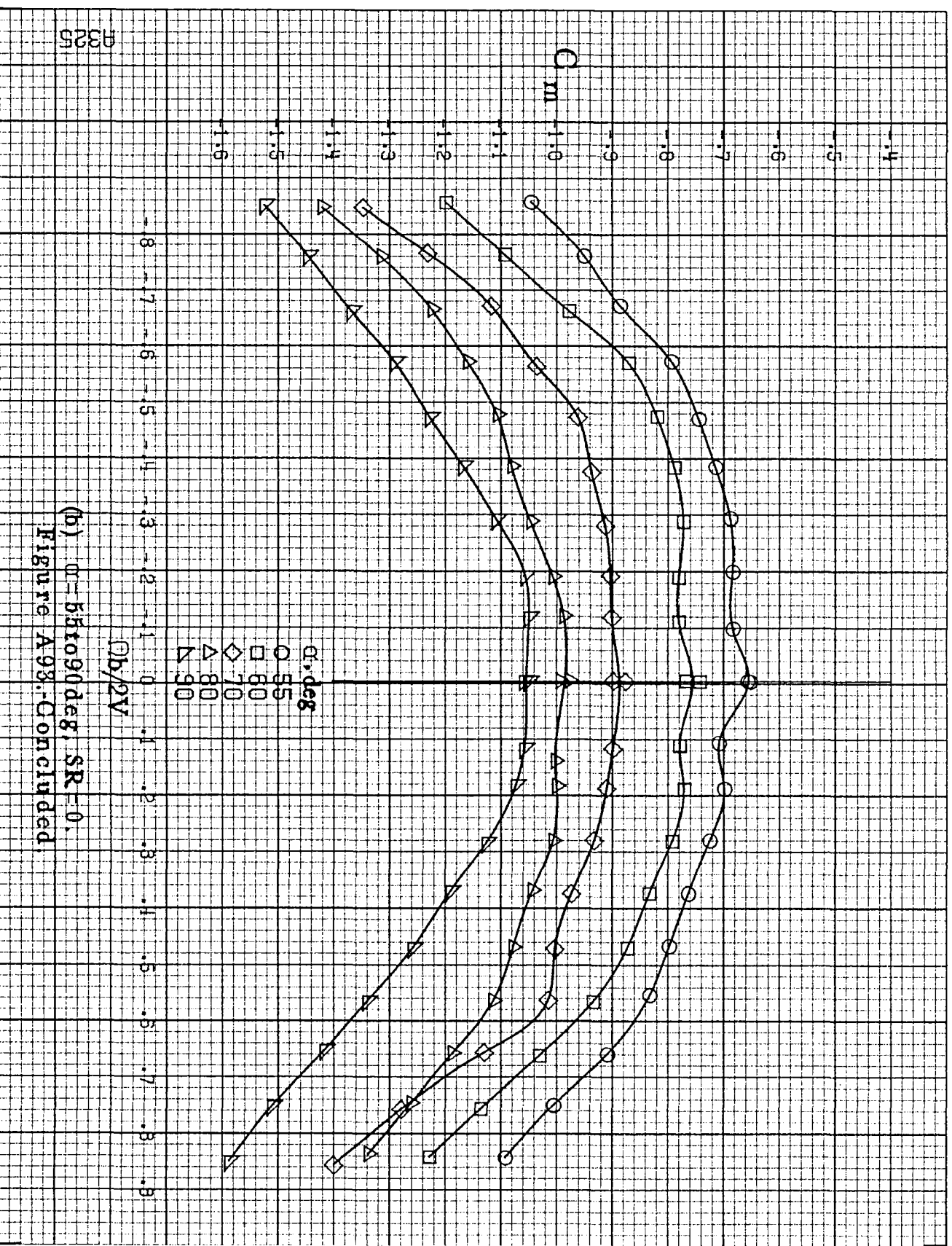
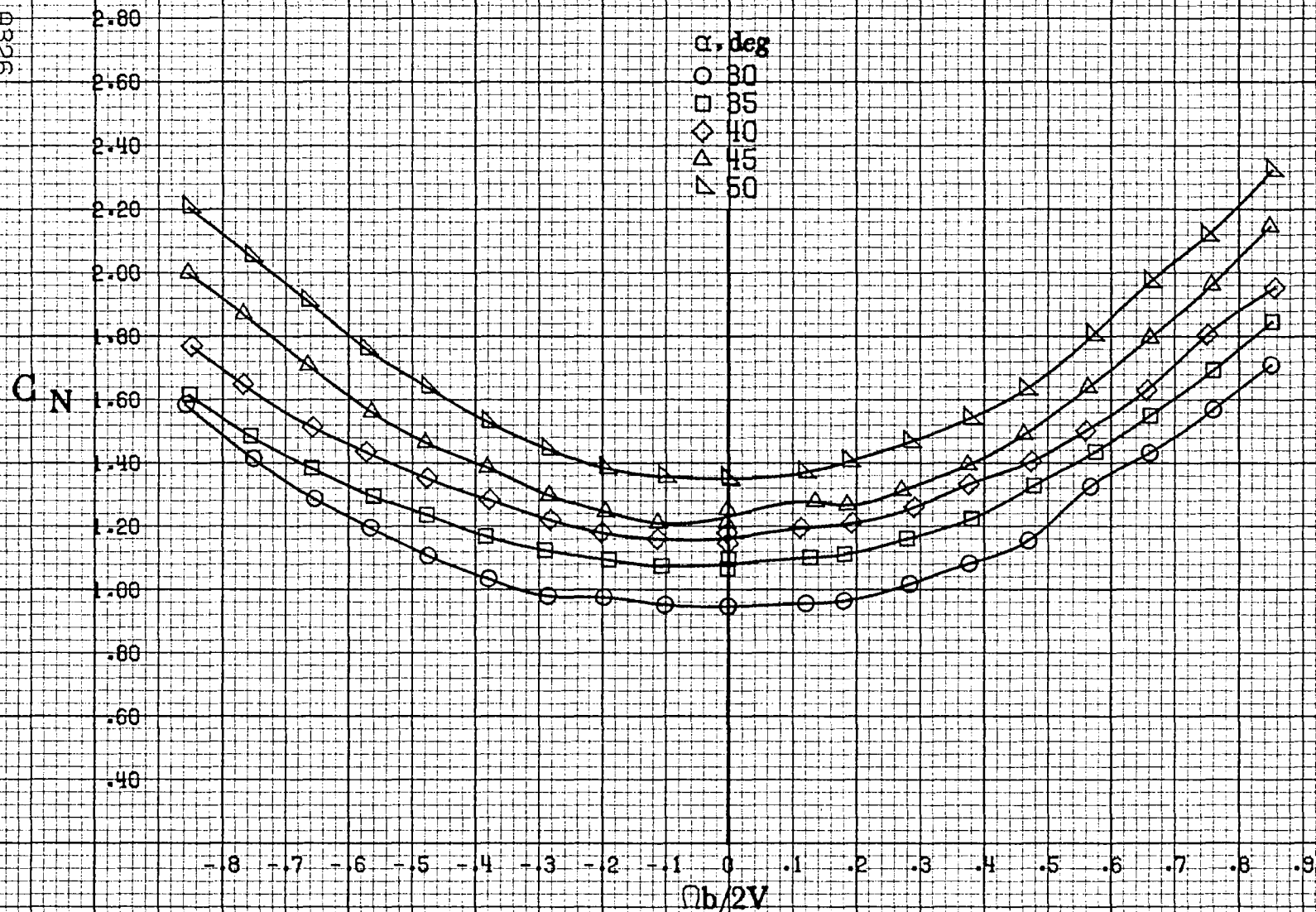
(a) $\alpha = 30$ to 50 deg, $SR = 0$.

Figure A93.-Effect of rotation rate and angle of attack on pitching-moment coefficient for no. 3 horizontal tail configuration with rounded fuselage bottom aft of wing T.E. $\delta_e = 0^\circ$, $\delta_s = 0^\circ$, $\delta_r = 0^\circ$, $\beta = 0^\circ$.



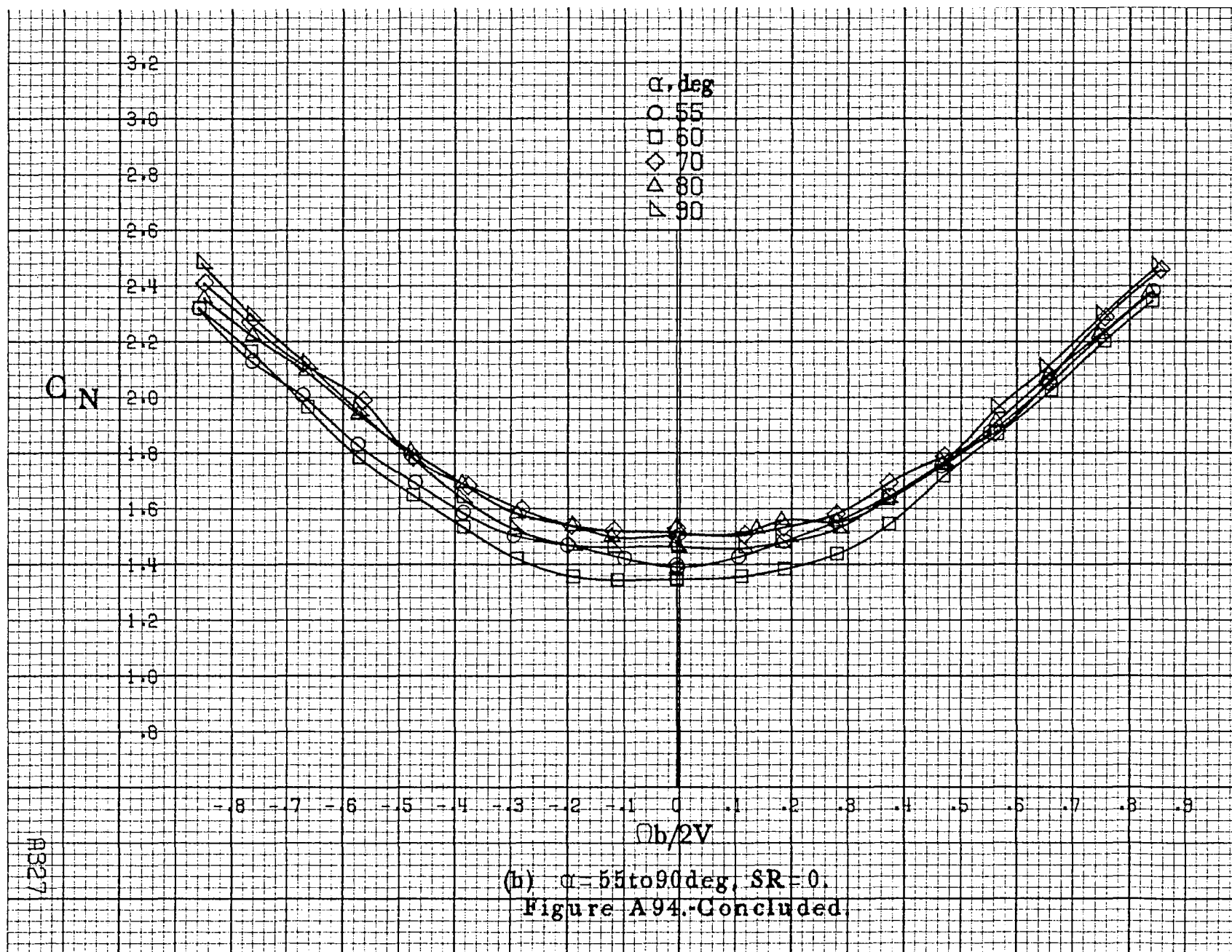
(b) $\omega = 5\pi \times 10^9$ deg, SR = 0.
Figure A93. Concluded.

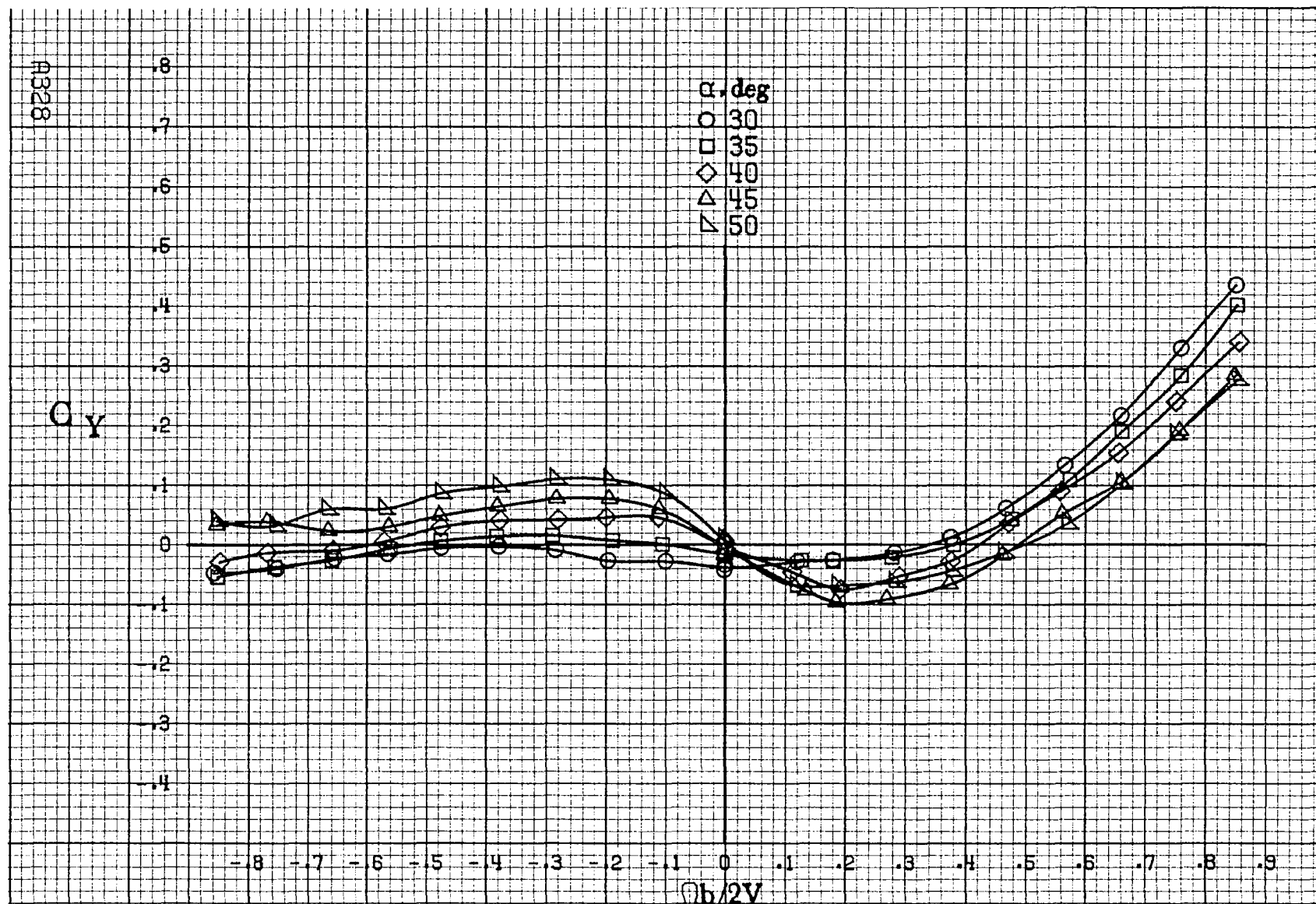
1326



(a) $\alpha = 30$ to 50 deg, $SR = 0$.

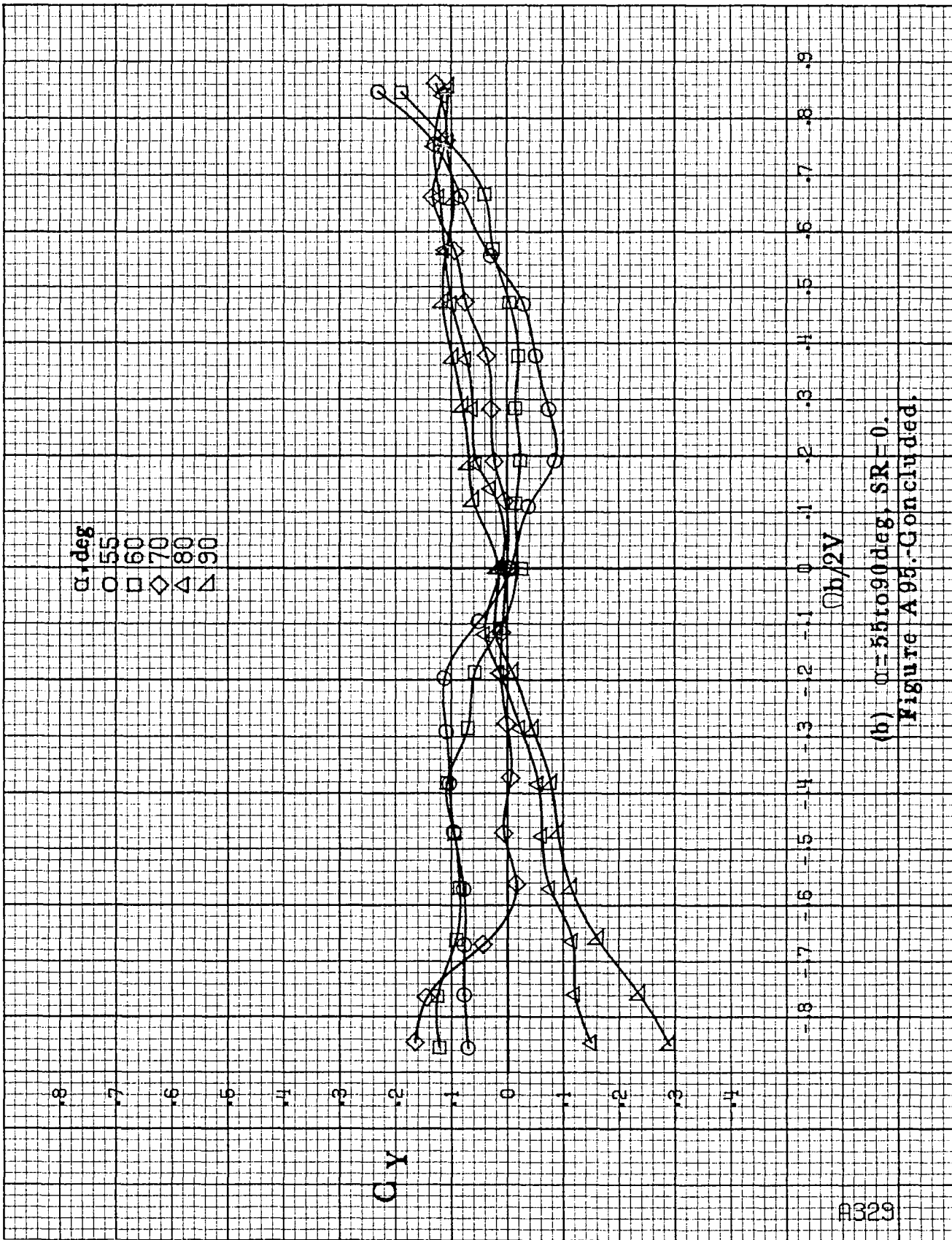
Figure A94. Effect of rotation rate and angle of attack on normal-force coefficient for no. 3 horizontal tail configuration with rounded fuselage bottom aft of wing T.E. $\delta_e = 0^\circ$, $\delta_a = 0^\circ$, $\delta_r = 0^\circ$, $\beta = 0^\circ$.



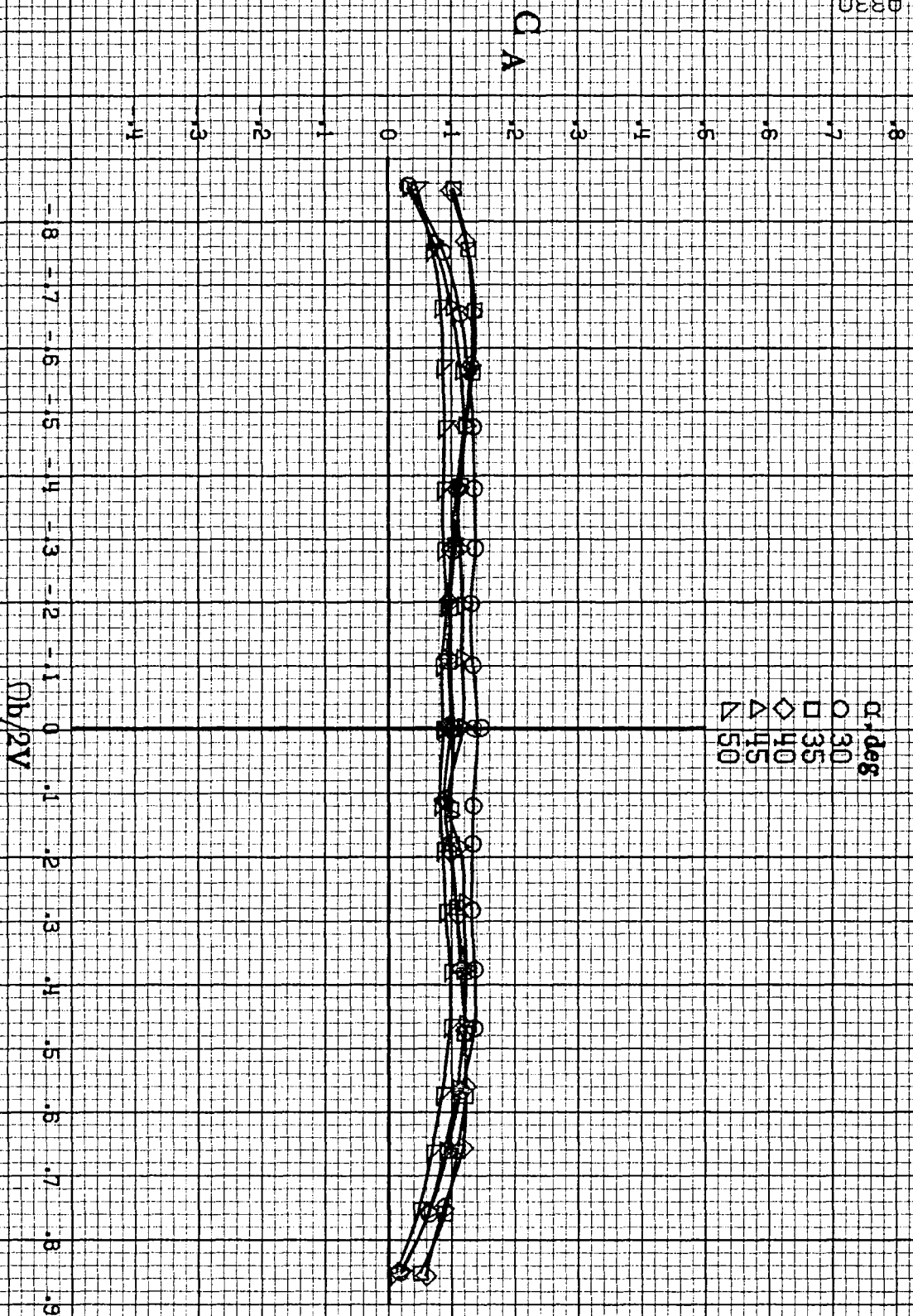


(a) $\alpha=30$ to 50° , $SR=0$.

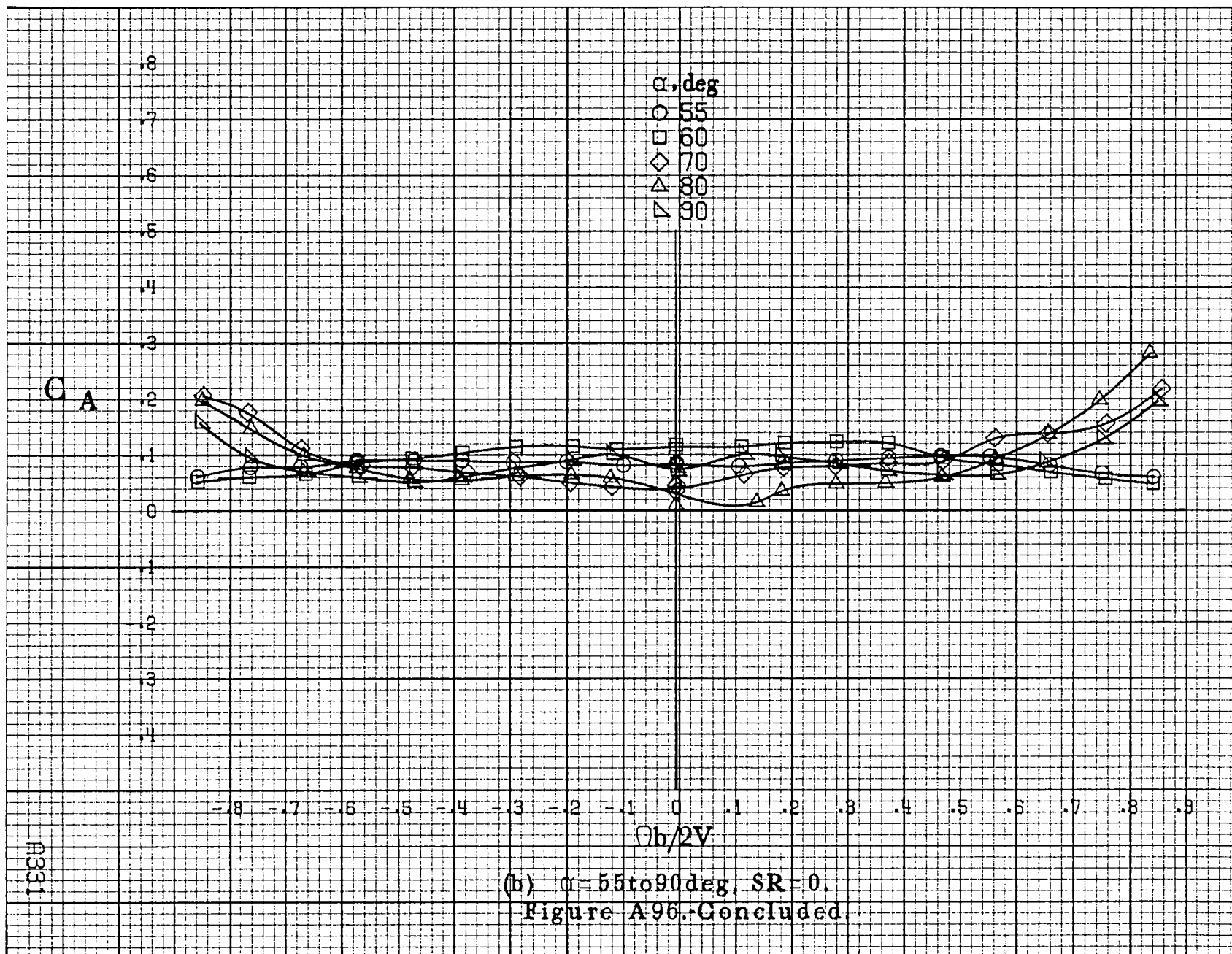
Figure A95. Effect of rotation rate and angle of attack on side-force coefficient for no. 3 horizontal tail configuration with rounded fuselage bottom aft of wing T.E. $\delta_a=0^\circ$, $\delta_s=0^\circ$, $\delta_r=0^\circ$, $\beta=0^\circ$.

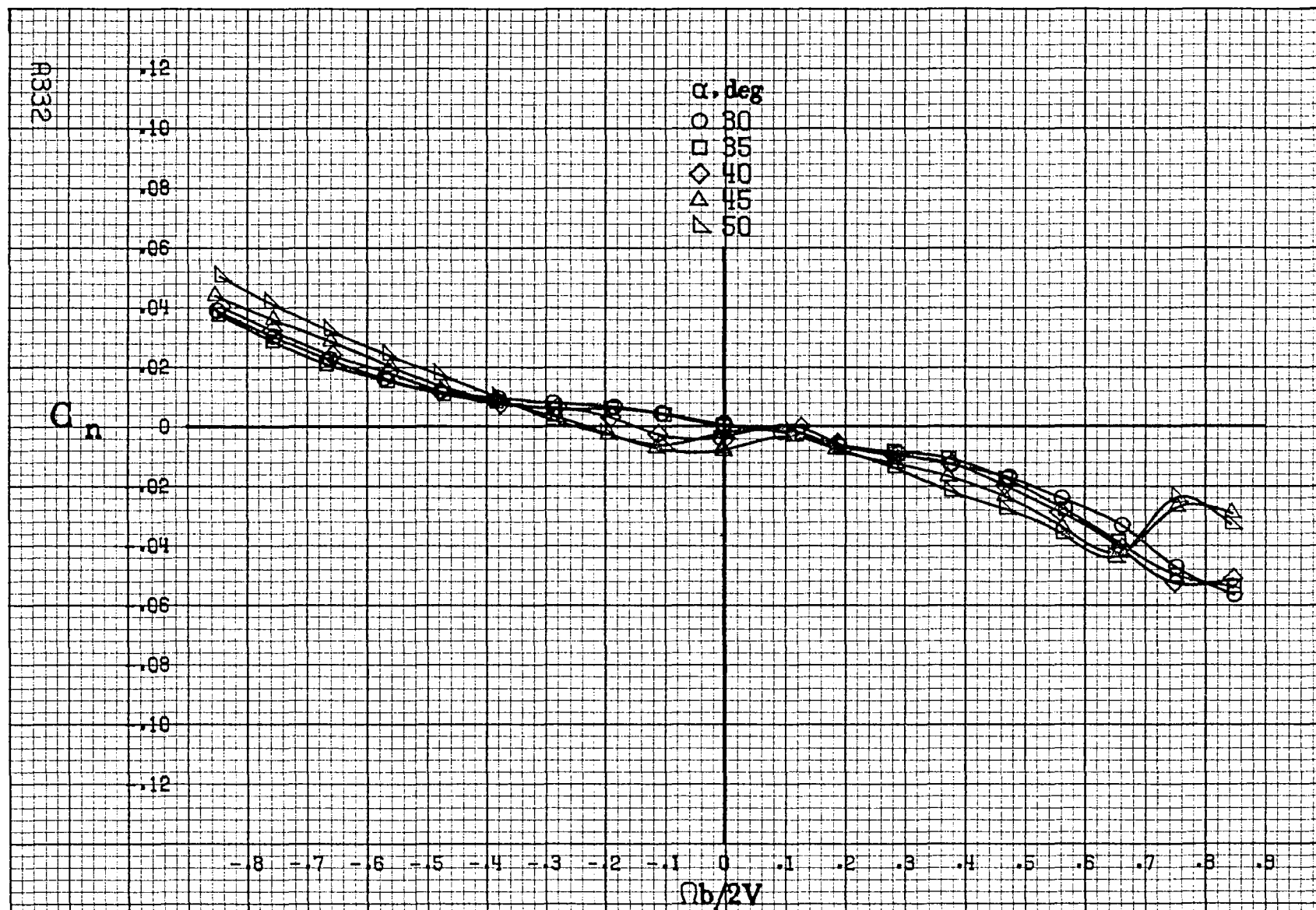


(b) $\alpha=55$ to 90° , $SR=0$.
Figure A95.-Concluded.



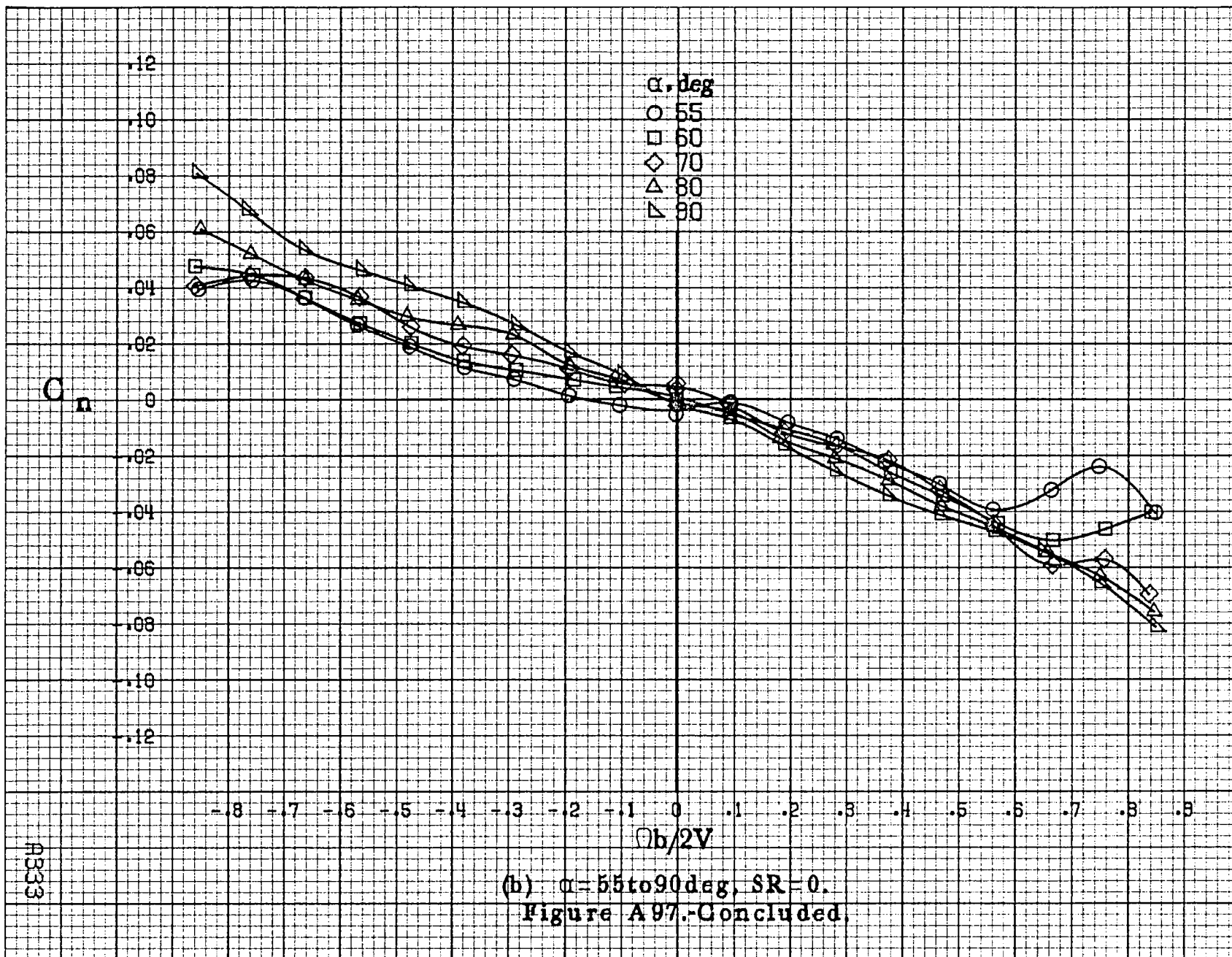
(a) $\alpha = 30$ to 50 deg, $SR = 0$.

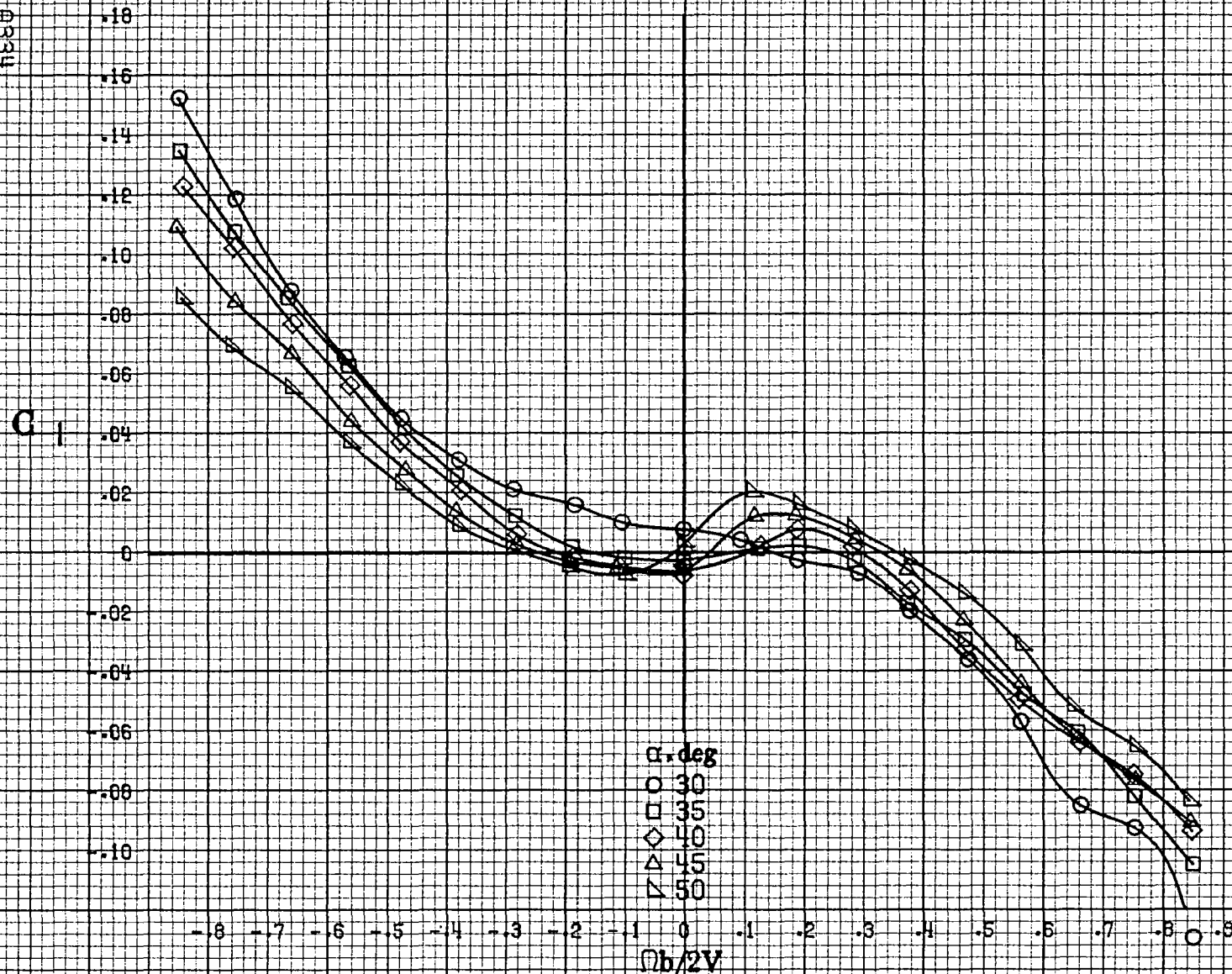




(a) $\alpha = 30$ to 50 deg, $SR = 0$.

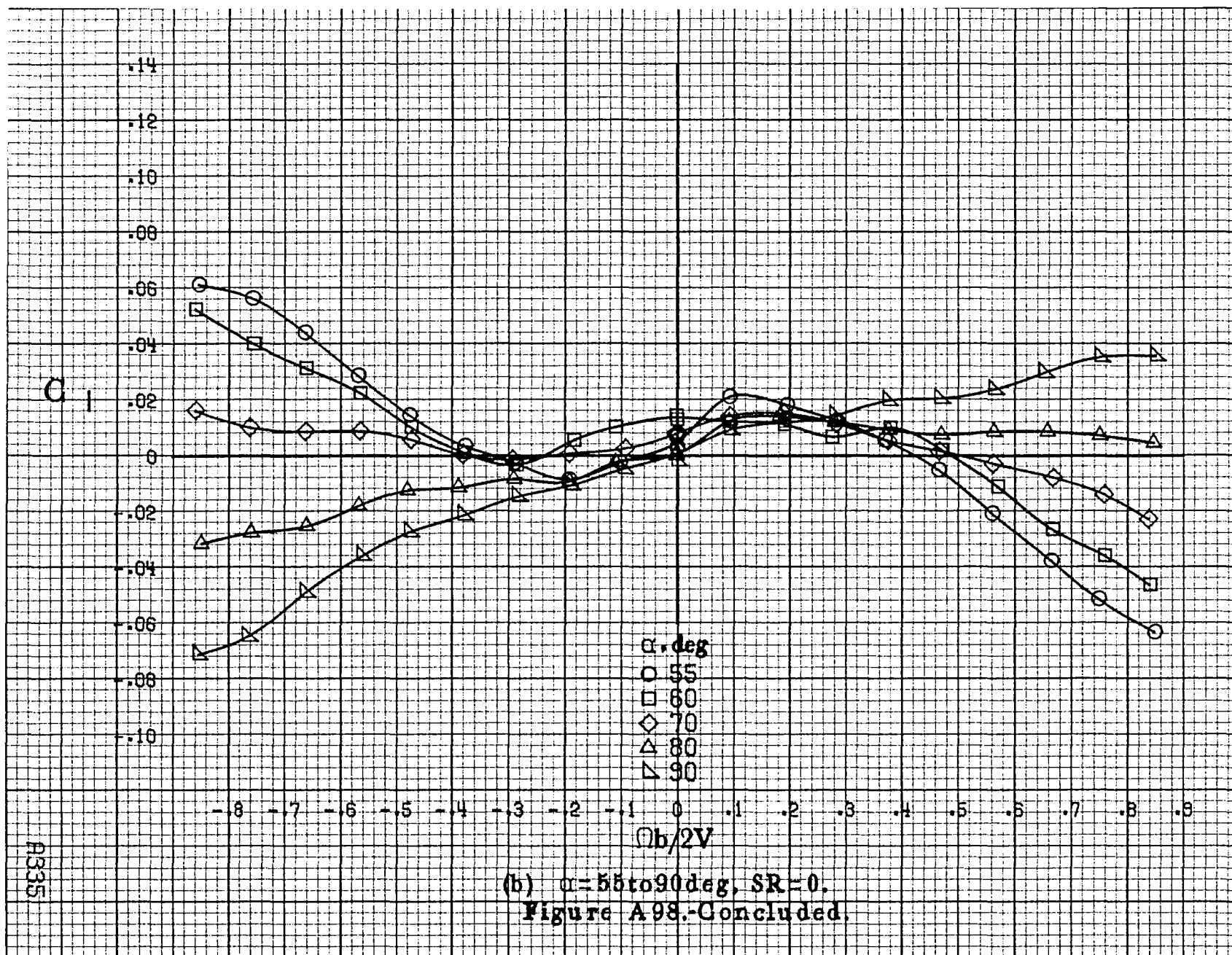
Figure A97. Effect of rotation rate and angle of attack on yawing-moment coefficient for no. 3 horizontal tail configuration with rounded fuselage bottom aft of engine cowlings. $\delta_e = 0^\circ$, $\delta_a = 0^\circ$, $\delta_r = 0^\circ$, $\beta = 0^\circ$.





(a) $\alpha=80$ to 50° , $SR=0$.

Figure A98.-Effect of rotation rate and angle of attack on rolling-moment coefficient for no. 3 horizontal tail configuration with rounded fuselage bottom aft of engine cowling. $\delta_e=0^\circ$, $\delta_a=0^\circ$, $\delta_r=0^\circ$, $\beta=0^\circ$.



A9336

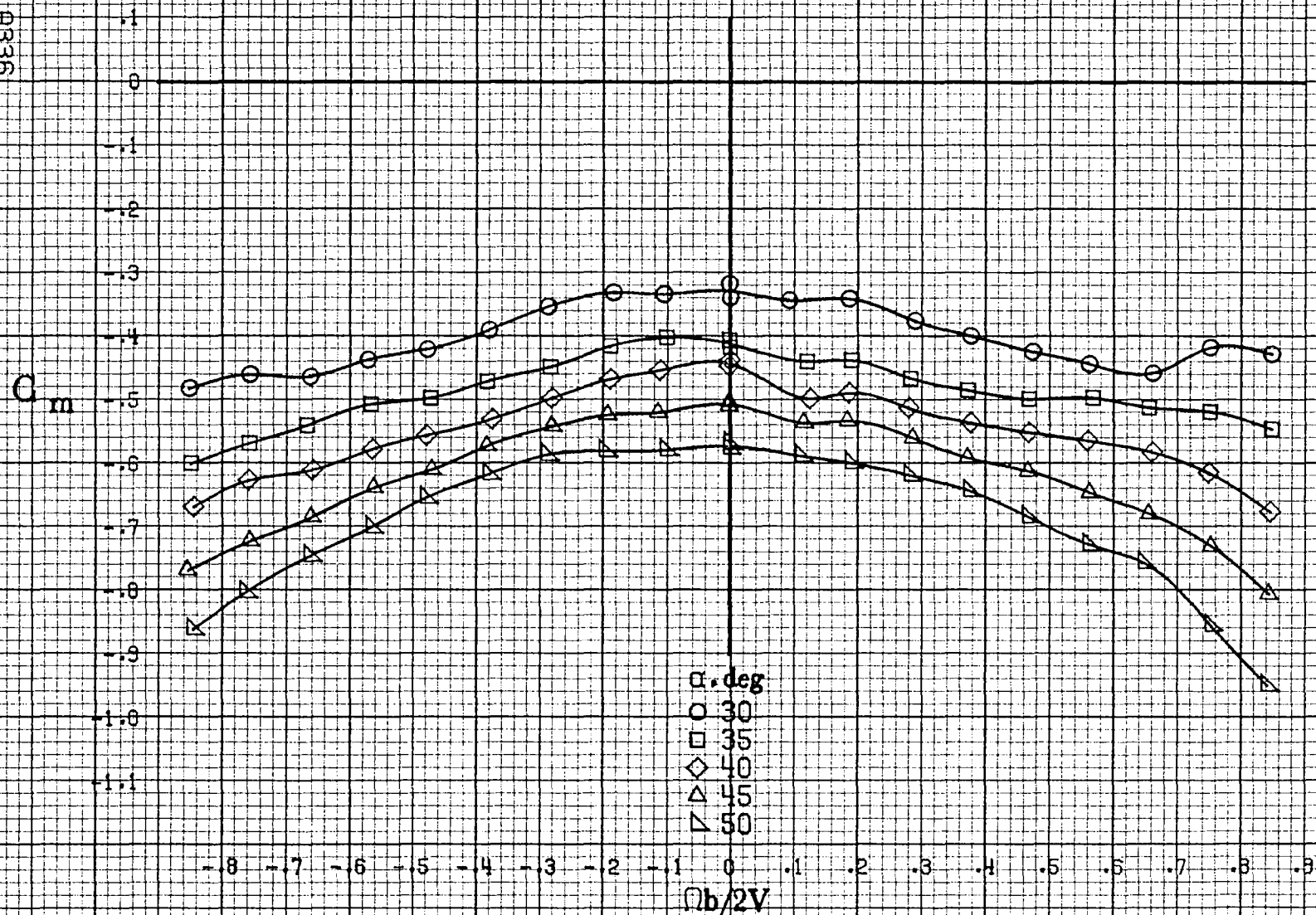
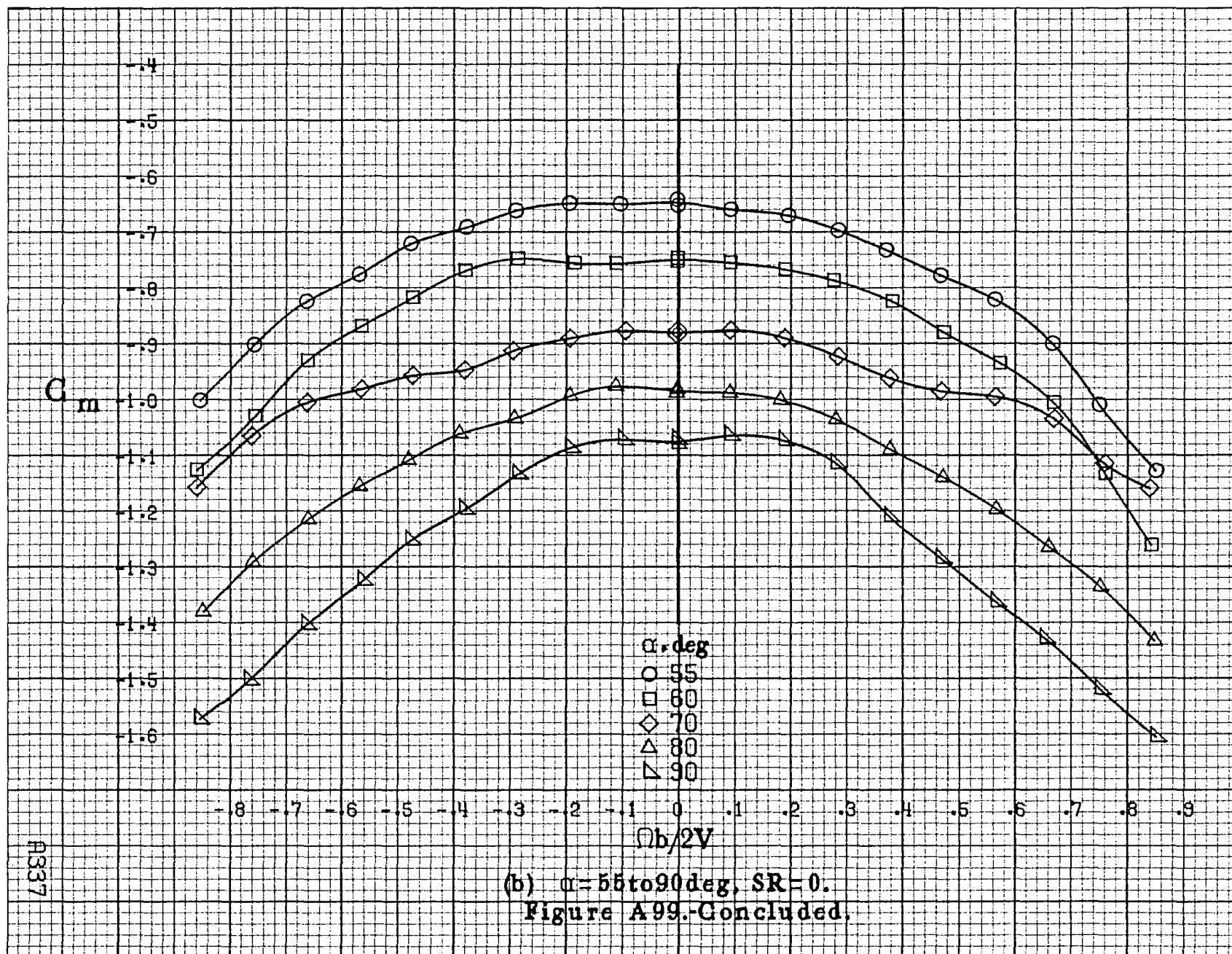
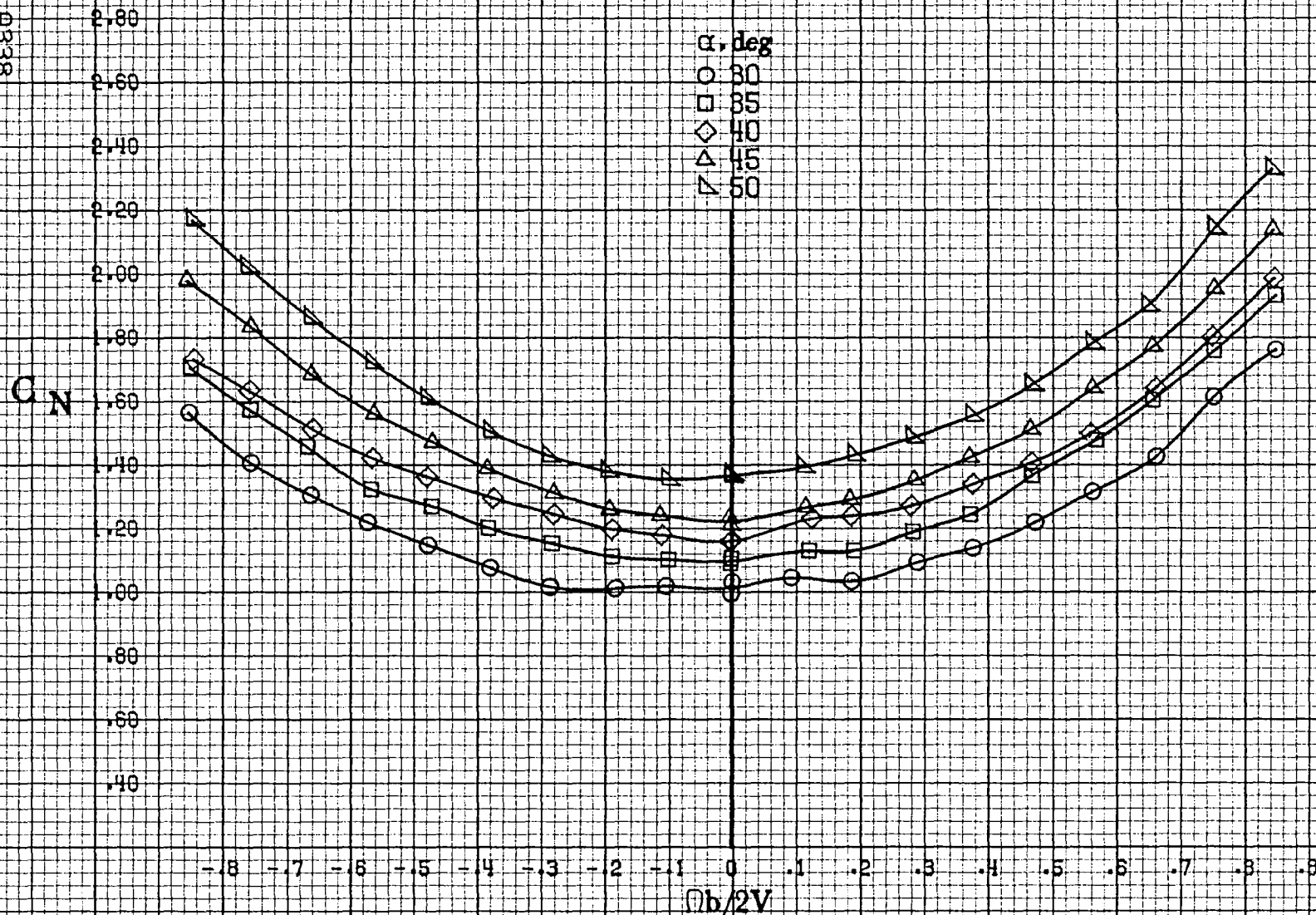
(a) $\alpha = 30$ to 50 deg, $SR = 0$.

Figure A99. Effect of rotation rate and angle of attack on pitching-moment coefficient for no. 8 horizontal tail configuration with rounded fuselage bottom aft of engine cowling. $\delta_e = 0^\circ$, $\delta_a = 0^\circ$, $\delta_r = 0^\circ$, $\beta = 0^\circ$.

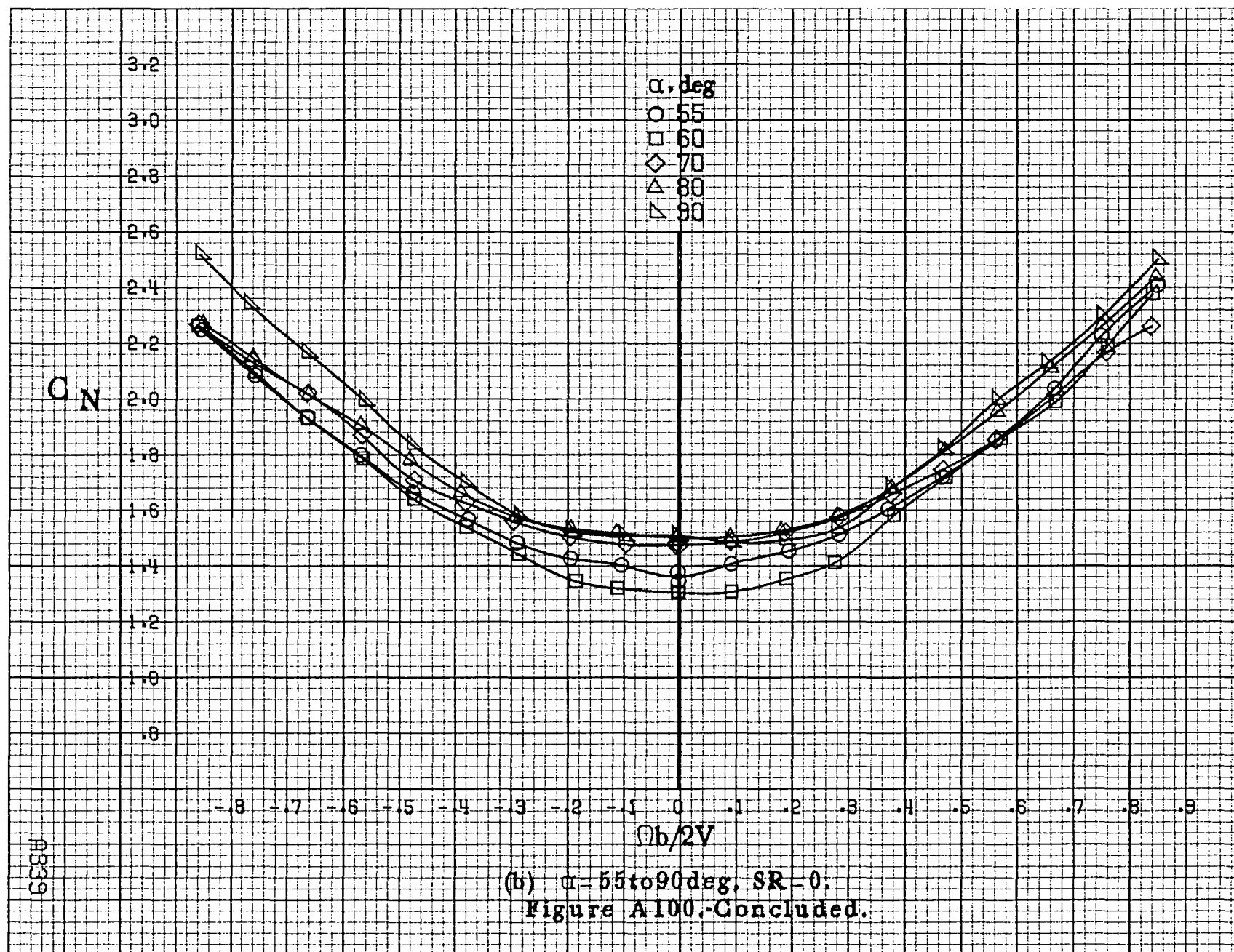


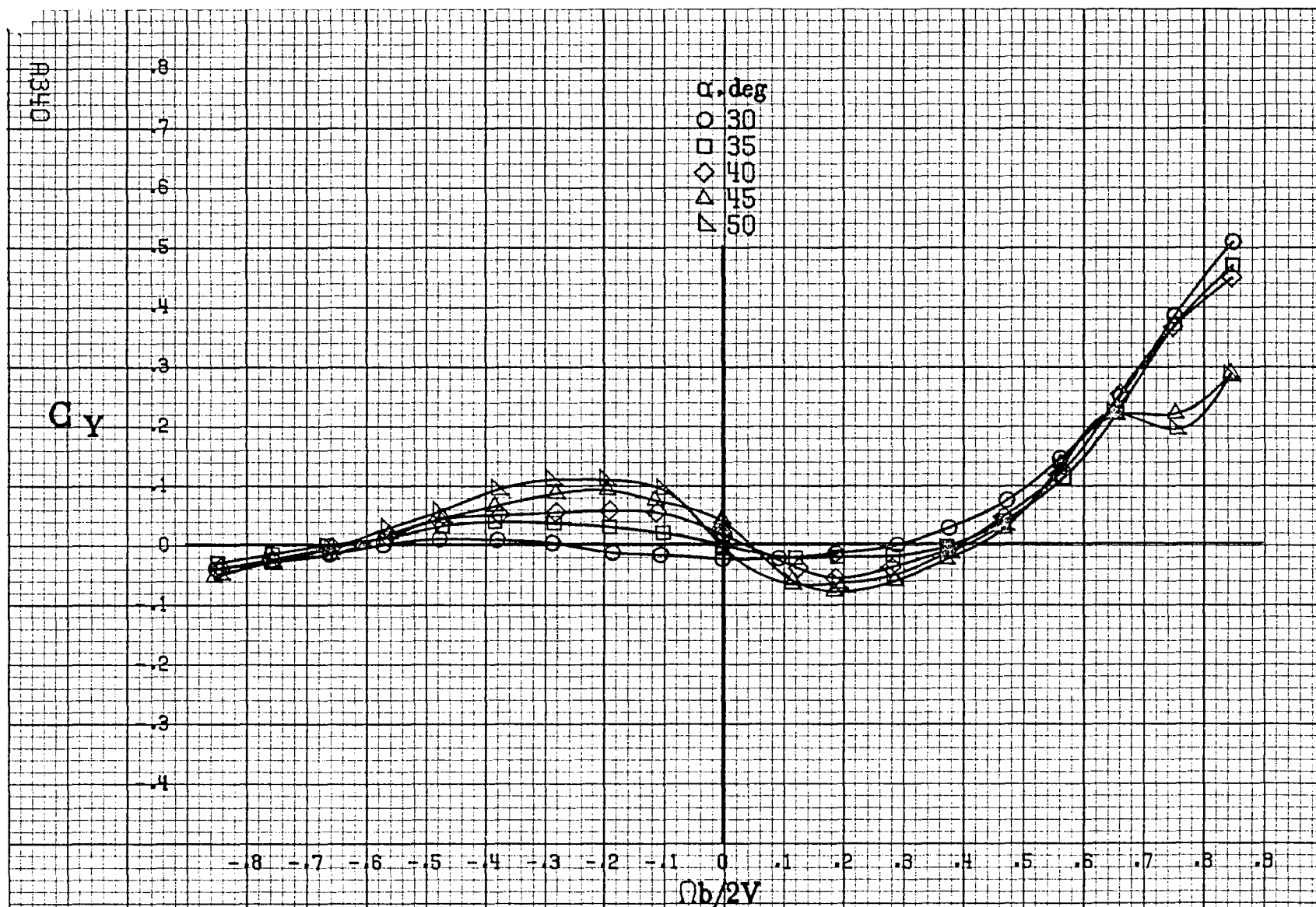
10338



(a) $\alpha = 30$ to 50 deg, $SR = 0$.

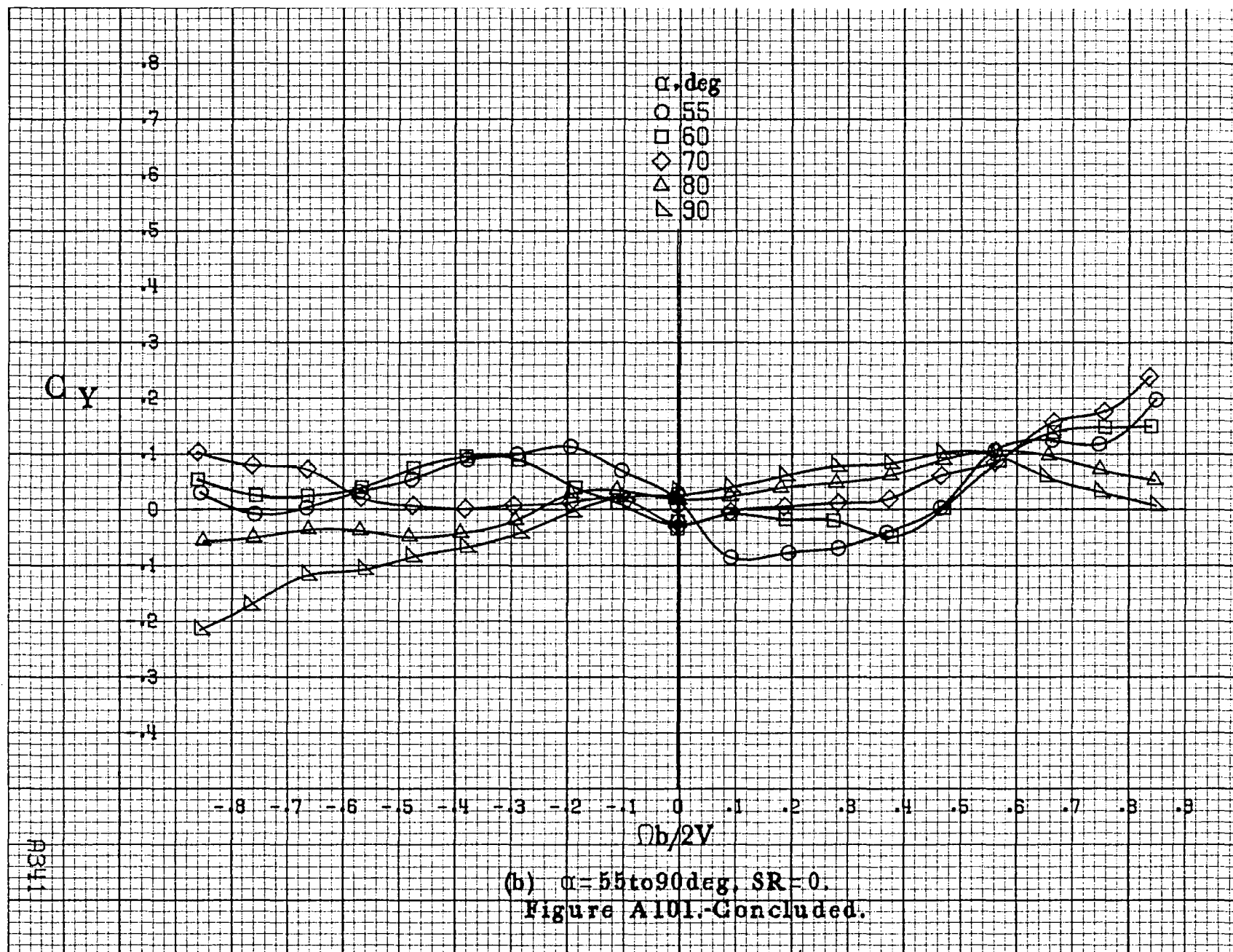
Figure A100.-Effect of rotation rate and angle of attack on normal-force coefficient for no. 3 horizontal tail configuration with rounded fuselage bottom aft of engine cowlings. $\delta_e = 0^\circ$, $\delta_a = 0^\circ$, $\delta_r = 0^\circ$, $\beta = 0^\circ$.

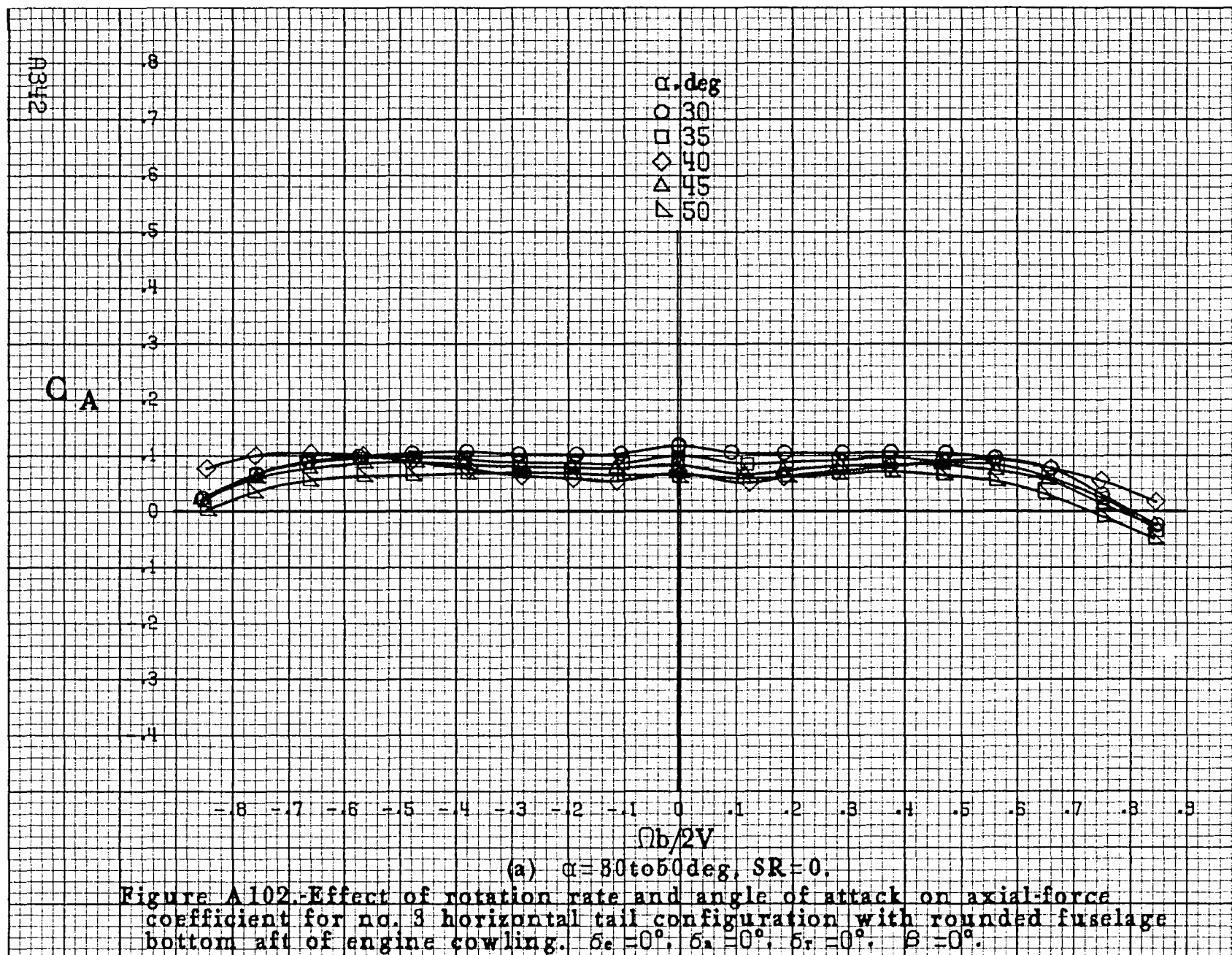


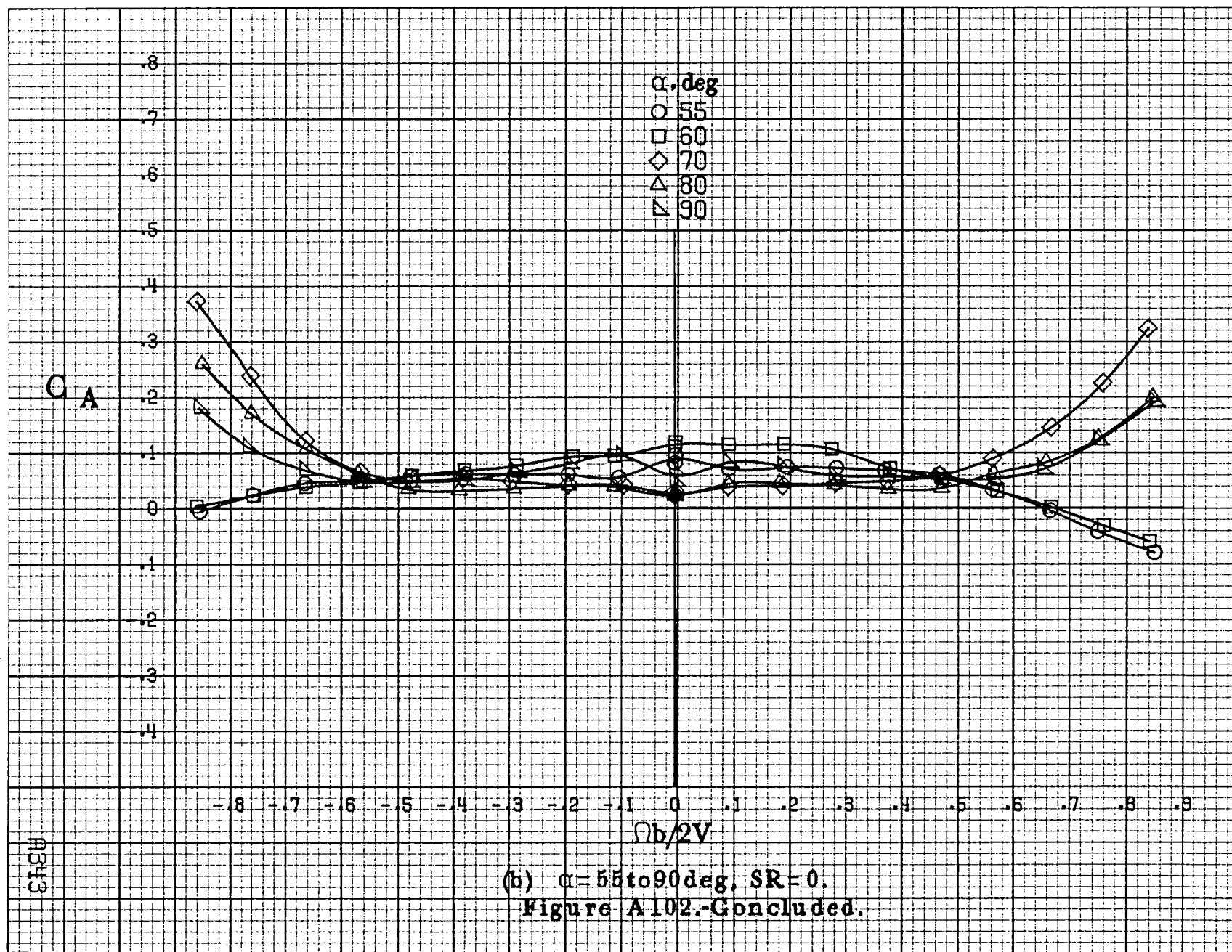


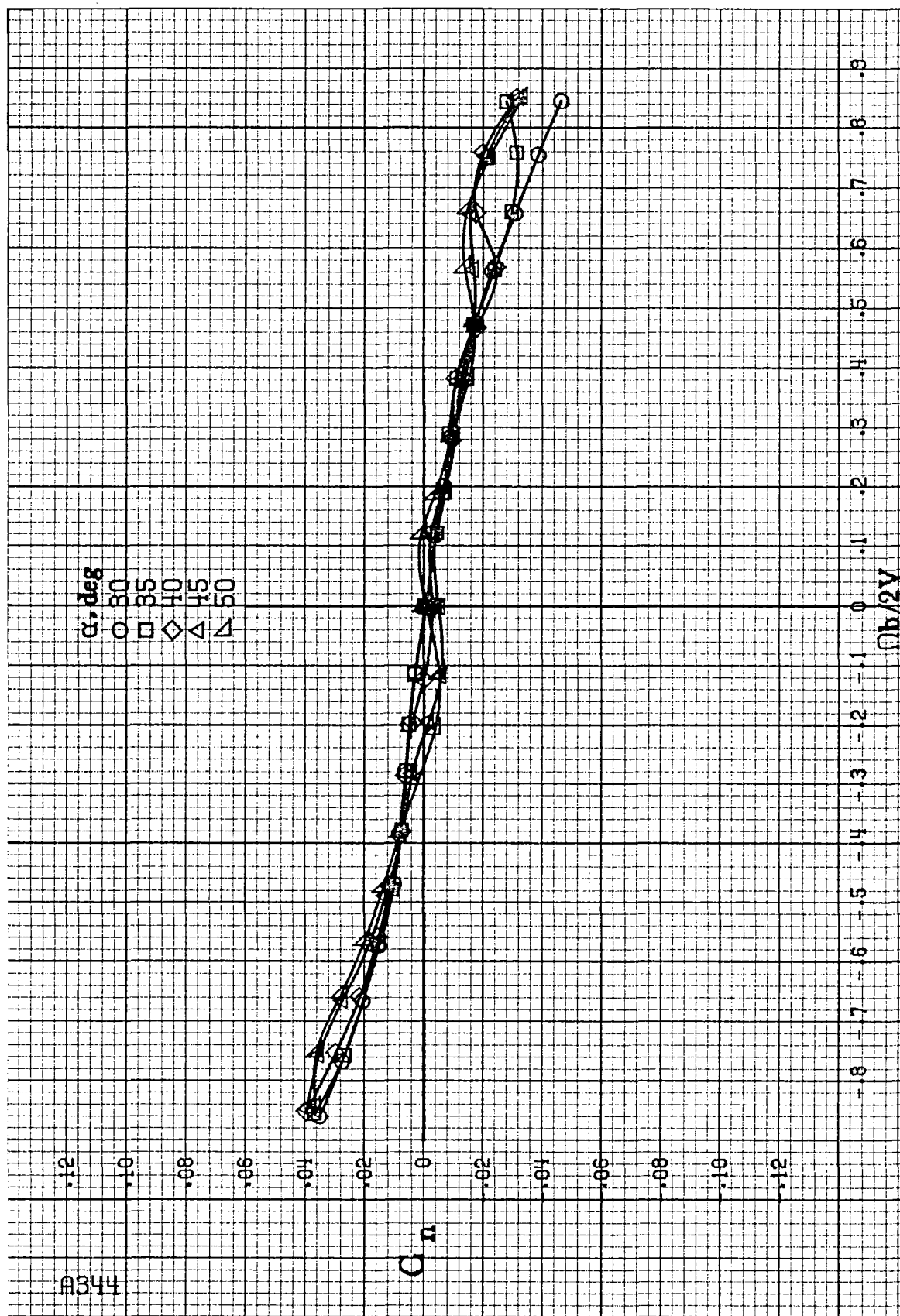
(a) $\alpha = 30$ to 50° , $SR = 0$.

Figure A101.-Effect of rotation rate and angle of attack on side-force coefficient for no. 3 horizontal tail configuration with rounded fuselage bottom aft of engine cowlings. $\delta_e = 0^\circ$, $\delta_a = 0^\circ$, $\delta_r = 0^\circ$, $\beta = 0^\circ$.



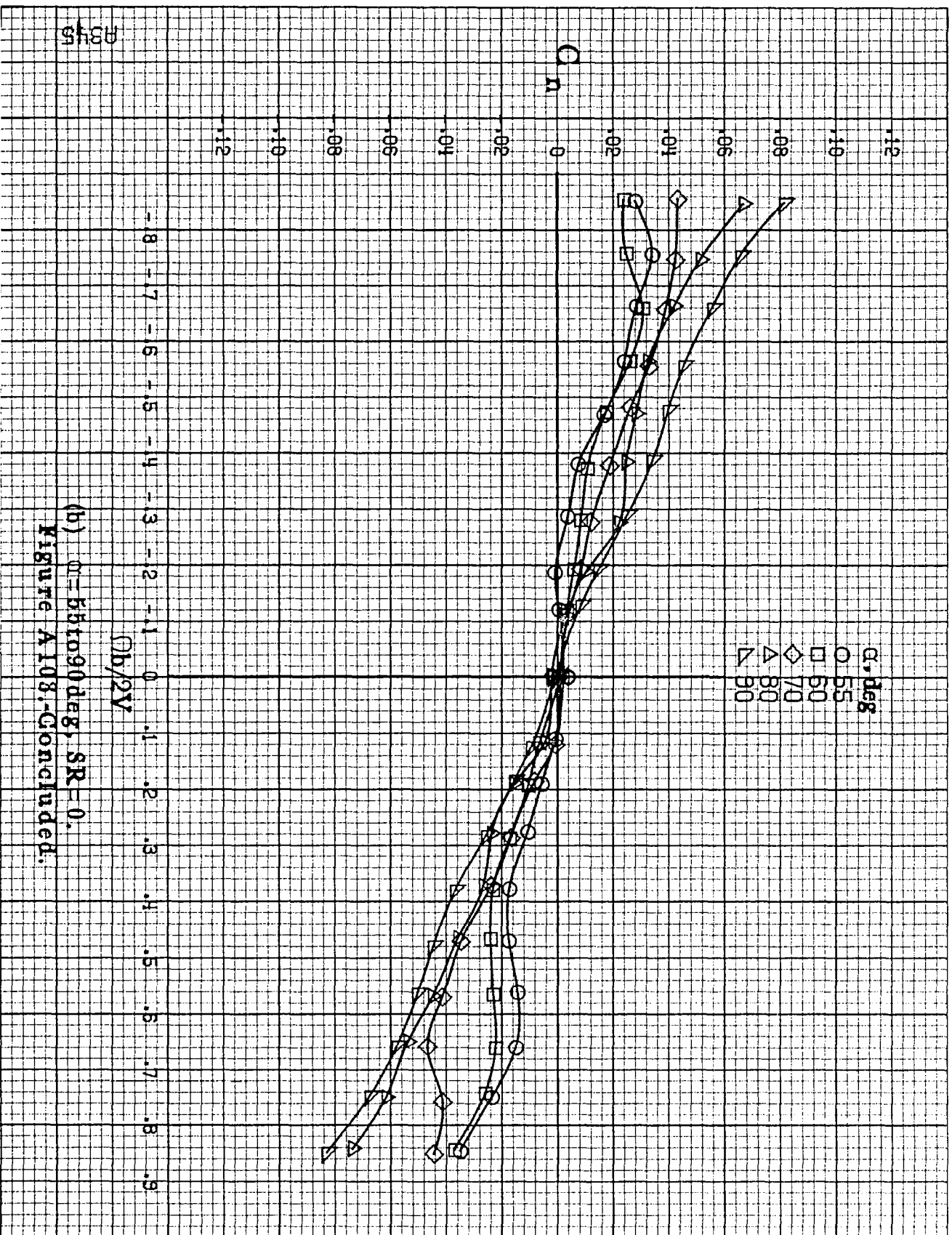






(a) $\alpha=30$ to 50 deg, $SR=0$.

Figure A108.-Effect of rotation rate and angle of attack on yawing-moment coefficient for no. 3 horizontal tail configuration with rounded fuselage bottom aft of wing TE, wing fairings removed. $\delta_e=0^\circ$, $\delta_r=0^\circ$, $\beta=0^\circ$.



8345

(b) $\alpha = 55$ to 90° , $SR = 0$.
Figure A108-Concluded.

A8346

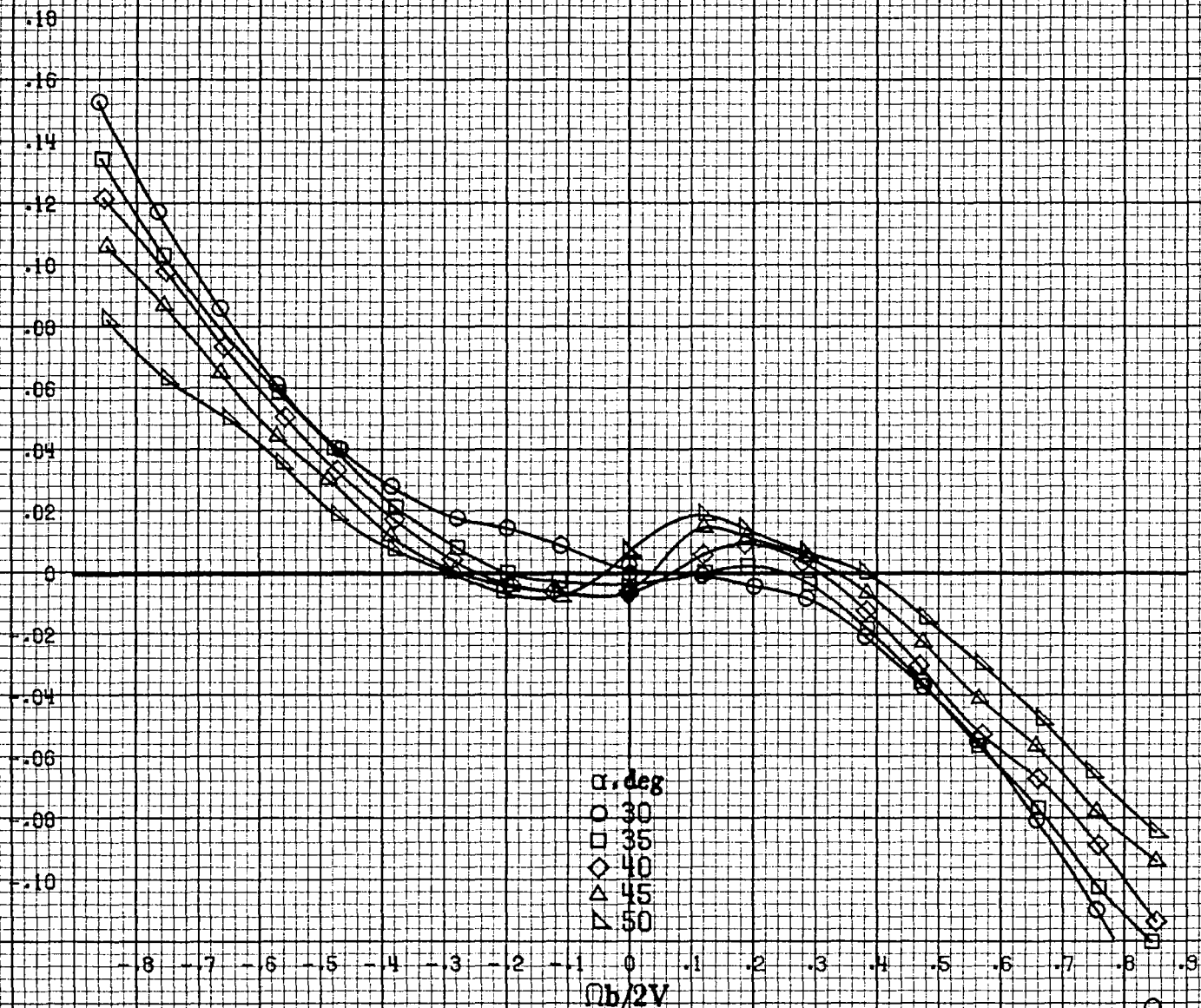
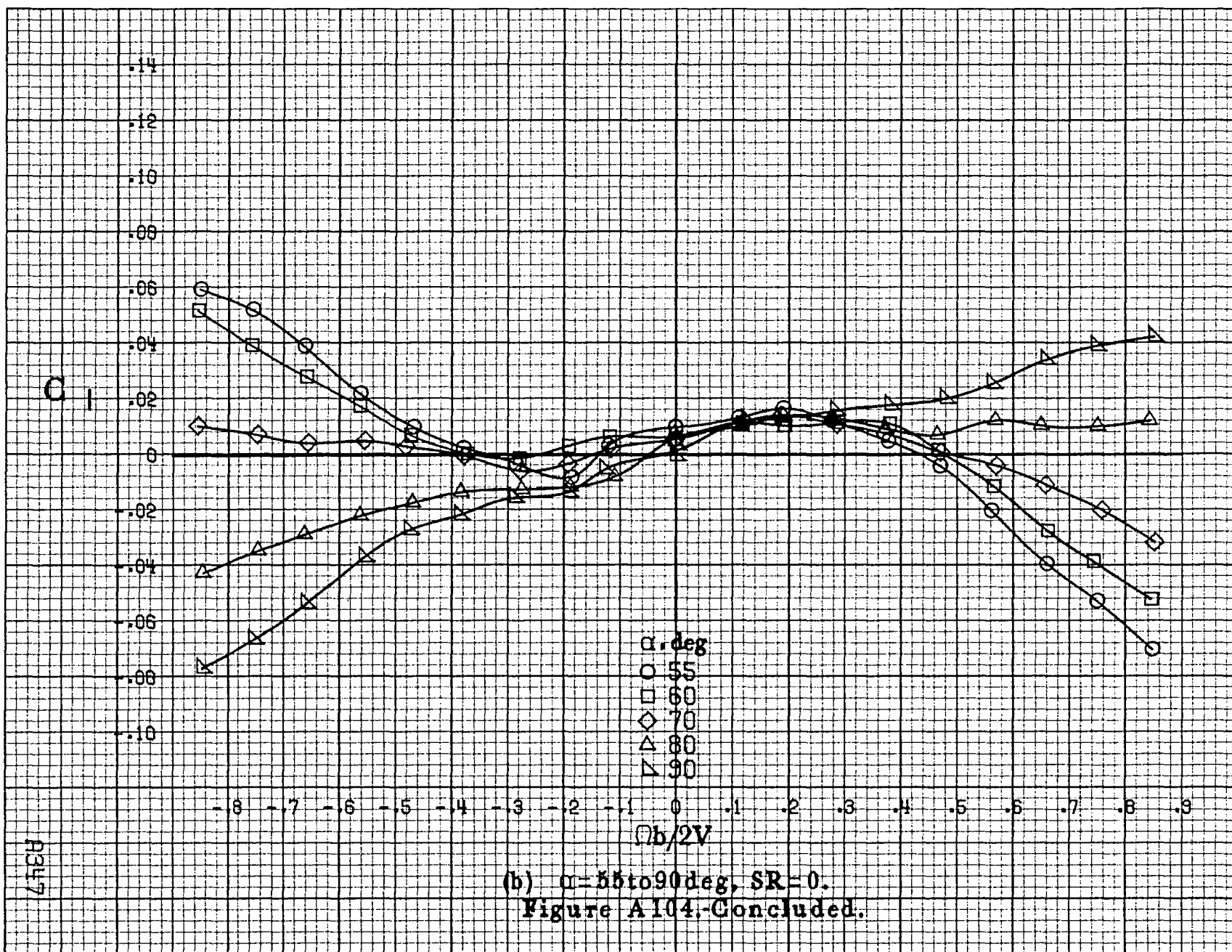
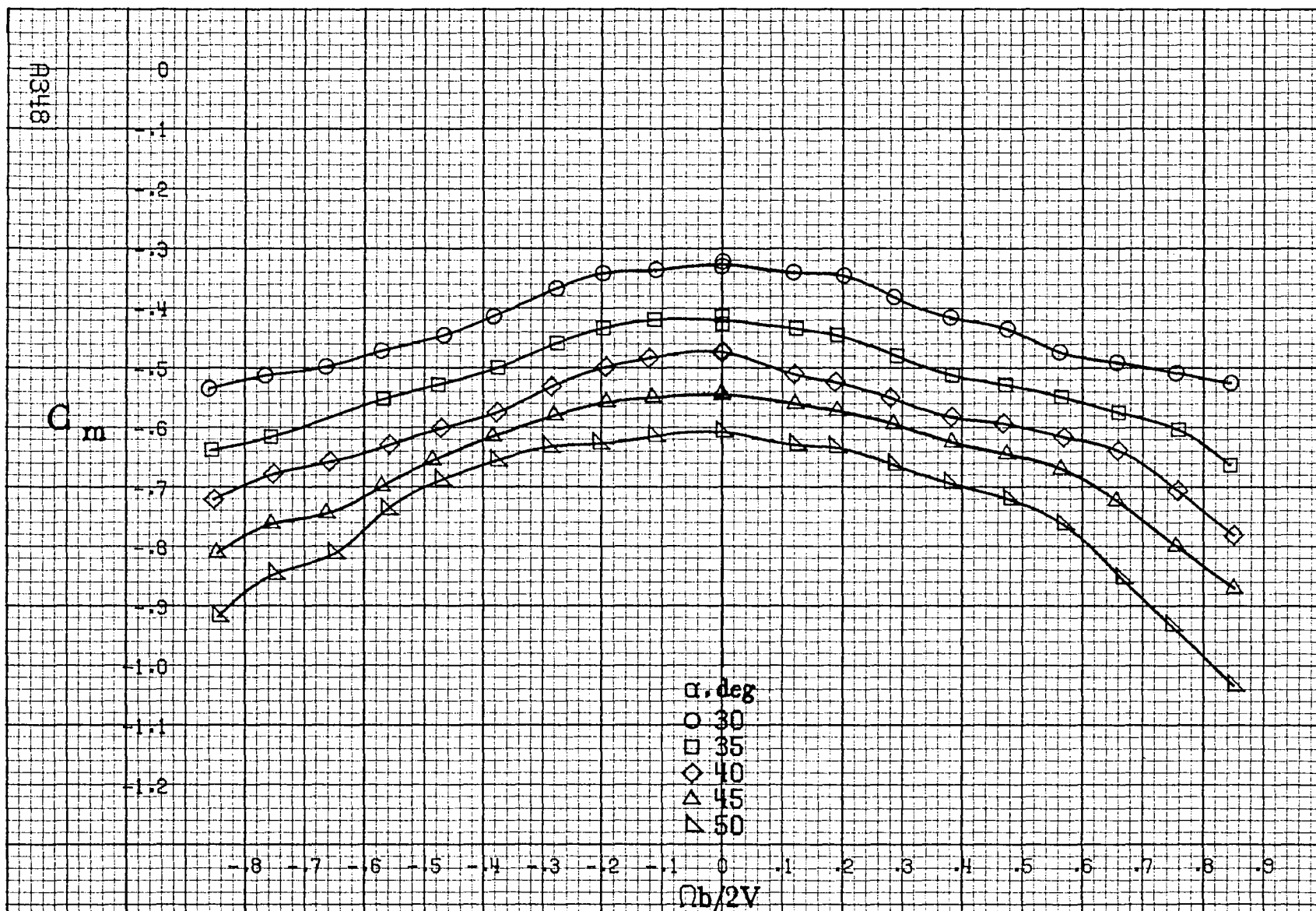
 C_l (a) $\alpha = 30$ to 50° , $SR = 0$.

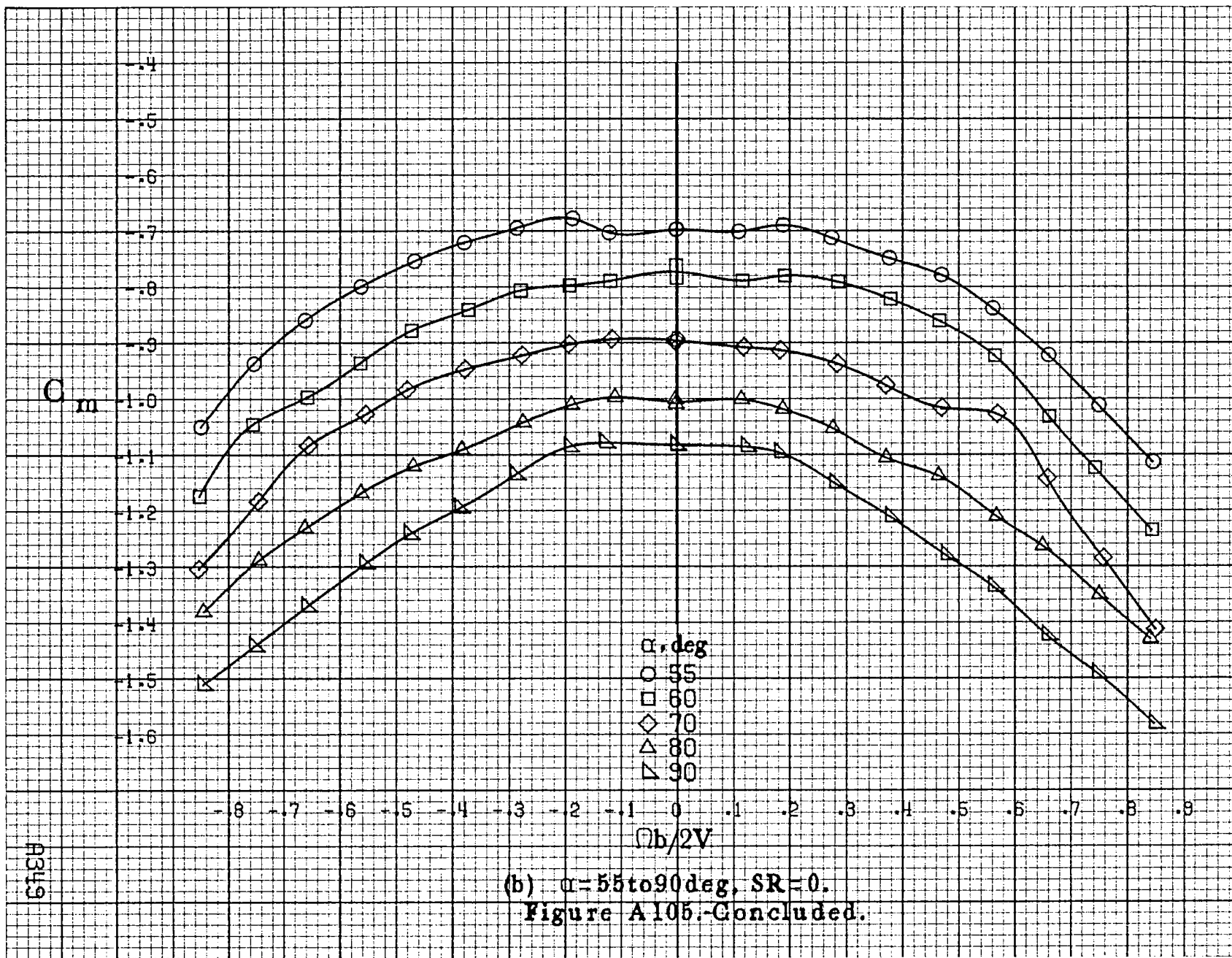
Figure A104.-Effect of rotation rate and angle of attack on rolling-moment coefficient for no. 3 horizontal tail configuration with rounded fuselage bottom aft of wing TE, wing fairings removed. $\delta_a = 0^\circ$, $\delta_s = 0^\circ$, $\delta_r = 0^\circ$, $\beta = 0^\circ$.





(a) $\alpha = 30$ to 50 deg, $SR = 0$.

Figure A105.-Effect of rotation rate and angle of attack on pitching-moment coefficient for no. 3 horizontal tail configuration with rounded fuselage bottom aft of wing TR, wing fairings removed. $\delta_e = 0^\circ$, $\delta_a = 0^\circ$, $\delta_r = 0^\circ$, $\beta = 0^\circ$.



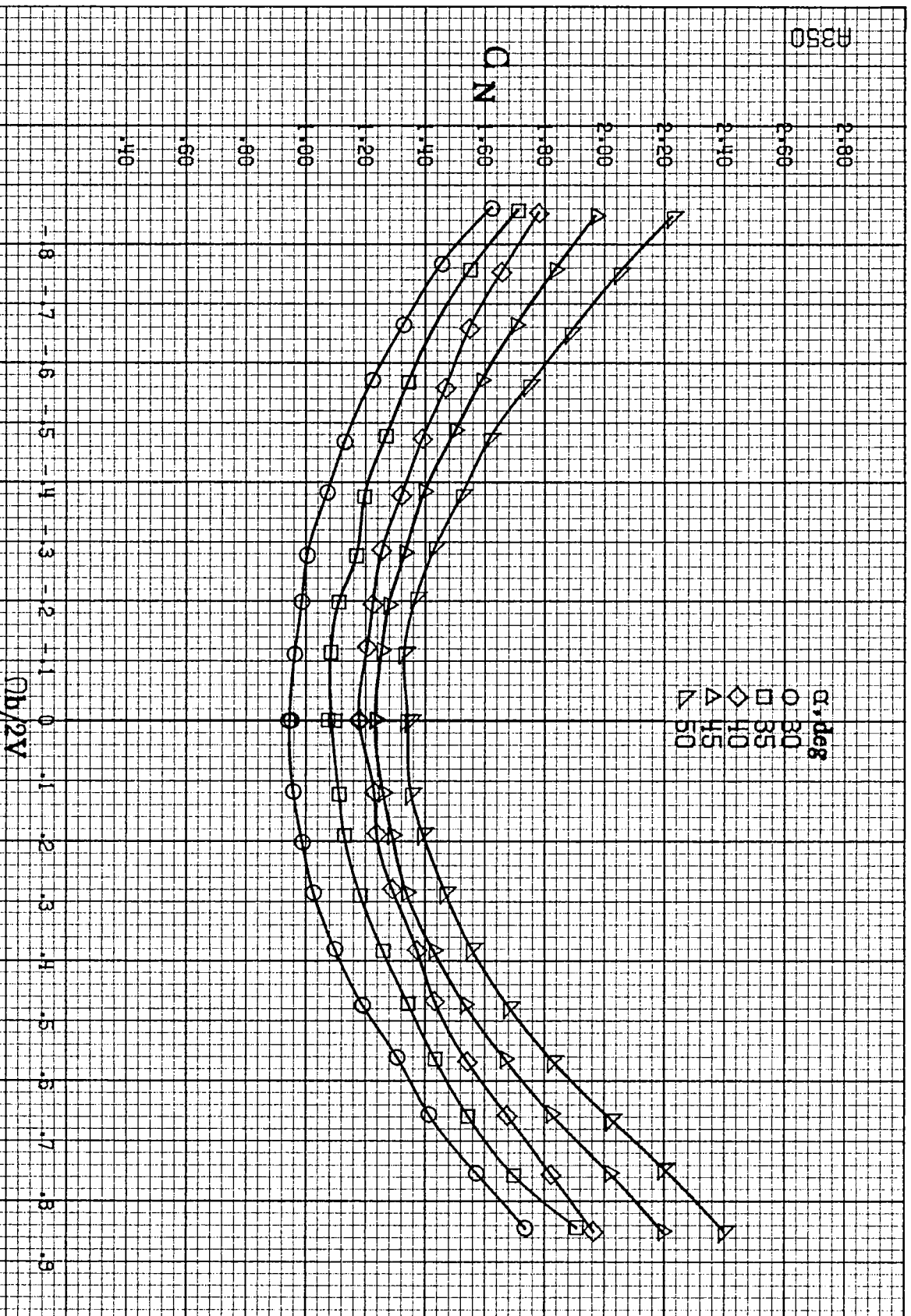
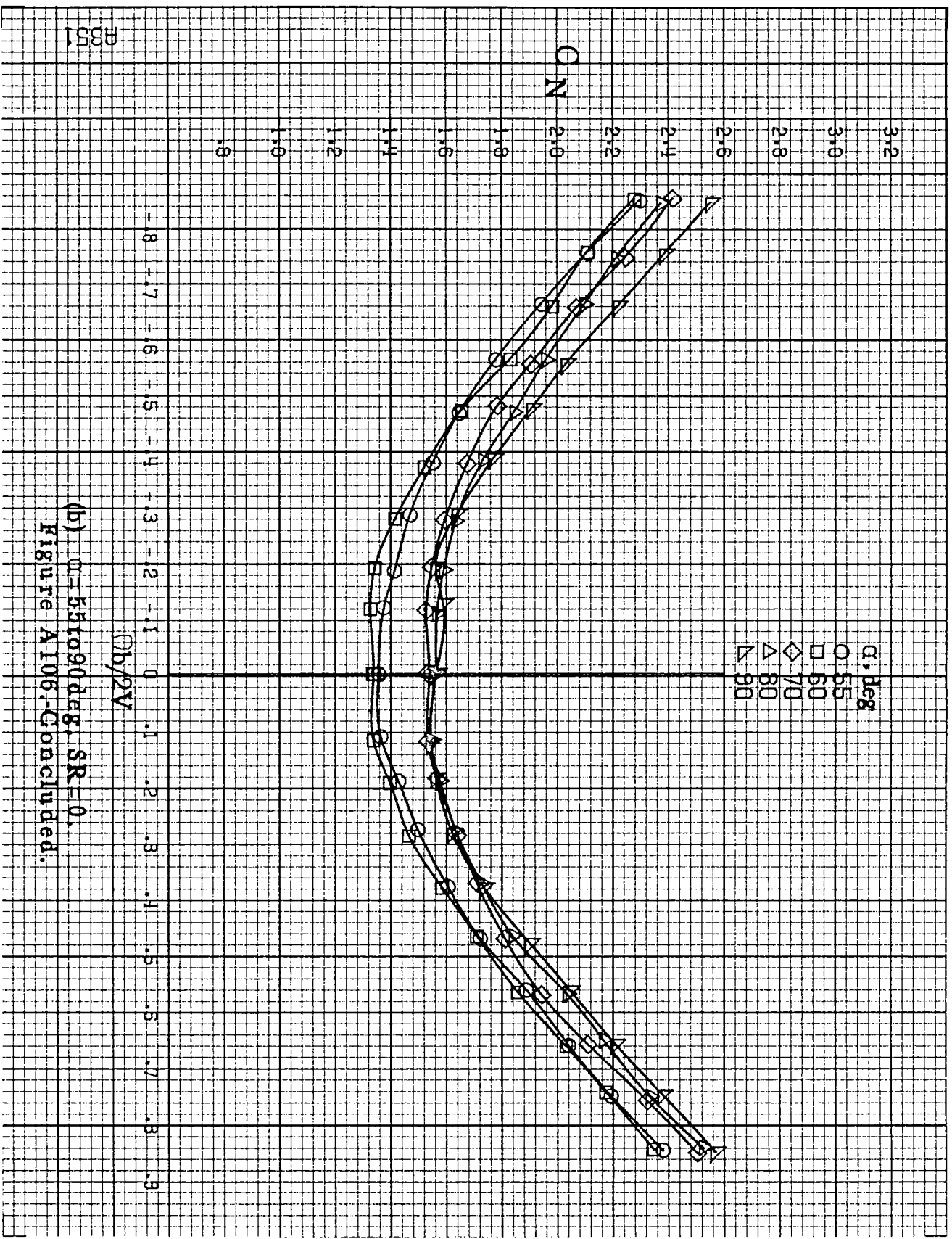
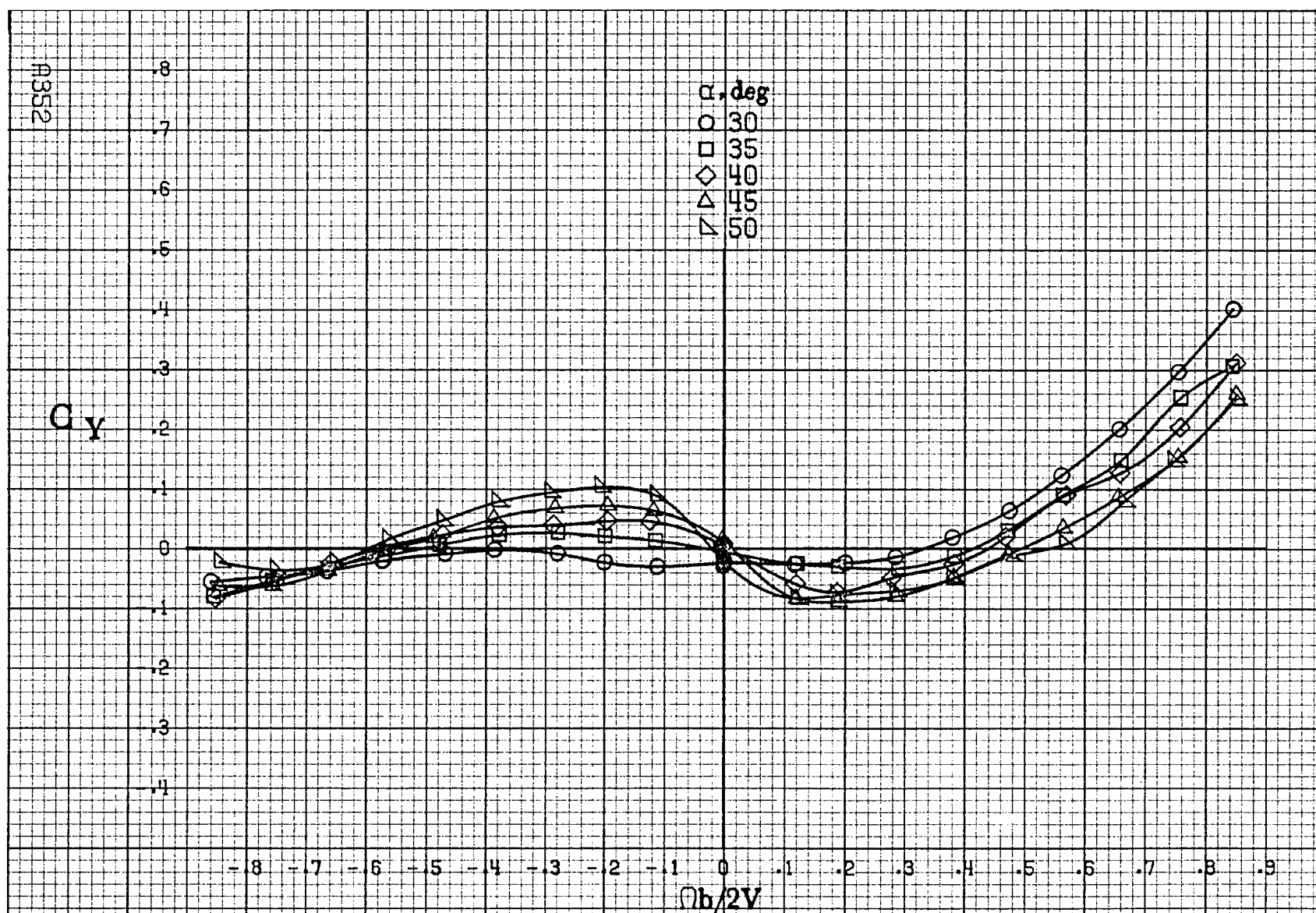


Figure A106.-Effect of rotation rate and angle of attack on normal-force coefficient for no. 3 horizontal tail configuration with rounded fuselage bottom aft of wing TF, wing fairings removed. $\alpha_e = 0^\circ$, $\alpha_a = 0^\circ$, $\alpha_f = 0^\circ$, $\beta = 0^\circ$.

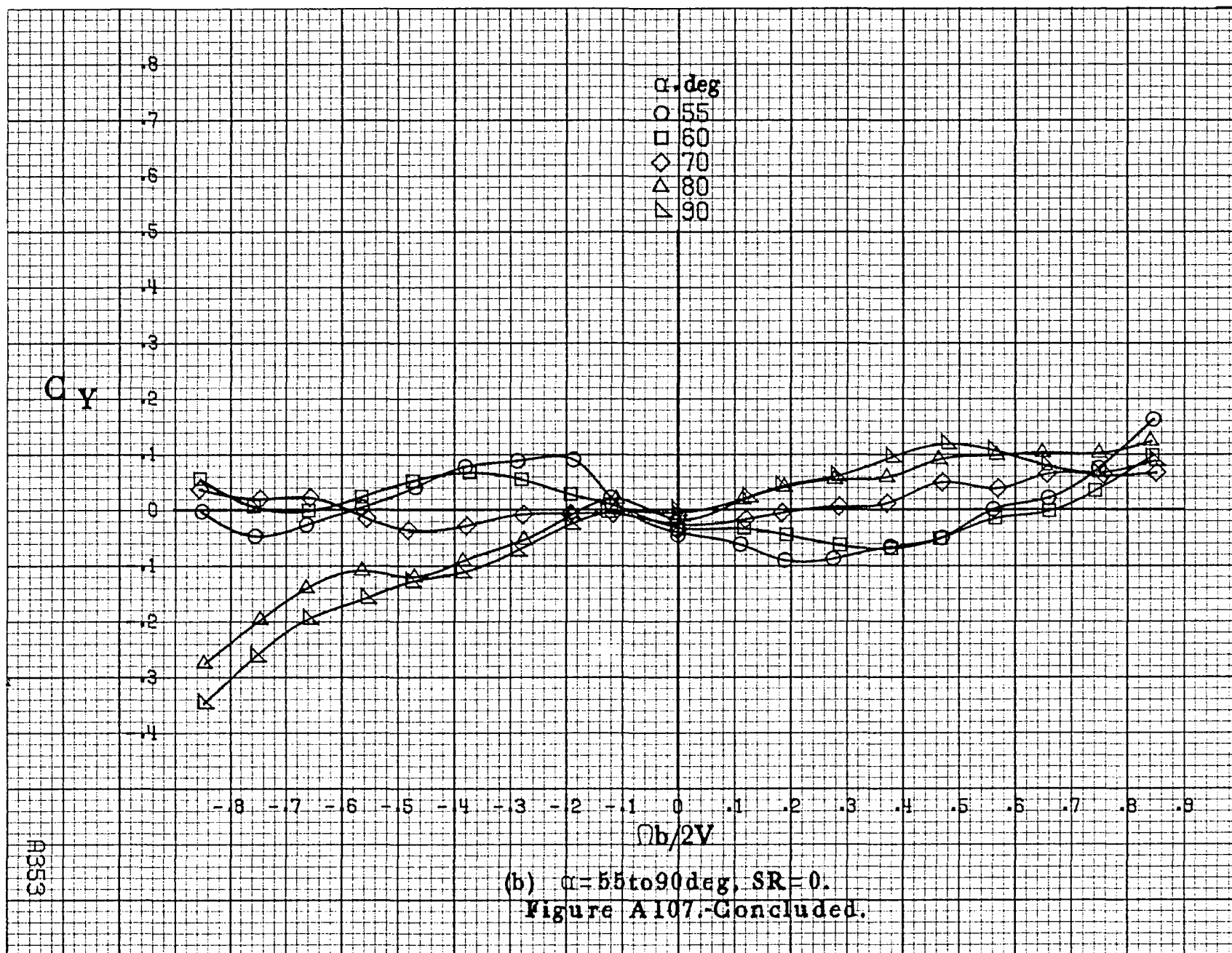


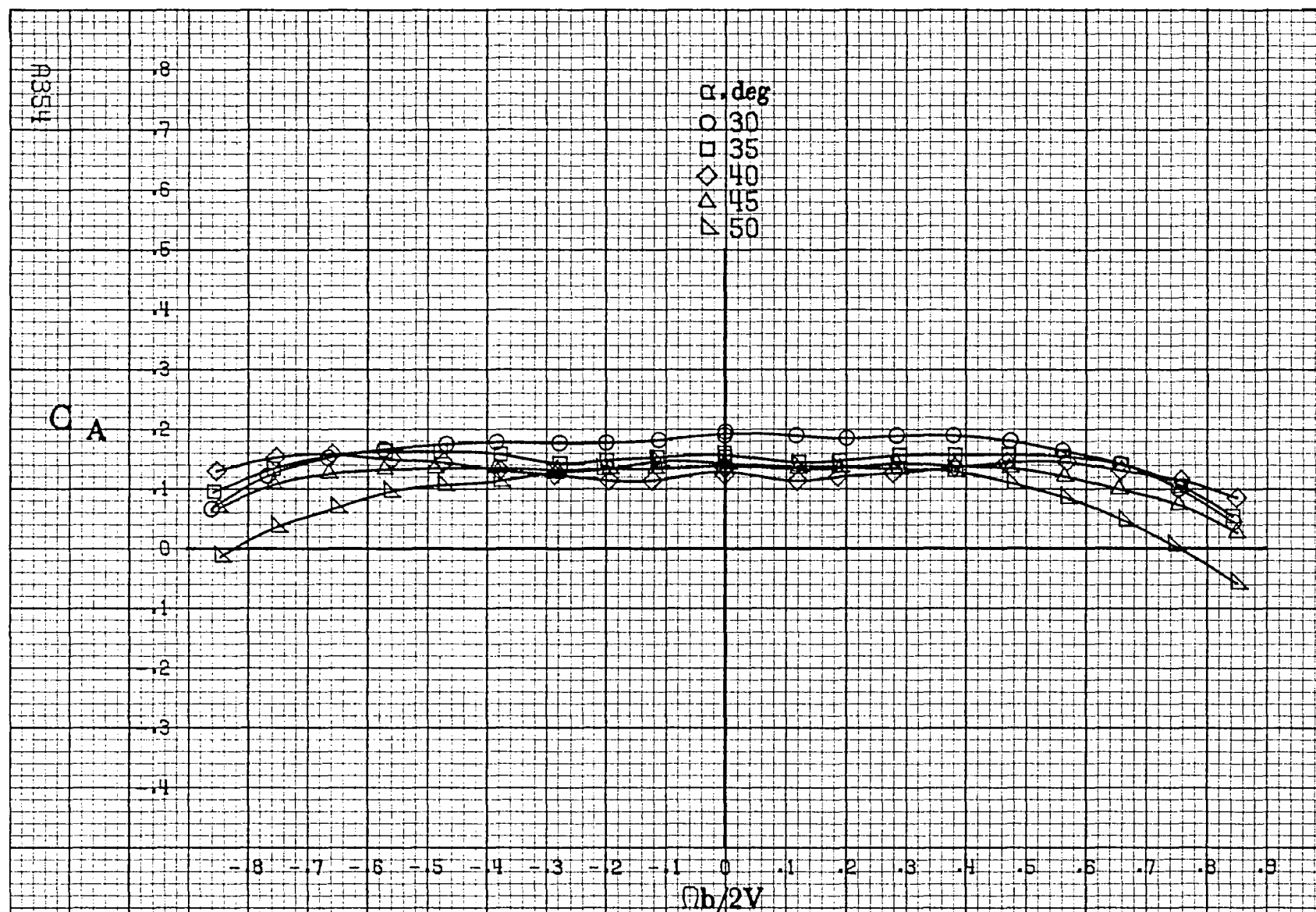
(b) $\alpha = 55$ to 90° , $SR = 0$,
Figure A106-C concluded.



(a) $\alpha = 30 \text{ to } 50 \text{ deg}$, $SR = 0$.

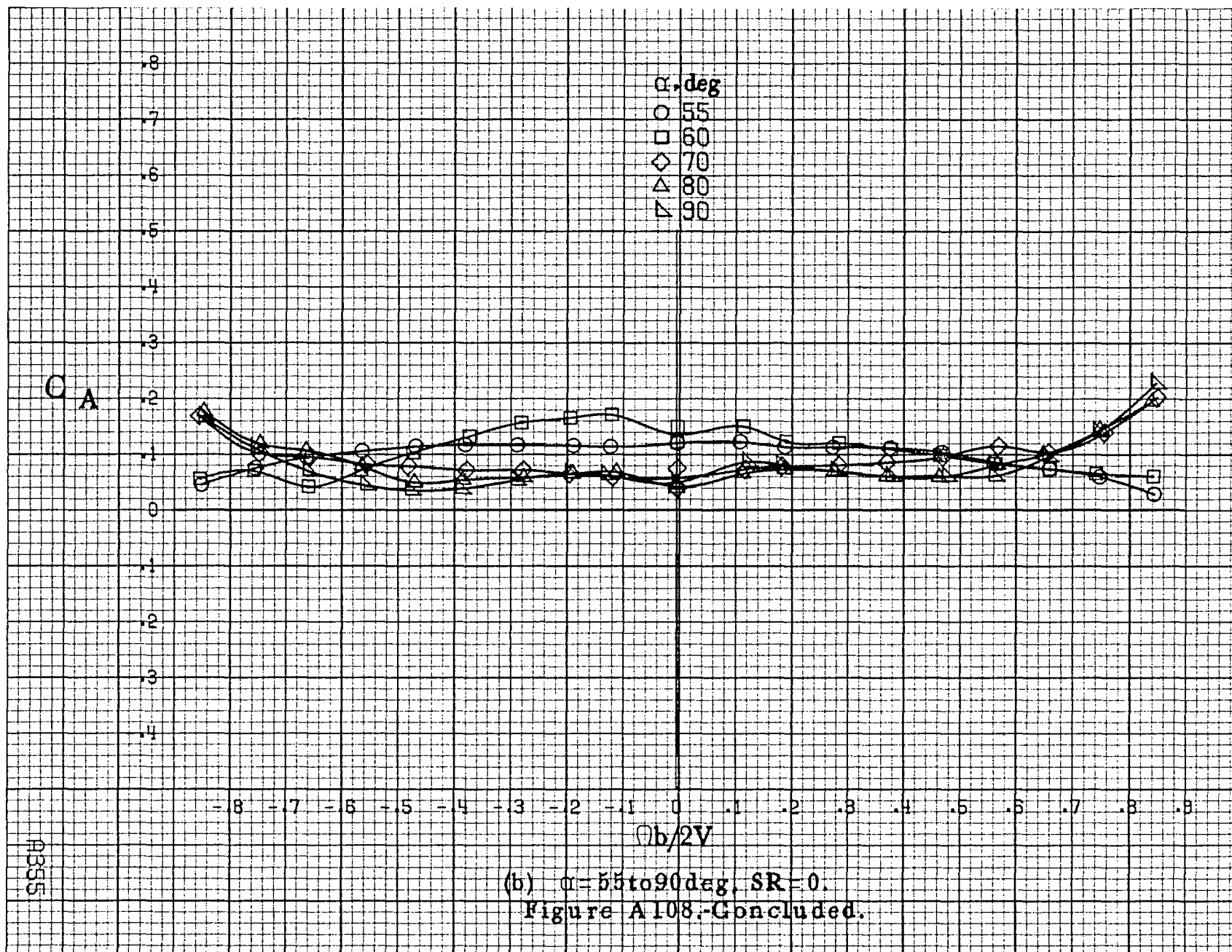
Figure A107.-Effect of rotation rate and angle of attack on side-force coefficient for no. 3 horizontal tail configuration with rounded fuselage bottom aft of wing T.E., wing fairings removed. $\delta_c = 0^\circ$, $\delta_s = 0^\circ$, $\delta_r = 0^\circ$, $\beta = 0^\circ$.

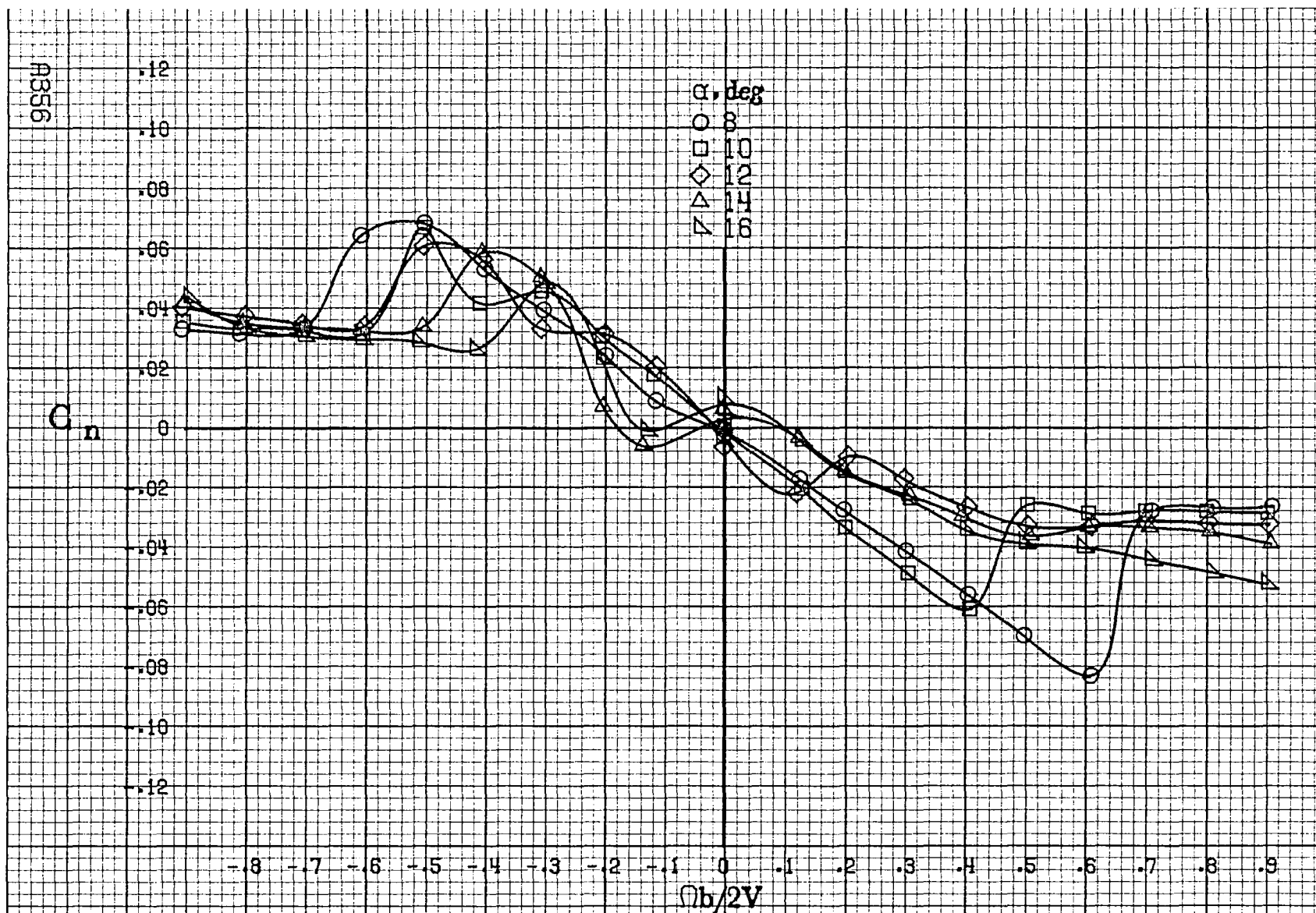




(a) $\alpha=30$ to 50° , $SR=0$.

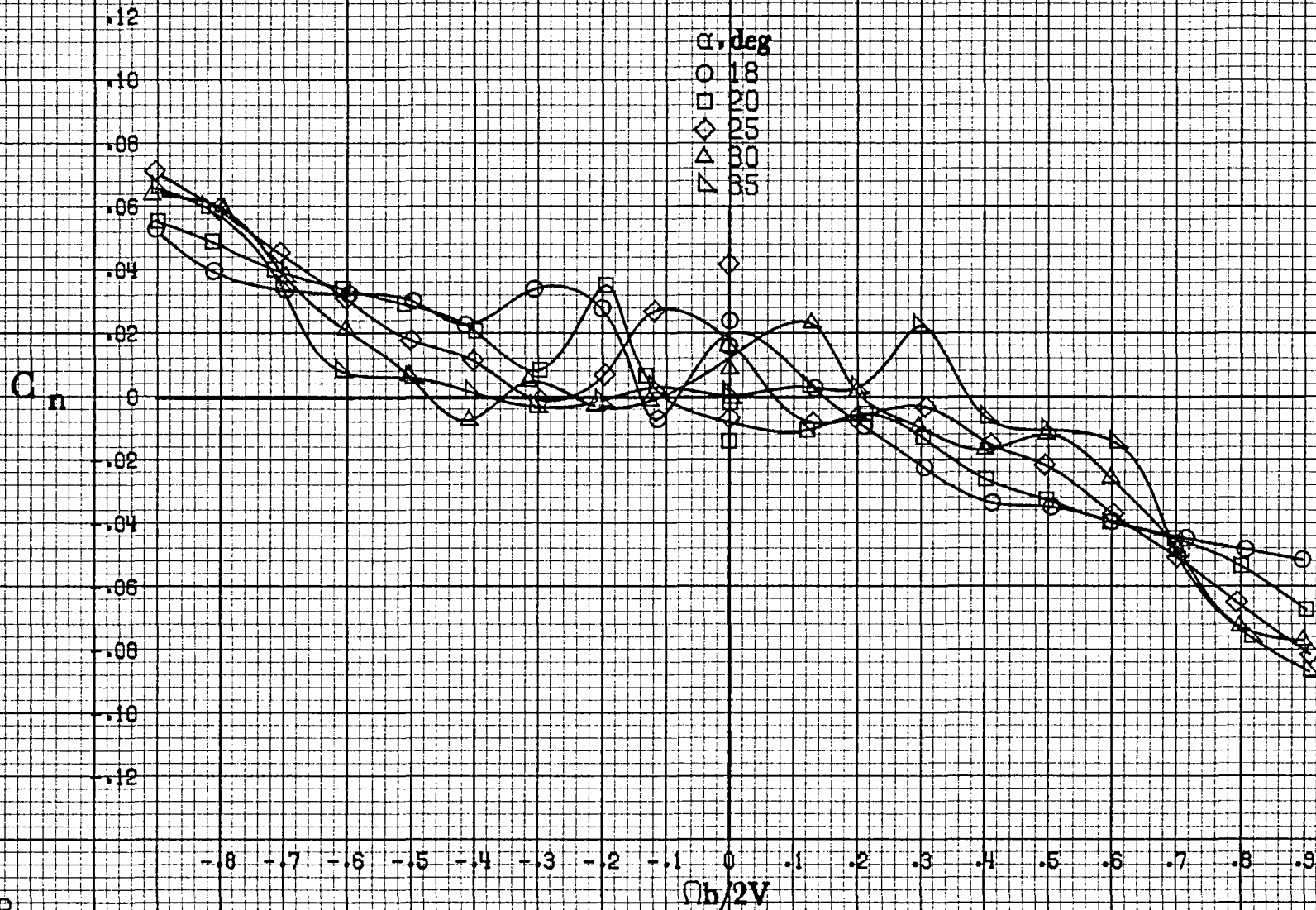
Figure A108.-Effect of rotation rate and angle of attack on axial-force coefficient for no. 3 horizontal tail configuration with rounded fuselage bottom aft of wing TE, wing fairings removed. $\delta_e=0^\circ$, $\delta_a=0^\circ$, $\delta_r=0^\circ$, $\beta=0^\circ$.



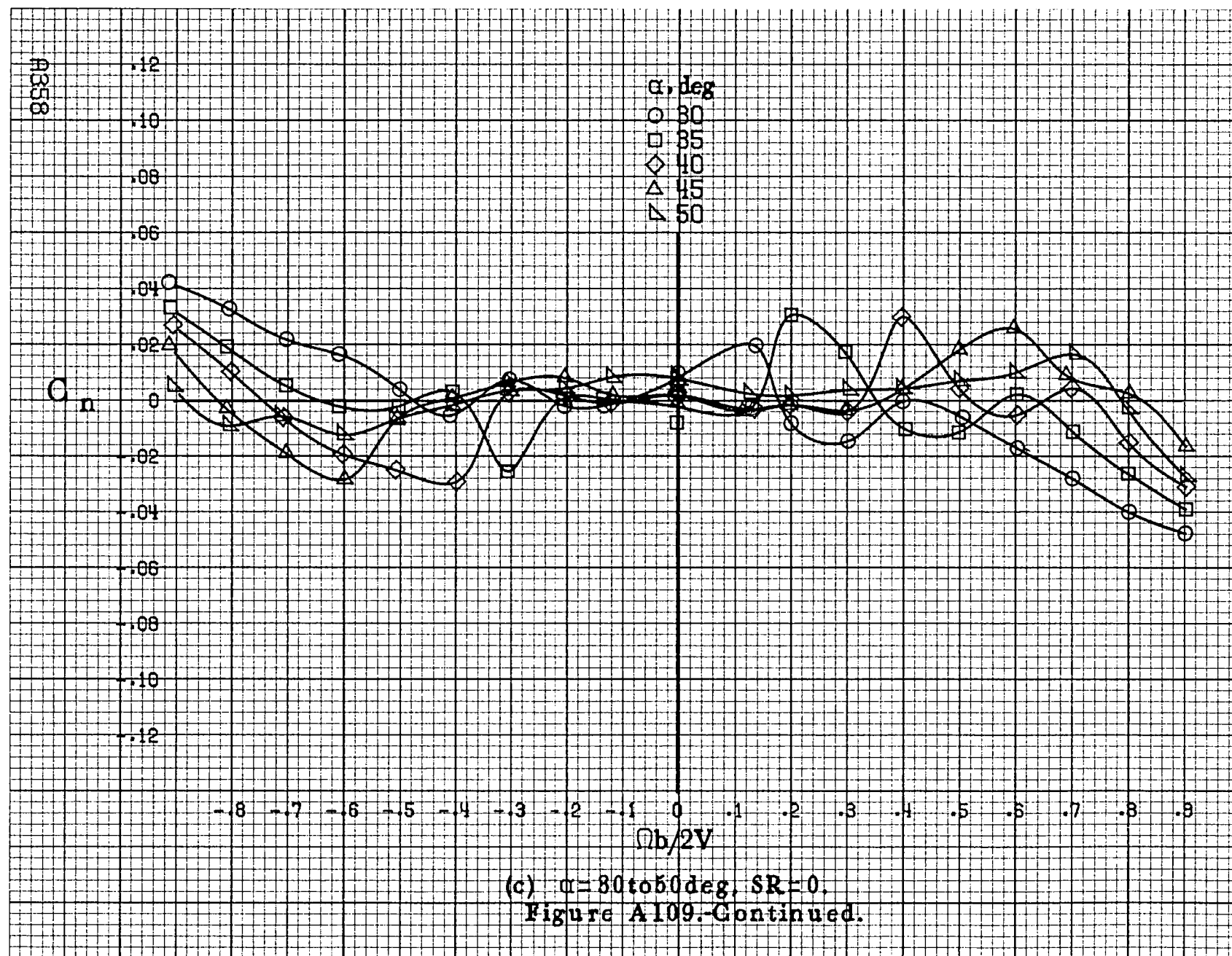


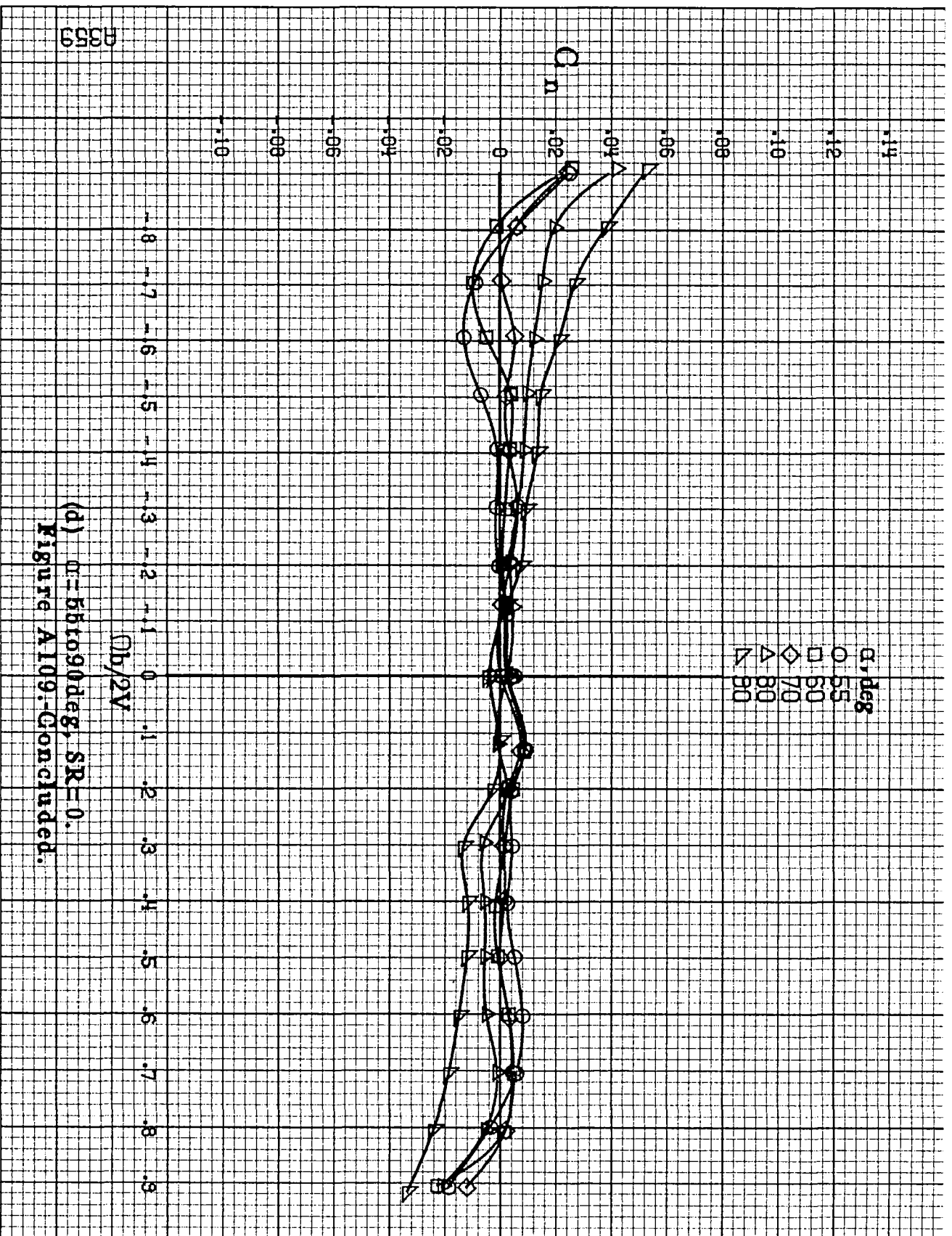
(a) $\alpha = 8 \text{ to } 16 \text{ deg}$, $SR = 76 \text{ cm (30 in)}$.

Figure A109.-Effect of rotation rate and angle of attack on yawing-moment coefficient for no. 3 horizontal tail configuration with full-span wing LE droop. $\delta_s = 0^\circ$, $\delta_a = 0^\circ$, $\delta_r = 0^\circ$, $\beta = 0^\circ$.



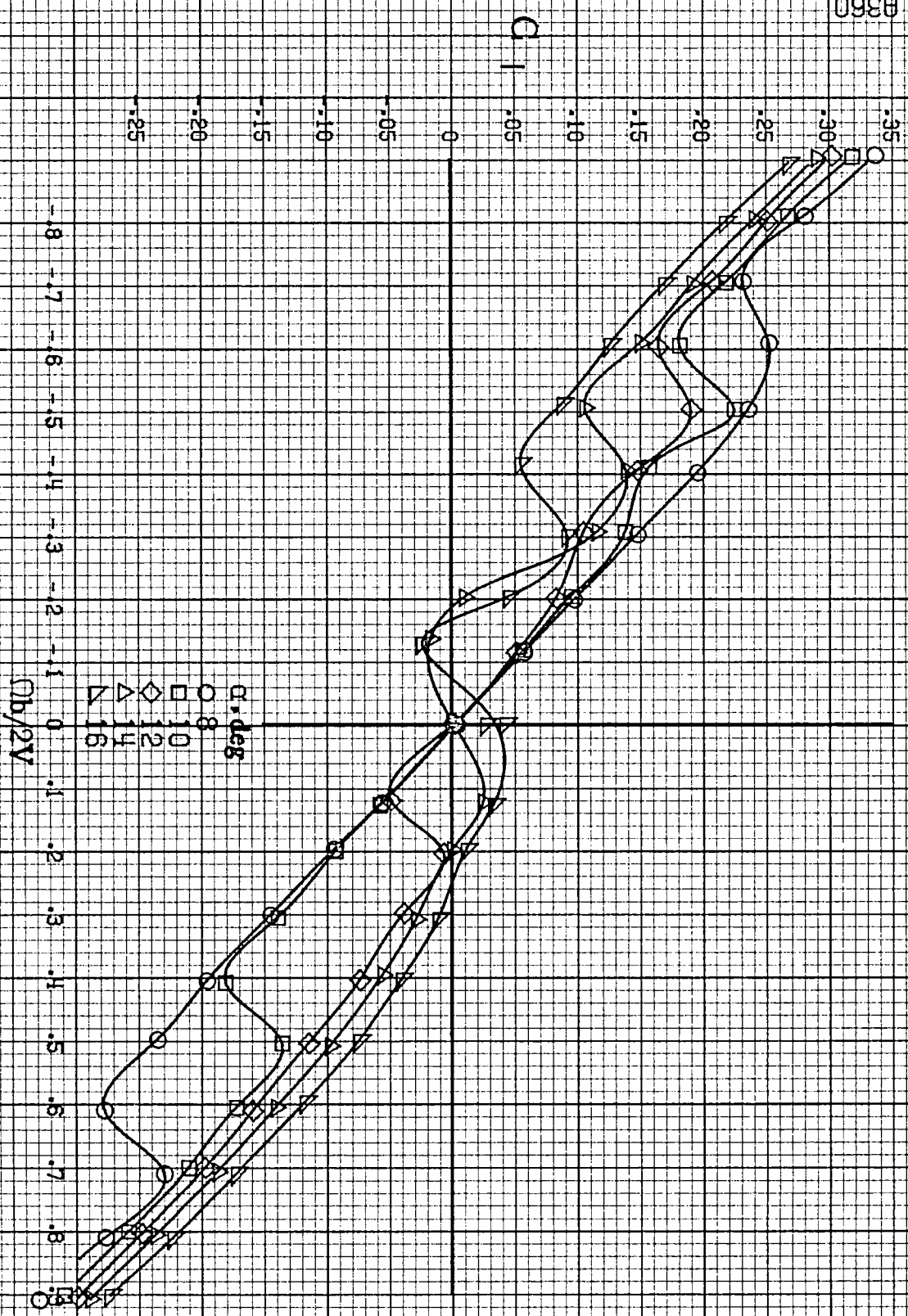
(b) $\alpha = 18$ to 35° , $SR = 76\text{cm}$ (30in).
Figure A109-Continued.





(d) $\alpha=55$ to 90 deg, $SR=0$.
Figure A109:-Concluded.

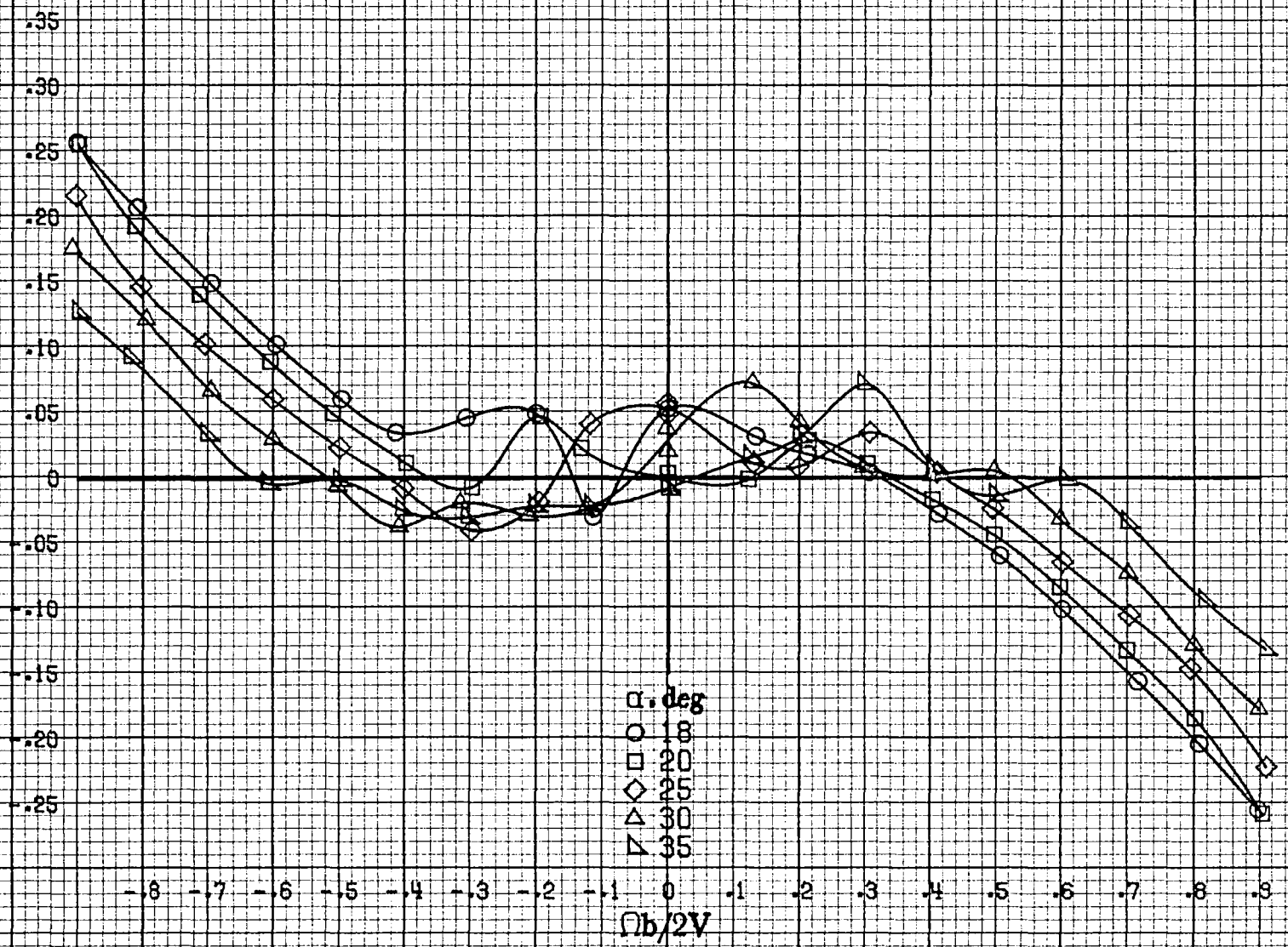
A360



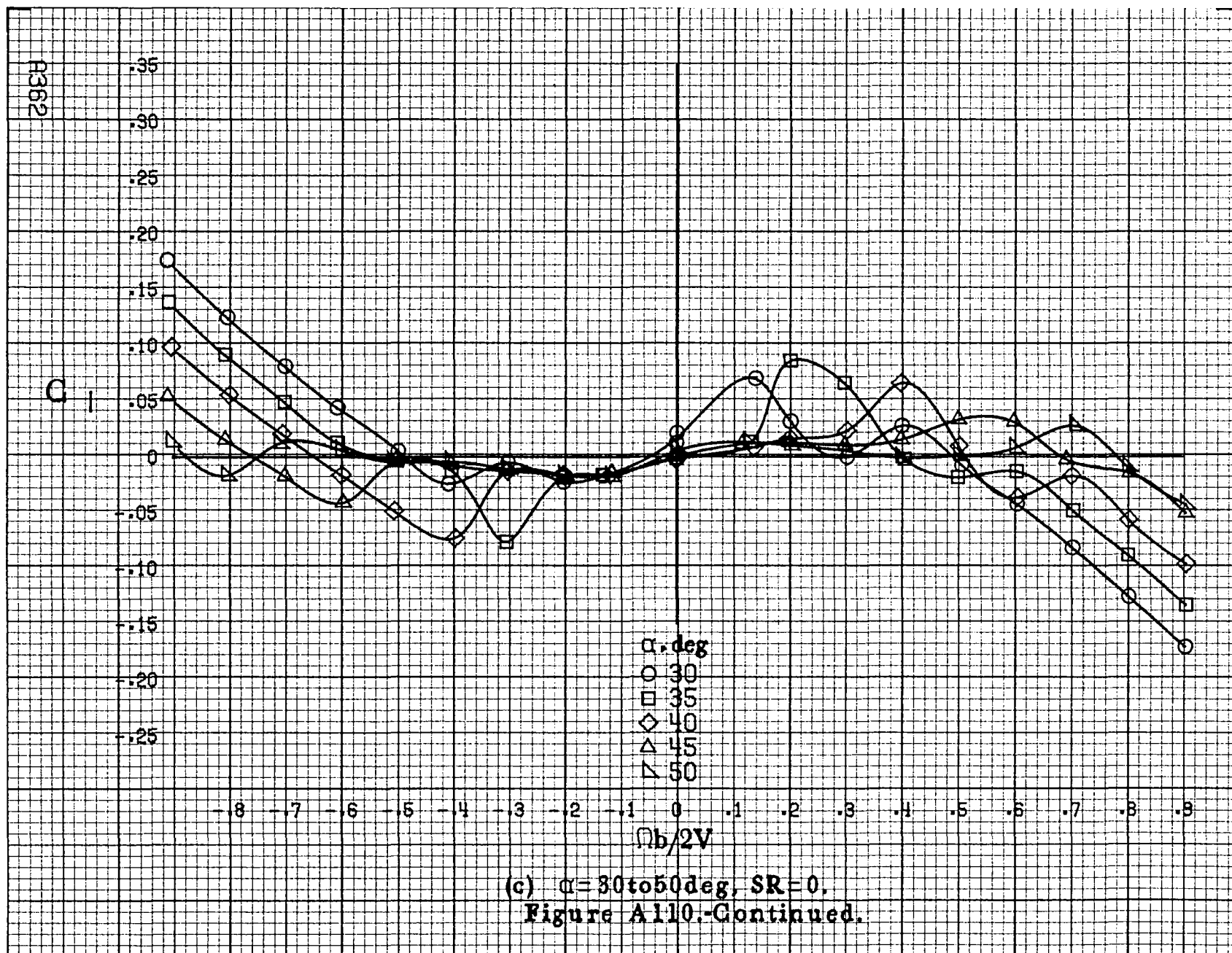
(a) $\alpha = 8$ to 16 deg, $SR = 76$ cm (30 in.).

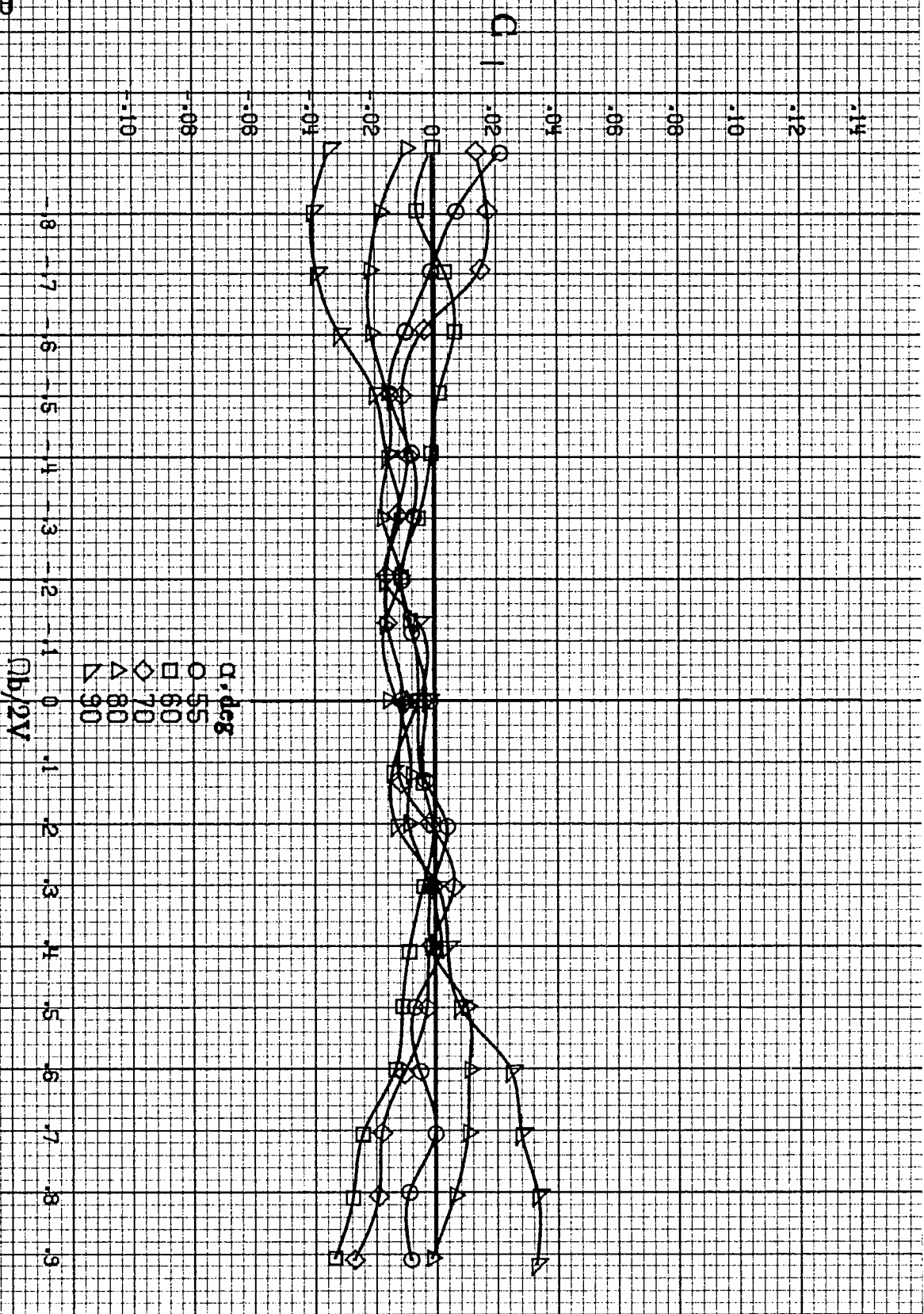
Figure A110.-Effect of rotation rate and angle of attack on rolling-moment coefficient for no. 3 horizontal tail configuration with full-span wing LT droop. $\delta_s = 0^\circ$, $\delta_t = 0^\circ$, $\delta_r = 0^\circ$, $B = 10^\circ$.

C_1

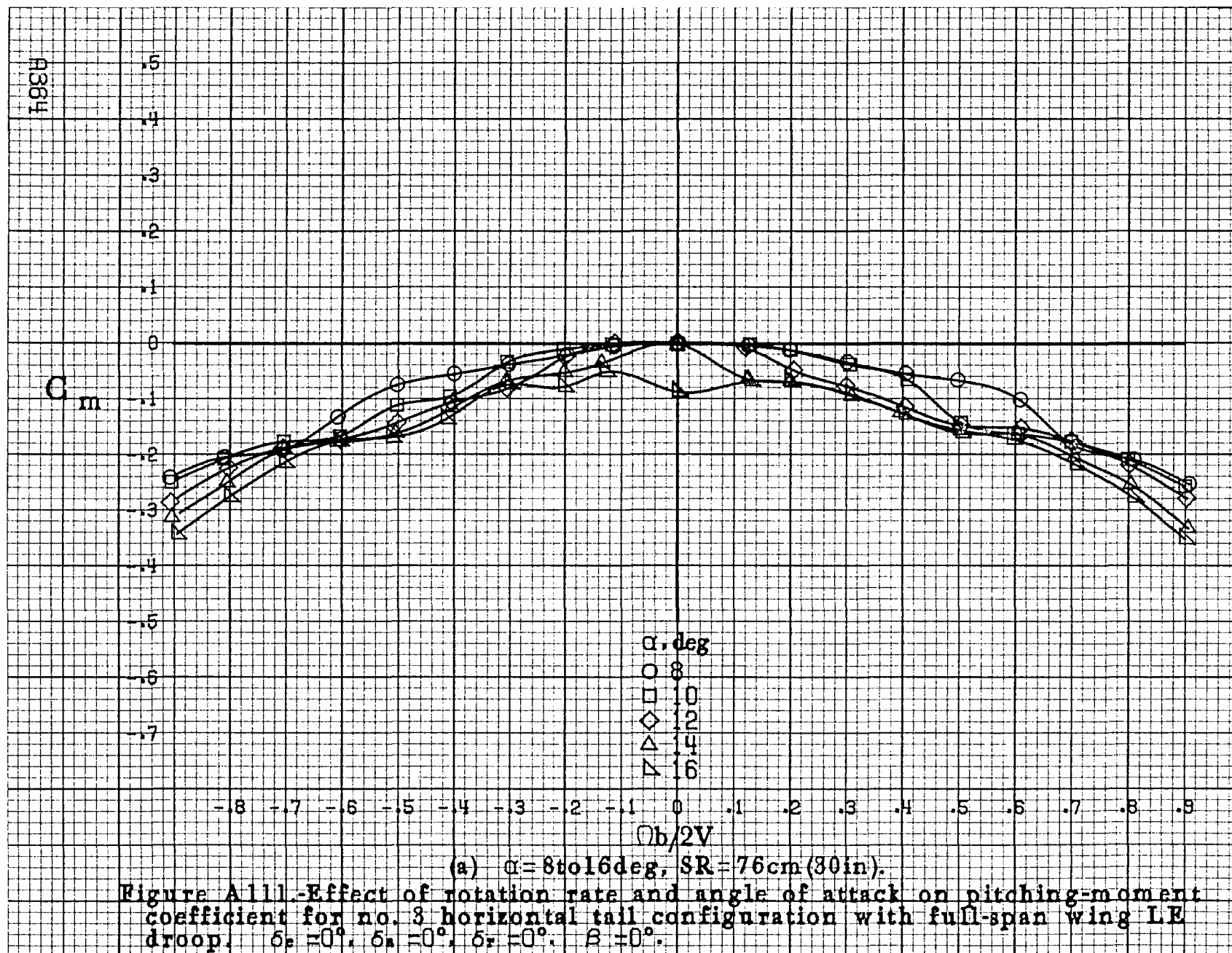


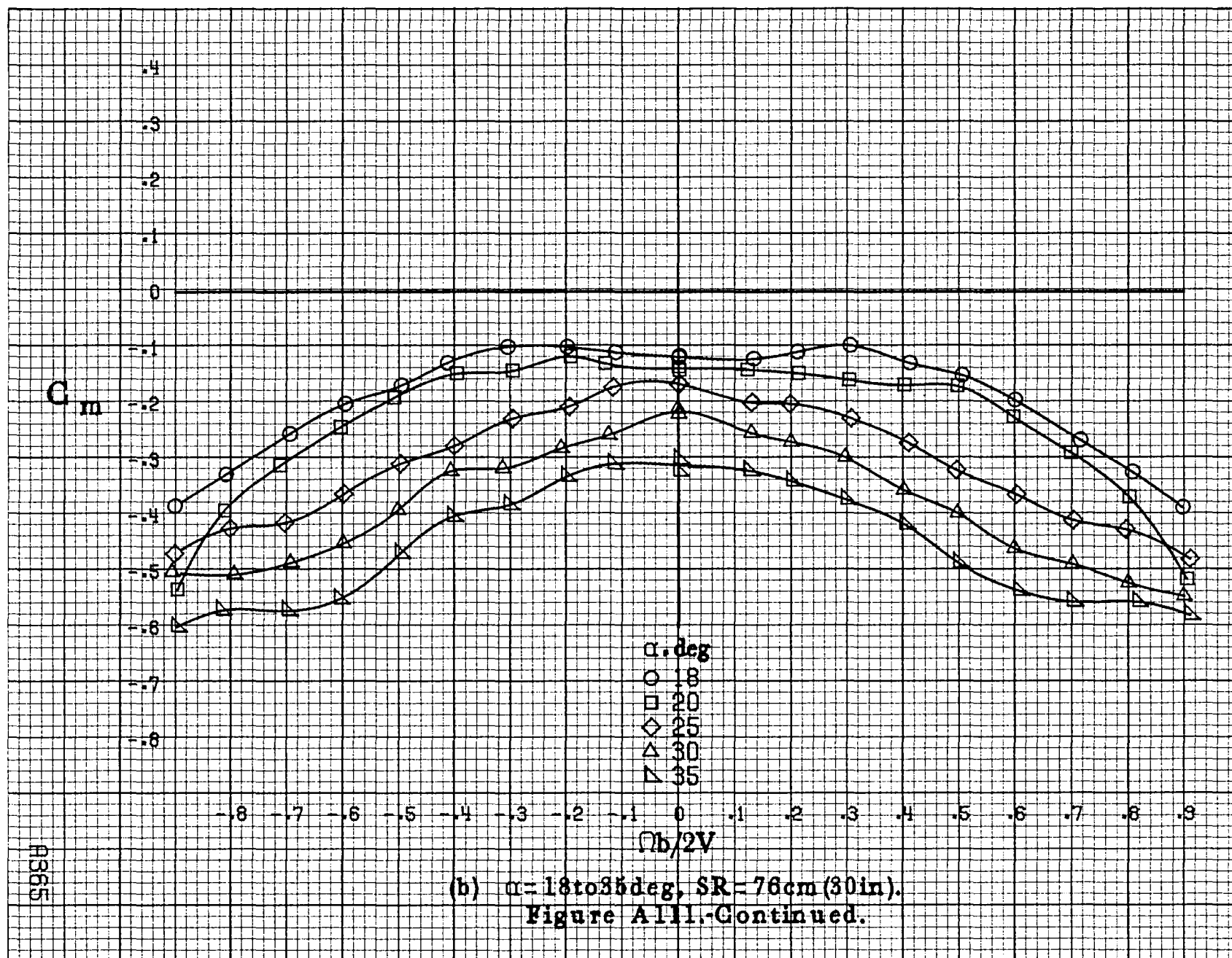
(b) $\alpha=18$ to 35 deg, $SR=76$ cm (30 in).
Figure A110.-Continued.

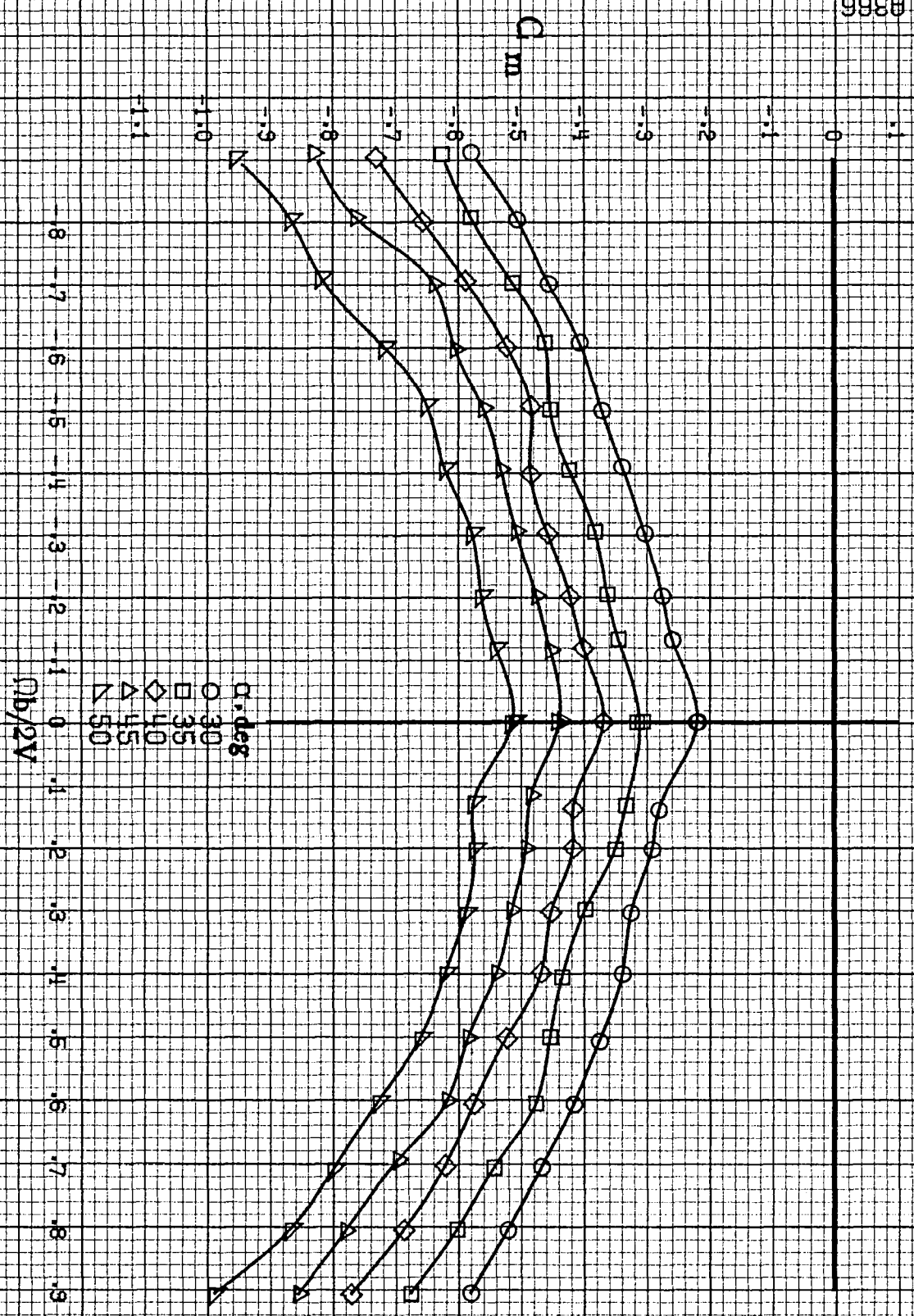




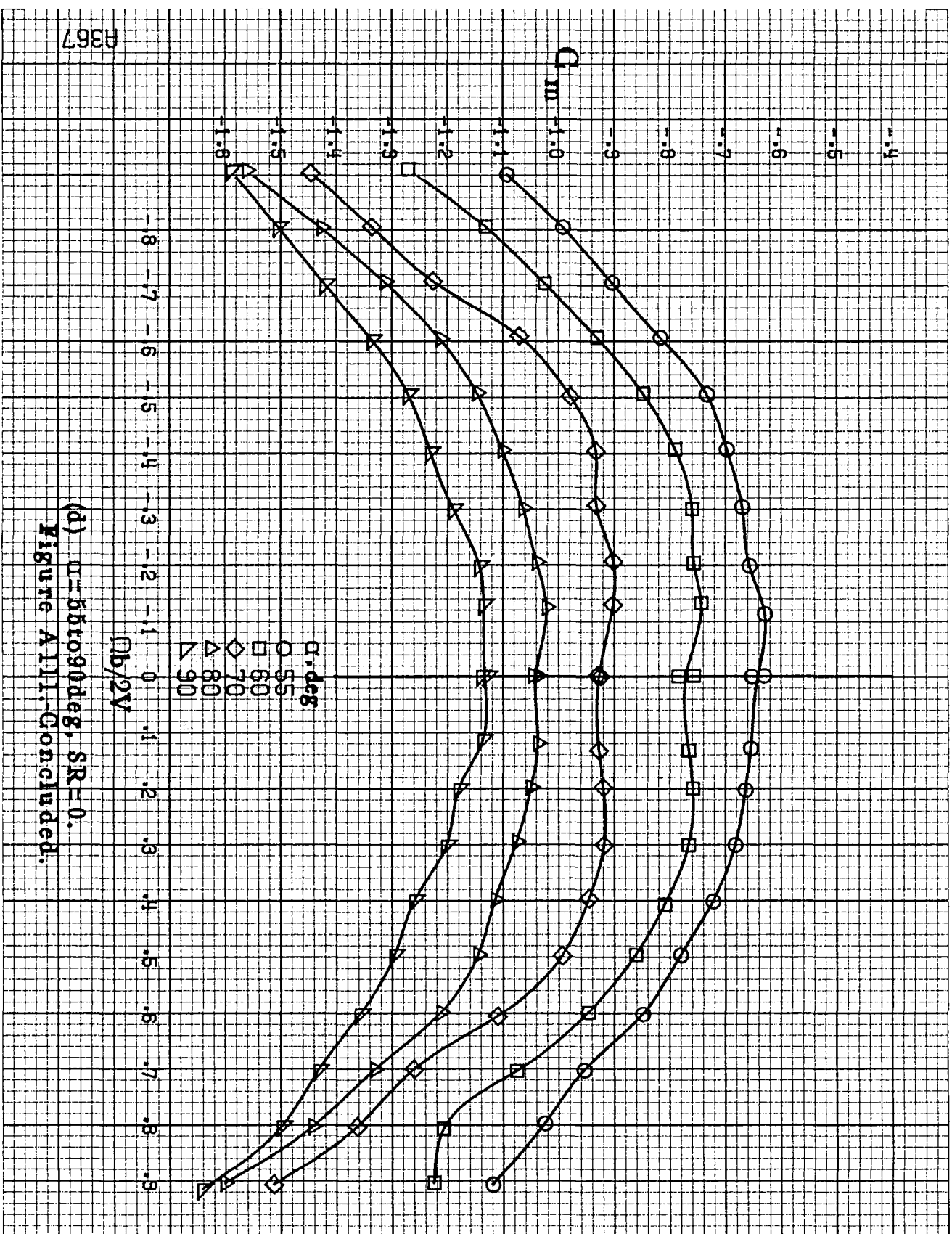
(d) $\alpha=56.1090deg, SR=0.$
 Figure A110-Concluded.



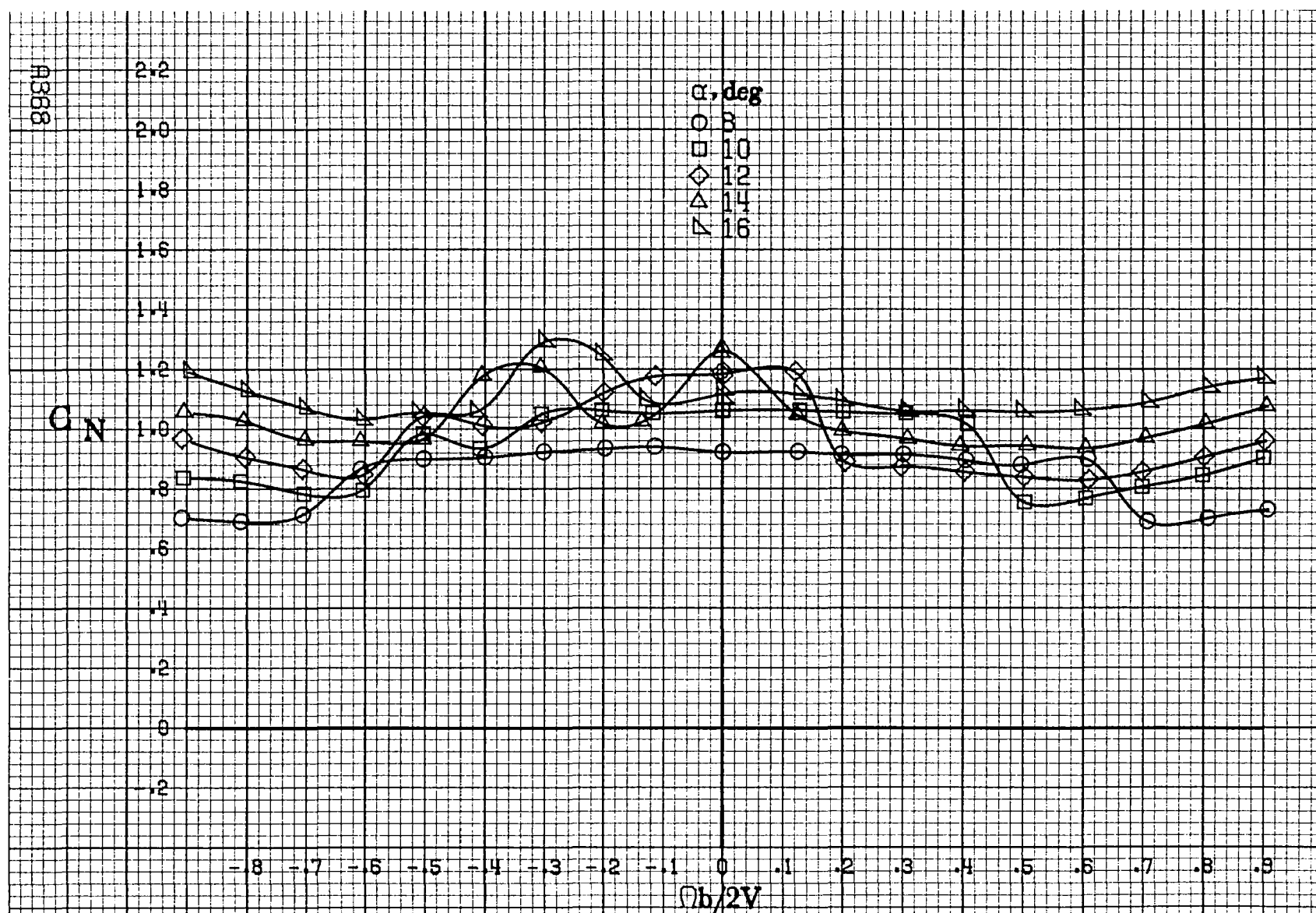




(c) $\alpha = 30$ to 50 deg, $SR = 0$.
Figure A111-Continued.

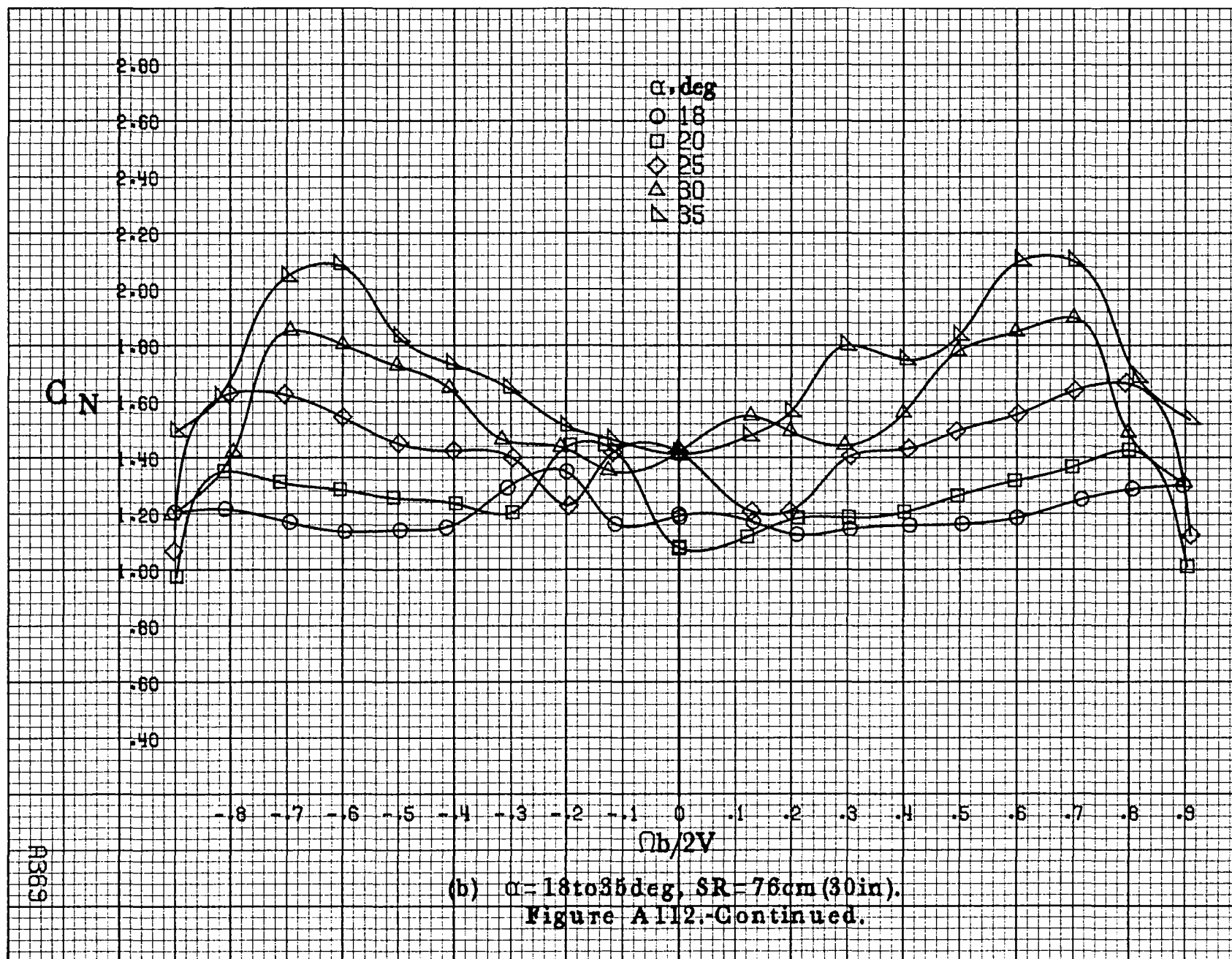


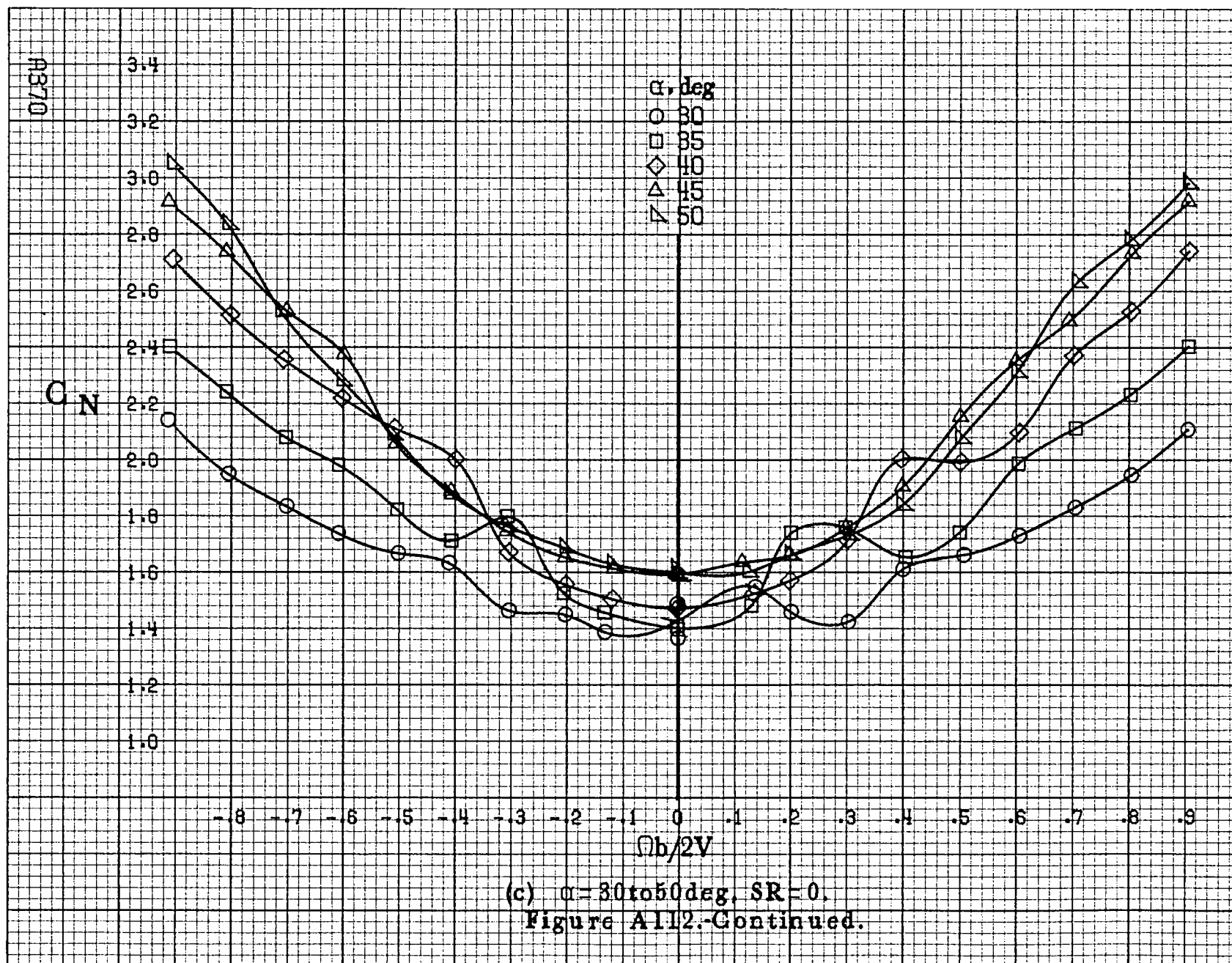
(d) $\alpha=55$ to 90° , $SR=0$.
Figure A1111-Concluded.

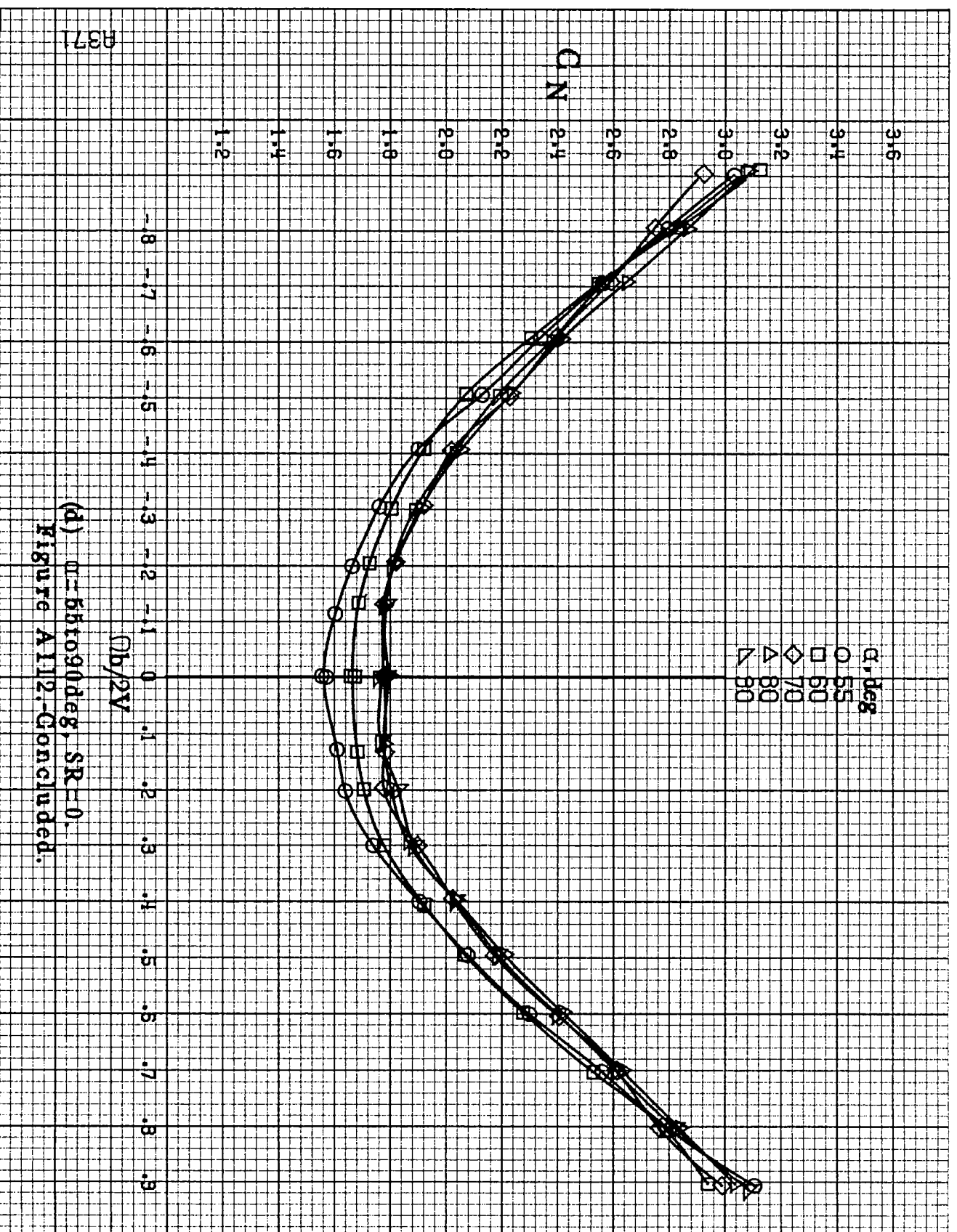


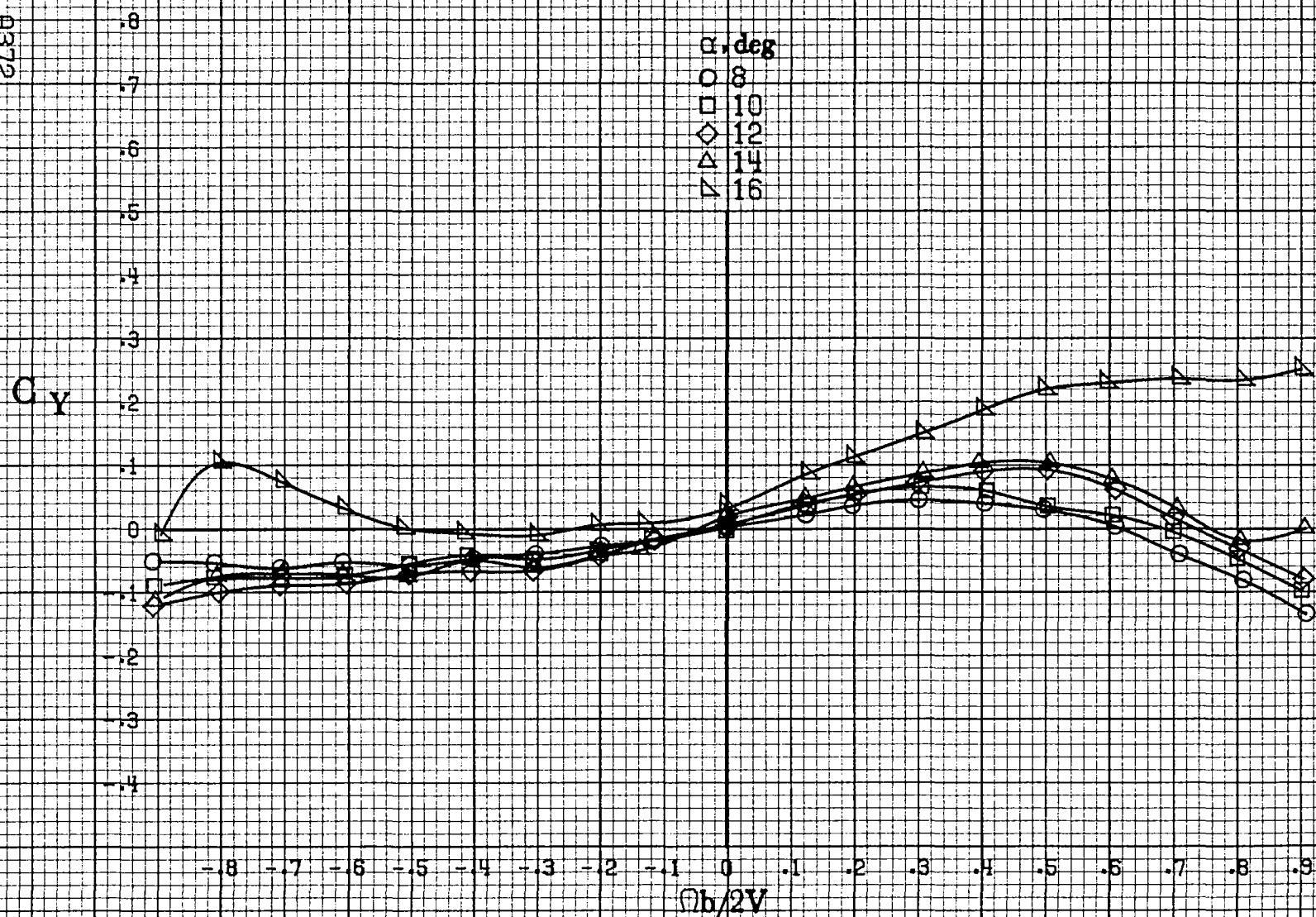
(a) $\alpha = 8 \text{ to } 16 \text{ deg}$, $SR = 76 \text{ cm (80 in)}$.

Figure A112.-Effect of rotation rate and angle of attack on normal-force coefficient for no. 3 horizontal tail configuration with full-span wing LE droop. $\delta_e = 0^\circ$, $\delta_a = 0^\circ$, $\delta_r = 0^\circ$, $\beta = 0^\circ$.



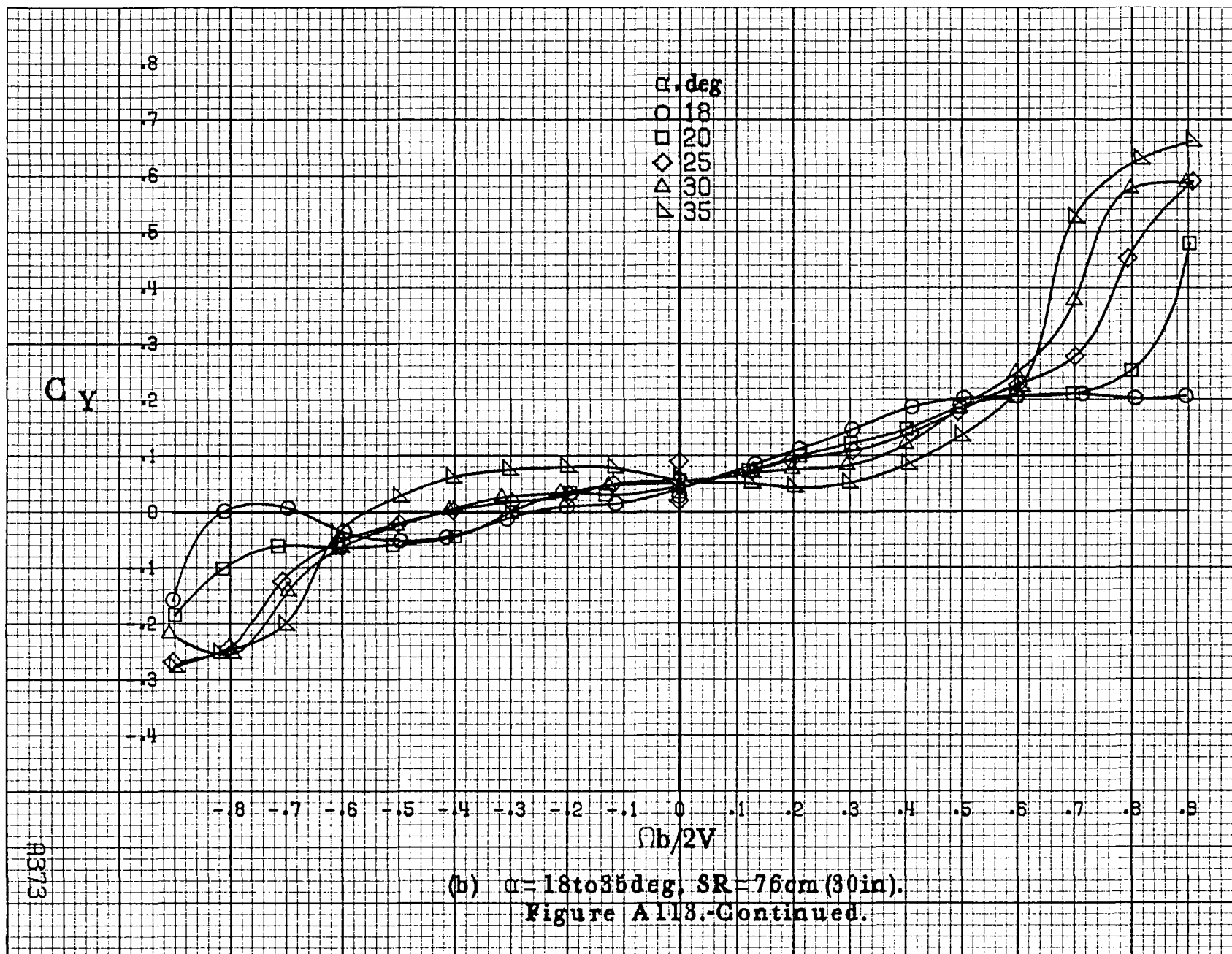


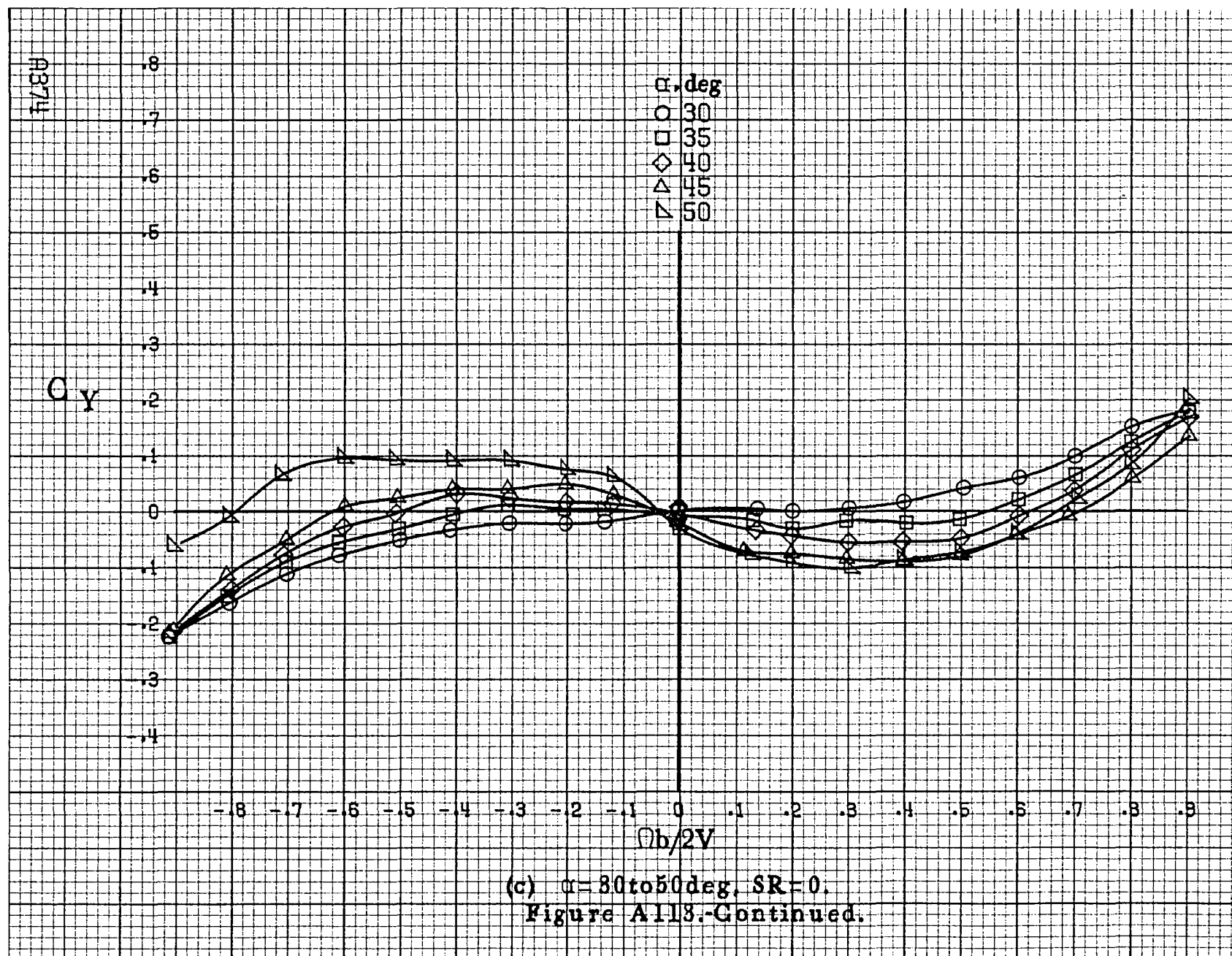


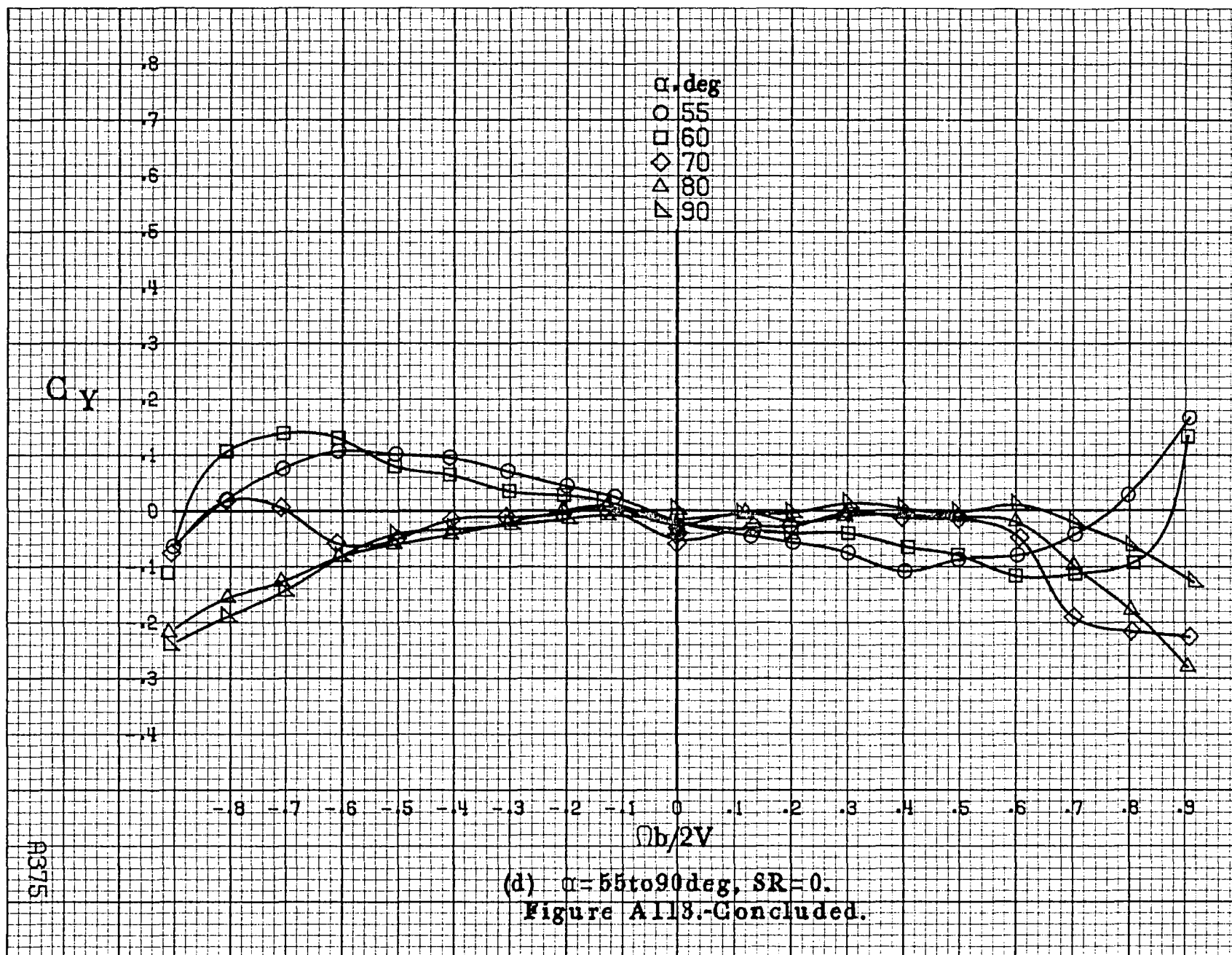


(a) $\alpha = 8$ to 16 deg, $SR = 76$ cm (30 in).

Figure A113.-Effect of rotation rate and angle of attack on side-force coefficient for no. 3 horizontal tail configuration with full-span wing LE drop. $\delta_e = 0^\circ$, $\delta_a = 0^\circ$, $\delta_r = 0^\circ$, $\beta = 0^\circ$.

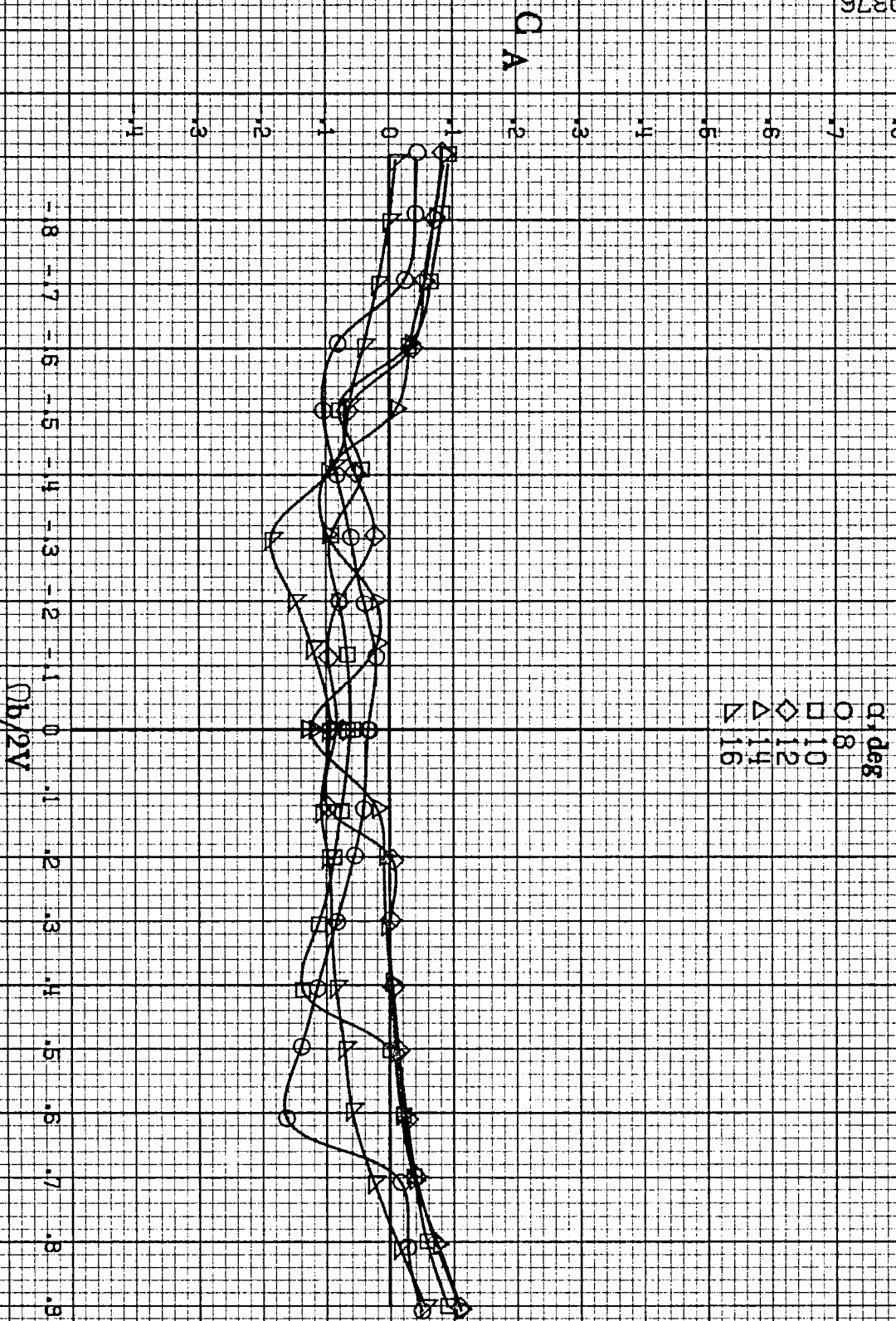






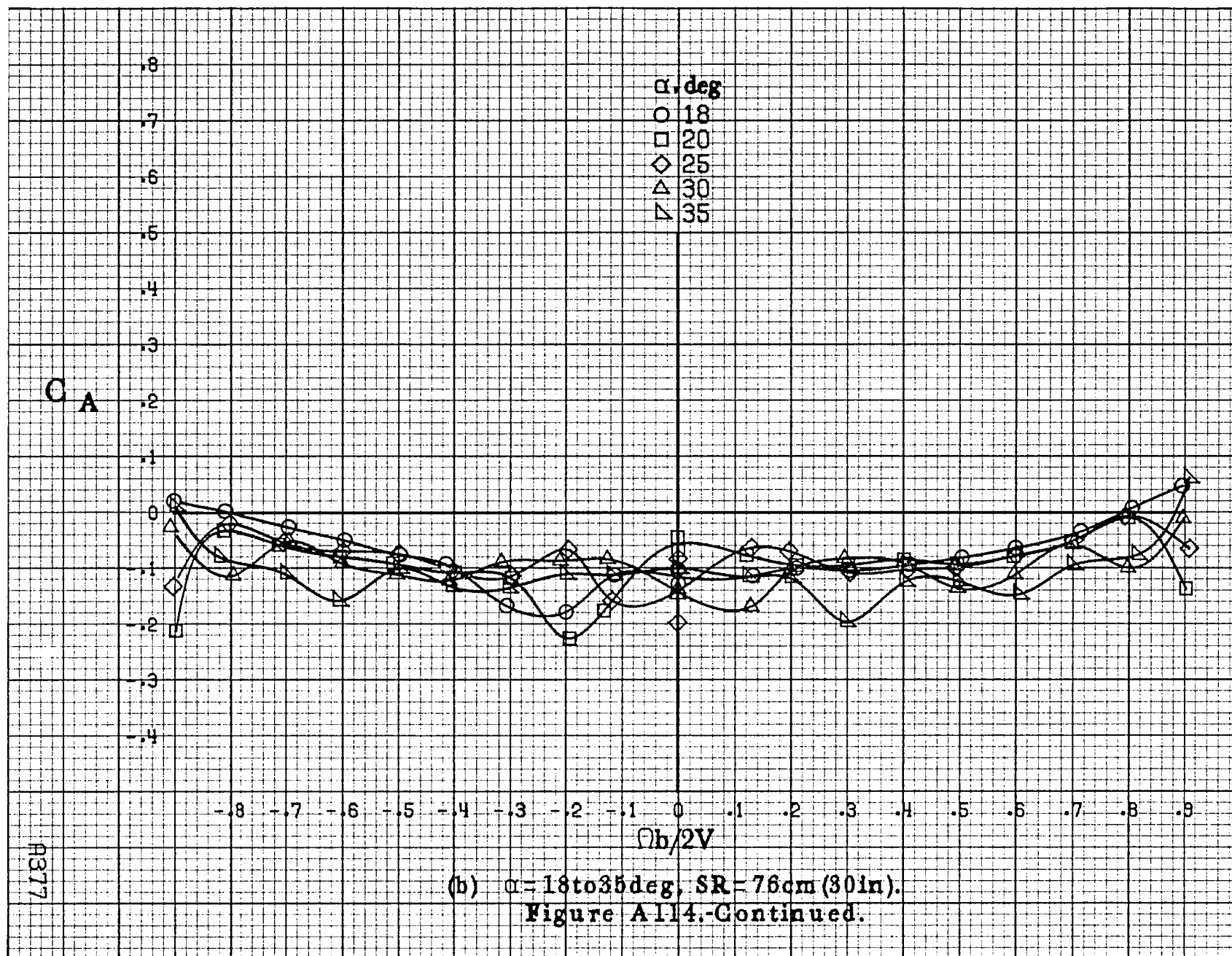
(d) $\alpha=55$ to 90° , $SR=0$.
Figure A118.-Concluded.

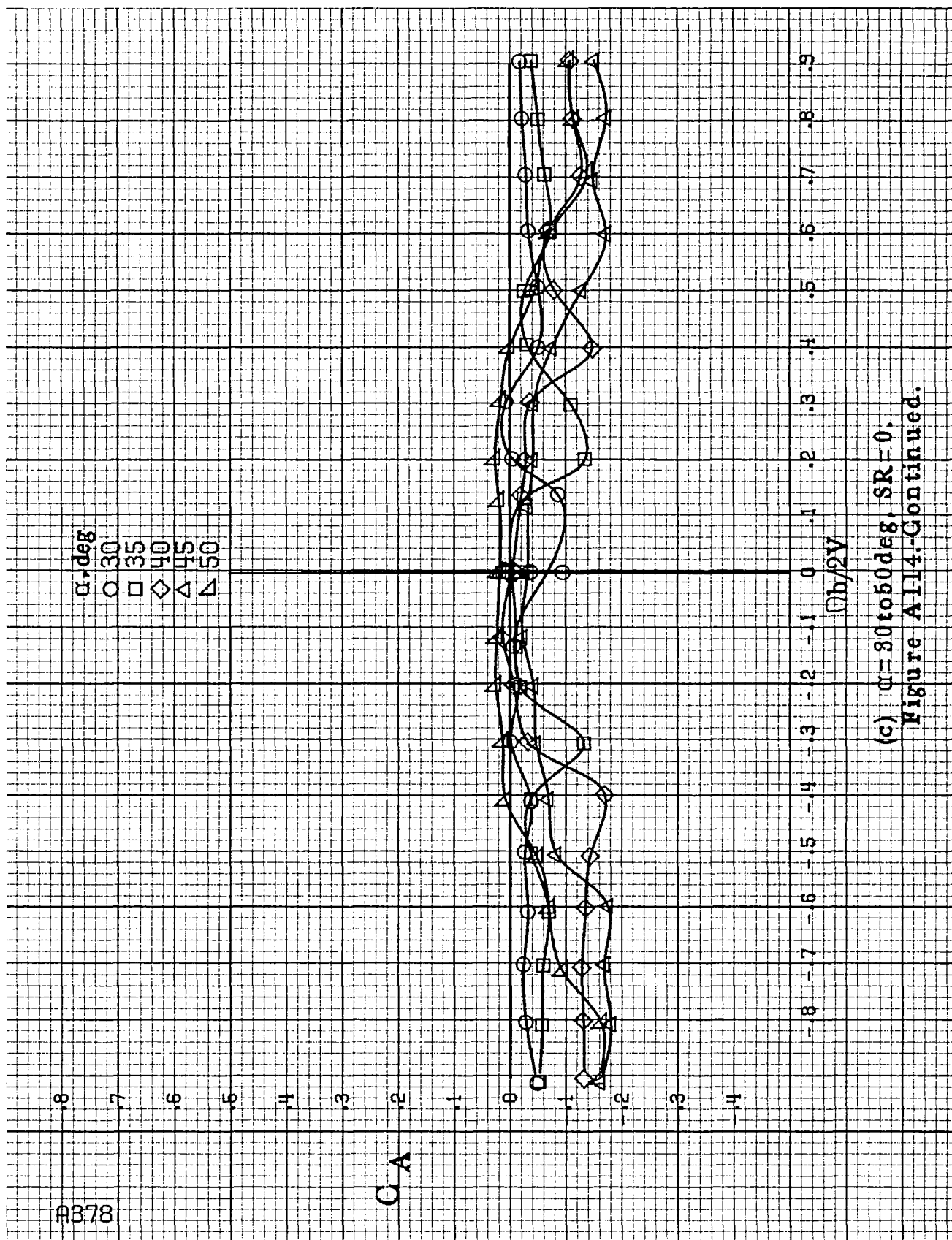
A375

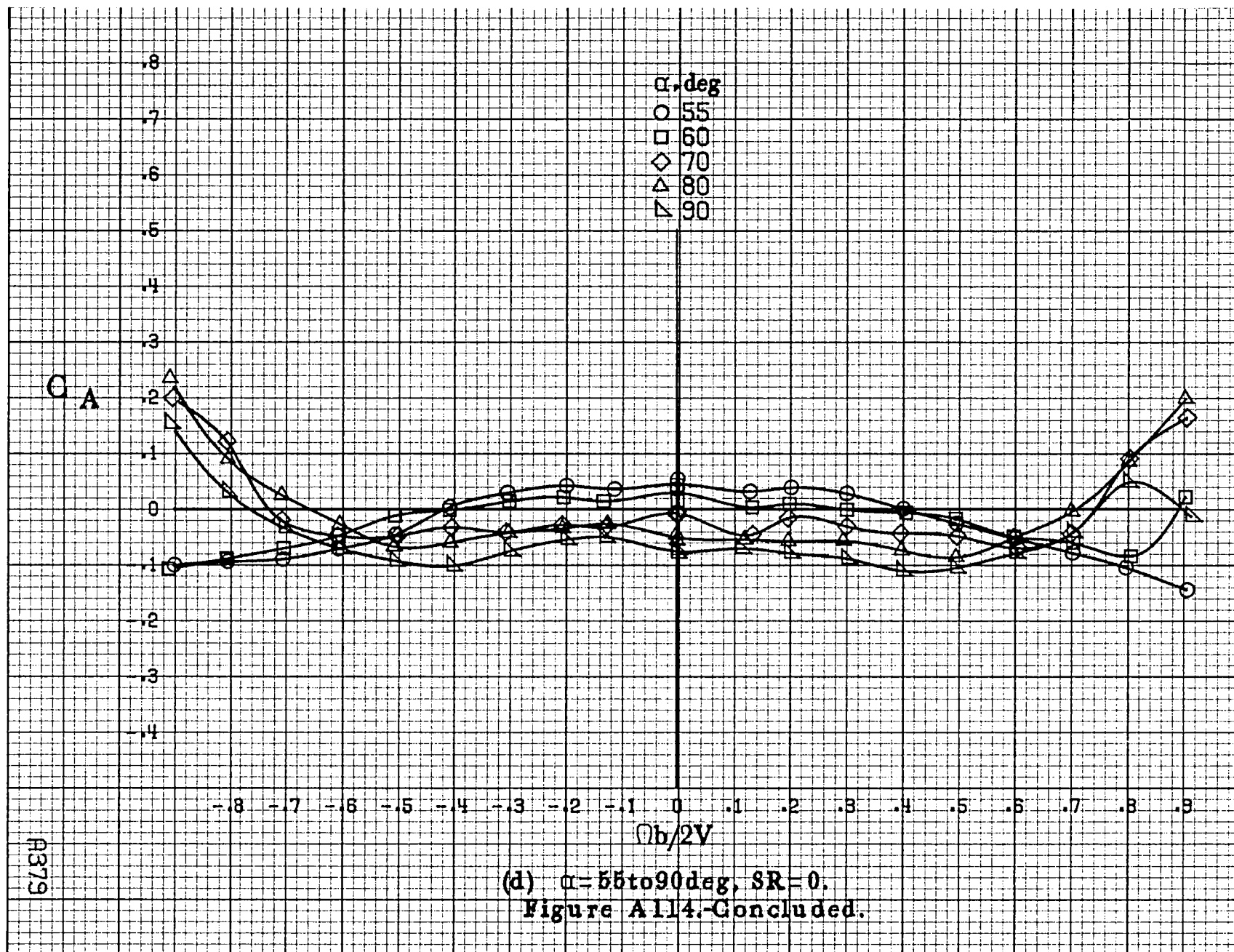


(a) $\alpha = 8$ to 16 deg, $SR = 76$ cm (30 in).

Figure A114.-Effect of rotation rate and angle of attack on axial-force coefficient for no. 3 horizontal tail configuration with full-span wing L.E. droop. $\delta_e = 0^\circ$, $\delta_n = 0^\circ$, $\delta_r = 0^\circ$, $\beta = 0^\circ$.







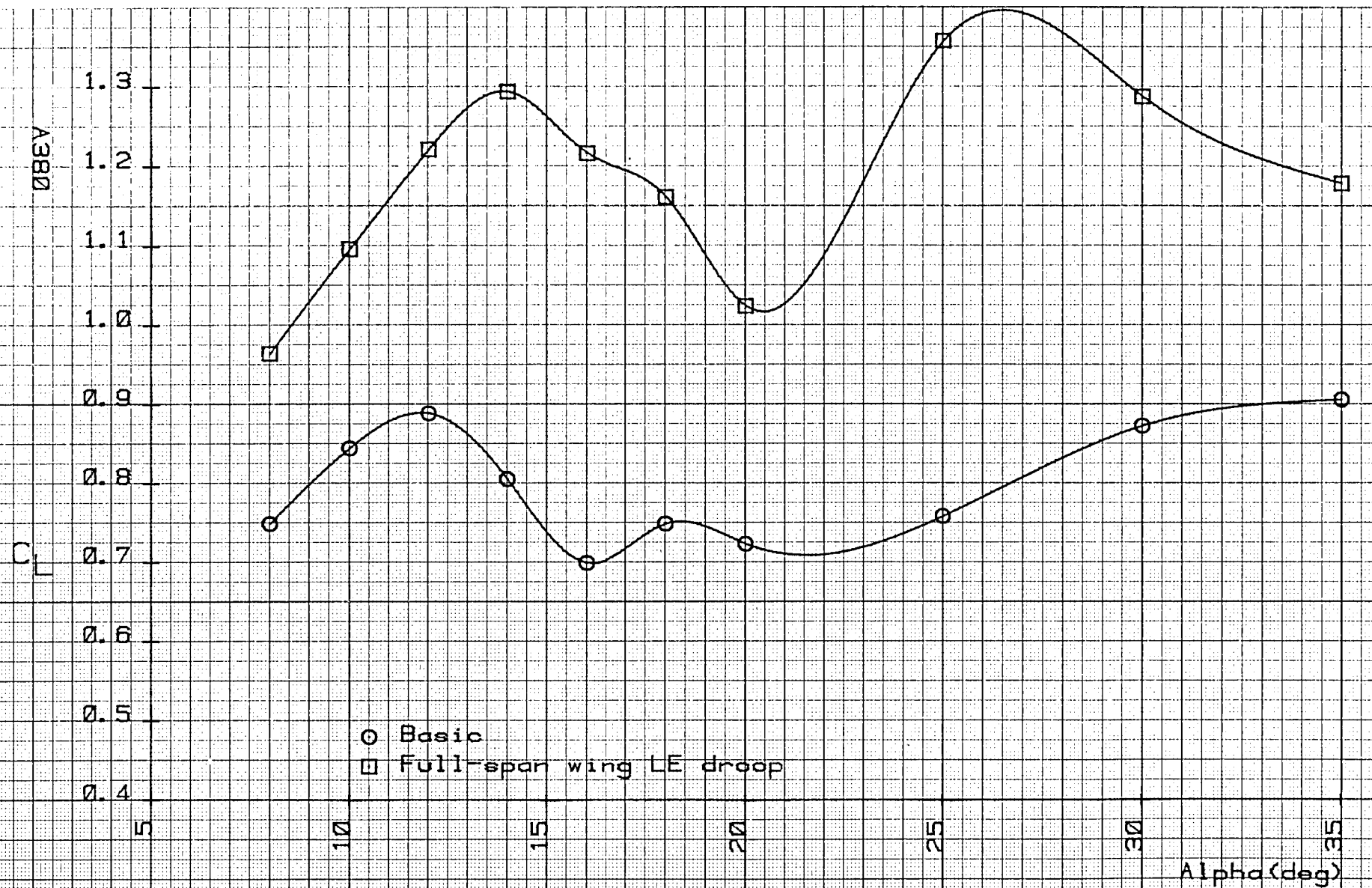


Figure A115.— Lift coefficient as a function of angle of attack for various model configurations.

1. Report No. NASA CR-3100		2. Government Accession No.		3. Recipient's Catalog No.	
4. Title and Subtitle Rotary Balance Data for a Typical Single-Engine General Aviation Design for an Angle-of-Attack Range of 8° to 90°. I - Low-Wing Model A				5. Report Date February 1980	
				6. Performing Organization Code	
7. Author(s) Randy S. Hultberg William Mulcay				8. Performing Organization Report No.	
				10. Work Unit No. 505-10-13-07	
9. Performing Organization Name and Address Bihle Applied Research, Inc. 400 Jericho Turnpike Jericho, New York 11753				11. Contract or Grant No. NAS1-14849, Task 31	
				13. Type of Report and Period Covered Contractor Report	
12. Sponsoring Agency Name and Address National Aeronautics and Space Administration Washington, DC 20546				14. Sponsoring Agency Code	
15. Supplementary Notes Langley Technical Monitor: James S. Bowman, Jr. Topical report					
16. Abstract Aerodynamic characteristics obtained in a rotational flow environment utilizing a rotary balance located in the Langley Spin Tunnel are presented in plotted form for a 1/5-scale, single-engine, low-wing, general aviation airplane model. The configuration tested included the basic airplane, various control deflections, tail designs, fuselage shapes and wing leading edges. Data are presented without analysis for an angle-of-attack range of 8° to 90° and clockwise and counter-clockwise rotations covering an $\frac{\Omega b}{2V}$ range from 0 to 0.85.					
17. Key Words (Suggested by Author(s)) General Aviation Spinning Rotary Balance High angle-of-attack wind tunnel data				18. Distribution Statement Unlimited - unclassified	
				Subject Category 02	
19. Security Classif. (of this report) Unclassified		20. Security Classif. (of this page) Unclassified		21. No. of Pages 398	
				22. Price* \$13.00	

National Aeronautics and
Space Administration

SPECIAL FOURTH CLASS MAIL
BOOK

Postage and Fees Paid
National Aeronautics and
Space Administration
NASA-451



Washington, D.C.
20546

Official Business

Penalty for Private Use, \$300

NASA

POSTMASTER: If Undeliverable (Section 158
Postal Manual) Do Not Return
